

2018

Utilising Cyclopropane Scaffolds in Synthetic Methodology and Syntheses of Prodrugs

Yi Sing Gee
University of Wollongong

Follow this and additional works at: <https://ro.uow.edu.au/theses1>

University of Wollongong

Copyright Warning

You may print or download ONE copy of this document for the purpose of your own research or study. The University does not authorise you to copy, communicate or otherwise make available electronically to any other person any copyright material contained on this site.

You are reminded of the following: This work is copyright. Apart from any use permitted under the Copyright Act 1968, no part of this work may be reproduced by any process, nor may any other exclusive right be exercised, without the permission of the author. Copyright owners are entitled to take legal action against persons who infringe their copyright. A reproduction of material that is protected by copyright may be a copyright infringement. A court may impose penalties and award damages in relation to offences and infringements relating to copyright material.

Higher penalties may apply, and higher damages may be awarded, for offences and infringements involving the conversion of material into digital or electronic form.

Unless otherwise indicated, the views expressed in this thesis are those of the author and do not necessarily represent the views of the University of Wollongong.

Recommended Citation

Gee, Yi Sing, Utilising Cyclopropane Scaffolds in Synthetic Methodology and Syntheses of Prodrugs, Doctor of Philosophy thesis, School of Chemistry, University of Wollongong, 2018. <https://ro.uow.edu.au/theses1/423>

Research Online is the open access institutional repository for the University of Wollongong. For further information contact the UOW Library: research-pubs@uow.edu.au

Utilising Cyclopropane Scaffolds in Synthetic Methodology and Syntheses of Prodrugs

A thesis submitted in fulfilment of the requirements for the award of the degree:

DOCTOR OF PHILOSOPHY

from

The University of Wollongong



by

Yi Sing Gee, BSc (Hons)

Supervisors: Dr Christopher J. T. Hyland, Dr Lezanne Ooi

School of Chemistry

June 2018

Declaration

I, Yi Sing GEE, declare that this thesis is submitted in fulfilment of the requirements for the conferral of the degree Doctor of Philosophy, from the University of Wollongong, is wholly my own work unless otherwise referenced or acknowledged. This document has not been submitted for qualifications at any other academic institution.

Yi Sing GEE

June 2018

*To dad, mum,
and my twenties*

Acknowledgements

I would like to express my sincere gratitude to the following people for their contributions throughout my PhD research, I could not have possibly made it to this day without their generous support and assistance.

First and foremost, I would like to thank my principal supervisor Dr Christopher Hyland for his patience and guidance over the last seven years. Ever since I was an undergraduate student, he has always been patient with all my endless questions. Up until now he still graciously points me to the right direction during my PhD research. He cheered the loudest over my achievements, and he taught me to pick up my pieces when I shattered. Having the opportunity to work and learn from him over all these years perhaps was one of the best thing that ever happened to me, and I will truly miss that part of my life.

Next, I would like to thank my co-supervisor Dr Lezanne Ooi for her expertise and guidance in neurobiology. I would also like to thank Dr Martin Engel and Dale Cross for testing my synthesised prodrugs on glioblastoma multiforme cell lines.

Special thanks to Dr Michael Gardiner for performing X-ray crystallography studies and Dr Jack Ryan for his expert opinion in organic chemistry. I would also like to express my appreciation to Professor Takayoshi Suzuki and co-workers for performing the LSD1 and MAOs inhibition assay.

I would like to acknowledge the efforts of all the chemists I collaborated during my PhD research: Niels Goertz, Dr Steven Wales, and especially Daniel Rivinoja. A special shout-out to all current and previous Hyland Group members for their friendship and support over all these years.

I am also grateful to the following staffs from UOW School of Chemistry: Dr Wilford Lie and Hairuddin Idris for the technical support in NMR; Dr Alan Maccarone, Dr Celine Kelso and Karin Maxwell for the technical support in mass spectrometry; Roza Dimeska for the technical support in IR.

Last but definitely not the least, I would like to thank my friends and family in Malaysia for their continuing love and support over the last nine years while I was studying in Australia. Thanks for making my dream come true.

Abstract

The ring-opening process of cyclopropane derivatives is prominent in biological processes and synthetic methodology. The reactivity of bifunctional three-membered rings is attributed to the ring-strain and the attached functional groups which can stabilise their ring-opened counterparts. This thesis reports the use of cyclopropane derivatives in synthetic methodology and syntheses of prodrugs – an overview of the thesis is provided in Chapter 1.

Chapter 2 reports the development of tumour selective prodrug Q-PAC, which liberates a 2-phenylcyclopropylamine moiety (2-PCPA, LSD1 inhibitor) and quinone methide (antioxidant scavenger) upon activation in GBM where ROS is abundant. As expected, prodrug Q-PAC selectively inhibited cell growth of GBM cells while healthy astrocytes remained unaffected.

Chapter 3 reports the preparation of metallocene derivatives for 2-PCPA. While the ferrocenyl derivatives unexpectedly underwent facile ring-opening to form β -hydroxyamides, the ruthenocenyl derivative was stable and displayed superior LSD1 inhibitory activity ($IC_{50} = 1.43 \mu\text{M}$) compared to its parent compound ($IC_{50} = 23.0 \mu\text{M}$).

The cyclopenta[*b*]indoline scaffold is featured in many bioactive compounds. Although many methods have been reported to prepare this scaffold, the resulting cyclopenta[*b*]indoline lacks of functional groups to allow further derivatisation. Chapter 4 reports the study of palladium-catalysed dearomative [3 + 2] cycloaddition of 3-nitroindoles with vinylcyclopropanes (VCPs). Using this method that we developed, densely functionalised cyclopenta[*b*]indolines were synthesised in good yield and moderate diastereoselectivity (up to 88% yield and 4.3:1 *dr*).

Abbreviations

2-PCPA	<i>trans</i> -2-Phenylcyclopropylamine/Tranlycypromine
4OHT	4-Hydroxytamoxifen
AIBN	Azobisisobutyronitrile
AML	Acute myeloid leukemia
ASAP	Atmospheric solids analysis probe
ATP	Adenosine triphosphate
ATRA	All- <i>trans</i> -retinoic acid
BBB	Blood brain barrier
Bn	Benzyl
Boc	<i>tert</i> -Butyloxycarbonyl
BPhen	Bathophenanthroline
BSO	Buthionine sulfoximine
Bz	Benzoyl
CLL	Chronic lymphocytic leukemia
CNS	Central nervous system
Cp	Cyclopentadienyl
Cy	Cyclohexyl
DA	Donor-acceptor
dba	Dibenzylideneacetone
DMAP	4-Dimethylaminopyridine
DPPA	Diphenylphosphoryl azide
<i>dr</i>	Diastereoselectivity
<i>ee</i>	Enantiomeric excess
EI	Electron ionisation
ESI	Electrospray ionisation
FAD	Flavin adenine dinucleotide
Fc	Ferrocene/Ferrocenyl
FDA	Food and Drug Administration
GBM	Glioblastoma multiforme
GSH	Glutathione
GSSG	Glutathione disulfide
H3K4me1/2	Mono- or dimethylated lysine 4 of histone 3

HDAC	Histone deacetylases
HMEC	Human mammary epithelial cells
HPLC	High-performance liquid chromatography
HRMS	High resolution mass spectrometry
IC ₅₀	Half maximal inhibitory concentration
IR	Infrared spectroscopy
K_i	Inhibitor constant
LSD1	Lysine-specific demethylase 1
MAOs	Monoamine oxidases
MNC	Mononuclear cells
MS	Mass spectrometry
NBS	<i>N</i> -Bromosuccinimide
NMR	Nuclear magnetic resonance spectroscopy
PBE	4-(Hydroxymethyl)phenylboronic acid pinacol ester
PCR	Polymerase chain reaction
PEITC	β -Phenylethyl isothiocyanate
QM	Quinone methide
ROS	Reactive oxygen species
SERM	Selective estrogen receptor modulator
SET	Single electron transfer
SOD	Superoxide dismutase
Tf	Trifluoromethanesulfonate
TFA	Trifluoroacetic acid
TFAA	Trifluoroacetic anhydride
TLC	Thin layer chromatography
TMM	Trimethylenemethane
Ts	Tosyl/Toluenesulfonyl
VCP	Vinylcyclopropane

Table of contents

Declaration	ii
Acknowledgements	iv
Abstract	v
Abbreviations	vi
<u>CHAPTER 1: UTILISING CYCLOPROPANE SCAFFOLDS IN SYNTHETIC METHODOLOGY AND SYNTHESSES OF PRODRUGS: THESIS OVERVIEW</u>	
1.1 Thesis overview	1
1.2 References	4
<u>CHAPTER 2: DESIGN AND SYNTHESIS OF A NOVEL DUAL-ACTION PRODRUG TO TARGET GLIOBLASTOMA MULTIFORME VIA LYSINE- SPECIFIC DEMETHYLASE (LSD1) INHIBITION AND GLUTATHIONE DEPLETION</u>	
2.1 Introduction	5
2.1.1 Glioblastoma multiforme (GBM)	5
2.1.2 Reactive oxygen species (ROS), glutathione (GSH) and the antioxidant system in cancers, such as GBM	7
2.1.3 Utilisation of reactive oxygen species (ROS) in cancer therapeutic strategies	11
2.1.4 Function of lysine-specific demethylase 1 (LSD1) and its role in cancers	17
2.1.5 Inhibition of LSD1 using trans-2-phenylcyclopropylamine (2- PCPA) analogues	20
2.1.6 Clinical trials involving 2-PCPA-based LSD1 Inhibitors	26
2.1.7 Other classes of LSD1 inhibitors	27
2.2 Aim and research plan	30
2.3 Results and discussion	33
2.3.1 Syntheses of prodrugs Q-PAC, Q-BrAC and QAC	33
2.3.2 Utilisation of mass spectrometry for the detection of Q-PAC active components upon activation	36
2.3.3 Evaluation of prodrugs on viability and migration in U87 glioblastoma cells	39

2.3.4 Higher selectivity of Q-PAC for GBM over healthy astrocytes	44
2.3.5 Effect of Q-PAC on histone modifications	48
2.3.6 Reduction of GSH levels in GBM cells after Q-PAC treatment	51
2.3.7 Q-PAC induced apoptosis in GBM by increasing caspase 3/7 activity	52
2.3.8 Proposed mechanism for the Q-PAC induced caspase-dependent apoptosis	55
2.3.9 Preparation and biological evaluation of iodinated prodrugs	56
2.3.10 Biological evaluation of reported LSD1 inhibitors on GBM cells	62
2.4 Conclusions and future work	70
2.5 Experimental	73
2.5.1 General experimental details for organic syntheses	74
2.5.2 Preparation of Q-PAC and its precursors	75
2.5.3 Preparation of Q-BrAC and its precursors	78
2.5.4 Preparation of QAC	80
2.5.5 Preparation of Q-2IAC and its precursors	81
2.5.6 Preparation of Q-3IAC and its precursors	85
2.5.7 Preparation of Q-4IAC and its precursor	89
2.5.8 Preparation of 11 and its precursors	91
2.5.9 Preparation of 12 and its precursors	92
2.5.10 Preparation of 13 and its precursor	95
2.5.11 Preparation of bizine and its precursors	97
2.5.12 ESI-MS experiment for prodrug activation	100
2.5.13 Culture details for cell culture assays	101
2.5.14 Confluence assay	102
2.5.15 Migration assay	102
2.5.16 Invasion assay	103
2.5.17 Cell viability assay	103
2.5.18 Apoptosis assay	103
2.5.19 Immunocytochemistry	104
2.5.20 Western blot	104
2.5.21 GSH assay	105
2.5.22 Reactive oxygen species (ROS) quantification	105

2.5.23 Statistical analysis	106
2.6 References	106
<u>CHAPTER 3: SYNTHESIS AND BIOLOGICAL EVALUATION OF METALLOCENE DERIVATIVES OF CYCLOPROPYLAMINES</u>	
3.1 Introduction	112
3.1.1 Oxidative ring-opening of cyclopropylamines	112
3.1.2 Application of ferrocene in medicinal chemistry	124
3.2 Aim and research plan	127
3.3 Results and discussion	130
3.3.1 Preparation of 2-PCPA derivatives	130
3.3.2 Oxidative ring-opening of ferrocenylmethylcyclopropylamines	132
3.3.3 Proposed mechanism for the formation of β -hydroxyamides derived from oxidative ring-opening of ferrocenylmethylcyclopropylamines	134
3.3.4 Role of stable radical intermediate in the oxidative ring-opening of ferrocenylmethylcyclopropylamines	137
3.3.5 Trapping benzylic radical intermediate 68 in [3 + 2] cycloaddition	139
3.3.6 Preparation of ruthenocene derivatives of 2-PCPA	141
3.3.7 Selectivity and potency of ruthenocetyl-2-PCPA 76 in LSD1 inhibition	143
3.4 Conclusion and future work	144
3.5 Experimental	146
3.5.1 Esterification of cinnamic acids	147
3.5.2 Corey–Chaykovsky cyclopropanation of ethyl cinnamates	151
3.5.3 Basic hydrolysis of esters	157
3.5.4 Curtius rearrangement of carboxylic acids with <i>t</i> -BuOH + Deprotection of Boc-group	162
3.5.5 Oxidative ring-opening of ferrocenylmethylcyclopropylamines	169
3.5.6 Preparation of <i>N</i> -(ferrocenylmethyl)-cyclopropylamine 73	179
3.5.7 Preparation of ruthenocene derivatives	180
3.5.8 X-ray crystallography	182
3.5.9 In vitro assay of ruthenocetyl-2-PCPA 76	183
3.6 References	183

**CHAPTER 4: PALLADIUM-CATALYSED DEAROMATIVE [3 + 2]
CYCLOADDITION OF 3-NITROINDOLES WITH VINYL-CYCLOPROPANE
DICARBOXYLATES**

4.1 Introduction	186
4.1.1 Activation of vinylcyclopropanes by Pd catalysts in cycloadditions	186
4.1.2 Vinylcyclopropanes in nucleophilic additions catalysed by Pd(0)	199
4.1.3 Indoline-derived heterocycles	204
4.2 Aim and research plan	208
4.3 Results and discussion	211
4.3.1 Optimisation of reaction conditions	211
4.3.2 Reaction scope	223
4.3.2.1 Preparation of indole and VCP substrates	223
4.3.2.2 Scope of reaction	225
4.3.3 Chemical transformation of cyclopenta[<i>b</i>]indolines and pyrroloindoline	232
4.3.4 Proposed reaction mechanism	238
4.4 Conclusion and future work	241
4.5 Experimental	245
4.5.1 Preparation of 2-vinylcyclopropane-1,1-dicarboxylates	245
4.5.2 Preparation of indole substrates	249
4.5.3 Typical procedure for Pd-catalyzed dearomative [3 + 2] cycloaddition of 3-nitroindoles with 2-vinylcyclopropane-1,1-dicarboxylates	255
4.5.4 Chemical transformation of cyclopenta[<i>b</i>]indoline derivatives	275
4.5.5 X-ray crystallographic information	283
4.6 References	284
<u>APPENDIX 1: SUPPORTING FIGURE FOR CHAPTER 2</u>	287
<u>APPENDIX 2: NMR SPECTRA FOR CHAPTER 2</u>	289
<u>APPENDIX 3: NMR SPECTRA FOR CHAPTER 3</u>	317
<u>APPENDIX 4: NMR SPECTRA FOR CHAPTER 4</u>	352
<u>APPENDIX 5: PUBLICATIONS</u>	405

Chapter 1

Utilising cyclopropane scaffolds in synthetic methodology and syntheses of prodrugs:

Thesis overview

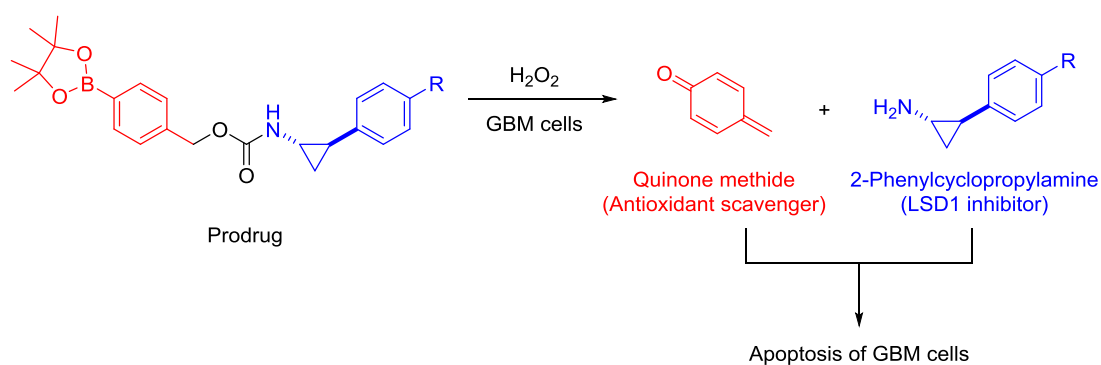
1.1 Thesis overview

Bifunctional three-membered rings, such as cyclopropylamines and vinylcyclopropanes (VCP), are useful scaffolds in synthetic methodologies and medicinal chemistry. Apart from the intrinsic ring-strain in cyclopropane (strain energy = 27.5 kcal/mol)¹ that acts as a thermodynamic driving force, their reactivities are greatly influenced by the functional groups present on the ring. These spring-loaded scaffolds can participate in reactions upon chemical activation, or biological processes when interacting with cellular enzymes.

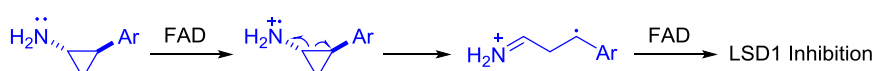
Glioblastoma multiforme (GBM) is the most aggressive form of brain cancer with poor survival rate,² unfortunately current available treatments either have difficulty in administration or undesired side effects after treatment. Various cancers, including GBM, express elevated level of lysine-specific demethylase 1 (LSD1) which causes abnormal demethylation of histone proteins and subsequently suppression of tumour suppressor genes.³ Therefore, 2-phenylcyclopropylamine (2-PCPA)-based LSD1 inhibitors were studied and they demonstrated promising outcome in cancer treatment studies. The FAD cofactor in the active site of LSD1 carries out the single electron oxidation of amine nitrogen on 2-PCPA which leads to the ring-opening of cyclopropane. As a result, the ring-opened distonic radical cation fuses with FAD and irreversibly inhibits LSD1 (Scheme 1). Meanwhile, boronate-containing compounds also recently emerged as a new class of prodrug which selectively target cancer cells

with release of toxic quinone methides. In Chapter 2, inspired by the potency and selectivity of these motifs towards cancer cells, we designed and created a prodrug hybrid of these two motifs to harness the reactive distonic radical cation and quinone methide, which was subjected to in vitro evaluation on GBM cells and healthy astrocytes (Scheme 1).

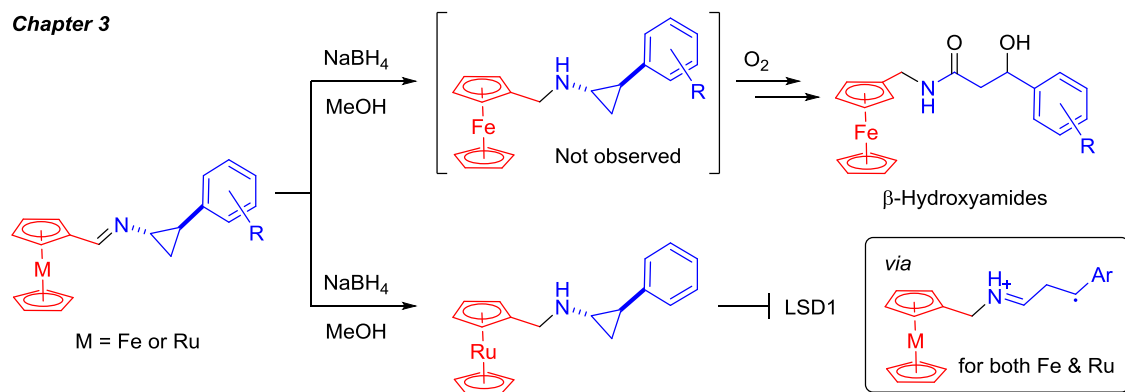
Chapter 2



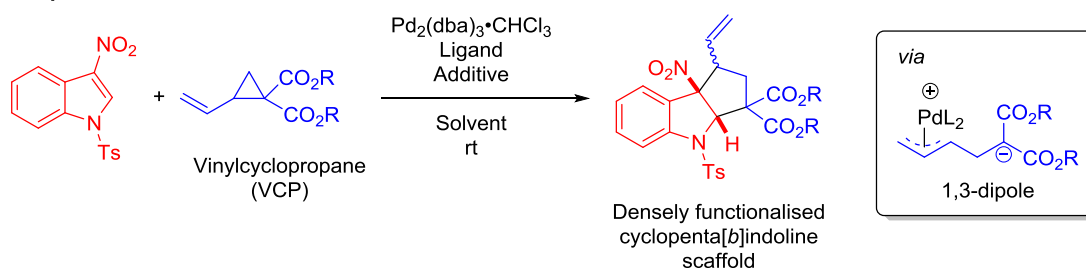
Single electron oxidation of 2-PCPA leads to ring-opening & LSD1 inhibition



Chapter 3



Chapter 4



Scheme 1: Thesis overview.

Incorporation of redox active metallocenes into existing drugs has been reported to enhance drug potency and provide a secondary mechanism to induce cytotoxicity, for example, the ferrocene derivatives of the breast cancer drug tamoxifen (namely ferrocifen) demonstrated remarkable antiproliferative effect on hormone-independent breast cancer cell line MDA-MB-231 while hydroxytamoxifen (the active metabolite of tamoxifen) was inactive.⁴ Syntheses of metallocene derivatives of 2-PCPA will be discussed in Chapter 3 (Scheme 1). It was revealed that ferrocene-derivatives of 2-PCPA were susceptible to spontaneous oxidative ring-opening in air to form β -hydroxyamides, where the reaction mechanism was similar to that of 2-PCPA with FAD/LSD1 except molecular oxygen was the oxidant in this case. Chapter 3 discusses the substrate scope of this ring-opening process that proceeds via proposed distonic radical cation, and also the preparation and in vitro evaluation of air-stable ruthenocene derivative of 2-PCPA (Scheme 1).

The cyclopenta[*b*]indoline scaffold is featured in many bioactive compounds, such as diazepinoindoline (treatment and prevention of central nervous system disorders)⁵ and polyveoline (antitrypanosomal alkaloid)⁶. Although many methods have been reported to prepare this scaffold in high yield, the resulting cyclopenta[*b*]indoline lacks functional groups to allow further derivatisation, which poses a challenge to access structures with higher complexity. A solution to this problem is found in the cycloaddition of 3-nitroindoles with vinylcyclopropanes (VCPs) that affords densely functionalised cyclopenta[*b*]indolines. Pd(0) catalyses the formation of zwitterionic 1,3-dipoles from VCPs, which then react with 3-nitroindoles in a [3 + 2] cycloaddition fashion to yield the cyclopenta[*b*]indolines (Scheme 1). Chapter 4 reports the study of Pd-catalysed dearomative and diastereoselective [3 + 2] cycloaddition of 3-nitroindoles with VCPs, which details the reaction optimisation, substrate scope and proposed

reaction mechanism. This chapter also demonstrates the utility of these densely functionalised cyclopenta[*b*]indoline in further chemical transformations.

1.2 References

- (1) Seiser, T.; Saget, T.; Tran, D. N.; Cramer, N. *Angew. Chem. Int. Ed.* **2011**, *50*, 7740.
- (2) Singh, M. M.; Manton, C. A.; Bhat, K. P.; Tsai, W. W.; Aldape, K.; Barton, M. C.; Chandra, J. *Neuro. Oncol.* **2011**, *13*, 894.
- (3) Suzuki, T.; Miyata, N. *J. Med. Chem.* **2011**, *54*, 8236.
- (4) Top, S.; Vessières, A.; Leclercq, G.; Quivy, J.; Tang, J.; Vaissermann, J.; Huché, M.; Jaouen, G. *Chem. - Eur. J.* **2003**, *9*, 5223.
- (5) Welmaker, G. S.; Sabalski, J. E.; Smith, M. D. US20020058689A1, 2002.
- (6) Ngantchou, I.; Nyasse, B.; Denier, C.; Blonski, C.; Hannaert, V.; Schneider, B. *Bioorg. Med. Chem. Lett.* **2010**, *20*, 3495.

Chapter 2

Design and synthesis of a novel dual-action prodrug to target glioblastoma multiforme via lysine-specific demethylase 1 (LSD1) inhibition and glutathione depletion

2.1 Introduction

2.1.1 Glioblastoma multiforme (GBM)

Glial cells are a broad class of non-neuronal cells that provide physical support and protection to neurons in the central and peripheral nervous systems. The name was derived from the ancient Greek word “glía” which means glue. This class of cells are regarded as the “glue” to hold neurons together, they also supply oxygen and nutrients to neurons while removing neurotoxic substances. Half of the brain volume is comprised of different glial cells, such as astrocytes, oligodendrocytes and microglia.¹ The star-shaped cells, astrocytes, are the most abundant cell types in the human brain. They are mainly responsible for the distribution of neurotransmitters around synapses, maintenance of ion balance and detoxification of xenobiotics.² Oligodendrocytes produce the myelin sheath, which is a fatty substance that wraps around axons – this myelin sheath acts as insulation to the axon so that electrical messages can be delivered faster. As the main immune defence in the central nervous system (CNS), microglia are macrophages that protect the CNS from pathogens, toxins and remove dead or damaged cells from the CNS.

Glioblastoma multiforme (GBM) is the most aggressive and fatal form of brain cancer. GBM patients have a median survival of 12 to 15 months after diagnosis, while the five-year survival rate is merely 5%.³⁻⁵ The life expectancy is significantly reduced to 3 months if left untreated.⁶ This glioma was observed to grow rapidly and invade

neighbouring tissue easily, hence it is notorious for its highly malignant character and frequent reoccurrence in patients even after treatment.

Higher incidence of GBM is recorded in senior citizens, Caucasians and males.⁷ The aetiology and cause for this disease remain unclear. Although the cell of origin for glioblastoma remains inconclusive, recent studies suggested that astrocytes and oligodendrocyte progenitor cells could serve as the cell of origin.^{8,9}

Although treatment options for GBM are available, these options possess difficulty in execution and often cause undesirable side effects. First lines of defence are surgery, radiation therapy, anti-angiogenic agents and chemotherapy. In surgical removal, the tumour is often surrounded by sensitive brain cells which have low capacity in self-repair, therefore it is challenging to access the tumour and remove it completely without damaging the surrounding tissue. Also, metastasis to other parts of the brain means that surgery alone is often unsuccessful. In terms of challenges in chemotherapy, the intrinsic defence of the brain, the blood brain barrier (BBB), hinders some drug molecules from entering the target site, therefore reducing the efficacy of chemotherapy. Therefore chemotherapeutic drugs need to be designed to cross the BBB or other strategies employed to deliver them directly to the brain. Temozolomide is an FDA approved oral chemotherapy drug that alkylates DNA and triggers apoptosis. Moreover, administration of temozolomide was observed to sensitise tumours for radiotherapy.¹⁰ However, significant toxicities and side effects are associated with administration of temozolomide, such as thrombocytopenia, lymphopenia, neutropenia and myelodysplastic syndrome.¹¹ In a treatment trial combining radiotherapy and temozolomide, 15 to 20% of all patients in this regimen were affected by at least one of the side effects stated above, which resulted in premature discontinuance in treatment in some cases.¹² Nevertheless, it is still less toxic than other alkylator-based chemotherapies, such as nitrosoureas.¹¹

In addition to the challenges and side effects in GBM treatments, the prognosis for GBM is notoriously poor even with therapies. Furthermore, despite innovative therapies being introduced for the treatment of GBM (such as molecularly targeted agents, immunotherapy and gene therapy),¹³ there has been a lack of significant improvement on extending patient survival over the last few decades. From 2009 to 2013, Australians diagnosed with brain and other CNS cancer had an average of 25% chance of surviving for 5 years compared with others in the general population, and this rate has remained steady over the last 30 years.¹⁴ In order to improve patient survival rate, there is a pressing need to develop novel and efficient treatment options that can either prevent or minimise undesired side effects.

2.1.2 Reactive oxygen species (ROS), glutathione (GSH) and the antioxidant system in cancers, such as GBM

Reactive oxygen species (ROS) is a broad term covering reactive chemical species that are oxygen-containing, such as the superoxide anion radical ($O_2^{\bullet-}$), the hydroxyl radical (HO^{\bullet}) and hydrogen peroxide (H_2O_2). ROS in living organisms can be derived from exogenous sources, such as tobacco¹⁵, pollutants¹⁶ and radiation¹⁷, or from endogenous sources, as a by-product of the electron transport chain during mitochondrial respiration. During the synthesis of ATP by the electron transport chain, electrons are transferred between proteins in a process that ultimately reduces oxygen to water. A small proportion of the electrons can leak from the chain and partially reduce oxygen molecules to superoxide. It has been estimated that around 0.2 – 2% of the molecular oxygen consumed by mitochondria is converted to superoxide.¹⁸ Subsequently, superoxide dismutase (SOD) can carry out the dismutation of superoxide into oxygen and hydrogen peroxide. Other biological processes can also give rise to ROS as by-products, for

example during β -oxidation in peroxisomes, synthesis of prostaglandin or metabolism reactions by cytochrome P450.¹⁹

Excessive amounts of ROS can exert oxidative damage to cellular contents such as DNA, proteins and lipids. Although ROS can be harmful in organisms due to their high reactivity, a moderate amount of ROS is essential for biological functions. ROS is involved in signalling and regulation of cellular functions, such as cell proliferation, differentiation, metabolism and the DNA damage response.²⁰

Intrinsic antioxidant or ROS-scavenging systems are in place to prevent oxidative cellular damage. SOD, glutathione peroxidase and catalase are examples of enzymes that detoxify ROS in cells. Furthermore, the tripeptide antioxidant, glutathione (GSH, consisting glutamate, cysteine and glycine, Figure 1) is one of the main antioxidants, in which the cysteine thiol group acts as the reducing agent. GSH is oxidised to glutathione disulfide (GSSG) upon reducing superoxide and hydroxyl radicals.²¹ The conversion of GSH to GSSG also occurs when GSH peroxidases reduce hydrogen peroxide and organic peroxides. GSSG reductase converts GSSG back to GSH in order to counteract further ROS.

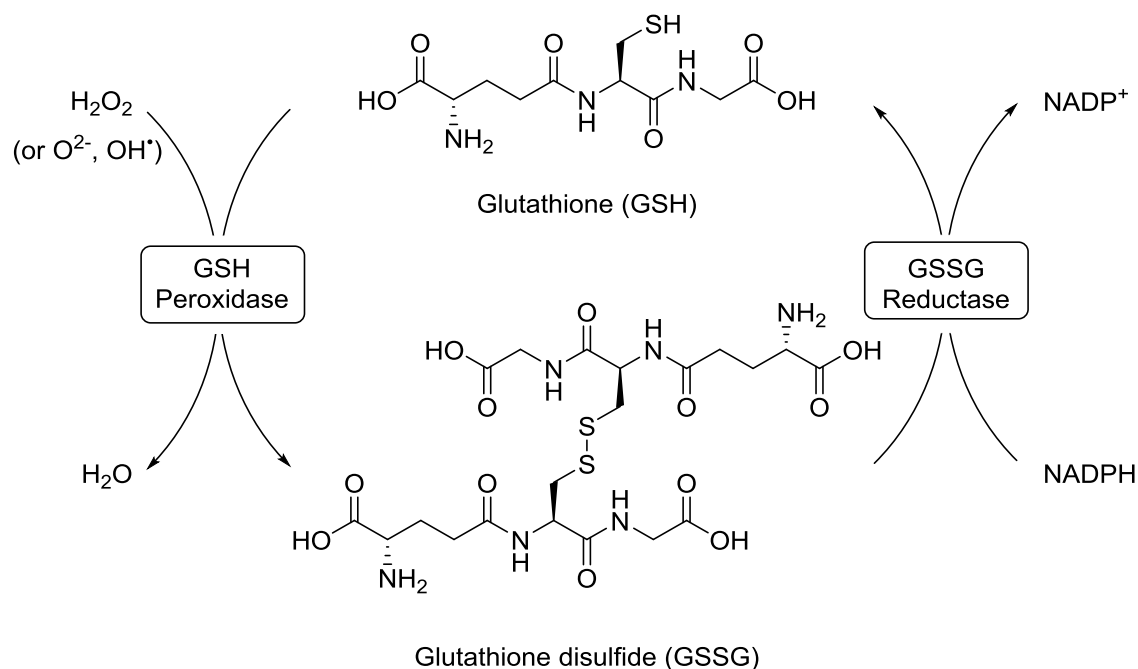


Figure 1: Antioxidant glutathione (GSH) is converted to glutathione disulfide (GSSG) while reducing ROS (such as H_2O_2 , O_2^- and OH^\bullet). GSSG is then reduced to GSH in order to counteract further oxidative stress.

When the ROS balance within the cells is disrupted by elevated level of ROS and/or reduced capacity in antioxidant, the cells are said to be under oxidative stress. Growing evidence has shown that various types of cancers have increased level of ROS.²²⁻²⁴ The intracellular concentration of H_2O_2 in normal cells ranges between 1 – 700 nM, where 1 μM is considered toxic.²⁵ On the other hand, cancer cells can withstand a higher H_2O_2 concentration of 10 – 100 μM , which is more than 10 fold higher than in normal cells.²⁶ These highly reactive ROS damage nucleic acids, proteins and lipids, therefore they can lead to DNA mutations, cancer cell proliferation, metastasis and angiogenesis.²⁷

It has been postulated that while cancer cells generate higher ROS levels they also upregulate antioxidant systems to maintain the redox homeostasis.¹⁹ This adaptive mechanism is vital for cancer cells to survive under the high oxidative stress conditions by regulating ROS levels within the range where severe oxidative damage and apoptosis

can be avoided. For instance, *H-Ras*-transformed ovarian epithelial T29H cells with high concentrations of ROS were found to have elevated levels of the antioxidants peroxiredoxin-3 and thioredoxin peroxidase, compared to their non-tumorigenic equivalents.²⁸ *Ras*-transformed cells were also found to be prone to cell death upon glutathione depletion, implying the vital role of GSH to maintain their survival.²⁹ As such, interfering with the redox balance by suppression of the antioxidant system could be a feasible avenue for cancer treatment.

Due to the significant role GSH plays in cancer cell survival, several studies have been focussing on scavenging GSH or inhibiting its production to allow ROS accumulation and hence induce apoptosis. β -Phenylethyl isothiocyanate (PEITC, Figure 2) conjugates with GSH, therefore depleting the GSH pool. Trachootham et al. showed that when *Ras*-transformed ovarian epithelial cells T72 (T72Ras) were treated with PEITC, substantial increase in ROS and concomitant cell death were observed.²⁹ An in vivo study also showed that PEITC treatment extends animal survival.²⁹ Without treatment, mice inoculated with T72Ras cells have a median survival time of 25 days. The median survival time was significantly improved to 48 days when mice were treated with PEITC by i.p. injection (50 mg/kg, five times per week).

γ -Glutamylcysteine synthetase is another attractive target for impairing cancer cells antioxidant system as it ligates glutamate and cysteine and is the rate-limiting enzyme in the production of GSH. As buthionine sulfoximine (BSO, Figure 2) inhibits γ -glutamylcysteine synthetase, Maeda et al. investigated the synergistic effect of BSO and arsenic trioxide (As_2O_3 , ROS generator) on 11 cancer cell lines and it was observed that the growth inhibition effect was enhanced by 1.2 to 52.5-fold compared to administration of As_2O_3 alone.³⁰

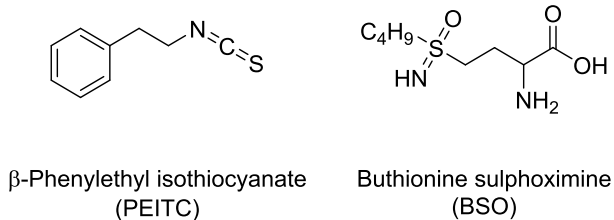


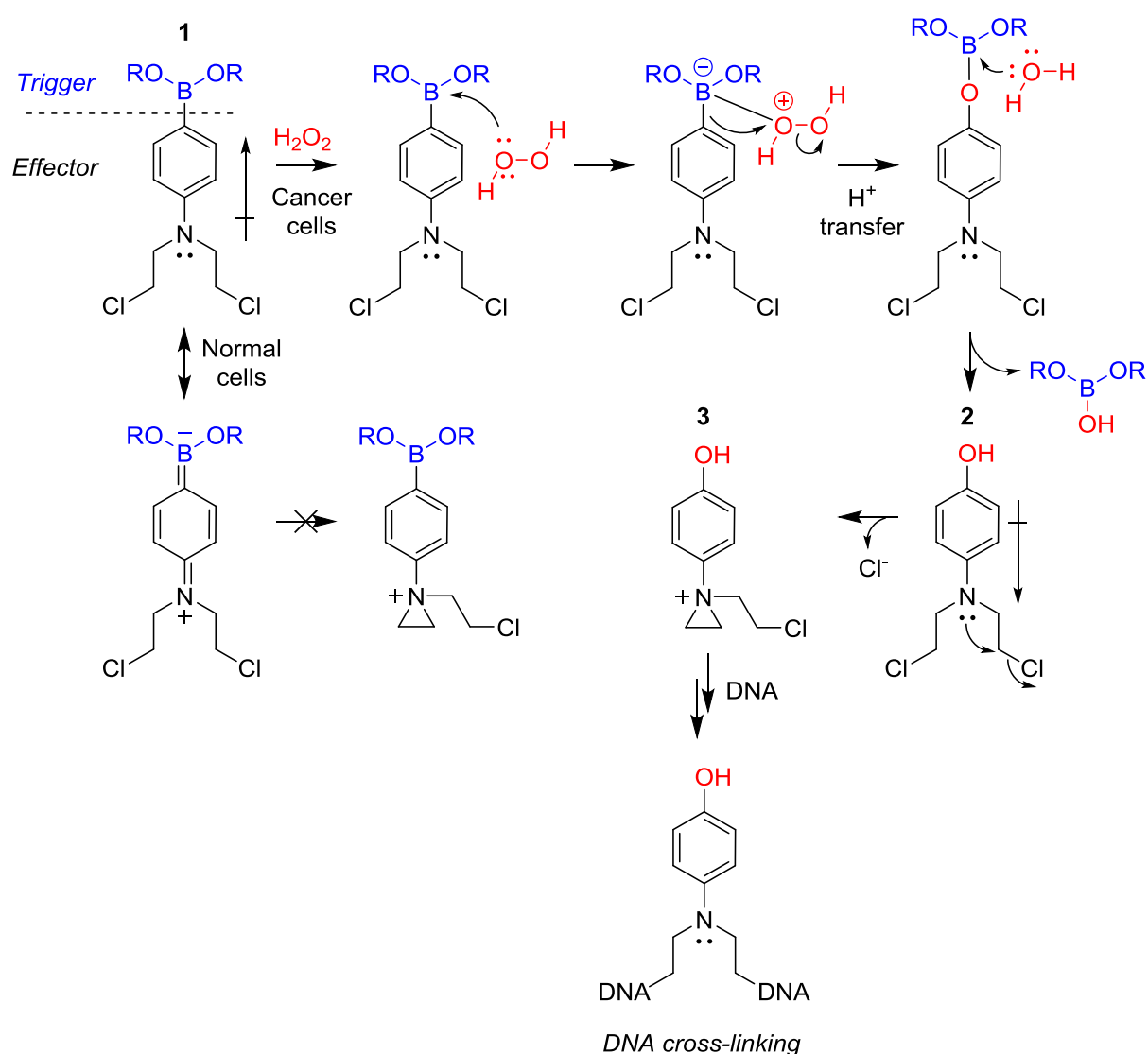
Figure 2: Inhibitors of the antioxidant system (PEITC and BSO).

2.1.3 Utilisation of reactive oxygen species (ROS) in cancer therapeutic strategies

The presence of elevated ROS associated with cancer cells has been harnessed to develop selective anti-cancer treatments. Several research groups have exploited the high ROS content of cancer cells to develop cancer-specific prodrugs. These prodrugs usually consist of a “trigger” moiety and an “effector”/“drug” moiety. The trigger moiety is initiated only upon exposure to H_2O_2 , which subsequently leads to activation of the effector unit to induce cytotoxicity in cancer cells.²⁷ Aryl boronates have been commonly utilised as a trigger unit in these cases because they are readily available and can be oxidatively cleaved selectively by H_2O_2 , which is abundant in cancer cells. As the activation of an aryl boronate prodrug relies on the concentration of H_2O_2 , cytotoxicity should be lower in healthy cells that maintain reduced levels of ROS, compared to cancer cells.

Peng and co-workers developed a series of ROS-initiated DNA cross-linking agents (nitrogen mustards) that selectively induced apoptosis in chronic lymphocytic leukemia (CLL) over normal lymphocytes (Scheme 2).³¹ Once the carbon-boron bond of these aryl boronate prodrugs **1** is oxidised by H_2O_2 and transformed into alcohol **2**, the electron density on the aromatic ring is increased – inducing the formation of a highly electrophilic aziridinium ring **3**, which is susceptible to cross-linking with DNA. Without

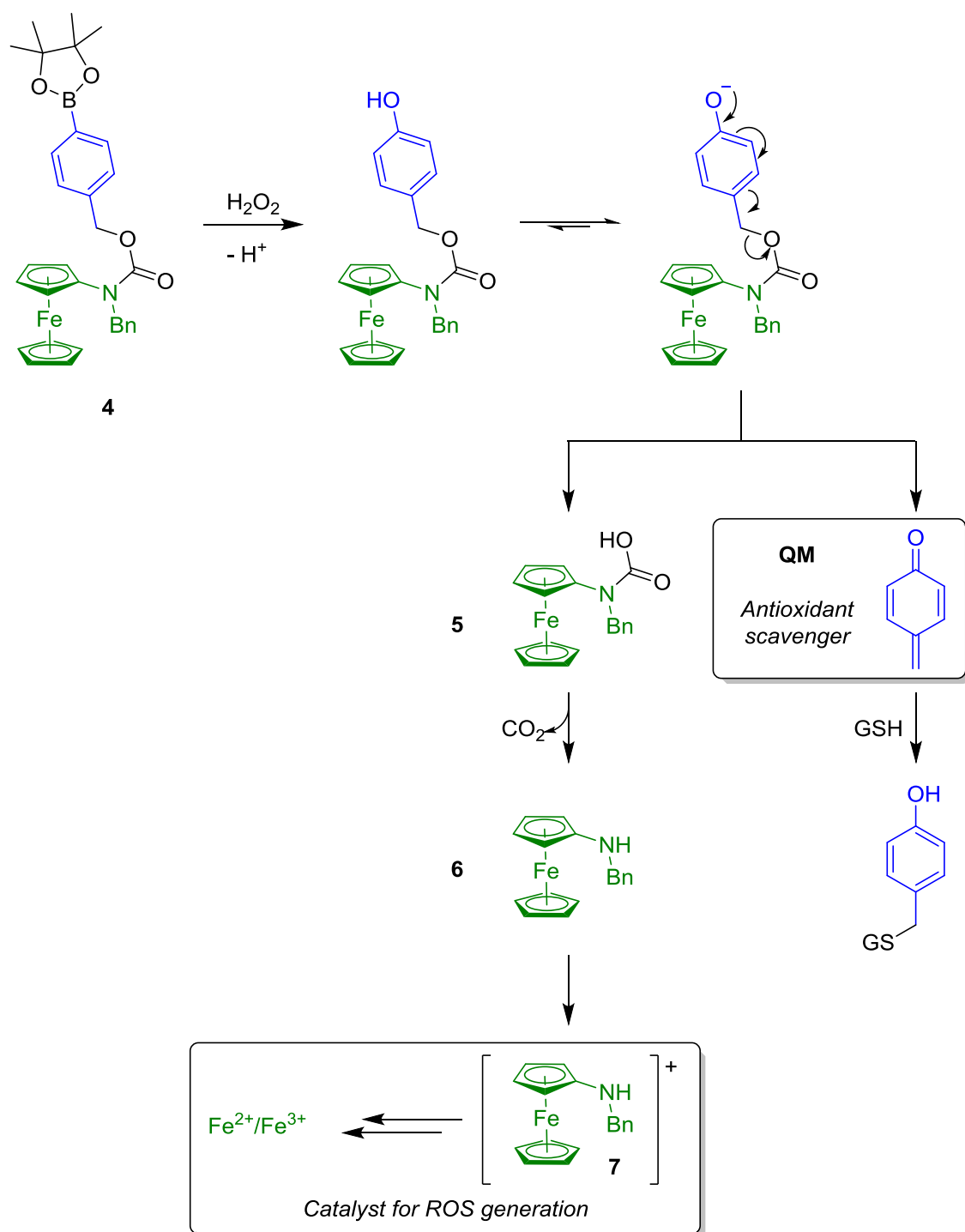
exposure to H_2O_2 , the lone pair on the nitrogen mustard is unavailable for aziridinium formation as it is delocalised into the benzene ring, due to the presence of an electron-withdrawing boronate group attached to the ring, therefore these prodrugs will not affect normal cells. As a result, the most potent analogue in this study had an IC_{50} value of 5 – 6 μM in CLL, while normal lymphocytes remained unaffected.



Scheme 2: Mechanism of DNA cross-linking by ROS-induced nitrogen mustards.^{31,32}

Recent interest in aryl boronate prodrugs has been focussing on dual action to induce cytotoxicity. Mokhir and co-workers reported several studies on dual-action prodrugs (**4**), which give rise to catalysts for ROS generation *and* antioxidant scavengers

upon activation (Scheme 3).^{26,33-35} Upon entering cancer cells and exposure to H₂O₂, the aryl boronate group of **4** is converted into a phenol, which is in equilibrium with the corresponding phenolate. The phenolate can then undergo 1,6-elimination to give compound **5** and *p*-quinone methide (QM). Compound **5** is unstable and undergoes decarboxylation to yield compound **6**, followed by oxidation of the ferrocene moiety to yield ferrocinium ion **7** that can serve as a catalyst for ROS production. Furthermore, **7** eventually decomposes in water to give Fe²⁺/Fe³⁺, which can also generate ROS catalytically. Meanwhile, GSH is quenched through the nucleophilic addition to QM, the antioxidant scavenger. The high electrophilicity of QM is attributed to the activated conjugated system, which aromatises upon nucleophilic attack, therefore making it susceptible to nucleophilic addition of GSH. As a result, the death of cancer cells is accelerated as the antioxidant level is decreasing, while the ROS concentration is increasing. The most potent prodrug **4** in these studies is toxic towards several cancer cell lines (IC₅₀ = 1.5 – 27 μM), and non-toxic towards non-malignant cells such as fibroblasts and mononuclear cells (MNC) (Table 1).^{26,33,35} In vivo experiments also revealed that prodrug **4** (6 daily doses of 26 μg/kg) extended the survival of BDF1 hybrid mice (DBA/2,♀ × C57Bl/6,♂) implanted with L1210 leukemia from 13.7 ± 0.6 days to 17.5 ± 0.7 days.³⁴



Scheme 3: Activation mechanism of aminoferrocene-based prodrugs in cancer cells with higher concentration of ROS. Upon activation, electrophilic QM will be generated to scavenge GSH, therefore leaving oxidative stress unsuppressed. At the same time ferrocenium 7 and inorganic iron species will be generated to generate ROS and hence amplifying oxidative stress.

Table 1: Cytotoxicities and selectivities of aminoferrocene-based prodrug **4** in cancer cells.^{26,33,35}

Malignant/Normal Cells	Cell Lines	IC₅₀ (μM)
Malignant	HL-60 (Human promyelocytic leukemia)	9
	U373 (Human glioblastoma-astrocytoma)	25
	CLL (Chronic lymphocytic leukemia)	1.5
	DU145 (Prostate cancer)	18 - 27
	LNCaP (Prostate cancer)	11 - 17
Normal	Fibroblasts	> 100
	MNC (Mononuclear cells)	> 10

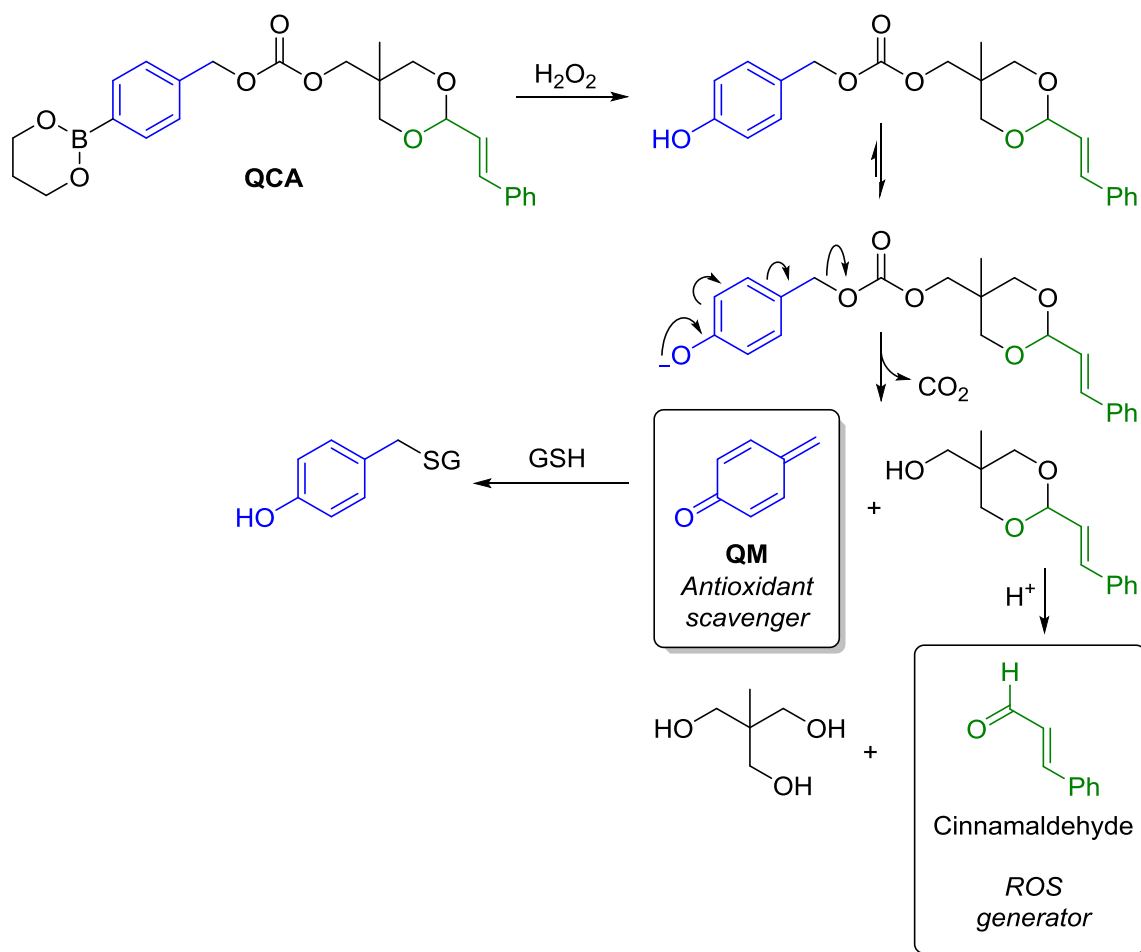
Noh et al. recently reported the dual stimuli-responsive hybrid anticancer drug QCA (Scheme 4).³⁶ The prodrug relied on not only ROS, but also acidic pH for activation, which is a property displayed in the extracellular microenvironment of cancer cells due to rapid glycolysis and lactic acid production.³⁷ Similar to the work from Mokhir and co-workers, upon prodrug activation, QM will be liberated from QCA as the antioxidant scavenger but with cinnamaldehyde as the ROS generator. Cinnamaldehyde induces ROS production in mitochondria and inhibits growth of cancer cells. More importantly, it possesses minimal cytotoxicity to normal cells. However the use of cinnamaldehyde in clinical applications has been limited by its poor bioavailability due to the aldehyde group being prone to rapid oxidation. Therefore, masking cinnamaldehyde in the form of acetal in prodrug QCA extends its bioavailability, due to the stability of this moiety under non-acidic aqueous conditions. The prodrug activation mechanism is similar to the above study from Mokhir and co-workers – after 1,6-elimination and decarboxylation, QM and an acetal-protected cinnamaldehyde are released. The acetal-protected cinnamaldehyde can then be unmasked under aqueous acidic conditions to release the ROS-generating

cinnamaldehyde. The acetal-deprotection selectively occurs in cancer cells as the extracellular pH of cancer cells ranges from 6.2 – 6.9 whereas the value of that in normal cells is usually 7.3 – 7.4.³⁸

In the studied cell lines, human prostate cancer DU145 was found to have the highest level of H₂O₂ and GSH, while normal mouse fibroblast NIH3T3 had the least amount of these species.³⁶ As a result, a remarkable decrease in GSH level was observed in DU145 cells following treatment with QCA. QCA induced cytotoxicity in DU145 (IC₅₀ = 48 µM) and colon cancer SW620 (IC₅₀ = 76 µM) cells, while minimal cytotoxicity was found in normal NIH3T3 cells (IC₅₀ = 182 µM). Even though the selectivity towards human cancer cell lines was promising, perhaps normal human cells should be used as comparison, rather than using mouse fibroblast NIH3T3.

In the *in vivo* study, mice were subcutaneously injected with SW620 or DU145 cells and treated with QCA at a physiologically relevant dose of 2 mg/kg every 3 days for 22 days. Mice treated with QCA had a significantly smaller tumour mass compared to mice treated with cinnamaldehyde and/or quinone methide-generator. Furthermore, no observable damages or lesions were found in the heart or liver, therefore suggesting that QCA can exhibit anticancer effects without inducing off-target cytotoxicity.

In order to create a safety profile for QCA, normal mice were administered with QCA at the same dosage of 2 mg/kg every other day for 10 days. A biomarker for liver health (alanine transaminase) was monitored and there was no difference in treated and untreated normal mice. There was also no histological evidence indicating toxicity in the heart, indicating that QCA had limited toxicity in normal mice.



Scheme 4: Activation mechanism of dual stimuli-responsive prodrug QCA.³⁶

Redox-active anticancer prodrugs have just recently been investigated but are clearly showing promising results in cellular and mouse models, due to their ability to target cancer cells over healthy cells.

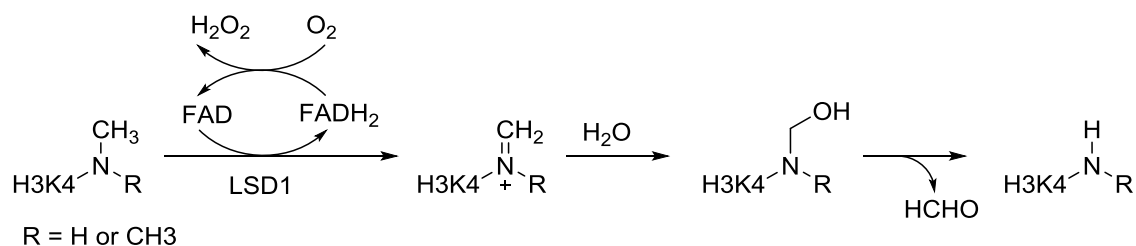
2.1.4 Function of lysine-specific demethylase 1 (LSD1) and its role in cancers

Lysine-specific demethylase 1 (LSD1) can alter chromatin compactness and gene expression. As such, LSD1 plays an important role in cancer progression. Chromatin is made up of DNA and histone proteins. Histones are octamers consisting two H2A-H2B dimers and one H3-H4 tetramer.³⁹ Approximately 146 base pairs of DNA surround this histone protein to form a nucleosome.⁴⁰ The polynucleosome string is composed of a

series of nucleosomes linked with a short segment of linker DNA (10 to 80 base pairs)⁴¹, which undergoes a few rounds of folding to compress the chromatin structure. Importantly, the compactness of chromatin is associated with gene repression.⁴¹

The structure of the chromatin and gene expression are influenced by post-translational modifications on histone tails, which protrude from the nucleosome surface. For example, methylated lysine 4 at histone 3 (H3K4), H3K36 and H3K79 is generally associated to transcriptional activation; whereas methylated H3K9, H3K27 and H4K20 is mostly related with transcriptional repression.⁴²

The methylation status of these histone lysines can be modified by enzymes, and hence gene expression will be altered as well. Histone lysine methyltransferases install methyl groups on histone lysine residues, and while several enzymes of this class had been identified by 2003,⁴³ it was only in 2004 that the lysine-specific demethylase 1 (LSD1) was reported by Shi et al.⁴⁴ LSD1 was the first reported histone demethylase which carries out the demethylation of mono- and dimethylated lysine 4 of histone 3 (H3K4me_{1/2}). The demethylation process involves flavin adenine dinucleotide (FAD) dependent enzymatic oxidation (Scheme 5).⁴⁴ Firstly, FAD oxidises H3K4me_{1/2} to form an iminium cation, while itself converts into FADH₂. The unstable iminium cation then undergoes hydrolysis and deformylation to yield the demethylated lysine. Meanwhile, FAD can be regenerated through oxidation of FADH₂ with molecular oxygen, hence repeating the demethylation process.⁴⁵ A lone pair of electrons on the substrate's nitrogen atom is required during the flavin-dependent amine oxidation, therefore LSD1 can only demethylate H3K4me_{1/2}, but not H3K4me₃.⁴⁵



Scheme 5: Mechanism of H3K4me1/2 demethylation catalysed by LSD1.

Corepressor protein CoREST was found to bind with LSD1 and it was essential in H3K4 demethylation.⁴⁶ The crystal structure of LSD1-CoREST-H3 revealed that H3 adopts three consecutive γ -turns and fits nicely inside the LSD1 active site, therefore generating many sequence-specific interactions with LSD1.⁴⁷ Furthermore, this creates an ideal side chain spacing, which orientates the H3 *N*-terminus into an anionic pocket, while placing H3K4me1/2 towards FAD for catalysis. The catalytic site of LSD1 is incapable to accommodate more than three residues on the methylated lysine *N*-terminal, therefore providing specificity towards H3K4.

In a prostate cell line, when LSD1 complexes with the androgen receptor, it carries out the demethylation of H3K9me1/2 instead.⁴⁸ Different from the demethylation of H3K4me1/2 (where LSD1 is bound to CoREST), demethylation of H3K9me1/2 promotes gene activation.⁴⁸ Therefore when binding to different partners, LSD1 can have different target of demethylation and hence different transcription outcome. Apart from histone protein demethylation, LSD1 can also carry out the demethylation of non-histone proteins to regulate cellular functions. For instance, LSD1 can demethylate p53 on K370me1/2 to inhibit its roles as a transcriptional activator and tumour suppressor.⁴⁹ Moreover, LSD1 catalysed the demethylation of DNA methyltransferase 1 to stabilise it for the regulation of global DNA methylation.⁵⁰

Overexpression of LSD1 was observed in various cancers, such as GBM,⁵¹ acute myeloid leukemia (AML),⁵² neuroblastoma,⁵³ prostate cancer,^{48,54} breast cancer,⁵⁵ lung cancer,⁵⁶ and bladder cancer cells.⁵⁶ As a result of LSD1 overexpression, abnormal demethylation of H3K4me1/2 leads to inhibition of tumour suppressor genes.⁵⁷ LSD1 is also responsible for tumorigenesis by suppressing p53-mediated apoptosis.^{56,58} Fortunately, elevated H3K4 methylation and suppression of cancer cell growth were observed in studies involving inhibition or RNAi-mediated knockdown of LSD1.^{53,59,60} Due to the fact that LSD1 inhibition leads to the suppression of carcinogenesis, inhibiting LSD1 could be a potential option for cancer therapy.^{61,62}

2.1.5 Inhibition of LSD1 using *trans*-2-phenylcyclopropylamine (2-PCPA) analogues

Due to the potential role of LSD1 in cancer highlighted in the previous section, several classes of LSD1 inhibitors have been studied. Similar to LSD1, monoamine oxidases (MAOs) A and B are also flavin-dependent enzymes. MAOs are involved in degradation of important neurotransmitters, and their inhibition has been widely investigated for treatment in neurological disorders, such as Parkinson's disease and depression.⁶³ As the active site in LSD1 shares partial homology with MAOs,⁶⁴ a few classes of MAO inhibitors were shown to inhibit LSD1 as well. These include *trans*-2-phenylcyclopropylamine (2-PCPA),⁶⁵ pargyline (**8**),⁴⁸ and phenelzine (**9**) (Figure 3).⁴³

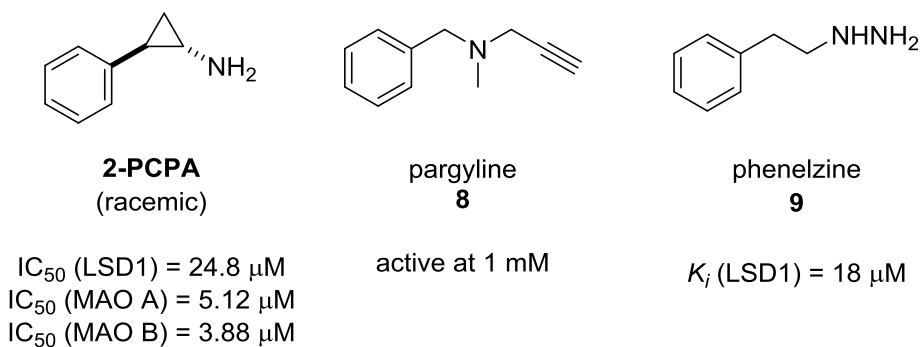


Figure 3: Examples of MAO inhibitors that also inhibit LSD1.^{43,66}

2-PCPA and its derivatives are the most studied LSD1 inhibitors.⁴³ Even though 2-PCPA is a potent MAO inhibitor and antidepressant drug,⁶³ its clinical use is restricted due to several undesirable side effects, including headaches, dizziness, orthostatic hypotension, and sexual dysfunction.^{63,67} Despite these unfavourable side effects, 2-PCPA demonstrated promising results in LSD1 inhibition, therefore it could be useful in cancer treatment. For instance, 2-PCPA was reported to suppress androgen receptor-dependent transcription and growth of bladder cancer cells.⁶⁸ Furthermore, 2-PCPA induced global H3K4 methylation and growth inhibition in neuroblastoma cells.⁵³ Inhibition of xenograft growth was observed in a mouse neuroblastoma model, after administering i.p. injection of 2-PCPA (2 mg/kg) daily for 21 days.⁵³

Schmidt et al. conducted kinetic studies and mass spectrometry (MS) analyses, the study indicated that 2-PCPA is a time-dependent, mechanism-based irreversible LSD1 inhibitor.⁶⁴ It was postulated that through single-electron transfer (SET) mechanism, 2-PCPA forms a covalent C–C bond with FAD at C(4a) in the catalytic site of LSD1, followed by concomitant ring-opening of the cyclopropyl ring (Figure 4).⁶⁴ Two possible adducts of 2-PCPA (atropaldehyde or cinnamaldehyde adducts) can be formed depending on which C–C bond in the cyclopropyl ring is cleaved (Figure 4).⁶⁴ Structural and MS analyses performed by Yang et al. revealed that the proposed cinnamaldehyde

adduct can then be transformed into a five-membered ring structure, which is the major 2-PCPA-FAD adduct obtained in LSD1 inhibition (Figure 4).⁶⁹ Based on the crystal structure analysis reported by Mimasu et al., the five-membered ring adduct is not the sole adduct formed during LSD1 inhibition and an intermediate N(5) adduct **A** was proposed.⁷⁰ Subsequently, Binda et al. demonstrated that (1*R*,2*S*)-2-PCPA provides the N(5) adduct **A**, while (1*S*,2*R*)-2-PCPA provides N(5) adduct **B** (Figure 4).⁷¹ In summary, no matter which 2-PCPA-FAD adduct is formed, covalent alteration of FAD decreases the availability of FAD to oxidise H3K4me1/2. Importantly, demethylation of H3K4me1/2 by LSD1 is obstructed due to the depletion of functional FAD.

Despite 2-PCPA exhibiting promising results in LSD1 inhibition and the mechanism being known, its use for LSD1 inhibition suffers from poor inhibitory activity ($K_i = 243 \mu\text{M}$).⁶⁴ In addition, 2-PCPA is more selective towards MAO than LSD1.⁶⁴ To overcome this selectivity issue, there is an urgent need to alter the 2-PCPA structure to improve its inhibitory activity and selectivity against LSD1. Towards this goal, many studies reported 2-PCPA derivatives with enhanced inhibitory activity and selectivity towards LSD1 compared to the parent compound (Figure 5).⁷¹⁻⁸⁰ The active sites in MAO A and MAO B are less spacious than LSD1, and hence their active sites are less likely to accommodate large substituents on the phenyl moiety of 2-PCPA.^{60,81} Therefore substitution on the phenyl ring of 2-PCPA is one of the common modifications reported to achieve LSD1 selectivity by size exclusion. Furthermore, alkylation on the 2-PCPA amine nitrogen was also found to improve selectivity and potency in LSD1 inhibition.

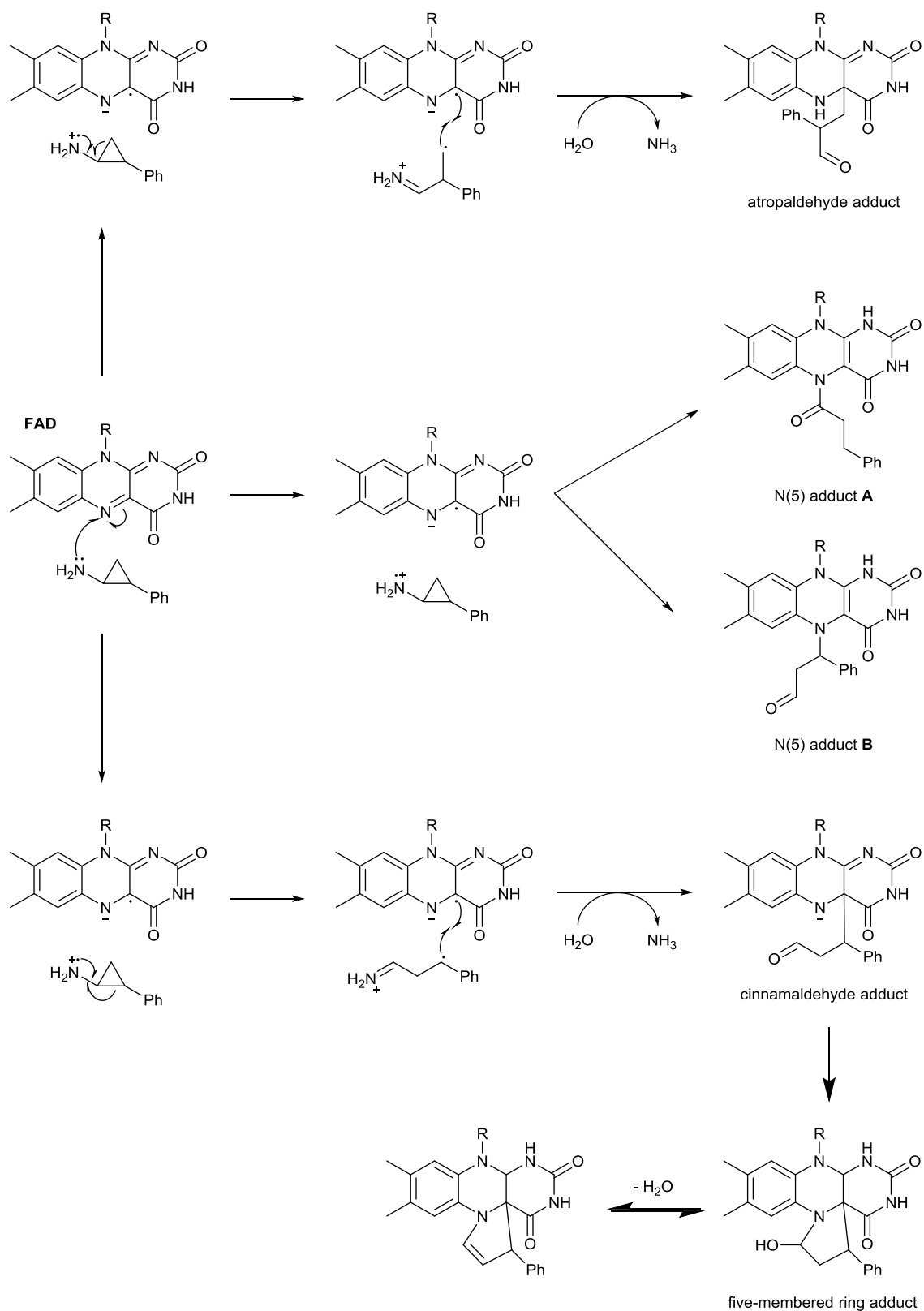


Figure 4: LSD1 inhibition by 2-PCPA through irreversible covalent modification of FAD.

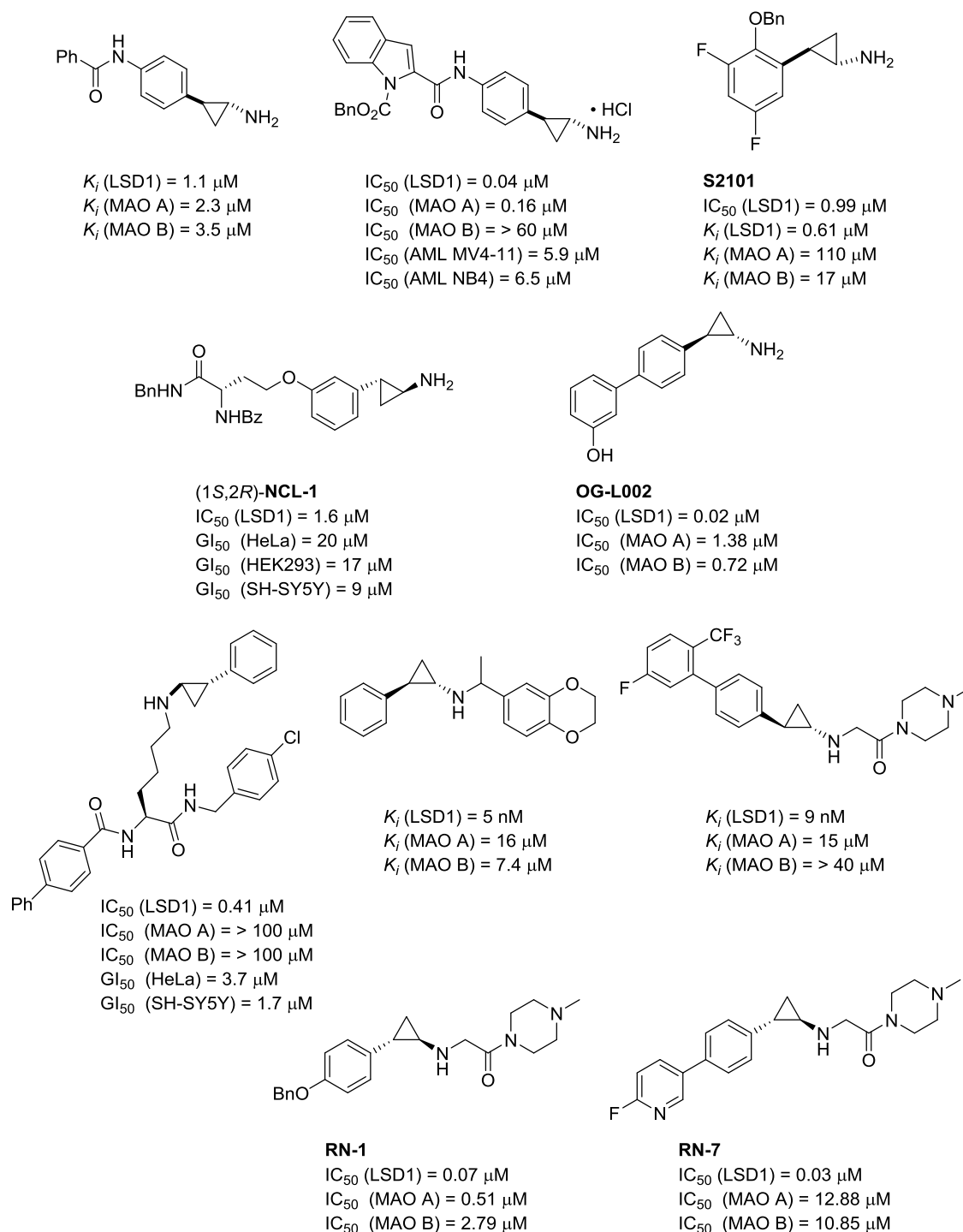
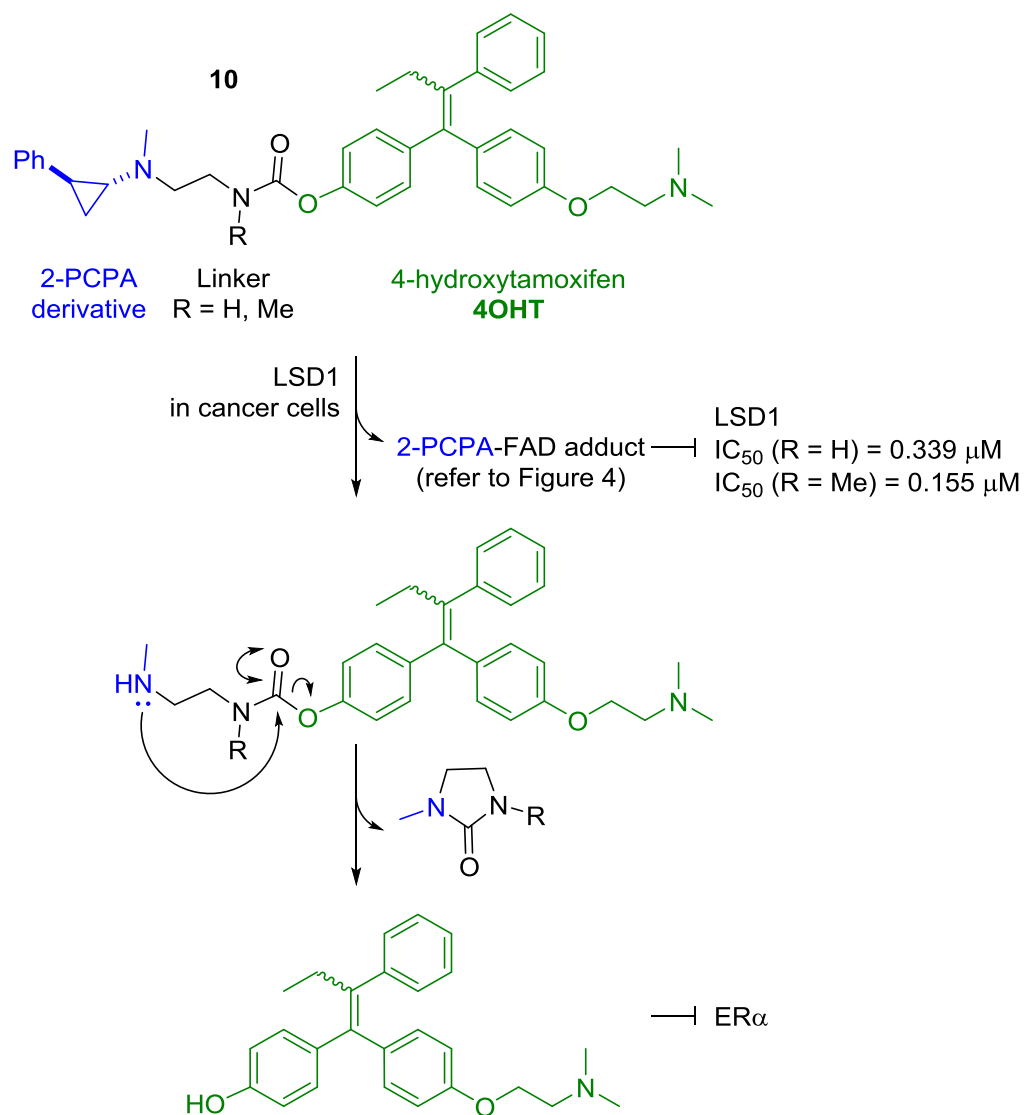


Figure 5: Selected examples of reported 2-PCPA derivatives as LSD1 inhibitors.⁷¹⁻⁸⁰

Very few LSD1-based prodrugs have been reported, but recently in seminal work Suzuki and co-workers reported novel prodrugs **10** that consisted of 2-PCPA and 4-hydroxytamoxifen (4OHT) moieties covalently linked together (Scheme 6).⁶⁶ Once the 2-PCPA moiety of this prodrug interacts with the LSD1 active site, activation to liberate

4OHT – an anti-estrogen agent for the treatment of breast cancer – occurs. Therefore, in breast cancer cells where LSD1 is overexpressed, the anticancer effect is achieved through inhibition of LSD1 and estrogen receptor α (ER α) synergistically. Prodrug **10** also serves as a selective treatment due to the difference in LSD1 expression in cancer and normal cells. In ER α -positive breast cancer MCF7 cells, prodrugs **10** exerted cytotoxicity and significantly reduced cell growth at 0.1 μ M. When non-cancerous human mammary epithelial cells (HMEC) were treated with **10**, the viability of the cells was not affected at concentrations up to 2.5 μ M, therefore suggesting that prodrug **10** is selective towards breast cancer cells. To date, prodrug **10** remained as the first and only reported prodrug based on the LSD1 inhibitor 2-PCPA.



Scheme 6: Activation mechanism of prodrug **10** to exert dual action on ER α -positive breast cancer cells.⁶⁶

2.1.6 Clinical trials involving 2-PCPA-based LSD1 Inhibitors

Since the discovery of LSD1 in 2004 and multiple studies on its inhibitors, there are currently several on-going clinical trials targeting LSD1 inhibition by 2-PCPA based derivatives. The combination of 2-PCPA and retinoid all-*trans*-retinoic acid (ATRA) is currently in a Phase I study to investigate a new treatment paradigm in AML (ClinicalTrials.gov Identifier: NCT02273102). Notably, it was proposed that LSD1

inhibition sensitises non-acute promyelocytic leukemia AML towards ATRA treatment, which was a challenge due to drug resistance.⁸² Oryzon developed the *N*-alkylated 2-PCPA analogue ORY-1001 (Figure 6), which is currently in Phase I/IIa study in patients with relapsed acute leukemia (EudraCT Number: 2013-002447-29). ORY-1001 displayed excellent selectivity, LSD1 inhibitory activity and oral bioavailability in rodents.⁸³ Furthermore, no off-target toxicity was observed in 28 days rat toxicology studies. Subsequently, GlaxoSmithKline also enrolled an *N*-alkylated 2-PCPA analogue GSK2879552 (Figure 6) into Phase I study for AML treatment (ClinicalTrials.gov Identifier: NCT02177812).

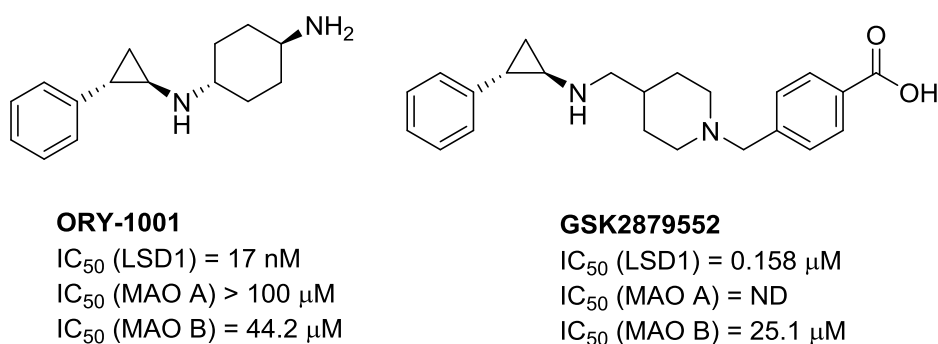


Figure 6: 2-PCPA derivatives that are currently in clinical trials (as of 28th December 2017).⁸³⁻⁸⁵

2.1.7 Other classes of LSD1 inhibitors

Other than investigating derivatisation of 2-PCPA, another strategy to identify potential LSD1 inhibitors is to shift away from the 2-PCPA template and search for other core structures that may interact with LSD1. Hence in recent years, structural diversity was observed in the literature on LSD1 inhibitors.⁸⁶ Non-2-PCPA based LSD1 inhibitors may have a different mode of action in LSD1 inhibition, therefore providing an alternative avenue for cancer treatment.

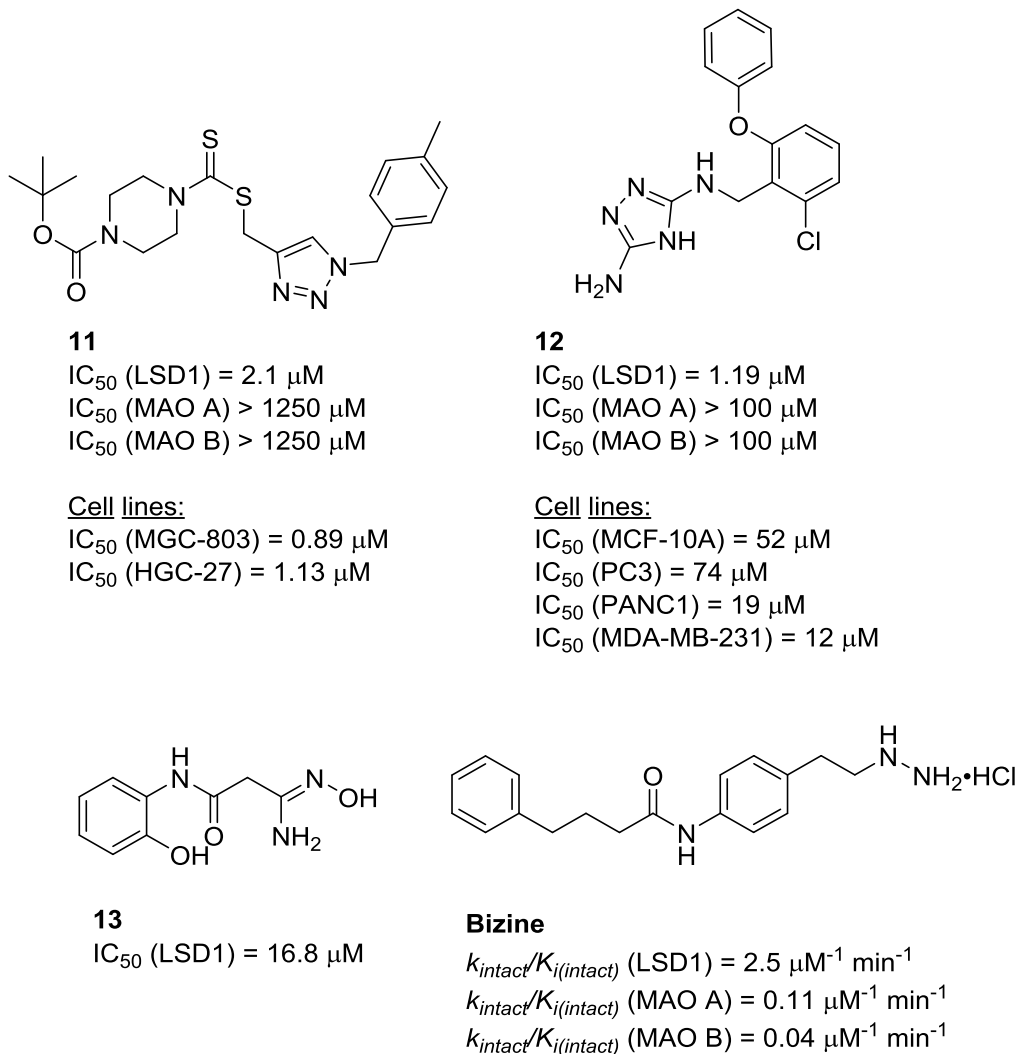


Figure 7: Selected examples of other classes of LSD1 inhibitors.⁸⁷⁻⁹⁰

Similar to 2-PCPA, phenelzine **9** is also a mechanism-based LSD1 inhibitor which can covalently fused to FAD in the active site, however in this case the key initiating step involves hydrazine rather than cyclopropylamine oxidation.⁹¹ The use of the MAO inhibitor phenelzine **9** in LSD1 inhibition is underexplored, however, Cole and co-workers reported bizine, an analogue of phenelzine **9**, as a superior LSD1 inhibitor compared to its parent compound (Figure 7).⁸⁹ Bizine was found to be selective and potent towards LSD1 compared to MAO, and it demonstrated antiproliferative effects in lung cancer H460 (IC_{50} = 14 μ M) and prostate cancer LNCaP (IC_{50} = 16 μ M) cell lines. Furthermore, LSD1 inhibition by bizine provided neuroprotection to neurons under

oxidative stress. Neurons were treated with homocysteic acid to induce oxidative stress (via GSH depletion) and then treated with bizine. As a result, significantly enhanced survival of neurons was observed with 0.5 μM of bizine.

Zheng et al. reported the triazole–dithiocarbamate based molecule **11**, which was potent and selective against LSD1 (Figure 7).⁹⁰ Unlike 2-PCPA, it was proposed that **11** is a reversible LSD1 inhibitor and it inhibited LSD1 by causing FAD ejection. Compound **11** demonstrated excellent LSD1 inhibitory activity in gastric cancer cell lines MGC-803 ($\text{IC}_{50} = 0.89 \mu\text{M}$) and HGC-27 ($\text{IC}_{50} = 1.13 \mu\text{M}$). It was also demonstrated that **11** induced apoptosis and inhibited cell migration in MGC-803 cells. Due to lower LSD1 expression in gastric cancer cell line SGC-7901, the LSD1 inhibitory effect of **11** was significantly lower than the previous cell lines ($\text{IC}_{50} = 89.5 \mu\text{M}$). As expected, **11** did not show marked effects on normal gastric epithelial cell line GES-1. When treating MGC-803-implanted mice (xenograft model) with **11** at a dose of 20 mg/kg, tumour weight was reduced by 68.5%, while no apparent body weight was lost during treatment, suggesting that **11** is efficient in suppressing tumour growth without inducing global toxicity.

By virtual screening of the Maybridge Hitfinder 5 compound library for the identification of LSD1 inhibitors, Woster and co-workers reported the triazole-based molecule **12** as a potent and reversible LSD1 inhibitor (Figure 7). Molecular modelling studies reveal that **12** forms several key interactions with the LSD1 active site through hydrogen bonding and FAD through π -stacking, therefore effectively hindering substrate binding. Compound **12** was potent and selective towards LSD1 ($\text{IC}_{50} = 1.19 \mu\text{M}$), and it induced cytotoxicity in several cancer cell lines (IC_{50} ranges from 12 μM – 74 μM).

Woster and co-workers also reported amidoxime **13** as LSD1 inhibitor in a separate study identified through virtual screening (Figure 7).⁸⁷ In silico analysis

suggested that **13** binds to precisely the same region as H3K4 of the histone tails. Furthermore, a combination of both hydrophobic and hydrophilic interactions stabilises the LSD1/CoREST complex with **13** such that the latter is placed directly in front of FAD, preventing it from accessing other substrates. Compound **13** significantly increased the methylation level of H3K4me2 in the human lung carcinoma cell line Calu-6. Furthermore, through quantitative PCR significant upregulation in the expression level of aberrantly silenced tumour suppressor genes (*SFRP2*, *HCAD* and *GATA4*) was observed in the Calu-6 cell treated with **13**.

2.2 Aim and research plan

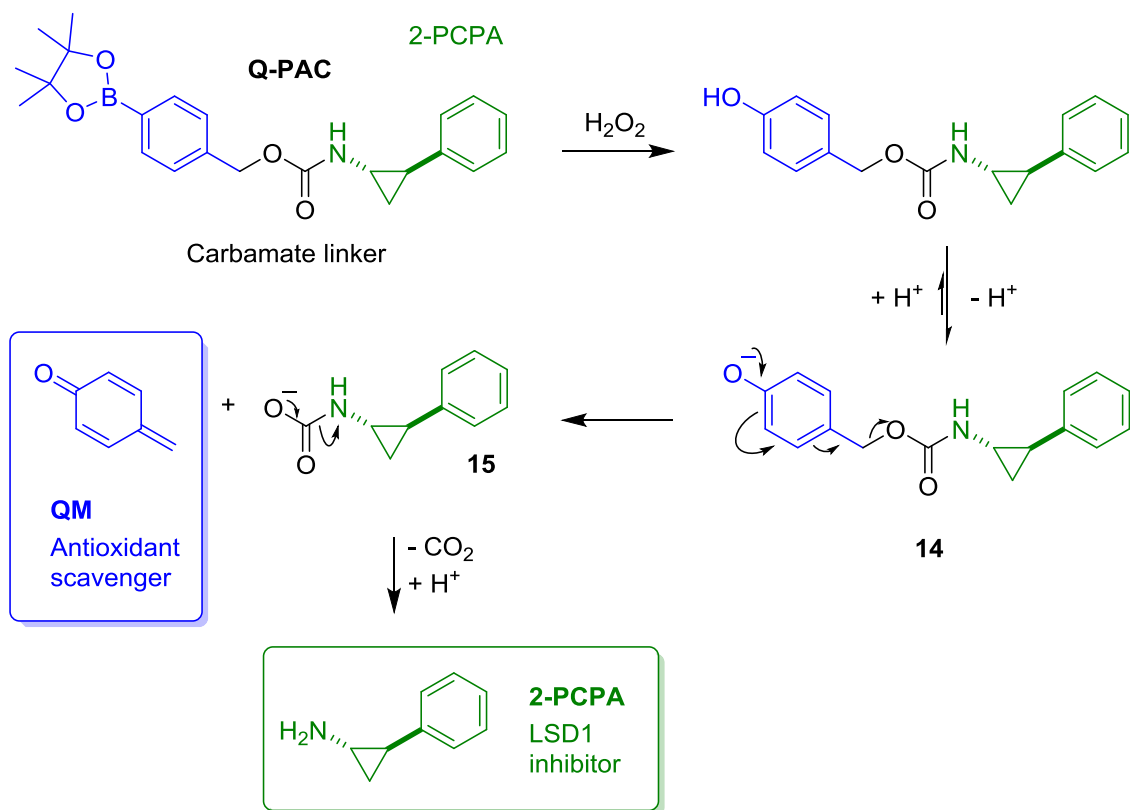
The survival rate of GBM patients has not been improved in the past few decades and current available treatment options have their limitations and undesired side-effects. Therefore, there is a pressing need to develop new treatment options for GBM to overcome these issues.

In the literature, the difference in ROS concentration between cancer and normal cells has been utilised to develop cancer-selective prodrugs. Upon activation by the high concentration of ROS in cancer cells, these prodrugs mainly induce cytotoxicity in these cells by suppression of antioxidant systems (e.g. inhibition of GSH by QM) and amplification of ROS. Under these synergistic effects, cancer cells will be more susceptible to further ROS insults therefore leading to cell death. On the other hand, 2-PCPA based LSD1 inhibitors have demonstrated promising outcomes in cancer treatment, notably there are two *N*-alkylated 2-PCPA analogues currently in active clinical trials.

Given that prodrugs based on LSD1 inhibitor have been scarcely reported, in this study, we aim to develop a GBM-selective prodrug which will liberate QM (antioxidant scavenger) and 2-PCPA (LSD1 inhibitor) upon activation by ROS. The prodrug we have designed consists of an aryl boronate trigger and 2-PCPA joined by a carbamate linker as is named Q-PAC (quinone-methide-phenylaminocyclopropane) (Scheme 7). It is anticipated that upon entering cancer cells, activation of Q-PAC would occur by excess H₂O₂, converting the aryl boronate moiety into a phenol - the phenolate counterpart **14** then undergoes 1,6-elimination to give QM and intermediate **15**. Ultimately, 2-PCPA would be obtained after decarboxylation of **15**. While the formation of phenolate **14** depends on its equilibrium with phenol, the decarboxylation of intermediate **15** will promote the equilibrium shifting towards the phenolate. As discussed above QM is highly electrophilic and is anticipated to quench the antioxidant GSH, therefore further obstructing the cancer cells' ability to counteract oxidative stress which subsequently allows the accumulation of ROS. Concurrently, we would expect 2-PCPA to inhibit LSD1 which is overexpressed in GBM, thus reducing the suppression of tumour suppressor genes and limiting cancer cell proliferation and survival. In summary, the novel prodrug is expected to have a dual-action of antioxidant scavenging and LSD1 inhibition.

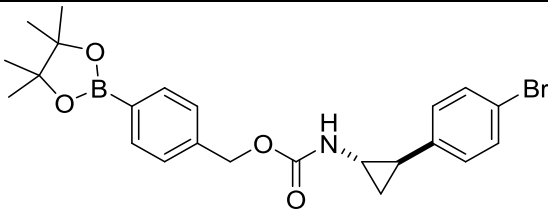
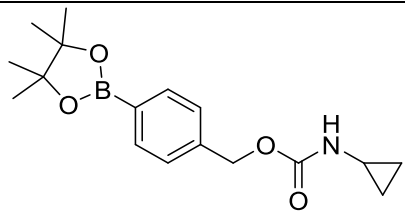
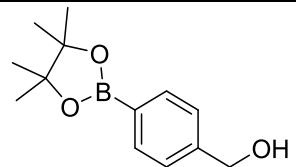
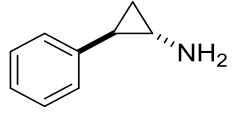
The research plan will involve testing the cytotoxicity of Q-PAC on the immortalised GBM cell line U87. Furthermore, in order to demonstrate clinical significance of Q-PAC, testing on three different primary GBMs of different GBM subtypes (RN1: classical, JK2: proneural, SJH1: neural) is necessary. The selectivity of Q-PAC against GBM is also important to ascertain, so healthy astrocytes will also be treated with Q-PAC to determine this. Several analogues and individual components of Q-PAC will be prepared and assessed in parallel to gain an understanding of what portions of the molecule are important for activity (Table 2).

Aryl boronate trigger



Scheme 7: Proposed activation mechanism of Q-PAC to release QM and 2-PCPA.

Table 2: Analogues and fragments of Q-PAC to obtain SAR information.

Molecules	Purpose
 <p style="text-align: center;">Q-BrAC (Quinone-methide- bromophenylaminocyclopropane)</p>	<p>To study the effect of having a halogen substituent at the <i>para</i> position on phenyl ring of 2-PCPA.</p>
 <p style="text-align: center;">QAC (Quinone-methide-aminocyclopropane)</p>	<p>To study the effect of solely QM in the absence of LSD1 inhibitor (2-PCPA). Upon activation by ROS, QAC will generate QM and cyclopropylamine, instead of 2-PCPA. Cyclopropylamine is not an LSD1 inhibitor.</p>
 <p style="text-align: center;">PBE (Phenyl boronate ester)</p>	<p>To study the effect of solely QM in the absence of LSD1 inhibitor (2-PCPA). Upon activation by ROS, PBE can potentially generate QM solely.</p>
 <p style="text-align: center;">2-PCPA</p>	<p>To study the effect of solely LSD1 inhibitor in the absence of antioxidant scavenger (QM). Racemic mixture of 2-PCPA was used.</p>

2.3 Results and discussion

2.3.1 Syntheses of prodrugs Q-PAC, Q-BrAC and QAC

The preparation of prodrugs Q-PAC and Q-BrAC were initiated with Corey–Chaykovsky cyclopropanation of commercially available ethyl cinnamates (Scheme 8).

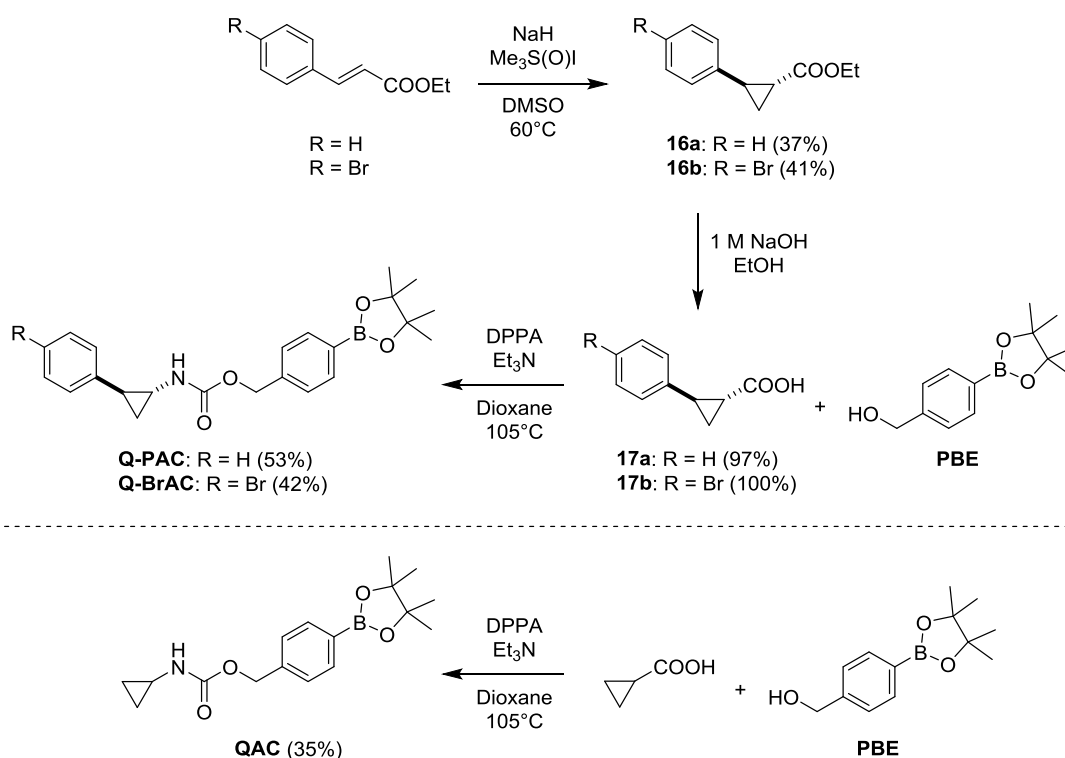
The reaction proceeded through the deprotonation of Me₃S(O)I with NaH to generate sulfoxonium ylide, followed by methylene transfer from the ylide to the ethyl cinnamate substrates (reaction mechanism and *trans* diastereoselectivity will be discussed in Chapter 3 Section 3.3.1). In the ¹H NMR spectrum of cyclopropane **16a**, the cyclopropanation of ethyl cinnamates was indicated by the absence of olefin protons (doublets at 7.67 and 6.43 ppm) and the presence of cyclopropane protons (2.53 – 2.50, 1.90, 1.59, 1.33 – 1.26 ppm). Similarly in the ¹³C NMR spectrum of **16a**, absence of olefin carbon signals (144.5 and 118.4 ppm) and presence of cyclopropane carbon signals (26.2, 24.2 and 17.1 ppm) indicated that the cyclopropanation was successful.

The resulting cyclopropyl esters **16a-b** were then subjected to basic hydrolysis to yield carboxylic acids **17a-b** in excellent-quantitative yields. In the ¹³C NMR spectrum of carboxylic acid **17a**, the absence of OCH₂CH₃ signals (60.7 and 14.3 ppm) indicated that the basic hydrolysis was successful.

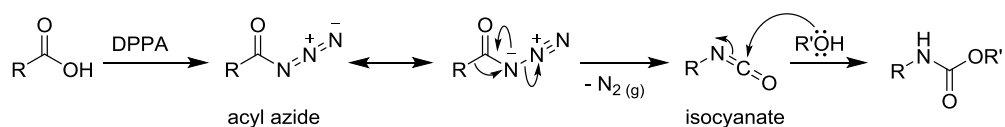
The carboxylic acids **17a-b** were then subjected to Curtius rearrangement with PBE, which furnished the proposed prodrugs Q-PAC and Q-BrAC. Mechanistically, the Curtius rearrangement involves formation of an acyl azides upon treatment of carboxylic acids with diphenylphosphoryl azide (DPPA). At elevated temperature, acyl azides underwent thermal decomposition, rearrangement and liberation of nitrogen gas to form the isocyanate intermediates. Lastly, nucleophilic attack of hydroxyl group from PBE to the isocyanates created the carbamate linker between two substrates.

In the ¹H NMR spectrum of Q-PAC, the OCH₂ proton signal was shifted downfield from 4.66 ppm (PBE)⁹² to 5.12 ppm. Meanwhile in the ¹³C NMR spectrum of Q-PAC, the carbonyl signal (156.6 ppm) from the carbamate linker supported that the linking of two building blocks was successful. It should be noted that prodrug Q-PAC

was obtained as a racemic mixture, therefore two enantiomers of 2-PCPA will be liberated upon oxidative activation of Q-PAC, namely (1*S*,2*R*)-2-PCPA and (1*R*,2*S*)-2-PCPA. The fact that two enantiomers of 2-PCPA will be generated should not pose difficulty in the interpretation of biological evaluation results because Benelkebir et al. showed that the two *trans* enantiomers possess similar LSD1 inhibition activity: $K_i = 28.1 \mu\text{M}$ for (1*S*,2*R*)-2-PCPA and $K_i = 26.6 \mu\text{M}$ for (1*R*,2*S*)-2-2-PCPA.⁹³



Mechanism of Curtius rearrangement



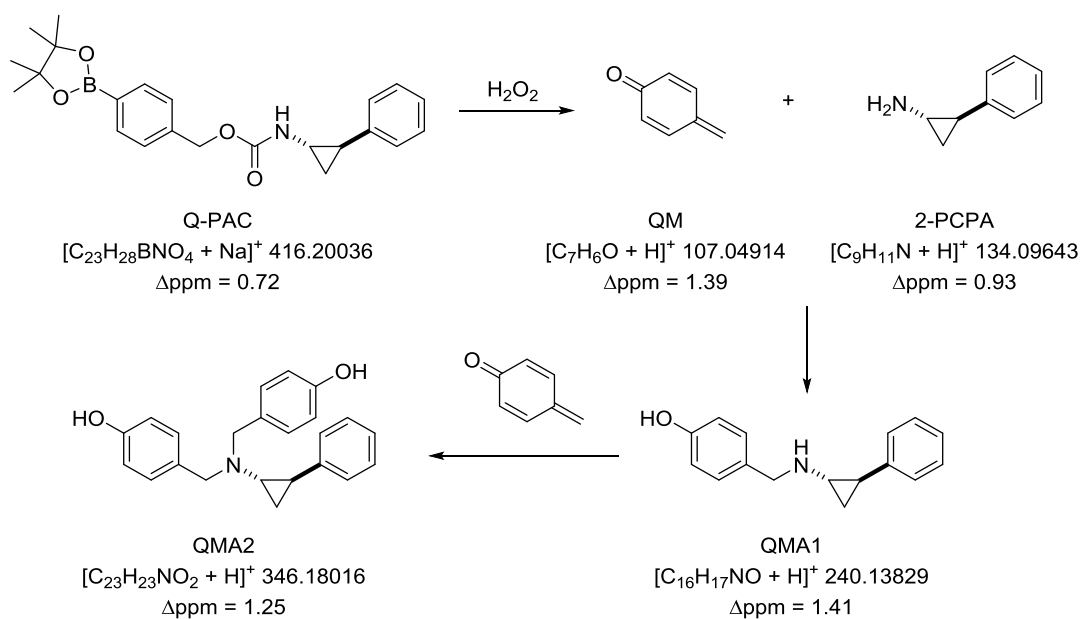
Scheme 8: Synthetic route to prepare prodrugs Q-PAC, Q-BrAC and QAC.

Similar to the preparation of Q-PAC and Q-BrAC, prodrug QAC was synthesised by Curtius rearrangement using commercially available cyclopropanecarboxylic acid and PBE in 35% yield. Some key features in the NMR spectra of QAC was similar to that of Q-PAC, the down-field chemical shift of OCH₂ (from 4.66 to 5.11 ppm) in ¹H NMR and

the presence of carbonyl signal (157.0 ppm) in ^{13}C NMR indicated that the Curtius rearrangement had proceeded smoothly.

2.3.2 Utilisation of mass spectrometry for the detection of Q-PAC active components upon activation

As a proof of concept for prodrug activation, Q-PAC was treated with hydrogen peroxide and the generated active species were detected using electrospray ionisation mass spectrometry (ESI-MS). It was envisaged that prodrug Q-PAC activation via hydrogen peroxide would yield QM and 2-PCPA (Scheme 9). In the absence of GSH, QM can react with 2-PCPA to yield adduct QMA1, which can then further react with another QM to form adduct QMA2.



Scheme 9: Activation of Q-PAC by H_2O_2 to liberate QM and 2-PCPA. In the absence of other nucleophilic species (such as GSH), subsequent formation of QMA1 and QMA2 adducts was detected. Exact mass/charge (m/z) values and corresponding MS accuracy (Δppm) of detected species are stated above.

Positive-mode ESI-MS was utilised to examine this activation process. Prior to H₂O₂ addition to an Q-PAC solution a signal detected at m/z 416 is assigned to [Q-PAC + Na]⁺ (Figure 8a). Under identical instrument conditions the appearance of m/z 107 and 134 following 5 minutes treatment with hydrogen peroxide indicates the presence of initial products QM and 2-PCPA, respectively (Figure 8b). Analysis following longer reaction times results in Figure 8 spectra (c) and (d) which indicate: (1) further relative increase in QM and 2-PCPA; (2) production of QMA1 and QMA2 adducts evidenced by m/z 240 and 346 signals, respectively. These results are consistent to the activation mechanism and adduct formation illustrated in Scheme 9. In a separate Q-PAC solution where hydrogen peroxide was not added, the sample was analysed with ESI-MS three days after preparation. Q-PAC was detected intact while QM, 2-PCPA, QMA1 and QMA2 were not detected, suggesting that hydrogen peroxide is required for the activation of prodrug.

Experiments were repeated on a LTQ XL Orbitrap for high resolution mass analysis to further support assignment (spectra not shown). Experimental errors from those theoretical m/z values shown in Scheme 9 are included for each putative elemental ionic composition where all fall within 2 ppm.

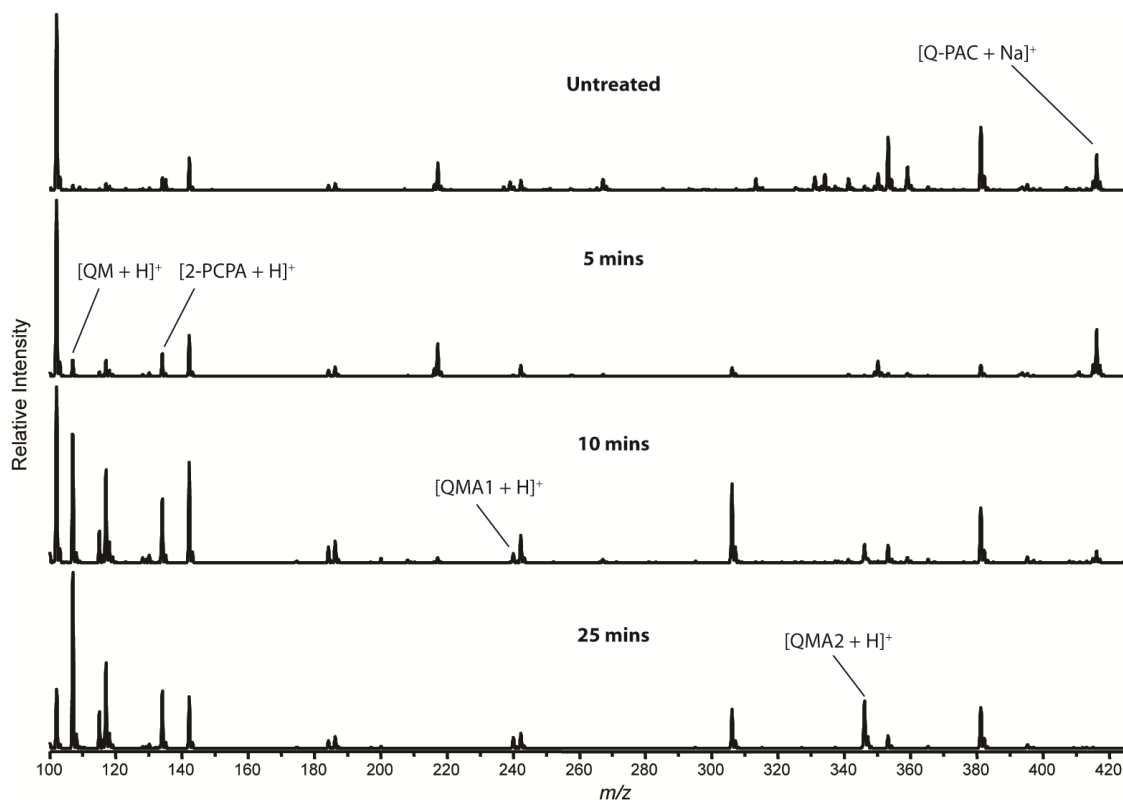


Figure 8: Low resolution (+)ESI-MS data collected at increasing times after Q-PAC treatment with H₂O₂. The sodiated Q-PAC m/z 416 is labelled in the spectrum resulting from analysis of the untreated prodrug. Mass spectra were collected after 5, 10 and 25 minutes of Q-PAC treatment time. Signals corresponding to activation products and adducts (as shown in Scheme 9) are labelled in the spectra; all other peaks have been accounted for as background with the exception of m/z 306, which could be the sodiated phenol intermediate after the oxidative hydrolysis of Q-PAC and prior to 1,6-elimination.

In this mass spectrometry assay, prodrug Q-PAC was treated with 9 mM of hydrogen peroxide, which was consistent to the condition employed by Hagen et al.²⁶ While this oxidant concentration was higher than physiological level, it was necessary in order to observe the activation process in a practical timeframe. In experiments using physiological level of hydrogen peroxide (100 μM and 1 mM), the activation occurred in a significantly slower rate where prodrug was still present even after a day. It should also

be pointed out that the level of hydrogen peroxide in this assay declined as time progressed due to reaction with the prodrug or decomposition; while the ROS level in cancer cells would elevate due to the ROS production in mitochondria and the antioxidant-scavenging action of QM.

While this mass spectrometry study was not a kinetic assay, it was confirmed that prodrug Q-PAC was able to undergo H₂O₂ induced oxidative cleavage of its boronate trigger and 1,6-elimination to release QM, 2-PCPA and QM-derived adducts (QMA1 and QMA2). This was critical given the desired dual action of the drug that required QM to reduce the antioxidant inhibitor GSH while 2-PCPA simultaneously inhibits LSD1. The obtained result is consistent with the report of Mokhir and co-workers, who demonstrated a similar breakdown of aminoferrocene-based prodrugs with H₂O₂.²⁶ Unlike Mokhir and co-workers however, we were able to directly detect QM. Given the concentration of GSH in cells is higher than the effective concentration of Q-PAC,⁹⁴ the desired reaction between GSH and QM would negate the formation of QM-derived adducts QMA1/QMA2 and therefore reduce the antioxidant ability of the cell.

2.3.3 Evaluation of prodrugs on viability and migration in U87 glioblastoma cells

With the synthesis of the prodrugs in hand and mechanistic information obtained, attention was turned towards biological testing. Much of this work was carried out experimentally by collaborators Dr M. Engel and D. Cross (Illawarra Health & Medical Research Institute).

The immortalised GBM cell line U87 is commonly used to assess novel GBM treatments and it was employed for the preliminary screening of the prodrug prepared in this study. Interestingly, Q-PAC reduced U87 confluence and hence proliferation in a

dose-dependent manner within 24 h ($F(7, 42)=73.94, P<0.0001$; Figure 9A). Cell viability was quantified through a Resazurin-based fluorometric assay, and it was found that U87 cell viability was also reduced dose-dependently after 24 h ($F(6,35)=51.34, P<0.0001$) and 48 h ($F(6,28)=9.47, P<0.0001$) (Figure 9D). In scratch-wound assay where an area of the U87 cells was removed to create a gap for cells to migrate, Q-PAC was found to dose-dependently inhibit the migration of U87 cells ($F(6, 13)=16.93, P<0.0001$; Figure 9B). 3D Cell invasion through matrigel after Q-PAC treatment was measured by electrical impedance, and it was discovered that the migration and invasion were suppressed ($F(4, 14)=5.324, P = 0.0081$; Figure 9C). Consistent to the observed results, the cell morphology displayed distinct change after Q-PAC treatment of 10 μM and 100 μM , where treated cells were clearly shrinking compared to cells that were only treated with ethanol vehicle (Figure 9E-G). In summary, Q-PAC dose-dependently reduced the cell proliferation, viability, migration and invasion of U87 cells.

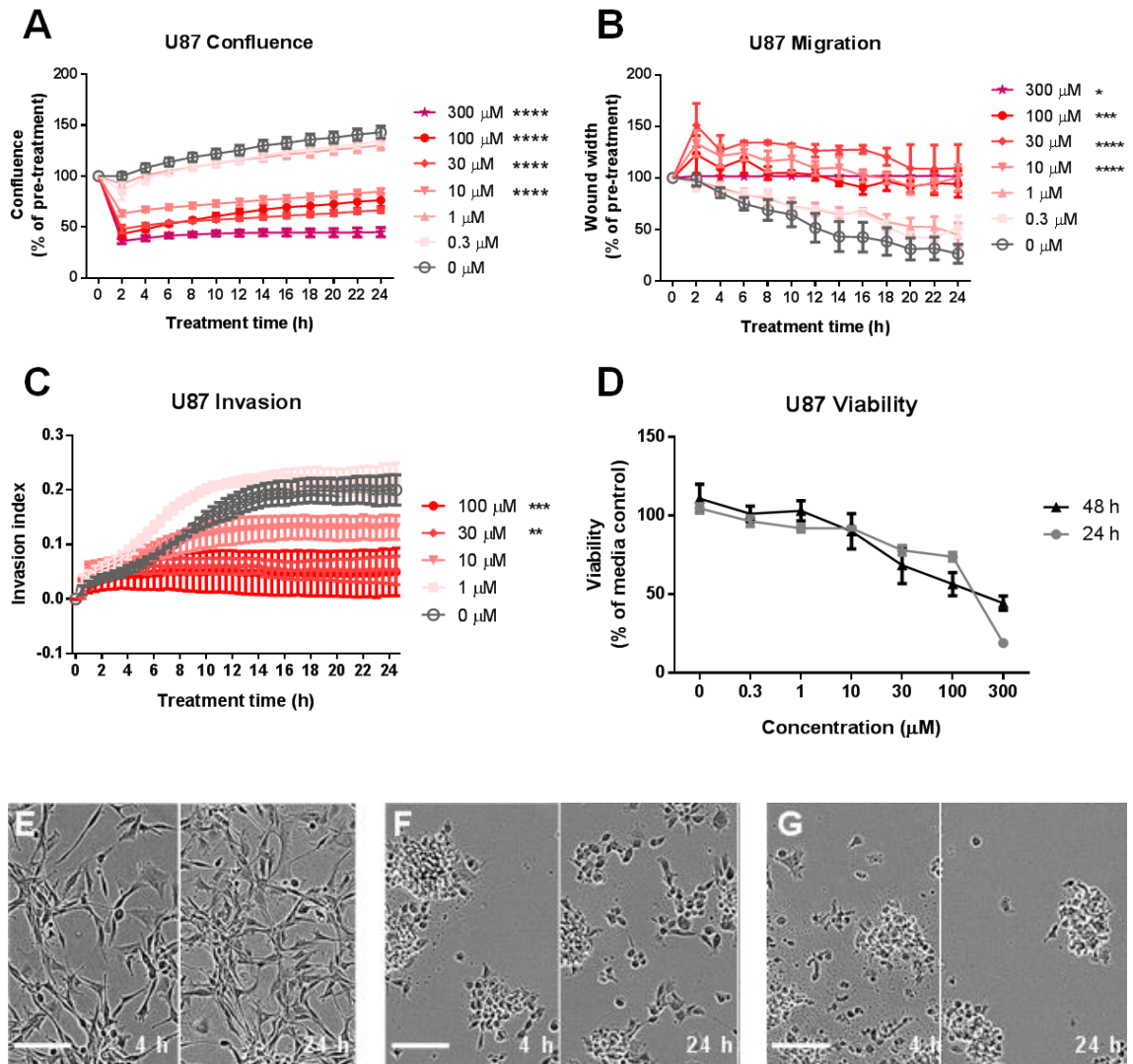


Figure 9: *Q-PAC impairs viability and mobility of U87 glioblastoma cells. (A) Confluence of U87 cultures treated with Q-PAC. Algorithm-based confluence analysis of phase-contrast microscope images at 10x magnification every 2 h over a 24 h period following Q-PAC treatment (n=6 per concentration), normalised to culture confluence prior treatment. (B) 2D migration of U87 cells treated with Q-PAC. Algorithm-based scratch wound analysis of phase-contrast microscope images at 10x magnification every 2 h over a 24 h period following scratch wound and Q-PAC treatment (n=4 per concentration), normalised to wound width prior treatment. (C) 3D invasion of U87 cells treated with Q-PAC. Invasion through matrigel was measured via electrical impedance every 30 min over a 24 h period following Q-PAC treatment (n=4 per concentration). (D)*

*Viability of U87 cultures treated for either 24 h (grey circles) or 48 h (black triangles) with Q-PAC (0 to 300 μ M). Cell viability was quantified via a Resazurin-based fluorometric assay ($n = 5$), with readings normalised to media-only cultures. Data represent mean \pm SEM, * $P < 0.05$, ** $P < 0.01$, *** $P < 0.001$, **** $P < 0.0001$ compared to vehicle control. (E-G) Representative images of U87 cultures treated with Q-PAC. Cultures treated with vehicle (E, EtOH), 10 μ M (F) and 100 μ M (G) were captured in phase-contrast images 4 h and 24 h after treatment at 10x magnification (scale bar = 50 μ m). In vitro assays were performed by Dr M. Engel and D. Cross (Illawarra Health & Medical Research Institute).*

Analogues and fragments of Q-PAC were then examined on U87 cell line. Interestingly, Q-BrAC (brominated version of Q-PAC) did not affect U87 confluence (F (6, 14)=5.220, $P = 0.0052$) and viability (F (6, 14)=2.634, $P = 0.0635$). Upon hydrogen peroxide-induced activation, Q-BrAC was hypothesised to liberate QM and a brominated version of 2-PCPA (Br-PCPA). Since both Q-PAC and Q-BrAC generate QM upon activation, the difference in cell proliferative inhibition could be due to the difference in LSD1 inhibition by 2-PCPA and Br-PCPA. In a report from Binda et al. and Benelkebir et al., Br-PCPA was found to be more potent than 2-PCPA by having a lower K_i (4.6 – 9.6 fold difference).^{71,93} However Gooden et al. reported that 2-PCPA was slightly more potent in LSD1 inhibition than Br-PCPA (1.2 fold difference). The discrepancies in results between each study could be due to differences in assays and experimental condition. Results from our examination of Q-BrAC implied that Br-PCPA may be a weaker LSD1 inhibitor compare to 2-PCPA, consistent to the findings from Gooden et al.⁸¹

Results from several studies indicated that *para*-substituted 2-PCPA analogues were more potent in LSD1 inhibition than the mother compound, as shown in Figure

5.^{71,72,75} These reported *para*-substituents were larger and bulkier than bromine atom, which may suggest that the decrease in LSD1 inhibitory action of Br-PCPA may not be due to steric clash with LSD1 active site, however the actual reason for inactivity remained unclear.

Since Q-PAC demonstrated promising results in the preliminary evaluation on U87 cell line, individual fragments of Q-PAC as listed in Table 2 were then evaluated on U87 to investigate the importance of each components. These include 2-PCPA (LSD1 inhibitor), CPA (phenyl-free version of 2-PCPA), PBE (weak QM generator) and QAC (generates QM and CPA upon activation by H₂O₂). None of these four fragments affected the confluence, viability or migration ability of U87 cells for up to 300 μ M (Appendix 1, Figure A1). This data suggests that by inhibiting LSD1 or GSH alone could not achieve the same anticancer effect Q-PAC demonstrated. Moreover, co-treatment of 2-PCPA and PBE did not affect the confluence and viability for U87 cultures (Appendix 1, Figure A1), which implies that the delivery of these two fragments in the form of Q-PAC is essential for the suppression of U87 cell growth. As a suggestion for future work, co-treatment of QAC (QM source) and 2-PCPA (LSD1 inhibitor) is advised to investigate the importance of linking the two active components with carbamate linker. Even if the same cytotoxicity can be achieved, it is unlikely to deliver these two compounds to patients due to the undesired effect of 2-PCPA.

In this study, the 2-PCPA-based prodrug Q-PAC impaired several cancer properties of U87 cells at concentration as low as 10 μ M, while even 300 μ M of 2-PCPA was ineffective against the immortalised GBM cells. Even though the use of 2-PCPA in cancer treatment was reported in several studies,^{53,55} a high concentration was usually required, with up to 20-fold higher than the IC₅₀. Moreover, 2-PCPA was shown to be ineffective against immortalised GBM cultures even at a high concentration of 1 mM,

despite high expression of LSD1 in these cells.⁵¹ Not only Q-PAC performed better than 2-PCPA in reducing viability in U87 cells, it also suppressed the migration and invasion phenotype of U87 cells, which are the most notorious cancerous features of GBM.⁹⁵

2.3.4 Higher selectivity of Q-PAC for GBM over healthy astrocytes

Inspired by the promising results of Q-PAC in U87 cell lines, the investigation was further extended to primary GBM cultures. The primary GBM cultures were grown from untreated human biopsy samples of three different subtypes (RN1: classical; JK2: proneural; SJH1: neural), which were previously characterised.⁹⁶ Consistent to the results observed in U87 cell line, Q-PAC dose-dependently reduced confluence in primary GBMs ($P < 0.001$ for each cell line, Figure 10A-C), and suppressed migration in the scratch-wound assay ($P < 0.001$ for each cell line, Figure 10E-G). Even though the three tested primary GBMs displayed different proliferation and migration rates, Q-PAC inhibited both tumour properties at concentrations above 10 μM . GBM culture viability reduced within 48 h of Q-PAC treatment at concentrations of 30 μM and above (Figure 11). On the other hand, Q-BrAC did not reduce the confluence or viability of RN1 cells (Figure 12), consistent to the results from U87 cultures.

Next, primary cerebral astrocyte cultures (human and mouse) were treated with Q-PAC to probe for the prodrug selectivity against GBMs. In contrast to the GBM cultures, healthy astrocytes treated with Q-PAC at concentrations up to 300 μM for 48 h did not show reduction in cell viability (human astrocytes: $F(6, 53)=0.56$, $P=0.76$; mouse astrocytes: $F(6, 36)=0.91$, $P=0.49$; Figure 11A), nor a change in their migratory behaviour ($F(6, 12)=0.47$, $P = 0.82$; Figure 10H). Although the confluence of primary astrocyte cultures differed after Q-PAC treatment ($F(6, 38)=15.3$, $P < 0.0001$; Figure 10D), only 30

μM Q-PAC resulted in cell confluence reduction (80.1 % of vehicle after 48 h, $P < 0.001$; Figure 10D), it was a smaller reduction than for any of the GBM cultures at the same concentration (RN1: 32.7%, JK2: 64.6% and SJH1: 62.7% of vehicle; Figure 10A-C). These data show that primary GBM cells are more vulnerable to Q-PAC treatment than healthy astrocytes, therefore Q-PAC can be a potential and selective treatment for GBM.

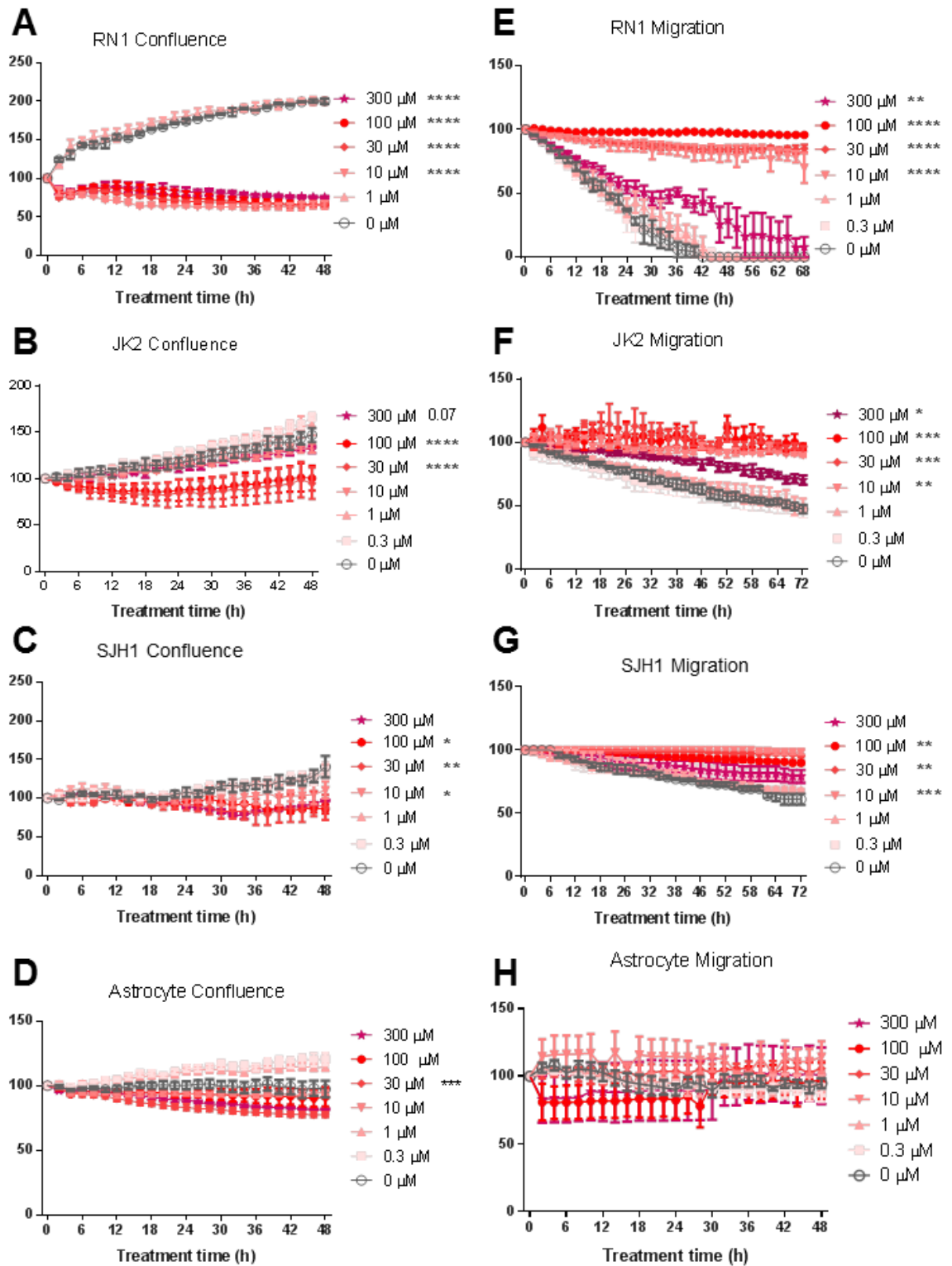


Figure 10: *Q-PAC impairs proliferation and mobility of primary glioblastoma (GBM) cells but not healthy astrocytes. Confluence of primary human GBM (A-C) and astrocyte (D) cultures treated with Q-PAC was quantified via algorithm-based analysis of phase-contrast microscope images at 10x magnification over a 48 h period (n=3 per*

concentration & culture), normalised to culture confluence prior treatment. 2D migration of human GBM (E-G) and astrocyte (H) cultures treated with Q-PAC. Scratch wound width was quantified through algorithm-based analysis of phase-contrast microscope images at 10x magnification following scratch wound and Q-PAC treatment (n=3 per concentration and culture), normalised to wound width prior treatment. Data represent mean \pm SEM, * $P < 0.05$, ** $P < 0.01$, *** $P < 0.001$, **** $P < 0.0001$ compared to vehicle control.

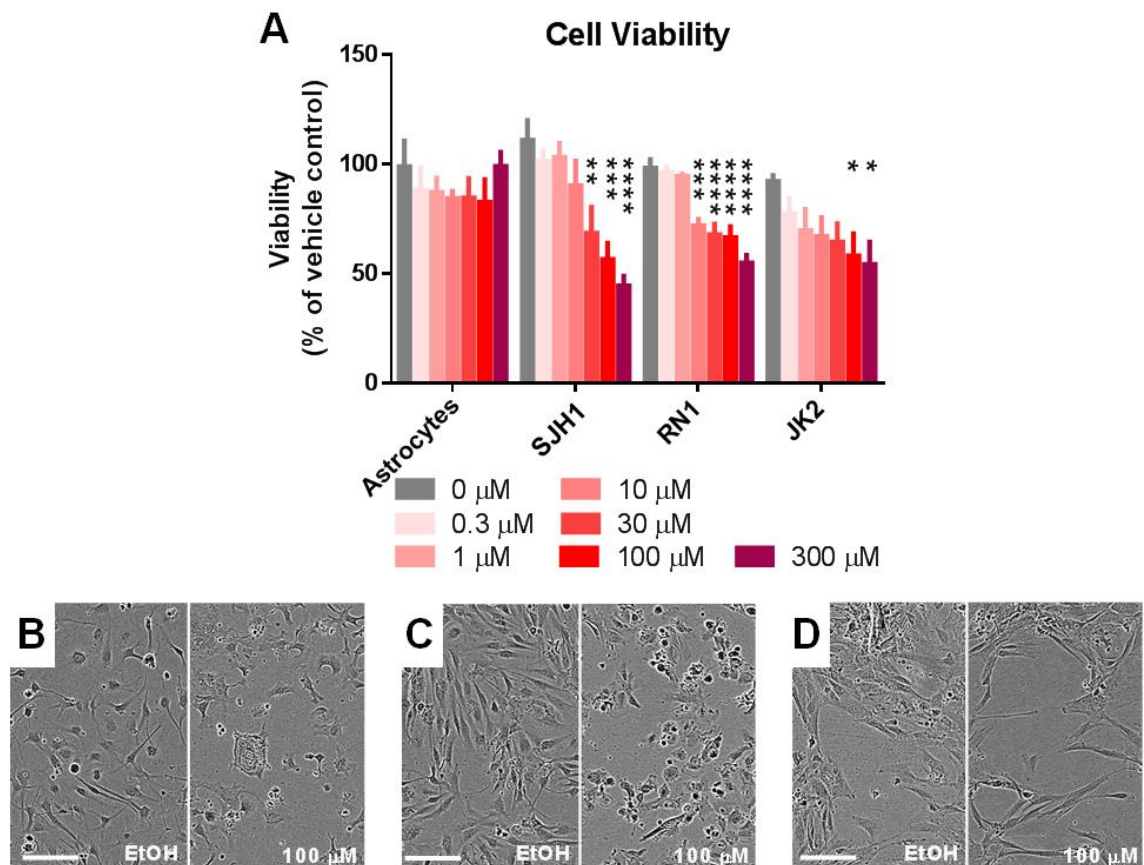


Figure 11: (A) Viability of primary cultures treated with Q-PAC for 48 h. Cell viability was quantified via a Resazurin-based fluorometric assay in cultures treated for 48 h (n = 4). Readings were normalised to media-only cultures. Data represent mean \pm SEM, * $P < 0.05$, ** $P < 0.01$, *** $P < 0.001$, **** $P < 0.0001$ compared to vehicle control. (B-D) Representative images of human SJH1 primary glioblastoma (B), RN1 primary

glioblastoma (C) and healthy astrocyte (D) cultures treated Q-PAC. Cells treated with vehicle (EtOH), or 100 μ M Q-PAC were captured in phase-contrast 24 h after treatment at 10x magnification (scale bar = 50 μ m).

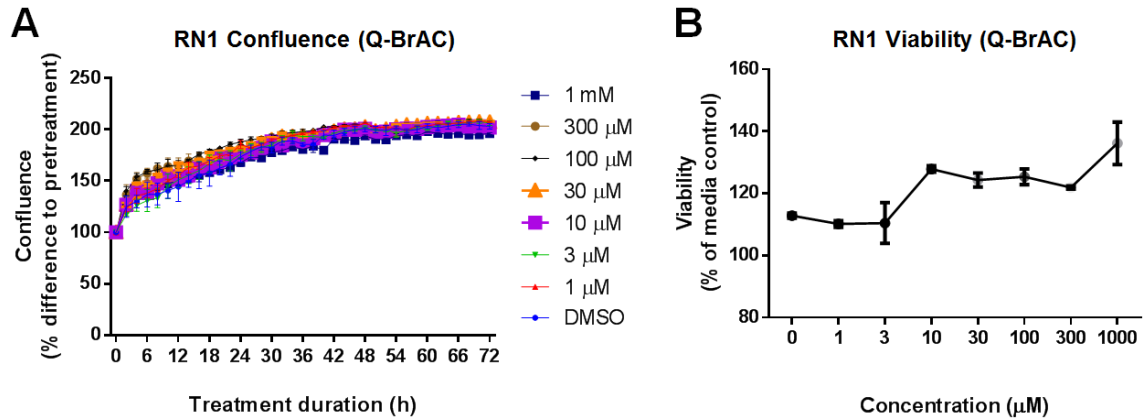


Figure 12: (A) Confluence of primary human GBM RN1 cultures treated with Q-BrAC was quantified via algorithm-based analysis of phase-contrast microscope images at 10x magnification over a 72 h period ($n = 2$ per concentration & culture), normalised to culture confluence prior treatment. (B) Viability of primary GBM RN1 culture treated with Q-BrAC for 48 h. Cell viability was quantified via a Resazurin-based fluorometric assay in cultures treated for 48 h ($n = 2$). Readings were normalised to media-only cultures. Data represent mean \pm SEM.

2.3.5 Effect of Q-PAC on histone modifications

Intrigued by the promising results as observed in the U87 cell line and primary GBMs, the underlying mechanisms of Q-PAC treatment were then investigated. Firstly, the epigenetic profile of histones was studied as LSD1 demethylates H3K4me1/2.

The histone demethylase LSD1 was reported to overexpress in GBM,^{51,97} therefore the expression of LSD1 in GBM cultures of this study was quantified by western

blot analysis. As expected, primary GBMs RN1 and SJH1 expressed higher levels of LSD1 compared to healthy astrocytes (Figure 13A). Interestingly, the LSD1 expression in U87 and JK2 did not differ compared to healthy astrocytes (Figure 13A).

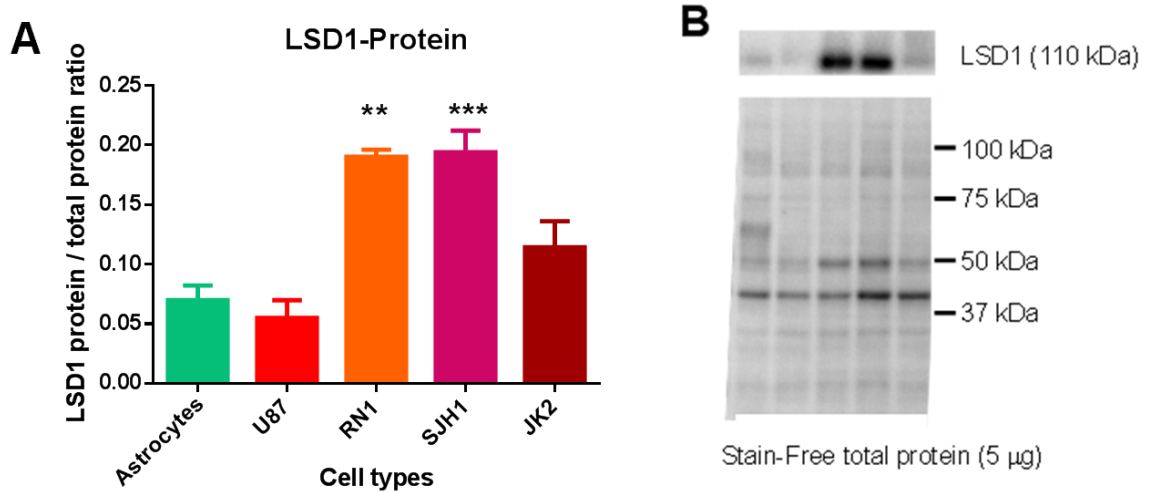


Figure 13: (A) LSD1 protein levels in human astrocytes and glioblastoma cells (established cell line: U87MG; primary patient samples: RN1, SJH1, JK2) were quantified via immunoblotting ($n=3$ per cell type), normalised to total protein content of each sample. (B) Representative immunoblot for LSD1 (detected at 110 kDa) and total protein for each cell type (healthy astrocytes, U87, RN1, SJH1 and JK2).

As a proxy to measure the degree of LSD1 inhibition induced by Q-PAC, the expression of H3K4me1/2 in U87 (basal LSD1 level) and RN1 (overexpressed LSD1 level) were quantified by western blot analysis 4 h after Q-PAC treatment. The duration of 4 h was chosen because changes in confluence and migration were observed within 4 h in response to Q-PAC treatment. In treated U87 cells, no effect was observed in the levels of H3K4me1 ($F(5, 18)=1.024$, $P=0.43$) and H3K4me2 ($F(5, 12)=0.25$, $P=0.93$) (Figure 14A). On the other hand in RN1 culture, the levels of H3K4me1 ($F(5,12)=3.18$, $P=0.05$) and H3K4me2 ($F(5,12)=2.74$, $P=0.07$) increased and peaked at 10 µM of Q-PAC, while not differing to control level at lower or higher concentrations (Figure 14B).

Lastly, 10 μM of Q-PAC did not affect the level of H3K4me2 ($t=0.26$, $df=6$, $P=0.814$; data not shown) in healthy astrocytes (H3K4me1 was not detected in the human astrocytes).

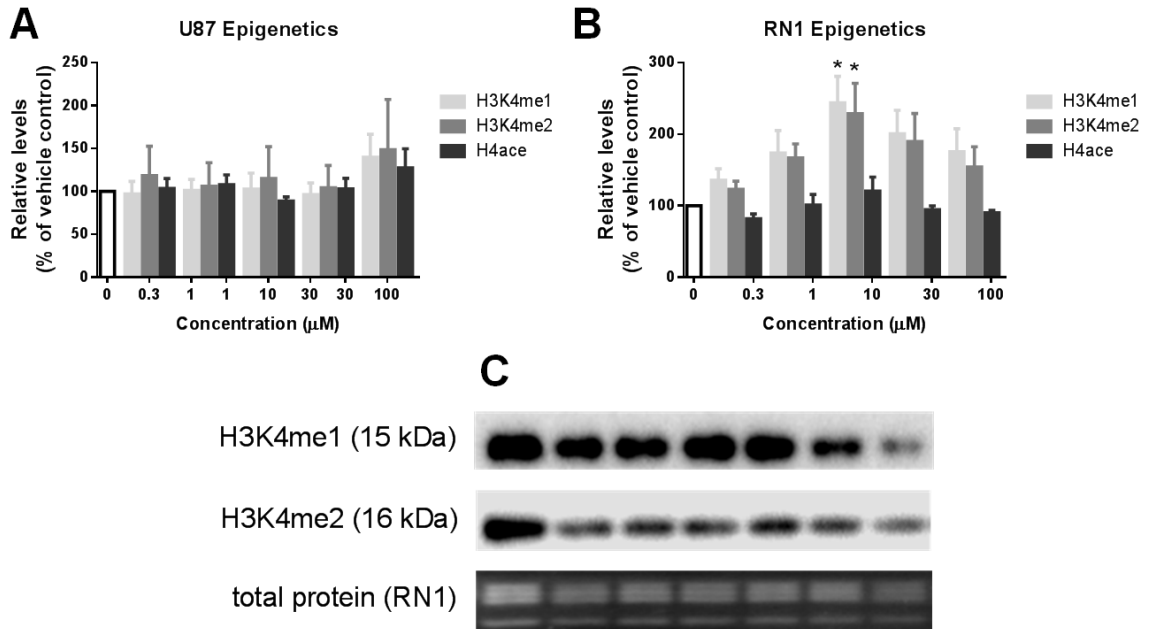


Figure 14: (A-B) H3K4 monomethylation (me1), dimethylation (me2) and H4 acetylation (ace) levels quantified via immunoblotting in U87MG (A, $n=4$) and RN1 cells (B, $n=3$) cells after 4 h treatment with Q-PAC (0 to 100 μM). Immunoblot intensities were adjusted to total loaded protein and normalised to vehicle control cultures. Data represent mean \pm SEM, * $P<0.05$ compared to vehicle control. (C) Representative immunoblot for RN1 cell samples, blotted for H3K4me1 (detected at 15 kDa), H3K4me2 (detected at 16 kDa), and total protein (segment depicting 8 to 20 kDa) for each Q-PAC concentration (0 to 100 μM).

Apart from H3K4me1/2, H4 pan acetylation in treated U87 and RN1 cultures was also quantified by western blot, as this histone modification has been reported to control chromosome assembly and transcription.⁹⁸ However no changes in H4 acetylation was

observed in U87 ($F(5, 17)=1.13$, $P=0.38$; Figure 14A) and RN1 ($F(5, 12)=1.51$, $P=0.26$; Figure 14B).

The 2-PCPA-based prodrug Q-PAC displayed better treatment response in U87 cells compared to 2-PCPA, therefore this attracts the question whether Q-PAC retained its LSD1 inhibitor function. While an inverted U-shaped concentration-dependent effect on H3K4me1/2 was observed in primary GBM cells, with the peak difference at 10 μM ; the H3K4me1/2 levels were surprisingly unaffected by Q-PAC treatment in immortalised U87 cells. The unchanged H3K4me1/2 levels in U87 cells were unexpected as both U87 and primary GBM cultures demonstrated decrease in cell confluence after Q-PAC treatment. This finding may suggest that Q-PAC only cause minor global methylation changes, or gene-specific methylation changes are likely.^{82,99}

2.3.6 Reduction of GSH levels in GBM cells after Q-PAC treatment

Q-PAC was designed to not only inhibit LSD1 but also suppress antioxidant system by quenching GSH. Therefore, the GSH and ROS levels in GBM cultures were quantified 4 h after Q-PAC treatment, where onset of treatment effects on confluence and migration were observed. Through a fluorometric assay, it was discovered that Q-PAC dose-dependently reduced GSH concentration in U87 and RN1 cells, but not in healthy astrocytes (Figure 15A). Similarly, ROS level elevated dose-dependently with Q-PAC concentration in U87 ($F(7, 33)=5.03$, $P<0.001$) and RN1 ($F(6, 28)=5.76$, $P<0.001$) cells within the same treatment timeframe (Figure 15B). In summary, suppression of antioxidant system to increase ROS was observed in Q-PAC treated GBM cells but not in healthy astrocytes.

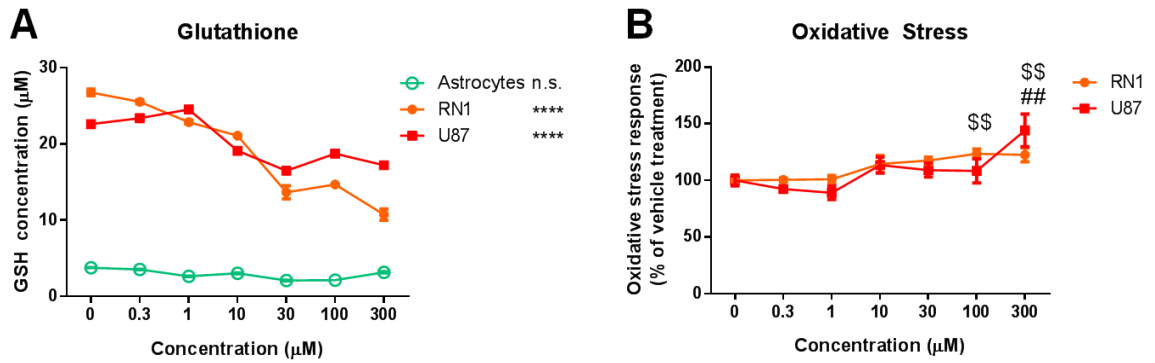


Figure 15: *Q-PAC increases oxidative stress and reduces GSH in GBM cells but not healthy astrocytes. (A) Intracellular GSH concentration was quantified via fluorometric assay 4 h after Q-PAC treatment (0 to 300 μM) in human established GBM cells (U87MG), primary GBM cells (RN1) and primary astrocytes (n=3 per concentration and cell type). (B) Oxidative stress levels were quantified via a cell-permeant fluorogenic probe 4 h after Q-PAC treatment (0 to 300 μM) in human established GBM cells (U87MG) and primary GBM cells (RN1), normalized to vehicle treated cultures (n=3 per concentration and cell type). Data represent mean ± SEM, ****P<0.0001 compared to vehicle control; \$\$P<0.01 compared vehicle control (RN1); ##P<0.01 compared to vehicle control (U87MG).*

2.3.7 Q-PAC induced apoptosis in GBM by increasing caspase 3/7 activity

In order to gain further insight into the underlying mechanism of Q-PAC reducing confluence and cell viability in GBM, we next investigated if Q-PAC induced cell cycle arrest, since LSD1 inhibitors have been reported to induce cell cycle arrest in breast cancer cells.¹⁰⁰ Minichromosome maintenance 2 (MCM2) is part of the DNA replication machinery which is only expressed in proliferating cells.¹⁰¹ 48 h of Q-PAC treatment did not affect the proportion of MCM2-positive U87 or primary GBM cultures (Figure 16),

suggesting that the reduction in viable cells may not be due to cancer cells driving out of the cell cycle.

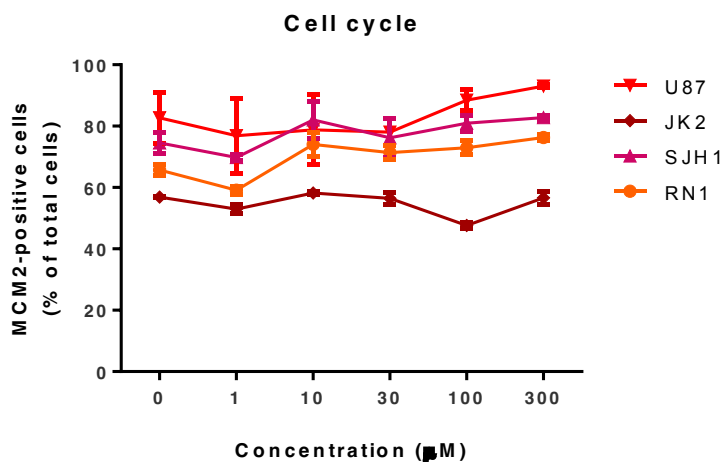


Figure 16: Reduction in GBMs cell viability was not due to cell cycle arrest. Cells positive for minichromosome maintenance 2 expression (MCM2, part of the DNA replication machinery that is only expressed in proliferating cells), were counted in cultures treated with Q-PAC (0 to 300 μM) for 48 h (n=4 per concentration and type). MCM2-positive cells were quantified via antibody-based immunofluorescence labelling in microscope images at 20x magnification and presented as % of total cell number.

Caspase 3/7 play essential roles in executing cell apoptosis.¹⁰² It is well documented that apoptosis is closely related to ROS concentration, and GSH depletion induced activation of caspase 3.^{103,104} Furthermore, LSD1 inhibition was also reported to induce caspase-dependent apoptosis in AML,⁵² Ewing sarcoma¹⁰⁵ and endometrial carcinoma,¹⁰⁶ therefore caspase 3/7 activity was monitored in GBM cells and healthy astrocytes after Q-PAC treatment. Q-PAC does-dependently increased caspase 3/7 activity in U87 (F(6, 11)=24.30, P < 0.0001; Figure 17A), RN1 (F(5, 22)=6.2, P=0.001; Figure 17B), JK2 (F(5, 6)=5.7, P = 0.027; Figure 17C) and SJH1 (F(6, 7)=4.83, P=0.028; Figure 17D) cultures, without affecting caspase 3/7 activity in healthy astrocytes (F(5,

12)=2.67, $P=0.08$; Figure 17E). The increase in caspase 3/7 activity suggest that the reduction in GBMs cell viability was due to caspase-mediated apoptosis induced by Q-PAC, while the basal caspase activity in healthy astrocytes was consistent to the observed unaffected viability.

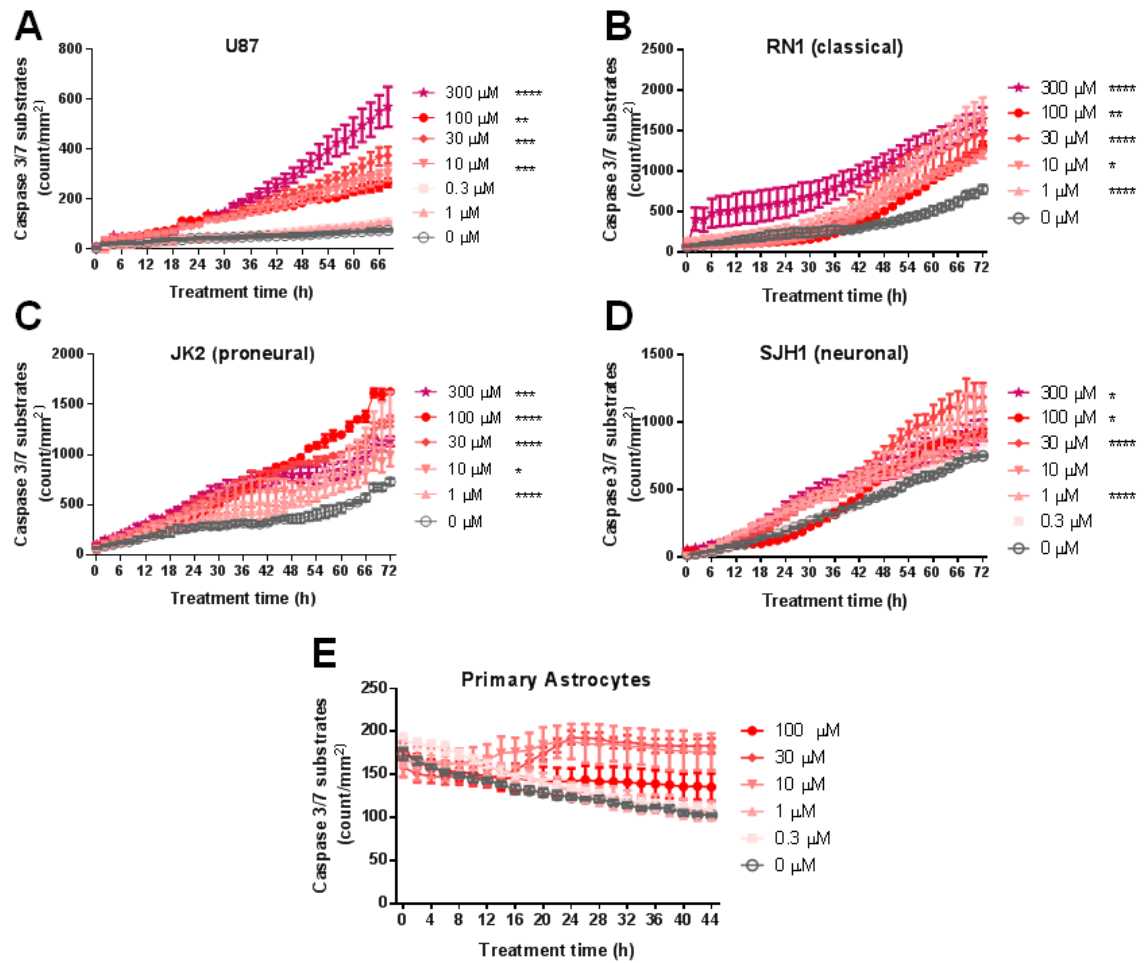


Figure 17: Q-PAC triggers caspase-dependent apoptosis in primary GBM cells but not in healthy astrocytes. Caspase activity of established U87 GBM cells (A), primary human GBM cultures (B-D) and primary human astrocytes cultures (E) after treatment with Q-PAC. Apoptosis was quantified through counting of green-fluorescent caspase 3/7 substrates per mm^2 in microscope images at 20x magnification over time ($n=3$ per concentration & culture). Data represent mean \pm SEM, * $P<0.05$, ** $P<0.01$, *** $P<0.001$, **** $P<0.0001$ compared to vehicle control.

2.3.8 Proposed mechanism for the Q-PAC induced caspase-dependent apoptosis

Due to the difference in cellular ROS concentration, prodrug Q-PAC selectively targeted GBM cells over healthy astrocytes (Section 2.3.4). Upon activation by hydrogen peroxide, Q-PAC liberated 2-PCPA (LSD1 inhibitor) and QM (GSH scavenger) which reduced viability in GBM cells. In this study, Q-PAC inhibited LSD1 in primary GBM RN1 as shown from the increased H3K4me1/2 levels at 10 μ M (Section 2.3.5), GSH depletion and oxidative stress elevation were also observed in GBM cells upon Q-PAC treatment (Section 2.3.6). As a result, the synergistic effect of LSD1 inhibition and GSH depletion likely induced caspase 3/7-mediated apoptosis in GBM cells (Section 2.3.7).

Due to the fact that the cytochrome c-initiated pathway is the main caspase activation pathway in mammalian cells, we proposed that cytochrome c plays a major role in the apoptosis of GBM cells through activation of caspase 9 and subsequently caspase 3/7 (Figure 18).¹⁰⁷ The release of cytochrome c from mitochondria is normally suppressed by Bcl-2 to prevent apoptosis.^{107,108} Since reduced expression of Bcl-2 was reported in LSD1 inhibition,^{109,110} this led us to believe that the release of cytochrome c is favoured and hence inducing caspase-dependent apoptosis in GBM cells treated with Q-PAC. Furthermore, release of cytochrome c is promoted under elevated oxidative stress caused by GSH depletion.¹⁰⁴ Therefore, we proposed that the dual-action prodrug Q-PAC promotes the liberation of cytochrome c from mitochondria by simultaneously increasing oxidative stress (via QM-induced GSH depletion) and suppressing the expression of Bcl-2 (via LSD1 inhibition). To verify this hypothesis, the expression of Bcl-2 can be quantified by Western blot analysis while the release of cytochrome c can be measured by immunodetection in the future.^{110,111}

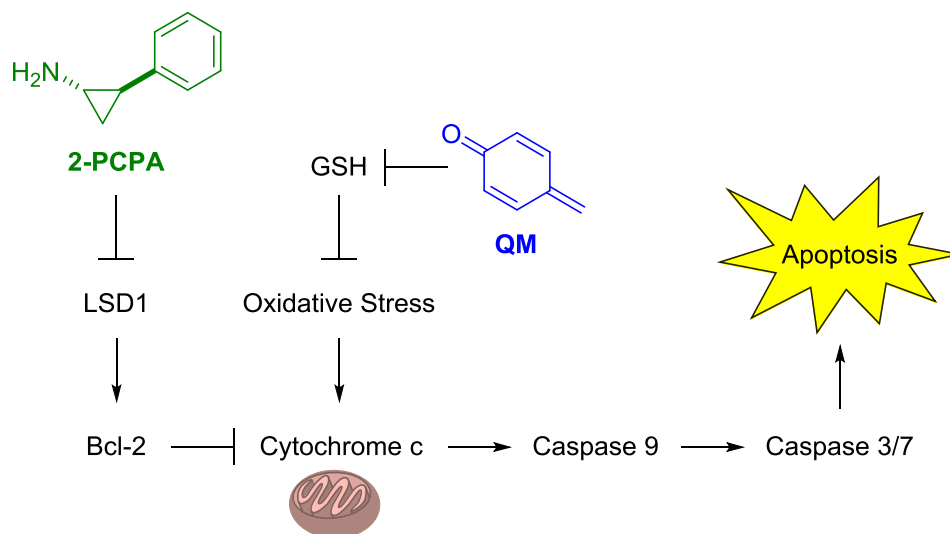


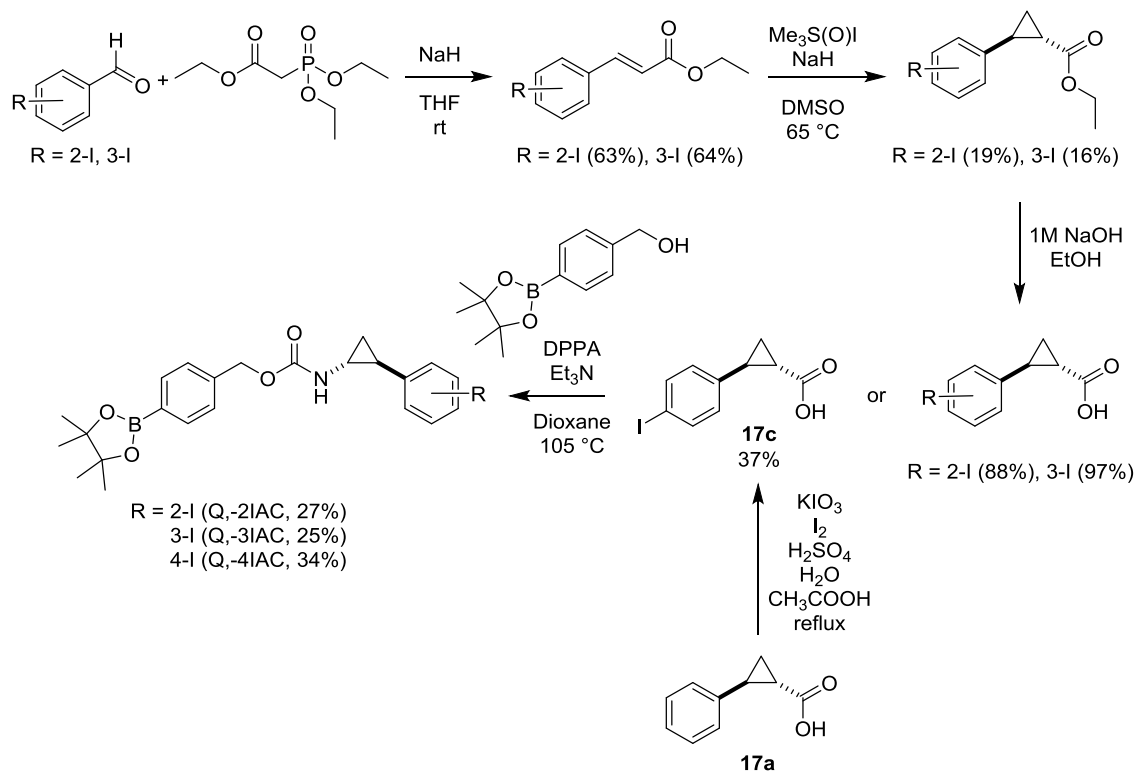
Figure 18: Proposed mechanism of caspase-dependent apoptosis induced by 2-PCPA and QM (generated from Q-PAC).

2.3.9 Preparation and biological evaluation of iodinated prodrugs

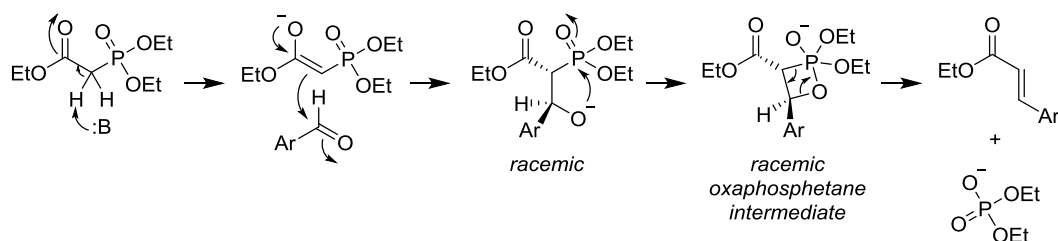
The capability to pass through BBB is an essential criterion for drugs targeting GBM, and this is reflected by the log BB parameter.^{112,113} The calculated log BB value for Q-PAC is 0.10, which is above the -0.3 cut-off for BBB permeability,¹¹⁴ suggesting that Q-PAC will pass through the blood brain barrier. Inspired by the promising and selective treatment effect demonstrated by Q-PAC in GBMs, and to gain insight into the biodistribution and metabolic stability, we aimed to radiolabel Q-PAC with ^{124}I in order to proceed forward with mice model. Isotope ^{124}I was chosen because this isotope has a relatively long half-life (4.2 days), which is feasible for prolonged in vivo studies.¹¹⁵

Prior to radiolabelling, three non-radioactive iodo-derivatives of prodrug Q-PAC were synthesised and tested in vitro to observe if the anticancer properties can still be retained with the presence of iodine atom, especially since Q-BrAC (the bromo-analogue of Q-PAC) did not show the same anticancer effect as observed with Q-PAC. Iodine atom

was located on the 2-PCPA phenyl moiety at different position in these three derivatives (namely Q-2IAC, Q-3IAC and Q-4IAC).



Mechanism of Horner–Wadsworth–Emmons reaction



Scheme 10: Preparation for the iodo-analogues of prodrug Q-PAC.

Ethyl cinnamates with iodine on the phenyl ring are not commercially available, therefore the syntheses of Q-2IAC and Q-3IAC started from Horner–Wadsworth–Emmons reaction of iodobenzaldehydes to yield the corresponding ethyl cinnamates (Scheme 10). NaH deprotonated triethyl phosphonoacetate to form the phosphonate carbanion, which then attacked the carbonyl in iodobenzaldehydes to yield the oxaphosphetane intermediate, followed by elimination of diethoxyphosphate salt to yield

the desired ethyl cinnamates. During the formation of oxaphosphetane intermediate, the ester group was placed *anti* to the aromatic ring to minimise steric hindrance. As a result, (*E*) olefin isomer was obtained solely as the product – indicated by the ¹H NMR analysis discussed below.

For the 2-iodo ethyl cinnamate, its formation was indicated by the absence of singlet at 9.97 ppm (R-CHO) in ¹H NMR spectrum, while the signals at 7.91 – 7.88 and 6.31 ppm were assigned as the olefin protons. The doublet at 6.31 ppm had a coupling constant of 15.5 Hz, which corresponded to an (*E*) alkene – consistent to the mechanism of Horner–Wadsworth–Emmons reaction.

Similar to the preparation of Q-PAC and Q-BrAC, the obtained iodo ethyl cinnamates were subjected to Corey–Chayvosky cyclopropanation, basic hydrolysis and ultimately Curtius rearrangement with PBE to yield the prodrugs Q-2IAC and Q-3IAC (Scheme 10). Among all the synthetic steps, low yields of 16 – 19% were obtained during the Corey–Chayvosky cyclopropanation. As the ethyl cinnamate substrates were not detected after the reaction, it was proposed that decomposition of reaction intermediates might have occurred – possibly a result of lower electrophilicity of the esters compare to the more commonly used aldehyde substrates.

On the other hand, Q-4IAC can be easily prepared from the iodination of *trans*-2-phenylcyclopropane-1-carboxylic acid **17a** follow by Curtius rearrangement with PBE (Scheme 10). Under acidic conditions, the triiodine cation (I₃⁺) was formed upon treatment of I₂ with IO₃⁻, the I₃⁺ then acted as an iodinating agent for the phenyl ring in **17a** to yield **17c**.¹¹⁶ In the ¹H NMR spectrum of **17c**, two distinct doublets with total integration of four protons were observed at 7.60 and 6.86 ppm (*J* = 8.0 Hz for both doublets), which is a feature of *para* disubstituted phenyl ring. The success in iodination

was also indicated in the ^{13}C NMR spectrum of **17c**, where an up-field shift was observed for the iodinated carbon (from 128.6 – 126.3 ppm in **17a** to 91.7 ppm in **17c**).

Immortal U87 cultures were then treated with these three iodo-prodrugs and cell confluence was assessed. Q-4IAC reduced cell confluence at concentrations of 100 μM or higher (Figure 19C). Although Q-2IAC also reduced U87 cell confluence at 100 μM in the first two hours after treatment, the cell confluence was observed to recover after four hours of treatment (Figure 19A). Meanwhile, Q-3IAC only reduced U87 cell confluence at a higher concentration of 300 μM (Figure 19B). The migratory ability of U87 cells was also assessed through a scratch-assay. The results of scratch-assay for the three iodo-prodrugs are consistent to the cell confluence, except Q-2IAC was able to reduce migration of U87 cells at a lower concentration of 30 μM rather than 100 μM (Figure 19D-F). In summary, cell proliferation and migratory ability of U87 cells were impaired by Q-4IAC and Q-2IAC, but at higher concentrations compared to Q-PAC.

Interestingly, although Q-4IAC displayed a reduced anticancer effect compared to Q-PAC, Q-4IAC was still more potent than Q-BrAC in the inhibition of U87 cell proliferation, and they are only differed in the halogen atoms on the 2-PCPA phenyl moiety. Since iodine atom is larger than bromine atom in size, this further supports the hypothesis that the lack of anticancer activity shown in Q-BrAC was not due to the steric clash of brominated 2-PCPA in the LSD1 active site.

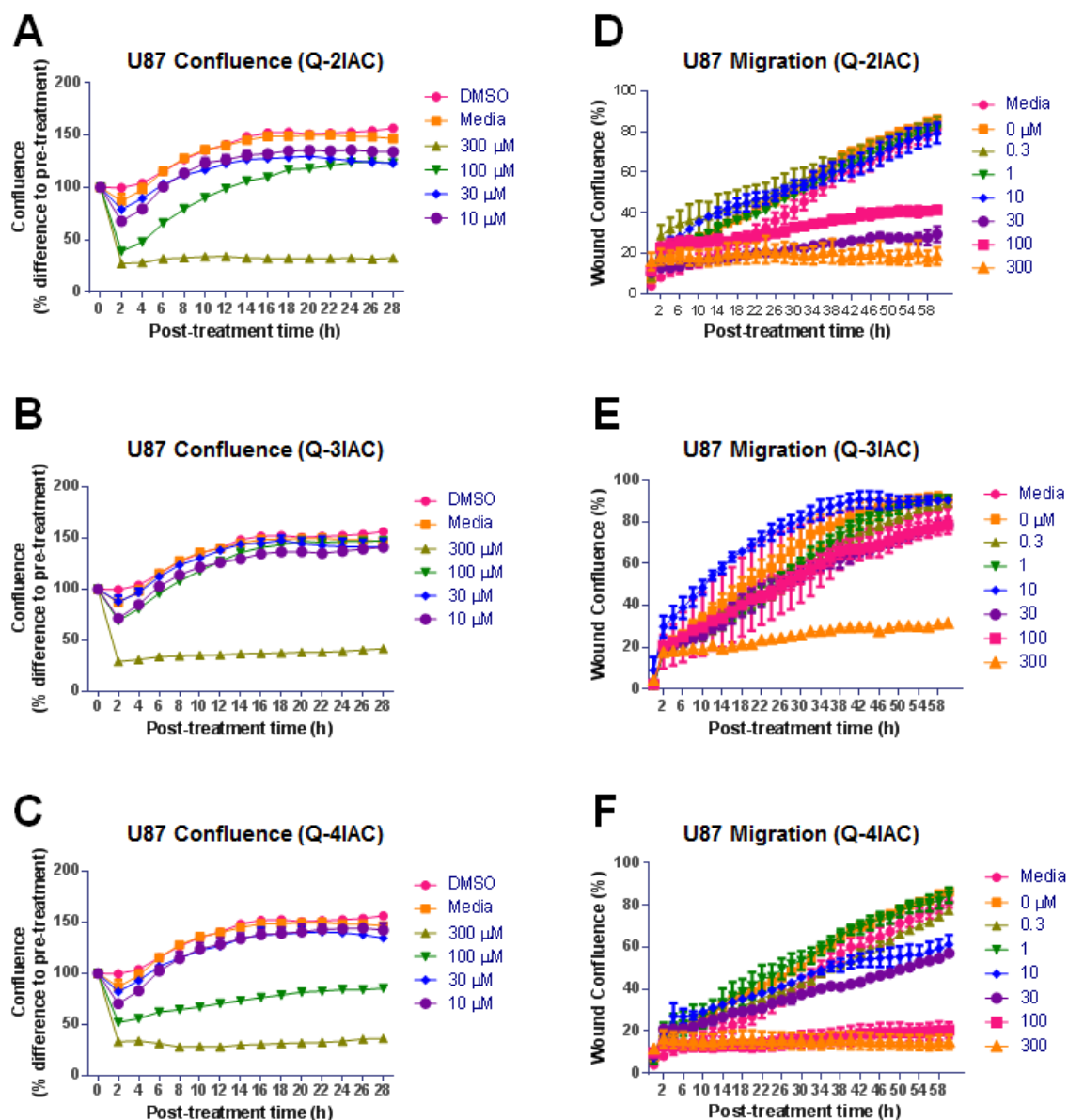


Figure 19: (A-C) Confluence of primary human GBM RN1 cultures treated with Q-2IAC (A), Q-3IAC (B) and Q-4IAC (C) were quantified via algorithm-based analysis of phase-contrast microscope images at 10x magnification over a 28 h period ($n=3$ per concentration & culture), normalised to culture confluence prior treatment. (D-F) 2D migration of human GBM RN1 cultures treated with Q-2IAC (D), Q-3IAC (E) and Q-4IAC (F). Scratch wound width was quantified through algorithm-based analysis of phase-contrast microscope images at 10x magnification following scratch wound and Q-

PAC treatment (n=3 per concentration and culture), normalised to wound width prior treatment. Data represent mean \pm SEM.

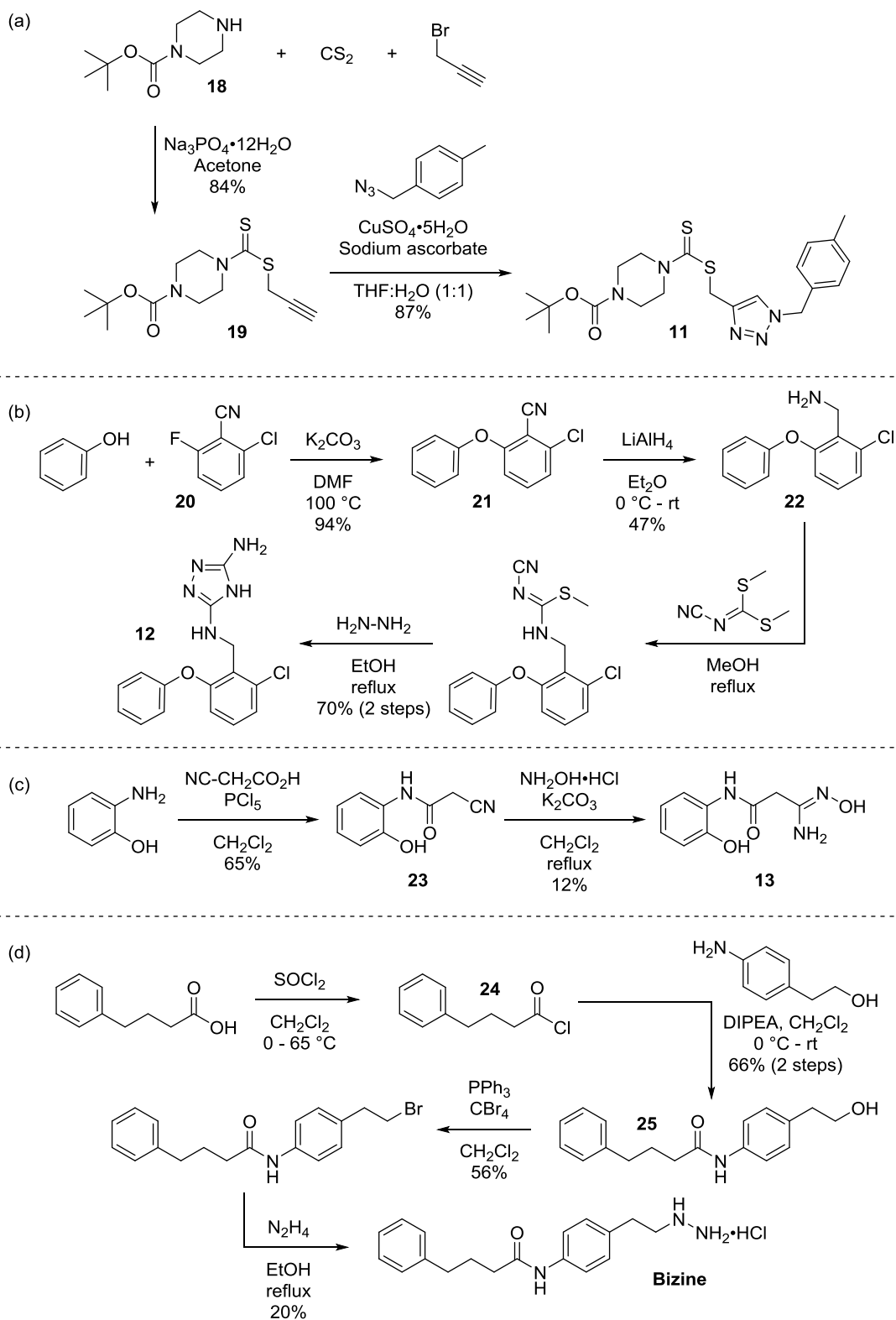
In order to access radiolabelled prodrugs, the stannylated derivatives of prodrugs needed to be prepared as precursors for radioiodination. The understanding of the prodrug's stability is vital to decide if preparation of stannylated derivatives should commence. As the prodrugs in this study were novel and their stability under radioiodination was unknown, Q-4IAC was subjected to radioiodination conditions to understand its molecular stability under these conditions. Experiments were conducted by Dr I. Greguric (Australian Nuclear Science and Technology Organisation). Prodrug Q-4IAC was subjected to two different radioiodination conditions: (i) Chloramine-T (100 μ g/100 μ L in H₂O) + 1.0 M HCl + 1 crystal of NaI; (ii) 2% peracetic acid/acetic acid + 1 crystal of NaI. The integrity of prodrug Q-4IAC was monitored via HPLC after treatments with radioiodination conditions. Based on the HPLC chromatograms after treatment, less than 3% of prodrug Q-4IAC remained while more than two decomposed species were present in each condition. The decomposed species were not identical in each condition as shown from the difference in retention time. Although it is possible that hydrolysis of the boronic ester to the acid took place, hydrolysis of the carbamate linkage could also be possible.

In summary, while prodrug Q-4IAC moderately decreased U87 cell confluence and migration, radiolabelling of Q-4IAC under these conditions is unlikely to be possible, with the degradation perhaps due to the oxidative aqueous acidic conditions used during radioiodination, which might cause both oxidation and/or hydrolysis of the boronate functionality. Therefore alternative milder radiolabelling approaches should be attempted in the future.¹¹⁷

2.3.10 Biological evaluation of reported LSD1 inhibitors on GBM cells

Since the discovery of LSD1 in 2004, 2-PCPA derivatives have been studied extensively in LSD1 inhibition, especially two of these derivatives are currently in clinical trials (Section 2.1.6). At the same time, potent and selective non-2-PCPA-based LSD1 inhibitors (**11-13**, bizine) have also been reported in literature (Section 2.1.7). Even though these non-2-PCPA-based LSD1 inhibitors demonstrated promising in vitro results in their respective studies, these inhibitors have not been assessed on GBM cell lines. In parallel to the GBM prodrug study, we investigated these reported non-2-PCPA-based LSD1 inhibitors in the treatment of GBM cells. Promising hits from this investigation could be incorporated into our prodrug platform to replace the 2-PCPA moiety in hope of improving LSD1 inhibitory activity.

Non-2-PCPA-based LSD1 inhibitors **11-13** and bizine were prepared based on their original reported literature (Scheme 11).⁸⁷⁻⁹⁰ During the course of preparing these inhibitors, it was discovered that several characterisation data for the reported inhibitors and their intermediates (such as ¹³C NMR, IR, HRMS and melting point) was missing from the literature. Therefore, these characterisation data were collected and reported in the experimental section of this chapter.



Scheme 11: Preparation of reported non-2-PCPA-based LSD1 inhibitors.

Inhibitor **11** was prepared in two steps (Scheme 11a). Firstly, intermediate **19** was prepared in one-pot from *tert*-butyl piperazine-1-carboxylate **18**, carbon disulfide and

propargyl bromide in the presence of $\text{Na}_3\text{PO}_4 \cdot 12\text{H}_2\text{O}$. Subsequently, a Huisgen 1,3-dipolar cycloaddition between the alkyne in **19** and 4-methylbenzyl azide yielded the desired inhibitor **11** in an overall yield of 73% over two steps. The ^1H NMR data of **11** was consistent with the literature.⁹⁰

Inhibitor **12** was prepared in four steps (Scheme 11b). After coupling phenol with 2-fluoro-6-chlorobenzonitrile **20** to form intermediate **21**, the nitrile group in **21** was reduced to amine **22** using LiAlH_4 . Subsequent reaction with *N*-cyanodithioiminocarbonate then hydrazine hydrate furnished the desired inhibitor **12**. The ^1H NMR data of **12** was consistent with the literature.⁸⁸ In the IR spectrum obtained from this study, the signals at 3352 and 3266 cm^{-1} were assigned as the N-H bonds in **12**. Moreover, the HRMS of **12** was acquired in this study with good accuracy ($\Delta\text{ppm} = 4.1$).

Inhibitor **13** was prepared in two steps (Scheme 11c). Intermediate **23** was obtained from the coupling of 2-aminophenol with cyanoacetic acid in the presence of phosphorus pentachloride. Subsequently, reaction of **23** with hydroxylamine hydrochloride and potassium carbonate provided the amidoxime inhibitor **13**. A low isolated yield of 12% was obtained in the final step, this could be due to the loss of material during recrystallisation. The ^1H NMR data of **13** was consistent with the literature.⁸⁷ While the ^{13}C NMR data was not reported, the ^{13}C NMR spectrum obtained in this study was consistent with the proposed structure. Due to the introduction of amine to nitrile via hydroxylamine hydrochloride, the $\text{H}_2\text{N}-\text{C}=\text{N}$ carbon signal shifted down-field from 115.8 ppm to 148.7 ppm. Similarly, the CH_2 signal shifted down-field from 27.2 ppm to 39.7 ppm due to the introduction of amine group to the adjacent carbon. Furthermore, the HRMS of **13** obtained in this study matched the proposed structure with great accuracy ($\Delta\text{ppm} = 1.0$).

Bizine was prepared in four steps (Scheme 11d). Firstly, 4-phenylbutyric acid was treated with thionyl chloride to form the acyl chloride intermediate **24**. This was followed by the nucleophilic addition of 2-(4-aminophenyl)ethanol to link the two fragments with an amide linkage. The resulting **25** intermediate was subjected to an Appel reaction with triphenylphosphine and tetrabromomethane, in order to convert the hydroxyl group to bromine. Eventually, the bromine atom was substituted by hydrazine to yield bizine. The ^1H NMR data of bizine was consistent with the literature.⁸⁹ While the IR data was not reported, the IR spectrum for bizine obtained in this study displayed signals at 3303 and 1684 cm^{-1} , corresponding to the N-H and C=O bonds in the molecule.

These LSD1 inhibitors and 2-PCPA were then subjected to treatment on primary GBM cell line RN1 which was found to overexpress LSD1 (Figure 13). Among the tested LSD1 inhibitors, only inhibitor **11** was found to affect RN1 cell confluency over a 48 h treatment period (Concentration: $F(5, 30)=25.80$, $P<0.001$; Time: $F(24, 720) = 568.3$, $P<0.001$), with concentrations of 10 μM and higher significantly lowering culture confluence (10 μM : $P=0.0005$, 30 μM : $P=0.0029$, 100 μM : $P<0.0001$) (Figure 20). Moreover, treatment of inhibitor **11** also impaired the migration of RN1 cells (Concentration: $F(5, 30)=34.36$, $P<0.001$; Time: $F(22, 660)=104.3$, $P<0.0001$) at concentrations of 10 μM and higher ($P<0.0001$ vs vehicle) (Figure 21). No effect on cell confluence or migration was observed when RN1 cells were treated with inhibitors **12**, **13**, bizine and 2-PCPA (Figure 20, Figure 21). Consistent to the reduction in RN1 cell confluence and migration, inhibitor **11** treatment dose-dependently reduced RN1 viability at concentration of 10 μM and higher (10 μM : $P=0.0168$, 30 μM : $P<0.0001$, 100 μM : $P<0.001$ vs vehicle) after 48 h of treatment (Figure 22).

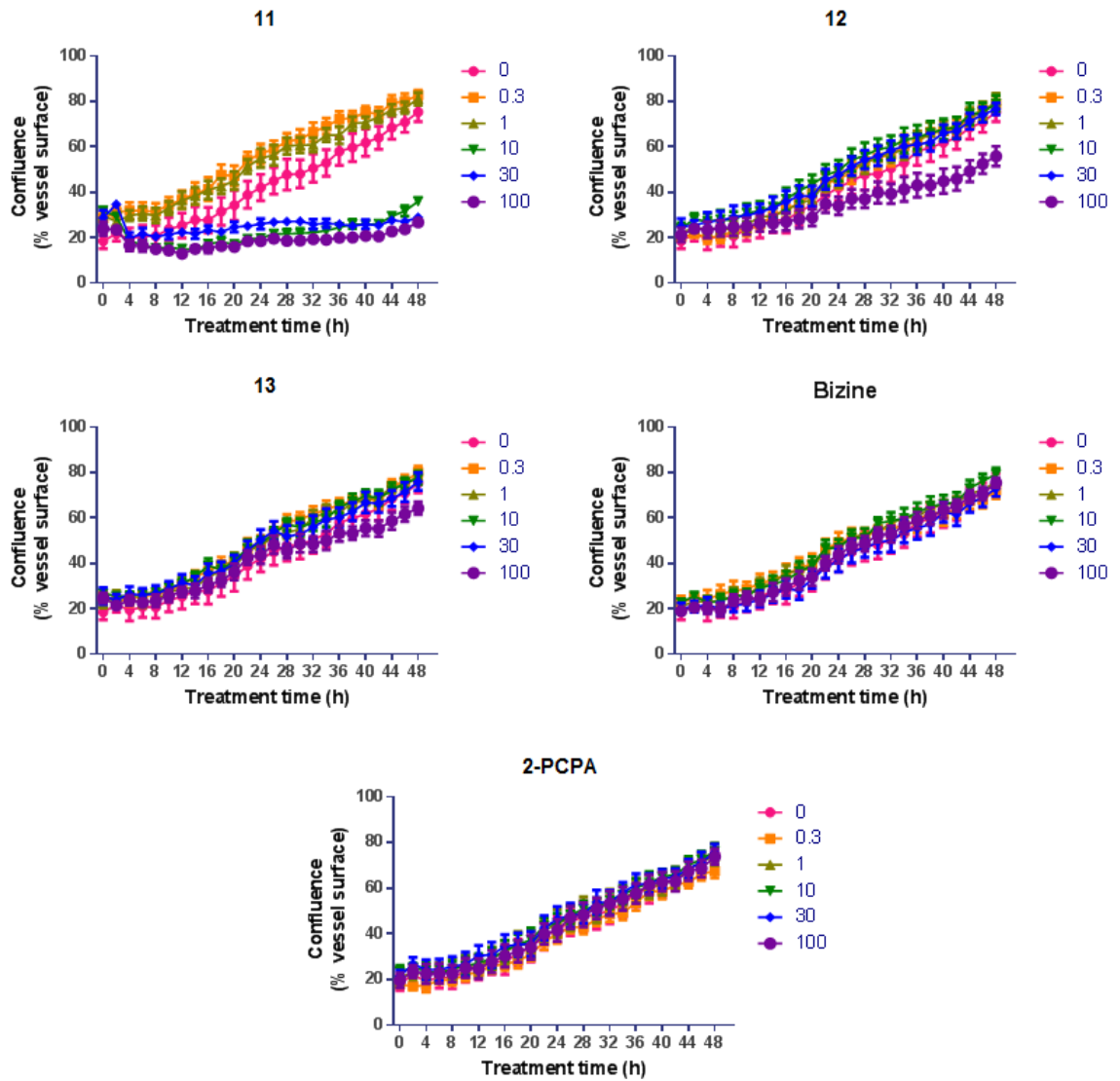


Figure 20: Confluence of RNI cultures treated with different reported LSD1 inhibitors. Algorithm-based confluence analysis of phase-contrast microscope images at 10x magnification every 2 h over a 48 h period following LSD1 inhibitor treatment ($n=3$ per concentration). Data represent mean \pm SEM.

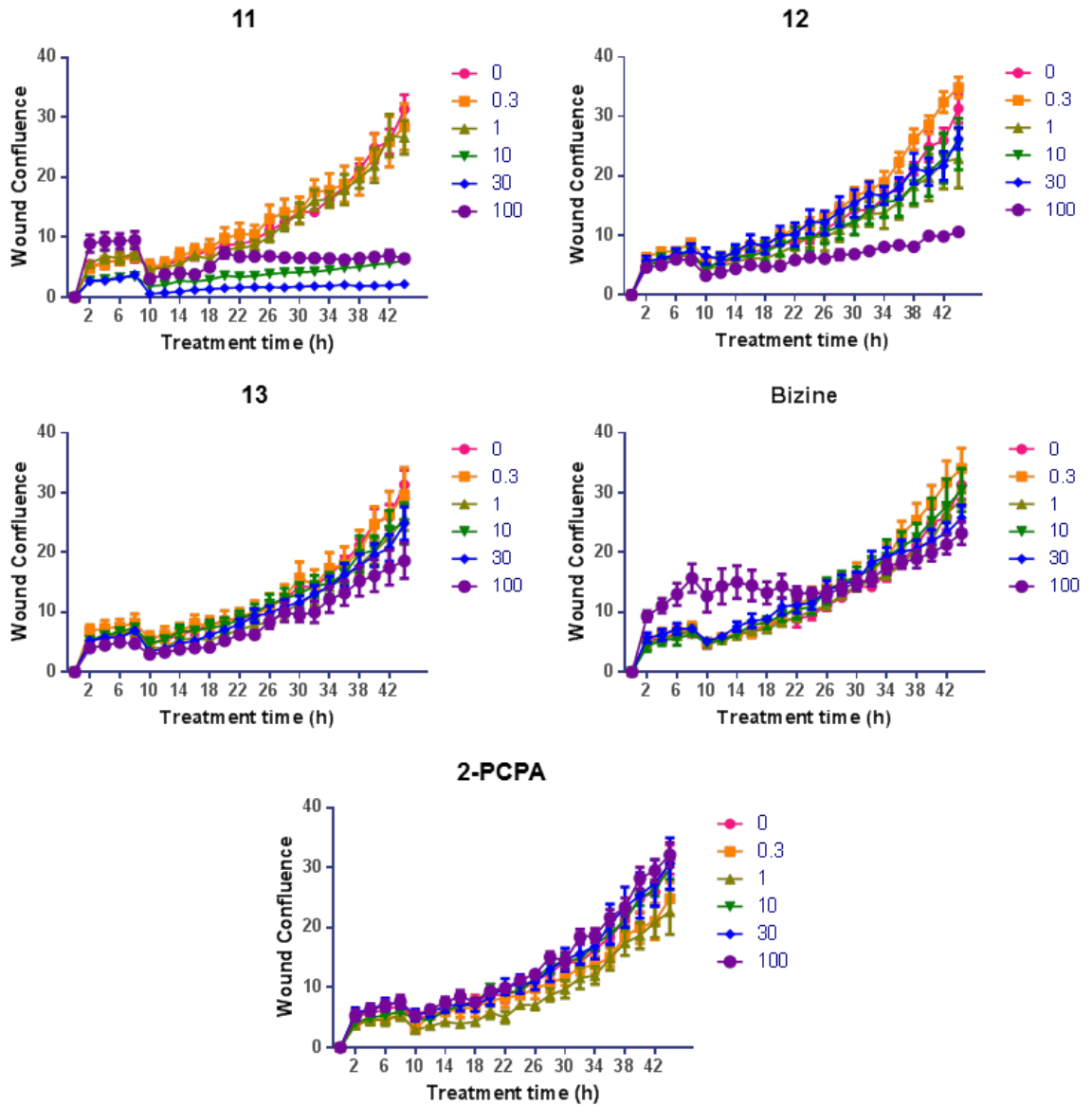


Figure 21: 2D migration of RNI cells treated with reported LSD1 inhibitors. Algorithm-based scratch wound analysis of phase-contrast microscope images at 10x magnification every 2 h over a 48 h period following scratch wound and LSD1 inhibitor treatment ($n=3$ per concentration). Data represent mean \pm SEM.

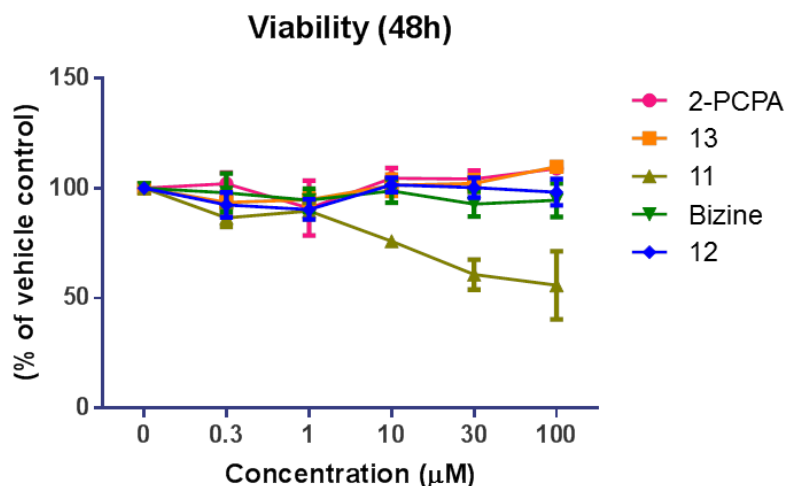


Figure 22: After treatment of reported LSD1 inhibitors, cell viability of RN1 culture was quantified via a Resazurin-based fluorometric assay ($n = 4$), with readings normalised to vehicle treated cultures. Data represent mean \pm SEM.

Since our 2-PCPA-based prodrug Q-PAC was found to induce caspase-mediated apoptosis in GBM cells, the caspase 3/7 activity was also monitored after RN1 cells were treated with these reported LSD1 inhibitors. Consistent to the observed reduction in RN1 cell viability, inhibitor **11** dose-dependently increased caspase 3/7 activity in RN1 cells (Concentration: $F(5, 30)=38.67$, $P<0.0001$; Time: $F(24, 720)=1157$, $P<0.0001$) at concentration of 10 μM or higher (10 μM : $P=0.0016$, 30 μM : $P<0.0001$, 100 μM : $P<0.0001$) (Figure 23). This result may suggest that the observed reduction in cell confluence and migration were caused by caspase-dependent apoptosis triggered by LSD1 inhibition and subsequently Bcl-2 suppression and cytochrome c release.¹⁰⁸⁻¹¹⁰ Similarly, no effect on caspase 3/7 activity was observed when RN1 cells were treated with inhibitors **12**, **13**, bizine and 2-PCPA (Figure 23).

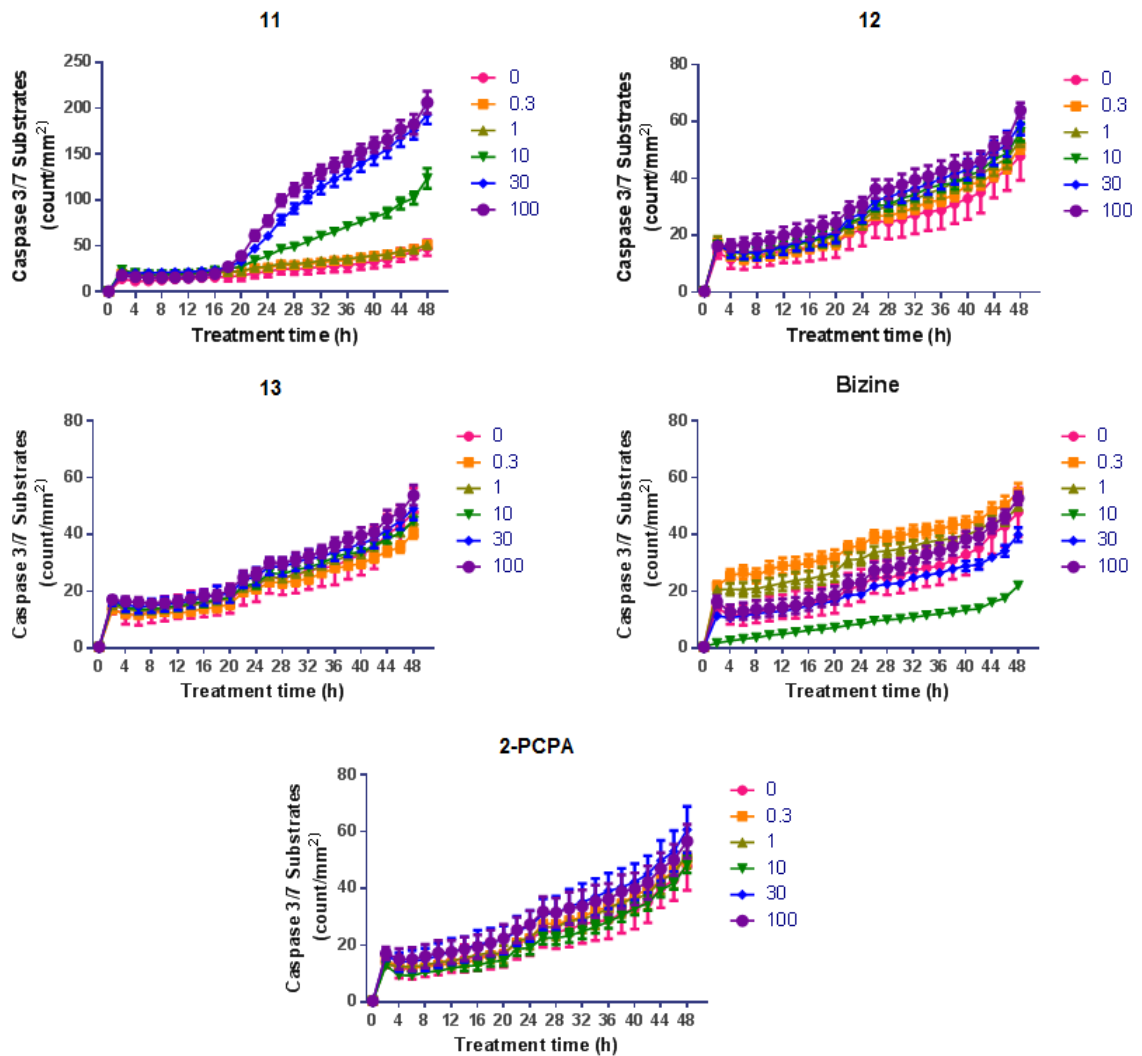


Figure 23: Apoptosis of primary GBM RN1 cultures treated with reported LSD1 inhibitors. Apoptosis was quantified through counting of green-fluorescent caspase 3/7 substrates per mm² in microscope images at 20x magnification over time ($n=3$ per concentration).

Among the tested LSD1 inhibitors, only inhibitor **11** displayed anticancer effect on primary GBM RN1 cells by inducing caspase-dependent apoptosis triggered by LSD1 inhibition. This demonstrated the potential of this inhibitor as a lead for further development and incorporation into the concept of dual-action prodrug described in this chapter.

2.4 Conclusions and future work

The dual-action prodrug Q-PAC described in this chapter utilised the high ROS concentration in tumour cells as an activation method to selectively target GBM cells over healthy astrocytes. Upon activation by hydrogen peroxide, Q-PAC releases 2-PCPA (LSD1 inhibitor) and QM (antioxidant scavenger), as verified from mass spectrometry experiments. LSD1 inhibition may lead to the suppression of Bcl-2 which allows the release of cytochrome c from mitochondria. At the same time, the liberation of cytochrome c is promoted when cells are under oxidative stress induced by GSH depletion. The release of cytochrome c from mitochondria is crucial in the caspase-dependent apoptosis pathway where caspase 9 is activated follow by caspase 3/7. As a result of caspase-dependent apoptosis induced by Q-PAC, the confluence, migration and cell viability of GBM cells were found to be reduced dose-dependently, while healthy astrocytes remained unaffected.

The selectivity of Q-PAC towards GBM cells over healthy astrocytes is mainly attributed to the aryl boronate functionality. Despite boronic esters having been described to have low hydrolytic stability in biological media,^{118,119} our results demonstrated that the boronic ester-containing Q-PAC was able to induce apoptosis in GBM selectively at micromolar range. In fact, the hydrolysed aryl boronic acid can also be oxidised to the phenol intermediate in the presence of H₂O₂.¹²⁰ Furthermore, Mokhir and co-workers have also reported promising results on aryl boronate-containing prodrugs.^{26,33,35} In the future, a more hydrolytic stable analogue of Q-PAC can be prepared in order to investigate if hydrolytic stability plays a role in the prodrug activity or its pharmacokinetics. Bernardini et al. reported that introducing steric hindrance to the diol moiety of boronic ester can slow down the hydrolysis rate (Figure 24a), presumably by blocking the attack of water molecule towards the boron p-orbital.¹¹⁸ Based on this

reported observation, we proposed the preparation of a hydrolytic stable analogue of Q-PAC with fused-cyclohexanes at the diol moiety (**26**, Figure 24b). Prodrugs Q-PAC and **26** can then be subjected to GBM treatment to observe if there is any difference in drug activity, as such the role of hydrolytic stability can be understood.

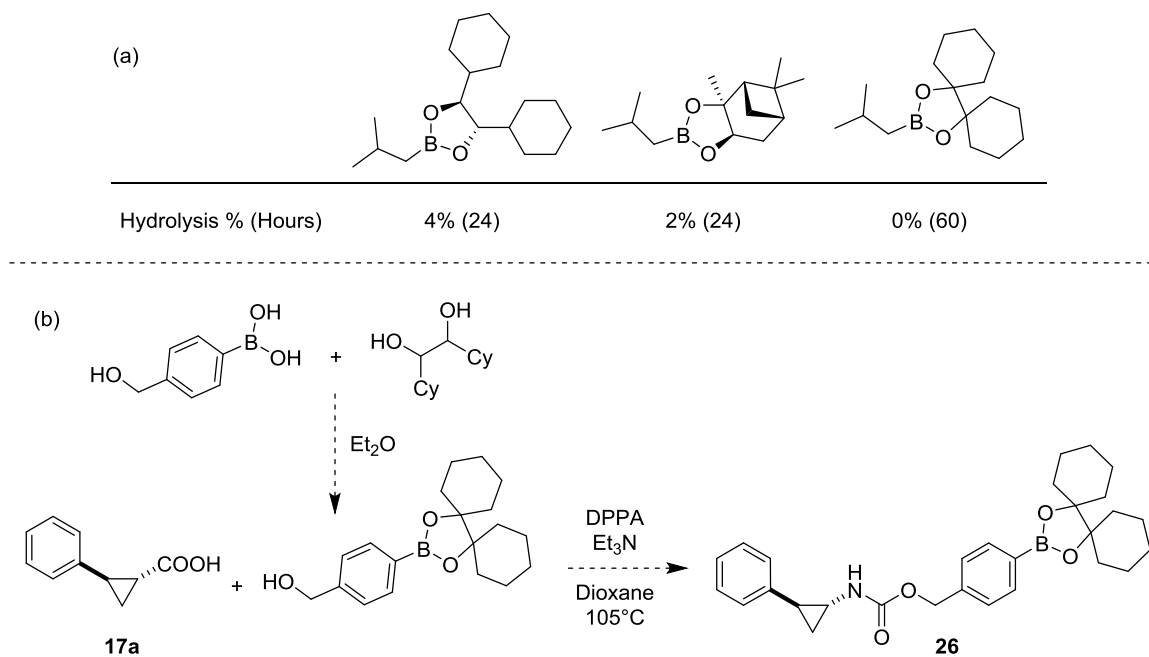
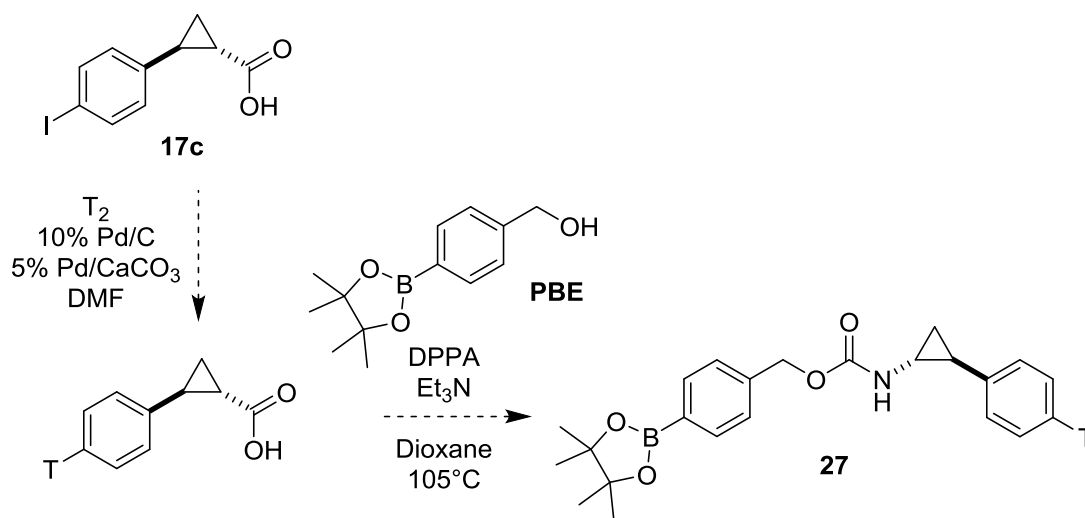


Figure 24: (a) Introduction of steric hindrance around the diol moiety in boronic esters was found to minimise hydrolysis.¹¹⁸ (b) Proposed preparation of hydrolytic stable analogue of Q-PAC (**26**).

Since Q-PAC demonstrated promising results in primary GBM cultures, the study should be preceded with in vitro studies. Radioiodination of the prodrug enable the study of biodistribution and metabolic stability in animal models. However preliminary results from this chapter suggest that the prodrug was unstable in the radioiodination conditions, therefore other radiolabelling methods should be considered. For example, tritium is another commonly used radioisotope in drug discovery.¹²¹ The tritium labelling of Q-PAC can be completed in two steps: Pd-catalysed iodine exchange of carboxylic acid precursor **17c** follow by the Curtius rearrangement with PBE (Scheme 12). The boronate

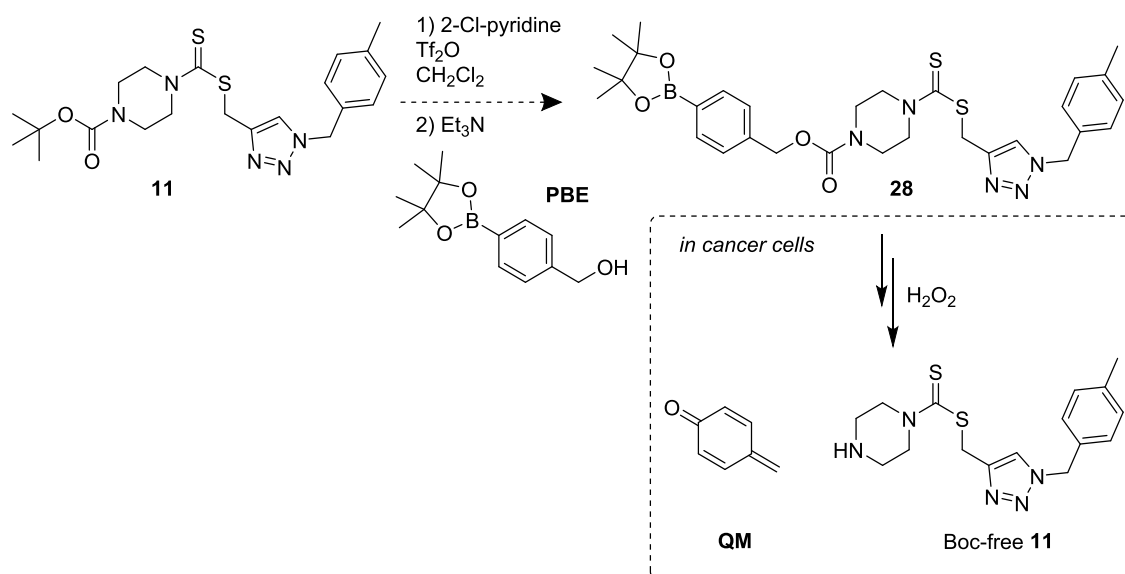
functionality is unlikely to be affected from the radiolabelling by introducing the tritium label before the aryl boronate. Moreover, due to the similar size of hydrogen atom and tritium, the tritium-labelled Q-PAC **27** is expected to have similar anticancer effect compared to Q-PAC but better than Q-4IAC.



Scheme 12: Proposed preparation of tritium-labelled Q-PAC.

In parallel to the prodrug study, reported LSD1 inhibitor **11** was found to induce caspase-dependent apoptosis in primary GBM RN1 cells, therefore reducing cell confluence, migration and viability. Encouraged by the promising results exhibited by LSD1 inhibitor **11**, and to enhance the LSD1 inhibitory action of prodrug, we proposed to replace the 2-PCPA moiety of Q-PAC with **11**. The designated prodrug **28** can be easily prepared from the coupling of **11** and PBE in one-pot (Scheme 13).¹²² In cancer cells where higher ROS concentration is present, prodrug **28** is proposed to release QM and a Boc-free analogue of inhibitor **11**. According to the literature, the Boc-free analogue of **11** was still able to inhibit LSD1, however its inhibitory activity was poorer than **11** (IC₅₀ for **11**: 2.1 μM; IC₅₀ for Boc-free **11**: 28.9 μM).⁹⁰ Nevertheless, based on available SAR information from the literature, the functionalisation of carbamate moiety in **11** is the most practical approach to prepare dual-action prodrug without completely diminishing

the LSD1 inhibitor property.⁹⁰ Furthermore, due to the structural homology between **11** and its Boc-free counterpart, the selectivity towards LSD1 over MAOs could be retained in the latter. Besides, the presence of GSH-scavenging QM might be able to compensate the reduction in LSD1 inhibitory activity.



Scheme 13: Proposed preparation of prodrug **28** which will liberate QM and a Boc-free analogue of **11** in cancer cells.

2.5 Experimental

All organic syntheses and molecule characterisation were performed by Y. S. Gee. Mass spectrometry experiments were conducted by Y. S. Gee and Dr A. Maccarone (University of Wollongong). In vitro assays were performed by Dr M. Engel and D. Cross (Illawarra Health & Medical Research Institute). The log BB value of prodrug Q-PAC was calculated by Dr H. Yu (University of Wollongong). Radioiodination and HPLC analysis of prodrug Q-4IAC were conducted by Dr I. Greguric (Australian Nuclear Science and Technology Organisation).

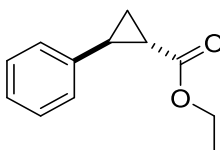
2.5.1 General experimental details for organic syntheses

Unless stated specifically, all chemicals were purchased from commercial suppliers and used without purification. All reactions were conducted in oven-dried glassware under nitrogen atmosphere. Reaction solvents were dried by passing through a column of activated alumina and then stored over 4Å molecular sieves. Progress of reactions was tracked by TLC and was performed on aluminium backed silica gel sheets (Grace Davison, UV254). TLC plates were visualised under UV lamp at 254 nm and/or by treatment with one of the following TLC stains: Phosphomolybdic acid (PMA) stain: PMA (10 g), absolute EtOH (100 mL); Potassium permanganate stain: KMnO_4 (1.5 g), 10% NaOH (1.25 mL), water (200 mL); Vanillin stain: Vanillin (15 g), concentrated H_2SO_4 (2.5 mL), EtOH (250 mL). For NMR spectroscopy analytes were dissolved in deuterated chloroform or stated otherwise. NMR spectra for each compound were collected from one of the following instrument: Mercury 2000 spectrometer operates at 500 and 125 MHz for ^1H and ^{13}C NMR respectively; Bruker spectrometer operates at 400, 100 and 470 MHz for ^1H , ^{13}C and ^{19}F NMR respectively; Varian spectrometer operates at 300 and 75 MHz for ^1H and ^{13}C NMR respectively. NMR data are expressed in parts per million (ppm) and referenced to the solvent (7.26 ppm for ^1H NMR and 77.16 ppm for ^{13}C NMR). The following abbreviations are used to assign the multiplicity of the ^1H NMR signal: s = singlet; bs = broad singlet; d = doublet; t = triplet; q = quartet; quin = quintet; dd = doublet of doublets; m = multiplet. NMR assignments were made on the basis of HMBC, HSQC, COSY and DEPT experiments. For mass spectrometry analytes were dissolved in HPLC grade methanol or dichloromethane. High-resolution mass spectra were collected from a Waters Xevo G1 QTOF mass spectrophotometer (ESI or ASAP) or Thermo Scientific LTQ Orbitrap XL (ESI). Infrared spectra were obtained from

a Shimadzu IRAffinity-1 Fourier transform infrared spectrophotometer with ATR attachment. Melting point measurements were taken on a Buchi M-560.

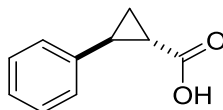
2.5.2 Preparation of Q-PAC and its precursors

Ethyl 2-phenylcyclopropane-1-carboxylate (16a)



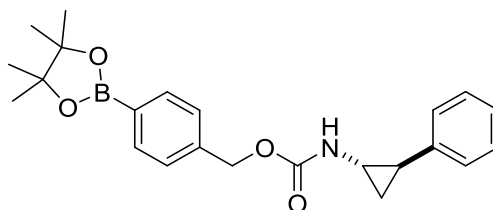
A suspension of trimethylsulfoxonium iodide (3.75 g, 17.0 mmol, 1.2 equiv) and sodium hydride (60% in mineral oil, 685 mg, 17.1 mmol, 1.2 equiv) in anhydrous DMSO (14 mL) were stirred for 1 h before the addition of ethyl cinnamate (2.40 mL, 2.52 g, 14.3 mmol, 1 equiv). After the reaction was heated at 60 °C overnight, the reaction solution was poured into brine solution (50 mL) and extracted with ethyl acetate (4 × 30 mL). The combined organic extracts were washed with water (50 mL) and brine solution (50 mL). After drying the solution with magnesium sulfate, the solution was concentrated under reduced pressure to give a pale yellow oil crude which was later subjected to column chromatography (10% ethyl acetate/hexane). The title compound was collected as a pale yellow oil (1.01 g, 5.30 mmol) in 37% yield. ¹H NMR (500 MHz, CDCl₃): δ 7.29 – 7.26 (m, 2H, CH_{Ar}), 7.21 – 7.18 (m, 1H, CH_{Ar}), 7.10 (d, *J* = 7 Hz, 2H, CH_{Ar}), 4.17 (q, *J* = 7 Hz, 2H, OCH₂), 2.53 – 2.50 (m, 1H, CH-Ar), 1.90 (ddd, *J* = 8.7, 4.5, 4.5 Hz, 1H, CH-COOEt), 1.59 (ddd, *J* = 9.4, 4.8, 5.0 Hz, 1H, CH₂-CH-Ar), 1.33 – 1.26 (m, 4H, CH₂-CH-Ar and OCH₂CH₃) ppm. ¹³C NMR (125 MHz, CDCl₃): δ 173.4 (C=O), 140.1 (C_{Ar}), 128.5 (CH_{Ar}), 126.5 (CH_{Ar}), 126.2 (CH_{Ar}), 60.7 (OCH₂), 26.2 (CH-Ar), 24.2 (CH-COOEt), 17.1 (CH₂-CH-Ar), 14.3 (CH₃) ppm. NMR data consistent with literature.^{123,124}

2-Phenylcyclopropane-1-carboxylic acid (17a)



1 M Sodium hydroxide solution (3.2 mL, 3.2 mmol, 2 equiv) was added to a solution of **16a** (304 mg, 1.60 mmol, 1 equiv) in ethanol (6 mL). The reaction was left stirring at room temperature for 24 h and then quenched with 2 M hydrochloric acid (2.4 mL, 4.8 mmol, 3 equiv) and water (5.43 mL) at 0 °C. The solution was stirred for 5 min before extraction with ethyl acetate (4 × 15 mL). Combined organic fractions were washed with water (10 mL) then brine (10 mL). The organic extracts were dried with magnesium sulfate and the solvent evaporated under reduced pressure to yield the product as a white solid that required no further purification (251 mg, 1.55 mmol) in 97% yield. **¹H NMR** (500 MHz, CDCl₃): δ 7.30 – 7.27 (m, 2H, CH_{Ar}), 7.23 – 7.20 (m, 1H, CH_{Ar}), 7.11 (d, *J* = 8 Hz, 2H, CH_{Ar}), 2.62 – 2.58 (m, 1H, CH-Ar), 1.91 (ddd, *J* = 8.4, 4.5, 4.5 Hz, 1H, CH-COOH), 1.66 (ddd, *J* = 9.2, 4.8, 5.0 Hz, 1H, CH₂), 1.43 – 1.39 (m, 1H, CH₂) ppm. **¹³C NMR** (125 MHz, CDCl₃): δ 179.8 (C=O), 139.5 (C_{Ar}), 128.6 (CH_{Ar}), 126.7 (CH_{Ar}), 126.3 (CH_{Ar}), 27.1 (CH-Ar), 24.0 (CH-COOH), 17.5 (CH₂) ppm. **Melting point:** 82.9 – 84.9 °C. NMR data consistent with literature.¹²⁵

4-(4,4,5,5-Tetramethyl-1,3,2-dioxaborolan-2-yl)benzyl (2-phenylcyclopropyl)carbamate
(Q-PAC)

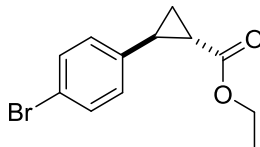


Triethylamine (0.400 mL, 0.290 g, 2.87 mmol, 1.2 equiv) and diphenylphosphoryl azide (0.580 mL, 742 mg, 2.70 mmol, 1.1 equiv) were added to a solution of **17a** (0.400 g, 2.46 mmol, 1 equiv) and 4-(hydroxymethyl)phenylboronic acid pinacol ester (638 mg, 2.72 mmol, 1.1 equiv) in dry dioxane (5 mL). The reaction solution was heated at 105 °C for 4 h then cooled to room temperature. Solvent was evaporated under reduced pressure and the compound was purified by column chromatography (25% ethyl acetate/hexane). The title compound was obtained as a colourless oil (514 mg, 1.31 mmol) in 53% yield. **¹H NMR** (500 MHz, CDCl₃): δ 7.79 (d, *J* = 7.5 Hz, 2H, CH_{Ar-B(OR)₂}), 7.33 (d, *J* = 7.5 Hz, 2H, CH_{Ar-B(OR)₂}), 7.25 – 7.23 (m, 2H, CH_{Ar}), 7.17 – 7.09 (m, 3H, CH_{Ar}), 5.23 (bs, 1H, NH), 5.12 (s, 2H, OCH₂), 2.75 (bs, 1H, CH-NH), 2.06 (bs, 1H, CH-Ar), 1.33 (s, 12H, CH₃), 1.18 (bs, 2H, CH₂-CHNH) ppm. **¹³C NMR** (75 MHz, CDCl₃)^a: δ 156.8 (C=O), 140.5 (C_{Ar}), 139.5 (C_{Ar-B(OR)₂}), 135.1 (CH_{Ar-B(OR)₂}), 128.4 (CH_{Ar}), 127.2 (CH_{Ar-B(OR)₂}), 126.6 (CH_{Ar}), 126.2 (CH_{Ar}), 83.9 (C-Me₂), 66.7 (OCH₂), 32.7 (CH-NH), 24.9 (CH₃ and CH-Ar), 16.2 (CH₂-CHNH) ppm. **IR** (Neat): 3318, 2977, 1706 cm⁻¹. **HRMS** (ESI) *m/z*: [M]⁺ Calcd for C₂₃H₂₈BNO₄ 393.2111; Found 393.2102.

^a The carbon directly attached to boron was not detected, this is probably due to quadropolar relaxation.¹²⁶

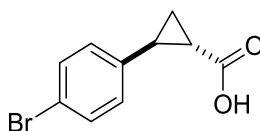
2.5.3 Preparation of Q-BrAC and its precursors

Ethyl 2-(p-bromophenyl)cyclopropane-1-carboxylate (16b)



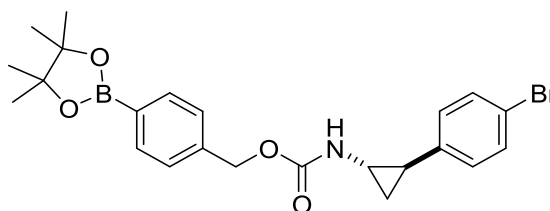
A suspension of trimethylsulfoxonium iodide (3.61 g, 16.4 mmol, 1.2 equiv) and sodium hydride (60% in mineral oil, 664 mg, 16.6 mmol, 1.2 equiv) in anhydrous DMSO (12 mL) were stirred for 1 h before the addition of ethyl (*E*)-3-(*p*-bromophenyl)-2-propenoate (3.48 g, 13.6 mmol, 1 equiv) in anhydrous DMSO (12 mL). After the reaction was heated at 60 °C for 36 h, the reaction solution was poured into brine solution (50 mL) and extracted with ethyl acetate (4 × 30 mL). The combined organic extracts were washed with water (50 mL) and brine solution (50 mL). After drying the solution with magnesium sulfate, the solution was concentrated under reduced pressure to give a brown oil crude which was later subjected to column chromatography (10% ethyl acetate/hexane). The title compound was collected as a colourless oil (1.52 g, 5.64 mmol) in 41% yield. **¹H NMR** (500 MHz, CDCl₃): δ 7.39 (d, *J* = 8 Hz, 2H, CH_{Ar}), 6.97 (d, *J* = 8 Hz, 2H, CH_{Ar}), 4.17 (q, *J* = 7 Hz, 2H, OCH₂), 2.49 – 2.45 (m, 1H, CH-Ar), 1.86 (ddd, *J* = 8.4, 4.5, 4.5 Hz, 1H, CH-COOEt), 1.60 (ddd, *J* = 9.3, 4.8, 5 Hz, 1H, CH₂-CH-Ar), 1.29 – 1.25 (m, 4H, CH₂-CH-Ar and CH₃) ppm. **HRMS** (ASAP) *m/z*: [M + H]⁺ Calcd for C₁₂H₁₄O₂Br 269.0177; Found 269.0164. ¹H NMR data are consistent with literature.¹²⁷

2-(p-Bromophenyl)cyclopropane-1-carboxylic acid (17b)



Sodium hydroxide solution (1 M, 6.9 mL, 6.9 mmol, 2 equiv) was added to a solution of **16b** (922 mg, 3.43 mmol, 1 equiv) in ethanol (12 mL). After the solution was left stirring overnight at room temperature, hydrochloric acid solution (2 M, 5.20 mL, 10.4 mmol, 3 equiv) and water (5 mL) were added to the reaction solution at 0 °C. The solution was extracted with ethyl acetate (3 × 30 mL) and washed with brine solution (2 × 30 mL). After drying the solution with magnesium sulfate, the solution was concentrated under reduced pressure to give the title compound as a white solid (823 mg, 3.41 mmol) in 100% yield. **¹H NMR** (500 MHz, CDCl₃): δ 7.41 (d, *J* = 8.5 Hz, 2H, CH_{Ar}), 6.98 (d, *J* = 8 Hz, 2H, CH_{Ar}), 2.57 – 2.53 (m, 1H, CH-Ar), 1.88 (ddd, *J* = 8.2, 4.2, 4.0 Hz, 1H, CH-COOH), 1.66 (ddd, *J* = 9.2, 4.8, 5.0 Hz, 1H, CH₂), 1.39 – 1.35 (m, 1H, CH₂) ppm. **¹³C NMR** (75 MHz, CDCl₃): δ 179.3 (C=O), 138.8 (C_{Ar}), 131.7 (CH_{Ar}), 128.2 (CH_{Ar}), 120.5 (C_{Ar}), 26.5 (CH-Ar), 24.2 (CH-COOH), 17.5 (CH₂) ppm. **IR** (Neat): 2923, 1681 cm⁻¹. **HRMS** (ASAP) *m/z*: [M + H]⁺ Calcd for C₁₀H₁₀O₂Br 240.9864; Found 240.9865. **Melting point** : 118.5 – 122.4 °C.

4-(4,4,5,5-Tetramethyl-1,3,2-dioxaborolan-2-yl)benzyl (2-(*p*-
bromophenyl)cyclopropyl)carbamate (*Q-BrAC*)



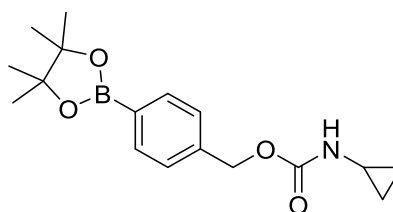
Triethylamine (0.380 mL, 276 mg, 2.73 mmol, 1.1 equiv) and diphenylphosphoryl azide (0.590 mL, 755 mg, 2.74 mmol, 1.1 equiv) were added to a solution of **17b** (0.600 g, 2.49 mmol, 1 equiv) and 4-(hydroxymethyl)phenylboronic acid pinacol ester (641 mg, 2.74

mmol, 1.1 equiv) in anhydrous dioxane (5 mL). The reaction solution was heated at 105 °C for 2.5 h before it was concentrated under reduced pressure. After purification using column chromatography (25% ethyl acetate/hexane), the title compound was obtained as white powder (498 mg, 1.05 mmol) in 42% yield. **¹H NMR** (500 MHz, CDCl₃): δ 7.79 (d, *J* = 7.5 Hz, 2H, CH_{Ar-B(OR)₂}), 7.33 (d, *J* = 7.5 Hz, 4H, CH_{Ar-B(OR)₂} and CH_{Ar}), 7.02 – 6.84 (m, 2H, CH_{Ar}), 5.12 (bs, 3H, OCH₂ and NH), 2.70 (bs, 1H, CH-NH), 2.04 (bs, 1H, CH-Ar), 1.34 (s, 12H, CH₃), 1.16 (bs, 2H, CH₂-CH-NH) ppm. **¹³C NMR** (125 MHz, CDCl₃)^a: δ 156.6 (C=O), 139.4 (C_{Ar}), 139.3 (C_{Ar}), 135.0 (CH_{Ar-B(OR)₂}), 131.3 (CH_{Ar}), 128.4 (CH_{Ar}), 127.2 (CH_{Ar-B(OR)₂}), 119.8 (C_{Ar}), 83.9 (C-Me₂), 66.6 (OCH₂), 32.6 (CH-NH), 24.8 (CH₃ and CH-Ar), 15.9 (CH₂-CH-NH) ppm. **IR** (Neat): 3314, 2978, 1710 cm⁻¹. **HRMS** (ESI) *m/z*: [M + Na]⁺ Calcd for C₂₃H₂₇BBrNO₄Na 494.11142; Found 494.11037. **Melting point**: 117.3 – 122.9 °C.

^a The carbon directly attached to boron was not detected, this is probably due to quadropolar relaxation.¹²⁶

2.5.4 Preparation of QAC

4-(4,4,5,5-Tetramethyl-1,3,2-dioxaborolan-2-yl)benzyl cyclopropylcarbamate (QAC)



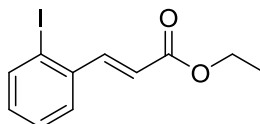
Cyclopropanecarboxylic acid (0.190 mL, 205 mg, 2.39 mmol, 1 equiv), triethylamine (0.360 mL, 261 mg, 2.58 mmol, 1.1 equiv) and diphenylphosphoryl azide (0.550 mL, 702 mg, 2.55 mmol, 1.1 equiv) were added to a solution of 4-(hydroxymethyl)phenylboronic

acid pinacol ester (599 mg, 2.56 mmol, 1.1 equiv) in anhydrous dioxane (4.5 mL). After the solution was left stirring at 105 °C overnight, it was concentrated under reduced pressure and the crude mixture was subjected to column chromatography (30% ethyl acetate in petroleum spirit). The title compound was obtained as a white solid (266 mg, 0.838 mmol) in 35% yield. **¹H NMR** (500 MHz, CDCl₃): δ 7.79 (d, *J* = 7.5 Hz, 2H, CH_{Ar}), 7.34 (d, *J* = 7 Hz, 2H, CH_{Ar}), 5.11 (s, 2H, OCH₂), 4.99 (bs, 1H, NH), 2.60 (bs, 1H, CH-NH), 1.34 (s, 12H, CH₃), 0.71 (d, *J* = 6 Hz, 2H, CH₂), 0.52 (bs, 2H, CH₂) ppm. **¹³C NMR** (125 MHz, CDCl₃)^a: δ 157.0 (C=O), 139.6 (C_{Ar}), 135.0 (CH_{Ar}), 127.1 (CH_{Ar}), 83.8 (C-Me₂), 66.5 (OCH₂), 24.9 (CH₃), 23.2 (CH-NH), 6.9 (CH₂-CH-NH) ppm. **IR** (Neat): 3362, 2980, 1726 cm⁻¹. **HRMS** (ESI) *m/z*: [M + Na]⁺ Calcd for C₁₇H₂₄NO₄BNa 340.16961; Found 340.16915. **Melting point**: 96.7 – 97.2 °C.

^a The carbon directly attached to boron was not detected, this is probably due to quadropolar relaxation.¹²⁶

2.5.5 Preparation of Q-2IAC and its precursors

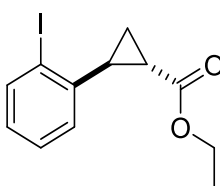
Ethyl (E)-3-(2-iodophenyl)acrylate



Triethyl phosphonoacetate (0.750 mL, 848 mg, 3.78 mmol, 1.1 equiv) was slowly added to a suspension of NaH (60% in mineral oil, 217 mg, 5.42 mmol, 1.6 equiv) in anhydrous THF (34 mL). The suspension was stirred for 10 mins before the addition of 2-iodobenzaldehyde (802 mg, 3.46 mmol, 1 equiv). After the reaction solution was stirred overnight at room temperature, the reaction was quenched with solid ammonium chloride

and 1 M HCl (10 mL) then diluted with ethyl acetate (10 mL) and water (10 mL). The aqueous fraction was isolated and extracted with ethyl acetate (2 × 10 mL) and the combined organic fractions were washed with saturated NaHCO₃ solution (20 mL) then brine (20 mL). The solution was then dried with magnesium sulfate and concentrated under reduced pressure. The crude product was purified with column chromatography (5% ethyl acetate/hexane) to give the title compound as a pale yellow oil (653 mg, 2.16 mmol) in 63% yield. **¹H NMR** (500 MHz, CDCl₃): δ 7.91 – 7.88 (m, 2H, HC=CH-COOEt and CH_{Ar}), 7.56 (d, *J* = 7.5 Hz, 1H, CH_{Ar}), 7.36 (t, *J* = 7.5 Hz, 1H, CH_{Ar}), 7.05 (t, *J* = 7.5 Hz, 1H, CH_{Ar}), 6.31 (d, *J* = 15.5 Hz, 1H, HC=CH-COOEt), 4.29 (q, *J* = 7 Hz, 2H, OCH₂), 1.35 (t, *J* = 7.5 Hz, 3H, CH₃) ppm. **¹³C NMR** (125 MHz, CDCl₃): δ 166.3 (C=O), 147.7 (HC=CH-COOEt), 140.0 (CH_{Ar}), 137.9 (C_{Ar}), 131.1 (CH_{Ar}), 128.5 (CH_{Ar}), 127.4 (CH_{Ar}), 121.3 (HC=CH-COOEt), 101.1 (C_{Ar}), 60.7 (OCH₂), 14.3 (CH₃) ppm. **IR** (Neat): 1707 cm⁻¹. **HRMS** (ASAP) *m/z*: [M + H]⁺ Calcd for C₁₁H₁₂IO₂ 302.9882; Found 302.9881.

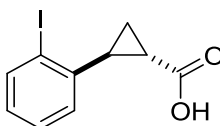
Ethyl 2-(2-iodophenyl)cyclopropane-1-carboxylate



A suspension of trimethylsulfoxonium iodide (610 mg, 2.77 mmol, 1.4 equiv) and sodium hydride (60% in mineral oil, 115 mg, 2.88 mmol, 1.5 equiv) in anhydrous DMSO (3 mL) were stirred for 30 mins before the addition of ethyl (*E*)-3-(2-iodophenyl)acrylate (597 mg, 1.97 mmol, 1 equiv) in anhydrous DMSO (2 mL). After the reaction was heated at 60 °C overnight, the reaction solution was poured into brine solution (25 mL) and extracted with ethyl acetate (3 × 15 mL). The combined organic extracts were washed

with water (50 mL) and brine solution (50 mL). After drying the solution with magnesium sulfate, the solution was concentrated under reduced pressure to give a brown oil crude which was later subjected to column chromatography (5% ethyl acetate/hexane). The title compound was collected as a colourless oil (116 mg, 368 μmol) in 19% yield. **$^1\text{H NMR}$** (500 MHz, CDCl_3): δ 7.85 (d, $J = 8$ Hz, 1H, CH_{Ar}), 7.26 (t, $J = 9$ Hz, 1H, CH_{Ar}), 7.00 (d, $J = 7.5$ Hz, 1H, CH_{Ar}), 6.93 (t, $J = 7.5$ Hz, 1H, CH_{Ar}), 4.27 – 4.17 (m, 2H, OCH_2), 2.62 – 2.58 (m, 1H, CH-Ar), 1.78 – 1.73 (m, 1H, CH-COOEt), 1.63 (ddd, $J = 9.2, 4.8, 5.0$ Hz, 1H, $\text{CH}_2\text{-CH-Ar}$), 1.34 – 1.29 (m, 4H, $\text{CH}_2\text{-CH-Ar}$ and CH_3) ppm. **$^{13}\text{C NMR}$** (125 MHz, CDCl_3): δ 173.2 (C=O), 142.2 (C_{Ar}), 139.2 (CH_{Ar}), 128.4 (CH_{Ar}), 128.2 (CH_{Ar}), 127.4 (CH_{Ar}), 102.6 (C_{Ar}), 60.7 (OCH_2), 31.8 (CH-Ar), 23.7 (CH-COOEt), 16.2 ($\text{CH}_2\text{-CH-Ar}$), 14.4 (CH_3) ppm. **IR** (Neat): 1719 cm^{-1} . **HRMS** (ASAP) m/z : $[\text{M} + \text{H}]^+$ Calcd for $\text{C}_{12}\text{H}_{14}\text{IO}_2$ 317.0039; Found 317.0027.

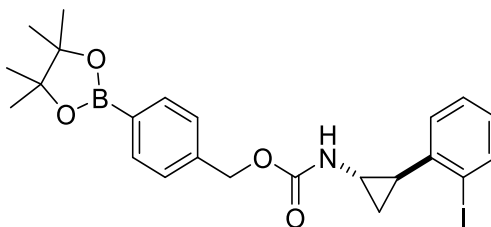
2-(2-Iodophenyl)cyclopropane-1-carboxylic acid



Sodium hydroxide solution (1 M, 0.64 mL, 0.64 mmol, 2 equiv) was added to a solution of ethyl 2-(2-iodophenyl)cyclopropane-1-carboxylate (101 mg, 0.320 mmol, 1 equiv) in ethanol (5 mL). After the solution was left stirring overnight at room temperature, hydrochloric acid solution (2 M, 0.48 mL, 0.96 mmol, 3 equiv) and water (10 mL) were added to the reaction solution at 0 $^{\circ}\text{C}$. The solution was extracted with diethyl ether (3 \times 20 mL) and washed with brine solution (30 mL). After drying the solution with magnesium sulfate, the solution was concentrated under reduced pressure to give the title

compound as a white solid (81.0 mg, 0.280 mmol) in 88% yield. **¹H NMR** (500 MHz, CDCl₃): δ 7.84 (d, *J* = 8 Hz, 1H, CH_{Ar}), 7.27 (d, *J* = 7.5 Hz, 1H, CH_{Ar}), 7.01 (d, *J* = 7.5 Hz, 1H, CH_{Ar}), 6.94 (td, *J* = 7.5, 1.0 Hz, 1H, CH_{Ar}), 2.71 – 2.67 (m, 1H, CH-Ar), 1.78 – 1.77 (m, 1H, CH-COOH), 1.71 (ddd, *J* = 9.2, 4.7, 5.0 Hz, 1H, CH₂), 1.43 – 1.39 (m, 1H, CH₂) ppm. **¹³C NMR** (125 MHz, CDCl₃): δ 179.9 (C=O), 141.8 (C_{Ar}), 139.3 (CH_{Ar}), 128.7 (CH_{Ar}), 128.3 (CH_{Ar}), 127.7 (CH_{Ar}), 102.8 (C_{Ar}), 32.7 (CH-Ar), 23.7 (CH-COOH), 17.2 (CH₂) ppm. **IR** (Neat): 1685 cm⁻¹. **HRMS** (ESI) *m/z*: [M - H]⁻ Calcd for C₁₀H₈IO₂ 286.9569; Found 286.9577. **Melting point**: 97.8 – 104.4 °C.

4-(4,4,5,5-Tetramethyl-1,3,2-dioxaborolan-2-yl)benzyl (2-(2-iodophenyl)cyclopropyl)carbamate (Q-2IAC)

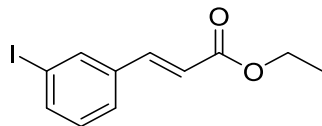


Triethylamine (0.100 mL, 72.6 mg, 0.717 mmol, 2.8 equiv) and diphenylphosphoryl azide (0.100 mL, 128 mg, 0.464 mmol, 1.8 equiv) were added to a solution of 2-(2-iodophenyl)cyclopropane-1-carboxylic acid (74.0 mg, 0.257 mmol, 1 equiv) and 4-(hydroxymethyl)phenylboronic acid pinacol ester (69.3 mg, 0.296 mmol, 1.2 equiv) in dry dioxane (1 mL). The reaction solution was heated at 105 °C for 2 h 15 mins then cooled to room temperature. Solvent was evaporated under reduced pressure and the compound was purified by column chromatography (25% ethyl acetate/hexane). The title compound was obtained as a colourless oil (36.2 mg, 69.7 μmol) in 27% yield. **¹H NMR** (500 MHz, CDCl₃): δ 7.81 (app t, *J* = 7.5 Hz, 3H, CH_{Ar}), 7.36 (d, *J* = 8.0 Hz, 2H, CH_{Ar}),

7.26 (bs, 1H, CH_{Ar}), 7.08 (bs, 1H, CH_{Ar}), 6.91 (t, *J* = 7.5 Hz, 1H, CH_{Ar}), 5.36 (bs, 1H, NH), 5.14 (s, 2H, OCH₂), 2.71 (d, *J* = 2.5 Hz, 1H, CHNH), 2.13 – 2.09 (m, 1H, CH-Ar), 1.34 (s, 12H, CH₃), 1.26 – 1.21 (m, 2H, CH₂-CH-NH) ppm. ¹³C NMR (125 MHz, CDCl₃): δ 156.7 (C=O), 142.3 (C_{Ar}), 139.3 (C_{Ar}), 138.9 (CH_{Ar}), 135.0 (CH_{Ar}), 128.3 (CH_{Ar}), 128.2 (CH_{Ar}), 128.0 (CH_{Ar}), 127.2 (CH_{Ar}), 102.5 (C_{Ar}), 83.8 (C-Me₂), 66.7 (OCH₂), 32.5 (CH-NH), 30.5 (CH-Ar), 24.8 (CH₃), 16.4 (CH₂-CH-NH) ppm. IR (Neat): 3317, 2976, 2923, 1700 cm⁻¹. HRMS (ESI) *m/z*: [M + Na]⁺ Calcd for C₂₃H₂₇BINO₄Na 542.09755; Found 542.09612.

2.5.6 Preparation of Q-3IAC and its precursors

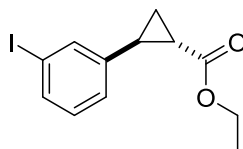
Ethyl (E)-3-(3-iodophenyl)acrylate



Triethyl phosphonoacetate (0.580 mL, 655 mg, 2.92 mmol, 0.8 equiv) was slowly added to a suspension of NaH (60% in mineral oil, 163 mg, 4.07 mmol, 1.2 equiv) in anhydrous THF (26 mL). The suspension was stirred for 10 mins before the addition of 3-iodobenzaldehyde (804 mg, 3.46 mmol, 1 equiv). After the reaction solution was stirred for 1 h at room temperature, the reaction was quenched with solid ammonium chloride then 1 M HCl (10 mL) and water (10 mL). The aqueous fraction was isolated and extracted with ethyl acetate (2 × 10 mL) and the combined organic fractions were washed with saturated NaHCO₃ solution (20 mL) then brine (20 mL). The solution was then dried with magnesium sulfate and concentrated under reduced pressure to give a crude yellow oil. ¹H NMR spectrum of the crude yellow oil indicated that starting material was still present therefore it was further treated with a solution of triethyl phosphonoacetate (0.230

mL, 260 mg, 1.16 mmol, 0.3 equiv) and NaH (60% in mineral oil, 79.5 mg, 1.99 mmol, 0.6 equiv) in THF following the procedure above. The crude product was purified with column chromatography (5% ethyl acetate/hexane) to give the title compound as a pale yellow oil (666 mg, 2.20 mmol) in 64% yield. **¹H NMR** (500 MHz, CDCl₃): δ 7.88 (d, *J* = 1.5 Hz, 1H, CH_{Ar}), 7.70 (d, *J* = 7.5 Hz, 1H, CH_{Ar}), 7.57 (d, *J* = 16 Hz, 1H, HC=CH-COOEt), 7.47 (d, *J* = 7.5 Hz, 1H, CH_{Ar}), 7.12 (t, *J* = 7.5 Hz, 1H, CH_{Ar}), 6.42 (d, *J* = 16 Hz, 1H, HC=CH-COOEt), 4.27 (q, *J* = 7 Hz, 2H, OCH₂), 1.34 (t, *J* = 7.5 Hz, 3H, CH₃) ppm. **¹³C NMR** (125 MHz, CDCl₃): δ 166.5 (C=O), 142.7 (HC=CH-COOEt), 138.9 (CH_{Ar}), 136.7 (CH_{Ar}), 136.6 (C_{Ar}), 130.5 (CH_{Ar}), 127.2 (CH_{Ar}), 119.6 (HC=CH-COOEt), 94.7 (C_{Ar}), 60.7 (OCH₂), 14.3 (CH₃) ppm. **IR** (Neat): 3059, 1707 cm⁻¹. **HRMS** (ASAP) *m/z*: [M + H]⁺ Calcd for C₁₁H₁₂IO₂ 302.9882; Found 302.9879.

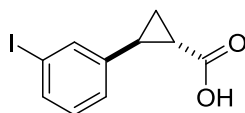
Ethyl 2-(3-iodophenyl)cyclopropane-1-carboxylate



A suspension of trimethylsulfoxonium iodide (577 mg, 2.62 mmol, 1.4 equiv) and sodium hydride (60% in mineral oil, 0.110 g, 2.76 mmol, 1.5 equiv) in anhydrous DMSO (4 mL) were stirred for 45 mins before the addition of ethyl (*E*)-3-(3-iodophenyl)acrylate (559 mg, 1.85 mmol, 1 equiv). After the reaction was heated at 60 °C overnight, the reaction solution was poured into brine solution (20 mL) and extracted with ethyl acetate (3 × 15 mL). The combined organic extracts were washed with water (50 mL) and brine solution (50 mL). After drying the solution with magnesium sulfate, the solution was concentrated under reduced pressure to give a light brown film crude which was later subjected to

column chromatography (5% ethyl acetate/hexane). The title compound was collected as a colourless oil (91.9 mg, 291 μmol) in 16% yield. **$^1\text{H NMR}$** (500 MHz, CDCl_3): δ 7.53 (d, $J = 7.5$ Hz, 1H, CH_{Ar}), 7.45 (s, 1H, CH_{Ar}), 7.06 (d, $J = 7.5$ Hz, 1H, CH_{Ar}), 7.00 (t, $J = 8$ Hz, 1H, CH_{Ar}), 4.17 (q, $J = 7$ Hz, 2H, OCH_2), 2.47 – 2.43 (m, 1H, CH-Ar), 1.88 (ddd, $J = 8.3, 4.2, 4.5$ Hz, 1H, CH-COOEt), 1.61 – 1.57 (m, 1H, $\text{CH}_2\text{-CH-Ar}$), 1.28 (t, $J = 7$ Hz, 4H, $\text{CH}_2\text{-CH-Ar}$ and CH_3) ppm. **$^{13}\text{C NMR}$** (125 MHz, CDCl_3): δ 173.0 (C=O), 142.6 (C_{Ar}), 135.6 (CH_{Ar}), 135.3 (CH_{Ar}), 130.1 (CH_{Ar}), 125.6 (CH_{Ar}), 94.4 (C_{Ar}), 60.8 (OCH_2), 25.4 (CH-Ar), 24.1 (CH-COOEt), 16.9 ($\text{CH}_2\text{-CH-Ar}$), 14.3 (CH_3) ppm. **IR** (Neat): 1718 cm^{-1} . **HRMS** (ASAP) m/z : $[\text{M} + \text{H}]^+$ Calcd for $\text{C}_{12}\text{H}_{14}\text{IO}_2$ 317.0039; Found 317.0025.

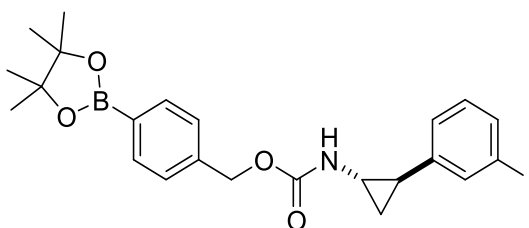
2-(3-Iodophenyl)cyclopropane-1-carboxylic acid



Sodium hydroxide solution (1 M, 0.48 mL, 0.48 mmol, 2 equiv) was added to a solution of ethyl 2-(3-iodophenyl)cyclopropane-1-carboxylate (75.5 mg, 0.240 mmol, 1 equiv) in ethanol (4 mL). After the solution was left stirring overnight at room temperature, hydrochloric acid solution (2 M, 0.36 mL, 0.72 mmol, 3 equiv) and water (10 mL) were added to the reaction solution at 0 °C. The solution was extracted with diethyl ether (3 \times 20 mL) and washed with brine solution (30 mL). After drying the solution with magnesium sulfate, the solution was concentrated under reduced pressure to give the title compound as a white solid (66.6 mg, 0.231 mmol) in 96% yield. **$^1\text{H NMR}$** (500 MHz, CDCl_3): δ 7.54 (d, $J = 8$ Hz, 1H, CH_{Ar}), 7.46 (s, 1H, CH_{Ar}), 7.06 (d, $J = 7.5$ Hz, 1H, CH_{Ar}), 7.01 (t, $J = 7.5$ Hz, 1H, CH_{Ar}), 2.53 (bs, 1H, CH-Ar), 1.89 (bs, 1H, CH-COOH), 1.65 – 1.65 (m, 1H, CH_2), 1.37 (bs, 1H, CH_2) ppm. **$^{13}\text{C NMR}$** (125 MHz, CDCl_3): δ 179.5

(C=O), 141.9 (C_{Ar}), 135.8 (CH_{Ar}), 135.4 (CH_{Ar}), 130.1 (CH_{Ar}), 125.6 (CH_{Ar}), 94.5 (C_{Ar}), 26.3 (CH-Ar), 24.1 (CH-COOH), 17.3 (CH₂) ppm. **IR** (Neat): 1685 cm⁻¹. **HRMS** (ESI) m/z: [M - H]⁻ Calcd for C₁₀H₈IO₂ 286.9569; Found 286.9568. **Melting point**: 83.4 – 86.3 °C.

4-(4,4,5,5-Tetramethyl-1,3,2-dioxaborolan-2-yl)benzyl (2-(3-iodophenyl)cyclopropyl)carbamate (**Q-3IAC**)

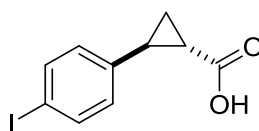


Triethylamine (0.100 mL, 72.6 mg, 0.717 mmol, 2.5 equiv) and diphenylphosphoryl azide (0.100 mL, 128 mg, 0.465 mmol, 1.6 equiv) were added to a solution of 2-(3-iodophenyl)cyclopropane-1-carboxylic acid (83.1 mg, 0.288 mmol, 1 equiv) and 4-(hydroxymethyl)phenylboronic acid pinacol ester (74.2 mg, 0.317 mmol, 1.1 equiv) in dry dioxane (1 mL). The reaction solution was heated at 105 °C for 2 h then cooled to room temperature. Solvent was evaporated under reduced pressure and the compound was purified by column chromatography (25% ethyl acetate/hexane). The title compound was obtained as a colourless oil (36.9 mg, 71.1 μmol) in 25% yield. **¹H NMR** (400 MHz, CDCl₃): δ 7.79 (d, *J* = 8.4 Hz, 2H, CH_{Ar}), 7.51 – 7.47 (m, 2H, CH_{Ar}), 7.34 (d, *J* = 8.0 Hz, 2H, CH_{Ar}), 7.12 – 7.10 (m, 1H, CH_{Ar}), 7.01 – 6.95 (m, 1H, CH_{Ar}), 5.12 (bs, 2H, OCH₂), 2.74 (bs, 1H, CHNH), 2.01 (bs, 1H, CH-Ar), 1.34 (s, 12H, CH₃), 1.19 – 1.15 (m, 2H, CH₂-CH-NH) ppm. **¹³C NMR** (100 MHz, CDCl₃): δ 156.7 (C=O), 142.8 (C_{Ar}), 139.3 (C_{Ar}), 135.6 (CH_{Ar}), 135.2 (CH_{Ar}), 135.0 (CH_{Ar}), 130.0 (CH_{Ar}), 127.2 (CH_{Ar}), 126.0

(CH_{Ar}), 94.4 (C_{Ar}), 83.8 (C-Me₂), 66.7 (OCH₂), 32.7 (CH-NH), 24.9 (CH₃ and CH-Ar), 16.1 (CH₂-CH-NH) ppm. **IR** (Neat): 3316, 2979, 1710 cm⁻¹. **HRMS** (ESI) m/z: [M + Na]⁺ Calcd for C₂₃H₂₇BINO₄Na 542.09755; Found 542.09676.

2.5.7 Preparation of Q-4IAC and its precursor

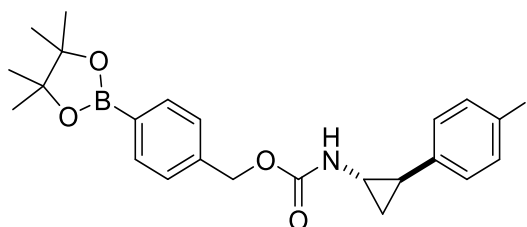
2-(4-Iodophenyl)cyclopropane-1-carboxylic acid (**17c**)



2-Phenylcyclopropanecarboxylic acid **17a** (151 mg, 930 μmol, 1 equiv), iodine (150 mg, 592 μmol, 0.64 equiv), potassium iodate (49.1 mg, 229 μmol, 0.25 equiv) were added to a solution of concentrated sulfuric acid (0.2 mL) in water (1 mL) and glacial acetic acid (4 mL). The solution was heated to reflux and glacial acetic acid (6 mL) was added portion-wise over 4 h to rinse down iodine from the condenser. The reaction was quenched with 1 M Na₂S₂O₄ solution (1 mL) and water (24 mL). The solution was extracted with ethyl acetate (4 × 15 mL) then the extracts were washed with brine (2 × 30 mL) and dried over sodium sulfate. After recrystallization of the crude product, the title compound was collected as a white solid (98.5 mg, 342 μmol) in 37% yield. **¹H NMR** (500 MHz, CDCl₃): δ 7.60 (d, *J* = 8 Hz, 2H, CH_{Ar}), 6.86 (d, *J* = 8 Hz, 2H, CH_{Ar}), 2.54 (bs, 1H, CH-Ar), 1.87 (bs, 1H, CH-COOH), 1.67 – 1.65 (m, 1H, CH₂), 1.38 – 1.36 (m, 1H, CH₂) ppm. **¹³C NMR** (125 MHz, CDCl₃): δ 179.4 (C=O), 139.2 (C_{Ar}), 137.5 (CH_{Ar}), 128.3 (CH_{Ar}), 91.7 (C_{Ar}), 26.6 (CH-Ar), 24.0 (CH-COOH), 17.4 (CH₂) ppm. **IR** (Neat): 1685 cm⁻¹. **HRMS** (ESI) m/z: [M - H]⁻ Calcd for C₁₀H₈IO₂ 286.9569; Found 286.9565. **Melting point**: 155.9 – 157.5 °C.

4-(4,4,5,5-Tetramethyl-1,3,2-dioxaborolan-2-yl)benzyl
iodophenyl)cyclopropyl)carbamate (*Q-4IAC*)

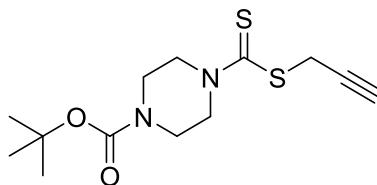
(2-(4-



Triethylamine (0.100 mL, 72.6 mg, 0.717 mmol, 2.2 equiv) and diphenylphosphoryl azide (0.100 mL, 128 mg, 0.465 mmol, 1.4 equiv) were added to a solution of **17c** (95.2 mg, 0.330 mmol, 1 equiv) and 4-(hydroxymethyl)phenylboronic acid pinacol ester (87.0 mg, 0.372 mmol, 1.1 equiv) in dry dioxane (1 mL). The reaction solution was heated at 105 °C for 24 h then cooled to room temperature. Solvent was evaporated under reduced pressure and the compound was purified by column chromatography (25% ethyl acetate/hexane). The title compound was obtained as a colourless oil (58.0 mg, 0.112 mmol) in 34% yield. **¹H NMR** (500 MHz, CDCl₃): δ 7.79 (d, *J* = 8.0 Hz, 2H, CH_{Ar}), 7.55 (bs, 2H, CH_{Ar}), 7.33 (d, *J* = 7.5 Hz, 2H, CH_{Ar}), 6.89 – 6.71 (m, 2H, CH_{Ar}), 5.20 (bs, 1H, NH), 5.11 (s, 2H, OCH₂), 2.70 (bs, 1H, CHNH), 2.01 (bs, 1H, CH-Ar), 1.34 (s, 12H, CH₃), 1.15 (bs, 2H, CH₂-CH-NH) ppm. **¹³C NMR** (125 MHz, CDCl₃): δ 156.6 (C=O), 140.1 (C_{Ar}), 139.3 (C_{Ar}), 137.3 (CH_{Ar}), 135.0 (CH_{Ar}), 128.7 (CH_{Ar}), 127.2 (CH_{Ar}), 91.0 (C_{Ar}), 83.8 (C-Me₂), 66.6 (OCH₂), 32.6 (CH-NH), 24.8 (CH₃ and CH-Ar), 15.9 (CH₂-CH-NH) ppm. **IR** (Neat): 3261, 2978, 1704 cm⁻¹. **HRMS** (ESI) *m/z*: [M + Na]⁺ Calcd for C₂₃H₂₇BINO₄Na 542.09755; Found 542.09673. **Melting point**: 138.7 – 140.6 °C.

2.5.8 Preparation of 11 and its precursors

tert-Butyl 4-((prop-2-yn-1-ylthio)carbonothioyl)piperazine-1-carboxylate (**19**)

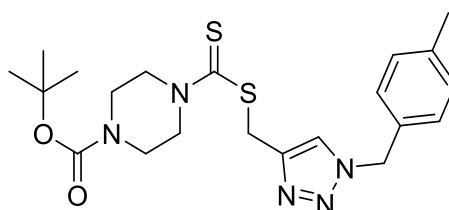


Carbon disulfide (0.200 mL, 253 mg, 3.33 mmol, 3 equiv) was added dropwise to a solution of *tert*-butyl piperazine-1-carboxylate (209 mg, 1.12 mmol, 1 equiv) and Na₃PO₄ · 12 H₂O (247 mg, 0.650 mmol, 0.6 equiv) in dry acetone (4.3 mL). After stirring for 30 mins at room temperature, propargyl bromide (80 wt. % in toluene, 0.140 mL, 0.150 g, 1.26 mmol, 1.1 equiv) was added dropwise to the solution. After the reaction was left stirring at room temperature for 30 mins, it was filtered and the filtrate was concentrated in vacuo. The residue was dissolved in ethyl acetate (10 mL) and washed with water (10 mL) then brine (10 mL). The organic solution was dried over magnesium sulfate and concentrated under reduced pressure to yield the title compound as a milky white solid (284 mg, 0.944 mmol) in 84% yield. ¹H NMR (300 MHz, CDCl₃): δ 4.12 (d, *J* = 2.4 Hz, 2H, CH₂-S), 3.56 (t, *J* = 5.4 Hz, 4H, CH₂-CH₂), 2.26 (t, *J* = 2.4 Hz, 1H, C≡CH), 1.48 (s, 9H, CH₃) ppm. IR (Neat): 1734, 1683, 1653 cm⁻¹. **Melting point:** 91.7 – 97.1 °C.

tert-Butyl

4-(((1-(4-methylbenzyl)-1H-1,2,3-triazol-4-yl)-

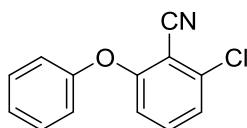
methylthio)carbonothioyl)piperazine-1-carboxylate (**11**)



A solution of **19** (99.1 mg, 0.330 mmol, 1 equiv), 4-methylbenzyl azide (61.4 mg, 0.417 mmol, 1.3 equiv), copper(II) sulfate (5.70 mg, 35.7 μ mol, 0.1 equiv) and sodium ascorbate (8.80 mg, 44.4 μ mol, 0.1 equiv) in a mixture of THF and water (1:1 ratio), was stirred for 2 h at room temperature. Water (1.4 mL) was added to the reaction and the mixture was extracted with ethyl acetate (3 \times 5 mL). The combined organic fractions were washed with brine solution (10 mL), dried over magnesium sulfate and concentrated under reduced pressure to give the title compound as a yellow solid (129 mg, 0.288 mmol) in 87% yield. $^1\text{H NMR}$ (300 MHz, CDCl_3): δ 7.55 (s, 1H, C=CH-N), 7.17 (s, 4H, CH_{Ar}), 5.44 (s, 2H, CH_2), 4.67 (s, 2H, CH_2), 4.29 (bs, 2H, CH_2), 3.92 (bs, 2H, CH_2), 3.52 (t, J = 5.1 Hz, 4H, $\text{CH}_2\text{-CH}_2$), 2.35 (s, 3H, Tosyl CH_3), 1.47 (s, 9H, CH_3) ppm. **Melting point:** 168.2 – 172.2 $^\circ\text{C}$.

2.5.9 Preparation of **12** and its precursors

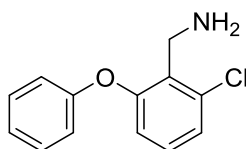
2-Chloro-6-phenoxybenzonitrile (21)



A solution of 2-fluoro-6-chlorobenzonitrile (775 mg, 4.98 mmol, 1 equiv), potassium carbonate (831 mg, 6.01 mmol, 1.2 equiv) and phenol (469 mg, 4.99 mmol, 1 equiv) in DMF (10.6 mL) was heated overnight at 100 $^\circ\text{C}$. The reaction solution was diluted with ethyl acetate (30 mL) and water (20 mL). The organic fraction was isolated then washed with brine (20 mL) and dried over magnesium sulfate. The solution was concentrated under reduced pressure to give the title compound as an orange solid (1.08 g, 4.69 mmol) in 94% yield. $^1\text{H NMR}$ (500 MHz, CDCl_3): δ 7.42 (t, J = 7.5 Hz, 2H, CH_{Ar}), 7.36 (t, J = 8.5 Hz, 1H, CH_{Ar}), 7.26 – 7.24 (m, 1H, CH_{Ar}), 7.17 (d, J = 8 Hz, 1H, CH_{Ar}), 7.10 (d, J =

8 Hz, 2H, CH_{Ar}), 6.73 (d, *J* = 8.5 Hz, 1H, CH_{Ar}) ppm. ¹³C NMR (125 MHz, CDCl₃): δ 161.4 (C_{Ar}), 154.5 (C_{Ar}), 138.1 (C_{Ar}), 134.1 (CH_{Ar}), 130.3 (CH_{Ar}), 125.6 (CH_{Ar}), 123.4 (CH_{Ar}), 120.3 (CH_{Ar}), 114.6 (CH_{Ar}), 113.1 (C≡N), 104.9 (C_{Ar}) ppm. IR (Neat): 3089, 1569, 1488, 1448, 1256 cm⁻¹. HRMS (ASAP) m/z: [M + H]⁺ Calcd for C₁₃H₉ClNO 230.0373; Found 230.0382. **Melting point:** 59.7 – 61.8 °C.

(2-Chloro-6-phenoxyphenyl)methanamine (22)

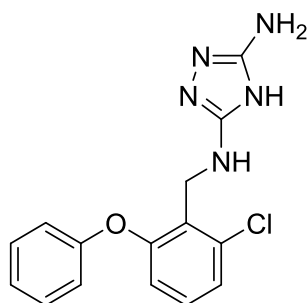


At 0 °C, a solution of 2-chloro-6-phenoxybenzotrile **21** (1.00 g, 4.35 mmol) in anhydrous diethyl ether (45 mL) was degassed by using nitrogen gas for 10 mins. LiAlH₄ (1 M in THF, 13.2 mL, 13.2 mmol, 3 equiv) was added dropwise to the solution over 10 mins at 0 °C and the reaction was left stirring at the same temperature for 2 h. The reaction was then gradually warmed to room temperature and left stirring overnight. At 0 °C, the reaction was quenched by the addition of Na₂SO₄ · 10 H₂O until no gas evolution was observed. The solution was left stirring for 30 mins before filtration through a plug of Celite. The filtrate was concentrated under reduced pressure to give a residue which was then purified using column chromatography (50% ethyl acetate/hexane). The title compound was obtained as a yellow oil (482 mg, 2.06 mmol) in 47% yield. ¹H NMR (500 MHz, CDCl₃): δ 7.34 (t, *J* = 7.5 Hz, 2H, CH_{Ar}), 7.18 – 7.10 (m, 3H, CH_{Ar}), 6.96 (d, *J* = 8.5 Hz, 2H, CH_{Ar}), 6.80 (d, *J* = 7.5 Hz, 1H, CH_{Ar}), 4.01 (s, 2H, CH₂) ppm. ¹³C NMR (125 MHz, CDCl₃)^a: δ 157.2 (C_{Ar}), 155.7 (C_{Ar}), 135.0 (C_{Ar}), 129.9 (CH_{Ar}), 128.5 (CH_{Ar}), 124.9 (CH_{Ar}), 123.5 (CH_{Ar}), 118.2 (CH_{Ar}), 117.7 (CH_{Ar}), 38.5 (CH₂) ppm. IR (Neat):

1587, 1569, 1488, 1447, 1256 cm^{-1} . **HRMS** (ASAP) m/z : $[\text{M} + \text{H}]^+$ Calcd for $\text{C}_{13}\text{H}_{13}\text{ClNO}$ 234.0686; Found 234.0686.

^a One of the aromatic quaternary carbon could not be accounted for, it could be overlapped with one of the observed aromatic quaternary carbon signal.

*N*³-(2-Chloro-6-phenoxybenzyl)-4*H*-1,2,4-triazole-3,5-diamine (**12**)



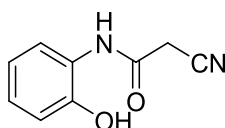
A solution of dimethyl *N*-cyanodithioiminocarbonate (348 mg, 2.38 mmol, 1.2 equiv) and (2-chloro-6-phenoxyphenyl)methanamine **22** (452 mg, 1.93 mmol, 1 equiv) in dry methanol (6 mL) was heated to reflux for 3 h. The reaction solution was concentrated under reduced pressure before the addition of dry ethanol (6 mL) and hydrazine hydrate (50 – 60%, 0.350 mL, 198 mg, 3.96 mmol). The reaction solution was heated to reflux for 1.5 h before concentrated under reduced pressure. After purifying the crude mixture with column chromatography (5% methanol in dichloromethane), the title compound was obtained as a white solid (426 mg, 1.35 mmol) in 70% yield. **¹H NMR** (500 MHz, DMSO): δ 7.39 (t, $J = 8$ Hz, 2H, CH_{Ar}), 7.31 – 7.24 (m, 2H, CH_{Ar}), 7.16 (t, $J = 7.5$ Hz, 1H, CH_{Ar}), 7.04 (d, $J = 8$ Hz, 2H, CH_{Ar}), 6.77 (d, $J = 7.5$ Hz, 1H, CH_{Ar}), 4.36 (d, $J = 5$ Hz, 2H, CH_2) ppm. **¹³C NMR** (100 MHz, DMSO)^a: δ 156.6 (C_{Ar}), 156.6 (C_{Ar}), 135.2 (C_{Ar}), 130.0 (CH_{Ar}), 129.7 (CH_{Ar}), 128.0 (C_{Ar}), 124.4 (CH_{Ar}), 123.8 (CH_{Ar}), 118.8 (CH_{Ar}), 117.1 (CH_{Ar}), 39.5 (CH_2) ppm. **IR** (Neat): 3352, 3266, 1658, 1489, 1448 cm^{-1} . **HRMS**

(ESI) m/z : $[M + H]^+$ Calcd for $C_{15}H_{15}ClN_5O$ 316.0965; Found 316.0978. **Melting point:** 192.9 – 200.4 °C.

^a Two of the aromatic quaternary carbons could not be accounted for, they could be overlapped with one/two of the observed aromatic quaternary carbon signals.

2.5.10 Preparation of 13 and its precursor

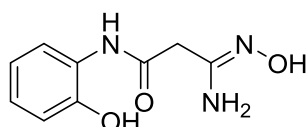
2-Cyano-N-(2-hydroxyphenyl)acetamide (23)



Cyanoacetic acid (0.400 g, 4.70 mmol, 1 equiv) was added to a suspension of phosphorus pentachloride (958 mg, 4.60 mmol, 1 equiv) in dry dichloromethane (84 mL). The suspension was heated to reflux for 45 mins then cooled down to room temperature and 2-aminophenol (504 mg, 4.60 mmol, 1 equiv) was added. The suspension was heated to reflux for 3.5 h before cooling down and solvent evaporation under reduced pressure. Water (20 mL) was added to the purplish white solid and the mixture was stirred for 10 mins. After filtration, the solid was washed with saturated sodium bicarbonate solution (10 mL) and water (2×10 mL). The title compound was collected as a purplish white solid (525 mg, 3.00 mmol) in 65% yield after drying. **¹H NMR** (400 MHz, $(CD_3)_2CO$): δ 9.07 (bs, 1H, OH or NH), 7.91 (d, $J = 8$ Hz, 1H, CH_{Ar}), 7.00 (td, $J = 8.0, 1.2$ Hz, 1H, CH_{Ar}), 6.92 (dd, $J = 7.8, 0.8$ Hz, 1H, CH_{Ar}), 6.84 (td, $J = 8.0, 1.2$ Hz, 1H, CH_{Ar}), 3.97 (s, 2H, CH_2) ppm. **¹³C NMR** (100 MHz, $(CD_3)_2CO$): δ 162.1 (C=O), 148.1 (C_{Ar}), 127.0 (C_{Ar}), 126.1 (CH_{Ar}), 122.4 (CH_{Ar}), 120.7 (CH_{Ar}), 116.7 (CH_{Ar}), 115.8 (C \equiv N), 27.2 (CH_2)

ppm. **IR** (Neat): 3314, 3268, 1670 cm^{-1} . **HRMS** (ASAP) m/z : $[M + H]^+$ Calcd for $\text{C}_9\text{H}_9\text{N}_2\text{O}_2$ 177.0664; Found 177.0665. **Melting point**: 200.9 – 204.9 $^\circ\text{C}$.

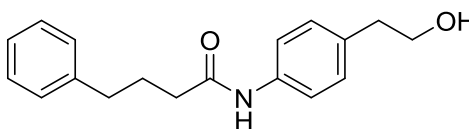
(3-Amino-3-(hydroxyimino)-N-[2-(hydroxyl)phenyl]propanamide) (13)



Hydroxylamine hydrochloride (93.8 mg, 1.35 mmol, 1.6 equiv) was added to a solution of potassium carbonate (148 mg, 1.07 mmol, 1.3 equiv) in water (0.45 mL). After the solution was diluted with methanol (4.5 mL), **23** (0.150 g, 0.850 mmol, 1 equiv) was added and the reaction solution was heated to reflux. After 2 h, the reaction solution was concentrated under reduced pressure and the resulting residue was added to a hot mixture of ethyl acetate and methanol (3:1 ratio). The mixture was filtered and the filtrate was concentrated under reduced pressure to give the crude product. The crude product was first purified using column chromatography (0 - 5% methanol in ethyl acetate), then recrystallisation (methanol/ethyl acetate). The title compound was obtained as a white solid (21.2 mg, 0.101 mmol) in 12% yield. **^1H NMR** (500 MHz, DMSO): δ 9.82 (bs, 1H, NH), 9.28 (s, 1H, OH), 9.10 (s, 1H, OH), 7.87 (d, $J = 8$ Hz, 1H, CH_{Ar}), 6.93 – 6.90 (m, 1H, CH_{Ar}), 6.86 – 6.84 (m, 1H, CH_{Ar}), 6.75 (t, $J = 7.5$ Hz, 1H, CH_{Ar}), 5.58 (s, 2H, NH_2), 3.13 (s, 2H, CH_2) ppm. **^{13}C NMR** (125 MHz, DMSO): δ 166.8 (C=O), 148.7 (C=N), 147.3 (C_{Ar}), 126.3 (C_{Ar}), 124.3 (CH_{Ar}), 121.2 (CH_{Ar}), 118.9 (CH_{Ar}), 115.2 (CH_{Ar}), 39.7 (CH_2) ppm. **IR** (Neat): 3420, 3329, 1653, 1550, 1454, 1281 cm^{-1} . **HRMS** (ASAP) m/z : $[M + H]^+$ Calcd for $\text{C}_9\text{H}_{12}\text{N}_3\text{O}_3$ 210.0879; Found 210.0877. **Melting point**: 156.5 – 157.2 $^\circ\text{C}$.

2.5.11 Preparation of bizine and its precursors

N-(4-(2-Hydroxyethyl)phenyl)-4-phenylbutanamide (**25**)

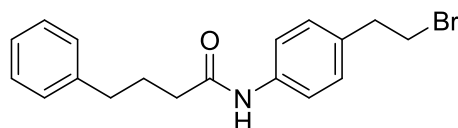


A solution of 4-phenylbutyric acid (2.00 g, 12.2 mmol, 1 equiv) in dichloromethane (3 mL) was cooled to 0 °C for 5 mins before the dropwise addition of thionyl chloride (4.50 mL, 7.34 g, 61.7 mmol, 5.1 equiv). The solution was stirred at 0 °C for 10 mins then heated to 55 °C. After 20 h, the reaction progress was monitored via TLC (2% MeOH in DCM with a few drops of glacial acetic acid) and small amount of starting material was still present, hence the temperature was raised to 65 °C. After 3 h, the reaction was monitored by TLC and small amount of starting material was still present. Solvent and remaining thionyl chloride were removed by distillation, then the residue was dried under reduced pressure. The acid chloride intermediate was collected as a brown liquid (2.06 g, 11.3 mmol). ¹H NMR (500 MHz, CDCl₃): δ 7.16 – 7.32 (m, 5H, CH_{Ar}), 2.89 (t, *J* = 7 Hz, 2H, CH₂-CH₂), 2.68 (t, *J* = 7 Hz, 2H, CH₂-CH₂), 2.04 (quin, *J* = 7.5 Hz, 2H, CH₂-CH₂-CH₂) ppm. NMR data consistent with literature.¹²⁸

To a cold solution of 2-(4-aminophenyl)ethanol (1.55 g, 11.3 mmol, 1 equiv) in dry dichloromethane (15.5 mL), *N,N*-diisopropylethylamine (13.8 mL, 10.2 g, 79.2 mmol, 7 equiv) was added dropwise, follow by the acid chloride intermediate (2.06 g, 11.3 mmol, 1 equiv). After 5 mins, the solution was left stirring at room temperature for 22 h. The solution was diluted by adding dichloromethane (75 mL) then washed with 2 N HCl (40 mL), saturated NaHCO₃ solution (75 mL) and brine (75 mL). After the solvent

evaporation under reduced pressure, the brown solid residue was dissolved in methanol (75 mL) and 1 M NaOH (35 mL) was added dropwise to the solution. The solution was left stirring under nitrogen atmosphere for 12 h. The reaction solution was concentrated in vacuo then diluted with ethyl acetate (100 mL). After washing the solution with 1 N HCl (80 mL), saturated NaHCO₃ solution (2 × 80 mL) and brine (80 mL), the solution was dried with magnesium sulfate and concentrated under reduced pressure. The title compound was collected as a brown solid (2.30 g, 8.11 mmol) in 66% yield. **¹H NMR** (500 MHz, CDCl₃): δ 7.43 (d, *J* = 8 Hz, 2H, CH_{Ar}), 7.31 – 7.28 (m, 2H, CH_{Ar}), 7.21 – 7.17 (m, 5H, CH_{Ar}), 7.04 (bs, 1H, NH), 3.84 (t, *J* = 6 Hz, 2H, CH₂-OH), 2.83 (t, *J* = 6 Hz, 2H, CH₂-CH₂), 2.72 (t, *J* = 7 Hz, 2H, CH₂-CH₂), 2.34 (t, *J* = 7.5 Hz, 2H, CH₂-CH₂), 2.08 (quin, *J* = 7 Hz, 2H, CH₂-CH₂-CH₂) ppm. **¹³C NMR** (500 MHz, CDCl₃): δ 171.3 (C=O), 141.4 (C_{Ar}), 136.3 (C_{Ar}), 134.5 (C_{Ar}), 129.4 (CH_{Ar}), 128.5 (CH_{Ar}), 128.4 (CH_{Ar}), 126.0 (CH_{Ar}), 120.3 (CH_{Ar}), 63.5 (CH₂OH), 38.6 (CH₂), 36.6 (CH₂), 35.1 (CH₂), 26.9 (CH₂) ppm. **IR** (Neat): 3326, 1654 cm⁻¹. **HRMS** (ASAP) *m/z*: [M + H]⁺ Calcd for C₁₈H₂₂NO₂ 284.1651; Found 284.1645. **Melting point**: 90.0 – 93.5 °C.

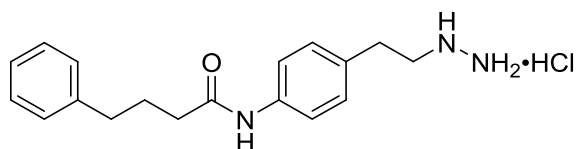
N-(4-(2-Bromoethyl)phenyl)-4-phenylbutanamide



Triphenylphosphine (1.85 g, 7.06 mmol, 2 equiv) and tetrabromomethane (2.34 g, 7.07 mmol, 2 equiv) were added to a solution of **25** (1.01 g, 3.56 mmol, 1 equiv) in dry dichloromethane (48 mL). After leaving the reaction stirring overnight at room temperature, the reaction was concentrated under reduced pressure and subjected to

column chromatography (40% ethyl acetate/hexane). The title compound was obtained as a pale yellow solid (687 mg, 1.98 mmol) in 56% yield. $^1\text{H NMR}$ (300 MHz, CDCl_3): δ 7.45 (d, $J = 8.4$ Hz, 2H, CH_{Ar}), 7.33 – 7.28 (m, 3H, CH_{Ar}), 7.23 – 7.15 (m, 4H, CH_{Ar}), 7.03 (bs, 1H, NH), 3.54 (t, $J = 7.5$ Hz, 2H, $\text{CH}_2\text{-Br}$), 3.12 (t, $J = 7.8$ Hz, 2H, $\text{CH}_2\text{-CH}_2$), 2.72 (t, $J = 7.5$ Hz, 2H, $\text{CH}_2\text{-CH}_2$), 2.34 (t, $J = 7.2$ Hz, 2H, $\text{CH}_2\text{-CH}_2$), 2.07 (quin, $J = 7.8$ Hz, 2H, $\text{CH}_2\text{-CH}_2\text{-CH}_2$) ppm. **IR** (Neat): 3298, 1654, 1604, 1535, 1514, 1411 cm^{-1} . **Melting point:** 64.0 – 68.2 $^\circ\text{C}$.

Bizine



Hydrazine hydrate (50 – 60%, 2.05 mL, 1.16 g, 23.2 mmol, 20 equiv) was added dropwise to a solution of *N*-(4-(2-bromoethyl)phenyl)-4-phenylbutanamide (401 mg, 1.16 mmol, 1 equiv) in ethanol (4 mL). The solution was heated to reflux for 1 h before concentrated under reduced pressure. After sodium hydroxide solution (1 M, 80 mL, 80 mmol, excess) was added to the residue, it was extracted with dichloromethane (3×80 mL) and concentrated in vacuo. The resulting yellow oil was dissolved in methanol (10 mL) and treated with hydrochloric acid (6 M, 2.0 mL, 12 mmol, excess) at 0 $^\circ\text{C}$. After stirring for 10 mins at 0 $^\circ\text{C}$, diethyl ether (5 mL) was added to the solution before it was concentrated under reduced pressure to yield a precipitate that was filtered and washed with cold diethyl ether. After drying the precipitate in a vacuum desiccator overnight, the title compound was obtained as a pale yellow solid (79.1 mg, 0.237 mmol) in 20% yield. $^1\text{H NMR}$ (500 MHz, DMSO): δ 9.88 (s, 1H, NH), 7.53 (d, $J = 8$ Hz, 2H, CH_{Ar}), 7.30 – 7.27

(m, 2H, CH_{Ar}), 7.21 – 7.17 (m, 3H, CH_{Ar}), 7.14 (d, $J = 8$ Hz, 2H, CH_{Ar}), 3.09 – 3.06 (m, 2H, CH₂-NH), 2.78 (bs, 2H, CH₂), 2.61 (t, $J = 8$ Hz, 2H, CH₂-CH₂), 2.31 (t, $J = 7.5$ Hz, 2H, CH₂-CH₂), 1.88 (quin, $J = 7.5$ Hz, 2H, CH₂-CH₂-CH₂) ppm. **IR** (Neat): 3303, 1684 cm⁻¹. **Melting point**: 173.4 – 177.1 °C.

2.5.12 ESI-MS experiment for prodrug activation

Following the procedure of Hagen et al.²⁶ a solvent system of 9:1 acetonitrile:water (v:v) was used to prepare a solution of Q-PAC and triethylamine (both 0.9 mM) for activation with hydrogen peroxide (9 mM). At 5 minute intervals out to 30 minutes aliquots were diluted 90-fold in solvent for analysis via electrospray ionization mass spectrometry on either a Thermo LTQ ion-trap or LTQ Orbitrap XL. Both utilized an Ion Max ESI source operated in positive mode with nitrogen as the desolvation gas. The following conditions were employed on the single-trap instrument: 5 µL/min infusion rate, 3.5 kV source voltage; sheath, auxillary and sweep gases set to 12, 0 and 0 (arbitrary flow), respectively; capillary temperature 200 °C and voltage 46 V; tube lens 130 volts. Settings for Orbitrap analysis: 10 µL/min infusion rate, 4.2 kV source voltage; sheath, auxillary and sweep gases set to 10, 0 and 0 (arbitrary flow), respectively; capillary held at 275 °C and 50 volts; tube lens 150 volts. The infusion syringe, tubing and ESI probe were rinsed with solvent until the ionized Q-PAC signal was reduced to background levels prior to analysis of a particular sample. Spectra reported here constitute the average between 50 and 100 scans and were analysed to monitor reaction species relative to Q-PAC as a function of reaction time.

2.5.13 Culture details for cell culture assays

U87MG cells (ECACC, Acc Nr.: 89081402, obtained in 2014, Female astrocytoma, identity confirmed via short tandem repeat profiling by Garvan Institute (Sydney, AU) in 2015) were maintained in Dulbecco's Modified Eagle Medium with F12 supplement (Life Technologies, #10565-018), 10% foetal bovine serum (Bovogen, #SFBS-F), and seeded at 20,000 cells/cm². Cells were used between passage 8 and 15, absence of mycoplasma confirmed every three month (MycoAlert, Lonza, AU).

Primary glioblastoma cultures provided by the Brain Cancer Research Unit of the QIMR Berghofer Medical Research Institute (2015) were established from untreated biopsy samples of different glioblastoma subtypes^{3,96} (SJH1: 72 years male, neural; RN1: 56 years male, classical; JK2: 75 years male, proneural). Approval for this study was obtained from the Human Research Ethics Committee of The University of Wollongong (HE16/324). Cells were maintained in Knockout-DMEM/F12 (Life Technologies, #12660-012) with StemPro supplement (Life Technologies, #A10508-01), human EGF (20 ng/ml) (Life Technologies, #PHG0314) and human FGF2 (10 ng/ml) (Life Technologies, #PHG0024), and seeded at 35,000 cells/cm² on matrigel (Corning, #354277, 1/100 dilution). Cells were used between passage 5 and 13 in 2015 and 2016, absence of mycoplasma confirmed every three month (MycoAlert, Lonza, AU).

Human astrocyte cultures were generated from human foetal brain tissue, which was obtained from 17 to 20-week-old fetuses collected after therapeutic termination following informed consent. Approval for this study was obtained from the Human Research Ethics Committee of Macquarie University (#5201200411). Written informed consent was obtained from the participants. Astrocytes were prepared using a protocol adapted from previously described methods¹²⁹ with slight modification. 1 g of brain was washed thrice with PBS containing 1% antibiotic/antimycotic to remove contaminating

blood. Visible blood vessels were removed with sterile scissors. Next, the tissue was placed in RPMI medium (Sigma-Aldrich, Australia) supplemented with 10% FBS and 2% antibiotic/antimycotic and dissociated mechanically by pipetting with a serological pipette. After one week in culture, the medium was removed and the culture was washed with PBS to remove unattached tissue fragments followed by addition of fresh medium. Once confluent, the culture was subjected to successive passage with trypsin-EDTA (0.25%) (Life Technologies) to remove contaminating cells and seeded at 20,000 cells/cm² for experiments. Cells were used between passage 2 and 5 in 2016, absence of mycoplasma confirmed every three month (MycoAlert, Lonza, AU).

2.5.14 Confluence assay

Culture confluence was monitored in 96 well plates (Greiner Bio-One CELLSTAR®) imaged every 2 h using an IncuCyte Zoom (Essen Bioscience) at 10x magnification (1.22 µm/pixel resolution) with three images per well. Pre- and post-treatment confluence was quantified through the inbuilt basic analyser algorithm (Essen Bioscience) adjusted to the individual morphology of each culture type.

2.5.15 Migration assay

For migration assays, cells were seeded into ImageLock 96-well Plates (Essen Biosciences) and maintained until 70% confluent. The 700-800 µm scratch wounds were made in each well using the 96 well WoundMaker (Essen Biosciences) directly prior to drug treatment. Plates were imaged every 2 h and migration into the wound area was quantified using the inbuilt Scratch Wound algorithm (Essen Biosciences), adjusted to the individual morphology of each culture type.

2.5.16 Invasion assay

Cell invasion was examined in real time using the xCELLigence RTCA DP System (Roche Applied Science). The xCELLigence system allows continuous quantitative monitoring of cellular behaviour including invasion by measuring electrical impedance at a porous membrane (pore size 8 μm). U87 cells were seeded at 22,500 cells/well into specialised two-layer Cell Invasion and Migration (CIM) plates coated with 20 μl matrigel (Corning, 1:30 dilution) and cultured without FBS for 24 h in the presence or absence of Q-PAC. Lower layer wells were filled with DMEM/F12 with 10% FBS as chemoattractant. Invasion was continuously monitored in real time over a period of 24 h. Data analysis was carried out using RTCA Software 1.2.1 supplied with the instrument.

2.5.17 Cell viability assay

Culture viability was assessed with the resazurin-based Presto Blue cell viability reagent (Life Technologies, #A13261) according to the manufacturer's instructions (2 h incubation) and quantified on a FLUOstar Optima (BMG labtech, excitation/emission 540 nm/580 nm).

2.5.18 Apoptosis assay

For apoptosis assays, the culture media was supplemented with caspase 3/7 NucView 488 enzyme substrate (2.5 μM final concentration, Biotium, #10402) 2 h prior to drug treatment. Phase contrast and fluorescent images were captured using an IncuCyte Zoom (green emission/excitation at 460 nm/524 nm) at 2 h intervals and 10x

magnification. Caspase substrates were quantified using the in-built basic analyser algorithm (Table 1) from a minimum of three images per well and time point.

2.5.19 Immunocytochemistry

Cultures were fixed (4% paraformaldehyde, 15 min) and blocked (5% goat serum, 1 h), before incubation with MCM2 polyclonal rabbit antibody (Cell Signalling Technologies, #4007, 1/500 in 5% BSA) overnight at 4 °C. This was followed by incubation with goat anti-rabbit IgG conjugated to Alexa 488 (Life Technologies, #A11008, 1/1000, 1%BSA) for 1 hr at room temperature and reddot2 (Biotium, #40061-1, 1/200) as a nuclear counterstain. Images were captured on an Incucyte Zoom in phase-contrast, green and red (emission/excitation 585 nm/635 nm) at 20x magnification with three images per well. The fraction of MCM2-positive cells was determined through automatic counting of reddot2 and MCM2 positive cells per image (see Table 1 for mask parameters).

2.5.20 Western blot

For histone modification quantification, cultures were lysed in triton extraction buffer (PBS containing 0.5% Triton X 100 (v/v), 1% protease inhibitor cocktail (P8340-1ML, Sigma-Aldrich) and 0.02% (w/v) NaN₃) and histones extracted in 0.2 M HCl at 4°C over 16 h. Reduced samples were separated on 15% polyacrylamide gels and transferred onto PVDF membranes (Millipore). Membranes were immunoblotted at 4 °C over 16 h for monomethylated H3K4 (5% milk block, Abcam #ab8895, 1:10,000 in 1% BSA), dimethylated H3K4 (5% milk block, Abcam #ab7766, 1:10,000 in 1%BSA) and acetylated H4 (3% milk block, Millipore #06-866, 1:4000 in 3% milk) followed by goat

anti-rabbit IgG-HRP (Millipore, #AP307P, 1:2500 in 1% milk) and detected by chemiluminescence. LSD1 expression was quantified in whole-cell lysates, separated on Criterion TGX Stain-Free Precast Gels (4-20%, Biorad #567-8095) and transferred onto PVDF membranes. Total protein loading was quantified by UV-imaging of trihalo transferred from the gels. Membranes were immunoblotted at 4 °C over 16 h for LSD1 (5% milk block, Cell Signalling #C69G12, 1:1,500 in 5% milk), followed by goat anti-rabbit IgG-HRP (Sigma, #A0545, 1:3,000 in 2.5% milk) and detected by chemiluminescence.

2.5.21 GSH assay

Reduced glutathione (GSH) of cell lysates was measured with a fluorometric kit, according to the manufacturer's instructions (Abcam, #ab138881) and fluorescence intensity monitored on a FLUOstar Optima (excitation/emission 490 nm/520 nm). Sample GSH concentration was determined through a serial-diluted GSH calibration curve (150 nM to 20 µM).

2.5.22 Reactive oxygen species (ROS) quantification

Oxidative stress in live cultures was assessed with CellROX Green (Life Technologies, #C10444), which remains non-fluorescent until oxidized by intracellular reactive oxygen species (ROS). The fluorescent signal intensity is proportional to the levels of intracellular free radicals. Cultures were plated in black optical bottom plates (Thermo Fisher, #NUN165305) and incubated in CellROX Green for 30 min after treatment, followed by 2x PBS washes prior to imaging. Images were captured on an Incucyte Zoom in phase-contrast and green at 20x magnification (0.61 µm/pixel

resolution) with three images per well. Mean Green Intensity was normalised to culture confluence for each image.

2.5.23 Statistical analysis

Analyses were performed using Graphpad Prism (Graphpad Software Inc.). Treatment effects were assessed using one-way or two-way analysis of variance (ANOVA) as relevant, followed by Bonferroni's multiple comparisons test where appropriate. All cell culture experiments were conducted with at least three independent biological replicates and at least two technical replicates each. Significance was accepted at $p < 0.05$ and data presented as mean \pm standard error of mean (SEM) for biological replicates.

2.6 References

- (1) Jessen, K. R. *Int. J. Biochem. Cell Biol.* **2004**, *36*, 1861.
- (2) Pitanga, B.; Nascimento, R.; Silva, V. D.; Costa, S. *Front. Pharmacol.* **2012**, *3*.
- (3) Verhaak, R. G.; Hoadley, K. A.; Purdom, E.; Wang, V.; Qi, Y.; Wilkerson, M. D.; Miller, C. R.; Ding, L.; Golub, T.; Mesirov, J. P.; Alexe, G.; Lawrence, M.; O'Kelly, M.; Tamayo, P.; Weir, B. A.; Gabriel, S.; Winckler, W.; Gupta, S.; Jakkula, L.; Feiler, H. S.; Hodgson, J. G.; James, C. D.; Sarkaria, J. N.; Brennan, C.; Kahn, A.; Spellman, P. T.; Wilson, R. K.; Speed, T. P.; Gray, J. W.; Meyerson, M.; Getz, G.; Perou, C. M.; Hayes, D. N. *Cancer Cell* **2010**, *17*, 98.
- (4) McLendon, R. E.; Halperin, E. C. *Cancer* **2003**, *98*, 1745.
- (5) Gallego, O. *Curr. Oncol.* **2015**, *22*, e273.
- (6) Schapira, A. H. V. *Neurology and Clinical Neuroscience E-Book*; Elsevier Health Sciences, 2006.
- (7) Agnihotri, S.; Burrell, K. E.; Wolf, A.; Jalali, S.; Hawkins, C.; Rutka, J. T.; Zadeh, G. *Arch. Immunol. Ther. Exp. (Warsz)*. **2013**, *61*, 25.
- (8) Zong, H.; Verhaak, R. G. W.; Canoll, P. *Expert Rev. Mol. Diagn.* **2012**, *12*, 383.
- (9) Zong, H.; Parada, L. F.; Baker, S. J. *Cold Spring Harbor Perspect. Biol.* **2015**, *7*, a020610.
- (10) Chamberlain, M. C.; Glantz, M. J.; Chalmers, L.; Van Horn, A.; Sloan, A. E. *J. Neurooncol.* **2007**, *82*, 81.
- (11) Chamberlain, M. C. *Expert Rev. Neurother.* **2010**, *10*, 1537.
- (12) Stupp, R.; Mason, W. P.; van den Bent, M. J.; Weller, M.; Fisher, B.; Taphoorn, M. J.; Belanger, K.; Brandes, A. A.; Marosi, C.; Bogdahn, U.; Curschmann, J.;

- Janzer, R. C.; Ludwin, S. K.; Gorlia, T.; Allgeier, A.; Lacombe, D.; Cairncross, J. G.; Eisenhauer, E.; Mirimanoff, R. O. *N. Engl. J. Med.* **2005**, *352*, 987.
- (13) Clarke, J.; Butowski, N.; Chang, S. *Arch. Neurol.* **2010**, *67*, 279.
- (14) “Brain and other central nervous system cancers,” Australian Institute of Health and Welfare, 2017.
- (15) Valavanidis, A.; Vlachogianni, T.; Fiotakis, K. *Int. J. Env. Res. Public Health* **2009**, *6*, 445.
- (16) Gurgueira, S. A.; Lawrence, J.; Coull, B.; Murthy, G. G. K.; González-Flecha, B. *Environ. Health Perspect.* **2002**, *110*, 749.
- (17) Yamamori, T.; Yasui, H.; Yamazumi, M.; Wada, Y.; Nakamura, Y.; Nakamura, H.; Inanami, O. *Free Radical Biol. Med.* **2012**, *53*, 260.
- (18) Madamanchi, N. R.; Runge, M. S. *Circ. Res.* **2007**, *100*, 460.
- (19) Trachootham, D.; Alexandre, J.; Huang, P. *Nat. Rev. Drug Discov.* **2009**, *8*, 579.
- (20) Gamaley, I. A.; Klyubin, I. V. In *Int. Rev. Cytol.*; Jeon, K. W., Ed.; Academic Press: 1999; Vol. 188, p 203.
- (21) Meister, A. *J. Biol. Chem.* **1988**, *263*, 17205.
- (22) Toyokuni, S.; Okamoto, K.; Yodoi, J.; Hiai, H. *FEBS Lett.* **1995**, *358*, 1.
- (23) Kawanishi, S.; Hiraku, Y.; Pinlaor, S.; Ma, N. *Biol. Chem.* **2006**, *387*, 365.
- (24) Szatrowski, T. P.; Nathan, C. F. *Cancer Res.* **1991**, *51*, 794.
- (25) Stone, J. R. *Arch. Biochem. Biophys.* **2004**, *422*, 119.
- (26) Hagen, H.; Marzenell, P.; Jentsch, E.; Wenz, F.; Veldwijk, M. R.; Mokhir, A. *J. Med. Chem.* **2011**, *55*, 924.
- (27) Peng, X.; Gandhi, V. *Ther Deliv* **2012**, *3*, 823.
- (28) Young, T. W.; Mei, F. C.; Yang, G.; Thompson-Lanza, J. A.; Liu, J.; Cheng, X. *Cancer Res.* **2004**, *64*, 4577.
- (29) Trachootham, D.; Zhou, Y.; Zhang, H.; Demizu, Y.; Chen, Z.; Pelicano, H.; Chiao, P. J.; Achanta, G.; Arlinghaus, R. B.; Liu, J.; Huang, P. *Cancer Cell* **2006**, *10*, 241.
- (30) Maeda, H.; Hori, S.; Ohizumi, H.; Segawa, T.; Kakehi, Y.; Ogawa, O.; Kakizuka, A. *Cell Death Differ.* **2004**, *11*, 737.
- (31) Chen, W.; Balakrishnan, K.; Kuang, Y.; Han, Y.; Fu, M.; Gandhi, V.; Peng, X. *J. Med. Chem.* **2014**, *57*, 4498.
- (32) Cao, S.; Christiansen, R.; Peng, X. *Chem. - Eur. J.* **2013**, *19*, 9050.
- (33) Marzenell, P.; Hagen, H.; Sellner, L.; Zenz, T.; Grinyte, R.; Pavlov, V.; Daum, S.; Mokhir, A. *J. Med. Chem.* **2013**, *56*, 6935.
- (34) Daum, S.; Chekhun, V. F.; Todor, I. N.; Lukianova, N. Y.; Shvets, Y. V.; Sellner, L.; Putzker, K.; Lewis, J.; Zenz, T.; de Graaf, I. A. M.; Groothuis, G. M. M.; Casini, A.; Zozulia, O.; Hampel, F.; Mokhir, A. *J. Med. Chem.* **2015**, *58*, 2015.
- (35) Schikora, M.; Reznikov, A.; Chaykovskaya, L.; Sachinska, O.; Polyakova, L.; Mokhir, A. *Bioorg. Med. Chem. Lett.* **2015**, *25*, 3447.
- (36) Noh, J.; Kwon, B.; Han, E.; Park, M.; Yang, W.; Cho, W.; Yoo, W.; Khang, G.; Lee, D. *Nat. Commun.* **2015**, *6*.
- (37) Kato, Y.; Ozawa, S.; Miyamoto, C.; Maehata, Y.; Suzuki, A.; Maeda, T.; Baba, Y. *Cancer Cell Int.* **2013**, *13*, 89.
- (38) Shirmanova, M. V.; Druzhkova, I. N.; Lukina, M. M.; Matlashov, M. E.; Belousov, V. V.; Snopova, L. B.; Prodanetz, N. N.; Dudenkova, V. V.; Lukyanov, S. A.; Zagaynova, E. V. *Biochimica et Biophysica Acta (BBA) - General Subjects* **2015**, *1850*, 1905.
- (39) Sharma, S. K.; Hazeldine, S.; Crowley, M. L.; Hanson, A.; Beattie, R.; Varghese, S.; Senanayake, T. M.; Hirata, A.; Hirata, F.; Huang, Y.; Wu, Y.; Steinbergs, N.;

- Murray-Stewart, T.; Bytheway, I.; Casero, R. A., Jr.; Woster, P. M. *MedChemComm* **2012**, *3*, 14.
- (40) Luger, K.; Mader, A. W.; Richmond, R. K.; Sargent, D. F.; Richmond, T. J. *Nature* **1997**, *389*, 251.
- (41) Felsenfeld, G.; Groudine, M. *Nature* **2003**, *421*, 448.
- (42) Hosseini, A.; Minucci, S. *Epigenomics* **2017**, *9*, 1123.
- (43) Suzuki, T.; Miyata, N. *J. Med. Chem.* **2011**, *54*, 8236.
- (44) Shi, Y.; Lan, F.; Matson, C.; Mulligan, P.; Whetstine, J. R.; Cole, P. A.; Casero, R. A.; Shi, Y. *Cell* **2004**, *119*, 941.
- (45) Forneris, F.; Binda, C.; Dall'Aglio, A.; Fraaije, M. W.; Battaglioli, E.; Mattevi, A. *J. Biol. Chem.* **2006**, *281*, 35289.
- (46) Lee, M. G.; Wynder, C.; Cooch, N.; Shiekhattar, R. *Nature* **2005**, *437*, 432.
- (47) Yang, M.; Culhane, J. C.; Szewczuk, L. M.; Gocke, C. B.; Brautigam, C. A.; Tomchick, D. R.; Machius, M.; Cole, P. A.; Yu, H. *Nat. Struct. Mol. Biol.* **2007**, *14*, 535.
- (48) Metzger, E.; Wissmann, M.; Yin, N.; Müller, J. M.; Schneider, R.; Peters, A. H.; Günther, T.; Buettner, R.; Schüle, R. *Nature* **2005**, *437*, 436.
- (49) Huang, J.; Sengupta, R.; Espejo, A. B.; Lee, M. G.; Dorsey, J. A.; Richter, M.; Opravil, S.; Shiekhattar, R.; Bedford, M. T.; Jenuwein, T. *Nature* **2007**, *449*, 105.
- (50) Wang, J.; Hevi, S.; Kurash, J. K.; Lei, H.; Gay, F.; Bajko, J.; Su, H.; Sun, W.; Chang, H.; Xu, G. *Nat. Genet.* **2008**, *41*, 125.
- (51) Singh, M. M.; Manton, C. A.; Bhat, K. P.; Tsai, W. W.; Aldape, K.; Barton, M. C.; Chandra, J. *Neuro. Oncol.* **2011**, *13*, 894.
- (52) Liu, S.; Lu, W.; Li, S.; Li, S.; Liu, J.; Xing, Y.; Zhang, S.; Zhou, J. Z.; Xing, H.; Xu, Y.; Rao, Q.; Deng, C.; Wang, M.; Wang, J. *Oncotarget* **2017**, *8*, 31901.
- (53) Schulte, J. H.; Lim, S.; Schramm, A.; Friedrichs, N.; Koster, J.; Versteeg, R.; Ora, I.; Pajtler, K.; Klein-Hitpass, L.; Kuhfittig-Kulle, S.; Metzger, E.; Schüle, R.; Eggert, A.; Buettner, R.; Kirfel, J. *Cancer Res.* **2009**, *69*, 2065.
- (54) Wissmann, M.; Yin, N.; Müller, J. M.; Greschik, H.; Fodor, B. D.; Jenuwein, T.; Vogler, C.; Schneider, R.; Günther, T.; Buettner, R.; Metzger, E.; Schüle, R. *Nat. Cell Biol.* **2007**, *9*, 347.
- (55) Lim, S.; Janzer, A.; Becker, A.; Zimmer, A.; Schüle, R.; Buettner, R.; Kirfel, J. *Carcinogenesis* **2010**, *31*, 512.
- (56) Hayami, S.; Kelly, J. D.; Cho, H.-S.; Yoshimatsu, M.; Unoki, M.; Tsunoda, T.; Field, H. I.; Neal, D. E.; Yamaue, H.; Ponder, B. A. J.; Nakamura, Y.; Hamamoto, R. *Int. J. Cancer* **2011**, *128*, 574.
- (57) Huang, Y.; Greene, E.; Murray Stewart, T.; Goodwin, A. C.; Baylin, S. B.; Woster, P. M.; Casero, R. A. *Proc. Natl. Acad. Sci. U.S.A.* **2007**, *104*, 8023.
- (58) Jin, L.; Hanigan, C. L.; Wu, Y.; Wang, W.; Park, B. H.; Woster, P. M.; Casero, R. A. *Biochem. J.* **2013**, *449*, 459.
- (59) Huang, Y.; Stewart, T. M.; Wu, Y.; Baylin, S. B.; Marton, L. J.; Perkins, B.; Jones, R. J.; Woster, P. M.; Casero Jr, R. A. *Clin. Cancer Res.* **2009**, *15*, 7217.
- (60) Ueda, R.; Suzuki, T.; Mino, K.; Tsumoto, H.; Nakagawa, H.; Hasegawa, M.; Sasaki, R.; Mizukami, T.; Miyata, N. *J. Am. Chem. Soc.* **2009**, *131*, 17536.
- (61) Lynch, J. T.; Harris, W. J.; Somerville, T. C. P. *Expert Opin. Ther. Targets* **2012**, *16*, 1239.
- (62) Stavropoulos, P.; Hoelz, A. *Expert Opin. Ther. Targets* **2007**, *11*, 809.
- (63) Khan, M. N. A.; Suzuki, T.; Miyata, N. *Med. Res. Rev.* **2013**, *33*, 873.
- (64) Schmidt, D. M. Z.; McCafferty, D. G. *Biochemistry* **2007**, *46*, 4408.

- (65) Lee, M. G.; Wynder, C.; Schmidt, D. M.; McCafferty, D. G.; Shiekhattar, R. *Chem. Biol.* **2006**, *13*, 563.
- (66) Ota, Y.; Itoh, Y.; Kaise, A.; Ohta, K.; Endo, Y.; Masuda, M.; Sowa, Y.; Sakai, T.; Suzuki, T. *Angew. Chem.* **2016**, *128*, 16349.
- (67) Khawam, E. A.; Laurencic, G.; Malone, D. A. *Cleve. Clin. J. Med.* **2006**, *73*, 351.
- (68) Kauffman, E. C.; Robinson, B. D.; Downes, M. J.; Powell, L. G.; Lee, M. M.; Scherr, D. S.; Gudas, L. J.; Mongan, N. P. *Mol. Carcinog.* **2011**, *50*, 931.
- (69) Yang, M.; Culhane, J. C.; Szewczuk, L. M.; Jalili, P.; Ball, H. L.; Machius, M.; Cole, P. A.; Yu, H. *Biochemistry* **2007**, *46*, 8058.
- (70) Mimasu, S.; Sengoku, T.; Fukuzawa, S.; Umehara, T.; Yokoyama, S. *Biochem. Biophys. Res. Commun.* **2008**, *366*, 15.
- (71) Binda, C.; Valente, S.; Romanenghi, M.; Pilotto, S.; Cirilli, R.; Karytinis, A.; Ciossani, G.; Botrugno, O. A.; Forneris, F.; Tardugno, M.; Edmondson, D. E.; Minucci, S.; Mattevi, A.; Mai, A. *J. Am. Chem. Soc.* **2010**, *132*, 6827.
- (72) Rodriguez, V.; Valente, S.; Rovida, S.; Rotili, D.; Stazi, G.; Lucidi, A.; Ciossani, G.; Mattevi, A.; Botrugno, O. A.; Dessanti, P.; Mercurio, C.; Vianello, P.; Minucci, S.; Varasi, M.; Mai, A. *MedChemComm* **2015**, *6*, 665.
- (73) Mimasu, S.; Umezawa, N.; Sato, S.; Higuchi, T.; Umehara, T.; Yokoyama, S. *Biochemistry* **2010**, *49*, 6494.
- (74) Ogasawara, D.; Suzuki, T.; Mino, K.; Ueda, R.; Khan, M. N. A.; Matsubara, T.; Koseki, K.; Hasegawa, M.; Sasaki, R.; Nakagawa, H. *Biorg. Med. Chem.* **2011**, *19*, 3702.
- (75) Liang, Y.; Quenelle, D.; Vogel, J. L.; Mascaro, C.; Ortega, A.; Kristie, T. M. *MBio* **2013**, *4*, e00558.
- (76) Ogasawara, D.; Itoh, Y.; Tsumoto, H.; Kakizawa, T.; Mino, K.; Fukuhara, K.; Nakagawa, H.; Hasegawa, M.; Sasaki, R.; Mizukami, T.; Miyata, N.; Suzuki, T. *Angew. Chem. Int. Ed.* **2013**, *52*, 8620.
- (77) Guibourt, N.; Ortega, M. A.; Castro-Palomino, L. J. WO2010084160A1, 2010.
- (78) Guibourt, N.; Ortega, M. A.; Castro-Palomino, L. J. WO2010043721A1, 2010.
- (79) Ortega, M. A.; Castro-Palomino, L. J.; Fyfe, M. C. T. WO2011035941A1, 2011.
- (80) Neelamegam, R.; Ricq, E. L.; Malvaez, M.; Patnaik, D.; Norton, S.; Carlin, S. M.; Hill, I. T.; Wood, M. A.; Haggarty, S. J.; Hooker, J. M. *ACS Chem. Neurosci.* **2012**, *3*, 120.
- (81) Gooden, D. M.; Schmidt, D. M.; Pollock, J. A.; Kabadi, A. M.; McCafferty, D. G. *Bioorg. Med. Chem. Lett.* **2008**, *18*, 3047.
- (82) Schenk, T.; Chen, W. C.; Göllner, S.; Howell, L.; Jin, L.; Hebestreit, K.; Klein, H.-U.; Popescu, A. C.; Burnett, A.; Mills, K.; Casero Jr, R. A.; Marton, L.; Woster, P.; Minden, M. D.; Dugas, M.; Wang, J. C. Y.; Dick, J. E.; Müller-Tidow, C.; Petrie, K.; Zelent, A. *Nat. Med.* **2012**, *18*, 605.
- (83) Maes, T.; Tirapu, I.; Mascaró, C.; Ortega, A.; Estiarte, A.; Valls, N.; Castro-Palomino, J.; Arjol, C. B.; Kurz, G. *J. Clin. Oncol.* **2013**, *31*, e13543.
- (84) Ortega Munoz, A.; Fyfe, M. C. T.; Martinell Pedemonte, M.; Estiarte Martinez, M. d. I. A.; Valls Vidal, N.; Kurz, G.; Castro Palomino Laria, J. C. WO2013057322A1, 2013.
- (85) Johnson, N. W.; Kaspavec, J.; Miller, W. H.; Rouse, M. B.; Suarez, D.; Tian, X. WO2012135113A2, 2012.
- (86) Zheng, Y.-C.; Ma, J.; Wang, Z.; Li, J.; Jiang, B.; Zhou, W.; Shi, X.; Wang, X.; Zhao, W.; Liu, H.-M. *Med. Res. Rev.* **2015**, *35*, 1032.
- (87) Hazeldine, S.; Pachaiyappan, B.; Steinbergs, N.; Nowotarski, S.; Hanson, A.; Casero, R. A.; Woster, P. M. *J. Med. Chem.* **2012**, *55*, 7378.

- (88) Kutz, C. J.; Holshouser, S. L.; Marrow, E. A.; Woster, P. M. *MedChemComm* **2014**, *5*, 1863.
- (89) Prusevich, P.; Kalin, J. H.; Ming, S. A.; Basso, M.; Givens, J.; Li, X.; Hu, J.; Taylor, M. S.; Cieniewicz, A. M.; Hsiao, P.-Y.; Huang, R.; Roberson, H.; Adejola, N.; Avery, L. B.; Casero, R. A.; Taverna, S. D.; Qian, J.; Tackett, A. J.; Ratan, R. R.; McDonald, O. G.; Feinberg, A. P.; Cole, P. A. *ACS Chem. Biol.* **2014**, *9*, 1284.
- (90) Zheng, Y.-C.; Duan, Y.-C.; Ma, J.-L.; Xu, R.-M.; Zi, X.; Lv, W.-L.; Wang, M.-M.; Ye, X.-W.; Zhu, S.; Mobley, D.; Zhu, Y.-Y.; Wang, J.-W.; Li, J.-F.; Wang, Z.-R.; Zhao, W.; Liu, H.-M. *J. Med. Chem.* **2013**, *56*, 8543.
- (91) Hayward, D.; Cole, P. A. *Methods Enzymol.* **2016**, *573*, 261.
- (92) Quin, C.; Robertson, L.; McQuaker, S. J.; Price, N. C.; Brand, M. D.; Hartley, R. C. *Tetrahedron* **2010**, *66*, 2384.
- (93) Benelkebir, H.; Hodgkinson, C.; Duriez, P. J.; Hayden, A. L.; Bulleid, R. A.; Crabb, S. J.; Packham, G.; Ganesan, A. *Biorg. Med. Chem.* **2011**, *19*, 3709.
- (94) Khan, M.; Yi, F.; Rasul, A.; Li, T.; Wang, N.; Gao, H.; Gao, R.; Ma, T. *IUBMB Life* **2012**, *64*, 783.
- (95) Demuth, T.; Berens, M. E. *J. Neurooncol.* **2004**, *70*, 217.
- (96) Day, B.; Stringer, B.; Wilson, J.; Jeffree, R.; Jamieson, P.; Ensbey, K.; Bruce, Z.; Inglis, P.; Allan, S.; Winter, C.; Tolleson, G.; Campbell, S.; Lucas, P.; Findlay, W.; Kadrian, D.; Johnson, D.; Robertson, T.; Johns, T.; Bartlett, P.; Osborne, G.; Boyd, A. *Cancers* **2013**, *5*, 357.
- (97) Sareddy, G. R.; Nair, B. C.; Krishnan, S. K.; Gonugunta, V. K.; Zhang, Q. G.; Suzuki, T.; Miyata, N.; Brenner, A. J.; Brann, D. W.; Vadlamudi, R. K. *Oncotarget* **2013**, *4*, 18.
- (98) Chahal, S. S.; Matthews, H. R.; Bradbury, E. M. *Nature* **1980**, *287*, 76.
- (99) Kidder, B. L.; Hu, G.; Zhao, K. *Genome Biol.* **2014**, *15*, R32.
- (100) Pollock, J. A.; Larrea, M. D.; Jasper, J. S.; McDonnell, D. P.; McCafferty, D. G. *ACS Chem. Biol.* **2012**, *7*, 1221.
- (101) Williams, G. H.; Stoeber, K. *Curr. Opin. Cell Biol.* **2007**, *19*, 672.
- (102) Riedl, S. J.; Shi, Y. *Nat. Rev. Mol. Cell Biol.* **2004**, *5*, 897.
- (103) Kim, C. K.; Kim, T.; Choi, I.-Y.; Soh, M.; Kim, D.; Kim, Y.-J.; Jang, H.; Yang, H.-S.; Kim, J. Y.; Park, H.-K.; Park, S. P.; Park, S.; Yu, T.; Yoon, B.-W.; Lee, S.-H.; Hyeon, T. *Angew. Chem. Int. Ed.* **2012**, *51*, 11039.
- (104) Gao, J.; Liu, X.; Rigas, B. *Proc. Natl. Acad. Sci. U. S. A.* **2005**, *102*, 17207.
- (105) Sankar, S.; Theisen, E. R.; Bearss, J.; Mulvihill, T.; Hoffman, L. M.; Sorna, V.; Beckerle, M. C.; Sharma, S.; Lessnick, S. L. *Clin. Cancer Res.* **2014**, *20*, 4584.
- (106) Theisen, E. R.; Gajiwala, S.; Bearss, J.; Sorna, V.; Sharma, S.; Janat-Amsbury, M. *BMC Cancer* **2014**, *14*, 752.
- (107) Jiang, X.; Wang, X. *Annu. Rev. Biochem.* **2004**, *73*, 87.
- (108) Yang, J.; Liu, X.; Bhalla, K.; Kim, C. N.; Ibrado, A. M.; Cai, J.; Peng, T.-I.; Jones, D. P.; Wang, X. *Science* **1997**, *275*, 1129.
- (109) Zou, Z.-K.; Huang, Y.-Q.; Zou, Y.; Zheng, X.-K.; Ma, X.-D. *Int. J. Mol. Med.* **2017**, *40*, 319.
- (110) Feng, S.; Jin, Y.; Cui, M.; Zheng, J. *Med. Sci. Monit.* **2016**, *22*, 4742.
- (111) Campos, C. B. L.; Paim, B. A.; Cosso, R. G.; Castilho, R. F.; Rottenberg, H.; Vercesi, A. E. *Cytometry Part A* **2006**, *69A*, 515.
- (112) Goodwin, J. T.; Clark, D. E. *J. Pharmacol. Exp. Ther.* **2005**, *315*, 477.
- (113) Clark, D. E. *J. Pharm. Sci.* **1999**, *88*, 815.

- (114) Rodríguez-Rodríguez, C.; Sánchez de Groot, N.; Rimola, A.; Álvarez-Larena, Á.; Lloveras, V.; Vidal-Gancedo, J.; Ventura, S.; Vendrell, J.; Sodupe, M.; González-Duarte, P. *J. Am. Chem. Soc.* **2009**, *131*, 1436.
- (115) Cascini, G. L.; Niccoli Asabella, A.; Notaristefano, A.; Restuccia, A.; Ferrari, C.; Rubini, D.; Altini, C.; Rubini, G. *BioMed. Res. Int.* **2014**, *2014*, 7.
- (116) Arotsky, J.; Darby, A. C.; Hamilton, J. B. A. *J. Chem. Soc., Perkin Trans. 2* **1973**, 595.
- (117) Li, L.; Liu, W.; Mu, X.; Mi, Z.; Li, C.-J. *Nat. Protoc.* **2016**, *11*, 1948.
- (118) Bernardini, R.; Oliva, A.; Paganelli, A.; Menta, E.; Grugni, M.; Munari, S. D.; Goldoni, L. *Chem. Lett.* **2009**, *38*, 750.
- (119) Achilli, C.; Ciana, A.; Fagnoni, M.; Balduini, C.; Minetti, G. *Cent. Eur. J. Chem.* **2013**, *11*, 137.
- (120) Gupta, S.; Chaudhary, P.; Seva, L.; Sabiah, S.; Kandasamy, J. *RSC Adv.* **2015**, *5*, 89133.
- (121) Lockley, W. J. S.; McEwen, A.; Cooke, R. *J. Labelled Compd. Radiopharmaceut.* **2012**, *55*, 235.
- (122) Kim, H.-K.; Lee, A. *Tetrahedron Lett.* **2016**, *57*, 4890.
- (123) Lyle, M. P. A.; Draper, N. D.; Wilson, P. D. *Org. Biomol. Chem.* **2006**, *4*, 877.
- (124) Minuth, T.; Irmak, M.; Groschner, A.; Lehnert, T.; Boysen, M. M. K. *Eur. J. Org. Chem.* **2009**, *2009*, 997.
- (125) Concellón, J. M.; Rodríguez-Solla, H.; Simal, C. *Org. Lett.* **2007**, *9*, 2685.
- (126) Wray, V. *Prog. Nucl. Magn. Reson. Spectrosc.* **1979**, *13*, 177.
- (127) Davi, M.; Lebel, H. *Chem. Commun.* **2008**, 4974.
- (128) Mühlman, A.; Lindberg, J.; Classon, B.; Unge, T.; Hallberg, A.; Samuelsson, B. *J. Med. Chem.* **2001**, *44*, 3407.
- (129) Guillemain, G.; Boussin, F. D.; Croitoru, J.; Franck-Duchenne, M.; Le Grand, R.; Lazarini, F.; Dormont, D. *J. Neurosci. Res.* **1997**, *49*, 576.

Chapter 3

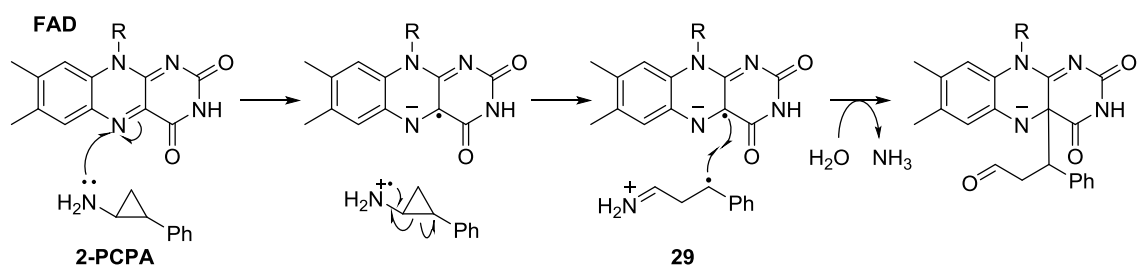
Synthesis and biological evaluation of metallocene derivatives of cyclopropylamines

3.1 Introduction

3.1.1 Oxidative ring-opening of cyclopropylamines

Cyclopropylamines are found in a broad variety of biologically active compounds, such as the broad-spectrum antibiotics Ciprofloxacin, Moxifloxacin and Trovafloxacin. As mentioned in the previous chapter, *trans*-2-phenylcyclopropylamine (2-PCPA) and its derivatives were reported to be LSD1 inhibitors, and they displayed potential as anticancer agents since two active clinical trials are currently in place. Over 200 patented pharmaceutically relevant molecules contain a cyclopropylamine moiety,¹ therefore much attention was drawn to the synthesis and reactivity of these moieties in recent years.^{2,3}

Cyclopropylamines also display interesting reactivity as they can undergo irreversible ring-opening reactions via a single-electron transfer mechanism to yield a β -carbon radical iminium ion **29** (Scheme 14). This ring-opening process is important in biological systems; for example, 2-PCPA inhibits LSD1 by oxidation of the cyclopropylamine nitrogen by FAD in the active site, subsequent ring-opening to **29** and covalent attachment to FAD (Scheme 14). In these systems it has been postulated that the ring-opened **29** reacts irreversibly with FAD in the active site to inactivate the enzyme.⁴ Their ability to undergo this ring-opening process has also seen them used as tools for studying biological amine-oxidation.^{5,6} However, to date, these oxidative ring-opening processes have not been greatly utilised as a tool in synthetic chemistry, but the process has been studied by several groups.

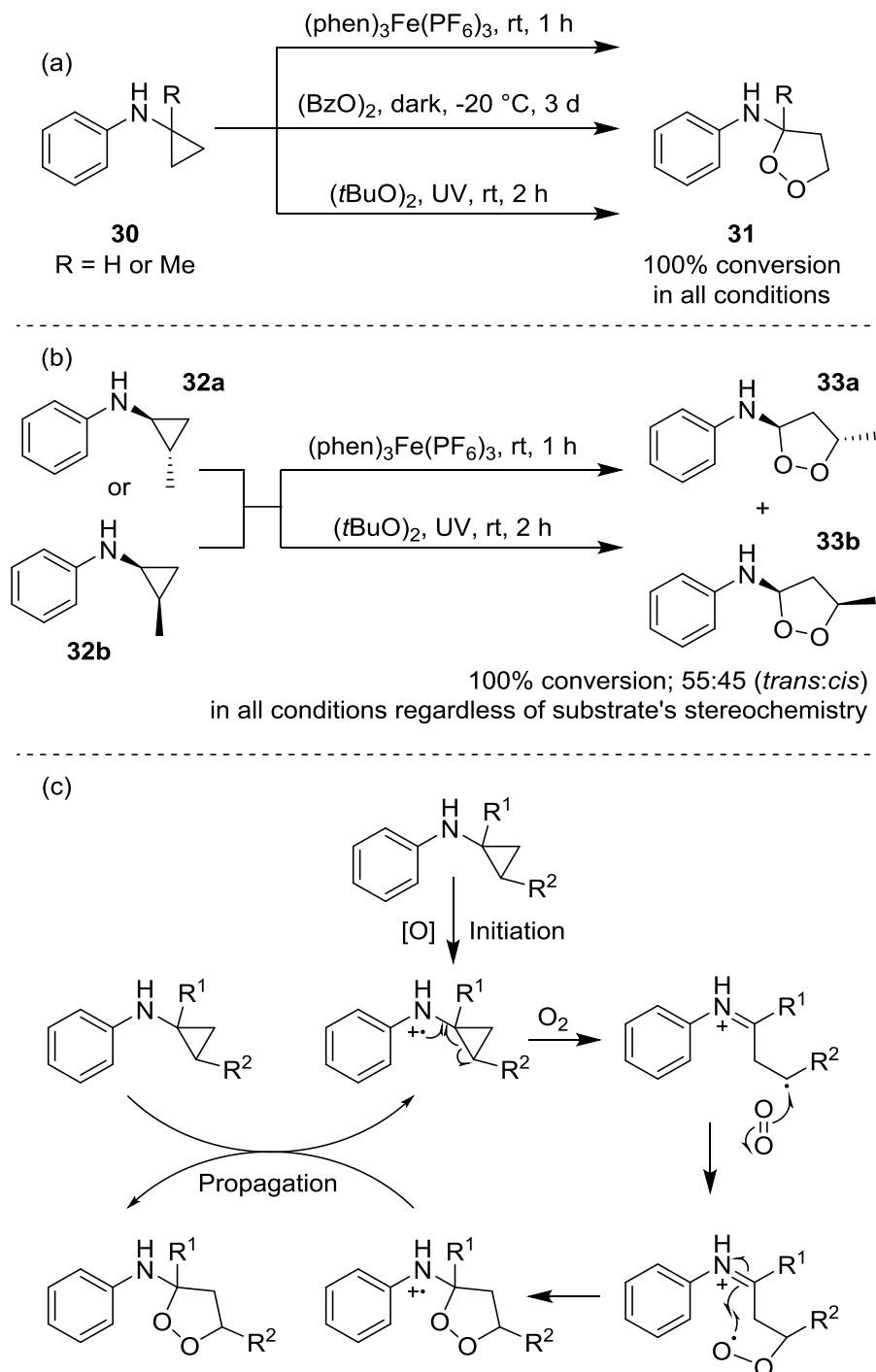


Scheme 14: An example of LSD1 inhibition through chemical modification of FAD by 2-PCPA. FAD induced single-electron oxidation on 2-PCPA nitrogen, and hence ring-opening of 2-PCPA occurs and the resulting benzylic radical covalently fused to FAD.

The single-electron oxidation of cyclopropylamine nitrogen can be achieved enzymatically (as seen in LSD1), chemically, photochemically and electrochemically.⁷ Wimalasena et al. reported the autocatalytic radical ring-opening of *N*-cyclopropyl-*N*-phenylamines **30** under aerobic conditions in the presence of (phen)₃Fe(PF₆)₃ (single-electron oxidant), benzoyl peroxide (hydrogen-abstrating reagent) or *t*-butyl peroxide/UV light (Scheme 15a).⁸ As a result of the oxidative ring-opening, 1,2-dioxolanes **31** were formed in all three conditions in high conversion, however isolated yields could not be accurately determined due to their instability during purification. When a methyl substituent was placed on a different carbon atom from the amine nitrogen (**32a** or **32b**), a mixture of dioxolane diastereomers **33a** and **33b** in a 55:45 (*trans*:*cis*) ratio was obtained, regardless of the substrate's stereochemistry (Scheme 15b).

The reaction was proposed to be initiated by a single-electron oxidation on the amine nitrogen facilitated by one of the three conditions (Scheme 15c). The formation of radical cation on the nitrogen induces ring-opening to the cyclopropane ring, followed by reaction with molecular oxygen to form the 1,2-dioxolane ring. The final step is an

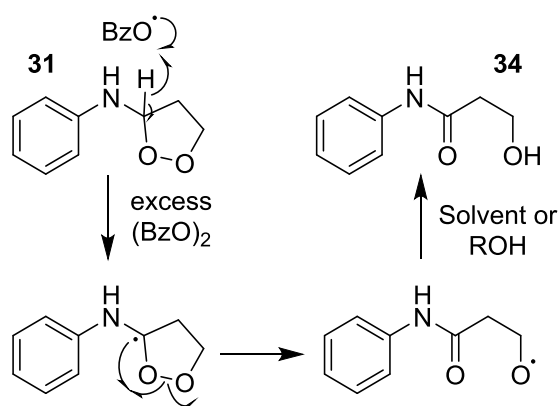
extraction of electron from the *N*-cyclopropyl-*N*-phenylamine substrate in order to propagate the cycle.



Scheme 15: (a) Autocatalytic radical ring-opening of *N*-cyclopropyl-*N*-phenylamines under aerobic conditions using different oxidants.⁸ Isolated yields of 1,2-dioxolanes could not be accurately determined due to instability during purification process. (b) When a

1,2-disubstituted cyclopropylamine was treated with the reaction condition, a mixture of diastereomers were obtained with a dr of 55:45 (*trans*:*cis*), regardless of the stereochemistry of the substrate. (c) Mechanism of oxidative ring-opening of *N*-cyclopropyl-*N*-phenylamines.

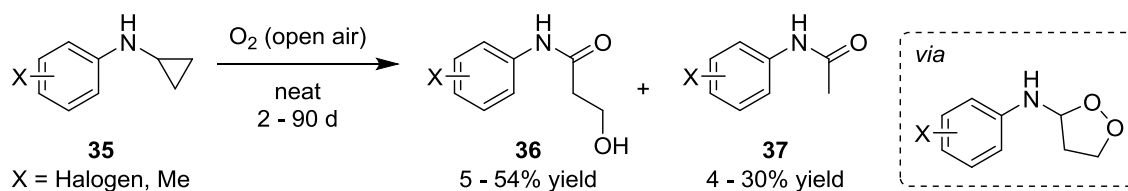
Interestingly, the 1,2-dioxolane product **31** underwent ring-opening and formed β -hydroxyamide **34** when excess benzoyl peroxide was used (Scheme 16). The excess benzoyl peroxide was proposed to extract the α -hydrogen from 1,2-dioxolane **31**, which led to the formation of a carbonyl bond and homolytic cleavage of the O–O bond. Subsequently, an extraction of proton from the solvent furnished the β -hydroxyamide **34**.



Scheme 16: Presence of excess $(\text{BzO})_2$ led to ring-opening of 1,2-dioxolane **31** and formation of β -hydroxyamide **34**.⁸

In a separate study conducted by Blackburn et al., the formation of β -hydroxyamides **36** was also observed even when neat *N*-cyclopropylanilines **35** were left in open air for prolonged period (2 – 90 days) without any chemical treatment (Scheme 17).⁹ The reaction was also proposed to proceed via an 1,2-dioxolane intermediate, however in this case, a small amount of the acetamide **37** was also formed. A control experiment was conducted where a mixture of β -hydroxyamide and *N*-cyclopropylaniline with different substituents on each phenyl ring was left in open air. As a result, the β -hydroxyamide

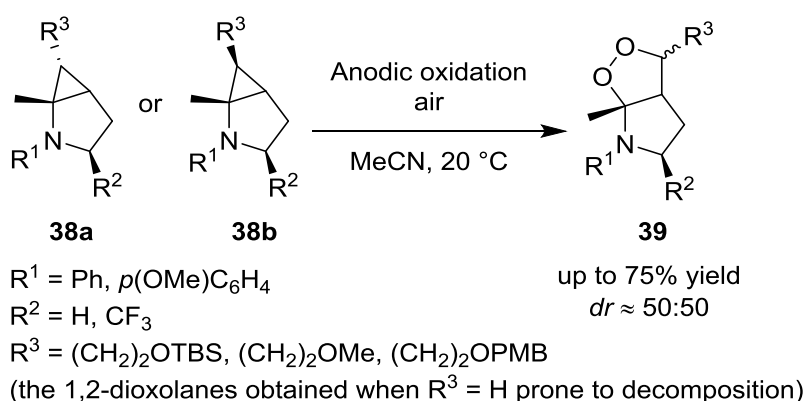
substrate remained intact, while the *N*-cyclopropylaniline gave rise to its corresponding β -hydroxyamide and acetamide. The outcome of this control experiment suggests that the formation of acetamide is derived from the reaction intermediate, rather than the deformylation of the β -hydroxyamide product. While this study possessed limited synthetic practicality due to the prolonged time needed in the absence of accelerants, it provided insight into the stability of these *N*-cyclopropylanilines and their susceptibility towards oxidation in open air.



Scheme 17: Oxidative ring-opening of *N*-cyclopropylanilines occurred slowly in open air without any chemical treatment.⁹ Three conditions were attempted and they all gave **36** and **37** in varied amount: (i) rt, 150 W lamp (ii) 50 °C, lab lighting (iii) rt, lab lighting.

Aiming to gain further insight into the reaction and to develop a more environmentally friendly method, Six and co-workers reported the electrochemical oxidative ring-opening of cyclopropylamines **38a/38b** to form 1,2-dioxolanes **39** (Scheme 18).^{10,11} In order to facilitate the single-electron oxidation of the amine nitrogen, the electrolyses were conducted in divided cells at constant potential values. The generated aminium cation radicals could then react with oxygen introduced by bubbling air through the anodic compartment. The electrolyses were followed by in situ cyclic voltammetry to ensure the consumption of cyclopropylamine substrates and formation of 1,2-dioxolane products **39**. In this study, several analogues of 1,2-dioxolane were found to be highly unstable and prone to decompose swiftly. Similar issues were encountered by Wimalasena et al. mentioned earlier, in which isolation yields could not be determined

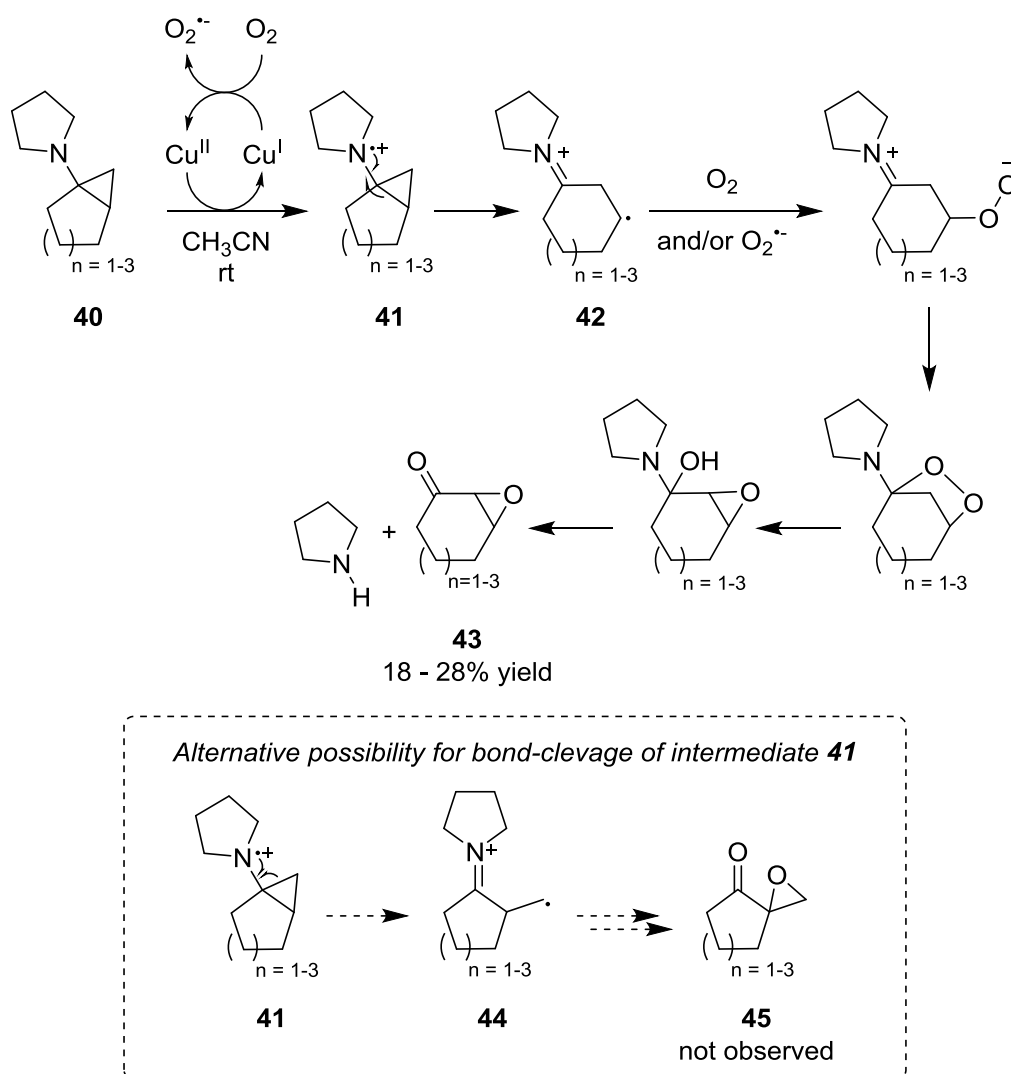
accurately due to decomposition during purification.⁸ Even though pure samples could be obtained in this case, significant loss of material was observed after flash chromatography (on silica gel or neutral alumina gel) or HPLC, therefore posing a challenge to synthetic utility. Nevertheless, the obtained 1,2-dioxolanes demonstrated moderate antimalarial activities against chloroquine-resistant FcB1 strains of *Plasmodium falciparum* ($IC_{50} = 1 - 13 \mu\text{M}$).



Scheme 18: Electrochemical approach to oxidatively ring-open cyclopropylamines and form 1,2-dioxolanes.^{10,11}

Itoh et al. reported one of the earliest works on the oxidative ring-opening of cyclopropylamines (Scheme 19).¹² The treatment of fused-cycloalkyl-cyclopropylamine **40** with CuCl_2 and oxygen led to the ring-opening and expansion of the cycloalkyl ring followed by subsequent oxidation to yield the epoxy ketone **43** in modest yield. Other copper halides and cobalt halides were also compatible with the reaction, however the reaction did not proceed when iron(III) chloride was used. After the single-electron oxidation of amine nitrogen, two possible bonds of intermediate **41** may undergo cleavage to give the ring-expanded **42** or branched-cycloalkane **44**. As epoxy ketone **43** was obtained as the sole product, it was postulated that the formation of intermediate **44** did not proceed. This data may suggest that radical intermediate **42** is more stable than **44** as

the extra adjacent alkyl chain provides further stabilisation to the carbon radical. Note that even though this reaction has 1,2-dioxolane as intermediate, epoxy ketone **43** was formed instead of a β -hydroxyamide or acetamide as observed from other studies. This could be due to the fact that the amine carbon in cyclopropane is tertiary instead of secondary, and hence no acidic proton to be liberated at the α position of 1,2-dioxolane. As a result, carbonyl formation and elimination of pyrrolidine occurred after the O–O bond cleavage in the 1,2-dioxolane.



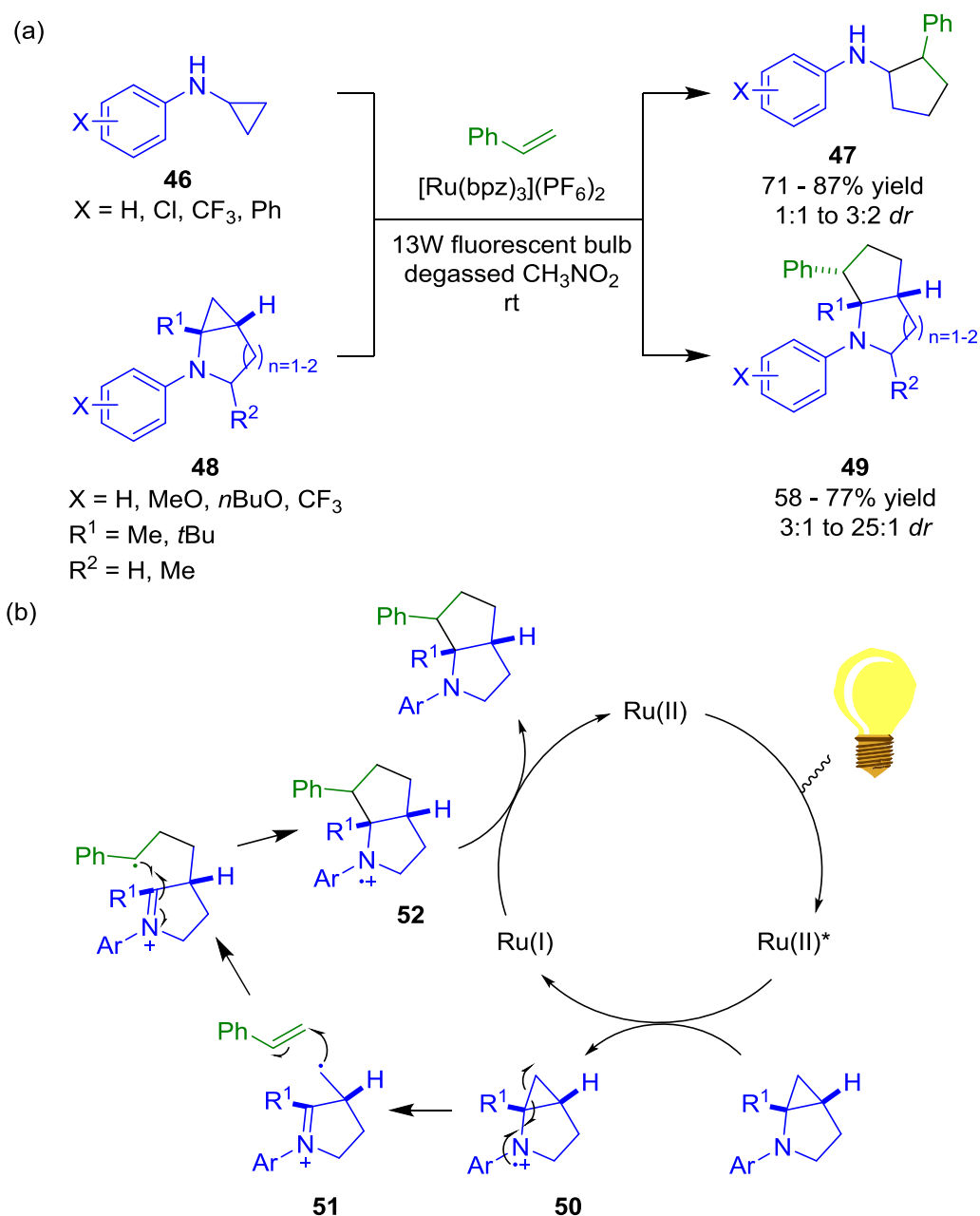
Scheme 19: *CuCl₂-catalysed oxidative ring-opening of fused-cycloalkyl-cyclopropylamine **40**, followed by ring-expansion and subsequent oxidation to yield epoxy ketone **43**.¹²*

Cyclopropylamines are susceptible to oxidative ring-opening which leads to the formation of distonic radical cation species, for instance **29** in Scheme 14 and **42** in Scheme 19. The examples demonstrated so far show that these distonic ion species can react with molecular oxygen to yield 1,2-dioxolanes, subsequently forming β -hydroxyamides, acetamides or epoxy ketones. Instead of allowing the distonic radical cation to react with molecular oxygen, Zheng and co-workers have demonstrated that this distonic ion species can be generated through photocatalysis, then trapped with a terminal olefin in a [3 + 2] cycloaddition to form five-membered carbocycles **47** or **49** (Scheme 20).¹³ In this study, the photocatalyst [Ru(bpz)₃](PF₆)₂ acts as the single-electron oxidant for amine nitrogen upon irradiation with visible light. During the optimisation of reaction conditions, it was discovered that degassing solvent is crucial for obtaining high reaction yield as molecular oxygen may intercept the distonic radical cation to form 1,2-dioxolane. The use of a 13W fluorescent light source was also found to be crucial to achieve high reaction yield. Zheng and co-workers also pointed out that the phenyl ring on cyclopropylamine nitrogen is necessary for the single-electron oxidation, as it lowers the redox potential of the amine nitrogen.

Initially, the reaction was conducted using monocyclic cyclopropylamines **46** with different substituted phenyl rings to give the product in good yields (71 – 87%) but poor diastereoselectivity (1:1 to 3:2) (Scheme 20a). The reaction conditions were then applied to bicyclic cyclopropylamines **48**, which were expected to exert steric hindrance during cycloaddition and hence increase the diastereoselectivity. The diastereoselectivity was indeed improved (3:1 to 25:1), however the reaction yield was slightly decreased (58 – 77% yield) (Scheme 20a). Notably, when R¹ on the cyclopropane was a *t*-Bu group instead of methyl group, an excellent diastereoselectivity of 25:1 was obtained, but with a poor yield of 28% (64% yield based on recovered cyclopropylamine substrate). This

result highlights the need to introduce steric hindrance in order to provide good diastereoselectivity in this reaction. Instead of using styrene-based substrates, the study also demonstrated that the photocatalytic condition can be extended to terminal olefins substituted with electron-withdrawing groups (52% yield, 1:1 *dr*) and conjugated dienes (40% yield, 2:1 *dr*). However, the reaction did not proceed using tertiary cyclopropylamines or internal olefins.

Mechanistically, upon irradiating the Ru(II) photocatalyst with 13W fluorescent light, the excited Ru(II)* species extracts an electron from the cyclopropylamine nitrogen and is concomitantly reduced to Ru(I). This results in the formation of a radical cation on the amine nitrogen **50** and hence subsequent ring-opening of the cyclopropane. The generated distonic cation radical **51** can then be added to an olefin substrate in a Giese reaction fashion. After the ring-formation is completed, the resulting nitrogen radical cation **52** extracts an electron from Ru(I), therefore allowing the catalytic cycle to continue.

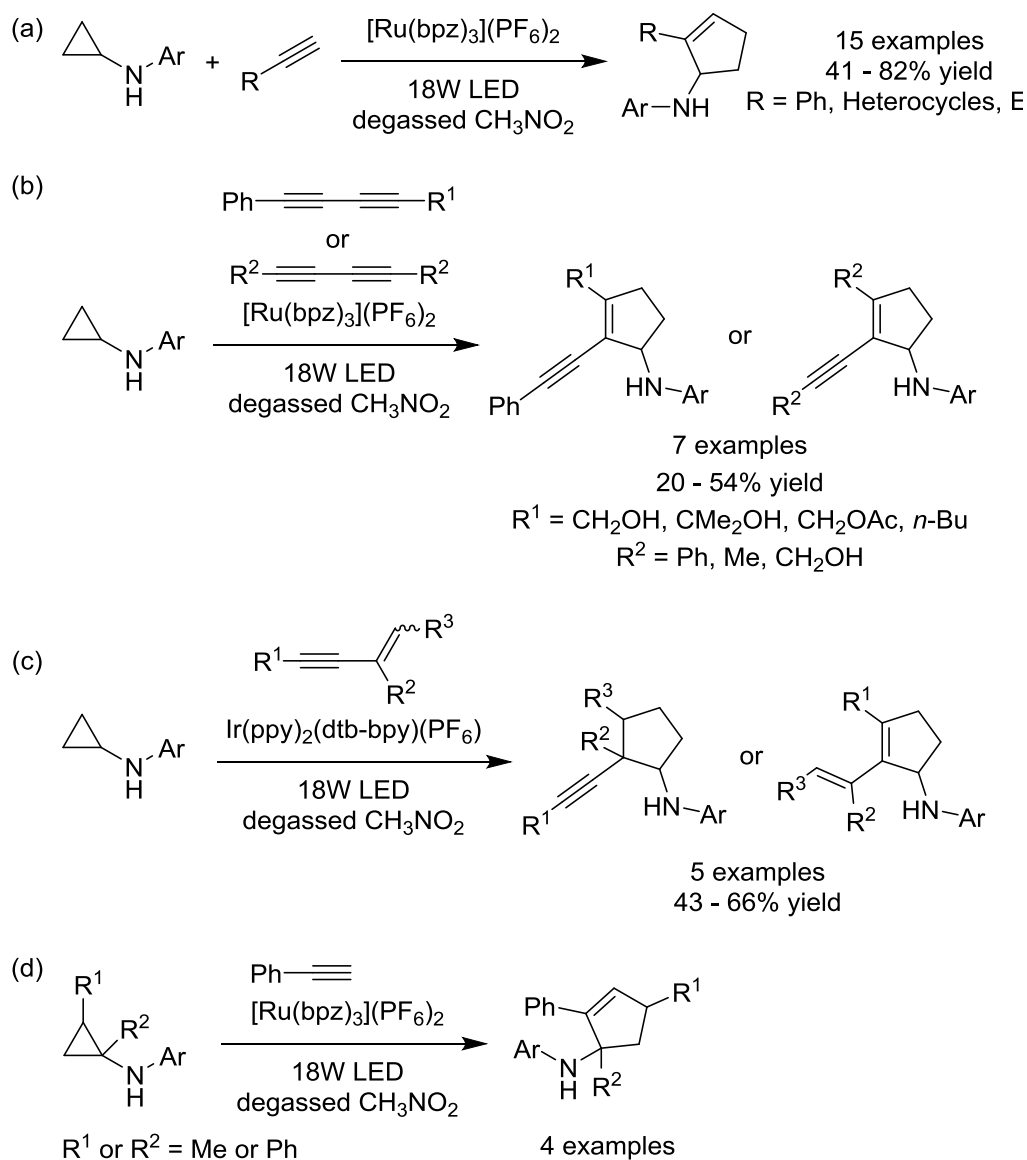


Scheme 20: (a) $[3 + 2]$ Cycloaddition of monocyclic and bicyclic cyclopropylamines with olefins under visible-light photocatalysis.¹³ (b) Proposed catalytic cycle.

In a separate study, Zheng and co-workers have demonstrated that the photocatalytic cycloaddition of cyclopropylamines can be extended to terminal alkynes (which have a lower reactivity), however a stronger light source of 18W LED was required to obtain higher yields (Scheme 21a).⁷ Terminal alkynes with various aromatic rings, heterocycles and electron-withdrawing groups were tolerated, while alkyl-

substituted terminal alkynes and internal alkynes were inert under the optimised conditions.

In order to further explore the substrate scope in this photocatalytic cycloaddition, Zheng and co-workers extended the scope to conjugated alkyne substrates, such as diynes and enynes (Scheme 21b-c).¹⁴ Moderate yields were obtained using symmetrical or asymmetrical diynes (Scheme 21b). In the case of asymmetrical diynes where one alkyne terminal was occupied with phenyl ring, the cycloaddition with cyclopropylamines occurred on the adjacent alkyne regioselectively. In the case of enynes, moderate yields were also obtained, but an issue of chemoselectivity became apparent (Scheme 21c). Generally within an enyne, the cycloaddition occurred on the olefin moiety provided minimal steric hindrance was present around the olefin. In the examples where sterically hindered olefins were employed, the cycloaddition with cyclopropylamines would then occur on the alkyne moiety. Lastly, substituted cyclopropylamines were also investigated as part of the substrate scope (Scheme 21d). Consistent with previous findings, tertiary cyclopropylamines failed to participate in cycloaddition with terminal alkynes. Substitution of a methyl group on any cyclopropane carbon was tolerated – giving the products in moderate yields.



Scheme 21: Photocatalytic [3 + 2] cycloaddition of *N*-arylcyclopropylamines with (a) terminal alkynes;⁷ (b) asymmetric and symmetric diynes;¹⁴ (c) enynes;¹⁴ (d) Photocatalytic [3 + 2] cycloaddition of substituted *N*-arylcyclopropylamines with terminal alkynes.¹⁴

Based on literature record, addition of external oxidants or an electrochemical approach was required to oxidatively ring-open cyclopropylamines in a facile manner. To date, cyclopropylamines with redox active organometallic moieties have been scarcely

studied, therefore we were intrigued to investigate the stability, reactivity and also the medical application of these derivatives.

3.1.2 Application of ferrocene in medicinal chemistry

Traditionally, organometallic complexes were perceived as toxic, unstable, and incompatible with aqueous or atmospheric environments. While this may be true in many cases, organometallic complexes that are non-toxic and stable in air or water do commonly exist. In fact, these stable organometallic complexes have gained attention in the field of medicinal chemistry, as they can enhance existing drug activity in different ways. In general, organometallic complexes are relatively lipophilic, therefore they can assist in drug delivery across cell membrane or blood brain barrier (BBB).¹⁵ Organometallic complexes also exhibit structural diversity that is not observed in hydrocarbon molecules, such as square planar, trigonal bipyramidal and octahedral geometry. This provides extra scope for SAR studies. Furthermore, the charge of the metal species can also vary depending on the cellular environment, and this may provide some control over drug activity or selectivity.¹⁶ The pharmacokinetic properties and cytotoxicities of the drugs can also be regulated through ligand hydrolysis rate by rational ligand design.¹⁷

Ferrocene is a redox-active metallocene composed of an Fe(II) core sandwiched between two cyclopentadienes, and its derivatives have been reported in different medical applications, such as a kinase inhibitor,¹⁸ a HDAC inhibitor,¹⁹ an antimalarial agent,²⁰ and an anticancer agent.²¹ Ferrocene is characterised by its capability to undergo single-electron oxidation, forming a ferrocenium cation – the redox reaction ($\text{Fe}^{2+} \leftrightarrow \text{Fe}^{3+}$) is reversible for most ferrocene derivatives.²¹ This unique reversible redox activity of

ferrocene could be harnessed to improve existing drug activity – an example of such an approach is now discussed.

In two-thirds of breast cancer patients, the tumorigenesis is attributed to the binding of estrogen (predominantly estradiol) with the alpha form of estrogen receptor ($ER\alpha$). This population of patients are classified as $ER(+)$ as they are hormone-dependent, while those patients who are hormone-independent are described as $ER(-)$. Tamoxifen (Figure 25a), which is a selective estrogen receptor modulator (SERM), has been clinically administered to $ER(+)$ breast cancer patients. Tamoxifen itself is a prodrug which releases hydroxytamoxifen (Figure 25a) to competitively bind to $ER\alpha$. Unfortunately, tamoxifen is not effective for $ER(-)$ due to the lack of $ER\alpha$ for binding. Even in the treatment for $ER(+)$ patients, expression of $ER\alpha$ may be progressively downregulated under treatment which renders the drug ineffective eventually.

Ferrocifens is an organometallic derivative of hydroxytamoxifen in which the β -phenyl ring is replaced with ferrocene (Figure 25a). With the introduction of the ferrocenyl moiety, ferrocifen was found to have a higher value of $\log P_{o/w}$ (4.3 – 4.5) compared to hydroxytamoxifen (3.2 – 3.4) and estradiol (3.5), indicating that it has superior cell permeability compared to hydroxytamoxifen and estradiol.²² In MCF7 cells which are $ER(+)$, the antiproliferative effect of ferrocifen was approximately 1.7-fold stronger than hydroxytamoxifen while ferrocene alone did not display any activity.²²

Interestingly, ferrocifen also displayed an antiproliferative effect on $ER(-)$ cell line MDA-MBA-231 which is immune to tamoxifen due to the lack of $ER\alpha$.²² This implies that ferrocifen possesses a secondary action other than being an antiestrogen. Through electrochemical experiments, Jaouen and co-workers proposed that the secondary action is attributed to the redox nature of ferrocenyl moiety and the conjugated

system.²³ These factors convert ferrocifen into a highly electrophilic quinone methide, which is susceptible to nucleophilic addition of glutathione (GSH) and nucleobases (Figure 25b), hence inducing cytotoxicity.

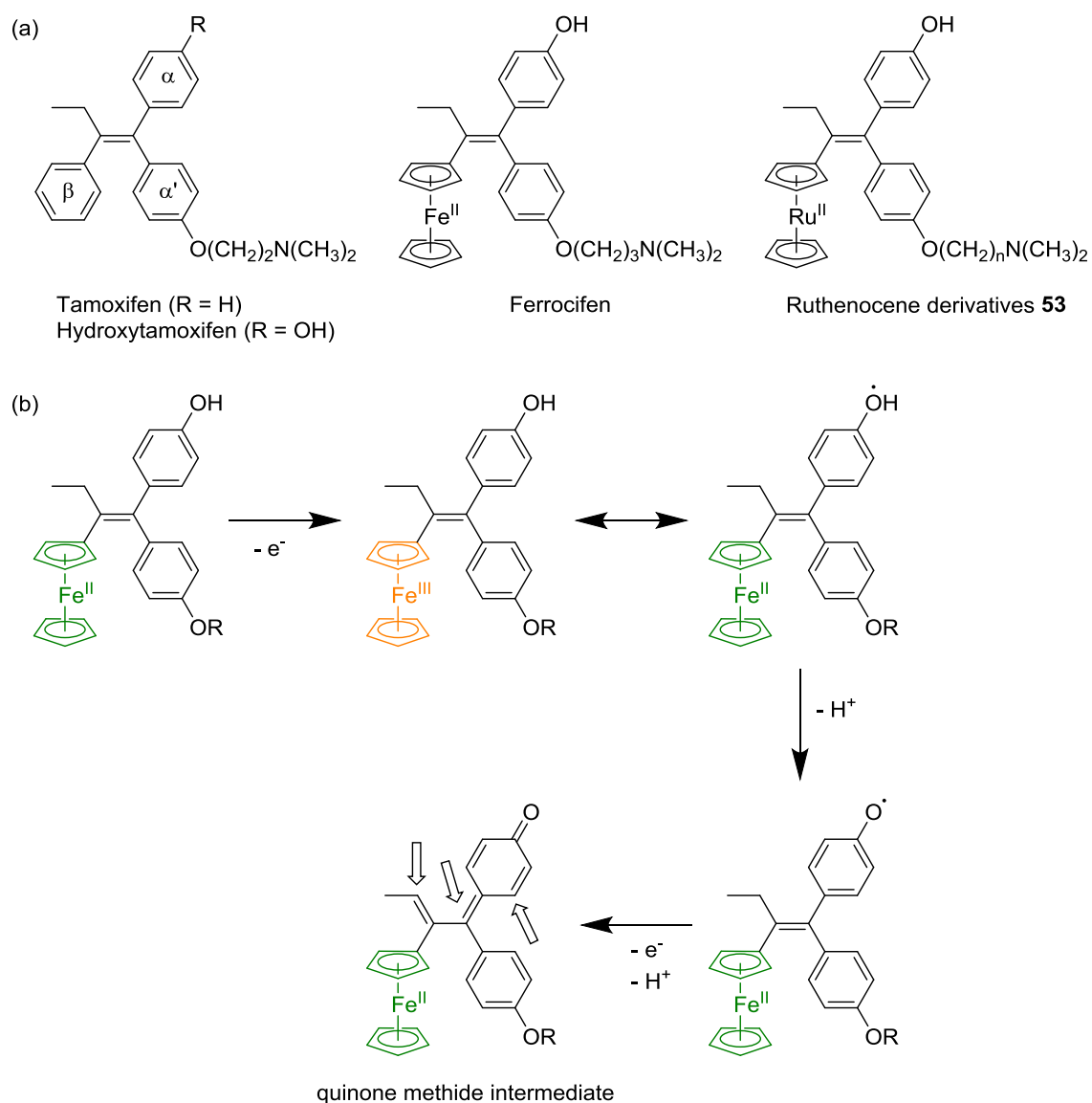


Figure 25: (a) SERMs: Tamoxifen, hydroxytamoxifen, ferrocifen and ruthenocene derivatives of hydroxytamoxifen **53**. (b) In ferrocifen, the redox active ferrocenyl moiety and conjugated system give rise to quinone methide intermediate which is prone to nucleophilic addition at positions indicated by arrows.

Since ruthenium is placed below iron in the periodic table, it was hypothesised that the ruthenocene derivatives of tamoxifen (**53**, Figure 25) could be easily oxidised therefore increasing antiproliferative effect on breast cancer cells. Jaouen and co-workers showed that the ruthenocene derivatives **53** indeed exhibited improved antiproliferative effect on ER(+) MCF7 cells compared to hydroxytamoxifen.²⁴ However unlike ferrocifen, the ruthenocene derivatives **53** did not display an antiproliferative effect on ER(-) MDA-MBA-231 cells, suggesting that the **53** may possess the antiestrogen nature of tamoxifen but not the cytotoxicity of ferrocifen. While ferrocene undergoes reversible redox reaction, electrochemical experiments revealed that the ruthenocenyl moiety was oxidised irreversibly and the resulting ruthenocenium species was unstable. Even though **53** only inhibits proliferation in ER(+) cells, it could still be useful in radioimaging for these cells due to the availability of γ -emitting isotopes ^{97}Ru and ^{103}Ru .²⁴

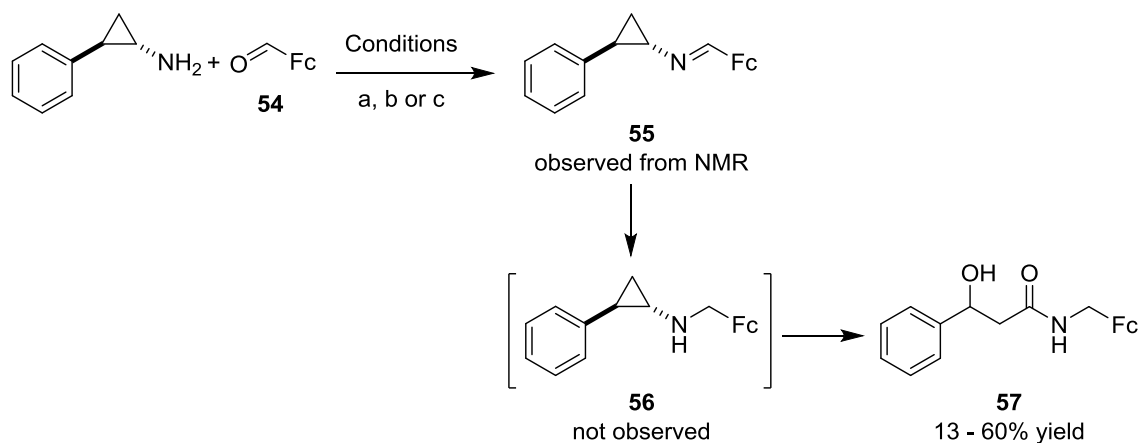
While organometallic derivatives of many structures are known, none (or few) are known for cyclopropylamine-based compounds. Since organometallics such as ferrocene has demonstrated redox activity, we were intrigued of the possibility for the catalytic ring-opening of cyclopropylamine in such derivatives.

3.2 Aim and research plan

As mentioned in the previous chapter sections 2.1.5 and 2.1.6, LSD1 inhibition using 2-PCPA analogues has attracted attention in the field of cancer research, especially two of the *N*-alkylated 2-PCPA derivatives are currently in clinical trials. Inspired by the potential of 2-PCPA in cancer treatment, and the utility of ferrocene in drug discovery, we originally aimed to prepare ferrocene derivatives of 2-PCPA. As a precursor to this comprehensive study, ferrocenecarboxaldehyde **54** and 2-PCPA were subjected to several

reductive amination conditions, however a ring-opened β -hydroxyamide **57** was obtained instead of the desired *N*-ferrocenylmethylcyclopropylamine **56** (Scheme 22).²⁵ Nevertheless, the formation of amine **56** was proposed as an intermediate because the C=N double bond in imine **55** was found to be reduced in amide **57**. Although the formation of β -hydroxyamide was similar to that in the study from Wimalasena et al.,⁸ this observation was unexpected due to the absence of external oxidant for the single-electron oxidation of amine nitrogen. Therefore, it was proposed that the ferrocene moiety acted as an internal oxidant to remove single electron from amine nitrogen, similar to that in ferrocifen. Furthermore, a study on dehydrogenative Heck reaction conducted by Pi et al. demonstrated that in the absence of external oxidant, the ferrocene substrates can oxidise the reduced Pd(0) catalyst back to Pd(II) and hence promote the catalytic cycle.²⁶

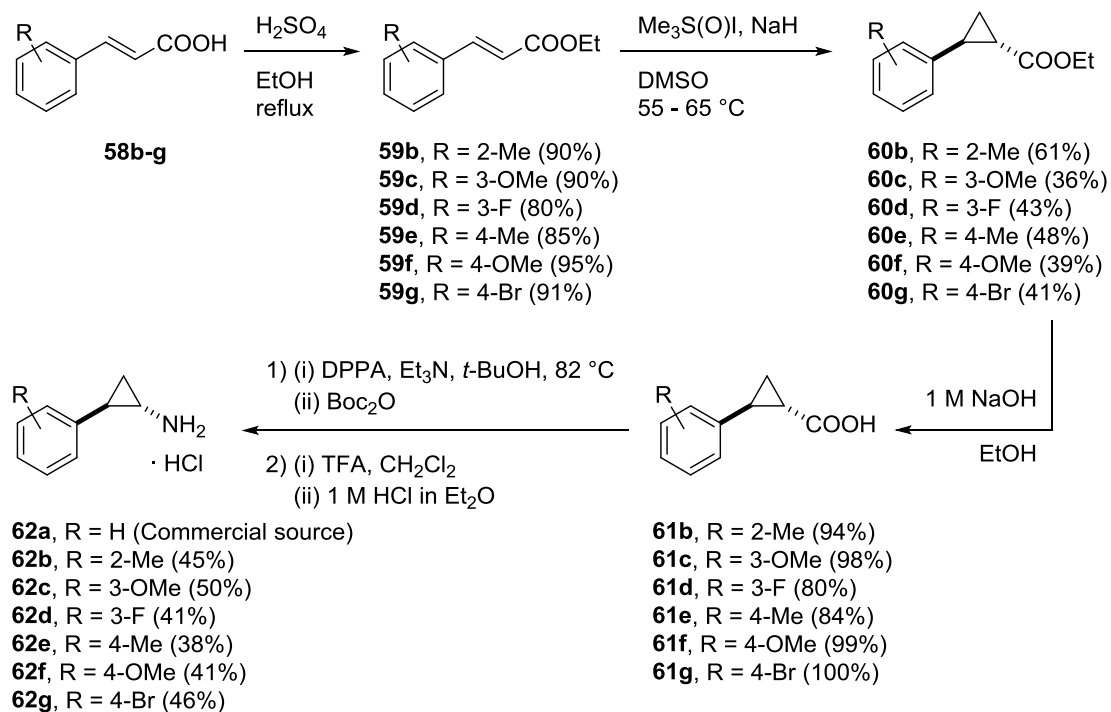
In this study, we aim to couple 2-PCPA derivatives with redox active metallocenes (such as ferrocene and ruthenocene) to both create medicinally relevant compounds and investigate the fundamental activity of these systems. This investigation should lead to a better understanding of the catalytic ring-opening process and the impact on bioactivity or organometallic cyclopropylamines. Firstly, the use of ferrocene as internal oxidant will be extended to other 2-PCPA derivatives with different substituents on the aromatic ring at various positions. In order to investigate the role of stable radical intermediate in the reaction, the reaction condition will be applied to cyclopropylamine which lacks of an aryl ring to stabilise the ring-opened radical cation intermediate. Lastly, ruthenocene derivative of 2-PCPA will be synthesised and subjected to LSD1 and MAOs inhibition assay to determine its potency and selectivity.



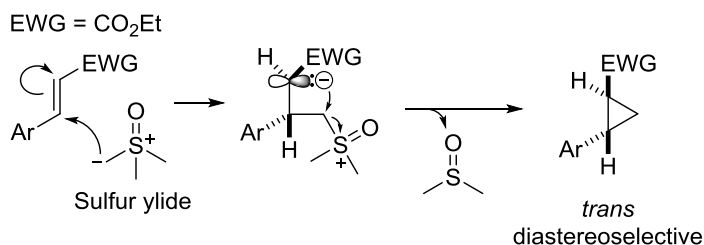
Scheme 22: Preliminary observation of ferrocenyl 2-PCPA ring-opening. Conditions: (a) (i) MgSO_4 , CH_2Cl_2 ; (ii) NaBH_4 , MeOH ; (b) Bu_3SnH , SiO_2 ; (c) (i) $\text{NaBH}(\text{OAc})_3$, 1,2-dichloroethane; (ii) LiBH_4 , EtOH . NaBH_3CN was attempted as reducing agent however neither amine **56** nor amide **57** was obtained.²⁵

3.3 Results and discussion

3.3.1 Preparation of 2-PCPA derivatives



Mechanism of Corey-Chaykovsky cyclopropanation



Scheme 23: Stepwise preparation of 2-PCPA derivatives with different substituents on phenyl ring.

While 2-PCPA is commercially available, 2-PCPA analogues with different substituents were prepared in a multi-step sequence (Scheme 23). Firstly, cinnamic acids **58b-g** underwent acid-catalysed esterification to yield ethyl cinnamates **59b-g** in excellent yields. In the ¹H NMR of ethyl cinnamates **59b-g**, the signals for OCH₂CH₃ can be clearly observed at approximately 4.27 (q, 2H) and 1.34 (t, 3H) ppm. The cyclopropyl

ring of **60b-g** was then constructed on the olefin of **59b-g** through Corey–Chaykovsky cyclopropanation. Sulfur ylide was generated through the deprotonation of trimethylsulfoxonium iodide with NaH, it was then added to the olefin moiety of **59b-g** and DMSO was eliminated during ring-closure. As a result of the cyclopropanation, the olefin proton signals in ^1H NMR disappeared (doublets at approximately 7.60 and 6.40 ppm), while cyclopropane proton signals were observed as multiplets in the aliphatic region (approximately 2.52 – 2.48, 1.92 – 1.88, 1.63 – 1.59 and 1.28 ppm, 1H for each multiplet).

Based on the mechanism of Corey–Chaykovsky cyclopropanation (Scheme 23), the use of an (*E*)-olefin substrate moulds the *trans* diastereoselectivity in the cyclopropane product. After the nucleophilic attack of the sulfur ylide to the olefin substrate, bond rotation to place the ester group *syn* to the aromatic ring is energetically undesirable due to steric hindrance, therefore *cis*-diastereomers of the cyclopropanes were not obtained. Furthermore, the ^1H NMR spectra of cyclopropanes **60b-g** were consistent with the literature where the *trans*-cyclopropanes were reported (except **60d** which was not reported in the literature).^{27,28}

This was followed by basic hydrolysis of **60b-g** to yield carboxylic acids **61b-g** (Scheme 23). Apart from the apparent change in physical appearance (from liquid to solid), the ^1H NMR spectra of **61b-g** lacked of signals for the OCH_2CH_3 moiety from the substrate (quartet at around 4.17 ppm and triplet at around 1.28 ppm), therefore indicating that the ester moiety was successfully hydrolysed.

The hydrochloride salts of 2-PCPA derivatives **62b-g** were obtained after Curtius rearrangement of **61b-g** with *t*-BuOH, acidic deprotection of the *N*-Boc-group and acidic salt precipitation (Scheme 23). Treatment of carboxylic acids **61b-g** led to the formation

of their corresponding acyl azides. The acyl azides then underwent decomposition, which involved evolution of nitrogen gas and rearrangement to form the isocyanate intermediate. Nucleophilic attack of *t*-BuOH to this isocyanate intermediate yielded the *N*-Boc carbamate product, where the presence of Boc group was evidenced by the singlet (9H) at around 1.45 ppm in ¹H NMR. After Boc-deprotection using TFA, the obtained amines were acidified using ethereal HCl to precipitate out the amine salts **62b-g**. In the ¹H NMR spectra of **62b-g**, singlet with 9H integration was not observed at around 1.45 ppm, indicating the Boc group was successfully removed. In samples where deuterated DMSO was used during NMR analysis, a broad singlet was observed at around 8.70 ppm, which was assigned as NH₃⁺ in **62b-g**.

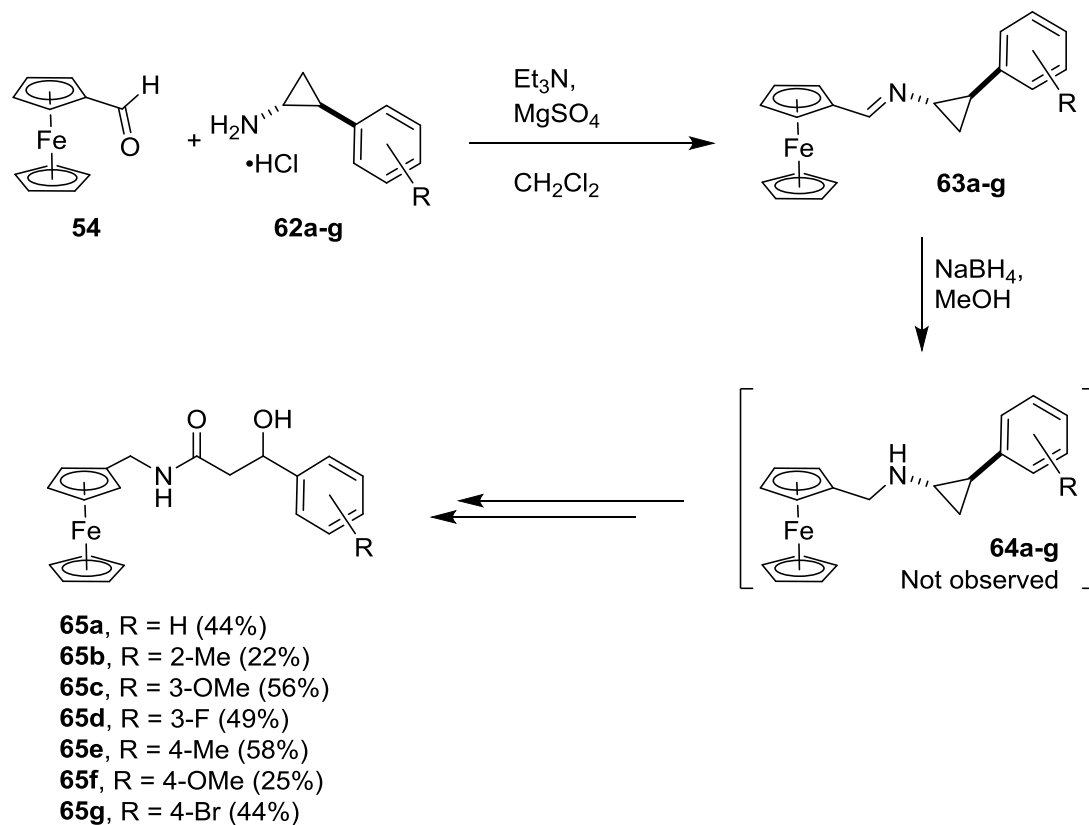
In the Curtius rearrangement of **61b-g**, instead of directly hydrolysing the isocyanate intermediates to amines, *t*-Bu carbamates were prepared and deprotected in order to access the amines **62b-g** as solid hydrochloride salts which were easier to handle/weigh out in the laboratory.

Although some of these 2-PCPA derivatives and their precursors were reported in literature and patents, not all of their characterisation data (such as NMR, IR, HRMS and melting point) were documented, and hence these data were collected and listed in the experimental section of this chapter.

3.3.2 Oxidative ring-opening of ferrocenylmethylcyclopropylamines

All 2-PCPA substrates **62a-g** were subjected to condensation with ferrocenecarboxaldehyde **54** to yield the corresponding imines **63a-g** (Scheme 24), which were then treated with sodium borohydride to form the corresponding β-hydroxyamides **65a-g** in moderate yields (22 – 58% over two steps from amine salt). This demonstrated

that the reaction is compatible with a range of electron-donating and electron-withdrawing substituents, at different positions of the aromatic rings.



Scheme 24: Oxidative ring-opening of 2-PCPA derivatives, two-steps yields (from 2-PCPA salts) were reported for β -hydroxyamides **65**.

From the ^1H NMR spectrum of β -hydroxyamide **65d** the absence of cyclopropane C-H signals (typically range from 1.30 – 1.90 ppm) indicated that the ring-opening had occurred. The β -hydroxyl carbon had originated from the cyclopropane (Ph-CH-CH₂), and the proton signal shifted downfield to 5.11 ppm due to the attachment of the hydroxyl group. The presence of an amide carbonyl was verified from the peak at 171.0 ppm in ^{13}C NMR and 1650 cm⁻¹ in the IR. Furthermore, the X-ray analysis of **65d** confirmed its assigned structure (Figure 26).

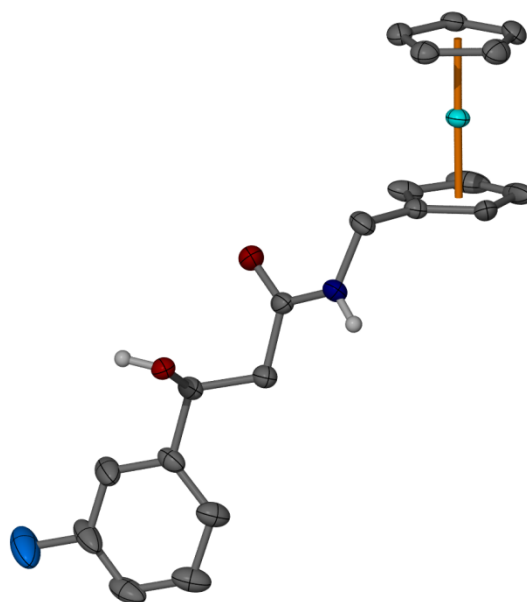
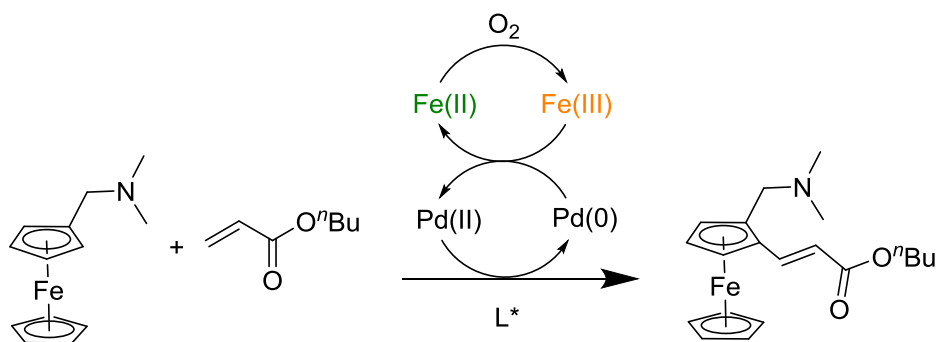


Figure 26: Crystal structure of β -hydroxyamide **65d**, collected by Dr M. Gardiner (University of Tasmania).

3.3.3 Proposed mechanism for the formation of β -hydroxyamides derived from oxidative ring-opening of ferrocenylmethylcyclopropylamines

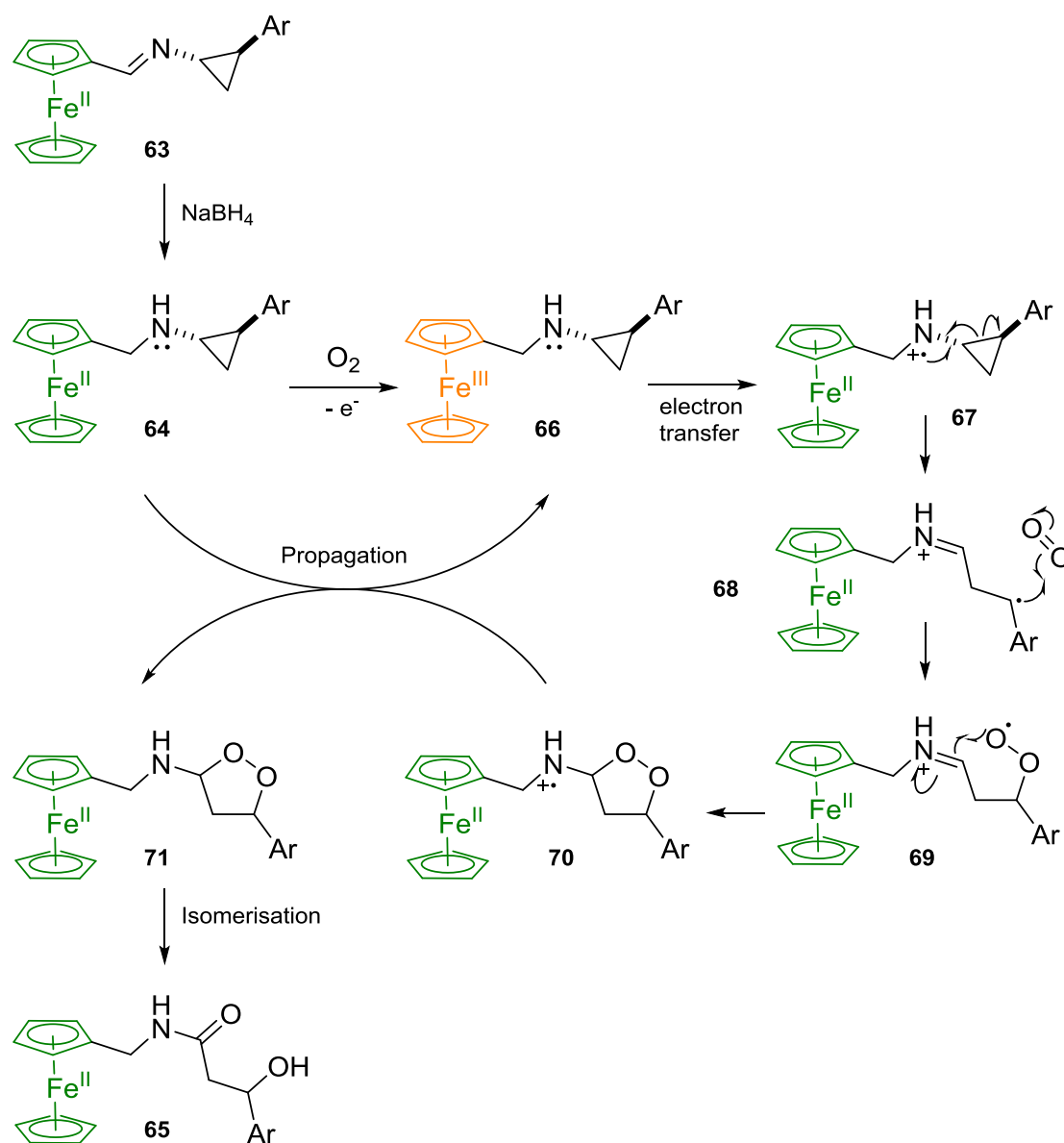
The reactivity of the ring-opening was attributed to the redox activity of the ferrocenyl moiety, especially as the corresponding benzyl-derivative has been reported to be air stable and subjected to biological studies.²⁹ The redox activity of ferrocene was not only observed in drugs like ferrocifen, it has been reported that air generated ferrocinium ions were utilised as the internal oxidant in asymmetric dehydrogenative Heck reactions (Scheme 25).²⁶



Scheme 25: The redox capability of ferrocene was utilised as an internal oxidant to recover Pd(II) from Pd(0) in a dehydrogenative Heck reaction.²⁶

Based on the proton NMR analysis of the obtained products, we proposed that the ferrocenylmethylcyclopropylamine **64** is formed in the first place due to the disappearance of imine N=CH-Fc signal at 8.25 ppm and presence of N-CH₂-Fc signal between 4.10 – 4.15 ppm. Note that the reaction was conducted under nitrogen atmosphere and there was no positive supply of oxygen gas to the system, thus the oxidation of ferrocenyl moiety in amine **64** may occur during workup where the amines are exposed to air (Scheme 26). As a result, the ferrocenium counterpart **66** is formed which led to the formation of radical cation **67** through single-electron oxidation of the amine nitrogen. The amine radical cation **67** prompts the ring-opening of cyclopropane by exclusively cleaving the C₁-C₂ bond, so that the more stable benzylic radical **68** can be formed. This is consistent with Wimalasena et al. who suggested the carbon-centered radical is a discrete intermediate in radical ring-opening of cyclopropylamines and therefore, ring-opening and molecular oxygen insertion are not concerted.⁸ The distonic radical cation **68** can then be trapped with molecular oxygen to yield adduct **69** and subsequently undergo 5-*exo-trig* cyclisation to radical cation **70**. The catalytic cycle is propagated by abstraction of an electron from amine **64** by radical cation **70**, which yields dioxolane **71** as an intermediate.

Dioxolane **71** was not observed in our current study, as it is likely undergoing isomerisation by concomitant O–O bond cleavage to yield *N*-ferrocenylmethyl β -hydroxyamide **65**, which is a facile process under basic conditions. This isomerisation step to the hydroxyamide could occur via several pathways. While it has been reported that 1,2-dioxolanes can undergo conversion to β -keto alcohols in the presence of silica gel,^{30,31} in our case this is unlikely as signals corresponding to the hydroxyamide were observed in the ¹H NMR of the crude reaction material prior to contact with silica gel. Therefore, it is more likely that the isomerisation occurs via base-mediated³² or radical abstraction⁸ of hydrogen. Of these two possibilities the base-mediated mechanism would appear more likely as no clear mechanism for generation of RO• is apparent and our conditions are intrinsically basic due to the presence of NaBH₄.



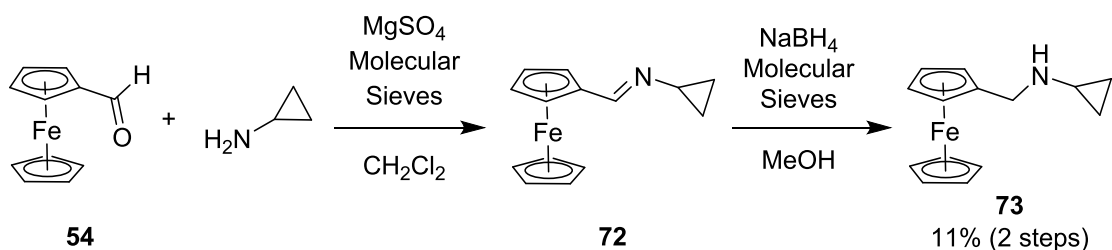
Scheme 26: Proposed mechanism of oxidative ring-opening of cyclopropylamines **64** to form β -hydroxyamides **65**.

3.3.4 Role of stable radical intermediate in the oxidative ring-opening of ferrocenylmethylcyclopropylamines

Apart from the redox capability of ferrocene, the reactivity of the ring-opening process could also be promoted by the release of ring-strain in cyclopropylamine intermediate **67** and subsequently the formation of radical intermediate **68** where the

radical is stabilised by the aromatic ring. This process is similar to the ring-opening process of 2-PCPA in LSD1 inhibition, where bond cleavage occurs exclusively between C1 and C2 to yield a stable benzylic radical **29** prior to covalent fusing with FAD (Scheme 14). Conversely, bond cleavage between C1 and C3 was not observed as the resulting methylene radical intermediate is less stable than benzylic radical **29**. In the work of Itoh et al. (Scheme 19), bond cleavage also occurred specifically between C1 and C2 in cyclopropylamine intermediate **41** as the resulting radical can be stabilised by two alkyl groups rather than one.¹² The stability of the radical intermediate seems to manipulate the ring-opening of cyclopropylamine.

To investigate the role of stable radical intermediate in this ring-opening process, cyclopropylamine which lacks of a stabilising phenyl ring, were subjected to condensation with ferrocenecarboxaldehyde **54** and formed cyclopropylimine **72** (Scheme 27). As such, it was anticipated that ferrocenylmethylcyclopropylamine **73** could form without subsequent ring-opening, due to the lack of phenyl ring to stabilise the radical intermediate if ring-opening occurs.



*Scheme 27: Oxidative ring-opening was not observed during the preparation of ferrocenylmethylcyclopropylamine **73** from the reduction of cyclopropylimine **72**.*

As expected, ring-opening was not observed after reducing cyclopropylimine **72** with sodium borohydride, and ferrocenylmethylcyclopropylamine **73** was obtained successfully. In the ¹H NMR spectrum of **73**, the cyclopropane proton signals were

located at 2.18 – 2.17 (1H, CH-NH), 0.44 – 0.43 (2H, CH₂-CH-NH) and 0.362 – 0.358 (2H, CH₂-CH-NH) ppm. Furthermore, an amide signal was not detected based on the absence of signals at around 171.0 ppm in ¹³C NMR and 1650 cm⁻¹ in IR, which further supports that oxidative ring-opening did not occur. Even though spectroscopic evidence support that ferrocenylmethylcyclopropylamine **73** was formed, the molecule slowly decomposed after column chromatography and leaving aside for a few days. The decomposition might not be solely due to ring-opening of cyclopropylamine because many unidentifiable peaks were observed within the aliphatic region in ¹H NMR spectrum.

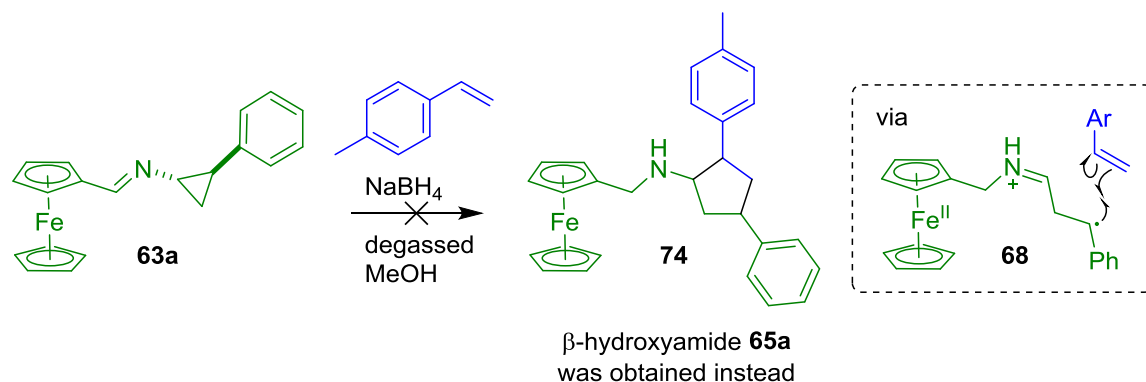
Due to the lack of phenyl group to stabilise the radical intermediate, it was observed that ferrocenylmethylcyclopropylamine **73** was more resistant to ring-opening compared to **64**, suggesting that the stability of ring-opened radical intermediate plays a role in the stability and reactivity of ferrocenylmethylcyclopropylamines.

3.3.5 Trapping benzylic radical intermediate **68** in [3 + 2] cycloaddition

Based on literature reports of cyclopropylamine ring-opening, together with the observed formation of β-hydroxyamides **65** derived from ferrocenylmethylcyclopropylamine **64**, we proposed that the benzylic radical **68** formed is a crucial reaction intermediate. Inspired by Zheng and co-workers' work in [3 + 2] cycloadditions of cyclopropylamines and olefins,³³ we attempted to trap benzylic radical **68** (generated through the reduction of cyclopropylimine **63a** with NaBH₄) using 4-methylstyrene, however the desired cycloaddition did not occur while β-hydroxyamides **65a** was obtained (Scheme 28).

Commercially sourced 4-methylstyrene was supplemented with 3,5-di-*tert*-butylcatechol as radical inhibitor to prevent polymerisation of 4-methylstyrene. It was assumed that this inhibitor may hinder the cycloaddition, therefore commercially sourced 4-methylstyrene was passed through an alumina plug to remove the inhibitor. Despite the removal of the inhibitor, the desired cycloaddition still did not occur while β -hydroxyamide **65a** was obtained again.

The cycloaddition was proven to be challenging, as the reaction required trace amount of oxygen to oxidise ferrocene to ferrocenium, while the generated benzylic radical **68** may have a higher affinity with molecular oxygen compared to 4-methylstyrene, which was added in abundance (5 equivalent). In summary, the trace amount of molecular oxygen required to initiate the oxidation could also be the interference for the cycloaddition to occur.



Scheme 28: Attempt to subject benzylic radical **68** to [3 + 2] cycloaddition with 4-methylstyrene. However, β -hydroxyamide **65a** was obtained, with or without removing 3,5-di-*tert*-butylcatechol (radical inhibitor) from 4-methylstyrene.

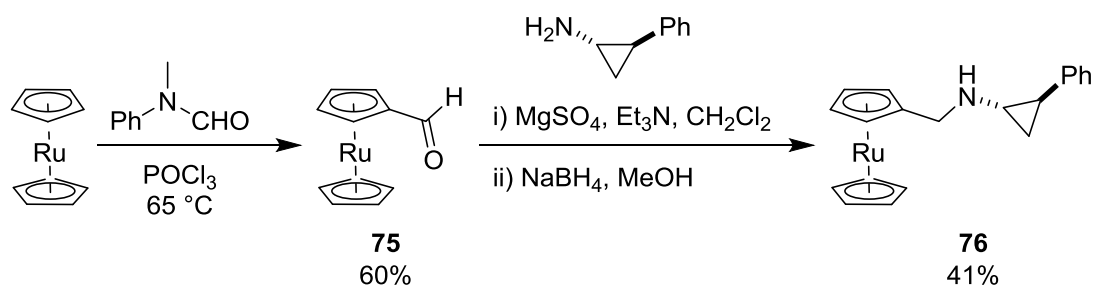
3.3.6 Preparation of ruthenocene derivatives of 2-PCPA

As ferrocenylmethylcyclopropylamines were intrinsically unstable and prone to ring-opening, ruthenocene analogues of 2-PCPA were the next focus of the project. In the study conducted by Jaouen and co-workers, ruthenocene analogues of ferrocifen (**53**, Figure 25) were found to retain the antiestrogen nature of hydroxytamoxifen but not the cytotoxicity exhibited by ferrocenyl group.²⁴ It was further pointed out that ruthenocene undergoes an irreversible oxidation, in contrast to the reversible redox activity observed in ferrocene. Therefore, we proposed that the ruthenocenylmethylcyclopropylamine **76** (Scheme 29) might be more stable in air than the ferrocenyl-counterpart – the latter transforming to a β -hydroxyamide via reversible Fe(II) oxidation. Despite this, it is possible that the redox active ruthenocene may enhance the FAD-mediated *N*-oxidation of **76** vs. 2-PCPA during LSD1 inhibition. Furthermore, the lipophilicity of ruthenocene moiety could facilitate the transport of **76** across the cell membrane.

LSD1 possesses a more spacious active site compared to MAOs based on the comparison of X-ray crystal structures,³⁴⁻³⁶ therefore **76**, which is larger than 2-PCPA in size, may be able to inhibit LSD1 selectively due to size exclusion by MAOs. Consistent to this hypothesis, *N*-alkylated 2-PCPA derivatives have demonstrated superior selectivity towards LSD1 compared to MAOs in literature and clinical trials.³⁷⁻⁴⁰

The synthesis of ruthenocenylmethylcyclopropylamine **76** requires the condensation of ruthenocenecarboxaldehyde **75** and 2-PCPA, follow by reduction of imine with sodium borohydride (Scheme 29). Unlike ferrocenecarboxaldehyde **54**, ruthenocenecarboxaldehyde **75** was not commercially available. The literature method to synthesise **75** from ruthenocene usually involved the use of *t*-BuLi/*t*-BuOK “super base” pair at low temperature ($-75\text{ }^{\circ}\text{C}$),⁴¹⁻⁴³ which posed a moderate to high risk in the laboratory. In order to access **75** more safely, ruthenocene was subjected to Vilsmeier–

Haack reaction with *N*-methylformanilide in a moderate yield of 60% (Scheme 29). *N*-Methylformanilide reacted with phosphorus oxychloride to generate a chloroiminium ion (Vilsmeier reagent), which then underwent electrophilic aromatic substitution with the electron rich ruthenocene, followed by hydrolysis to furnish the aldehyde moiety.



Scheme 29: Preparation of ruthenocencarboxaldehyde **75** and ruthenocenylmethylcyclopropylamine **76**.

Upon using NaBH₄ to reduce the imine resulting from the condensation of ruthenocencarboxaldehyde **75** and 2-PCPA, the desired ruthenocenylmethylcyclopropylamine **76** was obtained in a moderate yield of 41% (two steps yield from **75**), with no sign of ring-opening (Scheme 29). The obtained **76** was much more stable than ferrocenylmethylcyclopropylamine **73** (Scheme 27), in which the former passed through column chromatography without sign of decomposition or ring-opening. In the ¹H NMR of **76**, no aldehyde signal was detected at 9.73 ppm, indicating the complete consumption of substrate **75**. On the other hand, cyclopropane proton signals of **76** were observed at 2.44 (*CH*-NH), 1.91 (*CH*-Ar), 1.11 – 1.07 (*CH*₂-*CH*-NH) and 0.97 (*CH*₂-*CH*-NH) ppm. In terms of the Cp signals for ruthenocene in **76**, although the chemical shifts were slightly different from substrate **75**, the total proton integration matched the proposed structure of **76**. Moreover, the absence of carbonyl signals in ¹³C NMR and IR further support that **76** did not undergo oxidative ring-opening to a β-hydroxyamide.

3.3.7 Selectivity and potency of ruthenocenyl-2-PCPA **76** in LSD1 inhibition

Despite the fact that there are many literature examples of 2-PCPA derivatives in the studies of LSD1 inhibition, there is no reported precedent for organometallic analogues of 2-PCPA. Therefore, it was important to evaluate the LSD1 inhibitory activity and selectivity of ruthenocenyl-2-PCPA **76**, with 2-PCPA as a comparison control. This work was carried out by our collaborators at the Kyoto Prefectural University of Medicine (group of Prof T. Suzuki).

Using an LSD1 fluorometric drug discovery kit (BML-AK544-0001, Enzo), the IC_{50} of **76** in LSD1 inhibition was determined as 1.4 μ M, which is 16.4 times more potent than 2-PCPA (LSD1 IC_{50} = 23.0 μ M) (Table 3). Furthermore, **76** was determined to be inactive in MAO A and MAO B. These data demonstrated that ruthenocenyl-2-PCPA **76** is a potent and selective LSD1 inhibitor.

Table 3: Inhibitory activity of 2-PCPA and ruthenocene derivative **76** in LSD1 and MAOs.

	IC_{50} (μ M) ^a		
	LSD1	MAO A	MAO B
2-PCPA	23.0 \pm 3.4	6.00 \pm 1.38	6.54 \pm 0.51
Inhibitor 76	1.43 \pm 0.07	> 10	> 10

^a Values are means \pm SD of at least three experiments.

Inhibitor **76** demonstrated superior LSD1 inhibitory activity compared to its mother compound 2-PCPA. This could be due to the introduction of the bulky ruthenocene group on the cyclopropylamine nitrogen, as the two clinical trial candidates have bulky alkyl group on amine nitrogen as well (Section 2.1.6). Since the X-ray crystal structure of LSD1 revealed that this enzyme has a more capacious active site than MAOs,³⁴⁻³⁶ the selectivity towards LSD1 can be justified as the result of size exclusion from MAOs.

Ruthenocene derivatives of hydroxytamoxifen were found to have higher log $P_{o/w}$ values compared to hydroxytamoxifen, therefore assisting the drug to cross the cell membrane.²⁴ While the assay performed in this study was not a cellular assay, the ruthenocene in inhibitor **76** would be expected to aid the drug crossing cell membrane and hence achieve great potency in cancer cell lines. Due to the availability of γ -emitting isotopes ^{97}Ru and ^{103}Ru , ruthenocene derivative **76** can also be useful in the radioimaging of cancer cells, which will eliminate the challenge of radiolabelling.²⁴

This highly promising result lays the foundation for investigation of other analogues containing ruthenocene, which should be carried out in future studies.

3.4 Conclusion and future work

In conclusion, ferrocenylmethylcyclopropylamines **64** derived from 2-PCPA and ferrocenecarboxaldehyde **54** were prone to oxidative ring-opening and yield β -hydroxyamides **65**. This observation was consistent with different variation of substituents on the phenyl ring, so as different positions on the ring. β -Hydroxyamide moiety features in bioactive compounds, such as Cruentaren A (antifungal)⁴⁴ and

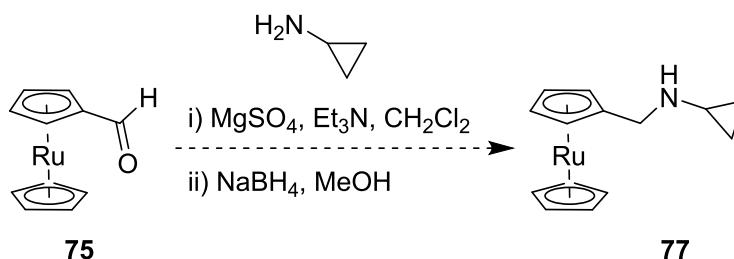
Ocreotide (growth hormone inhibitor)⁴⁵, organometallic analogues of this moiety can be potential interest to medicinal chemists. Further, this is the first study of an organometallic derivative of the biologically important cyclopropylamine moiety and will provide fundamental reactivity information to future workers in the medicinal organometallic field.

By replacing 2-PCPA with cyclopropylamine, in the Fc derivatives oxidative ring-opening did not occur due to the lack of phenyl ring to stabilise radical intermediate. However, the obtained ferrocenylmethylcyclopropylamine **73** slowly decomposed after purification and storage for a few days. Lastly, ruthenocene analogue of 2-PCPA **76** was successfully synthesised and subjected to in vitro assay. It was determined as a potent and selective LSD1 inhibitor ($IC_{50} = 1.4 \mu M$). The different fate of ferrocene and ruthenocene 2-PCPA analogues highlights the importance of metallocene redox potential, in which crucial to determine the ring-opening propensity. As such, the incorporation of ruthenocene to 2-PCPA created a LSD1 inhibitor that is air stable yet potent.

Preliminary results of **76** in the in vitro assay was promising and should be follow up with a cellular assay. The presence of ruthenocene increases the lipophilicity of the 2-PCPA analogue and hence an increase in cellular uptake is anticipated. Similar to 2-PCPA, it was assumed that **76** inhibits LSD1 by covalently fused to FAD in the active site. To verify this hypothesis, the **76**-FAD adduct generated during LSD1 inhibition can be detected using mass spectrometry.^{37,46} Furthermore, the H3K4me1/2 levels can be quantified by western blot. An increase in H3K4me1/2 levels is expected to occur if **76** successfully inhibits LSD1, due to the possible enhanced reactivity of ruthenocene towards the FAD-mediated ring-opening of **76**.

Although clinical trial candidates ORY-1001, GSK2879552 and **76** are all *N*-alkylated 2-PCPA derivatives with no substituent on the phenyl ring, it was not clear why the *N*-alkyl group increases potency in LSD1 inhibition. In silico docking study may shed a light on how these *N*-alkyl groups interact with the LSD1 active site and hence increase their inhibitory activities. Using this information with SAR analysis, a second generation of ruthenocene analogues can be developed, with derivatisation on ruthenocene and/or the phenyl ring.

A modified version of **76** without the phenyl ring can also be synthesised (**77**, Scheme 30), since ring-opening is unlikely to occur in this case. With such, we were intrigued to observe if ruthenocenylmethylcyclopropylamine **77** will still be able to inhibit LSD1 and induce cytotoxicity in cancer cells. This information can provide us some insight into the role of the ruthenocenyl moiety in LSD1 inhibition.



Scheme 30: Proposed preparation of ruthenocenylmethylcyclopropylamine **77** from the condensation and reductive amination of cyclopropylamine with ruthenocenecarboxaldehyde **75**.

3.5 Experimental

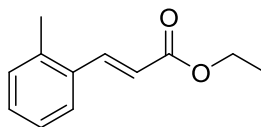
All organic syntheses and molecule characterisation listed below were performed by Y. S. Gee. The preparation of **62f**, **65f**, data acquisition of IR and HRMS for **65g**, were

assisted by an undergraduate student N. Goertz (University of Wollongong). X-ray crystallography was performed by Dr M. Gardiner (University of Tasmania). In vitro assay of ruthenocenyl-2-PCPA **76** was performed by Professor T. Suzuki and co-workers (Kyoto Prefectural University of Medicine).

General experimental details for organic syntheses and molecule characterisation are stated in Chapter 2 Section 2.5.1.

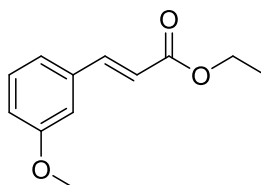
3.5.1 Esterification of cinnamic acids

Ethyl (E)-3-(o-tolyl)-2-propenoate (59b)



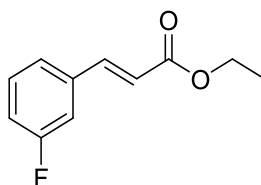
Concentrated sulfuric acid (~ 1 mL) was added to a solution of 2-methylcinnamic acid (2.01 g, 12.4 mmol) in ethanol (40 mL). After heating to reflux for 24 h, the reaction solution was concentrated *in vacuo* and diluted with ethyl acetate (40 mL). The solution was washed with 5% by mass NaHCO₃ aqueous solution (3 × 30 mL) and water (3 × 30 mL). After drying the solution with magnesium sulfate, the solution was concentrated under reduced pressure to give the title compound as a pale yellow oil (2.12 g, 11.1 mmol) in 90% yield. ¹H NMR (500 MHz, CDCl₃): δ 7.98 (d, *J* = 16 Hz, 1H, Ar-CH=CH), 7.55 (d, *J* = 7.5 Hz, 1H, CH_{Ar}), 7.29 – 7.26 (m, 1H, CH_{Ar}), 7.21 (t, *J* = 6.5 Hz, 2H, CH_{Ar}), 6.36 (d, *J* = 16 Hz, 1H, Ar-CH=CH), 4.27 (q, *J* = 7 Hz, 2H, OCH₂), 2.44 (s, 3H, Ar-CH₃), 1.34 (t, *J* = 7 Hz, 3H, CH₂CH₃) ppm. ¹H NMR data consistent with literature and the material is commercially available.^{47,48}

Ethyl (E)-3-(m-methoxyphenyl)-2-propenoate (59c)



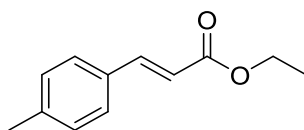
Concentrated sulfuric acid (~ 1 mL) was added to a solution of 3-methoxycinnamic acid (2.00 g, 11.2 mmol) in ethanol (38 mL). After heating to reflux for 24 h, the reaction solution was concentrated *in vacuo* and diluted with ethyl acetate (38 mL). The solution was washed with 5% by mass NaHCO₃ aqueous solution (3 × 30 mL) and water (3 × 35 mL). After drying the solution with magnesium sulfate, the solution was concentrated under reduced pressure to give the title compound as a pale yellow oil (2.09 g, 10.1 mmol) in 90% yield. ¹H NMR (500 MHz, CDCl₃): δ 7.65 (d, *J* = 16 Hz, 1H, Ar-CH=CH), 7.30 (t, *J* = 8 Hz, 1H, CH_{Ar}), 7.12 (d, *J* = 7.5 Hz, 1H, CH_{Ar}), 7.05 (s, 1H, CH_{Ar}), 6.93 (d, *J* = 8.5 Hz, 1H, CH_{Ar}), 6.43 (d, *J* = 16 Hz, 1H, Ar-CH=CH), 4.27 (q, *J* = 7 Hz, 2H, OCH₂), 3.83 (s, 3H, OCH₃), 1.34 (t, *J* = 7 Hz, 3H, CH₂CH₃) ppm. ¹H NMR data consistent with literature and the compound is commercially available.⁴⁹

Ethyl (E)-3-(m-fluorophenyl)-2-propenoate (59d)



Concentrated sulfuric acid (~ 1 mL) was added to a solution of 3-fluorocinnamic acid (1.51 g, 9.07 mmol) in ethanol (30 mL). After the solution was heated to reflux for 24 h, the reaction solution was concentrated *in vacuo* and diluted with ethyl acetate (30 mL). The solution was washed with 5% by mass NaHCO₃ aqueous solution (3 × 30 mL) and water (3 × 30 mL). After drying the solution with magnesium sulfate, the solution was concentrated under reduced pressure to give the title compound as a pale yellow oil (1.42 g, 7.29 mmol) in 80% yield. **¹H NMR** (500 MHz, CDCl₃): δ 7.64 (d, *J* = 15 Hz, 1H, Ar-CH=CH), 7.40 – 7.20 (m, 3H, CH_{Ar}), 7.08 (t, *J* = 11.5 Hz, 1H, CH_{Ar}), 6.43 (d, *J* = 18 Hz, 1H, Ar-CH=CH), 4.27 (q, *J* = 11.5 Hz, 2H, OCH₂), 1.34 (t, *J* = 12 Hz, 3H, CH₂CH₃) ppm. **¹³C NMR** (75 MHz, CDCl₃): δ 166.6 (C=O), 163.0 (d, *J* = 247.5 Hz, C_{Ar}), 143.2 (d, *J* = 2.25 Hz, Ar-CH=CH), 136.7 (d, *J* = 0.75 Hz, C_{Ar}), 130.4 (d, *J* = 8.25 Hz, CH_{Ar}), 124.0 (d, *J* = 1.5 Hz, CH_{Ar}), 119.7 (Ar-CH=CH), 117.1 (d, *J* = 21 Hz, CH_{Ar}), 114.3 (d, *J* = 21.8 Hz, CH_{Ar}), 60.7 (OCH₂), 14.3 (CH₃) ppm. **IR** (Neat): 1708 cm⁻¹. **HRMS** (ASAP) *m/z*: [M + H]⁺ Calcd for C₁₁H₁₂O₂F 195.0821; Found 195.0821. ¹H NMR data consistent with literature and the compound is commercially available.⁵⁰

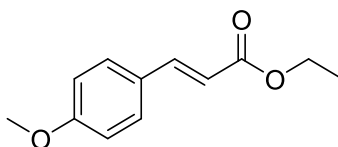
Ethyl (E)-3-(p-tolyl)-2-propenoate (59e)



Concentrated sulfuric acid (~ 1 mL) was added to a solution of 4-methylcinnamic acid (1.50 g, 9.26 mmol) in ethanol (31 mL). After heating to reflux for 24 h, the reaction solution was concentrated *in vacuo* and diluted with ethyl acetate (30 mL). The solution was washed with 5% by mass NaHCO₃ aqueous solution (3 × 30 mL) and water (3 × 30

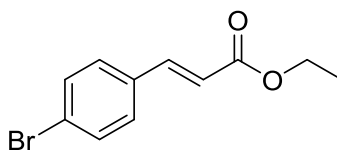
mL). After drying the solution with magnesium sulfate, the solution was concentrated under reduced pressure to give the title compound as a colourless oil (1.50 g, 7.86 mmol) in 85% yield. **¹H NMR** (500 MHz, CDCl₃): δ 7.66 (d, *J* = 16 Hz, 1H, Ar-CH=CH), 7.43 (d, *J* = 8 Hz, 2H, CH_{Ar}), 7.19 (d, *J* = 8 Hz, 2H, CH_{Ar}), 6.39 (d, *J* = 16 Hz, 1H, Ar-CH=CH), 4.26 (q, *J* = 7 Hz, 2H, OCH₂), 2.37 (s, 3H, Ar-CH₃), 1.34 (t, *J* = 10 Hz, 3H, CH₂CH₃) ppm. ¹H NMR data consistent with literature.⁵¹

Ethyl (E)-3-(p-methoxyphenyl)-2-propenoate (59f)



Concentrated sulfuric acid (~ 1 mL) was added to a solution of 4-methoxycinnamic acid (2.01 g, 11.3 mmol) in ethanol (35 mL). After heating to reflux for 24 h, the reaction solution was concentrated *in vacuo* and diluted with ethyl acetate (35 mL). The solution was washed with 5% by mass NaHCO₃ aqueous solution (3 × 30 mL) and water (3 × 30 mL). After drying the solution with magnesium sulfate, the solution was concentrated under reduced pressure to give the title compound as a colourless oil (2.20 g, 10.7 mmol) in 95% yield. **¹H NMR** (500 MHz, CDCl₃): δ 7.64 (d, *J* = 16 Hz, 1H, Ar-CH=CH), 7.48 (d, *J* = 8.5 Hz, 2H, CH_{Ar}), 6.90 (d, *J* = 8.5 Hz, 2H, CH_{Ar}), 6.31 (d, *J* = 16 Hz, 1H, Ar-CH=CH), 4.25 (q, *J* = 7.5 Hz, 2H, OCH₂), 3.84 (s, 3H, OCH₃), 1.33 (t, *J* = 7 Hz, 3H, CH₂CH₃) ppm. ¹H NMR data are consistent with literature.⁵²

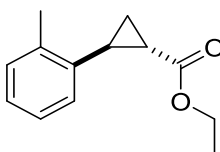
Ethyl (E)-3-(p-bromophenyl)-2-propenoate (59g)



Concentrated sulfuric acid (~ 1 mL) was added to a solution of 4-bromocinnamic acid (3.40 g, 15.0 mmol) in ethanol (50 mL). After heating to reflux for 24 h, the reaction solution was concentrated *in vacuo* and diluted with ethyl acetate (50 mL). The solution was washed with 5% by mass NaHCO₃ aqueous solution (3 × 30 mL) and water (3 × 30 mL). After drying the solution with magnesium sulfate, the solution was concentrated under reduced pressure to give a mixture of colourless oil and white precipitate. After hexane was added to the mixture, the colourless oil was dissolved in the solvent while the precipitate remained insoluble. After filtering the suspension, the filtrate was concentrated *in vacuo* to give the title compound as a pale yellow oil (3.48 g, 13.6 mmol) in 91% yield. ¹H NMR (300 MHz, CDCl₃): δ 7.61 (d, *J* = 15.9 Hz, 1H, Ar-CH=CH), 7.52 (d, *J* = 8.4 Hz, 2H, CH_{Ar}), 7.38 (d, *J* = 8.4 Hz, 2H, CH_{Ar}), 6.42 (d, *J* = 16.2 Hz, 1H, Ar-CH=CH), 4.27 (q, *J* = 7.2 Hz, 2H, OCH₂), 1.34 (t, *J* = 7.2 Hz, 3H, CH₂CH₃) ppm. ¹H NMR data are consistent with literature.⁵³

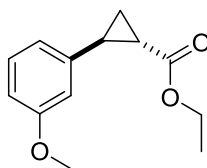
3.5.2 Corey–Chaykovsky cyclopropanation of ethyl cinnamates

Ethyl 2-(o-tolyl)cyclopropane-1-carboxylate (60b)



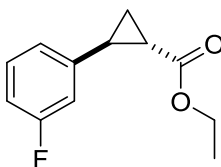
A suspension of trimethylsulfoxonium iodide (2.94 g, 13.4 mmol, 1.2 equiv) and sodium hydride (60% in mineral oil, 544 mg, 13.6 mmol, 1.2 equiv) in anhydrous DMSO (10 mL) were stirred for 1 h before the addition of **59b** (2.12 g, 11.1 mmol, 1 equiv) in anhydrous DMSO (10 mL). After the reaction was heated at 55 °C for 24 h, another suspension of trimethylsulfoxonium iodide (0.750 g, 3.41 mmol, 0.3 equiv) and sodium hydride (60% in mineral oil, 137 mg, 3.43 mmol, 0.3 equiv) in anhydrous DMSO (2.5 mL) was stirred for 1 h and added to the reaction solution. The reaction was then heated at 65 °C overnight before it was poured into brine solution (50 mL) and extracted with ethyl acetate (4 × 30 mL). The combined organic extracts were washed with water (50 mL) and brine solution (50 mL). After drying with magnesium sulfate, the solution was concentrated under reduced pressure to give a mixture of yellow oil and brown precipitate which was later subjected to column chromatography twice (5% ethyl acetate/hexane). The title compound was collected as a pale yellow oil (1.39 g, 6.78 mmol) in 61% yield. **¹H NMR** (500 MHz, CDCl₃): δ 7.15 – 7.11 (m, 3H, CH_{Ar}), 7.00 (d, *J* = 6 Hz, 1H, CH_{Ar}), 4.25 – 4.15 (m, 2H, OCH₂), 2.53 – 2.49 (m, 1H, CH-Ar), 2.38 (s, 3H, Ar-CH₃), 1.78 (ddd, *J* = 8.6, 4.5, 4.5 Hz, 1H, CH-COOEt), 1.59 – 1.56 (m, 1H, CH₂-CHCOOEt), 1.32 – 1.28 (m, 4H, CH₂-CHCOOEt and CH₂CH₃) ppm. **¹³C NMR** (75 MHz, CDCl₃): δ 174.0 (C=O), 138.1 (C_{Ar}), 138.0 (C_{Ar}), 130.0 (CH_{Ar}), 126.8 (CH_{Ar}), 126.0 (CH_{Ar}), 126.0 (CH_{Ar}), 60.8 (OCH₂), 24.8 (CH-Ar), 22.5 (CH-COOEt), 19.7 (Ar-CH₃), 15.5 (CH₂-CHCOOEt), 14.5 (CH₂CH₃) ppm. **IR** (Neat): 2923, 1724 cm⁻¹. **HRMS** (ASAP) *m/z*: [M + H]⁺ Calcd for C₁₃H₁₇O₂ 205.1229; Found 205.1230. ¹H and ¹³C NMR data are consistent with literature.²⁷

Ethyl 2-(m-methoxyphenyl)cyclopropane-1-carboxylate (60c)



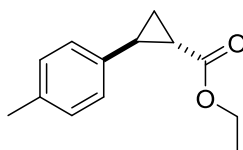
A suspension of trimethylsulfoxonium iodide (2.69 g, 12.2 mmol, 1.2 equiv) and sodium hydride (60% in mineral oil, 498 mg, 12.4 mmol, 1.2 equiv) in anhydrous DMSO (10 mL) were stirred for 1 h before the addition of **59c** (2.08 g, 10.1 mmol, 1 equiv) in anhydrous DMSO (10 mL). After the reaction was heated at 55 °C for 24 h, the reaction solution was poured into brine solution (50 mL) and extracted with ethyl acetate (3 × 30 mL). The combined organic extracts were washed with water (2 × 20 mL) and brine solution (2 × 20 mL). After drying with magnesium sulfate, the solution was concentrated under reduced pressure to give a yellow oil crude which was later subjected to column chromatography (10% ethyl acetate/hexane). The title compound was collected as a colourless oil (809 mg, 3.67 mmol) in 36% yield. ¹H NMR (500 MHz, CDCl₃): δ 7.19 (t, *J* = 8 Hz, 1H, CH_{Ar}), 6.74 (d, *J* = 8 Hz, 1H, CH_{Ar}), 6.69 (d, *J* = 7.5 Hz, 1H, CH_{Ar}), 6.65 (s, 1H, CH_{Ar}), 4.17 (q, *J* = 7 Hz, 2H, OCH₂), 3.79 (s, 3H, OCH₃), 2.51 – 2.47 (m, 1H, CH-Ar), 1.90 (ddd, *J* = 8.4, 4.5, 4.5 Hz, 1H, CH-COOEt), 1.60 – 1.57 (m, 1H, CH₂-CHCOOEt), 1.32 – 1.26 (m, 4H, CH₂-CHCOOEt and CH₂CH₃) ppm. ¹H NMR data are consistent with literature.²⁸

Ethyl 2-(m-fluorophenyl)cyclopropane-1-carboxylate (60d)



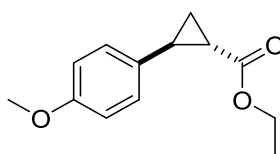
A suspension of trimethylsulfoxonium iodide (1.93 g, 8.78 mmol, 1.2 equiv) and sodium hydride (60% in mineral oil, 355 mg, 8.87 mmol, 1.2 equiv) in anhydrous DMSO (7.5 mL) were stirred for 1 h before the addition of **59d** (1.42 g, 7.29 mmol, 1 equiv) in anhydrous DMSO (7.5 mL). After heating at 55 °C for 24 h, the reaction solution was poured into brine solution (45 mL) and extracted with ethyl acetate (3 × 30 mL). The combined organic extracts were washed with water (4 × 20 mL) and brine solution (2 × 20 mL). After drying the solution with magnesium sulfate, the solution was concentrated under reduced pressure to give a yellow oil crude which was later subjected to column chromatography (5% ethyl acetate/hexane). The title compound was collected as a colourless oil (650 mg, 3.12 mmol) in 43% yield. **¹H NMR** (500 MHz, CDCl₃): δ 7.26 – 7.21 (m, 1H, CH_{Ar}), 6.91 – 6.87 (m, 2H, CH_{Ar}), 6.78 (d, *J* = 10 Hz, 1H, CH_{Ar}), 4.17 (q, *J* = 7 Hz, 2H, OCH₂), 2.52 – 2.48 (m, 1H, CH-Ar), 1.92 – 1.88 (m, 1H, CH-COOEt), 1.63 – 1.59 (m, 1H, CH₂-CHCOOEt), 1.28 (t, *J* = 7 Hz, 4H, CH₂-CHCOOEt and CH₂CH₃) ppm. **¹³C NMR** (125 MHz, CDCl₃): δ 172.7 (C=O), 162.8 (d, *J* = 245 Hz, C_{Ar}), 142.8 (d, *J* = 7.5 Hz, C_{Ar}), 129.7 (d, *J* = 8.8 Hz, CH_{Ar}), 121.8 (d, *J* = 2.5 Hz, CH_{Ar}), 113.1 (d, *J* = 21.3 Hz, CH_{Ar}), 112.7 (d, *J* = 22.5 Hz, CH_{Ar}), 60.5 (OCH₂), 25.5 (d, *J* = 1.3 Hz, CH-Ar), 24.1 (CH-COOEt), 16.9 (CH₂-CHCOOEt), 14.0 (CH₂CH₃) ppm. **IR** (Neat): 1718 cm⁻¹. **HRMS** (ESI) *m/z*: [M + H]⁺ Calcd for C₁₂H₁₄FO₂ 209.09778; Found 209.09770.

Ethyl 2-(p-tolyl)cyclopropane-1-carboxylate (60e)



A suspension of trimethylsulfoxonium iodide (1.30 g, 5.89 mmol, 1.2 equiv) and sodium hydride (60% in mineral oil, 243 mg, 6.07 mmol, 1.2 equiv) in anhydrous DMSO (5 mL) were stirred for 1 h before the addition of **59e** (932 mg, 4.90 mmol, 1 equiv) in anhydrous DMSO (5 mL). After the reaction was heated at 55 °C for 5 h, the reaction solution was poured into brine solution (30 mL) and extracted with ethyl acetate (3 × 20 mL). The combined organic extracts were washed with water (2 × 30 mL) and brine solution (30 mL). After drying the solution with magnesium sulfate, the solution was concentrated under reduced pressure to give a yellow oil crude which was later subjected to column chromatography (5% ethyl acetate/hexane). The title compound was collected as a colourless oil (481 mg, 2.35 mmol) in 48% yield. ¹H NMR (300 MHz, CDCl₃): δ 7.09 (d, *J* = 7.8 Hz, 2H, CH_{Ar}), 6.99 (d, *J* = 8.1 Hz, 2H, CH_{Ar}), 4.16 (q, *J* = 7.2 Hz, 2H, OCH₂), 2.52 – 2.45 (m, 1H, CH-Ar), 2.31 (s, 3H, Ar-CH₃), 1.86 (ddd, *J* = 8.7, 4.7, 4.2 Hz, 1H, CH-COOEt), 1.60 – 1.53 (m, 1H, CH₂-CHCOOEt), 1.27 (t, *J* = 7.2 Hz, 4H, CH₂-CHCOOEt and CH₂CH₃) ppm. HRMS (ASAP) *m/z*: [M + H]⁺ Calcd for C₁₃H₁₇O₂ 205.1229; Found 205.1228. ¹H NMR data are consistent with literature.²⁸

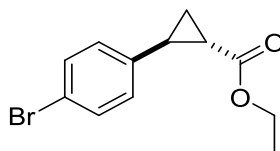
Ethyl 2-(p-methoxyphenyl)cyclopropane-1-carboxylate (60f)



A suspension of trimethylsulfoxonium iodide (2.83 g, 12.8 mmol, 1.2 equiv) and sodium hydride (60% in mineral oil, 537 mg, 13.4 mmol, 1.3 equiv) in anhydrous DMSO (10 mL) were stirred for 1 h before the addition of **59f** (2.21 g, 10.7 mmol, 1 equiv) in anhydrous DMSO (10 mL). After the reaction was heated at 55 °C for 24 h, another

suspension of trimethylsulfoxonium iodide (0.750 g, 3.41 mmol, 0.3 equiv) and sodium hydride (60% in mineral oil, 137 mg, 3.43 mmol, 0.3 equiv) in anhydrous DMSO (2.5 mL) was stirred for 1 h and added to the reaction solution. The reaction was then heated at 65 °C for 84 h before it was poured into brine solution (60 mL) and extracted with ethyl acetate (4 × 30 mL). The combined organic extracts were washed with water (50 mL) and brine solution (50 mL). After drying the solution with magnesium sulfate, the solution was concentrated under reduced pressure to give an orange-yellow solid crude which was later subjected to column chromatography (10% ethyl acetate/hexane). The title compound was collected as a white solid (919 mg, 4.17 mmol) in 39% yield. **¹H NMR** (500 MHz, CDCl₃): δ 7.03 (d, *J* = 8.5 Hz, 2H, CH_{Ar}), 6.82 (d, *J* = 9 Hz, 2H, CH_{Ar}), 4.16 (q, *J* = 7 Hz, 2H, OCH₂), 3.78 (s, 3H, OCH₃), 2.50 – 2.46 (m, 1H, CH-Ar), 1.82 (ddd, *J* = 8.5, 4.8, 5 Hz, 1H, CH-COOEt), 1.57 – 1.53 (m, 1H, CH₂-CHCOOEt), 1.29 – 1.23 (m, 4H, CH₂-CHCOOEt and CH₂CH₃) ppm. **HRMS** (ASAP) *m/z*: [M + H]⁺ Calcd for C₁₃H₁₇O₃ 221.1178; Found 221.1179. ¹H NMR data are consistent with literature.²⁸

Ethyl 2-(p-bromophenyl)cyclopropane-1-carboxylate (60g)

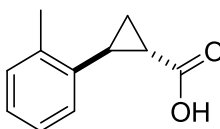


A suspension of trimethylsulfoxonium iodide (3.61 g, 16.4 mmol, 1.2 equiv) and sodium hydride (60% in mineral oil, 664 mg, 16.6 mmol, 1.2 equiv) in anhydrous DMSO (12 mL) were stirred for 1 h before the addition of **59g** (3.48 g, 13.6 mmol, 1 equiv) in anhydrous DMSO (12 mL). After the reaction was heated at 60 °C for 36 h, the reaction solution was poured into brine solution (50 mL) and extracted with ethyl acetate (4 × 30

mL). The combined organic extracts were washed with water (50 mL) and brine solution (50 mL). After drying the solution with magnesium sulfate, the solution was concentrated under reduced pressure to give a brown oil crude which was later subjected to column chromatography (10% ethyl acetate/hexane). The title compound was collected as a colourless oil (1.52 g, 5.64 mmol) in 41% yield. $^1\text{H NMR}$ (500 MHz, CDCl_3): δ 7.39 (d, $J = 8$ Hz, 2H, CH_{Ar}), 6.97 (d, $J = 8$ Hz, 2H, CH_{Ar}), 4.17 (q, $J = 7$ Hz, 2H, OCH_2), 2.49 – 2.45 (m, 1H, CH-Ar), 1.86 (ddd, $J = 8.4, 4.5, 4.5$ Hz, 1H, CH-COOEt), 1.60 (ddd, $J = 9.3, 4.8, 5$ Hz, 1H, $\text{CH}_2\text{-CHCOOEt}$), 1.29 – 1.25 (m, 4H, $\text{CH}_2\text{-CHCOOEt}$ and CH_2CH_3) ppm. **HRMS** (ASAP) m/z : $[\text{M} + \text{H}]^+$ Calcd for $\text{C}_{12}\text{H}_{14}\text{O}_2\text{Br}$ 269.0177; Found 269.0164. $^1\text{H NMR}$ data are consistent with literature.²⁸

3.5.3 Basic hydrolysis of esters

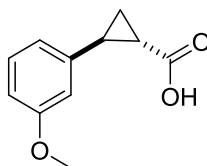
2-(o-Tolyl)cyclopropane-1-carboxylic acid (61b)



Sodium hydroxide solution (1 M, 9.5 mL, 9.5 mmol, 2 equiv) was added to a solution of **60b** (1.00 g, 4.91 mmol, 1 equiv) in ethanol (18 mL). After the solution was left stirring overnight at room temperature, hydrochloric acid solution (2 M, 7.10 mL, 14.2 mmol, 3 equiv) and water (5 mL) were added at 0 °C. The solution was extracted with ethyl acetate (50 mL + 2 × 30 mL) and washed with brine solution (2 × 30 mL). After drying the solution with magnesium sulfate, the solution was concentrated under reduced pressure to give the title compound as a white solid (816 mg, 4.63 mmol) in 94% yield. $^1\text{H NMR}$ (500 MHz, CDCl_3): δ 7.18 – 7.12 (m, 3H, CH_{Ar}), 7.01 (d, $J = 7$ Hz, 1H, CH_{Ar}), 2.63 –

2.59 (m, 1H, CH-Ar), 2.41 (s, 3H, CH₃), 1.81 – 1.77 (m, 1H, CH-COOH), 1.65 (ddd, $J = 9.1, 4.5, 5.0$ Hz, 1H, CH₂), 1.43 – 1.39 (m, 1H, CH₂) ppm. ¹³C NMR (125 MHz, CDCl₃): δ 180.4 (C=O), 138.1 (C_{Ar}), 137.3 (C_{Ar}), 130.0 (CH_{Ar}), 127.0 (CH_{Ar}), 126.0 (CH_{Ar}), 126.0 (CH_{Ar}), 25.6 (CH-Ar), 22.3 (CH-COOH), 19.6 (Ar-CH₃), 16.0 (CH₂) ppm. IR (Neat): 2926, 1685 cm⁻¹. HRMS (ASAP) m/z: [M + H]⁺ Calcd for C₁₁H₁₃O₂ 177.0916; Found 177.0944. **Melting point:** 67.3 – 69.7 °C.

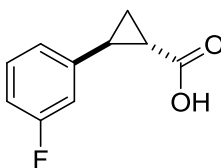
2-(m-Methoxyphenyl)cyclopropane-1-carboxylic acid (61c)



Sodium hydroxide solution (1 M, 7.35 mL, 7.35 mmol, 2 equiv) was added to a solution of **60c** (808 mg, 3.67 mmol, 1 equiv) in ethanol (14 mL). After the solution was left stirring overnight at room temperature, hydrochloric acid solution (2 M, 5.5 mL, 11 mmol, 3 equiv) and water (8.5 mL) were added to the reaction solution at 0 °C. The solution was extracted with ethyl acetate (55 mL + 2 × 30 mL) and washed with brine solution (2 × 30 mL). After drying the solution with magnesium sulfate, the solution was concentrated under reduced pressure to give the title compound as a white solid (690 mg, 3.59 mmol) in 98% yield. ¹H NMR (500 MHz, CDCl₃): δ 7.20 (t, $J = 8$ Hz, 1H, CH_{Ar}), 6.76 (d, $J = 8$ Hz, 1H, CH_{Ar}), 6.69 (d, $J = 7.5$ Hz, 1H, CH_{Ar}), 6.65 (s, 1H, CH_{Ar}), 3.79 (s, 3H, OCH₃), 2.60 – 2.56 (m, 1H, CH-Ar), 1.90 (ddd, $J = 8.4, 4.5, 4.5$ Hz, 1H, CH-COOH), 1.65 (ddd, $J = 9.5, 4.5, 5.0$ Hz, 1H, CH₂), 1.41 – 1.37 (m, 1H, CH₂) ppm. ¹³C NMR (125 MHz, CDCl₃): δ 179.7 (C=O), 159.8 (C_{Ar}), 141.2 (C_{Ar}), 129.6 (CH_{Ar}), 118.6 (CH_{Ar}), 112.3 (CH_{Ar}), 112.0 (CH_{Ar}), 56.2 (OCH₃), 27.1 (CH-Ar), 24.0 (CH-COOH), 17.5 (CH₂)

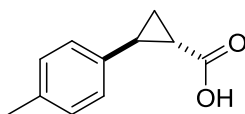
ppm. **IR** (Neat): 2934, 1684 cm^{-1} . **HRMS** (ESI) m/z : $[\text{M} - \text{H}]^-$ Calcd for $\text{C}_{11}\text{H}_{11}\text{O}_3$ 191.0708; Found 191.0699. **Melting point**: 94.3 – 95.1 $^{\circ}\text{C}$.

2-(m-Fluorophenyl)cyclopropane-1-carboxylic acid (61d)



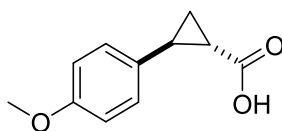
Sodium hydroxide solution (1 M, 5.1 mL, 5.1 mmol, 2 equiv) was added to a solution of **60d** (529 mg, 2.54 mmol, 1 equiv) in ethanol (45 mL). After the solution was left stirring overnight at room temperature, hydrochloric acid solution (2 M, 3.8 mL, 7.6 mmol, 3 equiv) and water (5 mL) were added to the reaction solution at 0 $^{\circ}\text{C}$. The solution was extracted with ethyl acetate (80 mL + 2 \times 20 mL) and washed with brine solution (2 \times 40 mL). After drying the solution with magnesium sulfate, the solution was concentrated under reduced pressure to give the title compound as a white solid (367 mg, 2.04 mmol) in 80% yield. **^1H NMR** (500 MHz, CDCl_3): δ 7.24 (d, $J = 6.5$ Hz, 1H, CH_{Ar}), 6.92 – 6.89 (m, 2H, CH_{Ar}), 6.79 (d, $J = 10$ Hz, 1H, CH_{Ar}), 2.61 – 2.57 (m, 1H, CH-Ar), 1.90 (ddd, $J = 8.4, 4.5, 4.5$ Hz, 1H, CH-COOH), 1.67 (ddd, $J = 9.6, 4.8, 5.0$ Hz, 1H, CH_2), 1.40 – 1.36 (m, 1H, CH_2) ppm. **^{13}C NMR** (125 MHz, CDCl_3): δ 179.5 (C=O), 163.0 (d, $J = 244$ Hz, C_{Ar}), 142.2 (d, $J = 7.5$ Hz, C_{Ar}), 130.0 (d, $J = 7.5$ Hz, CH_{Ar}), 122.1 (d, $J = 3.8$ Hz, CH_{Ar}), 113.7 (d, $J = 21.3$ Hz, CH_{Ar}), 113.2 (d, $J = 22.5$ Hz, CH_{Ar}), 26.6 (d, $J = 2.5$ Hz, CH-Ar), 24.1 (CH-COOH), 17.5 (CH_2) ppm. **IR** (Neat): 1685 cm^{-1} . **HRMS** (ESI) m/z : $[\text{M} - \text{H}]^-$ Calcd for $\text{C}_{10}\text{H}_8\text{FO}_2$ 179.05083; Found 179.05068. **Melting point**: 78.9 – 79.9 $^{\circ}\text{C}$.

2-(p-Tolyl)cyclopropane-1-carboxylic acid (61e)



Sodium hydroxide solution (1 M, 4.7 mL, 4.7 mmol, 2 equiv) was added to a solution of **60e** (477 mg, 2.33 mmol) in ethanol (43 mL). After the solution was left stirring overnight at room temperature, hydrochloric acid solution (2 M, 3.6 mL, 7.2 mmol) and water (21 mL) were added to the reaction solution at 0 °C. The solution was extracted with ethyl acetate (80 mL + 2 × 40 mL) and washed with brine solution (30 mL). After drying the solution with magnesium sulfate, the solution was concentrated under reduced pressure to give the title compound as a white solid (344 mg, 1.95 mmol) in 84% yield. **¹H NMR** (500 MHz, CDCl₃): δ 7.10 (d, *J* = 7.5 Hz, 2H, CH_{Ar}), 7.01 (d, *J* = 8 Hz, 2H, CH_{Ar}), 2.59 – 2.55 (m, 1H, CH-Ar), 2.32 (s, 3H, CH₃), 1.87 (ddd, *J* = 8.4, 4.5, 4.5 Hz, 1H, CH-COOH), 1.63 (ddd, *J* = 9.3, 4.8, 5 Hz, 1H, CH₂), 1.39 – 1.35 (m, 1H, CH₂) ppm. **Melting point:** 113.0 – 116.4 °C. ¹H NMR data are consistent with literature.⁵⁴

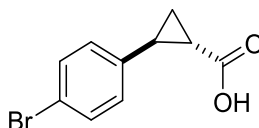
2-(p-Methoxyphenyl)cyclopropane-1-carboxylic acid (61f)



Sodium hydroxide solution (1 M, 8.5 mL, 8.5 mmol, 2 equiv) was added to a solution of **60f** (918 mg, 4.17 mmol, 1 equiv) in ethanol (15 mL). After the solution was left stirring overnight at room temperature, hydrochloric acid solution (2 M, 6.40 mL, 12.8 mmol, 3 equiv) and water (9 mL) were added at 0 °C. The solution was extracted with ethyl acetate

(50 mL + 2 × 30 mL) and washed with brine solution (2 × 30 mL). After drying the solution with magnesium sulfate, the solution was concentrated under reduced pressure to give the title compound as a white solid (791 mg, 4.12 mmol) in 99% yield. ¹H NMR (500 MHz, CDCl₃): δ 7.05 (d, *J* = 8.5 Hz, 2H, CH_{Ar}), 6.83 (d, *J* = 9 Hz, 2H, CH_{Ar}), 3.79 (s, 3H, OCH₃), 2.59 – 2.55 (m, 1H, CH-Ar), 1.83 (ddd, *J* = 8.4, 4.5, 4.5 Hz, 1H, CH-COOH), 1.62 (ddd, *J* = 9.5, 4.8, 4.5 Hz, 1H, CH₂), 1.37 – 1.34 (m, 1H, CH₂) ppm. **Melting point:** 109.9 – 113.3 °C. ¹H NMR data are consistent with literature.⁵⁴

*2-(p-Bromophenyl)cyclopropane-1-carboxylic acid (61g)*⁵⁵



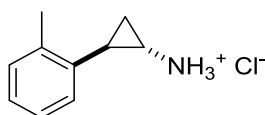
Sodium hydroxide solution (1 M, 6.9 mL, 6.9 mmol, 2 equiv) was added to a solution of **60g** (922 mg, 3.43 mmol, 1 equiv) in ethanol (12 mL). After the solution was left stirring overnight at room temperature, hydrochloric acid solution (2 M, 5.20 mL, 10.4 mmol, 3 equiv) and water (5 mL) were added to the reaction solution at 0 °C. The solution was extracted with ethyl acetate (3 × 30 mL) and washed with brine solution (2 × 30 mL). After drying the solution with magnesium sulfate, the solution was concentrated under reduced pressure to give the title compound as a white solid (823.1 mg, 3.41 mmol) in 100% yield. ¹H NMR (500 MHz, CDCl₃): δ 7.41 (d, *J* = 8.5 Hz, 2H, CH_{Ar}), 6.98 (d, *J* = 8 Hz, 2H, CH_{Ar}), 2.57 – 2.53 (m, 1H, CH-Ar), 1.88 (ddd, *J* = 8.2, 4.2, 4.0 Hz, 1H, CH-COOH), 1.66 (ddd, *J* = 9.2, 4.8, 5.0 Hz, 1H, CH₂), 1.39 – 1.35 (m, 1H, CH₂) ppm. ¹³C NMR (75 MHz, CDCl₃): δ 179.3 (C=O), 138.8 (C_{Ar}), 131.7 (CH_{Ar}), 128.2 (CH_{Ar}), 120.5 (C_{Ar}), 26.5 (CH-Ar), 24.2 (CH-COOH), 17.5 (CH₂) ppm. **IR** (Neat): 2923, 1681 cm⁻¹.

HRMS (ASAP) m/z : $[M + H]^+$ Calcd for $C_{10}H_{10}O_2Br$ 240.9864; Found 240.9865.

Melting point: 118.5 – 122.4 °C.

3.5.4 Curtius rearrangement of carboxylic acids with *t*-BuOH + Deprotection of Boc-group

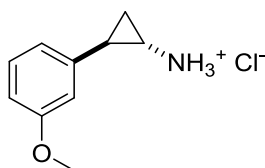
2-(*o*-Tolyl)cyclopropylamine hydrochloride (**62b**)



Diphenyl phosphoryl azide (1.10 mL, 1.38 g, 5.02 mmol, 1.2 equiv), triethylamine (0.950 mL, 0.692 g, 6.84 mmol, 1.6 equiv) and *tert*-butanol (8.80 mL, 6.76 g, 91.2 mmol, 21 equiv) were added to a solution of **61b** (749 mg, 4.25 mmol, 1 equiv) in dry toluene (25 mL). After the reaction was heated at 82 °C for 24 h, di-*tert*-butyl dicarbonate (1.15 g, 5.29 mmol, 1.2 equiv) was added and the reaction solution was allowed to stir for another 1.5 h before concentrating it under reduced pressure. The crude mixture was subjected to column chromatography (15% ethyl acetate/hexane) to give the intermediate *tert*-butyl (2-(*o*-tolyl)cyclopropyl)carbamate as a yellowish white solid (502 mg, 2.03 mmol). ¹H NMR (300 MHz, CDCl₃): δ 7.12 – 7.05 (m, 4H), 4.82 (bs, 1H), 2.78 (bs, 1H), 2.41 (s, 3H), 2.02 – 1.97 (m, 1H), 1.47 (s, 9H), 1.15 – 1.11 (m, 2H) ppm. Trifluoroacetic acid (5 mL) was added to a solution of *tert*-butyl (2-(*o*-tolyl)cyclopropyl)carbamate (495 mg, 2.00 mmol) in dichloromethane (1 mL). After the solution was stirred for 30 mins, solvent was removed under reduced pressure and ethereal HCl (1 M, 7 mL, 7 mmol, 3.5 equiv) was added to precipitate the product. Solvent was carefully removed using a glass pasteur pipette and the precipitate was washed with diethyl ether (3 × 10 mL). The title compound

was collected as a yellow solid (344 mg, 1.87 mmol) in 45% yield after two consecutive steps. **¹H NMR** (500 MHz, DMSO): δ 8.72 (br s, 3H, NH₃⁺), 7.16 (bs, 1H, CH_{Ar}), 7.12 – 7.09 (m, 2H, CH_{Ar}), 6.98 (d, J = 6 Hz, 1H, CH_{Ar}), 2.68 (bs, 1H, CH-NH₃⁺), 2.46 (m, 1H, CH-Ar), 2.38 (s, 3H, CH₃), 1.39 – 1.35 (m, 1H, CH₂), 1.20 – 1.16 (m, 1H, CH₂) ppm. **¹³C NMR** (125 MHz, DMSO): δ 137.2 (C_{Ar}), 136.9 (C_{Ar}), 129.6 (CH_{Ar}), 126.5 (CH_{Ar}), 125.9 (CH_{Ar}), 125.6 (CH_{Ar}), 29.6 (CH-NH₃⁺), 19.5 (CH₃), 18.9 (CH-Ar), 11.4 (CH₂) ppm. **IR** (Neat): 2898 cm⁻¹. **HRMS** (ESI) m/z : [M + H]⁺ Calcd for C₁₀H₁₄N 148.1126; Found 148.1130. **Melting point**: 173.7 – 175.4 °C.

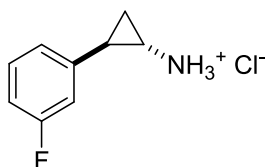
*2-(m-Methoxyphenyl)cyclopropylamine hydrochloride (62c)*⁵⁶



Diphenyl phosphoryl azide (0.850 mL, 1.09 g, 3.95 mmol, 1.2 equiv), triethylamine (0.750 mL, 0.545 g, 5.38 mmol, 1.7 equiv) and *tert*-butanol (7.00 mL, 5.43 g, 73.2 mmol, 22 equiv) were added to a solution of **61c** (627 mg, 3.26 mmol, 1 equiv) in dry toluene (20 mL). After the reaction was heated at 82 °C for 24 h, di-*tert*-butyl dicarbonate (1.06 g, 4.88 mmol, 1.5 equiv) was added and the reaction solution was allowed to stir for another 2 h before concentrating it under reduced pressure. The crude mixture was subjected to rapid column chromatography (20% ethyl acetate/hexane) to give the intermediate *tert*-butyl (2-(*m*-methoxyphenyl)cyclopropyl)carbamate as a white solid (459 mg, 1.74 mmol). **¹H NMR** (500 MHz, CDCl₃): δ 7.17 (t, J = 8 Hz, 1H), 6.72 (d, J = 8 Hz, 2H), 6.65 (bs, 1H), 4.82 (bs, 1H), 3.78 (s, 3H), 2.74 (bs, 1H), 2.03 – 1.99 (m, 1H), 1.45 (s, 9H), 1.17 – 1.15 (m, 2H) ppm. Trifluoroacetic acid (3 mL) was added to a solution

of *tert*-butyl (2-(*m*-methoxyphenyl)cyclopropyl)carbamate (458 mg, 1.74 mmol, 1 equiv) in dichloromethane (2 mL). After the solution was stirred for 50 mins, solvent was removed under reduced pressure and ethereal HCl (1 M, 6 mL, 6 mmol, 3.4 equiv) was added to precipitate the product. Solvent was carefully removed using a glass pasteur pipette and the precipitate was washed with diethyl ether (4 × 10 mL). The title compound was collected as a sandy brown solid (330 mg, 1.65 mmol) in 50% yield after two consecutive steps. **¹H NMR** (300 MHz, DMSO): δ 8.68 (br s, 3H, NH₃⁺), 7.19 (t, *J* = 7.8 Hz, 1H, CH_{Ar}), 6.77 – 6.70 (m, 3H, CH_{Ar}), 3.73 (s, 3H, OCH₃), 2.77 (bs, 1H, CH-NH₃⁺), 2.35 (bs, 1H, CH-Ar), 1.45 – 1.39 (m, 1H, CH₂), 1.22 – 1.15 (m, 1H, CH₂) ppm. **¹³C NMR** (75 MHz, DMSO): δ 159.4 (C_{Ar}), 140.9 (C_{Ar}), 129.4 (CH_{Ar}), 118.5 (CH_{Ar}), 111.9 (CH_{Ar}), 111.8 (CH_{Ar}), 55.0 (OCH₃), 30.5 (CH-NH₃⁺), 20.8 (CH-Ar), 13.2 (CH₂) ppm. **IR** (Neat): 3065, 2958, 2870 cm⁻¹. **HRMS** (ESI) *m/z*: [M + H]⁺ Calcd for C₁₀H₁₄ON 164.1075; Found 164.1076. **Melting point**: 146.5 – 147.8 °C.

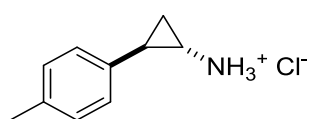
2-(m-Fluorophenyl)cyclopropylamine hydrochloride (62d)



Diphenyl phosphoryl azide (0.500 mL, 613 mg, 2.23 mmol, 1.2 equiv), triethylamine (0.420 mL, 308 mg, 3.04 mmol, 1.6 equiv) and *tert*-butanol (3.90 mL, 3.00 g, 40.5 mmol, 22 equiv) were added to a solution of **61d** (339 mg, 1.88 mmol, 1 equiv) in dry toluene (11 mL). After the reaction was heated at 82 °C for 22 h, di-*tert*-butyl dicarbonate (670 mg, 3.07 mmol, 1.6 equiv) was added and the reaction solution was allowed to stir for another 2 h before concentrating it under reduced pressure. The crude mixture was

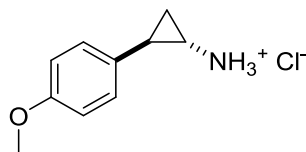
subjected to column chromatography (15% ethyl acetate/hexane) to give the intermediate *tert*-butyl (2-(*m*-fluorophenyl)cyclopropyl)carbamate as a white solid (203 mg, 0.809 mmol). ¹H NMR (500 MHz, CDCl₃): δ 7.21 (q, *J* = 6.5 Hz, 1H), 6.92 (d, *J* = 7.5 Hz, 1H), 6.87 – 6.80 (m, 2H), 4.84 (bs, 1H), 2.71 (bs, 1H), 2.05 – 2.02 (m, 1H), 1.45 (s, 9H), 1.16 (t, *J* = 7.5 Hz, 2H) ppm. Trifluoroacetic acid (2 mL) was added to a solution of *tert*-butyl (2-(*m*-fluorophenyl)cyclopropyl)carbamate (203 mg, 0.809 mmol, 1 equiv) in dichloromethane (3 mL). After the solution was stirred for 30 mins, solvent was removed under reduced pressure and ethereal HCl (1 M, 4 mL, 4 mmol, 4.9 equiv) was added to precipitate the product. Solvent was carefully removed using a glass pasteur pipette and the precipitate was washed with diethyl ether (3 × 10 mL). The title compound was collected as a white solid (146 mg, 0.776 mmol) in 41% yield after two consecutive steps. ¹H NMR (300 MHz, DMSO): δ 8.72 (br s, 3H, NH₃⁺), 7.32 (q, *J* = 6 Hz, 1H, CH_{Ar}), 7.02 (t, *J* = 6.9 Hz, 3H, CH_{Ar}), 2.84 – 2.79 (m, 1H, CH-NH₃⁺), 2.45 – 2.38 (m, 1H, CH-Ar), 1.50 – 1.43 (m, 1H, CH₂), 1.23 (m, 1H, CH₂) ppm. ¹³C NMR (125 MHz, DMSO): δ 162.3 (d, *J* = 241.3 Hz, C_{Ar}), 142.5 (d, *J* = 7.5 Hz, C_{Ar}), 130.2 (d, *J* = 8.8 Hz, CH_{Ar}), 122.7 (d, *J* = 2.5 Hz, CH_{Ar}), 113.0 (d, *J* = 17.5 Hz, CH_{Ar}), 112.9 (d, *J* = 18.8 Hz, CH_{Ar}), 30.7 (CH-NH₃⁺), 20.5 (d, *J* = 2.5 Hz, CH-Ar), 13.5 (CH₂) ppm. IR (Neat): 2990, 2945, 2863, cm⁻¹. HRMS (ASAP) *m/z*: [M + H]⁺ Calcd for C₉H₁₁NF 152.0876; Found 152.0906. **Melting point**: 173.8 – 175.4 °C

2-(p-Tolyl)cyclopropylamine hydrochloride (62e)



Diphenyl phosphoryl azide (0.500 mL, 0.640 g, 2.33 mmol, 1.2 equiv), triethylamine (0.410 mL, 298 mg, 2.94 mmol, 1.6 equiv) and *tert*-butanol (3.80 mL, 2.95 g, 39.7 mmol, 21 equiv) were added to a solution of **61e** (331 mg, 1.88 mmol, 1 equiv) in dry toluene (11 mL). After the reaction was heated at 82 °C for 24 h, di-*tert*-butyl dicarbonate (647 mg, 2.96 mmol, 1.6 equiv) was added and the reaction solution was allowed to stir for another 2 h before concentrating it under reduced pressure. The crude mixture was subjected to column chromatography (15% ethyl acetate/hexane) to give the intermediate *tert*-butyl (2-(*p*-tolyl)cyclopropyl)carbamate as a white solid (228 mg, 0.921 mmol). **¹H NMR** (500 MHz, CDCl₃): δ 7.07 (d, *J* = 8 Hz, 2H), 7.02 (d, *J* = 7.5 Hz, 2H), 4.84 (bs, 1H), 2.69 (bs, 1H), 2.30 (s, 3H), 2.02 – 1.98 (m, 1H), 1.45 (s, 9H), 1.14 – 1.12 (m, 2H) ppm. Trifluoroacetic acid (2 mL) was added to a solution of *tert*-butyl (2-(*p*-tolyl)cyclopropyl)carbamate (216 mg, 0.872 mmol, 1 equiv) in dichloromethane (2 mL). After the solution was stirred for 30 mins, solvent was removed under reduced pressure and ethereal HCl (1 M, 4 mL, 4 mmol, 4.6 equiv) was added to precipitate the product. Solvent was carefully removed using a glass pasteur pipette and the precipitate was washed with diethyl ether (2 × 10 mL). The title compound was collected as a yellow solid (124 mg, 0.675 mmol) in 38% yield after two consecutive steps. **¹H NMR** (500 MHz, DMSO): δ 8.67 (br s, 3H, NH₃⁺), 7.09 (d, *J* = 7.5 Hz, 2H, CH_{Ar}), 7.03 (d, *J* = 8 Hz, 2H, CH_{Ar}), 2.70 (bs, 1H, CH-NH₃⁺), 2.34 (bs, 1H, CH-Ar), 2.25 (s, 3H, CH₃), 1.41 – 1.37 (m, 1H, CH₂), 1.14 – 1.11 (m, 1H, CH₂) ppm. **¹³C NMR** (125 MHz, DMSO): δ 136.2 (C_{Ar}), 135.3 (C_{Ar}), 128.9 (CH_{Ar}), 126.1 (CH_{Ar}), 30.4 (CH-NH₃⁺), 20.6 (CH₃), 20.4 (CH-Ar), 13.0 (CH₂) ppm. **IR** (Neat): 2903 cm⁻¹. **HRMS** (ESI) *m/z*: [M + H]⁺ Calcd for C₁₀H₁₄N 148.11262; Found 148.11215. **Melting point**: 150.2 – 155.5 °C.

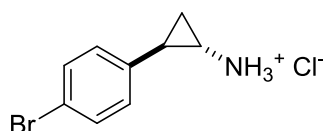
2-(*p*-Methoxyphenyl)cyclopropylamine hydrochloride (**62f**)



Diphenyl phosphoryl azide (0.970 mL, 1.24 g, 4.51 mmol, 1.2 equiv), triethylamine (0.850 mL, 0.620 g, 6.13 mmol, 1.6 equiv) and *tert*-butanol (7.80 mL, 6.06 g, 81.8 mmol, 21 equiv) were added to a solution of **61f** (746 mg, 3.88 mmol, 1 equiv) in dry toluene (24 mL). After the reaction was heated at 82 °C for 24 h, di-*tert*-butyl dicarbonate (991 mg, 4.54 mmol, 1.2 equiv) was added and the reaction solution was allowed to stir for another 2 h before concentrating it under reduced pressure. The crude mixture was subjected to column chromatography (20% ethyl acetate/hexane) to give the intermediate *tert*-butyl (2-(*p*-methoxyphenyl)cyclopropyl)carbamate as a white solid (608 mg, 2.31 mmol). ¹H NMR (500 MHz, CDCl₃): δ 7.08 (d, *J* = 8 Hz, 2H), 6.81 (d, *J* = 8 Hz, 2H), 4.81 (bs, 1H), 3.77 (s, 3H), 2.65 (bs, 1H), 2.00 (bs, 1H), 1.46 (s, 9H), 1.11 – 1.08 (m, 2H) ppm. Trifluoroacetic acid (2 mL) was added to a solution of *trans-tert*-Butyl-2-(*p*-methoxyphenyl)cyclopropylcarbamate (0.371 g, 1.41 mmol) in dichloromethane (2 mL). After the solution was stirred for 30 mins, solvent was removed under reduced pressure and ethereal HCl (1 M, 4 mL, 4 mmol, 2.9 equiv) was added to precipitate the product. Solvent was carefully removed using a glass pasteur pipette and the precipitate was washed with diethyl ether (5 × 10 mL). The title compound was collected as pale-yellow powder (225 mg, 1.13 mmol) in 41% yield after two consecutive steps. ¹H NMR (500 MHz, CD₃OD): δ 7.10 (d, *J* = 8 Hz, 2H, CH_{Ar}), 6.86 (d, *J* = 8 Hz, 2H, CH_{Ar}), 3.76 (s, 3H, OCH₃), 2.76 – 2.75 (m, 1H, CH-NH₃⁺), 2.35 (bs, 1H, CH-Ar), 1.39 – 1.36 (m, 1H, CH₂), 1.25 (q, *J* = 7 Hz, 1H, CH₂) ppm. ¹³C NMR (125 MHz, CD₃OD): δ 160.1 (C_{Ar}), 131.6 (C_{Ar}), 128.6 (CH_{Ar}), 115.1 (CH_{Ar}), 55.7 (OCH₃), 31.8 (CH-NH₃⁺), 21.9 (CH-Ar), 13.4

(CH₂) ppm. **IR** (Neat): 3128, 3037, 2884 cm⁻¹. **Melting point**: 176.4 – 179.4 °C. ¹H NMR data are consistent with literature.⁵⁰

2-(p-Bromophenyl)cyclopropylamine hydrochloride (62g)

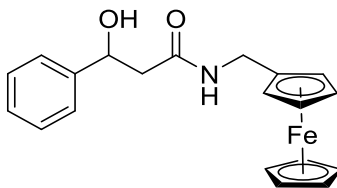


Diphenyl phosphoryl azide (0.800 mL, 1.02 g, 3.72 mmol, 1.5 equiv), triethylamine (0.700 mL, 508 mg, 5.02 mmol, 2 equiv) and *tert*-butanol (6.40 mL, 4.96 g, 66.9 mmol, 26 equiv) were added to a solution of **61g** (612 mg, 2.54 mmol, 1 equiv) in dry toluene (20 mL). After the reaction was heated at 82 °C for 24 h, di-*tert*-butyl dicarbonate (841 mg, 3.85 mmol, 1.5 equiv) was added and the reaction solution was allowed to stir for another 1 h before concentrating it under reduced pressure. The crude mixture was subjected to column chromatography (15% ethyl acetate/hexane) to give the intermediate *tert*-butyl (2-(*p*-bromophenyl)cyclopropyl)carbamate as a white solid (372 mg, 1.19 mmol). ¹H NMR (500 MHz, CDCl₃): δ 7.37 (d, *J* = 7.5 Hz, 2H), 7.02 (d, *J* = 7.5 Hz, 2H), 4.81 (bs, 1H), 2.67 (bs, 1H), 2.00 (bs, 1H), 1.45 (s, 9H), 1.15 – 1.12 (bs, 2H) ppm. Trifluoroacetic acid (4 mL) was added to a solution of *tert*-butyl (2-(*p*-bromophenyl)cyclopropyl)carbamate (372 mg, 1.19 mmol, 1 equiv) in dichloromethane (3 mL). After the solution was stirred for 30 mins, solvent was removed under reduced pressure and ethereal HCl (1 M, 5 mL, 5 mmol, 4.2 equiv) was added to precipitate the product. Solvent was carefully removed using a glass pasteur pipette and the precipitate was washed with diethyl ether (2 × 10 mL). The title compound was collected as an off white solid (287 mg, 1.16 mmol) in 46% yield after two consecutive steps. ¹H NMR (500

MHz, CD₃OD): δ 7.45 (d, $J = 8$ Hz, 2H, CH_{Ar}), 7.11 (d, $J = 8$ Hz, 2H, CH_{Ar}), 2.85 (ddd, $J = 7.6, 4, 4$ Hz, 1H, CH-NH₃⁺), 2.38 – 2.34 (m, 1H, CH-Ar), 1.46 – 1.42 (m, 1H, CH₂), 1.33 (q, $J = 7$ Hz, 1H, CH₂) ppm. ¹³C NMR (125 MHz, CD₃OD): δ 139.1 (C_{Ar}), 132.7 (CH_{Ar}), 129.4 (CH_{Ar}), 121.5 (C_{Ar}), 32.0 (CH-NH₃⁺), 22.1 (CH-Ar), 13.9 (CH₂) ppm. IR (Neat): 3013, 2884 cm⁻¹. **Melting point:** 191.0 – 194.7 °C. ¹H NMR data are consistent with literature.⁵⁰

3.5.5 Oxidative ring-opening of ferrocenylmethylcyclopropylamines

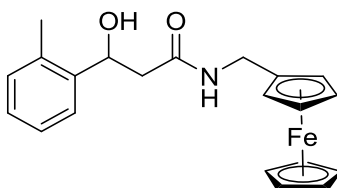
N-(Ferrocenylmethyl)-3-hydroxy-3-phenylpropanamide (**65a**)



Triethylamine (0.130 mL, 94.4 mg, 0.933 mmol, 1.9 equiv) was added to a suspension of *trans*-2-phenylcyclopropylamine hydrochloride (82.2 mg, 0.485 mmol, 1 equiv) and magnesium sulfate (219 mg, 1.82 mmol, 3.8 equiv) in dry dichloromethane (4 mL). This mixture was stirred for 10 minutes before ferrocenecarboxaldehyde (123 mg, 0.575 mmol, 1.2 equiv) was added. After 3 hours of stirring, another portion of ferrocenecarboxaldehyde (20.0 mg, 93.4 μ mol, 0.2 equiv) and one spatula of magnesium sulfate were added. The mixture was allowed to stir overnight after which another portion of ferrocenecarboxaldehyde (14.4 mg, 67.3 μ mol, 0.1 equiv) and a spatula of magnesium sulfate were added. After 2 hours of stirring, dry toluene (8 mL) was added to precipitate triethylamine hydrochloride and the mixture was filtered. After removal of solvents under reduced pressure, more triethylamine hydrochloride precipitated out, therefore dry toluene (10 mL) was added and the mixture was filtered again. After removal of solvents,

sodium borohydride (45.2 mg, 1.19 mmol, 2.5 equiv) was added to the solution of crude imine mixture (213 mg) in dry methanol (5 mL) at $-10\text{ }^{\circ}\text{C}$. After stirring for 15 minutes at $-10\text{ }^{\circ}\text{C}$, the reaction was left stirring at room temperature. Another portion of sodium borohydride (17.1 mg, 0.452 mmol, 0.9 equiv) was added after 45 mins at $-10\text{ }^{\circ}\text{C}$. After stirring for 15 minutes at $-10\text{ }^{\circ}\text{C}$, the reaction solution was left stirring overnight at room temperature. The reaction was quenched with water (5 mL) and methanol was evaporated under reduced pressure. After the aqueous layer was extracted with ethyl acetate ($3 \times 10\text{ mL}$), the combined organic extracts were washed with brine (10 mL) and dried over magnesium sulfate. This crude mixture was subjected to column chromatography (40-80% ethyl acetate/hexane) which yielded the title compound as a yellow-orange solid (77.8 mg, 0.214 mmol) in a 44% overall yield. **$^1\text{H NMR}$** (500 MHz, CDCl_3): δ 7.36 – 7.25 (m, 5H, CH_{Ar}), 6.08 (s, 1H, NH), 5.09 (dd, $J = 8.75, 3.5\text{ Hz}$, 1H, CH-OH), 4.14 – 4.12 (m, 11H, $\text{CH}_2\text{-NH}$ and CH_{Cp}), 2.59 – 2.50 (m, 2H, $\text{CH}_2\text{-CHOH}$) ppm. **$^{13}\text{C NMR}$** (125 MHz, CDCl_3): δ 171.1 (C=O), 143.1 (C_{Ar}), 128.5 (CH_{Ar}), 127.7 (CH_{Ar}), 125.6 (CH_{Ar}), 84.4 (C_{Cp}), 70.9 (CH-OH), 68.6 (CH_{Cp}), 68.2 (CH_{Cp}), 68.1 (CH_{Cp}), 44.7 ($\text{CH}_2\text{-CHOH}$), 38.8 ($\text{CH}_2\text{-NH}$) ppm. **IR** (Neat): 3300, 1646 cm^{-1} . **HRMS** (ASAP) m/z : $[\text{M}]^+$ Calcd for $\text{C}_{20}\text{H}_{21}\text{FeNO}_2$ 363.0922; Found 363.0914. **Melting point**: 114.7 – 116.9 $^{\circ}\text{C}$.

N-(Ferrocenylmethyl)-3-hydroxy-3-(*o*-methylphenyl)propanamide (**65b**)

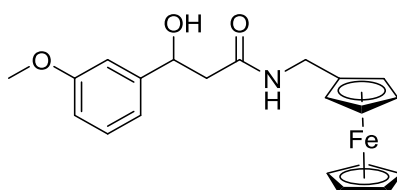


Triethylamine (0.150 mL, 109 mg, 1.08 mmol, 2 equiv) was added to a suspension of **62b** (101 mg, 0.550 mmol, 1 equiv) and magnesium sulfate (235 mg) in dry dichloromethane

(4 mL). This mixture was stirred for 10 minutes before ferrocenecarboxaldehyde (139 mg, 0.651 mmol, 1.2 equiv) was added. After 3 hours of stirring, another portion of ferrocenecarboxaldehyde (25.8 mg, 0.121 mmol, 0.2 equiv) and one spatula of magnesium sulfate were added. The mixture was allowed to stir overnight after which another portion of ferrocenecarboxaldehyde (12.1 mg, 56.5 μ mol, 0.1 equiv) and a spatula of magnesium sulfate were added. After 2 hours of stirring, dry toluene (8 mL) was added to precipitate triethylamine hydrochloride and the mixture was filtered. After removal of solvents under reduced pressure, more triethylamine hydrochloride precipitated out, therefore dry toluene (10 mL) was added and the mixture was filtered again. After removal of solvents, sodium borohydride (50.1 mg, 1.32 mmol, 2.4 equiv) was added to the solution of crude imine mixture (252 mg) in dry methanol (7 mL) at -10 °C. After stirring for 15 minutes at -10 °C, the reaction was left stirring at room temperature. Another portion of sodium borohydride (20.9 mg, 0.552 mmol, 1.7 equiv) was added after 4 h 30 mins at -10 °C. After stirring for 15 minutes at -10 °C, the reaction solution was left stirring overnight at room temperature. The reaction was quenched with water (4 mL) and methanol was evaporated under reduced pressure. After the aqueous layer was extracted with ethyl acetate (3×10 mL), the combined organic extracts were washed with brine (10 mL) and dried over magnesium sulfate. This crude mixture was subjected to column chromatography (40-80% ethyl acetate/hexane) which yielded the title compound as a brown-orange solid (46.1 mg, 0.122 mmol) in a 22% overall yield. **$^1\text{H NMR}$** (500 MHz, CDCl_3): δ 7.47 (d, $J = 7.5$ Hz, 1H, CH_{Ar}), 7.21 – 7.14 (m, 2H, CH_{Ar}), 7.10 – 7.09 (m, 1H, CH_{Ar}), 6.29 (bs, 1H, NH), 5.27 (d, $J = 9$ Hz, 1H, CH-OH), 4.14 – 4.12 (m, 11H, $\text{CH}_2\text{-NH}$ and CH_{Cp}), 2.50 – 2.40 (m, 2H, $\text{CH}_2\text{-CHOH}$), 2.29 (s, 3H, CH_3) ppm. **$^{13}\text{C NMR}$** (125 MHz, CDCl_3): δ 171.3 (C=O), 141.1 (C_{Ar}), 134.1 (C_{Ar}), 130.5 (CH_{Ar}), 127.5 (CH_{Ar}), 126.5 (CH_{Ar}), 125.3 (CH_{Ar}), 84.5 (C_{Cp}), 68.7 (CH_{Cp}), 68.3 (CH_{Cp}), 68.3 (CH_{Cp}), 67.5 (CH-

OH), 43.4 (CH₂-CHOH), 38.9 (CH₂-NH), 19.1 (CH₃) ppm. **IR** (Neat): 3305, 1636 cm⁻¹. **HRMS** (ESI) m/z: [M]⁺ Calcd for C₂₁H₂₃FeNO₂ 377.10782; Found 377.10726. **Melting point**: 103.2 – 107.3 °C.

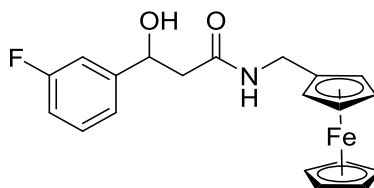
N-(Ferrocenylmethyl)-3-hydroxy-3-(*m*-methoxyphenyl)propanamide (**65c**)



Magnesium sulfate (231 mg, 1.92mmol, 3.8 equiv) was added to a solution of **62c** (101 mg, 0.506 mmol, 1 equiv) and triethylamine (0.210 ml, 1.51 mmol, 3 equiv) in dry dichloromethane (5 mL). This mixture was stirred for 15 mins before ferrocenecarboxaldehyde (0.130 g, 0.608 mmol, 1.2 equiv) was added. After 4 h of stirring, another portion of ferrocenecarboxaldehyde (19.7 mg, 0.0920 mmol, 0.2 equiv) and magnesium sulfate (103 mg, 0.859 mmol, 1.7 equiv) were added. The mixture was allowed to stir overnight after which another portion of ferrocenecarboxaldehyde (14.3 mg, 0.0668 mmol, 0.1 equiv) and a spatula of 4 Å molecular sieves were added. After 2 h of stirring, dry toluene (10 mL) was added to precipitate triethylamine hydrochloride and the mixture was filtered. After removal of solvents under reduced pressure, more triethylamine hydrochloride precipitated out, therefore dry toluene (4 mL) was added and the mixture was filtered again. After removal of solvents, sodium borohydride (41.1 mg, 1.09 mmol, 2.2 equiv) was added to the solution of crude imine mixture (240 mg) in dry methanol (3 mL) at -10 °C. After stirring for 15 mins at -10 °C, the reaction solution was left stirring overnight at room temperature. The reaction was quenched with water (5 mL) and methanol was evaporated by purging nitrogen gas through the flask. After the

aqueous layer was extracted with ethyl acetate (3 × 15 mL), the combined organic extracts were washed with brine (5 mL) and dried over magnesium sulfate. This crude mixture was subjected to column chromatography (40-80% ethyl acetate/hexane) which yielded the title compound as a brownish orange solid (112 mg, 0.284 mmol) in a 56% overall yield. **¹H NMR** (500 MHz, CDCl₃): δ 7.26 – 7.23 (m, 1H, CH_{Ar}), 6.94 – 6.91 (m, 2H, CH_{Ar}), 6.81 (d, *J* = 8 Hz, 1H, CH_{Ar}), 6.05 (bs, 1H, NH), 5.08 – 5.07 (m, 1H, CH-OH), 4.15 – 4.13 (m, 11H, CH₂-NH and CH_{Cp}), 3.80 (s, 3H, OCH₃), 2.56-2.54 (m, 2H, CH₂-CHOH) ppm. **¹³C NMR** (125 MHz, CDCl₃): δ 171.2 (C=O), 160.0 (C_{Ar}), 145.0 (C_{Ar}), 129.8 (CH_{Ar}), 118.0 (CH_{Ar}), 113.5 (CH_{Ar}), 111.3 (CH_{Ar}), 84.6 (C_{Cp}), 71.1 (CH-OH), 68.8 (CH_{Cp}), 68.4 (CH_{Cp}), 68.4 (CH_{Cp}), 68.4 (CH_{Cp}), 55.5 (OCH₃), 44.9 (CH₂-CHOH), 39.0 (CH₂-NH) ppm. **IR** (Neat): 3310, 1647 cm⁻¹. **HRMS** (ESI) *m/z*: [M + Na]⁺ Calcd for C₂₁H₂₃NO₃FeNa 416.0925; Found 416.0918. **Melting point**: 83.2 – 86.8 °C.

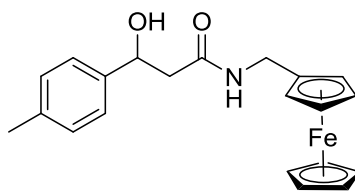
N-(Ferrocenylmethyl)-3-hydroxy-3-(*m*-fluorophenyl)propanamide (**65d**)



Magnesium sulfate (134 mg, 1.11 mmol, 5.8 equiv) was added to a solution of **62d** (35.4 mg, 0.189 mmol, 1 equiv) and triethylamine (0.0800 mL, 0.574 mmol, 3 equiv) in dry dichloromethane (2.0 mL). This mixture was stirred for 15 mins before ferrocenecarboxaldehyde (43.7 mg, 0.204 mmol, 1.1 equiv) was added. After 4 h of stirring, another portion of ferrocenecarboxaldehyde (4.50 mg, 0.0210 mmol, 0.1 equiv) and magnesium sulfate (100.6 mg, 0.836 mmol, 4.4 equiv) were added. The mixture was allowed to stir overnight after which another portion of ferrocenecarboxaldehyde (2.80

mg, 0.0131 mmol, 0.1 equiv) and a spatula of 4Å molecular sieves were added. After 2 h of stirring, dry toluene (5.0 mL) was added to precipitate triethylamine hydrochloride and the mixture was filtered. After removal of solvents under reduced pressure, more triethylamine hydrochloride salt precipitated out, so dry toluene (2.0 mL) was added and the mixture filtered again. After removal of solvents, sodium borohydride (11.6 mg, 0.306 mmol, 1.6 equiv) was added to the solution of crude imine mixture in dry methanol (1.0 mL) at $-10\text{ }^{\circ}\text{C}$. After stirring for 15 mins at $-10\text{ }^{\circ}\text{C}$, the reaction solution was left stirring overnight at room temperature. The reaction was quenched with water (5 mL) and methanol was evaporated by purging nitrogen gas through the flask. After the aqueous layer was extracted with ethyl acetate ($3 \times 10\text{ mL}$), the combined organic extracts were washed with brine (3 mL) and dried over magnesium sulfate. This crude mixture was subjected to column chromatography (40-70% ethyl acetate/hexane) which yielded the title compound as a brown solid (35.2 mg, 0.0923 mmol) in a 49% overall yield. **$^1\text{H NMR}$** (300 MHz, CDCl_3): δ 7.33 – 7.26 (m, 1H, CH_{Ar}), 7.13 – 7.10 (m, 2H, CH_{Ar}), 6.99 – 6.93 (m, 1H, CH_{Ar}), 5.93 (bs, 1H, NH), 5.11 (t, $J = 6.3\text{ Hz}$, 1H, CH-OH), 4.15 – 4.14 (m, 11H, $\text{CH}_2\text{-NH}$ and CH_{Cp}), 2.53 (d, $J = 6\text{ Hz}$, 2H, $\text{CH}_2\text{-CHOH}$) ppm. **$^{13}\text{C NMR}$** (125 MHz, CDCl_3): δ 171.0 (C=O), 163.0 (d, $J = 245\text{ Hz}$, C_{Ar}), 145.9 (d, $J = 7.5\text{ Hz}$, C_{Ar}), 130.1 (d, $J = 8.75\text{ Hz}$, CH_{Ar}), 121.2 (d, $J = 3.75\text{ Hz}$, CH_{Ar}), 114.5 (d, $J = 21.25\text{ Hz}$, CH_{Ar}), 112.7 (d, $J = 22.5\text{ Hz}$, CH_{Ar}), 84.3 (C_{Cp}), 70.3 (CH-OH), 68.7 (CH_{Cp}), 68.3 (CH_{Cp}), 68.3 (CH_{Cp}), 68.3 (CH_{Cp}), 44.5 ($\text{CH}_2\text{-CHOH}$), 38.9 ($\text{CH}_2\text{-NH}$) ppm. **IR** (Neat): 3238, 1650 cm^{-1} . **HRMS** (ESI) m/z : $[\text{M} + \text{Na}]^+$ Calcd for $\text{C}_{20}\text{H}_{20}\text{NO}_2\text{FeNa}$ 404.0725; Found 404.0710. **Melting point**: 112.3 – 116.3 $^{\circ}\text{C}$.

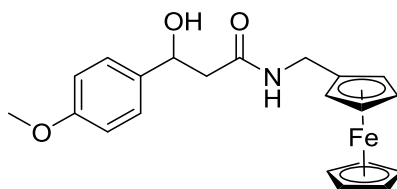
N-(Ferrocenylmethyl)-3-hydroxy-3-(*p*-methylphenyl)propanamide (**65e**)



Magnesium sulfate (252 mg, 2.09 mmol, 3.8 equiv) was added to a solution of **62e** (101 mg, 0.550 mmol, 1 equiv) and triethylamine (0.230 ml, 1.65 mmol, 3 equiv) in dry dichloromethane (5 mL). This mixture was stirred for 15 mins before ferrocenecarboxaldehyde (139 mg, 0.650 mmol, 1.2 equiv) was added. After stirring overnight, another portion of ferrocenecarboxaldehyde (23.1 mg, 0.108 mmol, 0.2 equiv) and magnesium sulfate (136 mg, 1.13 mmol, 2 equiv) were added. The mixture was allowed to stir for 2 more hours after which another portion of ferrocenecarboxaldehyde (11.7 mg, 0.0547 mmol, 0.1 equiv) and a spatula of 4Å molecular sieves were added. After stirring overnight, dry toluene (10 mL) was added to precipitate triethylamine hydrochloride and the mixture was filtered. After removal of solvents under reduced pressure, more triethylamine hydrochloride precipitated out, so dry toluene (4.0 mL) was added and the mixture was filtered again. After removal of solvent, sodium borohydride (62.4 mg, 1.65 mmol, 3 equiv) was added to the solution of crude imine mixture (251 mg) in dry methanol (3 mL) at $-10\text{ }^{\circ}\text{C}$. After stirring for 15 mins at $-10\text{ }^{\circ}\text{C}$, the reaction solution was left stirring overnight at room temperature. The reaction was quenched with water (5 mL) and methanol was evaporated by purging nitrogen gas through the flask. After the aqueous layer was extracted with ethyl acetate ($3 \times 15\text{ mL}$), the combined organic extracts were washed with brine (5 mL) and dried over sodium sulfate. This crude mixture was subjected to column chromatography (40-80% ethyl acetate/hexane) which yielded the title compound as a yellow oil (119 mg, 0.315 mmol) in 58% overall yield. $^1\text{H NMR}$ (500 MHz, CDCl_3): δ 7.25 (d, $J = 7.5\text{ Hz}$, 2H, CH_{Ar}), 7.15 (d, $J = 8\text{ Hz}$, 2H,

CH_{Ar}), 5.99 (bs, 1H, NH), 5.08 (d, *J* = 8.5 Hz, 1H, CH-OH), 4.15 – 4.13 (m, 11H, CH₂-NH and CH_{Cp}), 3.92 (bs, 1H, OH), 2.61 – 2.50 (m, 2H, CH₂-CHOH), 2.34 (s, 3H, CH₃) ppm. ¹³C NMR (125 MHz, CDCl₃): δ 171.1 (C=O), 140.1 (C_{Ar}), 137.4 (C_{Ar}), 129.2 (CH_{Ar}), 125.5 (CH_{Ar}), 84.4 (C_{Cp}), 70.9 (CH-OH), 68.6 (CH_{Cp}), 68.2 (CH_{Cp}), 68.2 (CH_{Cp}), 44.8 (CH₂-CHOH), 38.8 (CH₂-NH), 21.1 (CH₃) ppm. IR (Neat): 3299, 1636 cm⁻¹. HRMS (ESI) *m/z*: [M + Na]⁺ Calcd for C₂₁H₂₃NO₂FeNa 400.0976; Found 400.0979.

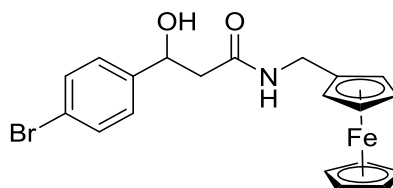
N-(Ferrocenylmethyl)-3-hydroxy-3-(*p*-methoxyphenyl)propanamide (**65f**)



Sodium sulfate (283 mg, 1.99 mmol, 3.7 equiv) was added to a solution of **62f** (107.4 mg, 0.538 mmol, 1 equiv) and triethylamine (0.230 mL, 1.65 mmol, 3 equiv) in dry dichloromethane (5.0 mL). The mixture was stirred for 15 mins before ferrocenecarboxaldehyde (138 mg, 0.647 mmol, 1.2 equiv) was added. After stirring overnight, another portion of ferrocenecarboxaldehyde (23.0 mg, 0.107 mmol, 0.2 equiv) and sodium sulfate (0.150 g, 1.06 mmol) were added. The mixture was stirred for 3 h after which another portion of ferrocenecarboxaldehyde (11.4 mg, 0.0533 mmol, 0.1 equiv) and a spatula of 4Å molecular sieves were added. After 2 h of stirring, dry toluene (10 mL) was added to precipitate triethylamine hydrochloride and the mixture was filtered. After removal of solvents under reduced pressure, more triethylamine hydrochloride precipitated out, therefore dry toluene (5.0 mL) was added and the mixture was filtered again. After removal of solvents, sodium borohydride (32.7 mg, 0.864 mmol, 1.6 equiv) was added to a solution of the crude imine mixture (240 mg) in dry methanol (3 mL) at

-10 °C. After stirring for 15 mins at -10 °C, the mixture was stirred overnight at room temperature. The reaction was quenched with water (5 mL) and methanol was evaporated by purging nitrogen gas through the flask. After the aqueous layer was extracted with ethyl acetate (3 × 15 mL), the combined organic extracts were washed with brine (5 mL) and dried over sodium sulfate. The crude mixture was subjected to column chromatography (40-80% ethyl acetate/hexanes) which yielded a 65.0 mg mixture of the title compound and an unknown impurity that was not removable by column chromatography (using either 50% ethyl acetate/hexanes or 5% methanol/dichloromethane), therefore preparative TLC was used to obtain the title compound (52.0 mg, 0.132 mmol) as a yellowish orange solid in 25% yield. **¹H NMR** (300 MHz, CDCl₃): δ 7.27 (d, *J* = 8.1 Hz, 2H, CH_{Ar}), 6.86 (d, *J* = 8.4 Hz, 2H, CH_{Ar}), 6.13 (bs, 1H, NH), 5.04 (d, *J* = 8.4 Hz, 1H, CH-OH), 4.15 – 4.14 (m, 11H, CH₂-NH and CH_{Cp}), 3.79 (s, 3H, OCH₃), 2.61 – 2.46 (m, 2H, CH₂-CHOH) ppm. **¹³C NMR** (75 MHz, CDCl₃): δ 171.3 (C=O), 159.2 (C_{Ar}), 135.4 (C_{Ar}), 127.0 (CH_{Ar}), 114.0 (CH_{Ar}), 84.5 (C_{Cp}), 70.7 (CH-OH), 68.8 (CH_{Cp}), 68.7 (CH_{Cp}), 68.3 (CH_{Cp}), 55.4 (OCH₃), 44.9 (CH₂-CHOH), 38.9 (CH₂-NH) ppm. **IR** (Neat): 3301, 1636 cm⁻¹. **HRMS** (ESI) *m/z*: [M + Na]⁺ Calcd for C₂₁H₂₃FeNO₃Na 416.0925; Found 416.0937. **Melting point**: 80.5 – 83.8 °C.

N-(Ferrocenylmethyl)-3-hydroxy-3-(*p*-bromophenyl)propanamide (**65g**)



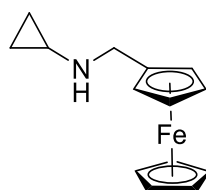
Triethylamine (0.110 mL, 79.9 mg, 0.789 mmol, 1.9 equiv) was added to a suspension of **62g** (106 mg, 0.426 mmol, 1 equiv) and magnesium sulfate (197 mg, 1.63 mmol, 3.8

equiv) in dry dichloromethane (4 mL). This mixture was stirred for 10 minutes before ferrocenecarboxaldehyde (104 mg, 0.487 mmol, 1.1 equiv) was added. After 3 hours of stirring, another portion of ferrocenecarboxaldehyde (18.0 mg, 0.0841 mmol, 0.2 equiv) and one spatula of magnesium sulfate were added. The mixture was allowed to stir overnight after which another portion of ferrocenecarboxaldehyde (9.60 mg, 0.0449 mmol, 0.1 equiv) and a spatula of magnesium sulfate were added. After 2 hours of stirring, dry toluene (8 mL) was added to precipitate triethylamine hydrochloride and the mixture was filtered. After removal of solvents under reduced pressure, more triethylamine hydrochloride precipitated out, therefore dry toluene (5 mL) was added and the mixture was filtered again. After removal of solvents, sodium borohydride (65.4 mg, 1.73 mmol, 4 equiv) was added to the solution of crude imine mixture (233 mg) in dry methanol (5 mL) at $-10\text{ }^{\circ}\text{C}$. After stirring for 15 minutes at $-10\text{ }^{\circ}\text{C}$, the reaction was left stirring at room temperature. Another portion of sodium borohydride (28.7 mg, 0.759 mmol, 1.8 equiv) was added after 45 mins at $-10\text{ }^{\circ}\text{C}$. After stirring for 15 minutes at $-10\text{ }^{\circ}\text{C}$, the reaction solution was left stirring overnight at room temperature. The reaction was quenched with water (3 mL) and methanol was evaporated under reduced pressure. After the aqueous layer was extracted with ethyl acetate ($3 \times 10\text{ mL}$), the combined organic extracts were washed with brine (10 mL) and dried over magnesium sulfate. This crude mixture was subjected to column chromatography (40-80% ethyl acetate/hexane) which yielded the title compound as a yellowish orange (82.5 mg, 0.187 mmol) in a 44% overall yield. **$^1\text{H NMR}$** (500 MHz, CDCl_3): δ 7.44 (d, $J = 8\text{ Hz}$, 2H, CH_{Ar}), 7.20 (d, $J = 8.5\text{ Hz}$, 2H, CH_{Ar}), 6.13 (bs, 1H, NH), 5.03 – 5.00 (m, 1H, CH-OH), 4.14 – 4.09 (m, 11H, $\text{CH}_2\text{-NH}$ and CH_{Cp}), 2.48 – 2.47 (m, 2H, $\text{CH}_2\text{-CHOH}$) ppm. **$^{13}\text{C NMR}$** (125 MHz, CDCl_3): δ 170.9 (C=O), 142.2 (C_{Ar}), 131.7 (CH_{Ar}), 127.4 (CH_{Ar}), 121.5 (C_{Ar}), 84.2 (C_{Cp}), 70.3 (CH-OH), 68.7 (CH_{Cp}), 68.4 (CH_{Cp}), 68.3 (CH_{Cp}), 68.3 (CH_{Cp}), 44.5 ($\text{CH}_2\text{-CHOH}$), 38.9 ($\text{CH}_2\text{-$

NH) ppm. IR (Neat): 3302, 1636 cm^{-1} . HRMS (ESI) m/z : $[\text{M} + \text{Na}]^+$ Calcd for $\text{C}_{20}\text{H}_{20}\text{BrFeNO}_2\text{Na}$ 463.9925; Found 463.9934. **Melting point:** 113.6 – 115.1 $^{\circ}\text{C}$.

3.5.6 Preparation of *N*-(ferrocenylmethyl)-cyclopropylamine **73**

N-(Ferrocenylmethyl)-cyclopropylamine (**73**)



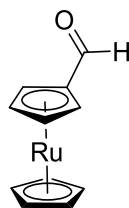
A suspension of ferrocenecarboxaldehyde (445 mg, 2.08 mmol, 1 equiv), magnesium sulfate (639 mg, 5.30 mmol, 1.7 equiv), and cyclopropylamine (0.120 mL, 98.9 mg, 1.73 mmol, 0.8 equiv) in dichloromethane (15 mL) was stirred for 5.5 h at room temperature before another portion of cyclopropylamine (0.100 mL, 82.4 mg, 1.44 mmol, 0.7 equiv) and magnesium sulfate (1 spatula) was added. After stirring overnight at room temperature, the reaction was filtered through a small plug of silica gel, using dichloromethane first to elute unreacted ferrocenecarboxaldehyde then ethyl acetate to elute a mixture of unreacted ferrocenecarboxaldehyde and imine intermediate **72**.

The ethyl acetate eluent was concentrated under reduced pressure then dissolved in anhydrous methanol with 4Å molecular sieves (6 spatula) added. The suspension was cooled to -10°C before sodium borohydride (72.0 mg, 1.90 mmol, 0.9 equiv) was added. The suspension was stirred at -10°C for another 5 mins then room temperature overnight. The reaction was quenched with water (10 mL), filtered then extracted with dichloromethane (3×20 mL). The combined organic extracts were dried over magnesium sulfate and concentrated under reduced pressure. After the crude mixture was purified by

column chromatography (1:1 ethyl acetate/hexane), the title compound was collected as a brown oil in 11% (60.5 mg, 0.237 mmol) yield. **¹H NMR** (500 MHz, CDCl₃): δ 4.17 (s, 2H, CH_{Cp}), 4.12 (s, 5H, CH_{Cp}), 4.10 (s, 2H, CH_{Cp}), 3.57 (s, 2H, CH₂-NH), 2.18 – 2.17 (m, 1H, CH-NH), 0.44 – 0.43 (m, 2H, CH₂-CH-NH), 0.362 – 0.358 (m, 2H, CH₂-CH-NH) ppm. **¹³C NMR** (125 MHz, CDCl₃): δ 86.9 (C_{Cp}), 68.5 (CH_{Cp}), 68.4 (CH_{Cp}), 67.8 (CH_{Cp}), 48.6 (CH₂-NH), 30.1 (CH-NH), 6.4 (CH₂-CH-NH) ppm. **IR** (Neat): 3086 cm⁻¹. **HRMS** (ASAP) m/z: [M]⁺ Calcd for C₁₄H₁₇FeN 255.0710; Found 255.0707.

3.5.7 Preparation of ruthenocene derivatives

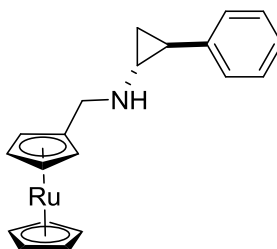
Ruthenocenecarboxaldehyde (75)



Ruthenocene (0.200 g, 0.864 mmol, 1 equiv) was added portion-wise to a mixture of phosphorus(V) oxychloride (0.160 mL, 265 mg, 1.73 mmol, 2 equiv) and *N*-methylformanilide (0.320 mL, 351 mg, 2.60 mmol, 3 equiv) over 30 mins. After stirring the mixture at room temperature for 1 h 30 mins, it was heated at 65 °C for 2 h and never exceeding 70 °C. After cooling the mixture to 0 °C, sodium acetate (672 mg) in water (16 mL) was slowly added and the mixture was stirred overnight at room temperature. The reaction mixture was extracted with diethyl ether (3 × 16 mL), then the combined organic extracts was washed with 1 M HCl (10 mL), brine (10 mL), saturated sodium carbonate solution (10 mL) and brine (10 mL). The combined organic extracts were dried over magnesium sulfate and concentrated under reduced pressure. After column

chromatography (40% hexane in diethyl ether), the title compound was collected as a yellow solid (135 mg, 0.522 mmol) in 60% yield. **¹H NMR** (400 MHz, CDCl₃): δ 9.73 (s, 1H, -CHO), 5.09 (t, *J* = 1.6 Hz, 2H, Cp), 4.86 (t, *J* = 2.0 Hz, 2H, Cp), 4.65 (s, 5H, Cp) ppm. **¹³C NMR** (100 MHz, CDCl₃): δ 190.1 (-CHO), 84.5 (C_{Cp}), 74.2 (CH_{Cp}), 72.0 (CH_{Cp}), 70.9 (CH_{Cp}) ppm. **IR** (Neat): 3094, 1669, 1654, 1457, 1373, 1246, 1102, 1033 cm⁻¹. **HRMS** (ESI) *m/z*: [M + H]⁺ Calcd for C₁₁H₁₁ORu 260.9853; Found 260.9850. **Melting point**: 99.9 – 101.6 °C. ¹H NMR spectrum and melting point are consistent with literature.⁵⁷

N-(Ruthenocenylmethyl)-2-phenylcyclopropan-1-amine (**76**)



A mixture of *trans*-2-phenylcyclopropylamine hydrochloride (25.6 mg, 0.151 mmol, 1 equiv), magnesium sulfate (141 mg, 1.17 mmol, 7.7 equiv), triethylamine (0.100 mL, 0.721 mmol) in dichloromethane (2 mL) was stirred at room temperature for 10 mins before the addition of ruthenocenecarboxaldehyde **75** (38.6 mg, 0.149 mmol, 1 equiv). After stirring the mixture at room temperature overnight, another portion of magnesium sulfate (72.0 mg, 0.598 mmol, 4 equiv) was added and the mixture was further stirred for an additional 4 h. The reaction mixture was diluted with toluene and filtered. The filtrate was concentrated under reduced pressure and used in further reaction without purification due to instability of the imine.

A solution of the imine in methanol (4 mL) was cooled to $-10\text{ }^{\circ}\text{C}$ before the addition of sodium borohydride (43.9 mg, 1.16 mmol, 7.7 equiv). The solution was stirred at $-10\text{ }^{\circ}\text{C}$ for 15 mins then room temperature overnight. The reaction solution was slowly quenched with water (1 ml), extracted with ethyl acetate ($3 \times 10\text{ mL}$) and dried over magnesium sulfate. After column chromatography (30% ethyl acetate/hexane), the title compound was obtained as a yellow oil (23.2 mg, 61.6 μmol) in 41% yield. **$^1\text{H NMR}$** (500 MHz, CDCl_3): δ 7.25 (t, $J = 5\text{ Hz}$, 2H, CH_{Ar}), 7.14 (t, $J = 7.5\text{ Hz}$, 1H, CH_{Ar}), 7.04 (d, $J = 8\text{ Hz}$, 2H, CH_{Ar}), 4.60 (s, 1H, CH_{Cp}), 4.58 (s, 1H, CH_{Cp}), 4.52 (s, 5H, CH_{Cp}), 4.47 (s, 2H, CH_{Cp}), 3.42 (s, 2H, $\text{CH}_2\text{-NH}$), 2.44 (bs, 1H, CH-NH), 1.91 (bs, 1H, CH-Ar), 1.11 – 1.07 (m, 1H, $\text{CH}_2\text{-CHNH}$), 0.97 (q, $J = 5.5\text{ Hz}$, 1H, $\text{CH}_2\text{-CHNH}$) ppm. **$^{13}\text{C NMR}$** (100 MHz, CDCl_3): δ 142.4 (C_{Ar}), 128.2 (CH_{Ar}), 125.8 (CH_{Ar}), 125.4 (CH_{Ar}), 91.3 (C_{Cp}), 70.9 (CH_{Cp}), 70.9 (CH_{Cp}), 70.4 (CH_{Cp}), 69.9 (CH_{Cp}), 47.9 ($\text{CH}_2\text{-NH}$), 41.3 (CH-NH), 25.2 (CH-Ar), 17.3 ($\text{CH}_2\text{-CH-Ar}$) ppm. **IR** (Neat): 3086, 3027, 2924, 1603, 1581, 1542, 1497, 1319, 1230, 1099 cm^{-1} . **HRMS** (ESI) m/z : $[\text{M} + \text{H}]^+$ Calcd for $\text{C}_{20}\text{H}_{22}\text{NRu}$ 378.0796; Found 378.0798.

3.5.8 X-ray crystallography

Crystals of **65d** were obtained from recrystallisation in ethyl acetate/hexanes. CCDC reference number 1434659. Data for **65d** were collected at $-173\text{ }^{\circ}\text{C}$ on crystals mounted on a Hampton Scientific cryoloop at the MX1 beamline of the Australian Synchrotron.⁵⁸ The structures were solved by direct methods with SHELXS-97, refined using full-matrix least-squares routines against F^2 with SHELXL-97,⁵⁹ and visualised using X-SEED.⁶⁰ All non-hydrogen atoms were refined anisotropically. All protons were clearly visible in difference maps during the refinement, including the amide N-H and alcohol O-H, but all were later placed in calculated positions and refined using a riding model with fixed C–H distances of 0.95 \AA ($sp^2\text{CH}$), 1.00 \AA ($sp^3\text{CH}$), 0.99 \AA (CH_2), 0.98

Å (CH₃), N–H distances of 0.88 Å and O–H distances of 0.84 Å The thermal parameters of all hydrogen atoms were estimated as $U_{\text{iso}}(\text{H}) = 1.2U_{\text{eq}}(\text{C})$ except for CH₃ where $U_{\text{iso}}(\text{H}) = 1.5U_{\text{eq}}(\text{C})$. A summary of crystallographic data is stated below.

Crystal data for **65d**: C₂₀H₂₀FFeNO₂, $M = 381.22$, monoclinic, $a = 10.5080(11)$, $b = 35.761(4)$, $c = 9.5150(16)$ Å, $\beta = 107.758(6)^\circ$, $U = 3405.2(8)$ Å³, $T = 100$ K, space group $P2_1/n$ (no. 14), $Z = 8$, 31981 reflections measured, 7745 unique ($R_{\text{int}} = 0.0460$), $6200 > 4s(F)$, $R = 0.0624$ (observed), $R_w = 0.1474$ (all data).

Data for the structure of complex **65d** were obtained on the MX1 beamline at the Australian Synchrotron, Victoria, Australia.

3.5.9 In vitro assay of ruthenoceny1-2-PCPA 76

LSD1 inhibitory activity of **76** was assessed using an LSD1 fluorometric drug discovery kit (BML-AK544-0001, Enzo), while MAO inhibition was determined using MAO-Glo assay system (V1401, Promega).

3.6 References

- (1) de Meijere, A. *Chem. Rev.* **2003**, *103*, 931.
- (2) Cao, B.; Xiao, D.; Joullié, M. M. *Org. Lett.* **1999**, *1*, 1799.
- (3) Denolf, B.; Mangelinckx, S.; Törnroos, K. W.; De Kimpe, N. *Org. Lett.* **2007**, *9*, 187.
- (4) Khan, M. N. A.; Suzuki, T.; Miyata, N. *Med. Res. Rev.* **2013**, *33*, 873.
- (5) Cerny, M. A.; Hanzlik, R. P. *J. Am. Chem. Soc.* **2006**, *128*, 3346.
- (6) Sun, Q.; Zhu, R.; Foss, F. W.; Macdonald, T. L. *Chem. Res. Toxicol.* **2008**, *21*, 711.
- (7) Nguyen, T. H.; Maity, S.; Zheng, N. *Beilstein J. Org. Chem.* **2014**, *10*, 975.
- (8) Wimalasena, K.; Wickman, Heang B.; Mahindaratne, Mathew P. D. *Eur. J. Org. Chem.* **2001**, *2001*, 3811.
- (9) Blackburn, A.; Bowles, D. M.; Curran, T. T.; Kim, H. *Synth. Commun.* **2011**, *42*, 1855.

- (10) Madelaine, C.; Buriez, O.; Crousse, B.; Florent, I.; Grellier, P.; Retailleau, P.; Six, Y. *Org. Biomol. Chem.* **2010**, *8*, 5591.
- (11) Madelaine, C.; Six, Y.; Buriez, O. *Angew. Chem. Int. Ed.* **2007**, *46*, 8046.
- (12) Itoh, T.; Kaneda, K.; Teranishi, S. *Tetrahedron Lett.* **1975**, *16*, 2801.
- (13) Maity, S.; Zhu, M.; Shinabery, R. S.; Zheng, N. *Angew. Chem. Int. Ed.* **2012**, *51*, 222.
- (14) Nguyen, T. H.; Morris, S. A.; Zheng, N. *Adv. Synth. Catal.* **2014**, *356*, 2831.
- (15) Hartinger, C. G.; Dyson, P. J. *Chem. Soc. Rev.* **2009**, *38*, 391.
- (16) Schluga, P.; Hartinger, C. G.; Egger, A.; Reisner, E.; Galanski, M.; Jakupec, M. A.; Keppler, B. K. *Dalton Trans.* **2006**, 1796.
- (17) Liu, Z.; Sadler, P. J. *Acc. Chem. Res.* **2014**, *47*, 1174.
- (18) Spencer, J.; Mendham, A. P.; Kotha, A. K.; Richardson, S. C. W.; Hillard, E. A.; Jaouen, G.; Male, L.; Hursthouse, M. B. *Dalton Trans.* **2009**, 918.
- (19) Spencer, J.; Amin, J.; Wang, M.; Packham, G.; Alwi, S. S. S.; Tizzard, G. J.; Coles, S. J.; Paranal, R. M.; Bradner, J. E.; Heightman, T. D. *ACS Med. Chem. Lett.* **2011**, *2*, 358.
- (20) Biot, C.; Nosten, F.; Fraisse, L.; Ter-Minassian, D.; Khalife, J.; Dive, D. *Parasite (Paris, France)* **2011**, *18*, 207.
- (21) Gasser, G.; Ott, I.; Metzler-Nolte, N. *J. Med. Chem.* **2011**, *54*, 3.
- (22) Top, S.; Vessières, A.; Leclercq, G.; Quivy, J.; Tang, J.; Vaissermann, J.; Huché, M.; Jaouen, G. *Chem. - Eur. J.* **2003**, *9*, 5223.
- (23) Hillard, E.; Vessières, A.; Thouin, L.; Jaouen, G.; Amatore, C. *Angew. Chem. Int. Ed.* **2006**, *45*, 285.
- (24) Pigeon, P.; Top, S.; Vessières, A.; Huché, M.; Hillard, E. A.; Salomon, E.; Jaouen, G. *J. Med. Chem.* **2005**, *48*, 2814.
- (25) Gee, Y. S. BSc (Hons) Thesis, University of Wollongong, 2013.
- (26) Pi, C.; Li, Y.; Cui, X.; Zhang, H.; Han, Y.; Wu, Y. *Chem. Sci.* **2013**, *4*, 2675.
- (27) Chen, Y.; Zhang, X. P. *J. Org. Chem.* **2007**, *72*, 5931.
- (28) Davi, M.; Lebel, H. *Chem. Commun.* **2008**, 4974.
- (29) Cho, S. J.; Jensen, N. H.; Kurome, T.; Kadari, S.; Manzano, M. L.; Malberg, J. E.; Caldarone, B.; Roth, B. L.; Kozikowski, A. P. *J. Med. Chem.* **2009**, *52*, 1885.
- (30) Feldman, K. S.; Simpson, R. E. *Tetrahedron Lett.* **1989**, *30*, 6985.
- (31) Iwama, T.; Matsumoto, H.; Ito, T.; Shimizu, H.; Kataoka, T. *Chem. Pharm. Bull.* **1998**, *46*, 913.
- (32) Zagorski, M. G.; Salomon, R. G. *J. Am. Chem. Soc.* **1980**, *102*, 2501.
- (33) Maity, S.; Zheng, N. *Angew. Chem. Int. Ed.* **2012**, *51*, 9562.
- (34) Yang, M.; Culhane, J. C.; Szewczuk, L. M.; Jalili, P.; Ball, H. L.; Machius, M.; Cole, P. A.; Yu, H. *Biochemistry* **2007**, *46*, 8058.
- (35) Mimasu, S.; Sengoku, T.; Fukuzawa, S.; Umehara, T.; Yokoyama, S. *Biochem. Biophys. Res. Commun.* **2008**, *366*, 15.
- (36) Binda, C.; Valente, S.; Romanenghi, M.; Pilotto, S.; Cirilli, R.; Karytinis, A.; Ciossani, G.; Botrugno, O. A.; Forneris, F.; Tardugno, M.; Edmondson, D. E.; Minucci, S.; Mattevi, A.; Mai, A. *J. Am. Chem. Soc.* **2010**, *132*, 6827.
- (37) Ogasawara, D.; Itoh, Y.; Tsumoto, H.; Kakizawa, T.; Mino, K.; Fukuhara, K.; Nakagawa, H.; Hasegawa, M.; Sasaki, R.; Mizukami, T.; Miyata, N.; Suzuki, T. *Angew. Chem. Int. Ed.* **2013**, *52*, 8620.
- (38) Ortega Munoz, A.; Fyfe, M. C. T.; Martinell Pedemonte, M.; Estiarte Martinez, M. d. I. A.; Valls Vidal, N.; Kurz, G.; Castro Palomino Laria, J. C. WO2013057322A1, 2013.

- (39) Maes, T.; Tirapu, I.; Mascaró, C.; Ortega, A.; Estiarte, A.; Valls, N.; Castro-Palomino, J.; Arjol, C. B.; Kurz, G. *J. Clin. Oncol.* **2013**, *31*, e13543.
- (40) Johnson, N. W.; Kaspavec, J.; Miller, W. H.; Rouse, M. B.; Suarez, D.; Tian, X. WO2012135113A2, 2012.
- (41) Sanders, R.; Mueller-Westerhoff, U. T. *J. Organomet. Chem.* **1996**, *512*, 219.
- (42) Malachowski, M. R.; Grau, M. F.; Thomas, J. M.; Rheingold, A. L.; Moore, C. E. *Inorg. Chim. Acta* **2010**, *364*, 132.
- (43) Alkan, A.; Gleede, T.; Wurm, F. R. *Organometallics* **2017**, *36*, 3023.
- (44) Kunze, B.; Steinmetz, H.; Höfle, G.; Huss, M.; Wiczorek, H.; Reichenbach, H. *J. Antibiot.* **2006**, *59*, 664.
- (45) Cozzi, R.; Attanasio, R. *Expert Rev. Clin. Pharmacol.* **2012**, *5*, 125.
- (46) Ueda, R.; Suzuki, T.; Mino, K.; Tsumoto, H.; Nakagawa, H.; Hasegawa, M.; Sasaki, R.; Mizukami, T.; Miyata, N. *J. Am. Chem. Soc.* **2009**, *131*, 17536.
- (47) Chen, Y.; Huang, L.; Ranade, M. A.; Zhang, X. P. *J. Org. Chem.* **2003**, *68*, 3714.
- (48) Masllorens, J.; Moreno-Manas, M.; Pla-Quintana, A.; Roglans, A. *Org. Lett.* **2003**, *5*, 1559.
- (49) Taber, D. F.; Nelson, C. G. *J. Org. Chem.* **2006**, *71*, 8973.
- (50) Benelkebir, H.; Hodgkinson, C.; Duriez, P. J.; Hayden, A. L.; Bulleid, R. A.; Crabb, S. J.; Packham, G.; Ganesan, A. *Biorg. Med. Chem.* **2011**, *19*, 3709.
- (51) Shimojoh, N.; Imura, Y.; Moriyama, K.; Togo, H. *Tetrahedron* **2011**, *67*, 951.
- (52) Concellón, J. M.; Concellón, C.; Méjica, C. *J. Org. Chem.* **2005**, *70*, 6111.
- (53) Lebel, H.; Davi, M. *Adv. Synth. Catal.* **2008**, *350*, 2352.
- (54) Concellón, J. M.; Rodríguez-Solla, H.; Simal, C. *Org. Lett.* **2007**, *9*, 2685.
- (55) Andreotti, D.; Arista, L.; Cardullo, F.; Spada, S.; Thewlis, K. M.; Ward, S. E. WO2006087169A1, 2006.
- (56) Arvidsson, L. E.; Johansson, A. M.; Hacksell, U.; Nilsson, J. L. G.; Svensson, K.; Hjorth, S.; Magnusson, T.; Carlsson, A.; Lindberg, P.; Andersson, B.; Sanchez, D.; Wikström, H.; Sundell, S. *J. Med. Chem.* **1988**, *31*, 92.
- (57) Joubert, C. C. Master of Science Thesis, University of the Free State, 2011.
- (58) McPhillips, T. M.; McPhillips, S. E.; Chiu, H.-J.; Cohen, A. E.; Deacon, A. M.; Ellis, P. J.; Garman, E.; Gonzalez, A.; Sauter, N. K.; Phizackerley, R. P.; Soltis, S. M.; Kuhn, P. *J. Synchrotron Radiat.* **2002**, *9*, 401.
- (59) Sheldrick, G. M. *SHELX97, Programs for Crystal Structure Analysis*; Universität Göttingen: Germany, 1998.
- (60) Barbour, L. J. *J. Supramol. Chem.* **2001**, *1*, 189.

Chapter 4

Palladium-catalysed dearomative [3 + 2] cycloaddition of 3-nitroindoles with vinylcyclopropane dicarboxylates

4.1 Introduction

4.1.1 Activation of vinylcyclopropanes by Pd catalysts in cycloadditions

Donor-acceptor (DA) three-membered rings, such as vinylcyclopropanes (VCPs) and vinylaziridines, are useful scaffolds in synthetic methodologies.¹⁻⁴ These DA three-membered rings are readily prepared and are generally stable to store and handle. Upon activation, they can be unmasked and reveal a reactive 1,3-dipole intermediates, which can participate in reactions such as cycloadditions and nucleophilic additions.

Apart from the strain energy present in the ring, the reactivity of DA three-membered rings can also be attributed to the functional groups present on the ring. One terminal on the ring would have a “donor” group to stabilise the cation formed upon activation, while the adjacent terminal would have an “acceptor” group to stabilise the anion. VCP dicarboxylate (Figure 27, boxed) is an example of DA three-membered ring. Upon activation to form 1,3-dipole, the vinyl group is the cation-stabilising donor group, while the adjacent diesters-carrying carbon stabilises the anion. Apart from esters, other electron withdrawing groups such as ketones and nitriles can also be used to stabilise the anion formed in 1,3-dipole.

Several methods have been reported to activate these three-membered rings (Figure 27). It has been reported that arylcyclopropanes, aziridines and less commonly VCPs can unleash a 1,3-dipole simply by thermal activation to cleave the C-C bond.⁵⁻⁷

Alternatively, Lewis acids can chelate with the acceptor group therefore polarising the bond between the donor and acceptor groups. The resulting dipole in each case can undergo reaction with a dipolarophile **78** to yield five-membered carbo- and heterocycles.⁸

For VCPs, metal catalysis is the more common approach for activation. Low valent metals such as Pd(0),⁹ Ni(0),^{10,11} Fe(0)¹² and Ir(0)¹³ have been reported to interact with the vinyl group to stabilise the cation formed in 1,3-dipole as a metal-allyl complex. This review will focus on studies that employ Pd-catalysis to create all-carbon zwitterionic 1,3-dipoles from VCP dicarboxylates.

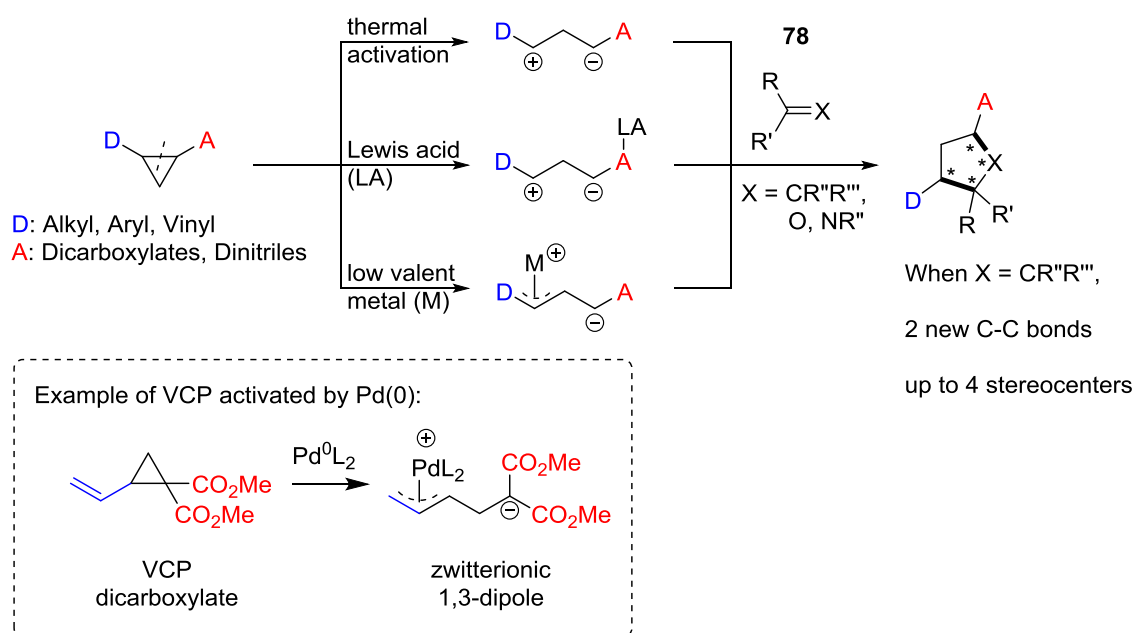
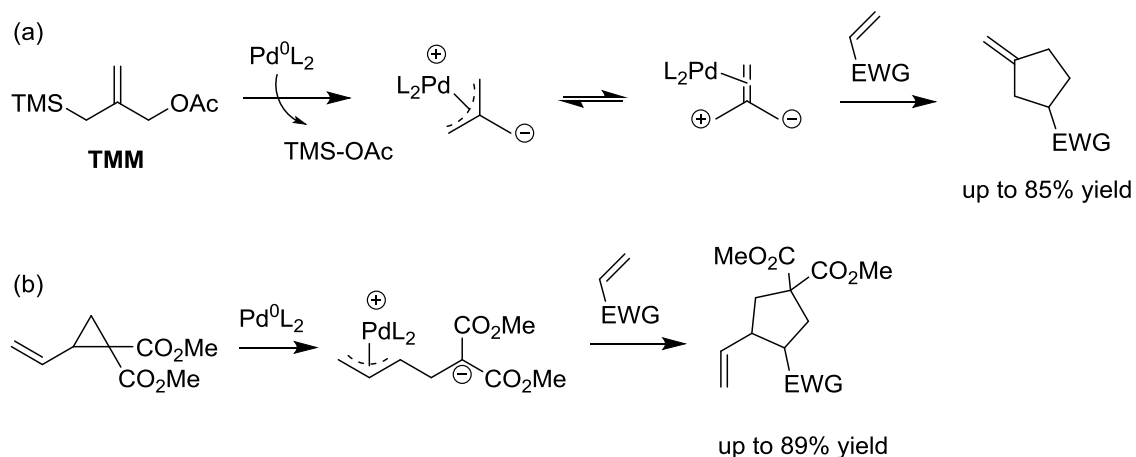


Figure 27: Methods to reveal 1,3-dipole from donor-acceptor three-membered ring.

The vinyl group in a vinylcyclopropane dicarboxylate provides a handle to interact with Pd(0), and hence prompting the ring-opening of cyclopropane via oxidative addition and the formation of a Pd-stabilised 1,3-dipole (Figure 27). This zwitterionic intermediate is composed of a cationic Pd- π -allyl complex and a dicarboxylate stabilised anion. As a result, this reactive intermediate can participate in [3 + 2] cycloaddition with

electron deficient olefins and other dipolarophiles. The resulting five-membered ring product has established two new C–C bonds and could have up to four stereocenters, therefore providing scope for asymmetric synthesis. Furthermore, preparation of a five-membered ring through this method provides high atom economy as all atoms in the substrates are preserved in the resulting product. For these reasons, the [3 + 2] cycloaddition of VCP dicarboxylates with dipolarophiles have been widely studied in the last few decades as a key method for preparing 5-membered carbocycles.

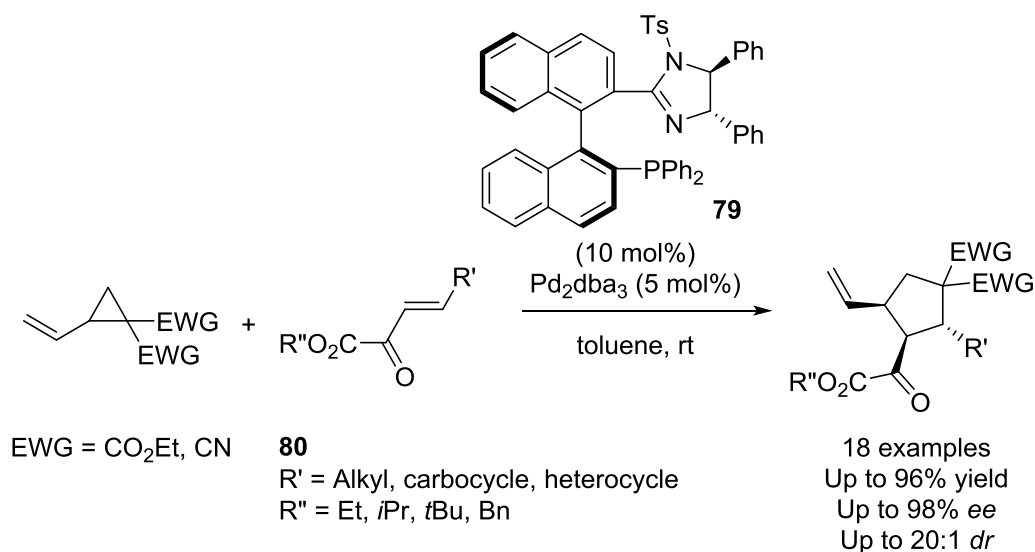
Prior to the discovery of VCP as 1,3-dipole in [3 + 2] cycloaddition, Trost et al. reported the use of trimethylenemethane (TMM) as 1,3-dipole to react with α,β -unsaturated ester and ketone (Scheme 31a).¹⁴ This method provided the five-membered ring product but with trimethylsilyl acetate as the by-product during the generation of TMM in situ. Later, Tsuji and colleagues introduced the use of VCP dicarboxylates in [3 + 2] cycloadditions with α,β -unsaturated esters and ketones (Scheme 31b).¹⁵ This method provided the cyclopentane product in good yield and it had superior atom economy compared to that of using TMM, as well as providing more functionality on the product ring.



Scheme 31: Construction of five-membered ring from the Pd-catalysed [3 + 2] cycloaddition of electron-poor olefin with: (a) trimethylenemethane (TMM); (b) vinylcyclopropane dicarboxylate.

As seen from Trost and Tsuji's work, α,β -unsaturated carbonyls and electron deficient olefins are attractive dipolarophiles for 1,3-dipoles as they are good Michael acceptors to yield the five-membered carbocycles. Given the success of asymmetric processes involving Pd-allyl complexes and the importance of enantiomerically pure structures in target synthesis, much effort has been paid to developing asymmetric variants of the process shown in Scheme 31b.

Shi et al. developed novel chiral imidazoline-phosphines with a 1,1'-binaphthalene framework as *N,P*-ligands **79** and applied them to the Pd-catalysed cycloaddition of VCP dicarboxylate and VCP dinitrile with β,γ -unsaturated α -keto esters **80** (Scheme 32).¹⁶ The resulting five-membered carbocycles were obtained in excellent yield, enantioselectivity and diastereoselectivity. In terms of substrate scope, this method favoured dipolarophiles with electron-rich aromatic rings or heterocycles at the γ position where good yields and excellent diastereoselectivities were obtained. No product was obtained when a strongly electron-deficient aromatic ring was present, such as *p*-NO₂C₆H₄.



Scheme 32: Asymmetric synthesis of functionalised cyclopentane through Pd-catalysed [3 + 2] cycloaddition of VCP with β,γ -unsaturated α -keto esters.

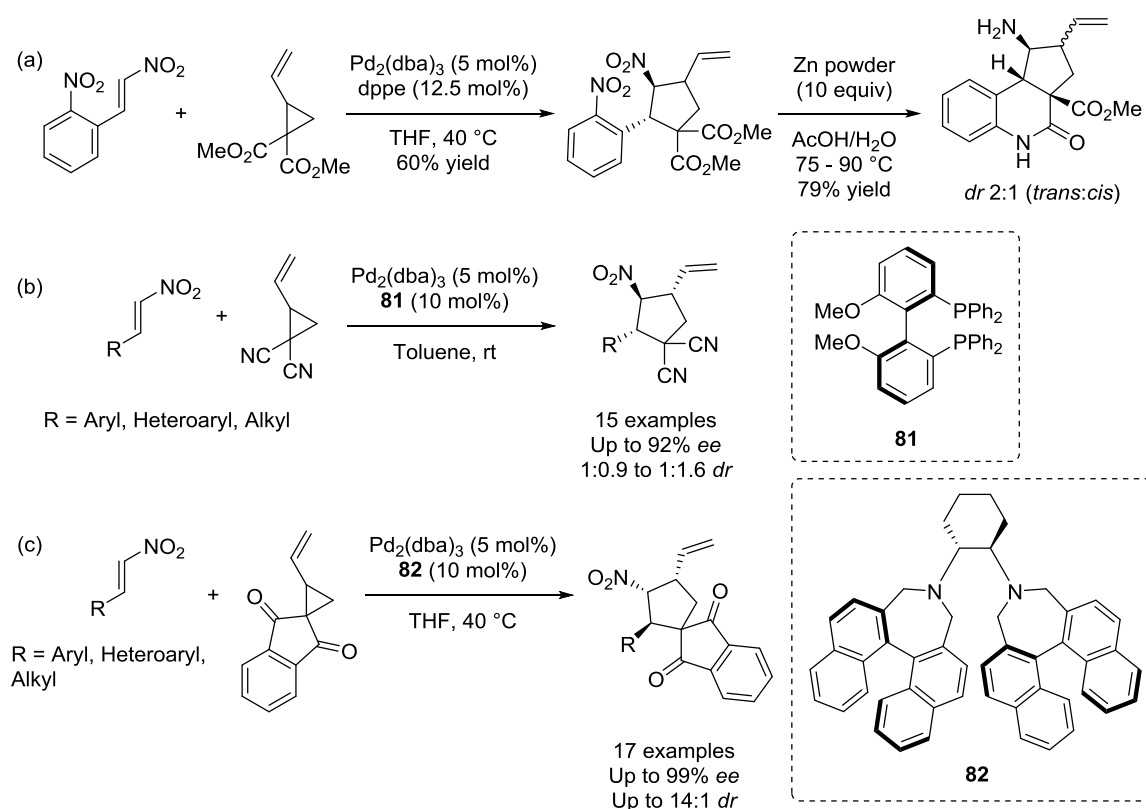
Apart from α,β -unsaturated carbonyls, nitroolefins are also excellent dipolarophiles for 1,3-dipoles, but have received scant attention to date. It's important to note that the use of nitroolefins as substrates provides a convenient avenue to ultimately install nitrogen-containing functional groups, such as amines and amides. For example, as part of a strategy to prepare the polycyclic *Melodinus* alkaloids, Goldberg et al. subjected $\beta,2$ -dinitrostyrene and VCP dicarboxylate to a Pd-catalysed [3 + 2] cycloaddition (Scheme 33a).¹⁷ The resulting nitrocyclopentane product was obtained as a mixture of inseparable diastereomers in 60% yield. The obtained cycloadducts were then subjected to zinc reduction of nitro groups to amines followed by in situ lactamisation to yield dihydroquinolinone products (Scheme 33a).

Later, Liu et al. reported the enantioselective Pd-catalysed cycloadditions of dicyano VCP with β -nitrostyrenes to yield nitrocyclopentanes (Scheme 33b).¹⁸ The reaction generally tolerated electron donating and electron withdrawing substituents at different positions on the ring to give good yields with moderate to good

enantioselectivities. Interestingly, this method could not generate the product when a strongly electron withdrawing nitro group is at the *ortho* position on the phenyl ring, which Goldberg et al. had employed in the previous study with VCP dicarboxylate.¹⁷ Even though the reaction gave poor diastereoselectivities of 1:0.9 to 1:1.6, the authors stated that the diastereomers could be separated by chromatography, therefore providing practicality to access both enantioenriched diastereomers individually.

VCPs can also be used to construct five-membered carbocycles with higher complexity, such as spirocycles. Spirocyclopentanes containing 1,3-indanedione moieties are common cores of many biologically active molecules, such as Fredericamycin A (antibiotics)¹⁹ and indacrinone (MK-196) (uricosuric diuretics)²⁰. In order to access this class of spirocycles, Liu and co-workers conducted a Pd-catalysed cycloaddition study using nitroolefins with a spirocyclic VCP containing 1,3-indanedione (Scheme 33c).²¹ A series of ligands were screened and it was discovered that *N,N*-ligands provided the best enantioselectivity, *P,P*-ligand provided moderate enantioselectivity, while *N,P*-ligands generated a racemic mixture. The reaction was compatible with heterocycles and aromatic rings with electron donating or electron withdrawing group, where desired products were obtained in good yield with moderate diastereoselectivity and excellent enantioselectivity. A sharp reduction in diastereoselectivity was observed when the substituent on the olefin was an unsaturated cycloalkane, while the excellent enantioselectivity remained unchanged.

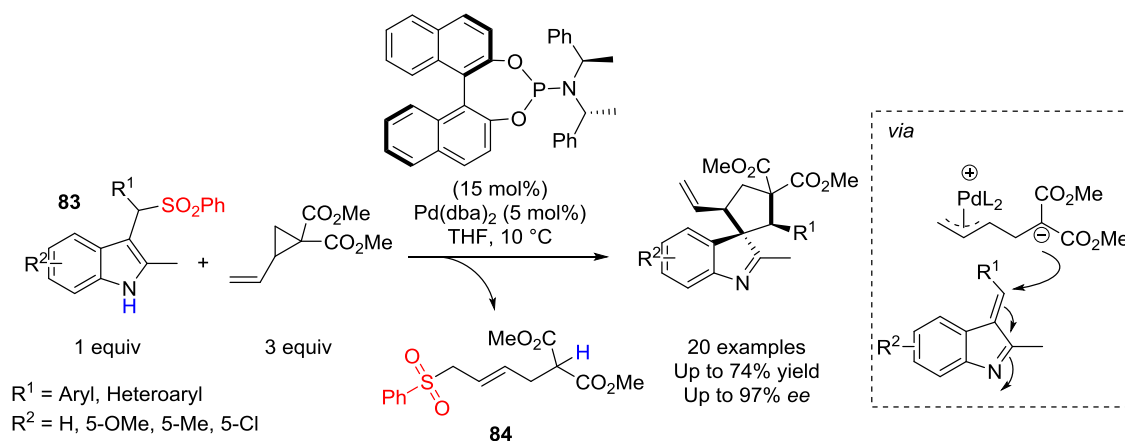
As the nitroolefin substrates and palladium catalyst depicted in Scheme 33 are essentially identical, the differences in the obtained diastereoselectivity could be attributed to the delicate balance in reaction parameters such as VCP substrates and/or ligands.



Scheme 33: Pd-catalysed [3 + 2] cycloaddition of VCPs with nitroolefins.

Spiroindolenines are another class of spirocycles that can be commonly found in biologically active compounds and commercial drugs.²²⁻²⁴ Similarly to spiro[4.5]deca-6,9-diene-8-ones, rapid approaches to access spiroindolenines are limited, thus Liu et al. reported the preparation of these spirocycles from the Pd-catalysed cycloaddition of VCP dicarboxylates and α,β -unsaturated imines, which were generated in situ from aryl sulfonyl indoles **83** (Scheme 34).²⁵ In general, spiroindolenines were prepared in good yield with excellent enantioselectivity and diastereoselectivity. The newly formed cyclopentane moiety had four stereocenters which two of them were quaternary carbons. The electronic nature of substituents had no significant effects on the reaction, however steric hindrance around the sulfonyl moiety did impact yields and enantioselectivities. A slight reduction in the enantioselectivities and a drastic drop in yields were observed when *ortho* substituted phenyl ring was around the sulfonyl moiety. Besides, substitution on the indole ring also slightly reduced the enantioselectivities of the products. The VCP played

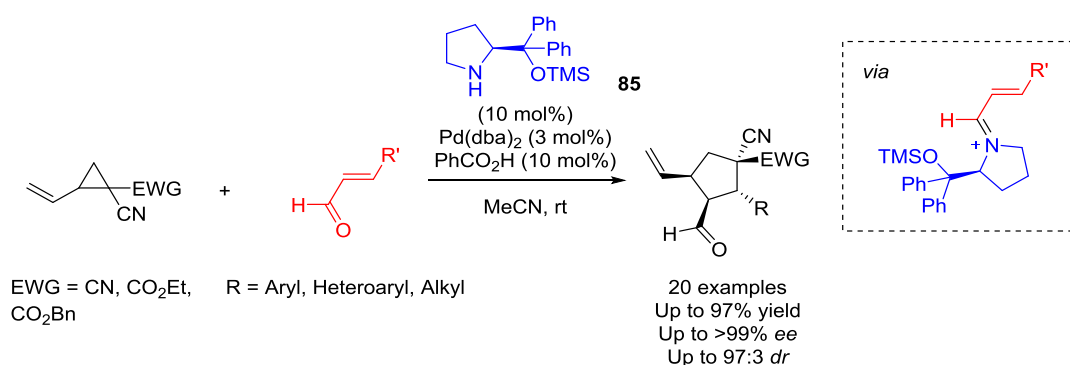
two roles in this reaction: firstly, the malonate anion of the 1,3-dipole deprotonated the indole which caused the formation of α,β -unsaturated imine and the liberation of benzenesulfinate anion. Once the malonate anion on the 1,3-dipole is protonated, the benzenesulfinate anion then attacked the Pd-allyl complex to form by-product **84**. On the other hand, another 1,3-dipole attacked the in situ generated α,β -unsaturated imine to form the desired cycloadduct in a [3 + 2] cycloaddition manner. Due to the consumption of 1,3-dipole for the initial indole deprotonation, excess VCP was required for this [3 + 2] cycloaddition.



Scheme 34: Pd-catalysed cycloaddition of VCPs with in situ generated unsaturated imines.

Instead of using chiral ligands, Jørgensen and colleagues conducted the stereoselective Pd-catalysed [3 + 2] cycloaddition of dicyano VCPs with α,β -unsaturated aldehydes in the presence of a chiral organocatalyst **85** (Scheme 35).²⁶ The role of the amine organocatalyst was to activate the aldehyde substrate as a reactive iminium ion intermediate and controls the sense of attack by the 1,3-dipole generated from the VCP by the achiral Pd-catalyst. Electron-donating and electron-withdrawing substituents can be accommodated at various positions on the β -phenyl ring of the aldehydes, although longer reaction time was required for substrates with *ortho* substituted phenyl rings,

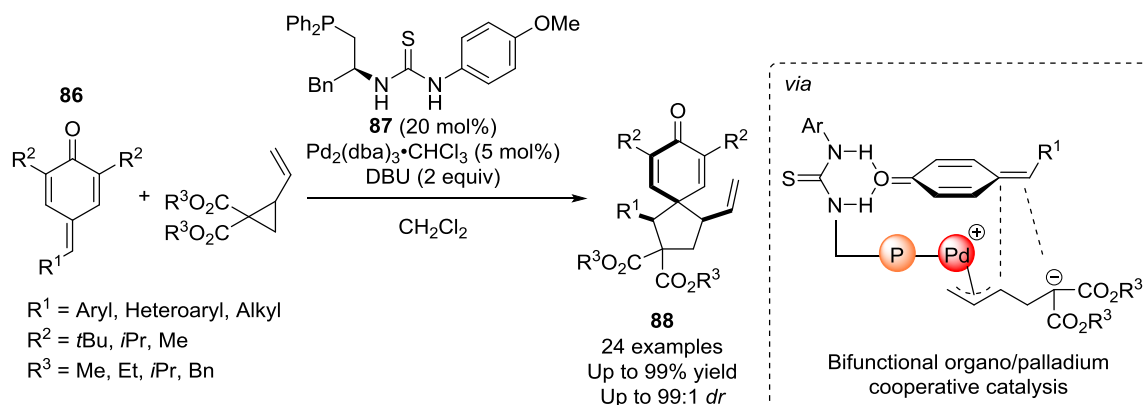
potentially due to steric hindrance. β -Heteroaryl and β -alkyl aldehyde substrates provided similar good yields but with slightly lower diastereoselectivity. Furthermore, VCPs with two different geminal electron-withdrawing groups were screened to yield the cyclopentane derivatives with four stereocenters. More importantly, the use of these VCPs created a quaternary stereocenter in the cycloadduct, which is a long-standing challenge in organic synthesis.²⁷⁻²⁹ The cycloaddition of these VCPs provided the cycloadducts in high yields, excellent enantioselectivity and good diastereoselectivity. In a separate study, Jørgensen et al. demonstrated that a similar Pd/organo dual catalysis method can be extended to vinylaziridines with α,β -unsaturated aldehydes, where good yields, high enantioselectivity and moderate diastereoselectivity were obtained.³⁰



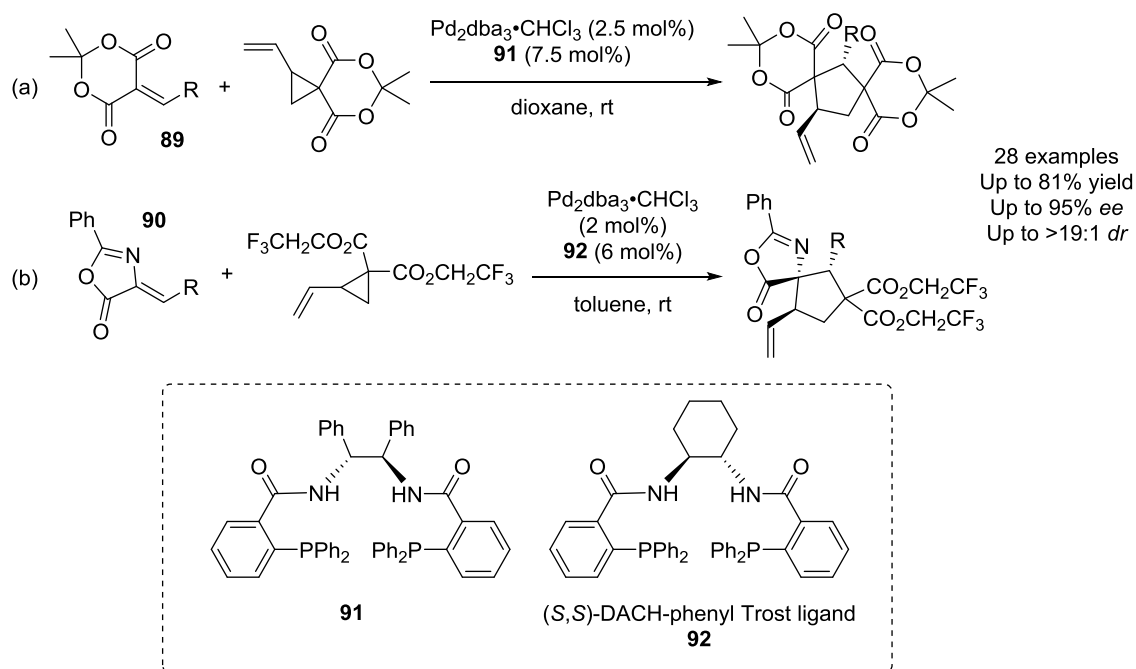
Scheme 35: Asymmetric [3 + 2] cycloaddition of VCPs and α,β -unsaturated aldehydes by synergistic palladium and organocatalysis.

Yao and colleagues also reported the utilisation of organo/palladium dual catalysis to construct spiro[4.5]deca-6,9-diene-8-ones **88** from the cycloaddition of VCP dicarboxylates and *para*-quinone methides **86** (Scheme 36).³¹ A series of phosphine-thiourea organocatalysts were examined at the start of the study. Changing the electronic nature of the thiourea-phenyl ring fine-tuned the acidity of thiourea, while the diastereoselectivity was not affected, the yield varied from 56 to 93%. As such, **87** bearing a *p*-methoxy group on the thiourea-phenyl ring was identified to provide the optimal yield

and diastereoselectivity. Even though moderate to good yields were obtained when standard monodentate and bidentate phosphine ligands were employed, the diastereoselectivity dropped significantly. These results highlight the need of bifunctional organo/metal catalysis to achieve diastereoselectivity. It was proposed that while the phosphine moiety of the organocatalyst activated the VCP into 1,3-dipole, the thiourea-NH moieties of the organocatalyst chelated to the oxygen of *para*-quinone methide **86** through hydrogen bonding. This method was applied to a range of VCP dicarboxylate and *para*-quinone methide substrates and it showed great functional group compatibility. Despite a chiral ligand **87** being employed, the reaction was not enantioselective and the authors aimed to investigate the enantioselective variant in a future study. Interestingly, when vinylaziridine was used instead of VCP, the diastereoselectivity declined drastically (76:24 *dr* when using vinylaziridine compared to 96:4 *dr* when using VCP).



Scheme 36: [3 + 2] cycloaddition of *para*-quinone methides with VCPs through metal/organo synergistic catalysis.



Scheme 37: Pd-catalysed cycloaddition of substituted VCPs with Meldrum's acid alkylidenes and azlactone alkylidenes.

Recently, Trost et al. investigated the stereoselective Pd-catalysed cycloaddition of substituted VCPs with Meldrum's acid alkylidenes **89** (Scheme 37a) and azlactone alkylidenes **90** (Scheme 37b).³² Pd- π -allyl species are known to isomerise between η^3 and η^1 haptomers – a process called π - σ - π interconversion (Figure 28a). When the η^3 haptomer isomerises to the η^1 haptomer, the latter can undergo a σ -bond rotation then isomerise to a η^3 isomer, which has the opposite configuration to the starting η^3 haptomer. This interconversion allows the stereoconvergence of both VCP enantiomers to enantioenriched products, thus Trost and co-workers employed the chiral ligands that they previously developed to create a chiral environment around the Pd centre, which can influence the π - σ - π interconversion and hence the stereoselectivity of the cycloaddition (Figure 28b). By having a chiral ligand as the mould for the Pd allyl complex, the sterically unfavoured η^3 haptomer is prompted to undergo π - σ - π interconversion to the sterically favoured η^3 haptomer. Promotion of π - σ - π interconversion is said to achieve

Curtin–Hammett conditions, where the interconversion between the diastereomeric complexes is more rapid than the irreversible ring closing step, therefore the interconversion is the crucial factor to control stereoselectivity. Curtin–Hammett principle stated that on the basis that the rates of conformational interconversion are faster than the rates of reaction, the relative amount of products formed from two critical conformations are entirely relied on the difference in transition states free energy, and not the relative populations of the conformations.³³

This concept was applied to two sets of substrates, Meldrum's acid derivatives of VCP with alkylidenes **89** and VCP dicarboxylate with azlactone alkylidenes **90** (Scheme 37). As a result, the obtained cycloadducts were highly substituted and stereoselective. Using the Meldrum's acid derivatives of VCP as example (as depicted in Figure 28a), conformers **A** and **F** are diastereomers with different free energies due to the steric interference between the substrate and ligand in **F**. Regardless of the relative population of these two conformers, conformer **F** rapidly converts to conformer **A** by undergoing π - σ - π interconversion. As this π - σ - π interconversion is faster than the reaction, the reaction achieves Curtin–Hammett conditions and selectively provides the major enantiomer and diastereomer based on conformer **A**.

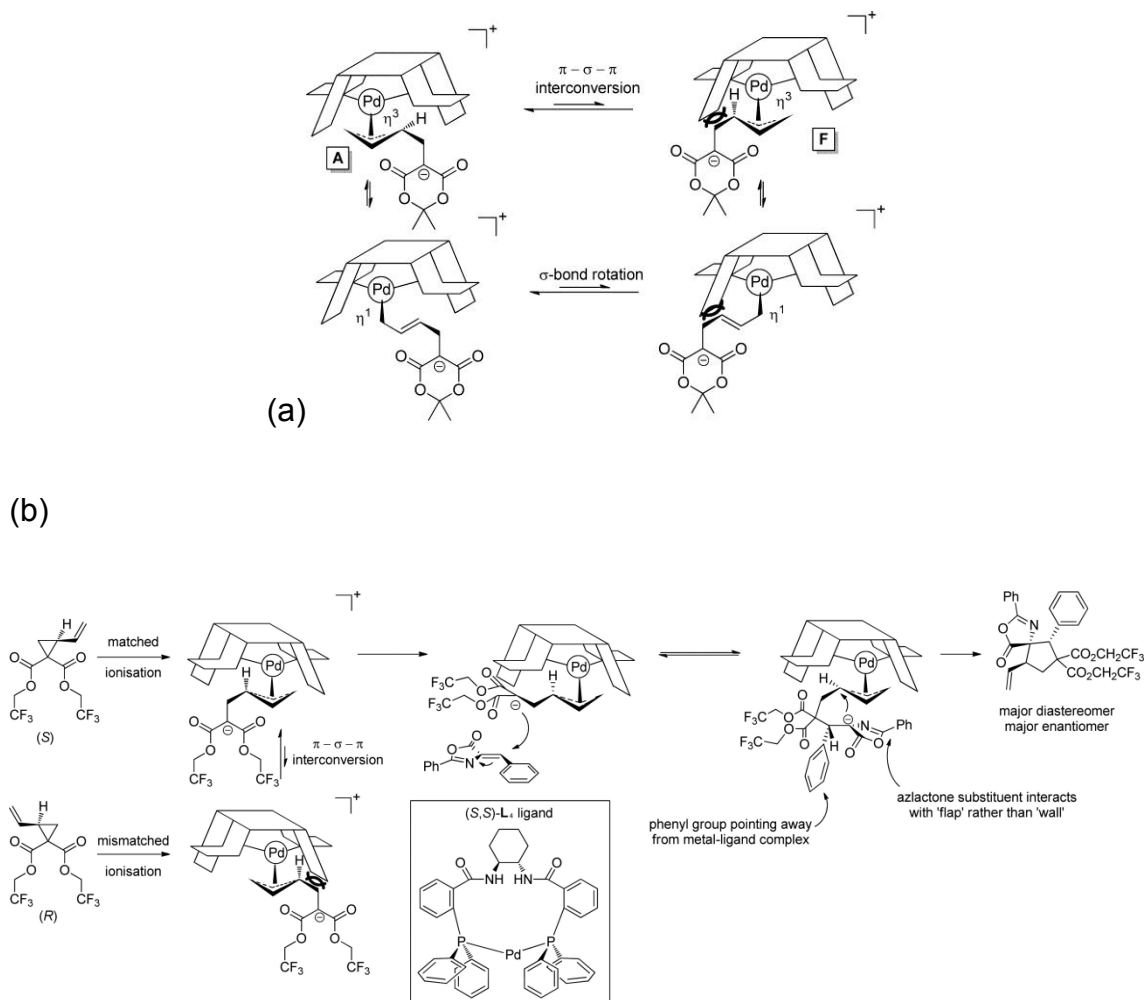
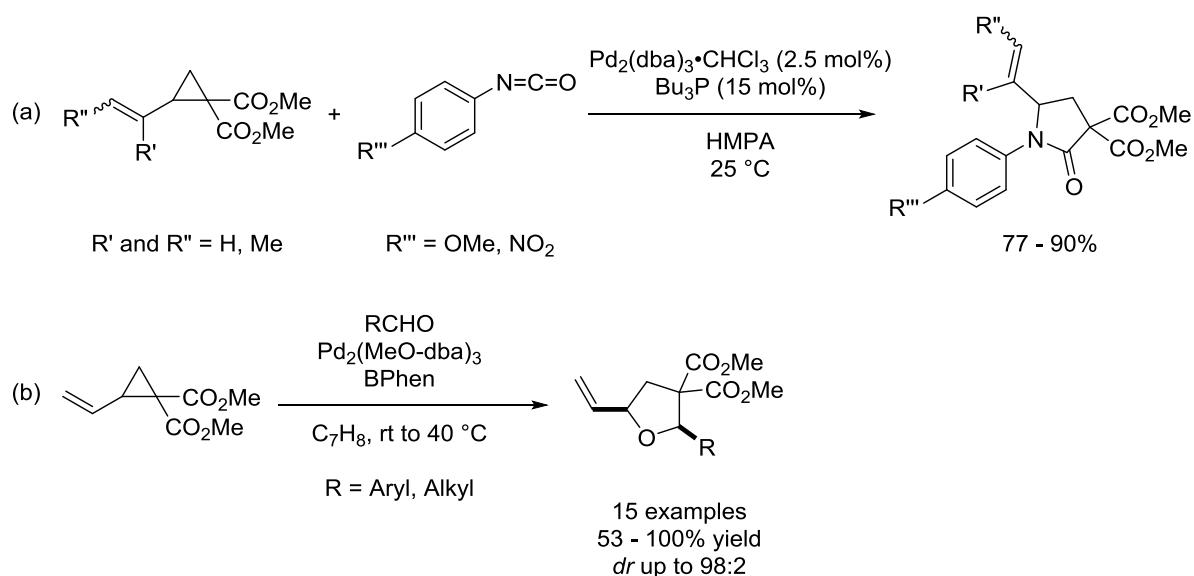


Figure 28: (a) Isomerisation of Pd- π -allyl complex through π - σ - π interconversion; (b) Stereoconvergent of Pd- π -allyl intermediates directed by Trost ligand through π - σ - π interconversion. (Figure was adapted from literature³²)

With variation in the dipolarophile, VCPs can access not only cyclopentane derivatives but also five-membered heterocycles. Tsuji et al. reported the [3 + 2] cycloaddition of VCP dicarboxylates with aryl isocyanates to prepare pyrrolidine derivatives in good yield (Scheme 38a).³⁴ VCP with mono- and disubstituted olefins, phenyl isocyanates with electron donating and electron withdrawing groups, were screened and they all provided good yield. However, no cyclisation product was obtained when alkyl isocyanates were attempted.

Johnson and co-workers have reported the diastereoselective preparation of tetrahydrofuran derivatives from the cycloaddition of VCP dicarboxylate with aldehydes (Scheme 38b).³⁵ Various ligands were screened in order to gain stereocontrol over the product and the diamine ligand bathophenanthroline (BPhen) was found to be the optimal ligand in their method to give the *cis* isomer as the major diastereomer. They reported high yields and short reaction times for electron-poor aldehydes. On the other hand, electron-rich aldehydes provided poor yields even though total consumption of VCP was observed. It was proposed that electron-rich aldehydes have lower electrophilicity, therefore disfavoring the nucleophilic attack of 1,3-dipole.

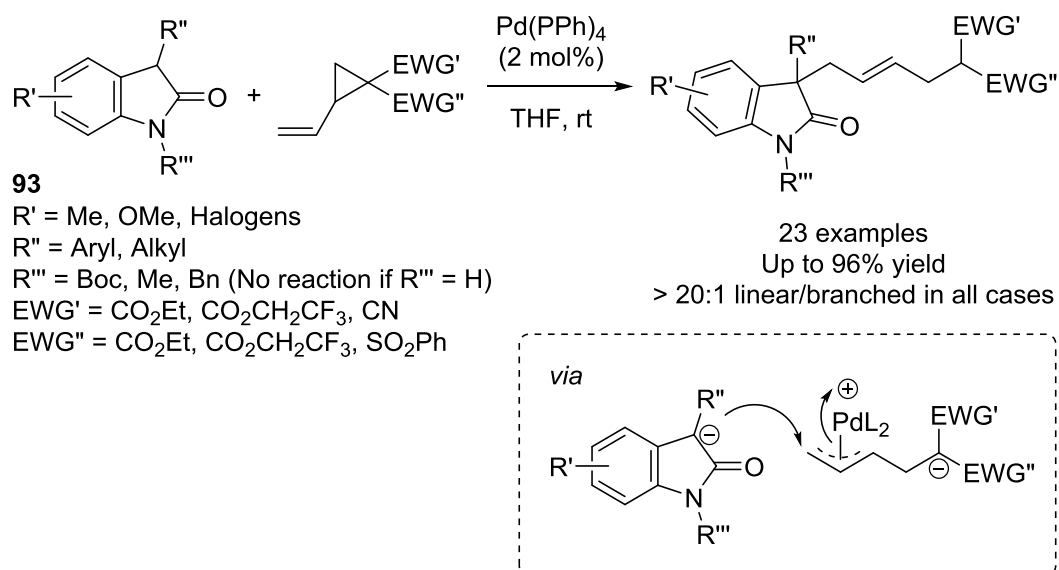


Scheme 38: Construction of five-membered heterocycles from Pd-catalysed cycloaddition of VCPs with: (a) aryl isocyanates; (b) aldehydes.

4.1.2 Vinylcyclopropanes in nucleophilic additions catalysed by Pd(0)

As seen above, Pd- π -allyl complexes derived from VCPs have been widely employed in [3 + 2] cycloaddition, however nucleophilic addition to π -allyl complexes forming acyclic products is less reported. Nucleophilic attack to π -allyl complexes gives

rise to acyclic products, which can be either linear or branched, therefore this provides the scope to study the regioselectivity. Jiang and colleagues utilised oxindoles **93** as the nucleophiles to attack Pd- π -allyl complexes derived from VCP dicarboxylates and found the reaction was highly regioselective towards the linear product (Scheme 39).³⁶ Various substituents could be accommodated at the oxindole aromatic ring and C3 position, products were obtained in good to excellent yields with > 20:1 linear/branched ratio. Similar yields and linear/branched ratios were observed when cyano and phenyl sulfonyl were used as the acceptor groups in VCPs.



Scheme 39: Pd-catalysed allylation of oxindoles with VCPs.

Werz et al. reported the Pd/Cu-catalysed three-component coupling of terminal alkynes, arynes and VCP dicarboxylate (Figure 29).³⁷ The aryne was generated in situ by treating 2-(trimethylsilyl)phenyl trifluoromethanesulfonate **94** with a fluoride source. Meanwhile, Cu(I) activated the terminal alkyne to form the copper acetylide nucleophile **95**, which then coupled to the aryne and formed a highly nucleophilic organocopper intermediate **96**. Eventually the nucleophilic intermediate **96** attacked the Pd- π -allyl complex to form the product and allowed the regeneration of Pd(0) and Cu(I). Aromatic,

heterocyclic and alkyl groups on terminal alkynes were found to give moderate to good yields with only the linear product obtained. However, when an ester group was installed on the terminal alkyne, no product was formed. It was proposed that this lack of reactivity was due to the electron-withdrawing group reducing the nucleophilicity of the acetylide. Notably, the regioselectivity could not be maintained when unsymmetrical arynes were used because the copper acetylide could attack either one of the two aryne carbons without any regio-control.

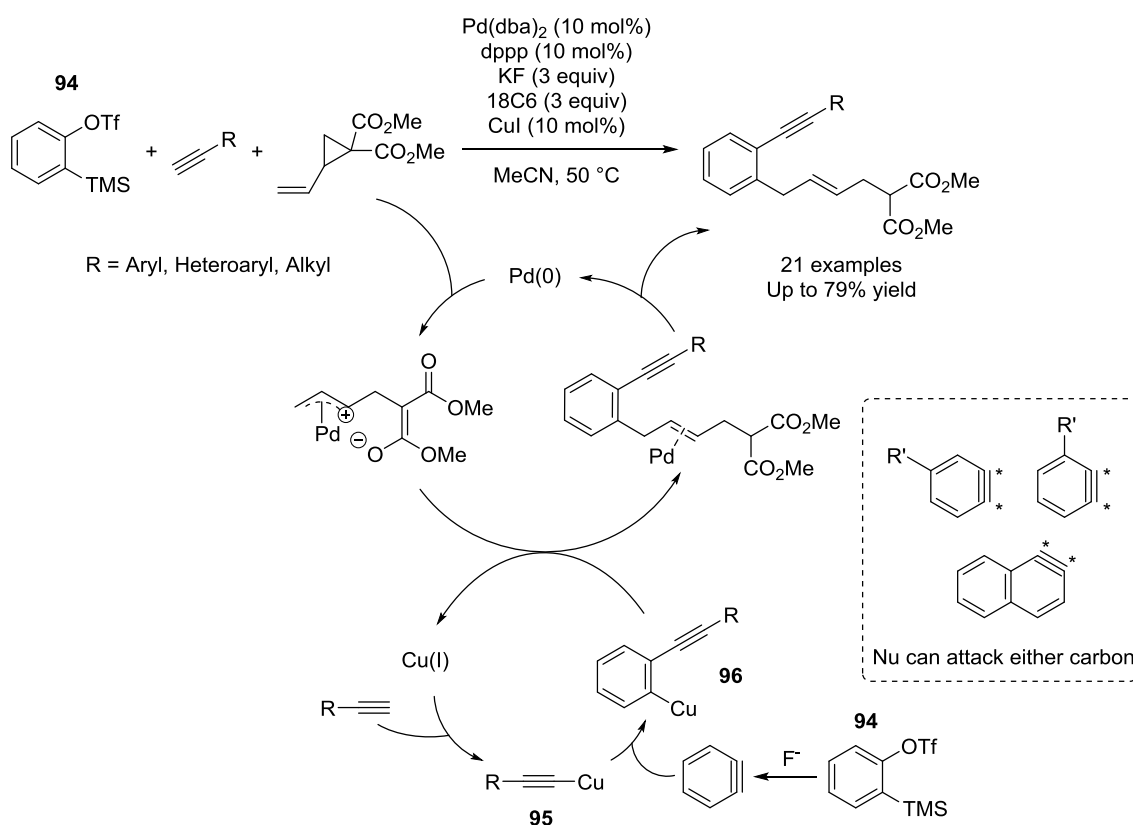


Figure 29: Pd-catalysed three-component coupling of terminal alkynes, arynes and VCP dicarboxylates.

Recently, the Hyland group has reported the Pd-catalysed addition of boronic acids to Pd- π -allyl complexes (Figure 30).³⁸ The reaction was conducted under mild conditions using neat water as the solvent, without the need of a ligand or additive.

Furthermore, the reactions regioselectivity depended on the 1,3-dipole source, being linear-selective for VCP dicarboxylates and branched-selective for styrenylcyclopropane dicarboxylates. It was proposed that Pd(0) nanoparticles (PdNPs) were formed in the presence of aryl boronic acids and these nanoparticles activated the VCPs into Pd- π -allyl complexes. Aryl boronic acids then underwent transmetallation with the Pd- π -allyl complexes, follow by reductive elimination to yield the products and regeneration of the Pd(0) catalyst. The regioselectivity was established during the reductive elimination based on the VCP substrates. When vinylcyclopropanes (R = H) were employed, linear products **97** were favoured as the terminal alkenes were more thermodynamically stable than internal alkene. Moreover, orientating the Pd-Ar complex towards terminal carbon minimises the steric repulsion against the VCP fragment during reductive elimination. On the other hand, the use of styrenylcyclopropane (R = Ar) provided branched products **98** selectively as these products had more stable conjugated systems.

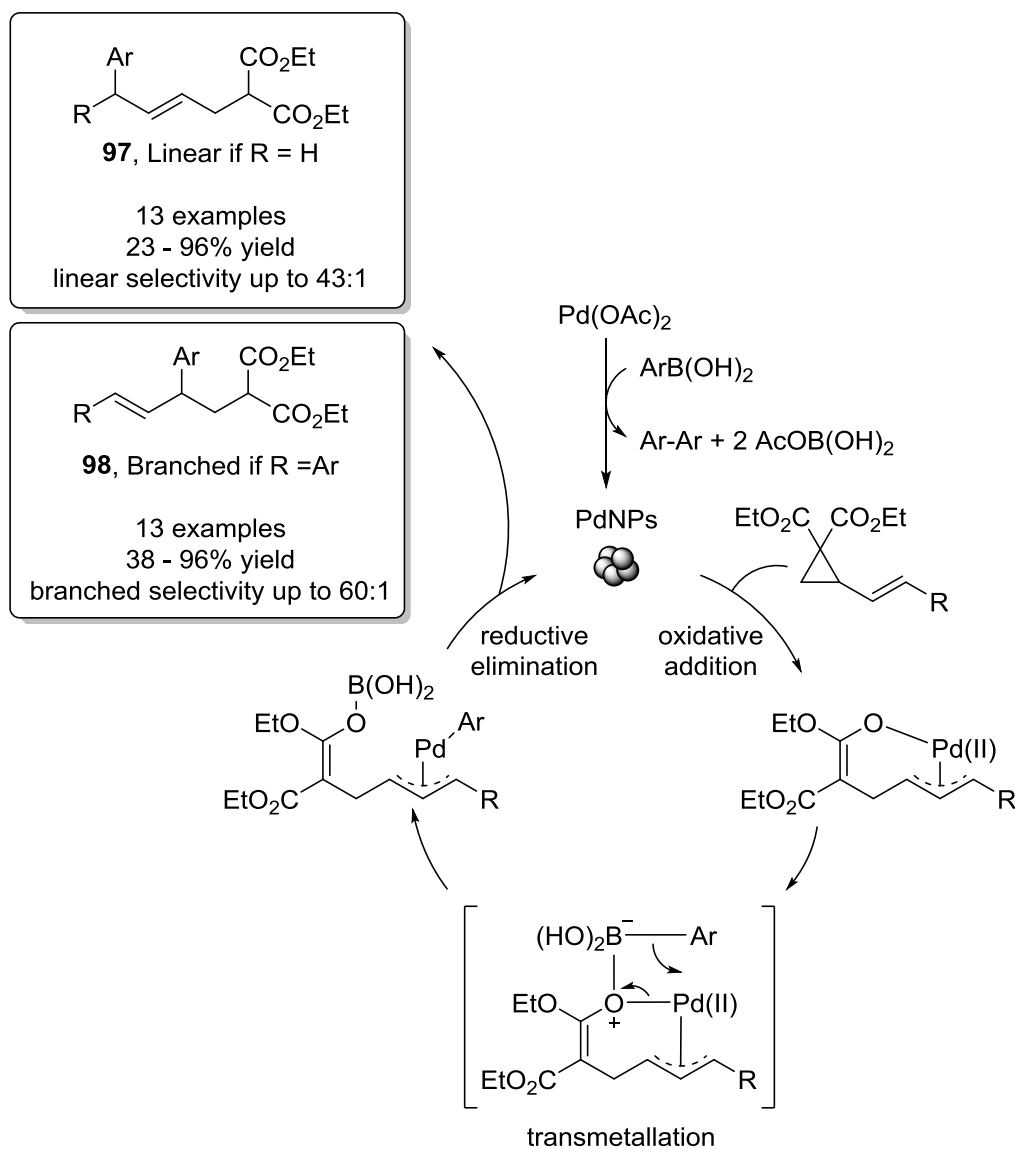


Figure 30: Pd-catalysed ring-opening of VCP dicarboxylates by boronic acids.

While the use of VCPs to generate 1,3-dipoles under Pd-catalysis have demonstrated great utility in the syntheses of five-membered rings and spirocycles via [3 + 2] cycloadditions to isolated π -systems, it has yet to be applied to prepare fused polycycles such as indoline-derived heterocycles. These fused systems would require the addition of 1,3-dipole to aromatic systems – a method that has not been well developed.

4.1.3 Indoline-derived heterocycles

Indoline-derived heterocycles are prevalent in a host of important biologically active molecules, therefore new methods for their preparation is a major area of investigation for synthetic chemists. The 2,3-fused pyrrolo derivatives (pyrroloindolines) feature a tricyclic skeleton with two *N*-heterocycles (Figure 31) and the preparation of these derivatives has been widely explored.³⁹ Notably, the construction of 3a-amino-pyrroloindolines is a particular interest due to their potent antibacterial properties.⁴⁰ Furthermore, these cores play a key role as intermediates for the preparation of heterodimeric C3a-C3a' linked cyclotryptamine-based alkaloids.⁴¹

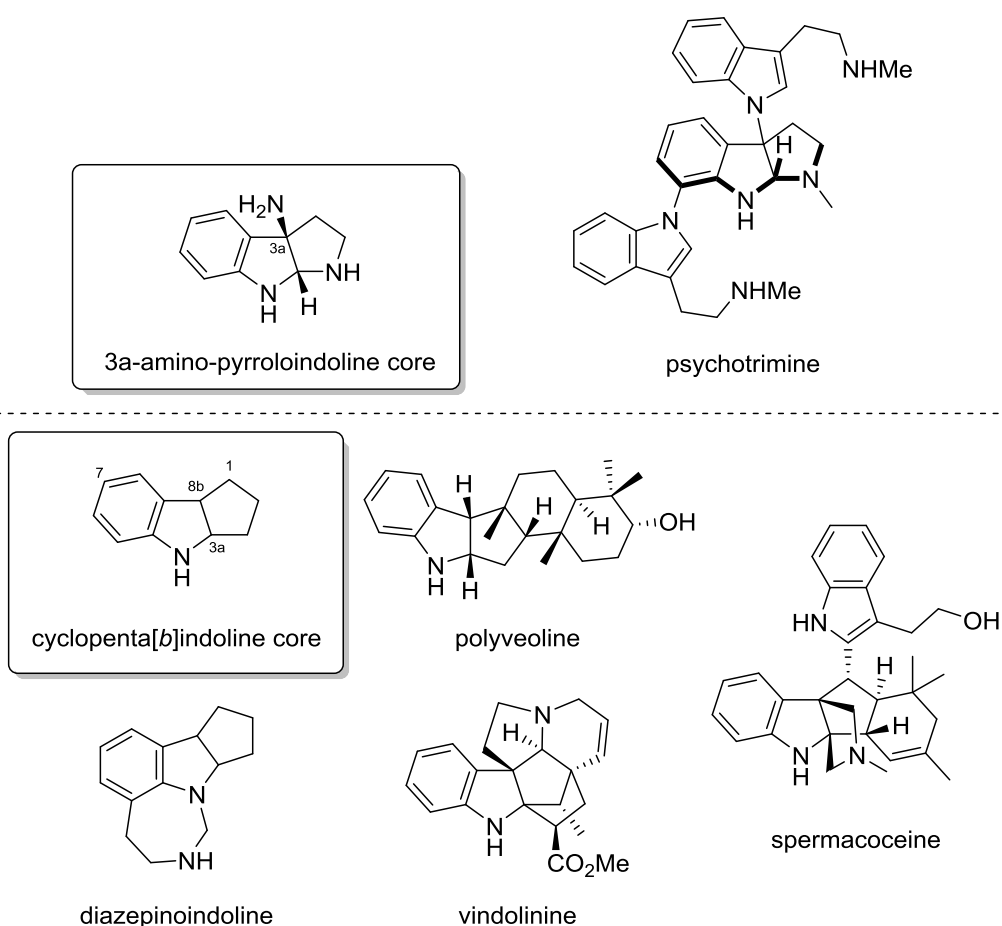
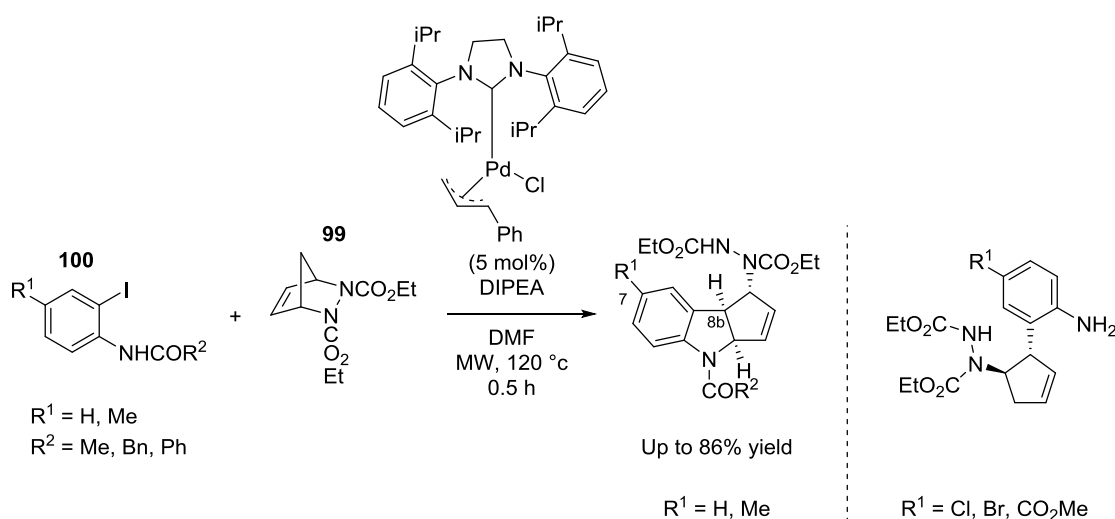


Figure 31: Representative examples of pyrroloindoline and cyclopenta[b]indoline cores.

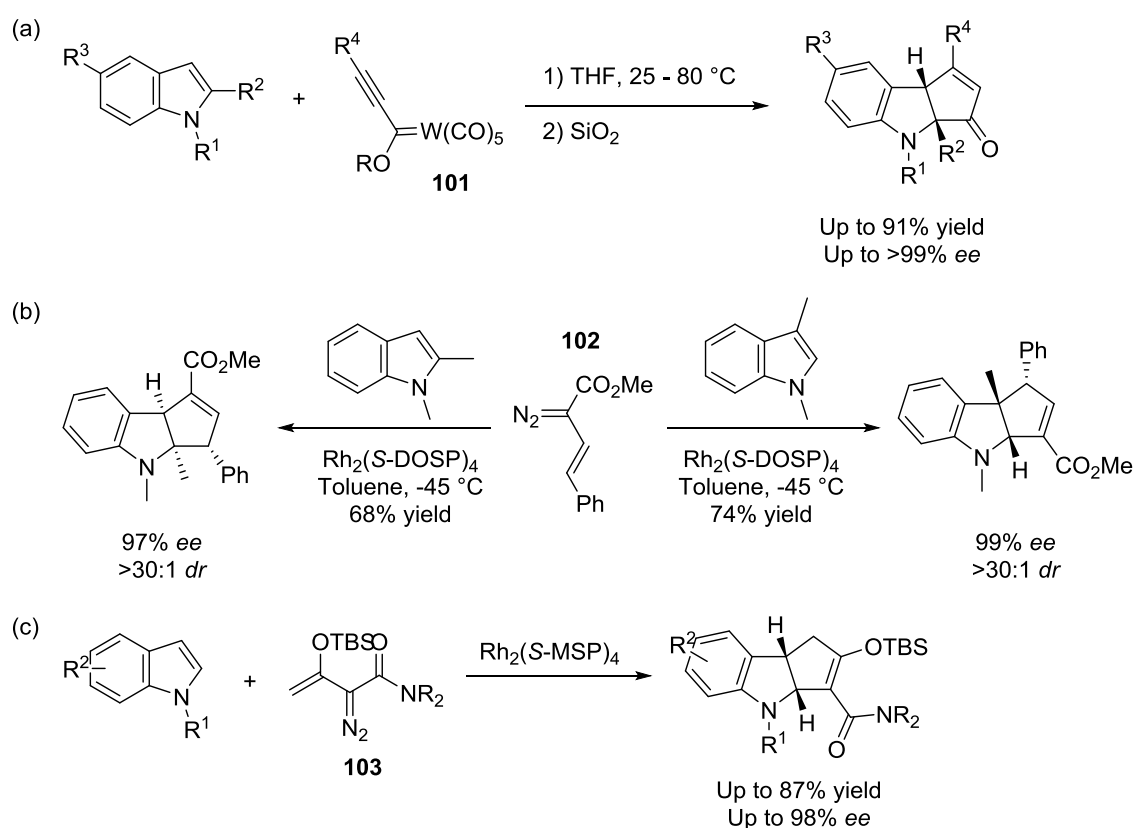
An important class of 2,3-fused cyclopentannulated indolines core (cyclopenta[*b*]indolines) are found in bioactive molecules such as diazepinoindoline (treatment and prevention of central nervous system disorders)⁴² and polyveoline (antitrypanosomal alkaloid)⁴³ (Figure 31). Despite being featured in various biologically active compounds, the construction of this indoline core has not been deeply investigated compared to the related pyrroloindolines.

Traditionally, cyclopenta[*b*]indolines were prepared in multiple steps by photochemical cyclization or heterocyclization of alkenylarylamines.⁴⁴⁻⁴⁷ Recently, Gilbertson and colleagues prepared cyclopenta[*b*]indoline in a step-efficient manner via a Pd-*N*-heterocyclic carbene-catalysed cyclopentannulation of diazabicyclic olefins **99** with *ortho*-functionalised aryl halides **100** (Scheme 40).⁴⁸ Although this method proceeded with high diastereoselectivity, it could not provide access to cyclopenta[*b*]indoline derivatives with electron-withdrawing groups or a halogen at C7, nor a substituent at C8b.



Scheme 40: Pd-NHC catalysed cycloaddition of diazabicyclic olefins **99** with *ortho*-functionalised aryl halides **100**.

Indole derivatives are readily available flat skeleton that can be converted into a three-dimensional structure through cycloaddition. Hence, the [3 + 2] dearomative cycloaddition of 1,3-dipoles to the indole skeleton could be the most atom-efficient method to prepare cyclopenta[*b*]indolines.⁴⁹ Alkynyl Fischer carbene complexes **101** have been used by Barluenga for the asymmetric [3 + 2] cyclopentannulation of indoles (Scheme 41a).⁵⁰ Lian and Davies reported a Rh-catalysed version of this reaction with vinyl diazoacetates **102** (Scheme 41b),⁵¹ while Doyle and co-workers developed an asymmetric Rh-catalysed variant with enoldiazoacetamides **103** (Scheme 41c).⁵² The cycloadditions of indoles with metal carbenoids gave excellent yields, however further functionalisation at C1 and C8b is limited.



Scheme 41: Construction of cyclopenta[*b*]indoline through the [3 + 2] dearomative cycloaddition of metal carbenoids to indole core.

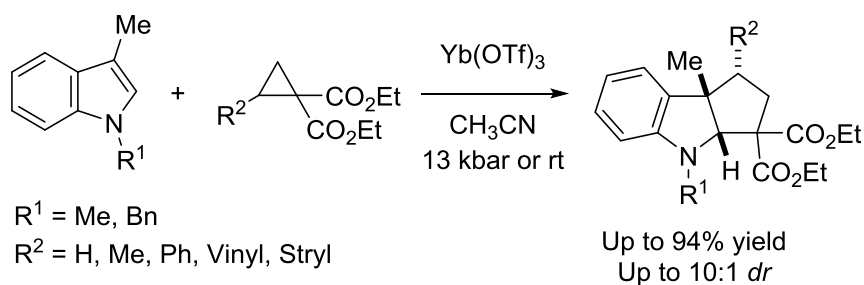
As demonstrated from the examples shown in Section 4.1.1 above, DA cyclopropanes are versatile and useful building blocks that generate 1,3-dipole to construct five-membered rings. Therefore, subjecting DA cyclopropanes to the [3 + 2] dearomative indole cycloaddition can be an atom efficient method to prepare cyclopenta[*b*]indolines. Kerr and colleagues reported the Yb(OTf)₃-catalysed formal [3 + 2] annulation of 3-alkylindoles with 1,1-cyclopropanediester as formal 1,3-dipoles to provide cyclopenta[*b*]indolines in high yield and diastereoselectivity (Scheme 42a).^{53,54} Besides, an enantioselective cycloaddition of electron-rich indoles with 1,1-cyclopropanediester using a BOX/Cu(II)-catalyst was also reported (Scheme 42b).⁵⁵ Although these reported methods are highly efficient for the construction of cyclopenta[*b*]indoline core, subsequent functionalisation at C1 is limited as it is occupied by alkyl or aryl groups.

While electron-rich indoles were employed in the several examples illustrated above, the reversal of polarity using electron-poor indoles as the cycloaddition partners is investigated to a lesser extent. Trost made an important contribution in this area with the [3 + 2] cycloaddition reactions of Pd-TMM to electron-deficient aromatics, including 3-nitro-1-phenylsulfonyl indoles to give cyclopenta[*b*]indolines (Scheme 42c).⁵⁶ By installing a nitro group on the C3 position and an electron-withdrawing group on the nitrogen, the typically nucleophilic indole was converted into an electrophilic Michael acceptor for the 1,3-dipole derived from TMM. Although this innovative method efficiently provides access to cyclopenta[*b*]indolines, further functionalisation at C1 is still restricted, similar to previous examples.

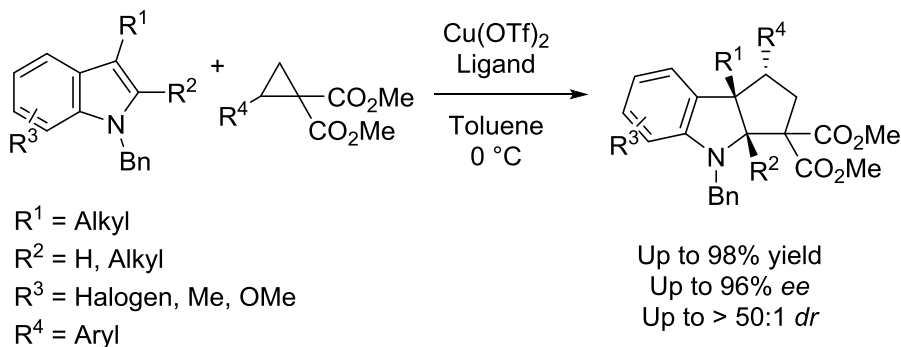
While TMM had been employed in [3 + 2] cycloaddition with aromatic systems such as nitroindoles, the versatile VCPs have not been used as partners with aromatic systems. The use of VCP dicarboxylates in [3 + 2] cycloaddition with aromatic systems

can provide functional groups as handles for further derivatisation, such as vinyl and ester groups. This strategy can be employed to overcome the limitation from reported studies where further derivatisation was restricted due to lack of manipulable functional groups.

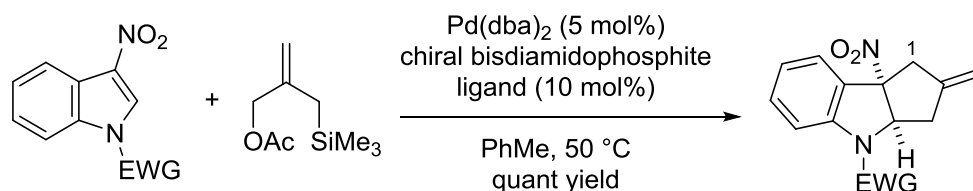
(a) Kerr et al. (racemic)



(b) Tang, Xie et al. (enantioselective)



(c) Trost et al.



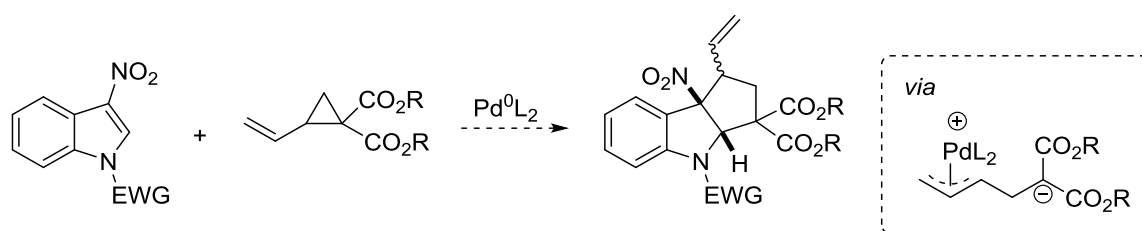
Scheme 42: Construction of cyclopenta[*b*]indoline through the [3 + 2] dearomative cycloaddition of indoles with 1,3-dipoles derived from: (a & b): DA cyclopropanes; (c) TMM.

4.2 Aim and research plan

Even though the preparation of cyclopenta[*b*]indoline core is less reported than the pyrroloindoline counterpart, existing methods provide access to this core in high yield

and excellent atom economy. However, the cycloadducts obtained from most of these studies have limited capacity to undergo further transformation due to lack of manipulable functional groups around the cyclopentane ring. Biologically active molecules that feature the cyclopenta[*b*]indoline core usually have higher complexity in their structures, hence there is a need to develop methods that can construct densely functionalised derivatives of this core in a step- and atom-economic manner. Furthermore, cyclopenta[*b*]indoline with amine group at C8b is analogous to 3a-amino-pyrroloindoline (Figure 31) which possessed antibacterial property. However, there is only one reported method that can provide access to cyclopenta[*b*]indolines with amine functionality at C8b.⁵⁶

Given this gap in the synthetic methodology, we aimed to construct densely functionalised cyclopenta[*b*]indolines from the cycloaddition of 3-nitroindoles with 1,3-dipoles generated from VCP dicarboxylates under Pd(0) catalysis (Scheme 43). The presence of a nitro group at C3 position serves two purposes: (1) to convert the indole into an electrophilic system such that the zwitterionic 1,3-dipole can act as the nucleophile towards C2 in a Michael addition fashion, and; (2) to install a handle for further reaction.



Scheme 43: Proposed reaction: Pd-catalysed [3 + 2] cycloaddition of 3-nitroindoles with VCP dicarboxylates.

The densely functionalised cycloadduct features a vinyl group at C1, geminal diesters at C3 and nitro group at C8b. Each of these functional groups has the potential to undergo further chemical transformation. For instance, the nitro group at C8b can be

reduced to an amine or removed entirely using radical nitration,⁵⁷ therefore the use of 3-nitroindole as substrate provides flexibility in further structural modification compared to 3-alkylindoles. The vinyl group can also undergo a Heck reaction,^{58,59} olefin metathesis⁶⁰ or cyclopropanation. As for the geminal diesters, they can undergo transesterification or basic hydrolysis as well as mono-decarboxylation. The presence of these functional groups provides the handle for further derivatisation, therefore this creates a path to access complex analogues of cyclopenta[*b*]indolines.

As mentioned earlier, cycloadditions utilising VCPs achieve excellent atom efficiency compared to TMM which have trimethylsilyl acetate as side product. Furthermore, the variation in olefin terminal and electron-withdrawing groups (carbonyls or nitriles) provides substrate scope for investigation.

This chapter will discuss the optimisation process to develop a diastereoselective [3 + 2] cycloaddition method for VCPs and 3-nitroindoles and investigation of the substrate scope. Subsequently, the obtained cyclopenta[*b*]indolines will be subjected to various chemical transformations to demonstrate their potential for further derivatisation.

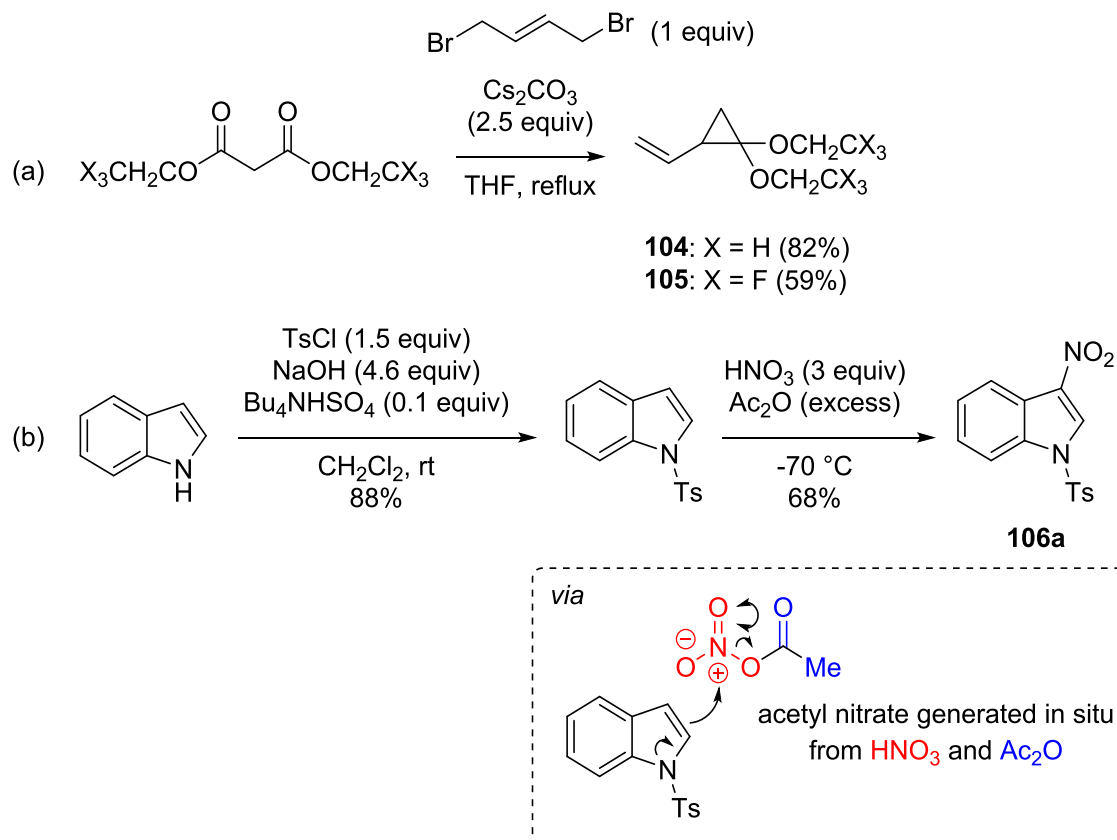
It is of note that as this study was conducted, a parallel study using vinylaziridine and 3-nitroindole to construct pyrroloindolines was performed at our lab.⁶¹ Partial results from that study, in particular the chemical transformation of pyrroloindoline, will be reported in this chapter. Also as this study was being concluded, Vitale and co-workers reported similar investigation with opposite stereochemical outcome,⁶² which will be discussed in the following section.

4.3 Results and discussion

4.3.1 Optimisation of reaction conditions

The study was initiated with 3-nitro-1-tosylindole **106a** and diethyl 2-vinylcyclopropane-1,1,-dicarboxylate **104** as reaction partners to investigate the proposed dearomative cycloaddition. Vinylcyclopropane **104** was prepared from commercially available diethyl malonate and *trans*-1,4-dibromo-2-butene under basic conditions in good yield – in both cases the spectra data obtained matched that reported in the literature (Scheme 44a). The ¹H NMR data of **104** was consistent with literature.⁶³

On the other hand, the electrophilic 3-nitroindole **106a** was prepared by the *N*-tosylation of indole, follow by a selective nitration at C3 position using in situ generated acetyl nitrate at –70 °C (Scheme 44b). The lone pair of electrons on indole nitrogen inductively accumulates electron density at C3 position and hence making it nucleophilic towards acetyl nitrate. However, it has been reported that nitration at C6 position can occur substantially at temperature higher than –50 °C (5% and 25% of C6 nitration at –50 °C and –10 °C respectively).⁶⁴ Similarly, this nitration method was employed instead of classical arene nitration method as the latter is not chemoselective and may nitrate the indole phenyl ring. The ¹H NMR data of **106a** was consistent with literature.⁶⁵

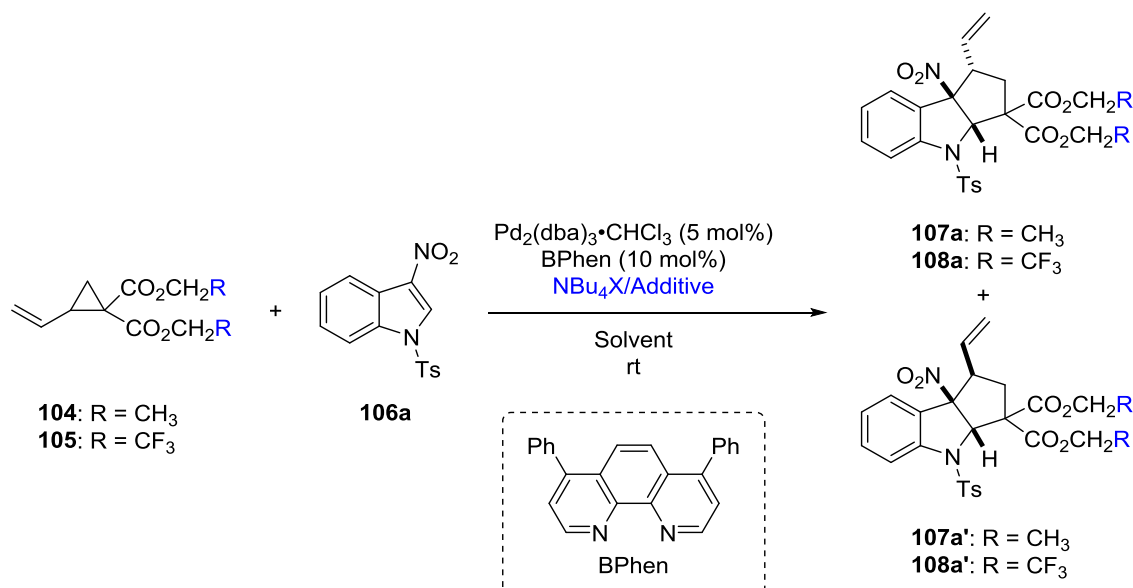


Scheme 44: Preparation of starting materials for dearomatisation reaction.

In a parallel study conducted in our lab using vinylaziridine in cycloaddition with 3-nitroindoles **106a**, the combination of BPhen and $\text{Pd}_2(\text{dba})_3 \cdot \text{CHCl}_3$ was identified as a suitable catalyst system for the reaction.⁶¹ Therefore, this catalyst and ligand combination was initially deployed in the proposed reaction. Gratifyingly, the reaction proceeded in good yield, providing the desired cyclopenta[*b*]indoline **107a/107a'**, but as a mixture of *cis* (favoured) and *trans* diastereoisomers in low *dr* (Table 4, entry 1). Due to the dearomatisation of the indole ring, the methine carbon adjacent to *N*-tosyl group was converted from sp^2 to sp^3 hybridisation and hence the corresponding singlets shifted up-field from 8.57 ppm (**106a**) to 6.36 (**107a'**) and 6.31 (**107a**) ppm in the ^1H NMR spectrum. Also, as a result of the reaction, the allylic methine proton experiences a deshielding effect due to the presence of nitro group in close proximity. In the ^1H NMR spectrum of **107a/107a'**, the corresponding signal was shifted down-field from 2.57 ppm (**104**) to 3.41

(**107a'**) and 3.30 ppm (**107a**). In the ^{13}C NMR spectrum of the mixture, the C-NO_2 signal shifted up-field from 133.2 ppm (**106a**) to 102.7 and 101.3 ppm (**107a/107a'**). More importantly, the signal of the methine carbon adjacent to *N*-tosyl group shifted up-field significantly from 127.8 ppm (**106a**) to 73.7 and 73.3 ppm (**107a/107a'**) as a result of the indole dearomatisation. The determination of their relative stereochemistry will be discussed later in the dearomatised cycloadducts **108a** and **108a'**.

Table 4: Optimisation of dearomative cycloaddition between vinylcyclopropane-1,1-dicarboxylates and 3-nitro-1-tosylindole: Effect of VCP electronics and additive.^a



Entry	R	NBu ₄ X/Additive (Equiv)	Solvent	<i>dr</i> (<i>trans</i> : <i>cis</i>) ^b	Yield ^c
1	CH ₃		MeCN	1:1.3	62
2	CF ₃		MeCN	1.3:1	95
3	CF ₃		THF	1.7:1	95
4 ^d	CF ₃	I (0.3)	THF	3.1:1	95
5 ^d	CF ₃	Br (0.3)	THF	2.8:1	97
6 ^d	CF ₃	Cl (0.3)	THF	2.6:1	92
7	CF ₃	I (1.0)	THF	3.7:1	74
8 ^d	CF ₃	I (0.5)	THF	4.3:1	(80)
9 ^d	CF ₃	LiI (0.5)	THF	N/A	Trace
10 ^d	CF ₃	ClO ₄ (0.5)	THF	2.0:1	75

^a Reactions carried out at 0.1 M, rt with 5 mol% Pd₂(dba)₃·CHCl₃ and 10 mol% BPhen with 1.0 eq. of VCP

104/105 and 1.3 eq. of indole **106a**. **107a/108a** refers to the *trans* diastereoisomer and **107a'/108a'** to the *cis* diastereoisomer. ^b Determined from the ¹H NMR of the crude reaction mixture. ^c Yield was calculated from ¹H NMR of the reaction mixture using mesitylene as an internal standard, with isolated yield in brackets where applicable. ^d 1:1 molar ratio of indole:VCP utilised.

It was postulated that the reversibility of the addition of the VCP-derived zwitterionic dipole to the 3-nitroindole could play a role in determining the ultimate diastereoselectivity of the reaction. As such the di(trifluoroethyl) ester analogue **105** was investigated as this would afford a more stable dipole and potentially facilitate this reversible addition.³² Interestingly, deploying **105** in the reaction reversed the sense of selectivity, favouring *trans* cyclopenta[*b*]indoline **108a** in MeCN, while switching the solvent to THF increased the *dr* moderately (Table 4, entries 2 and 3). In the ¹H NMR analysis of the crude mixture (Figure 32), the ratio of diastereoisomers was determined by measuring the integration ratio of the singlets at 6.32 (**108a'**) and 6.24 (**108a**) ppm, which were assigned as the methine protons adjacent to the NTs group (TsN-CH). Chromatographic purification and crystallisation of the mixture allowed the isolation of pure **108a**, which was later determined as the *trans* diastereoisomer by X-ray crystallography (Figure 33).

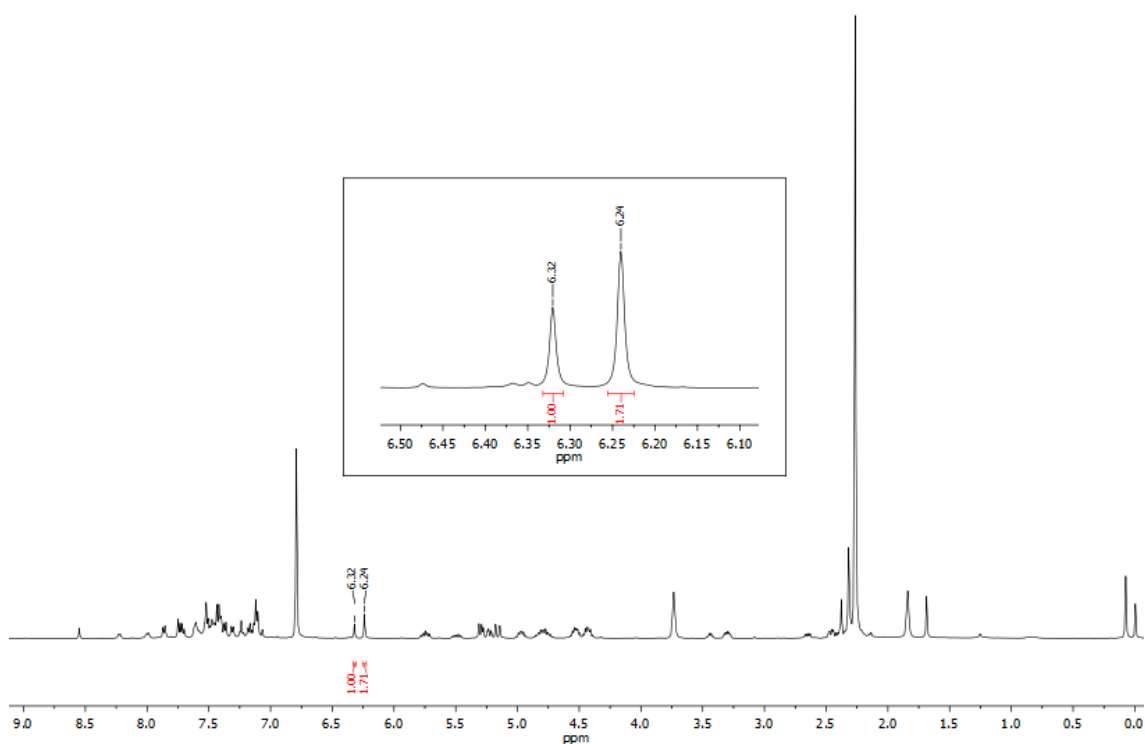


Figure 32: Determination of diastereoselectivity using ^1H NMR spectrum of the reaction crude for **108a/108a'**: The singlets at 6.32 (**108a'**) and 6.24 (**108a**) ppm correspond to the methine proton adjacent to NTs group ($\underline{\text{H}}\text{C-NTs}$), and the integration ratio of these two singlets reflect the diastereoselectivity of the reaction. Crude ^1H NMR spectrum in this figure was obtained from entry 3 (Table 4), which provided a dr of 1.7:1 (**108a**:**108a'**). After chromatographic purification and serial recrystallisation, a crystalline solid was obtained and its ^1H NMR spectrum only displayed the singlet at 6.24 ppm. Subsequent X-ray crystallography analysis revealed that the crystalline solid was the *trans* diastereomer **108a** (Figure 33), and hence the singlet at 6.24 ppm was assigned to the $\underline{\text{H}}\text{C-NTs}$ from **108a**.

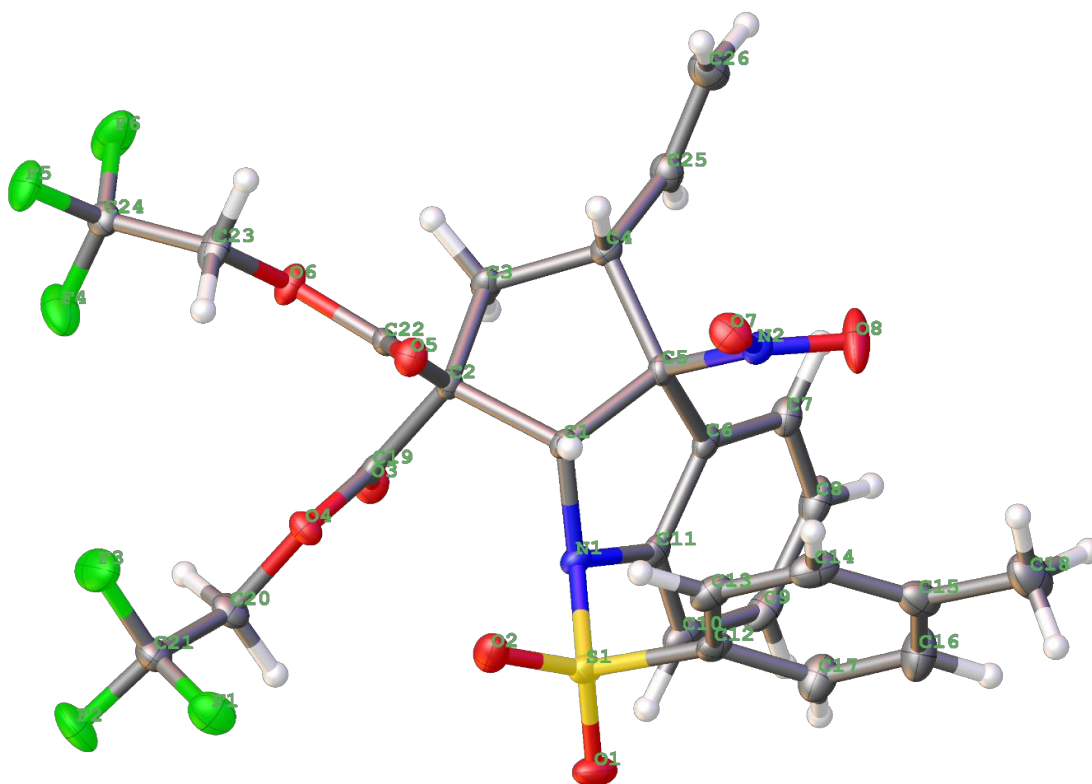


Figure 33: Thermal Ellipsoid Plot for the crystal structure of **108a**. Thermal ellipsoids are shown at the 50% probability level. All methyl and aromatic-ring hydrogen atoms are omitted for clarity.

It was postulated that π - σ - π interconversion between the two diastereomeric zwitterionic π -allylpalladium complexes derived from the vinylcyclopropane adding to the 3-nitroindole could be an important control factor in determining the *dr* of the reaction.⁶⁶ Given that halide additives are known to increase the rate of π - σ - π interconversion,⁶⁶ these were then investigated in the reaction (Figure 34). In line with this, it was found that the use of halide additives had a positive effect on the *dr* of the reaction (Table 4, entries 4-8), with 0.5 equiv of *n*Bu₄NI proving optimal (Table 4, entry 8).

The NBu₄I additive can play a role during the Michael addition and the subsequent intermediate Pd- π -allyl complex. During the Michael addition, NBu₄I stabilised the 1,3-

dipole derived from **105** (Figure 34), hence increasing the reversibility of Michael addition with indole **106a**. After the Michael addition and during the transition state, the tetrabutylammonium cation stabilised the anion, therefore decreasing the rate of nucleophilic attack (decreasing k_2 and k_2'). Meanwhile, the iodide allowed the interconversion between the η^3 and η^1 intermediates, therefore accelerating the π - σ - π interconversion between **TS1** and **TS2** (increasing k_1). Curtin–Hammett condition was achieved when $k_1 > k_2$ and k_2' , therefore the diastereoselectivity of the reaction relied solely on the free energy of **TS1** and **TS2**, where **TS1** was presumed to have a lower energy as **108a** was observed as the major diastereomer.

The individual effect of the tetrabutylammonium cation and iodide was then investigated. When LiI was introduced as the iodide source in the absence of tetrabutylammonium cation, only trace amount of product was detected (Table 4, entry 9). The low yield could be due to catalyst poisoning via palladate formation stabilised by Li^+ .⁶⁷ On the other hand, the introduction of tetrabutylammonium perchlorate as a source of NBu_4^+ without a halide only resulted in a slight increase in *dr* compared to that of when no additive was added (Table 4, entry 10). Therefore, both ionic species in NBu_4I were crucial to provide diastereoselective control.

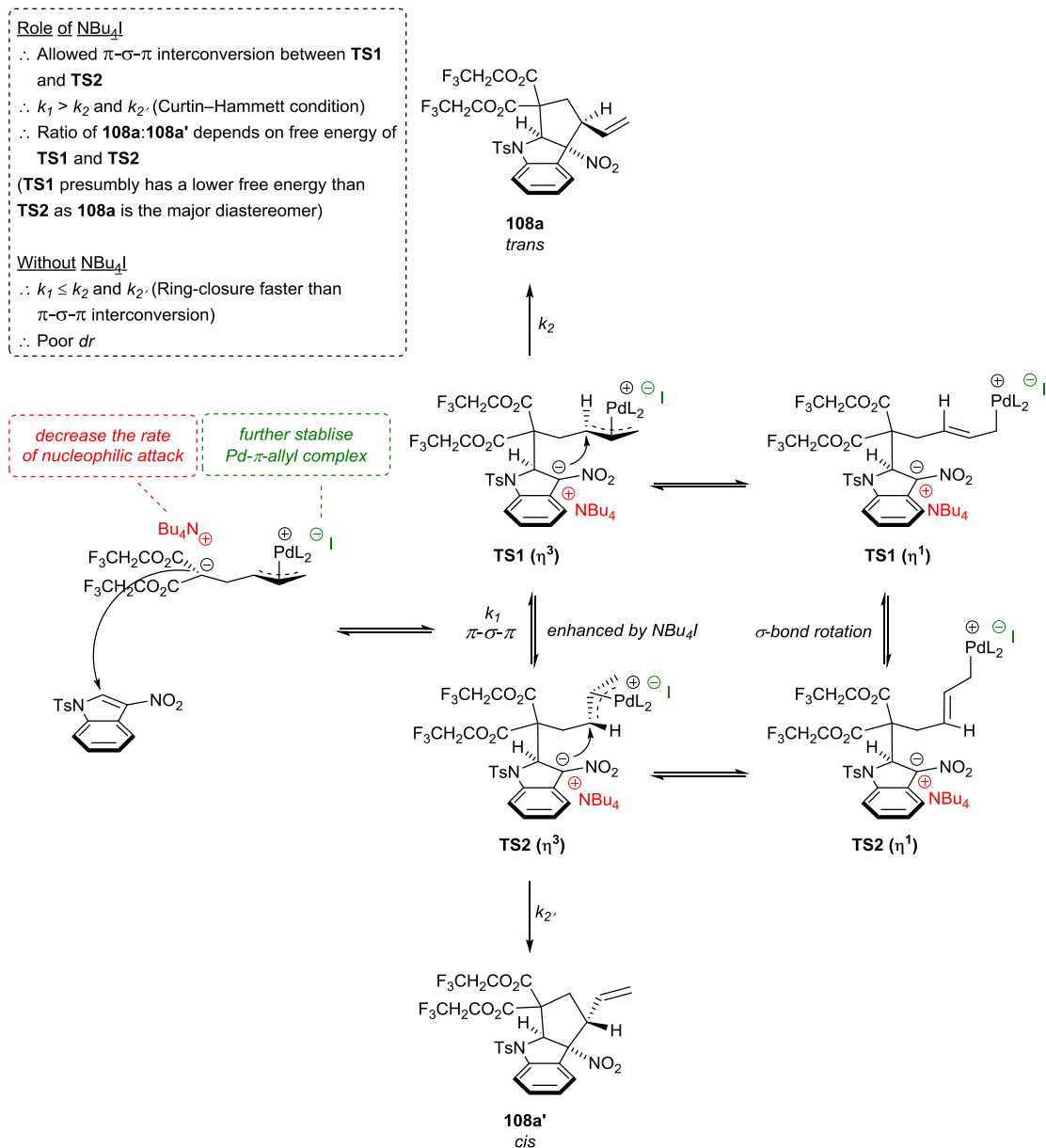
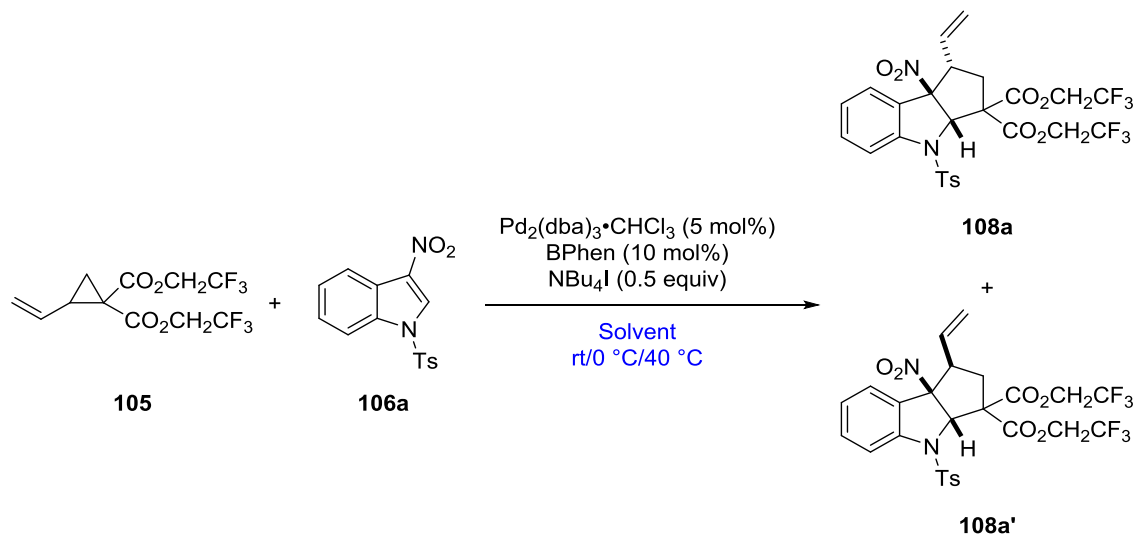


Figure 34: Addition of tetrabutylammonium iodide increases the rate of π - σ - π interconversion by stabilising **TS1** and **TS2**.

Lowering of the temperature (Table 5, entry 11) had no effect on the *dr*, but resulted in a slight decrease in yield while increasing the temperature to 40 °C (Table 5, entry 12) moderately reduced the *dr*. A screen of other solvents (Table 5, entries 13-16) resulted in lower yields and diastereoselectivity, indicating that THF was optimal.

Table 5: Optimisation of dearomative cycloaddition between vinylcyclopropane-1,1-dicarboxylates and 3-nitro-1-tosylindole: Temperature and solvent screening.^a



Entry	Solvent	Temperature	<i>dr</i> (<i>trans</i> : <i>cis</i>) ^b	Yield ^c
11	THF	0 °C	4.2:1	77
12	THF	40 °C	3.4:1	80
13	DCM	rt	1.7:1	74
14	Dioxane	rt	2.4:1	74
15	MeCN	rt	1.8:1	75
16	PhMe	rt	4.0:1	64

^a Reactions carried out at 0.1 M, rt with 5 mol% $\text{Pd}_2(\text{dba})_3 \cdot \text{CHCl}_3$ and 10 mol% BPhen with 1.0 eq. of VCP

105 and 1.3 eq. of indole **106a**. **108a** refers to the *trans* diastereoisomer and **108a'** to the *cis* diastereoisomer.

^b Determined from the ^1H NMR of the crude reaction mixture. ^c Yield was calculated from ^1H NMR of the reaction mixture using mesitylene as an internal standard. ^d 1:1 molar ratio of indole:VCP utilised.

Using THF as the solvent a selection of other ligands (Figure 35) were trialed in the reaction (Table 6, entries 17-27), including diphosphine, diamine and chiral Trost ligands, but while some resulted in an increased yield the *dr* was significantly lower than BPhen for all cases. Recent literature suggested that Pd(0) with electron-rich dba analogues displayed enhanced reactivity due to the destabilisation of back-bonding

therefore increasing dba ligand dissociation.⁶⁸ However in this study, the use of Pd₂(4,4'-OMe-dba)₃·CHCl₃ provided similar yield and *dr* to that of Pd₂(dba)₃·CHCl₃. As such, the reaction scope was investigated with the optimum conditions in entry 8 (Table 4). The catalyst/ligand loading can be lowered to 2.5 mol%/5 mol% respectively, however a noticeable drop in *dr* was observed (Table 6, entry 29).

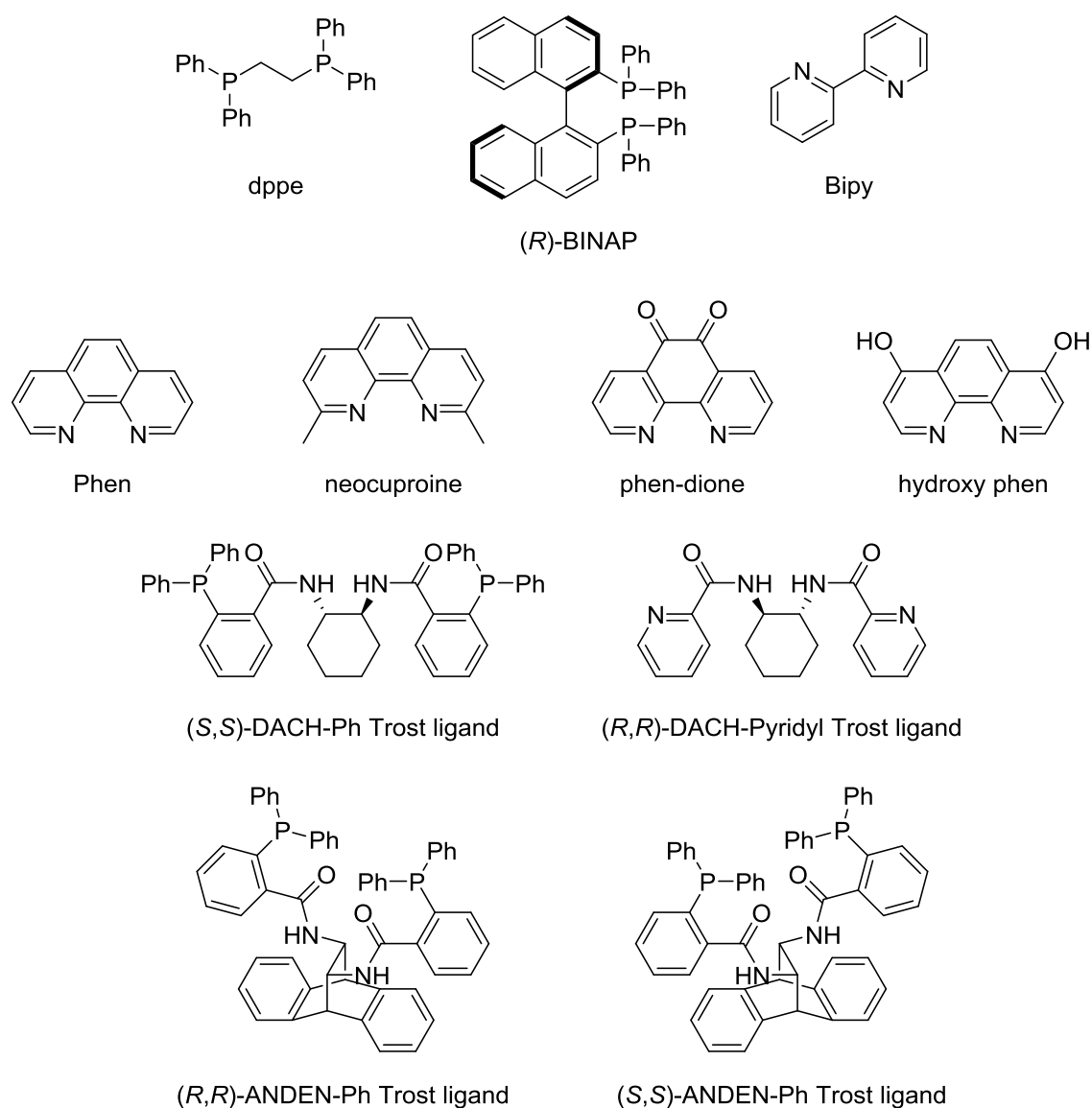
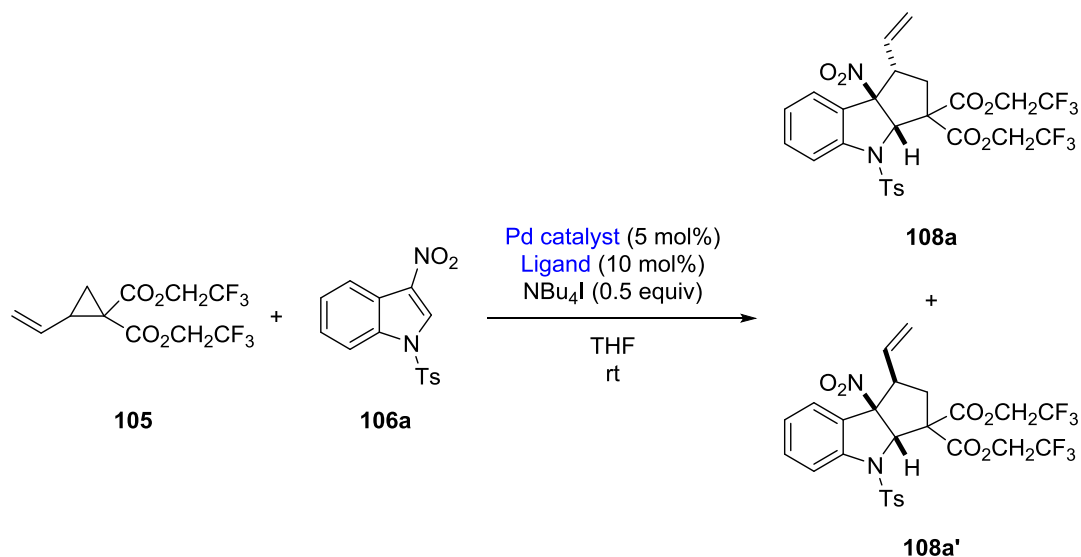


Figure 35: Candidates for ligand screening.

Table 6: Optimisation of dearomative cycloaddition between vinylcyclopropane-1,1-dicarboxylates and 3-nitro-1-tosylindole: Ligand and catalyst screening.^a



Entry	Catalyst	Ligand	<i>dr</i> (<i>trans</i> : <i>cis</i>) ^b	Yield ^c
17 ^d	Pd ₂ (dba) ₃ ·CHCl ₃	dppe	2.2:1	76
18 ^d	Pd ₂ (dba) ₃ ·CHCl ₃	(<i>R</i>)-BINAP	1.1:1	66
29 ^d	Pd ₂ (dba) ₃ ·CHCl ₃	Bipy	1.9:1	92
20 ^d	Pd ₂ (dba) ₃ ·CHCl ₃	Phen	2.7:1	97
21 ^d	Pd ₂ (dba) ₃ ·CHCl ₃	neocuproine	2.0:1	84
22 ^d	Pd ₂ (dba) ₃ ·CHCl ₃	phen-dione	1.9:1	25
23 ^d	Pd ₂ (dba) ₃ ·CHCl ₃	hydroxy phen	1.8:1	96
24 ^d	Pd ₂ (dba) ₃ ·CHCl ₃	(<i>S,S</i>)-DACH-Ph Trost ligand	1.6:1	67
25 ^d	Pd ₂ (dba) ₃ ·CHCl ₃	(<i>R,R</i>)-DACH-Pyridyl Trost ligand	1.5:1	100
26 ^d	Pd ₂ (dba) ₃ ·CHCl ₃	(<i>R,R</i>)-ANDEN-Ph Trost ligand	1.2:1	71
27 ^d	Pd ₂ (dba) ₃ ·CHCl ₃	(<i>S,S</i>)-ANDEN-Ph Trost ligand	1.2:1	83
28	Pd ₂ (4,4'-OMe-dba) ₃ ·CHCl ₃	BPhen	4.2:1	81
29 ^d	Pd ₂ (dba) ₃ ·CHCl ₃ ^e	BPhen ^e	3.1:1	82

^a Reactions carried out at 0.1 M, rt with 5 mol% Pd catalyst and 10 mol% ligand with 1.0 eq. of VCP **105** and 1.3 eq. of indole **106a**. **108a** refers to the *trans* diastereoisomer and **108a'** to the *cis* diastereoisomer. ^b

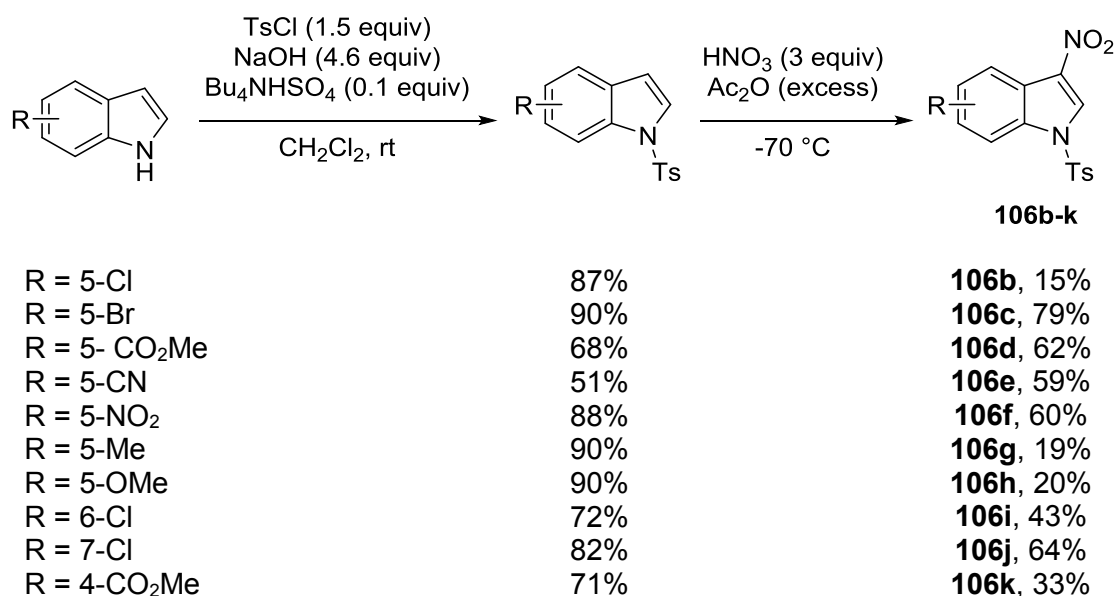
Determined from the ¹H NMR of the crude reaction mixture. ^c Yield was calculated from ¹H NMR of the

reaction mixture using mesitylene as an internal standard. ^d 1:1 molar ratio of indole:VCP utilised. ^e Pd₂(dba)₃·CHCl₃ (2.5 mol%), BPhen (5 mol%) (Halving catalyst & ligand loadings).

4.3.2 Reaction scope

4.3.2.1 Preparation of indole and VCP substrates

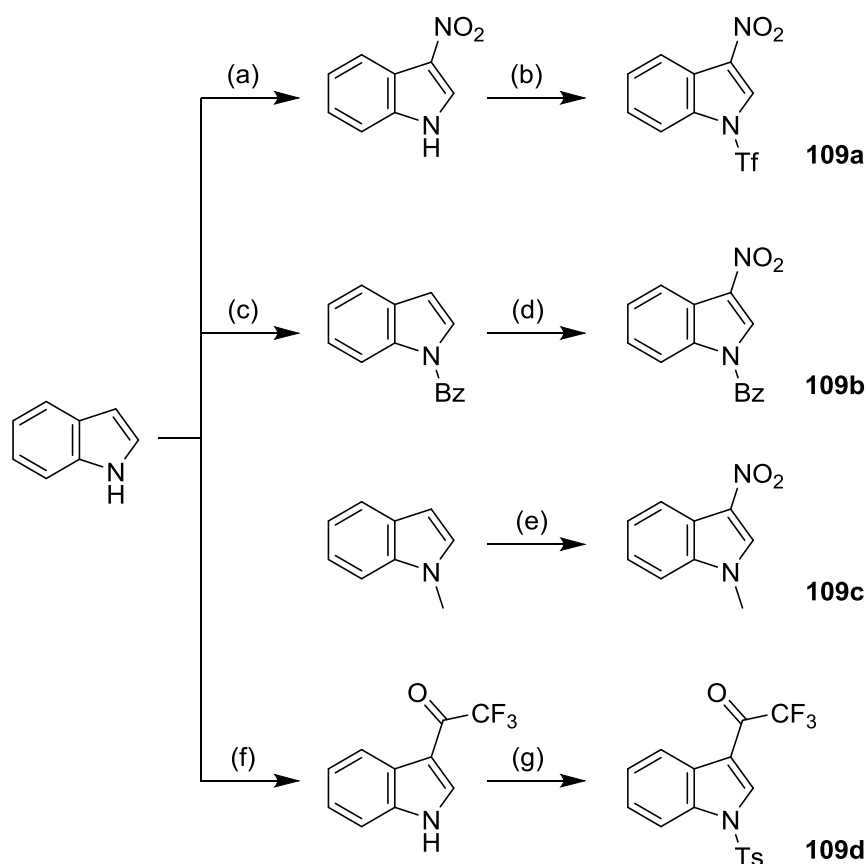
Derivatives of 3-nitroindoles and VCPs were prepared in order to explore the substrate scope of the dearomatisation reaction. Firstly, ten analogues of *N*-tosylated 3-nitroindoles were prepared (Scheme 45) using the same method as shown in Section 4.3.1.



Scheme 45: Two-step preparation of *N*-tosylated 3-nitroindoles **106b-k**, provided by D. Rivinoja (University of Wollongong).

Other indoles with different *N*-protecting groups and electron-withdrawing group on C3 were also prepared to investigate the tuning of the electron-withdrawing groups (Scheme 46). Nitro indole **109a** was prepared firstly by indole nitration at C3, followed by triflation on the indole nitrogen. In the ¹H NMR spectrum of nitro indole **109a**, the absence of doublet at 6.52 ppm suggested that the nitration of C3 was successful, while

the absence of broad singlet at 12.65 ppm indicated that the installation of triflate group on indole nitrogen was successful. Similarly in the ^1H NMR spectrum of indole **109d**, the absence of a doublet at 6.52 ppm and broad singlet at 12.70 ppm indicated that the installation of $-\text{C}(\text{O})\text{CF}_3$ at C3 and tosyl group on indole nitrogen were successful.

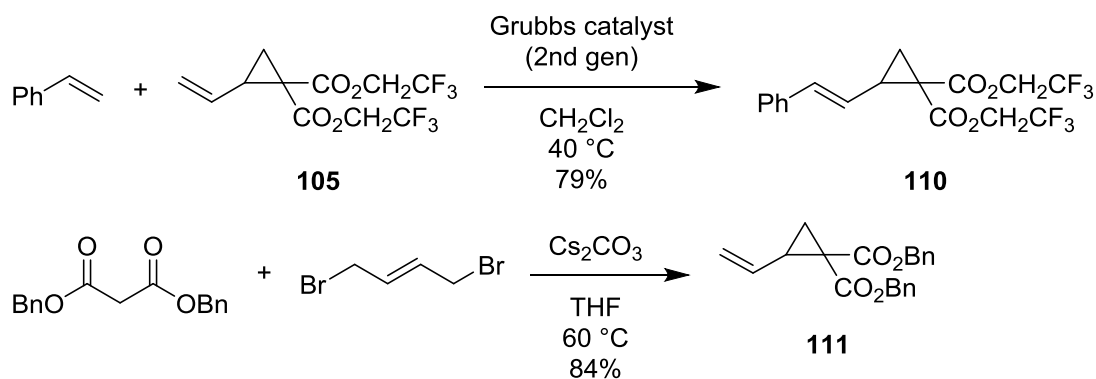


Scheme 46: Preparation of indole substrates with varied *N*-protecting groups and electron-withdrawing group on C3. Conditions: (a) NBS, AgNO_3 , MeCN, 16%. (b) DMAP, Et_3N , CH_2Cl_2 , trifluoromethanesulfonic anhydride, 65%. (c) BzCl , NaOH, *n*- Bu_4NHSO_4 , CH_2Cl_2 , 33%. (d) HNO_3 , Ac_2O , $-70\text{ }^\circ\text{C}$, 11%. (e) HNO_3 , Ac_2O , $-70\text{ }^\circ\text{C}$, 28%. (f) TFAA, DMF, 80%. (g) TsCl , NaOH, *n*- Bu_4NHSO_4 , CH_2Cl_2 , 7%. Indole substrates **109b** and **109c** were provided by D. Rivinoja (University of Wollongong).

As observed from Section 4.3.1, the change from VCP **104** to **105** significantly enhanced the diastereoselectivity due to increasing electron-withdrawing capability in

alkyl terminal and hence stabilisation of 1,3-dipole. In order to study the influence of substitution on the terminal vinyl position, a VCP analogue **110** was prepared from the Grubbs metathesis of **105** with styrene in a good yield of 79% (Scheme 47). In the ^1H NMR spectrum of **110**, the aromatic proton signals (7.30, 7.26 – 7.23 ppm) and olefin proton signals (doublet at 6.69 ppm for Ph-CH=CH and doublet of doublets at 5.83 ppm for Ph-CH=CH) suggested that the Grubbs metathesis was successful. The coupling constant for Ph-CH=CH) suggested that the Grubbs metathesis was successful. The coupling constant for the olefin proton signals was 15.5 – 16.0 Hz, indicating that the (*E*) olefin isomer was obtained as the sole product.

Besides, a VCP analogue **111** with dibenzyl esters was also synthesised in a good yield of 84% using similar preparation method of VCPs **104** and **105** (Scheme 47). In the ^1H NMR spectrum of **111**, the characteristic cyclopropane signals were observed at 2.63, 1.76, and 1.60 ppm.



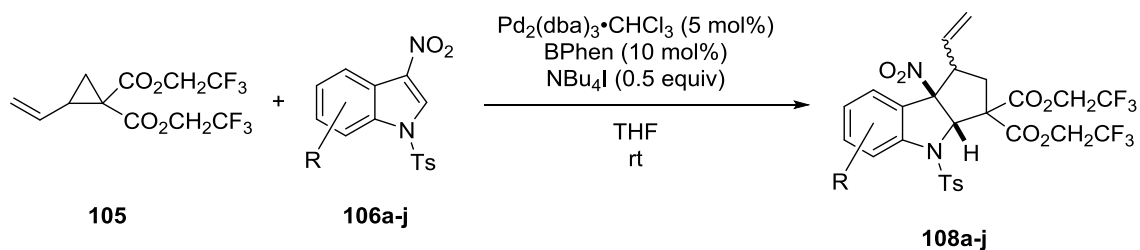
Scheme 47: Preparation of VCP derivatives **110** and **111**.

4.3.2.2 Scope of reaction

Using the optimised experimental conditions (entry 8, Table 4), various substituted *N*-tosyl-3-nitroindoles **106a-k** were subjected to the dearomatisation reaction with VCP **105** (Table 7). In most cases, the reaction proceeded in high yield (73 – 88%)

and good diastereoselectivity (3:1 to 4.3:1). Halogen substituents were tolerated by the Pd(0)-catalyst, providing products **108b**, **108c**, **108i** and **108j**. It is important that these halides were not affected by our catalyst system so that they can be amenable to further coupling reactions. Strongly electron-withdrawing groups (products **108d**, **108e** and **108f**) and an inductively donating methyl group (**108g**) also afforded the desired products. However, a 5-methoxy substituted 3-nitro-indole proved unreactive – presumably due to mesomeric donation rendering the indole insufficiently electron-poor to undergo dearomatisation.

Table 7: Substrate scope with various functionalised 3-nitroindoles.^a



<p>108a, 80% yield 4.3:1 <i>dr</i></p>	<p>108b, 88% yield 3:1 <i>dr</i></p>
<p>108c, 87% yield 3.4:1 <i>dr</i></p>	<p>108d, 84% yield 3.2:1 <i>dr</i></p>
<p>108e, 82% yield 3:1 <i>dr</i></p>	<p>108f, 73% yield 3.1:1 <i>dr</i></p>
<p>108g, 78% yield 3.1:1 <i>dr</i></p>	<p>108h, no reaction</p>
<p>108i, 88% yield 3.6:1 <i>dr</i></p>	<p>108j, 88% yield 3.2:1 <i>dr</i></p>

^a Diastereoselectivity (*trans:cis*) was determined from the ¹H NMR of the crude reaction mixture. All yields are for isolated products after chromatographic purification.

Curiously, when a methyl ester substituent was present at the 4-position of the starting indole **106k**, an inseparable mixture of unidentified products resulting from multiple VCP additions to the indole was obtained using the standard optimised conditions. This was suggested based on the ¹H NMR spectrum of the mixture, where a higher integration number was observed for CH_2CF_3 at approximately 4.50 ppm (Figure 36). Furthermore, all the olefin signals appeared as multiplets at around 5.00 – 5.50 ppm, which suggests internal alkene was present instead of terminal alkene. Besides, in the ¹³C NMR spectrum, five carbonyl signals were observed (165.4 – 168.0 ppm) while the proposed desired cycloadduct has only three carbonyls (Figure 36).

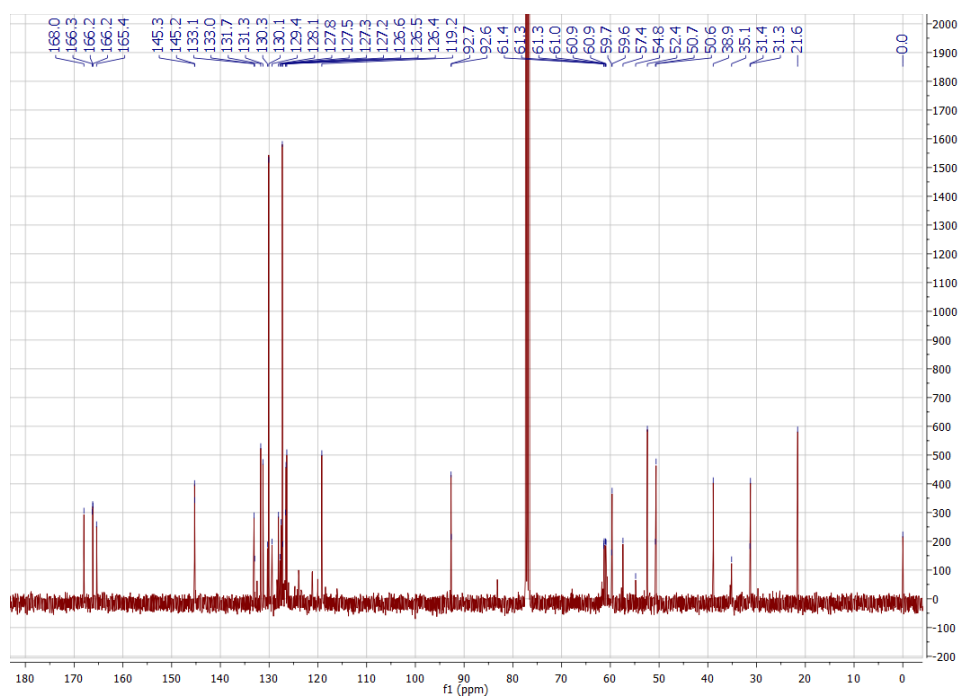
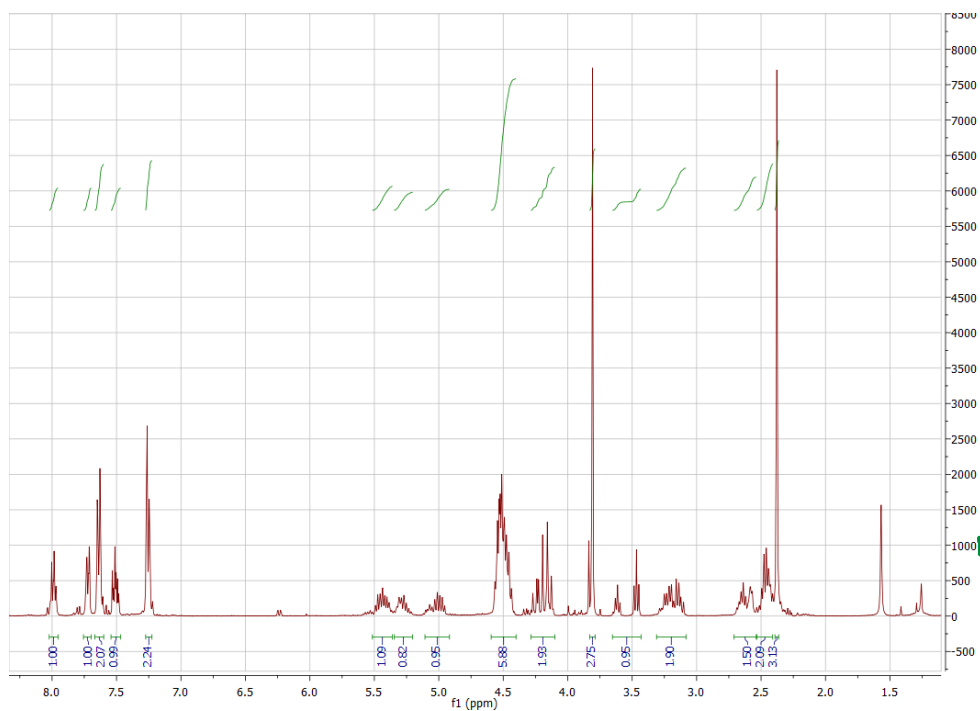
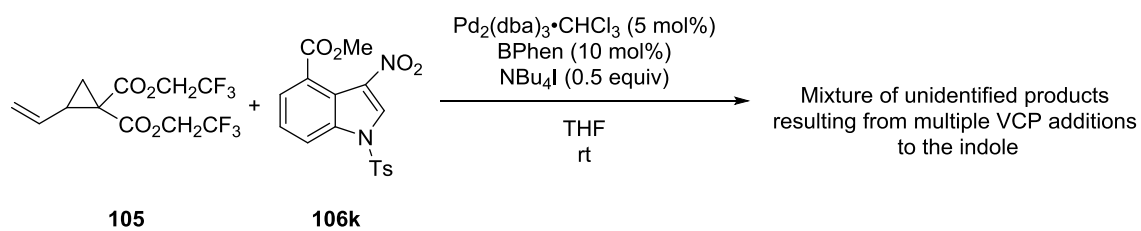
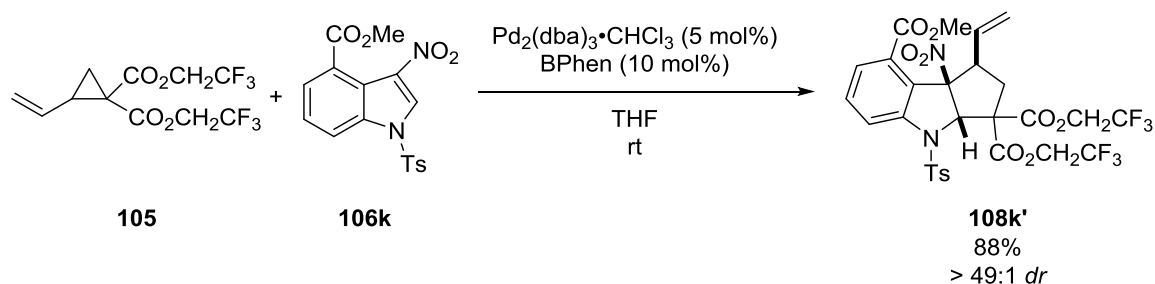


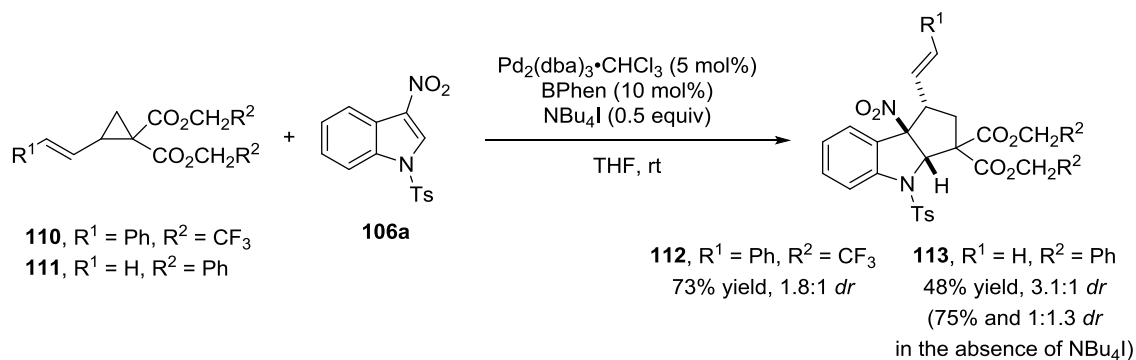
Figure 36: ^1H and ^{13}C NMR spectra of the product derived from the cycloaddition of VCP **105** and 3-nitroindole **106k** with methyl ester at C4.

However, when the NBu₄I additive was absent, the reaction proceeded smoothly but providing the *cis* diastereoisomer **108k'** with almost complete selectivity (Scheme 48). Unlike other substituents at C5, C6 or C7 of indole substrates, the methyl ester substituent at the C4 position of indole is in close proximity to the vinyl group or Pd- π -allyl complex during the reaction, and hence it may create steric hindrance which dictates the *cis* diastereoselectivity of the reaction – this is discussed in more detail below. The relative stereochemistry of product **108k'** was determined by X-ray crystallographic analysis of its ester hydrolysis product **120** (later in Section 4.3.3, Scheme 52b). A similar reversal in diastereoselectivity was observed with the analogous vinylaziridine substrate in another study conducted parallel to this study.⁶¹



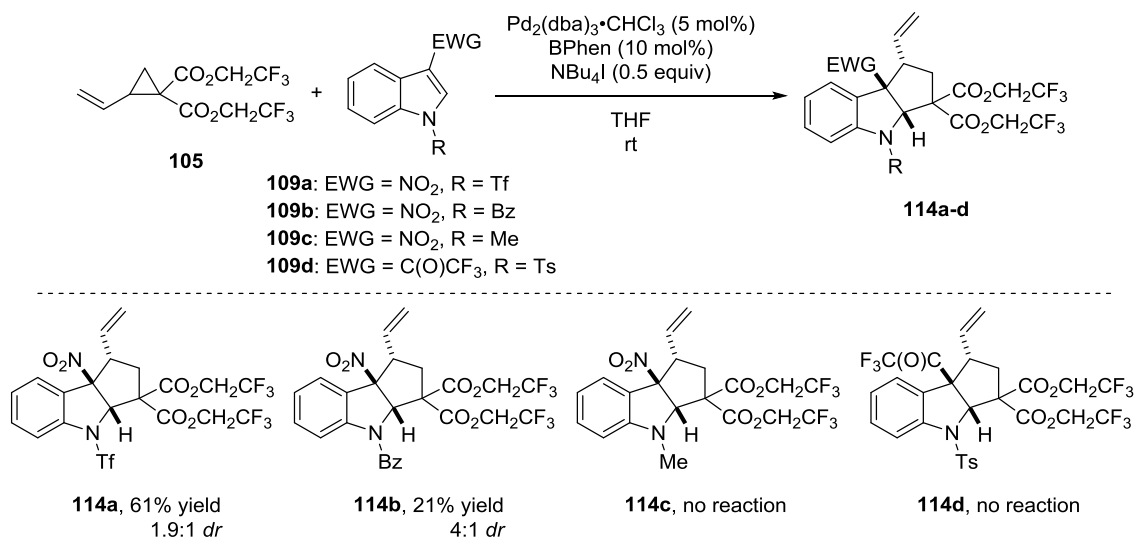
Scheme 48: Absence of NBu₄I additive reversed the diastereoselectivity of the reaction. Diastereoselectivity (*cis:trans*) was determined from the ¹H NMR of the crude reaction mixture.

Variation of the VCP was next investigated and interestingly, when a styryl-cyclopropane **110** was used, product **112** was obtained but a significant decrease in diastereoselectivity was observed (Scheme 49). Use of dibenzyl 2-vinylcyclopropane-1,1-dicarboxylate **111** gave the product **113** with slightly lowered *dr* and as expected, when the NBu₄I additive was absent, the *dr* dropped to 1:1.3 where the *cis* isomer is the major diastereomer. These two experiments provide additional evidence for our theory of reversible Michael attack and a π - σ - π interconversion being important for the selectivity.



Scheme 49: Variation of the vinylcyclopropane. Diastereoselectivity (*trans:cis*) was determined from the ¹H NMR of the crude reaction mixture. All yields are for isolated products after chromatographic purification.

The focus was then switched to the electron-withdrawing groups on the indole substrate, as they are likely crucial to the reactivity of the indole starting material to the dearomatisation process (Scheme 50). The reaction proceeds, but the diastereoselectivity decreases when the indole nitrogen is protected with a trifluoromethanesulfonate group (product **114a**, Scheme 50). Having an *N*-benzoyl-protected indole nitrogen gives similar diastereoselectivity to that of the tosyl counterpart but with a significantly poorer yield (product **114b**, Scheme 50). Furthermore, in the case of the *N*-Bz cycloadduct, the conditions reported here provide an improved diastereoselectivity compared to the reported diastereoselectivity of 1:1 where dppe ligand and acetonitrile were used in the absence of tetrabutylammonium halide.⁶² As a control experiment, no reaction occurred when the indole bears an *N*-methyl group, which increases the electron density of the indole substrate and hence reduces its electrophilicity for the Michael addition of 1,3-dipole (product **114c**, Scheme 50). Lastly, no conversion was observed when the nitro group at C3 was replaced with a trifluoroketone, suggesting that the nitro group at C3 could be essential for reactivity (product **114d**, Scheme 50).



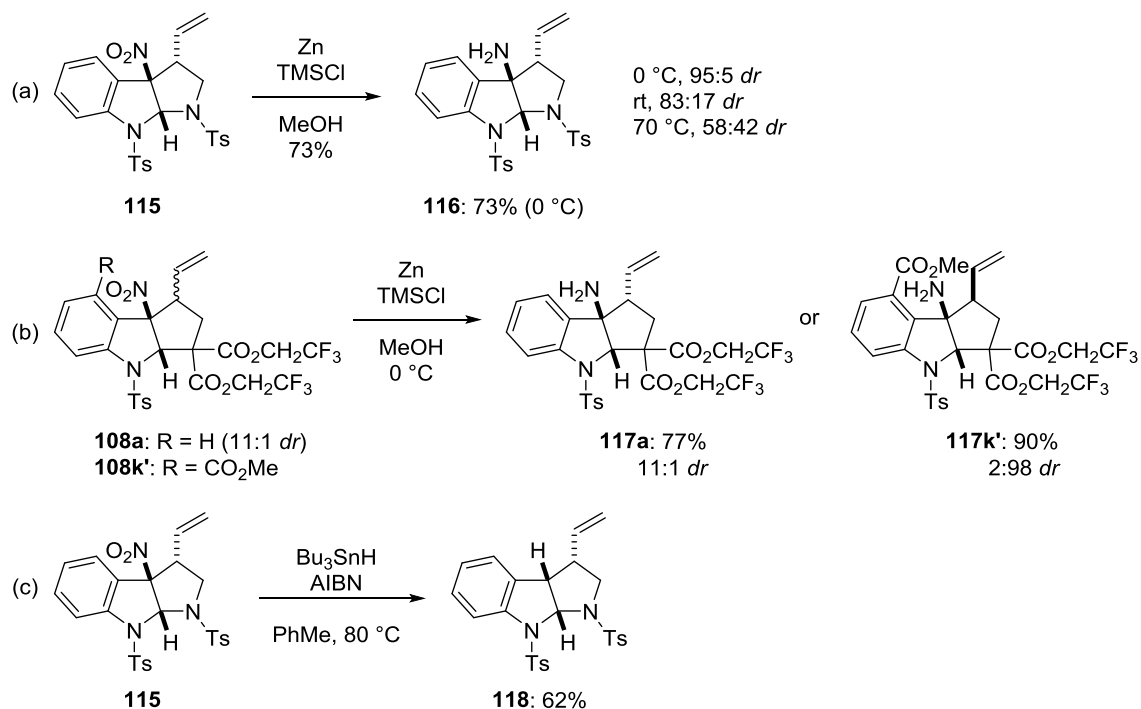
Scheme 50: Variation of the *N*-protecting groups and electron-withdrawing groups at C3 on the indole substrates. Diastereoselectivity (*trans*:*cis*) was determined from the ¹H NMR of the crude reaction mixture. All yields are for isolated products after chromatographic purification.

4.3.3 Chemical transformation of cyclopenta[*b*]indolines and pyrroloindoline

To demonstrate the synthetic utility of the densely cyclopenta[*b*]indolines and pyrroloindoline functionalised cycloadducts, the reduction of nitro group to an amine was first investigated. The reduction of the nitro group is of interest since pyrroloindolines with an amine group at C3a feature in natural bioactive compounds, such as psychotrimine (antibacterial).⁴⁰ Moreover, the installation of an amine group may allow diazotisation, which can allow replacement of the amine group with a halide for later substitution or coupling reactions.⁶⁹ The investigation was initiated using the *trans* diastereomer of pyrroloindoline **115** with a nitro group at C3a, which was obtained from a parallel study in our laboratory (Scheme 51a).⁶¹ Upon treatment of zinc powder under acidic condition, it was discovered that the nitro reduction was required to be performed

at low temperature (0 °C) or epimerisation of amine **116** could occur at room temperature or higher temperature. The degree of epimerisation is proportional to the temperature of the reaction. The zinc-mediated reduction of nitro group under acidic condition proceeds via a radical mechanism, where zinc powder acts as a reducing agent for the nitro group and subsequent intermediates through SET, while TMSCl in MeOH provides the proton source for the reaction intermediates and final product.

The same reduction conditions were then applied to **108a** and **108k'** which provided the corresponding amines **117a** and **117k'** in high yield and with the same *dr* as the starting cyclopent[*b*]indoline (Scheme 51b). In the ¹H NMR spectrum of **117a**, the signals for *HC*-NTs and *CH*-CH=CH₂ shifted up-field compared to the substrate **108a** due to the loss of two electronegative oxygens during reduction of nitro group (*HC*-NTs: shifted from 6.24 to 5.61 ppm; *CH*-CH=CH₂: shifted from 3.30 to 2.85 ppm). Similarly, in the ¹³C NMR spectrum of **117a**, the signal for *C*-NH₂ was detected at 79.7 ppm, which was shifted up-field from 100.8 ppm for *C*-NO₂ in substrate **108a**. Importantly, the presence of the newly formed amine group was indicated in the ¹H NMR (2H broad singlet at 4.08 ppm) and IR (3510 and 3263 cm⁻¹) spectra.

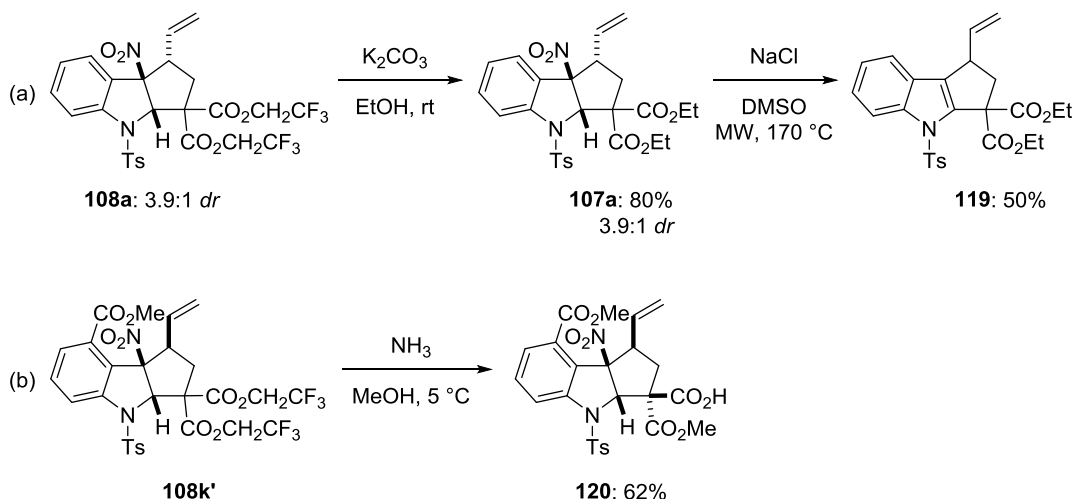


Scheme 51: Chemical transformation of nitro group in pyrroloindoline and cyclopenta[b]indolines: (a) Zinc-mediated reduction of nitro group in pyrroloindoline **115** under acidic condition. (b) Zinc-mediated reduction of nitro group in cyclopenta[b]indolines **108a** and **108k'** under acidic condition. (c) Radical denitration of pyrroloindoline **115**. Diastereoselectivity (*trans*:*cis*) was determined from the ¹H NMR of the crude reaction mixture.

Apart from reducing the nitro group to an amine, the nitro group can also be completely removed through radical denitration. Pyrroloindoline **115** was treated with Bu₃SnH and AIBN to yield the denitrated cycloadduct **118** in a moderate yield of 62% (Scheme 51c). The denitration also proceeds through a radical pathway where the [•]SnBu₃ radical (initiated by AIBN) adds on to one of the oxygen in nitro group, follow by fragmentation to eliminate the nitro-SnBu₃ chain, and eventually a hydrogen abstraction by Bu₃SnH to furnish the product **118**.⁷⁰ The formation of denitrated **118** was evidenced by its ¹H NMR spectrum, where signals for protons in close proximity to the substrate's nitro group were shifted up-field (NTs-CH-NTs: shifted from 7.07 to 6.44 ppm; CH-

CH=CH₂: shifted from 3.62 – 3.56 to 3.07 – 3.00 ppm). Notably, as the nitro group was replaced with a hydrogen sourced from Bu₃SnH, the relevant proton displayed a triplet at 3.68 ppm, which split the NTs-CH-NTs signal into a doublet in the spectrum at 6.44 ppm. Also due to the substitution of nitro group with hydride, the corresponding carbon shifted up-field significantly from 101.6 ppm to 49.7 ppm.

The use of diethyl ester VCP **104** in dearomatisation yielded cycloadducts **107a/107a'** in poor diastereoselectivity (Section 4.3.1). And hence cyclopent[*b*]indoline **108a** was subjected to transesterification in ethanol to access cycloadduct **107a** in diastereo-enriched form, where the *dr* remained the same as the substrate **108a** (Scheme 52a). The obtained cyclopent[*b*]indoline **107a** was then subjected to Krapcho decarboxylation conditions. However instead of undergoing decarboxylation, a rearomative denitration occurred to give rise to cyclopent[*b*]indole **119** (Scheme 52 a). In the ¹H NMR spectrum of **119**, no singlet was observed at 6.30 – 6.40 ppm, suggesting that the proton in Ts-N-CH was absent following rearomatisation. Besides, the proton integration values for OCH₂CH₃ remained the same as the substrate, indicating that decarboxylation did not take place. In the ¹³C NMR spectrum of **119**, a total of six quaternary aromatic carbon signals were detected, while no signal was detected around 100.0 and 73.0 ppm, suggesting that the signals for C-NO₂ and Ts-N-CH shifted down-field to the aromatic region due to rearomative denitration. The proposal of rearomative denitration to yield cyclopent[*b*]indole **119** was also supported by HRMS analysis where the sodiated adduct was detected with good accuracy. This cyclopent[*b*]indole features as the core unit of many alkaloids that display broad spectrum of pharmacological properties, such as paspaline (Maxi-K channel antagonist, potential treatment for Alzheimer's disease)⁷¹ and yuehchukene (antifertility agent)⁷².



Scheme 52: Chemical transformation of densely functionalised cyclopenta[*b*]indolines:

(a) Transesterification of **108a** to yield **107a**, follow by rearomative denitration to form cyclopent[*b*]indole **119**. (b) Face-selective hydrolysis of **108k'** to yield carboxylic acid **120**.

In order to demonstrate the utility of the geminal diesters, cyclopenta[*b*]indoline **108k'** was treated with ammonia in methanol to undergo basic hydrolysis (Scheme 52b). Interestingly, basic hydrolysis selectively occurred at the ester on the convex face (same face as the nitro and vinyl groups), while the ester on the opposite concave face underwent transesterification with the methanol solvent (Figure 37). It was hypothesised that both geminal diesters in the substrate **108k'** underwent transesterification with the methanol solvent in the first place, but subsequently the basic hydrolysis only occurred at the least hindered convex face to yield **120**. This result not only showcased the utility of the geminal diesters, but also the selective facial differentiation of these ester groups. Moreover, the resulting carboxylic acid **120** was also crystalline, which allowed the determination of the *cis*-relationship between the vinyl and nitro groups by X-ray crystallography (Figure 37). This thereby verifies the switch of diastereoselectivity when

indole substrate **106k** underwent dearomative cycloaddition with VCP **105** (Section 4.3.2.2).

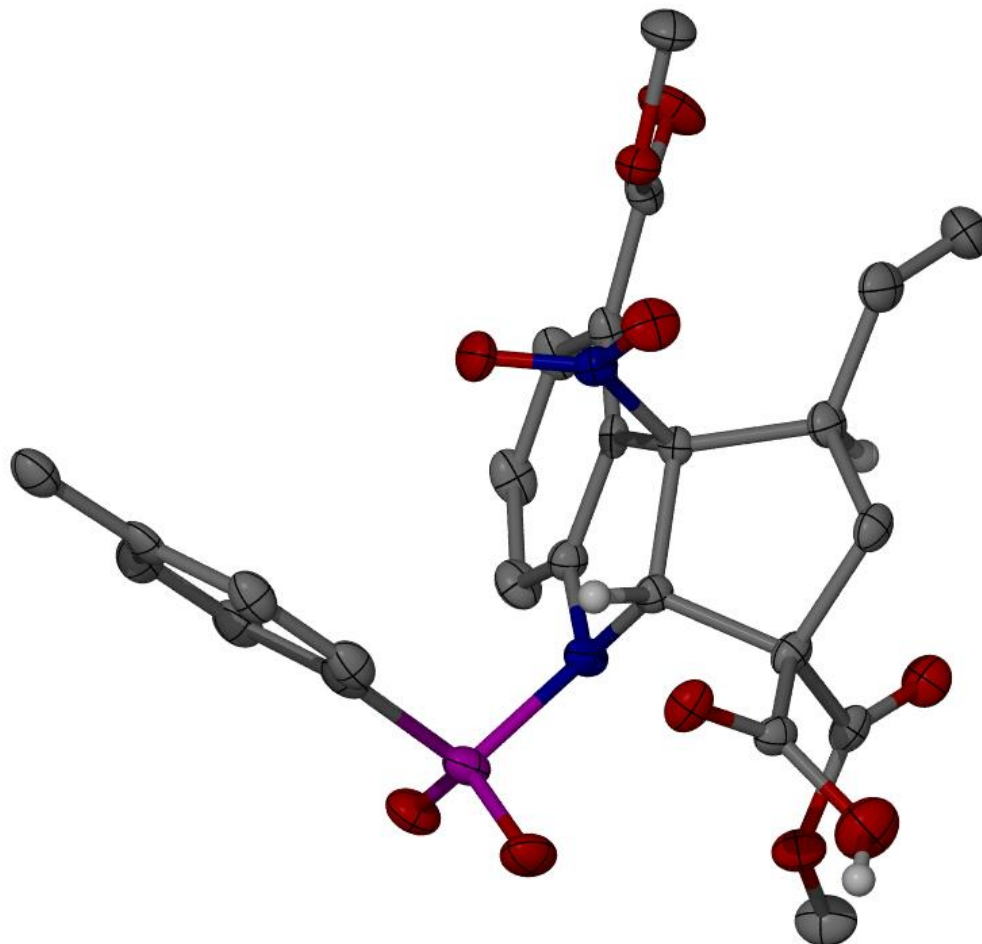


*Figure 37: Crystal structure of **120** obtained from the face-selective hydrolysis of **108k'**. As the nitro and vinyl groups are on the same face in **120**, this supports that **108k'** has *cis* relative stereochemistry.*

4.3.4 Proposed reaction mechanism

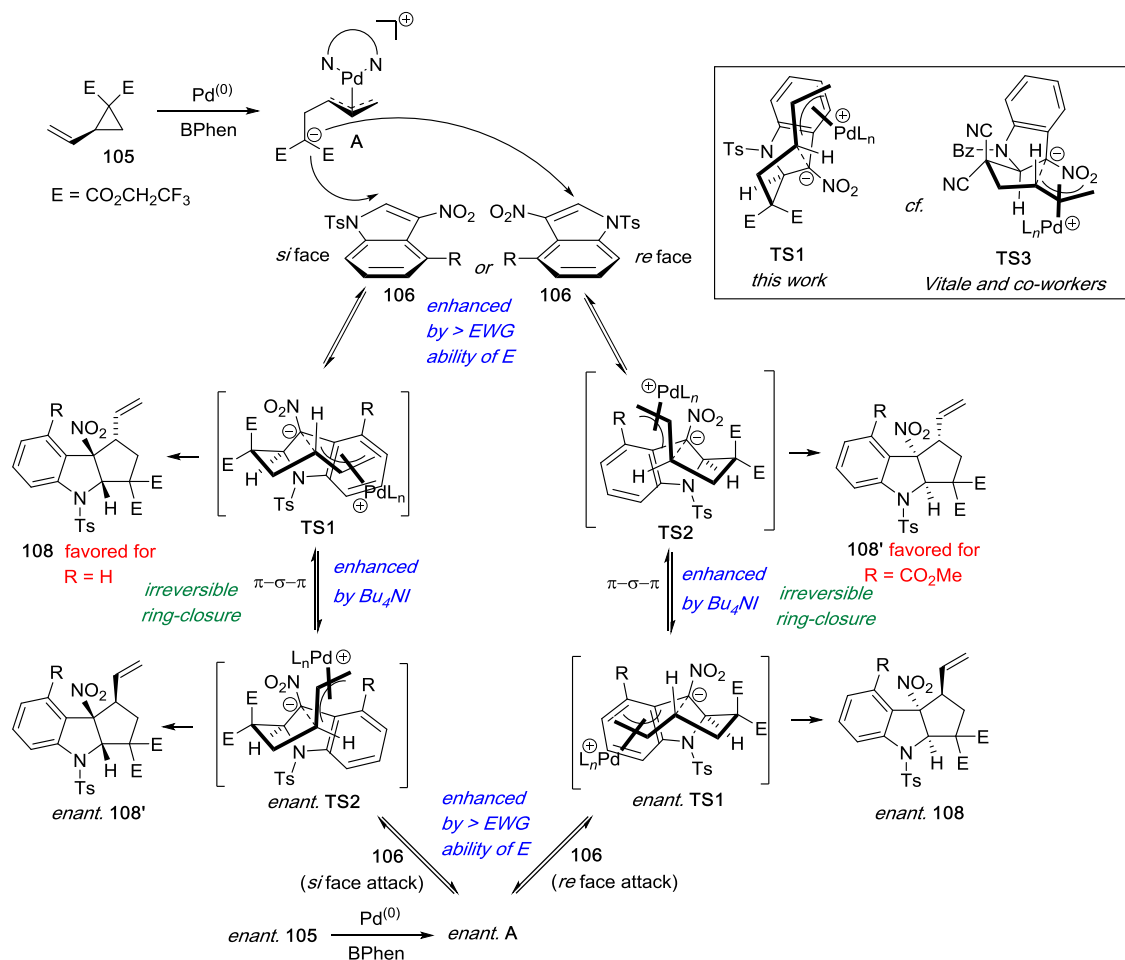
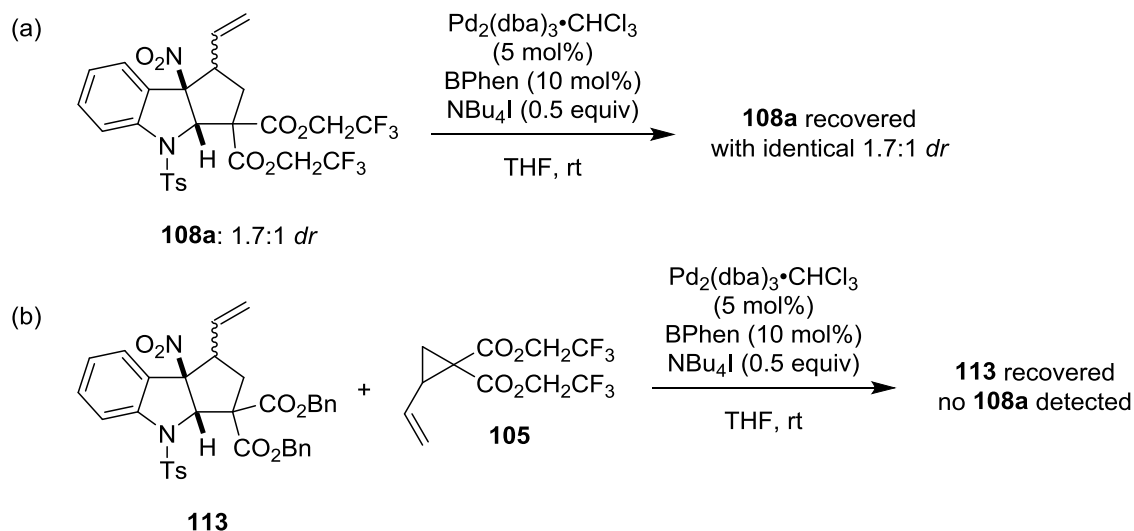


Figure 38: Proposed mechanism.

The reaction is likely initiated by Pd(0)-activation of the VCP by oxidative addition to form 1,3-dipole **A**, followed by a Michael addition with the electron-deficient indole **106** to form intermediates **TS1** or **TS2** (Figure 38). Subsequently, an irreversible ring-closure of **TS1** or **TS2** furnishes the cyclopenta[*b*]indoline products **108/108'**. The final ring-closure step was revealed as irreversible based on the observation of control experiments. The diastereomeric ratio remained the same after a mixture of **108a/108a'** (1.7:1 *dr*) was subjected to standard dearomatization conditions (Scheme 53a). Meanwhile, after subjecting **113** and **105** into standard dearomatization conditions, **113** was fully

recovered with no sign of **108a** detected (Scheme 53b), indicating that no incorporation of **105** and hence verifying that the ring-closure step is irreversible.



Scheme 53: Control experiments demonstrating irreversibility of the final ring-closure step.

The stereochemical outcome in this study attracts scope for discussion, especially as it is opposite to the concurrent report from Vitale and co-workers,⁶² where the *cis* diastereomer was the major product. Due to planar chirality, the Pd-stabilised zwitterionic 1,3-dipole **A** can either attack the *si* or *re* face of indole substrate **106**, therefore forming intermediates **TS1** or **TS2**. After Michael addition and prior to ring-closure, these intermediates can undergo π - σ - π facial interconversion. Although the current process provides a racemic mixture of products, both enantiomers of the dipole (**A** and *enant.* **A**) and their resultant Michael adducts, need to be acknowledged as they allow products of the same absolute configuration to emerge from opposite enantiomers of the dipole. Besides, an equilibrium between **A** and *enant.* **A** is also likely to be present due to π - σ - π interconversion. These factors are also crucial for the development of the future enantioselective variant of this study.

The *trans* diastereomer **108** is the major product for almost all cases in this study, suggesting that the irreversible ring-closure via **TS1** and *enant.* **TS1** is the favourable pathway, which is tentatively attributed to the stabilisation of **TS1** by a cation- π -interaction between the electron-rich indole backbone and the cationic π -allyl Pd complex.⁷³ Based on the results obtained during reaction optimisation, the *trans* diastereoselectivity is also attributed to the reversibility of the Michael addition (control via stabilisation of 1,3-dipole) and the facile π - σ - π interconversion between **TS1** and **TS2** with their enantiomers (mediated using NBu₄I additive). For instance, the formation of **113** is *trans* diastereoselective in the presence of halide additive but reverts back to a poorly diastereoselective reaction when the additive is absent. As proposed by Trost,⁶⁶ the halide additive results in a Curtin–Hammett scenario, where swift interconversion of the intermediate Pd-allyl complexes occurs, and hence funnelling the reaction to proceed via **TS1** selectively, which should be lower in energy than **TS2**.

Comparing the use of VCPs **104** and **105** in the absence of halide additives (entries 1 and 2, Table 4), a switch of diastereoselectivity is observed. This indicates that increasing stability of the malonyl-anion **A** (derived from **105**) allows for some interconversion between **TS1** and **TS2** outside of the π - σ - π pathway through reversible addition of the dipole.

For indole substrate **106k** where a methyl ester substituent is present at C4, the diastereoselectivity completely switches to the *cis* cycloadduct. This complete switch of diastereoselectivity is likely caused by a disfavoured steric interaction between the C4 ester and the Pd-allyl unit in **TS1** over-riding the π -stacking interaction, thereby promoting the reaction to proceed via **TS2** instead.

Vitale and co-workers postulated **TS3** (Figure 38, box) during the cycloaddition of dicyano VCP to 3-nitroindole in order to place the Pd-allyl moiety in a pseudo-equatorial position, therefore minimising diaxial interaction.⁶² However, this proposed transition state is probably unfavourable in our study due to steric reasons. One of the cyano group in **TS3** is in pseudo-axial position adjacent to the indole backbone, which is an unfavourable arrangement for the larger ester groups of the 1,1-diesters-derived VCPs.

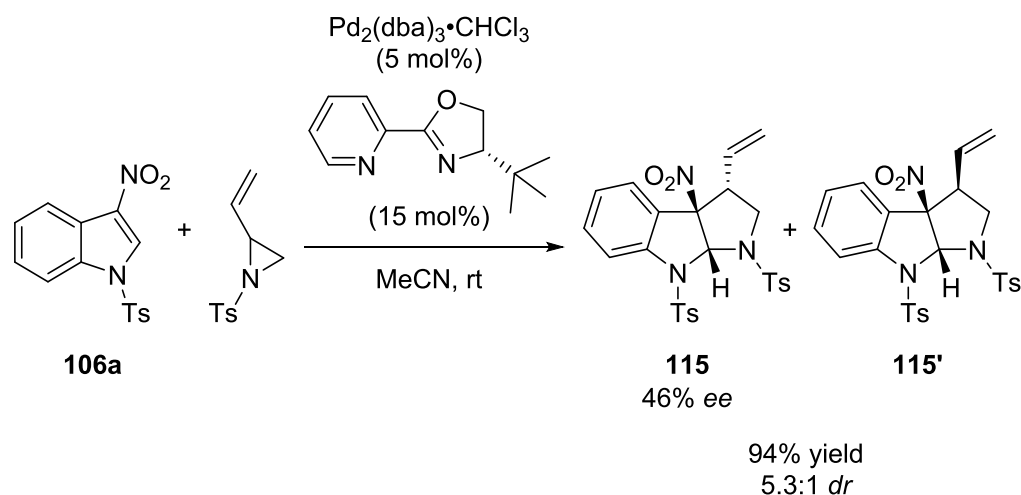
4.4 Conclusion and future work

In summary, the Pd-catalysed dearomative [3 + 2] cycloaddition of 3-nitroindoles with 2-vinylcyclopropane-1,1-dicarboxylates was achieved in high yields and moderate-good diastereoselectivity (up to 88% yield and 4.3:1 *dr*). Critically, this diastereoselectivity was complementary to the concurrent report on vinylcyclopropane addition to electron-deficient indoles, which is proposed to be due to the presence of a halide additive allowing for Curtin–Hammett control of the reaction. Furthermore, the densely functionalised cyclopenta[*b*]indoline products demonstrate potential to undergo further chemical transformation and provide access to other core structures. Of particular note is the facial differentiation of the geminal diester group, highlighting the versatility of 1,1-diesters-derived vinylcyclopropanes, which can also be prepared in a single step from commercial materials and are easily handled and stored.

In a related study in our research group, pyrroloindolines were constructed from the dearomative cycloaddition of vinylaziridine and 3-nitroindole in excellent *dr* (up to 98:2 for *trans* diastereomer), under similar reaction conditions to this study without the halide additive.⁶¹ In this study, even with the addition of halide additive, the magnitude of diastereoselectivity was lower than the parallel study. And hence computational studies can be conducted to understand the *dr* discrepancies in the use of vinylaziridine and VCP

as 1,3-dipole sources, in particular the free energy of each transition state between Michael addition and ring-closure. Moreover, computational studies can also provide insight into the contribution of nitro group in the reaction. It was hypothesised that the nitro group reverses the polarity of the indole core and tunes it into an electrophile. Due to the proximity between the nitro group and the Pd- π -allyl complex, it is possible that the nitro group can also have influence to the stereochemistry, either by steric or electronic effect. Thus the interaction between the nitro group and Pd- π -allyl complex should be modelled computationally to provide clearer insight to the reaction.

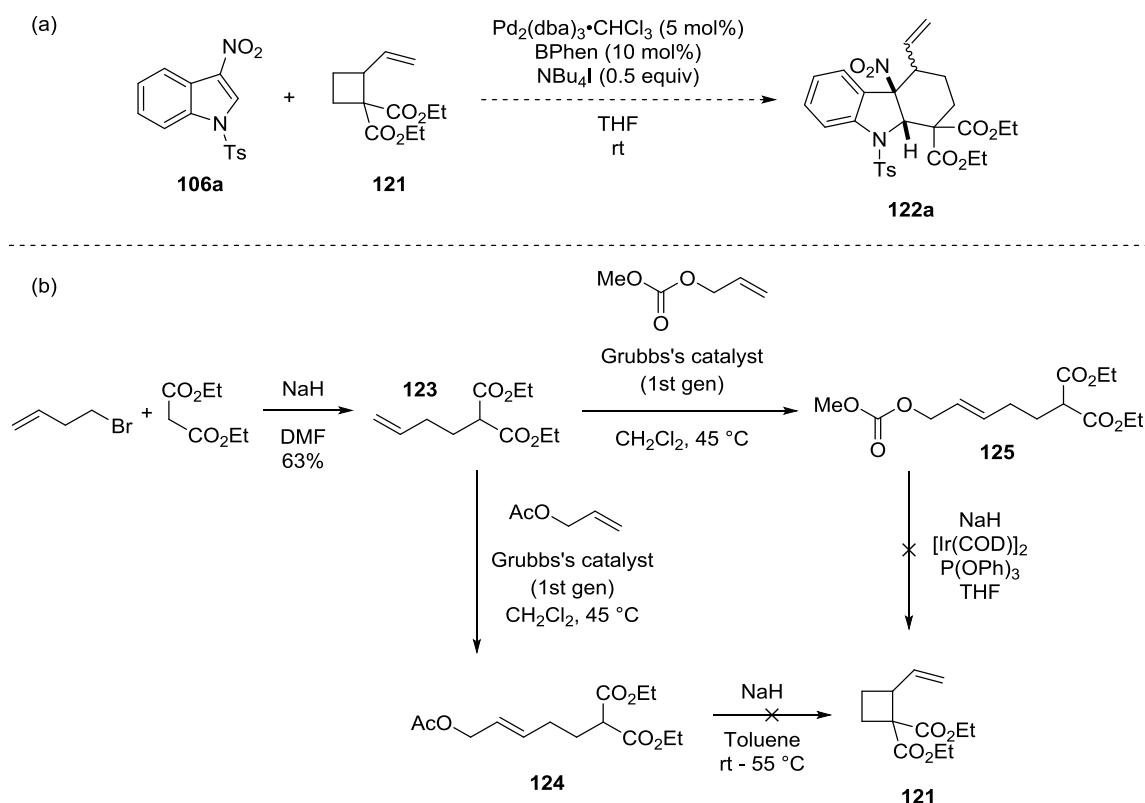
Furthermore, developing enantioselective variants of the reaction is also an important next phase of the study. Despite the poor diastereoselectivity obtained in the preliminary optimisation using chiral phosphorus ligand and Trost ligands (entries 18, 24 – 27, Table 6), there is still scope for other chiral ligands to develop an enantioselective and diastereoselective method for the preparation of cyclopenta[*b*]indolines. In a preliminary study from our group, instead of using BPhen as the ligand, diamine chiral ligand (*S*)-*t*-BuPyOx⁷⁴ was used in the synthesis of pyrroloindolines from vinylaziridines and 3-nitroindoles under Pd-catalysed dearomative cycloaddition (Scheme 54).⁷⁵ The bulky *t*-butyl group on the chiral carbon was hypothesised to provide facial selectivity in the transition state therefore establishing the enantioselectivity of the reaction. Although slight erosion was observed in diastereoselectivity compared to the BPhen counterpart, a promising initial *ee* of 46% was observed in the preliminary screening. This result is encouraging and the chiral ligand should be applied to the reaction described in this chapter. Since enantioselectivity is attributed to the bulky *t*-butyl group, other bulky group such as aryl group can be attempted in the condition screening.



Scheme 54: Enantioselective preparation of pyrroloindoline through Pd-catalysed cycloaddition of 3-nitroindoles with vinylaziridines using diamine chiral ligand (*S*)-*t*-BuPyOx.

The ring-strain present in three-membered rings granted these scaffolds the reactivity to participate in various reactions, especially in cycloaddition with dipolarophiles. While cyclobutane has a strain energy value of 26.7 kcal/mol, interestingly this value is fairly close to that of cyclopropane, which has a strain energy value of 27.5 kcal/mol.⁷⁶ Although the cycloaddition reactions of donor-acceptor cyclobutanes is less explored compared to the three-membered counterparts, existing literature mostly focusses on the use of Lewis acid catalysis to activate this four-membered ring.⁷⁷⁻⁸² To the best of our knowledge, Pd-catalysed cycloaddition of vinylcyclobutane with dipolarophiles has not been reported, therefore we were intrigued to investigate if vinylcyclobutane dicarboxylate **121** can be synthesised and subjected to the cycloaddition with 3-nitroindole **106a** to yield cycloadduct **122a** (Scheme 55a). Hexahydrocarbazole **122a** is featured in many bioactive alkaloids,⁸³ for instances strychnine⁸⁴ (toxin) and vindoline⁸⁵ (precursors for oncolytic agent vinblastine).

The preparation of vinylcyclobutane **121** was found to be challenging during a preliminary study conducted as part this investigation (Scheme 55b). Firstly, substrate dimerisation occurred during the olefin metathesis of **123** with allyl acetate or allyl methyl carbonate, and the undesired dimers were inseparable from their respective products **124** or **125**. Furthermore, conversion was not observed during the cyclisation step for both precursors **124** and **125**. In the future, optimisation of olefin metathesis should be carried out to minimise dimerisation and hence pure cyclisation precursors can be obtained. Besides, screening of alternative cyclisation method is also required to access vinylcyclobutane **121**. Due to time constraint, no further investigation was carried out to optimise these reaction conditions.



Scheme 55: (a) Proposed [4 + 2] cycloaddition of vinylcyclobutane dicarboxylate **121** with 3-nitroindole **106a**. (b) Attempted preparation of vinylcyclobutane dicarboxylate **121**.

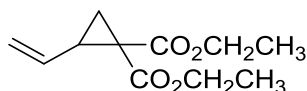
4.5 Experimental

Majority of the organic syntheses and molecule characterisation were performed by Y. S. Gee, with the exception of a few substrates which are stated as follow. Preliminary optimisation of reaction condition (entries 1 – 3, Table 4) was conducted by Dr S. Wales (University of Wollongong). VCP **104**, several indole substrates (**106b-k**, **109b-c**) and cycloadduct **107a/107a'** were provided by D. J. Rivinoja (University of Wollongong) in a collaborative project which was conducted concurrently with this study. X-ray crystallography was performed by Dr M. Gardiner (University of Tasmania).

General experimental details for organic syntheses and molecule characterisation are stated in Chapter 2 Section 2.5.1.

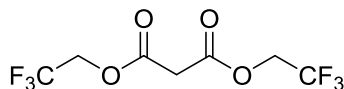
4.5.1 Preparation of 2-vinylcyclopropane-1,1-dicarboxylates

Diethyl 2-vinylcyclopropane-1,1-dicarboxylate (104)



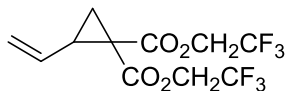
The title compound was prepared from reported method⁸⁶ as a colourless oil (1.71 g, 8.07 mmol) in 82% yield. **¹H NMR** (500 MHz, CDCl₃): δ 5.48 – 5.40 (m, 1H, CH=CH₂), 5.30 (d, *J* = 15.0 Hz, 1H, CH=CH₂), 5.13 (d, *J* = 10.0 Hz, 1H, CH=CH₂), 4.27 – 4.13 (m, 4H), 2.57 (q, *J* = 10.0 Hz, 1H), 1.69 (dd, *J* = 7.5, 5.0 Hz, 1H, CH₂), 1.55 (dd, *J* = 5.0, 4.0 Hz, 1H, CH₂), 1.28 – 1.25 (m, 6H, CH₃) ppm. NMR data consistent with literature.⁶³

Bis(2,2,2-trifluoroethyl) malonate



A suspension of malonic acid (2.00 g, 19.3 mmol, 1 equiv), magnesium sulfate (2.06 g, 17.1 mmol, 0.9 equiv), 2,2,2-trifluoroethanol (8.00 mL, 0.110 mol, 5.7 equiv) and sulfuric acid (0.450 mL) in benzene (10 mL) were heated to reflux for 48 h. The reaction suspension was cooled to room temperature and filtered, then the filtrate was diluted with benzene (20 mL) and washed with 10% sodium carbonate solution (3 × 20 mL), water (20 mL) and brine (20 mL). The solution was dried over sodium sulfate and concentrated under reduced pressure to yield the title product as a colourless oil (3.17 g, 11.8 mmol) in 61% yield. ¹H NMR (500 MHz, CDCl₃): δ 4.55 (q, *J* = 16.5 Hz, 4H, OCH₂), 3.61 (s, 2H, O=C-CH₂-C=O) ppm. ¹³C NMR (125 MHz, CDCl₃): δ 164.0 (C=O), 122.5 (q, *J* = 276.2 Hz, CF₃), 61.2 (q, *J* = 36.3 Hz, OCH₂), 40.2 (O=C-CH₂-C=O) ppm. NMR data consistent with literature.⁸⁷

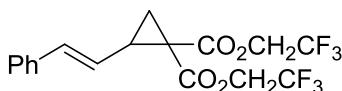
Bis(2,2,2-trifluoroethyl) 2-vinylcyclopropane-1,1-dicarboxylate (105)



A suspension of bis(2,2,2-trifluoroethyl) malonate (503 mg, 1.87 mmol, 1 equiv), *trans*-1,4-dibromo-2-butene (407 mg, 1.90 mmol, 1 equiv) and caesium carbonate (1.52 g, 4.66 mmol) in THF (38 mL) was heated at 60 °C for 24 h. The reaction suspension was cooled to room temperature and filtered, then the filtrate was diluted with ether (80 mL) and washed with saturated sodium bicarbonate solution (30 mL), water (30 mL) and brine (30

mL). After the solution was dried over sodium sulfate and concentrated under reduced pressure, column chromatography (50% dichloromethane in hexane) was performed to yield the title compound as a colourless oil (353 mg, 1.10 mmol) in 59% yield. **¹H NMR** (500 MHz, CDCl₃): δ 5.50 – 5.43 (m, 1H, CH=CH₂), 5.35 (d, *J* = 17 Hz, 1H, CH=CH₂), 5.23 (d, *J* = 10.5 Hz, 1H, CH=CH₂), 4.61 – 4.45 (m, 4H, CH₂CF₃), 2.74 (q, *J* = 8.5 Hz, 1H, CH-CH=CH₂), 1.90 (dd, *J* = 7.5, 5.5 Hz, 1H, CH₂-CH-CH=CH₂), 1.74 (dd, *J* = 9.0, 5.5 Hz, 1H, CH₂-CH-CH=CH₂) ppm. **¹³C NMR** (125 MHz, CDCl₃): δ 167.5 (C=O), 165.2 (C=O), 131.3 (CH=CH₂), 122.6 (q, *J* = 275 Hz, CF₃), 120.3 (CH=CH₂), 61.3 (q, *J* = 37.5 Hz, OCH₂), 61.2 (q, *J* = 37.5 Hz, OCH₂), 35.0 (C-(COOCF₃)₂), 32.9 (CH-CH=CH₂), 21.5 (CH₂-CH-CH=CH₂) ppm. NMR data consistent with literature.³²

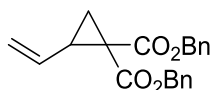
Bis(2,2,2-trifluoroethyl) (E)-2-styrylcyclopropane-1,1-dicarboxylate (110)



A solution of **105** (158 mg, 0.495 mmol, 1 equiv), Grubbs Catalyst 2nd Generation (10.2 mg, 12.0 μmol, 2.4 mol%) and styrene (1.10 mL, 997 mg, 9.57 mmol, 19.3 equiv) in dichloromethane (4 mL) was heated at 40 °C for 1 h then concentrated under reduced pressure. After column chromatography (5 – 20% ethyl acetate in hexane), the title compound was obtained as a colourless oil (155 mg, 0.392 mmol) in 79% yield. **¹H NMR** (500 MHz, CDCl₃): δ 7.30 (d, *J* = 4.5 Hz, 4H, CH_{Ar}), 7.26 – 7.23 (m, 1H, CH_{Ar}), 6.69 (d, *J* = 15.5 Hz, 1H, Ph-CH=CH), 5.83 (dd, *J* = 16.0, 8.5 Hz, 1H, Ph-CH=CH), 4.63 – 4.44 (m, 4H, OCH₂), 2.91 (q, *J* = 8.5 Hz, 1H, Ph-CH=CH-CH), 2.05 – 2.02 (m, 1H, CH₂-C(CO₂CH₂CF₃)₂), 1.85 (dd, *J* = 9.0, 5.0 Hz, 1H, CH₂-C(CO₂CH₂CF₃)₂) ppm. **¹³C NMR** (125 MHz, CDCl₃): δ 167.4 (C=O), 165.4 (C=O), 136.1 (C_{Ar}), 135.4 (Ph-CH=CH), 128.6

(CH_{Ar}), 128.0 (CH_{Ar}), 126.2 (CH_{Ar}), 122.4 (Ph-CH=CH), 61.3 (q, $J = 37.5$ Hz, OCH₂), 61.2 (q, $J = 36.3$ Hz, OCH₂), 35.3 (C(CO₂CH₂CF₃)₂), 33.4 (Ph-CH=CH-CH), 22.3 (CH₂-C(CO₂CH₂CF₃)₂) ppm. **IR** (Neat): 3033, 1743, 1412, 1273, 1159, 1113 cm⁻¹. **HRMS** (ESI) m/z: [M + Na]⁺ Calcd for C₁₇H₁₄F₆O₄Na 419.0694; Found 419.0686.

Dibenzyl 2-vinylcyclopropane-1,1-dicarboxylate (III)



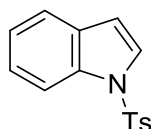
A suspension of dibenzyl malonate (0.440 mL, 0.500 g, 1.76 mmol, 1 equiv), *trans*-1,4-dibromo-2-butene (373 mg, 1.74 mmol, 1 equiv) and caesium carbonate (1.44 g, 4.42 mmol, 2.5 equiv) in THF (35 mL) was heated at 60 °C for 24 h. The suspension was cooled to room temperature and filtered. The filtrate was diluted with diethyl ether (70 mL) and washed with saturated sodium bicarbonate solution (50 mL), water (50 mL) then brine (50 mL). After the solution was dried over sodium sulfate and concentrated under reduced pressure, column chromatography (50% dichloromethane in hexane) was performed to yield the title compound as a colourless oil (495 mg, 1.47 mmol) in 84% yield. **¹H NMR** (500 MHz, CDCl₃): δ 7.32 – 7.26 (m, 10H, CH_{Ar}), 5.44 – 5.37 (m, 1H, CH=CH₂), 5.28 (d, $J = 17.0$ Hz, 1H, CH=CH₂), 5.08-5.20 (m, 5H, CH=CH₂ and 2 × OCH₂), 2.63 (q, $J = 8.5$ Hz, 1H, CH-CH=CH₂), 1.76 (dd, $J = 7.5, 5.0$ Hz, 1H, CH₂-C(CO₂Bn)₂), 1.60 (dd, $J = 9.0, 4.5$ Hz, 1H, CH₂-C(CO₂Bn)₂) ppm. **¹³C NMR** (100 MHz, CDCl₃): δ 169.4 (C=O), 167.2 (C=O), 135.5 (C_{Ar}), 135.4 (C_{Ar}), 132.8 (CH=CH₂), 128.5 (CH_{Ar}), 128.4 (CH_{Ar}), 128.3 (CH_{Ar}), 128.23 (CH_{Ar}), 128.21 (CH_{Ar}), 128.0 (CH_{Ar}), 118.8 (CH=CH₂), 67.4 (OCH₂), 67.3 (OCH₂), 35.9 (C-(CO₂Bn)₂), 31.7 (CH-CH=CH₂), 20.8 (CH₂-C-(CO₂Bn)₂) ppm. **IR** (Neat): 3034, 1722, 1498, 1455, 1379, 1317, 1266, 1189,

1123 cm^{-1} . **HRMS** (ESI) m/z : $[\text{M} + \text{Na}]^+$ Calcd for $\text{C}_{21}\text{H}_{20}\text{O}_4\text{Na}$ 359.1259; Found 359.1273.

4.5.2 Preparation of indole substrates

Indole derivatives **106b-k** and **109c** were prepared based on reported method.⁶¹

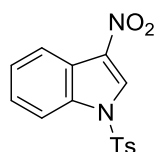
1-Tosyl-1H-indole



Ground sodium hydroxide pearls (1.56 g, 39.0 mmol, 4.6 equiv) was added to a solution of indole (996 mg, 8.50 mmol, 1 equiv) and tetrabutylammonium bisulfate (293 mg, 0.862 mmol, 0.1 equiv) in dichloromethane (85 mL). The solution was stirred for 10 mins before the addition of tosyl chloride (2.43 g, 12.8 mmol, 1.5 equiv). The reaction was left stirring for overnight before the addition of saturated ammonium chloride solution (50 mL). After stirring the mixture for 30 mins, the organic fraction was isolated while the aqueous fraction was extracted with dichloromethane (2×30 mL). The combined organic fractions were dried over magnesium sulfate and concentrated under reduced pressure. The title compound was collected as an off white solid (2.03 g, 7.49 mmol) in 88% yield after column chromatography (20% ethyl acetate in hexane). **^1H NMR** (500 MHz, CDCl_3): δ 7.99 (d, $J = 8.5$ Hz, 1H, CH_{Ar}), 7.75 (d, $J = 8$ Hz, 2H, CH_{Ar} Tosyl), 7.55 (d, $J = 3.5$ Hz, 1H, TsN-CH=CH), 7.51 (d, $J = 8$ Hz, 1H, CH_{Ar}), 7.30 (t, $J = 8$ Hz, 1H, CH_{Ar}), 7.22 – 7.18 (m, 3H, CH_{Ar} and $2 \times \text{CH}_{\text{Ar}}$ Tosyl), 6.64 (d, $J = 3.5$ Hz, 1H, TsN-CH=CH), 2.31 (s, 3H, CH_3) ppm. **^{13}C NMR** (125 MHz, CDCl_3): δ 144.9 (C_{Ar}), 135.4 (C_{Ar}), 134.9 (C_{Ar}),

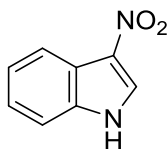
130.8 (C_{Ar}), 129.8 (CH_{Ar} Tosyl), 126.8 (CH_{Ar} Tosyl), 126.3 (TsN-CH=CH), 124.5 (CH_{Ar}), 123.2 (CH_{Ar}), 121.3 (CH_{Ar}), 113.5 (CH_{Ar}), 109.0 (TsN-CH=CH), 21.5 (CH₃) ppm. NMR data consistent with literature.^{88,89}

3-Nitro-1-tosyl-1H-indole (106a)



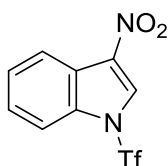
After the slow addition of acetic anhydride (1.00 mL, 1.08 g, 10.6 mmol) to 70% nitric acid (0.200 mL, 211 mg, 3.36 mmol, 3 equiv) at 0 °C, the solution was stirred at room temperature for 20 mins and then added to a solution of 1-tosyl-1H-indole (304 mg, 1.12 mmol, 1 equiv) in acetic anhydride (2 mL) at -78 °C for 2 h. The reaction was quenched with ice cold water (20 mL) at -78 °C, slowly warmed to rt and then extracted with ethyl acetate (3 × 20 mL). The organic extractions were concentrated under reduced pressure and the residue was dissolved in ethyl acetate (30 mL), washed with saturated sodium bicarbonate solution (5 × 20 mL) and dried over magnesium sulfate. After removal of solvent under reduced pressure, the crude solid was recrystallised in methanol to give the title compound as a beige solid (242 mg, 0.764 mmol) in 68% yield. ¹H NMR (500 MHz, CDCl₃): δ 8.57 (s, 1H, CH=C-NO₂), 8.24 (d, *J* = 7.5 Hz, 1H, CH_{Ar}), 8.00 (d, *J* = 7 Hz, 1H, CH_{Ar}), 7.88 (d, *J* = 7.5 Hz, 2H, CH_{Ar} Tosyl), 7.47 – 7.45 (m, 2H, CH_{Ar}), 7.33 (d, *J* = 8 Hz, 2H, CH_{Ar} Tosyl), 2.40 (s, 3H, CH₃) ppm. ¹³C NMR (125 MHz, CDCl₃): δ 146.8 (C_{Ar}), 133.9 (C_{Ar}), 133.6 (C_{Ar}), 133.2 (C-NO₂), 130.5 (CH_{Ar} Tosyl), 127.8 (HC=CNO₂), 127.5 (CH_{Ar} Tosyl), 126.8 (CH_{Ar}), 125.9 (CH_{Ar}), 121.8 (C_{Ar}), 121.2 (CH_{Ar}), 113.6 (CH_{Ar}), 21.7 (CH₃) ppm. NMR data consistent with literature.⁶⁵

3-Nitro-1H-indole



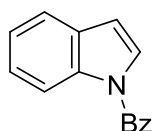
A solution of *N*-bromosuccinimide (1.60 g, 8.97 mmol, 1.05 equiv) in acetonitrile was heated at 82 °C for 10 mins prior to the addition of silver(I) nitrate (1.53 g, 8.99 mmol, 1.05 equiv) and indole (1.00 g, 8.54 mmol, 1 equiv). The reaction was heated to 102 °C for 2 h then filtered to remove silver bromide. The filtrate was concentrated under reduced pressure then dissolved in dichloromethane (90 mL) and washed with 4% sodium bicarbonate solution (2 × 45 mL). Insolubles were filtered, organic fraction was isolated and dried over magnesium sulfate. After column chromatography (40% ethyl acetate in hexane), the title compound was collected as a yellow solid (0.220 g, 1.35 mmol) in 16% yield. ¹H NMR (400 MHz, DMSO): δ 12.65 (bs, 1H, NH), 8.65 (d, *J* = 3.2 Hz, 1H, CH=C-NO₂), 8.11 – 8.07 (m, 1H, CH_{Ar}), 7.59 – 7.55 (m, 1H, CH_{Ar}), 7.39 – 7.32 (m, 2H, CH_{Ar}) ppm. ¹³C NMR (100 MHz, DMSO): δ 135.5 (C_{Ar}), 131.0 (CH=C-NO₂), 128.9 (C_{Ar}), 124.6 (CH_{Ar}), 124.2 (CH_{Ar}), 120.3 (C_{Ar}), 119.9 (CH_{Ar}), 113.8 (CH_{Ar}) ppm. NMR data consistent with literature.⁹⁰

3-Nitro-1-((trifluoromethyl)sulfonyl)-1H-indole (109a)



A solution of 3-nitro-1*H*-indole (101 mg, 0.622 mmol, 1 equiv), DMAP (81.9 mg, 0.670 mmol, 1.1 equiv) and triethylamine (0.350 mL, 254 mg, 2.51 mmol, 4 equiv) in dichloromethane (6 mL) was cooled to 0 °C prior to the addition of trifluoromethanesulfonic anhydride (0.350 mL, 587 mg, 2.08 mmol, 3.3 equiv). After the addition, the solution was allowed to warm to room temperature and stirred overnight. Reaction was quenched with ice-cold water (5 mL). Organic layer was isolated and the aqueous layer was extracted with ethyl acetate (3 × 20 mL). After the combined organic extracts were dried over sodium sulfate and concentrated under reduced pressure, column chromatography (20 – 40% ethyl acetate in hexane) was performed to yield the title compound as a yellow solid (118 mg, 0.401 mmol) in 65% yield. **¹H NMR** (500 MHz, CDCl₃): δ 8.37 – 8.34 (m, 2H, CH_{Ar} and HC=C-NO₂), 7.96 (d, *J* = 6.8 Hz, 1H, CH_{Ar}), 7.62 – 7.58 (m, 2H, CH_{Ar}) ppm. **¹³C NMR** (100 MHz, CDCl₃): δ 135.8 (C_{Ar}), 134.7 (C_{Ar}), 128.2 (CH_{Ar}), 127.7 (HC=C-NO₂), 127.3 (CH_{Ar}), 121.81 (C_{Ar}), 121.77 (CH_{Ar}), 119.3 (q, *J* = 320 Hz, CF₃), 113.9 (CH_{Ar}) ppm. **¹⁹F NMR** (470 Hz, CDCl₃): δ -74.64 (s, CF₃) ppm. **IR** (Neat): 3170, 1591, 1560, 1513, 1478, 1443, 1416, 1355, 1316, 1267, 1215, 1142, 1124, 1101, 1067 cm⁻¹. **HRMS** (ESI) *m/z*: [M + Na]⁺ Calcd for C₉H₅F₃N₂O₄SNa 316.9820; Found 316.9815. **Melting point**: 89.1 – 92.9 °C.

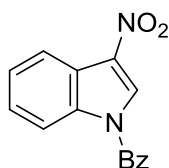
(1H-Indol-1-yl)(phenyl)methanone



The title compound was prepared from reported method⁶¹ as a colourless oil (141 mg, 0.636 mmol) in 33% yield. **¹H NMR** (500 MHz, CDCl₃): δ 8.40 (d, *J* = 8.3 Hz, 1H, CH_{Ar}),

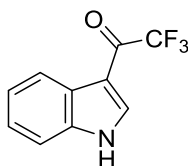
7.73 - 7.71 (m, 2H, CH_{Ar}), 7.59 (t, *J* = 7.3 Hz, 2H, CH_{Ar}), 7.51 (t, *J* = 7.5 Hz, 2H, CH_{Ar}), 7.39 - 7.36 (m, 1H, CH_{Ar}), 7.32 - 7.28 (m, 2H, overlapping CH_{Ar} & CH=CH-N), 6.60 (d, *J* = 3.7 Hz, 1H, CH=CH-N) ppm. NMR data consistent with literature.⁹¹

(3-Nitro-1H-indol-1-yl)(phenyl)methanone (109b)



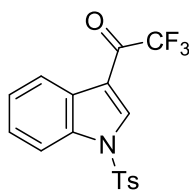
The title compound was prepared from (1*H*-indol-1-yl)(phenyl)methanone based on a reported method.⁶¹ Recrystallization from hot methanol gave the title compound as a white solid (132 mg, 0.496 mmol) in 11% yield. ¹H NMR (500 MHz, CDCl₃): δ 8.38-8.36 (m, 1H, CH_{Ar}), 8.32-8.31 (m, 1H, CH_{Ar}), 8.28 (s, 1H, NO₂C=CH-N), 7.79-7.77 (m, 2H, CH_{Ar}), 7.74-7.71 (m, 1H, CH_{Ar}), 7.61 (t, *J* = 7.7 Hz, 2H, CH_{Ar}), 7.55-7.51 (m, 2H, CH_{Ar}) ppm. ¹³C NMR (125 MHz, CDCl₃): δ 168.3 (C=O), 135.3 (C_{Ar}), 133.7 (CH_{Ar}), 133.3 (NO₂C=CH-N), 132.3 (C_{Ar}), 129.8 (CH_{Ar}), 129.4 (CH_{Ar}), 129.2 (NO₂C=CH-N), 127.3 (CH_{Ar}), 126.5 (CH_{Ar}), 121.9 (C_{Ar}), 120.9 (CH_{Ar}), 116.5 (CH_{Ar}) ppm. IR (Neat): 3141, 1708, 1545, 1479, 1450, 1387, 1370, 1317, 1299, 1213, 1145, 1120 cm⁻¹. NMR data consistent with the literature.⁶²

2,2,2-Trifluoro-1-(1H-indol-3-yl)ethan-1-one



The title compound was prepared as an off-white solid (727 mg, 3.41 mmol) in 80% yield based on reported method.⁹² **¹H NMR** (400 MHz, DMSO): δ 12.70 (bs, 1H, NH), 8.49 (q, $J = 0.5$ Hz, 1H, CH_{Ar}), 8.22 – 8.16 (m, 1H, CH_{Ar}), 7.62 – 7.57 (m, 1H, CH_{Ar}), 7.37 – 7.30 (m, 2H, CH_{Ar}) ppm. **¹³C NMR** (100 MHz, DMSO): δ 173.9 (q, $J = 30.0$ Hz, C(O)CF₃), 137.6 (CH=C), 136.6 (C_{Ar}), 125.7 (C_{Ar}), 124.3 (CH_{Ar}), 123.4 (CH_{Ar}), 121.1 (CH_{Ar}), 116.9 (q, $J = 290.0$ Hz, CF₃), 113.0 (CH_{Ar}), 108.8 (C_{Ar}) ppm. NMR data consistent with literature.⁹²

2,2,2-Trifluoro-1-(1-tosyl-1H-indol-3-yl)ethan-1-one (109d)



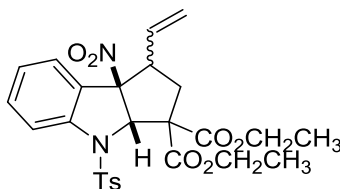
Ground sodium hydroxide pearls (206 mg, 5.15 mmol, 5.5 equiv) was added to a solution of 2,2,2-trifluoro-1-(1H-indol-3-yl)ethan-1-one (199 mg, 0.935 mmol, 1 equiv) and tetrabutylammonium bisulfate (32.8 mg, 0.0966 mmol, 0.1 equiv) in dichloromethane (10 mL). The solution was stirred for 10 mins before the addition of tosyl chloride (0.270 g, 1.42 mmol, 1.5 equiv). The reaction was left stirring overnight at room temperature. Tetrabutylammonium bisulfate (33.2 mg, 0.0978 mmol, 0.1 equiv) and ground sodium hydroxide pearls (0.180 g, 4.50 mmol, 4.8 equiv) were added to the suspension. The reaction was left stirring overnight at 55 °C before the addition of saturated ammonium chloride solution (20 mL). The solution was stirred for 2 h then the organic fraction was isolated and the aqueous fraction was extracted with dichloromethane (2 × 10 mL). The combined organic extracts were dried over magnesium sulfate and concentrated under reduced pressure. After column chromatography (20% ethyl acetate in hexane), the title

compound was collected as an oily white solid (22.6 mg, 0.0615 mmol) in 7% yield. NMR data consistent with literature.⁹²

4.5.3 Typical procedure for Pd-catalyzed dearomative [3 + 2] cycloaddition of 3-nitroindoles with 2-vinylcyclopropane-1,1-dicarboxylates

An oven-dried 3 mL reaction vial equipped with a magnetic stir bar was charged with the 2-vinylcyclopropane-1,1-dicarboxylate derivative (0.0500 mmol, 1.0 equiv), the indole derivative (0.0500 mmol, 1 equiv), Pd₂(dba)₃·CHCl₃ (2.60 mg, 0.00251 mmol, 5 mol %), BPhen (1.70 mg, 0.00500 mmol, 10 mol %) and NBu₄I (10.1 mg, 0.0273 mmol, 0.5 equiv). The vial was fitted with a septum cap and purged with N₂. Anhydrous THF (0.820 mL) was added and the reaction was stirred till the consumption of both substrates as indicated from TLC. The solvent was removed under reduced pressure and the crude residue was purified by column chromatography.

Diethyl (1S,3aS,8bR)-8b-nitro-4-tosyl-1-vinyl-1,3a,4,8b-tetrahydrocyclopenta[b]indole-3,3(2H)-dicarboxylate (107a/107a')



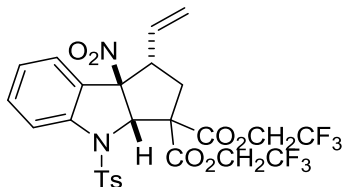
Based on the typical procedure, the title compound was obtained as a pale yellow oil (53.7 mg, 102 μmol) in 99% yield after column chromatography (20 % ethyl acetate in hexane). ¹H NMR (500 MHz, CDCl₃): δ 7.73 (t, *J* = 8.5 Hz, 2H, CH_{Ar}), 7.52 - 7.51 (m, 3H, CH_{Ar}), 7.47 - 7.43 (m, 2H, CH_{Ar}), 7.41 (d, *J* = 8.5 Hz, 2H, CH_{Ar}), 7.37 (d, *J* = 8.0 Hz,

1H, CH_{Ar}), 7.22 (t, *J* = 7.5 Hz, 1H, CH_{Ar}), 7.15 (t, *J* = 7.5 Hz, 1H, CH_{Ar}), 7.10 (dd, *J* = 13.5, 8.0 Hz, 3H, CH_{Ar}), 6.36 (s, 1H, Ts-N-CH_{Major}), 6.31 (s, 1H, Ts-N-CH_{Minor}), 5.78 (ddd, *J* = 17.4, 10.0, 7.5 Hz, 1H, CH=CH_{2Major}), 5.53 (dt, *J* = 17.0, 9.5 Hz, 1H, CH=CH_{2Minor}), 5.28 - 5.11 (m, 4H, CH=CH₂), 4.48 - 4.16 (m, 8H, OCH₂CH₃), 3.41 (app q, *J* = 7.0 Hz, 1H, CH-CH=CH_{2Major}), 3.30 (dt, *J* = 14.0, 6.5 Hz, 1H, CH-CH=CH_{2Minor}), 2.59 (dd, *J* = 13.5, 6.5 Hz, 1H, CHCH_{2Major}), 2.40 (dd, *J* = 13.5, 56.5 Hz, 1H, CHCH_{2Minor}), 2.31 - 2.28 (m, 7H, CH₃ and CHCH₂), 2.21 (app t, *J* = 14.0 Hz, 1H, CHCH_{2Major}), 1.40-1.31 (m, 12H, OCH₂CH₃) ppm. ¹³C NMR (125 MHz, CDCl₃): δ 169.8 (2 × overlapping C=O), 167.9 (C=O), 166.7 (C=O), 145.1 (C_{Ar}), 145.0 (C_{Ar}), 144.5 (C_{Ar}), 142.6 (C_{Ar}), 133.0 (C_{Ar}), 132.8 (CH=CH₂), 132.4 (CH=CH₂), 132.1 (CH_{Ar}), 132.0 (CH_{Ar}), 129.80 (CH_{Ar Tosyl}), 129.79 (CH_{Ar Tosyl}), 128.9 (CH_{Ar}), 128.6 (C_{Ar}), 127.8 (CH_{Ar Tosyl}), 127.7 (CH_{Ar Tosyl}), 126.5 (CH_{Ar}), 126.0 (CH_{Ar}), 125.3 (CH_{Ar}), 124.7 (C_{Ar}), 121.1 (CH=CH₂), 120.7 (CH=CH₂), 118.3 (CH_{Ar}), 117.8 (CH_{Ar}), 102.7 (C-NO₂), 101.3 (C-NO₂), 73.7 (Ts-N-CH), 73.3 (Ts-N-CH), 64.9 (C-(CO₂Et)₂), 64.1 (C-(CO₂Et)₂), 62.85 (OCH₂CH₃), 62.80 (OCH₂CH₃), 62.65 (OCH₂CH₃), 62.61 (OCH₂CH₃), 53.8 (CH-CH=CH₂), 50.5 (CH-CH=CH₂), 39.6 (CHCH₂), 37.5 (CHCH₂), 21.71 (CH₃), 21.70 (CH₃), 14.18 (CO₂CH₂CH₃), 14.14 (CO₂CH₂CH₃), 14.10 (CO₂CH₂CH₃), 14.08 (CO₂CH₂CH₃) ppm. **IR** (Neat): 2987, 1730, 1551, 1368, 1265, 1172, 1091, 734, 664 cm⁻¹. **HRMS** (ESI) *m/z*: [M + Na]⁺ Calcd for C₂₆H₂₈N₂O₈SNa 551.1464; Found 551.1445.

Bis(2,2,2-trifluoroethyl)

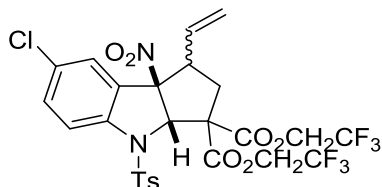
(3*a*S,8*b*R)-8*b*-nitro-4-tosyl-1-vinyl-1,3*a*,4,8*b*-

tetrahydrocyclopenta[*b*]indole-3,3(2*H*)-dicarboxylate (**108a**)



Based on the typical procedure, the title compound was obtained as a white solid (28.3 mg, 0.0445 mmol) in 80% yield after column chromatography (25 – 50% diethyl ether in hexane). The major isomer was isolated by recrystallization in methanol and dichloromethane. **¹H NMR** (500 MHz, CDCl₃): δ 7.75 (d, *J* = 8.5 Hz, 1H, CH_{Ar}), 7.49 (t, *J* = 8.0 Hz, 1H, CH_{Ar}), 7.43 (d, *J* = 8.5 Hz, 2H, CH_{Ar} Tosyl), 7.38 (d, *J* = 7.5 Hz, 1H, CH_{Ar}), 7.18 (t, *J* = 7.5 Hz, 1H, CH_{Ar}), 7.13 (d, *J* = 8.0 Hz, 2H, CH_{Ar} Tosyl), 6.24 (s, 1H, CH-NTs), 5.75 (ddd, *J* = 17.4, 10.5, 7.5 Hz, 1H, CH=CH₂), 5.31 (d, *J* = 10.5 Hz, 1H, CH=CH₂), 5.17 (d, *J* = 17.0 Hz, 1H, CH=CH₂), 5.02 – 4.95 (m, 1H, OCH₂CF₃), 4.84 – 4.77 (m, 1H, OCH₂CF₃), 4.57 – 4.50 (m, 1H, OCH₂CF₃), 4.47 – 4.40 (m, 1H, OCH₂CF₃), 3.30 (dt, *J* = 14.0, 6.5 Hz, 1H, CH-CH=CH₂), 2.47 (dd, *J* = 13.5, 5.5 Hz, 1H, CH₂-CH-CH=CH₂), 2.34 (s, 3H, CH₃), 2.28 (app t, *J* = 14.0 Hz, 1H, CH₂-CH-CH=CH₂) ppm. **¹³C NMR** (125 MHz, CDCl₃): δ 167.7 (C=O), 164.5 (C=O), 145.5 (C_{Ar}), 144.0 (C_{Ar}), 132.3 (CH_{Ar}), 132.1 (C_{Ar}), 131.6 (CH=CH₂), 129.8 (CH_{Ar} Tosyl), 128.6 (CH_{Ar}), 127.7 (CH_{Ar} Tosyl), 125.3 (CH_{Ar}), 123.9 (C_{Ar}), 122.5 (q, *J* = 275 Hz, CF₃), 122.4 (q, *J* = 270 Hz, CF₃), 121.2 (CH=CH₂), 117.9 (CH_{Ar}), 100.8 (C-NO₂), 73.6 (CH-NTs), 63.7 (C(CO₂CH₂CF₃)₂), 62.1 (q, *J* = 37.5 Hz, OCH₂CF₃), 61.9 (q, *J* = 37.5 Hz, OCH₂CF₃), 50.2 (CH-CH=CH₂), 37.4 (CH₂-CH-CH=CH₂), 21.6 (CH₃) ppm. **¹⁹F NMR** (470 Hz, CDCl₃): δ -73.61 (t, *J* = 8.0 Hz, CF₃), -73.75 (t, *J* = 8.9 Hz, CF₃) ppm. **IR** (Neat): 1751, 1551, 1461, 1420, 1370, 1285, 1241, 1157, 1072 cm⁻¹. **HRMS** (ESI) *m/z*: [M + Na]⁺ Calcd for C₂₆H₂₂F₆N₂O₈SNa 659.0899; Found 659.0928. **Melting point**: 185.2 – 187.2 °C.

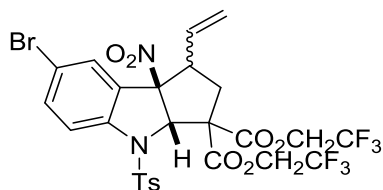
Bis(2,2,2-trifluoroethyl)(3aS,8bR)-7-chloro-8b-nitro-4-tosyl-1-vinyl-1,3a,4,8b tetrahydrocyclopenta[b]indole-3,3(2H)-dicarboxylate (108b/108b')



Based on the typical procedure, the title compound was obtained as a colourless film (31.1 mg, 0.0464 mmol) in 88% yield after column chromatography (10 – 20% ethyl acetate in hexane). ¹H NMR (400 MHz, CDCl₃): δ 7.69 – 7.65 (m, 2H, CH_{Ar} Major and CH_{Ar} Minor), 7.52 – 7.41 (m, 7H, 3 × CH_{Ar} Major and 4 × CH_{Ar} Minor), 7.34 (d, *J* = 2.0 Hz, 1H, CH_{Ar} Major), 7.18 – 7.16 (m, 4H, 2 × CH_{Ar} Major and 2 × CH_{Ar} Minor), 6.28 (s, 1H, Ts-N-CH Minor), 6.24 (d, *J* = 0.8 Hz, 1H, Ts-N-CH Major), 5.74 (ddd, *J* = 17.3, 10.2, 7.6 Hz, 1H, CH=CH₂ Major), 5.51 – 5.44 (m, 1H, CH=CH₂ Minor), 5.38 (d, *J* = 10.4 Hz, 1H, CH=CH₂ Major), 5.31 – 5.25 (m, 2H, CH=CH₂ Minor), 5.19 (d, *J* = 17.2 Hz, 1H, CH=CH₂ Major), 5.01 – 4.92 (m, 1H, OCH₂CF₃ Major), 4.88 – 4.70 (m, 1H of OCH₂CF₃ Major and 2H of OCH₂CF₃ Minor), 4.59 – 4.50 (m, 2H, OCH₂CF₃ Major and OCH₂CF₃ Minor), 4.47 – 4.37 (m, 2H, OCH₂CF₃ Major and OCH₂CF₃ Minor), 3.42 (app q, *J* = 6.8 Hz, 1H, CH-CH=CH₂ Minor), 3.29 (dt, *J* = 14.4, 6.4 Hz, 1H, CH-CH=CH₂ Major), 2.66 (dd, *J* = 14.0, 6.4 Hz, 1H, CH-CH₂ Minor), 2.50 (dd, *J* = 14.0, 4.4 Hz, 1H, CH-CH₂ Major), 2.40 (dd, *J* = 12.6, 5.6 Hz, 1H, CH-CH₂ Minor), 2.36 (s, 3H, CH₃ Tosyl Major), 2.35 (s, 3H, CH₃ Tosyl Minor), 2.28 (app t, *J* = 14.4 Hz, 1H, CH-CH₂ Major) ppm. ¹³C NMR (100 MHz, CDCl₃): δ 167.6 (C=O Major), 167.4 (C=O Minor), 165.9 (C=O Minor), 164.4 (C=O Major), 145.8 (C_{Ar} Major), 145.7 (C_{Ar} Minor), 142.7 (C_{Ar} Major), 140.9 (C_{Ar} Minor), 132.6 (CH_{Ar} Major), 132.4 (CH_{Ar} Minor), 132.0 (C_{Ar} Minor), 131.9 (C_{Ar} Major), 131.6 (C_{Ar} Minor), 131.3 (CH=CH₂ Minor), 130.94 (CH=CH₂ Major), 130.87 (C_{Ar} Major), 130.1 (CH_{Ar} Tosyl

Major), 130.0 (CH_{Ar} Tosyl Minor), 129.3 (C_{Ar} Minor), 129.0 (CH_{Ar} Minor), 128.6 (CH_{Ar} Major), 127.64 (CH_{Ar} Tosyl Major), 127.58 (CH_{Ar} Tosyl Minor), 125.5 (C_{Ar} Major), 122.5 (q, *J* = 275 Hz, CF₃ Major and CF₃ Minor), 122.4 (q, *J* = 276 Hz, CF₃ Major and CF₃ Minor), 122.2 (CH=CH₂ Minor), 121.9 (CH=CH₂ Major), 118.8 (CH_{Ar} Major), 118.7 (CH_{Ar} Minor), 101.7 (C-NO₂ Minor), 100.4 (C-NO₂ Major), 73.9 (Ts-N-CH Major and Ts-N-CH Minor), 64.6 (C-(CO₂CH₂CF₃)₂ Minor), 63.8 (C-(CO₂CH₂CF₃)₂ Major), 62.7 – 61.4 (m, CH₂CF₃ Major and CH₂CF₃ Minor), 53.8 (CH-CH=CH₂ Minor), 50.2 (CH-CH=CH₂ Major), 39.6 (CH-CH₂ Minor), 37.4 (CH-CH₂ Major), 21.6 (CH₃ Major and CH₃ Minor) ppm. **¹⁹F NMR** (470 Hz, CDCl₃): δ -73.51 (t, *J* = 8.0 Hz, CF₃ Minor), -73.61 (t, *J* = 7.5 Hz, CF₃ Major), -73.70 (t, *J* = 8.5 Hz, CF₃ Minor), -73.75 (t, *J* = 8.5 Hz, CF₃ Major) ppm. **IR** (Neat): 1751, 1553, 1472, 1419, 1373, 1285, 1241, 1158, 1105, 1091, 1068 cm⁻¹. **HRMS** (ESI) *m/z*: [M + Na]⁺ Calcd for C₂₆H₂₁ClF₆N₂O₈SNa 693.0509; Found 693.0511.

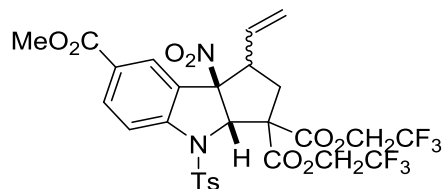
Bis(2,2,2-trifluoroethyl)(3aS,8bR)-7-bromo-8b-nitro-4-tosyl-1-vinyl-1,3a,4,8b-tetrahydrocyclopenta[b]indole-3,3(2H)-dicarboxylate (108c/108c')



Based on the typical procedure, the title compound was obtained as an off-white solid (34.6 mg, 0.0484 mmol) in 87% yield after column chromatography (15 – 40% ethyl acetate in hexane). **¹H NMR** (500 MHz, CDCl₃): δ 7.63 – 7.59 (m, 5H, 2 × CH_{Ar} Major and 3 × CH_{Ar} Minor), 7.52 (d, *J* = 8.0 Hz, 2H, CH_{Ar} Minor), 7.48 (d, *J* = 1.5 Hz, 1H, CH_{Ar} Major), 7.44 (d, *J* = 8.0 Hz, 2H, CH_{Ar} Major), 7.17 (d, *J* = 7.5 Hz, 4H, 2 × CH_{Ar} Major and 2 × CH_{Ar} Minor), 6.27 (s, 1H, Ts-N-CH Minor), 6.23 (s, 1H, Ts-N-CH Major), 5.74 (ddd, *J* = 17.3, 10.3,

7.5 Hz, 1H, $CH=CH_2$ Major), 5.50 – 5.43 (m, 1H, $CH=CH_2$ Minor), 5.38 (d, $J = 10.5$ Hz, 1H, $CH=CH_2$ Major), 5.31 – 5.25 (m, 2H, $CH=CH_2$ Minor), 5.19 (d, $J = 17.0$ Hz, 1H, $CH=CH_2$ Major), 5.00 – 4.93 (m, 1H, OCH_2CF_3 Major), 4.87 – 4.71 (m, 1H of OCH_2CF_3 Major and 2H of OCH_2CF_3 Minor), 4.58 – 4.50 (m, 2H, OCH_2CF_3 Major and OCH_2CF_3 Minor), 4.46 – 4.38 (m, 2H, OCH_2CF_3 Major and OCH_2CF_3 Minor), 3.42 (app q, $J = 8.5$ Hz, 1H, $CH-CH=CH_2$ Minor), 3.28 (dt, $J = 14.0, 6.5$ Hz, 1H, $CH-CH=CH_2$ Major), 2.66 (dd, $J = 14.0, 6.5$ Hz, 1H, $CH-CH_2$ Minor), 2.49 (dd, $J = 14.0, 4.5$ Hz, 1H, $CH-CH_2$ Major), 2.42 – 2.39 (m, 1H, $CH-CH_2$ Minor), 2.37 (s, 3H, CH_3 Tosyl Major), 2.36 (s, 3H, CH_3 Tosyl Minor), 2.28 (app t, $J = 14.0$ Hz, 1H, $CHCH_2$ Major) ppm. ^{13}C NMR (125 MHz, $CDCl_3$): δ 167.5 ($C=O$ Major), 165.8 ($C=O$ Minor), 164.4 ($C=O$ Major), 145.8 (C_{Ar} Major), 145.7 (C_{Ar} Minor), 143.2 (C_{Ar} Major), 141.4 (C_{Ar} Minor), 135.4 (CH_{Ar} Major), 135.3 (CH_{Ar} Minor), 132.0 (C_{Ar} Minor), 131.9 (C_{Ar} Major), 131.5 (CH_{Ar} Major), 131.2 ($CH=CH_2$ Minor), 130.9 ($CH=CH_2$ Major), 130.1 (CH_{Ar} Tosyl Major), 130.0 (CH_{Ar} Tosyl Minor), 129.6 (C_{Ar} Minor), 129.4 (CH_{Ar} Minor), 127.63 (CH_{Ar} Tosyl Major), 127.57 (CH_{Ar} Tosyl Minor), 125.7 (C_{Ar} Major), 122.5 (q, $J = 276$ Hz, CF_3 Major and CF_3 Minor), 122.4 (q, $J = 276$ Hz, CF_3 Major and CF_3 Minor), 122.2 ($CH=CH_2$ Minor), 121.9 ($CH=CH_2$ Major), 119.2 (CH_{Ar} Major), 119.0 (CH_{Ar} Minor), 118.9 (C_{Ar} Minor), 118.2 (C_{Ar} Major), 101.7 ($C-NO_2$ Minor), 100.3 ($C-NO_2$ Major), 73.8 (Ts-N-CH Major and Ts-N-CH Minor), 64.6 ($C-(CO_2CH_2CF_3)_2$ Minor), 63.7 ($C-(CO_2CH_2CF_3)_2$ Major), 62.6 – 61.5 (m, CH_2CF_3 Major and CH_2CF_3 Minor), 53.8 ($CH-CH=CH_2$ Minor), 50.2 ($CH-CH=CH_2$ Major), 39.6 ($CH-CH_2$ Minor), 37.4 ($CH-CH_2$ Major), 21.7 (CH_3 Major and CH_3 Minor) ppm. ^{19}F NMR (470 Hz, $CDCl_3$): δ -73.51 (t, $J = 8.0$ Hz, CF_3 Minor), -73.61 (t, $J = 8.0$ Hz, CF_3 Major), -73.69 (t, $J = 8.5$ Hz, CF_3 Minor), -73.74 (t, $J = 8.5$ Hz, CF_3 Major) ppm. IR (Neat): 1751, 1559, 1555, 1472, 1419, 1370, 1283, 1250, 1161, 1103, 1068 cm^{-1} . HRMS (ESI) m/z : $[M + Na]^+$ Calcd for $C_{26}H_{21}BrF_6N_2O_8SNa$ 737.0004; Found 737.0034.

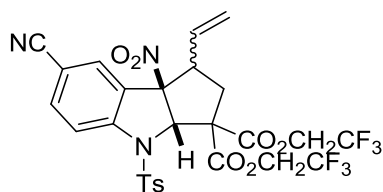
7-Methyl 3,3-bis(2,2,2-trifluoroethyl) (3a*S*,8b*R*)-8b-nitro-4-tosyl-1-vinyl-1,3a,4,8b-tetrahydrocyclopenta[*b*]indole-3,3,7(2*H*)-tricarboxylate (**108d/108d'**)



Based on the typical procedure, the title compound was obtained as a colourless film (30.5 mg, 0.0439 mmol) in 84% yield after column chromatography (20 – 30% ethyl acetate in hexane). ¹H NMR (400 MHz, CDCl₃): δ 8.21 – 8.15 (m, 3H, CH_{Ar} Major and 2 × CH_{Ar} Minor), 8.02 (d, *J* = 1.2 Hz, 1H, CH_{Ar} Major), 7.79 (d, *J* = 8.8 Hz, 1H, CH_{Ar} Major), 7.75 (d, *J* = 8.8 Hz, 1H, CH_{Ar} Minor), 7.56 (d, *J* = 8.0 Hz, 2H, CH_{Ar} Tosyl Minor), 7.48 (d, *J* = 8.4 Hz, 2H, CH_{Ar} Tosyl Major), 7.18 – 7.15 (m, 4H, 2 × CH_{Ar} Tosyl Major and 2 × CH_{Ar} Tosyl Minor), 6.39 (s, 1H, Ts-N-CH Minor), 6.29 (d, *J* = 0.8 Hz, 1H, Ts-N-CH Major), 5.80 (ddd, *J* = 17.3, 10.2, 7.2 Hz, 1H, CH=CH₂ Major), 5.57 – 5.49 (m, 1H, CH=CH₂ Minor), 5.39 (d, *J* = 10.4 Hz, 1H, CH=CH₂ Major), 5.31 (d, *J* = 16.8 Hz, 1H, CH=CH₂ Minor), 5.27 (d, *J* = 10.0 Hz, 1H, CH=CH₂ Minor), 5.20 (d, *J* = 17.2 Hz, 1H, CH=CH₂ Major), 5.01 – 4.91 (m, 1H, OCH₂CF₃ Major), 4.87 – 4.73 (m, 1H of OCH₂CF₃ Major and 2H of OCH₂CF₃ Minor), 4.60 – 4.50 (m, 2H, OCH₂CF₃ Major and OCH₂CF₃ Minor), 4.48 – 4.39 (m, 2H, OCH₂CF₃ Major and OCH₂CF₃ Minor), 3.92 (s, 3H, OCH₃ Minor), 3.91 (s, 3H, OCH₃ Major), 3.49 (app q, *J* = 7.2 Hz, 1H, CH-CH=CH₂ Minor), 3.35 (dt, *J* = 14.4, 6.4 Hz, 1H, CH-CH=CH₂ Major), 2.71 – 2.64 (m, 1H, CH-CH₂ Minor), 2.52 (ddd, *J* = 13.8, 5.4, 0.8 Hz, 1H, CH-CH₂ Major), 2.45 (dd, *J* = 14.0, 7.6 Hz, 1H, CH-CH₂ Minor), 2.34 (s, 3H, CH₃ Tosyl Major), 2.33 (s, 3H, CH₃ Tosyl Minor), 2.28 – 2.25 (m, 1H, CH-CH₂ Major) ppm. ¹³C NMR (100 MHz, CDCl₃): δ 167.6 (C=O Major), 167.5 (C=O Minor), 165.8 (C=O Minor), 165.6 (C=O Major), 164.4 (C=O Major), 147.7 (C_{Ar} Major), 145.9 (C_{Ar} Major), 145.81 (C_{Ar} Minor), 145.77 (C_{Ar} Minor), 134.0 (CH_{Ar} Major), 133.9 (CH_{Ar} Minor), 132.4 (C_{Ar} Minor), 132.1 (C_{Ar} Major), 131.4 (CH=CH₂ Minor), 131.1 (CH=CH₂ Major),

130.2 (CH_{Ar} Major), 130.1 (CH_{Ar} Tosyl Major and CH_{Ar} Tosyl Minor), 128.2 (CH_{Ar} Minor), 128.1 (C_{Ar} Minor), 127.8 (C_{Ar} Minor), 127.6 (CH_{Ar} Tosyl Major), 127.5 (CH_{Ar} Tosyl Minor), 127.4 (C_{Ar} Major), 124.2 (C_{Ar} Major), 122.5 (q, *J* = 280 Hz, CF₃ Major and CF₃ Minor), 122.4 (q, *J* = 280 Hz, CF₃ Major and CF₃ Minor), 122.1 (CH=CH₂ Minor), 121.7 (CH=CH₂ Major), 117.0 (CH_{Ar} Major), 116.7 (CH_{Ar} Minor), 101.8 (C-NO₂ Minor), 100.2 (C-NO₂ Major), 74.2 (Ts-N-CH Major), 73.9 (Ts-N-CH Minor), 64.6 (C-(CO₂CH₂CF₃)₂ Minor), 63.7 (C-(CO₂CH₂CF₃)₂ Major), 62.6 – 61.5 (m, CH₂CF₃ Major and CH₂CF₃ Minor), 53.4 (CH-CH=CH₂ Minor), 52.5 (OCH₃ Major and OCH₃ Minor), 49.9 (CH-CH=CH₂ Major), 39.7 (CH-CH₂ Minor), 37.5 (CH-CH₂ Major), 21.64 (CH₃ Major), 21.61 (CH₃ Minor) ppm. **¹⁹F NMR** (470 Hz, CDCl₃): δ -73.54 (t, *J* = 8.5 Hz, CF₃ Minor), -73.62 (t, *J* = 8.0 Hz, CF₃ Major), -73.68 (t, *J* = 8.0 Hz, CF₃ Minor), -73.74 (t, *J* = 8.0 Hz, CF₃ Major) ppm. **IR** (Neat): 1754, 1722, 1555, 1374, 1287, 1243, 1165, 1111, 1088 cm⁻¹. **HRMS** (ESI) *m/z*: [M + Na]⁺ Calcd for C₂₈H₂₄F₆N₂O₁₀SNa 717.0954; Found 717.0928.

Bis(2,2,2-trifluoroethyl) (3*aS*,8*bR*)-7-cyano-8*b*-nitro-4-tosyl-1-vinyl-1,3*a*,4,8*b*-tetrahydrocyclopenta[*b*]indole-3,3(2*H*)-dicarboxylate (**108e/108e'**)

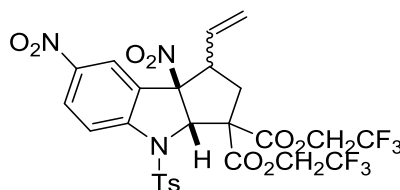


Based on the typical procedure, the title compound was obtained as a colourless film (31.0 mg, 0.0469 mmol) in 82% yield after column chromatography (20 – 30% ethyl acetate in hexane). **¹H NMR** (400 MHz, CDCl₃): δ 7.85 – 7.82 (m, 3H, CH_{Ar} Major and 2 × CH_{Ar} Minor), 7.77 – 7.74 (m, 2H, CH_{Ar} Major and CH_{Ar} Minor), 7.68 (d, *J* = 4.0 Hz, 1H, CH_{Ar} Major), 7.55 (d, *J* = 8.0 Hz, 2H, CH_{Ar} Minor), 7.47 (d, *J* = 8.0 Hz, 2H, CH_{Ar} Major), 7.22 – 7.19 (m,

4H, $2 \times \text{CH}_{\text{Ar Major}}$ and $2 \times \text{CH}_{\text{Ar Minor}}$, 6.30 (d, $J = 1.6$ Hz, 2H, Ts-N-CH_{Major} and Ts-N-CH_{Minor}), 5.74 (ddd, $J = 17.3, 10.4, 7.2$ Hz, 1H, CH=CH_{2 Major}), 5.51 – 5.42 (m, 1H, CH=CH_{2 Minor}), 5.43 (d, $J = 10.4$ Hz, 1H, CH=CH_{2 Major}) 5.35 – 5.30 (m, 2H, CH=CH_{2 Minor}), 5.23 (d, $J = 17.2$ Hz, 1H, CH=CH_{2 Major}), 4.99 – 4.89 (m, 1H, OCH₂CF_{3 Major}), 4.87 – 4.76 (m, 2H, OCH₂CF_{3 Major} and OCH₂CF_{3 Minor}), 4.74 – 4.67 (m, 1H, OCH₂CF_{3 Minor}), 4.61 – 4.52 (m, 2H, OCH₂CF_{3 Major} and OCH₂CF_{3 Minor}), 4.49 – 4.38 (m, 2H, OCH₂CF_{3 Major} and OCH₂CF_{3 Minor}), 3.43 (app q, $J = 8.0$ Hz, 1H, CH-CH=CH_{2 Minor}), 3.33 (dt, $J = 16.0, 8.0$ Hz, 1H, CH-CH=CH_{2 Major}), 2.68 (dd, $J = 16.0, 8.0$ Hz, 1H, CH-CH_{2 Minor}), 2.57 (ddd, $J = 14.0, 5.6, 1.2$ Hz, 1H, CH-CH_{2 Major}), 2.44 (dd, $J = 13.8, 9.6$ Hz, 1H, CH-CH_{2 Minor}), 2.37 (s, 3H, CH_{3 Tosyl Major}), 2.36 (s, 3H, CH_{3 Tosyl Minor}), 2.26 (app t, $J = 14.8$ Hz, 1H, CH-CH_{2 Major}) ppm. **¹³C NMR** (100 MHz, CDCl₃): δ 167.3 (C=O_{Major}), 167.2 (C=O_{Minor}), 165.9 (C=O_{Minor}), 164.3 (C=O_{Major}), 147.5 (C_{Ar Major}), 146.3 (C_{Ar Major}), 146.2 (C_{Ar Minor}), 145.6 (C_{Ar Minor}), 136.2 (CH_{Ar Major}), 136.0 (CH_{Ar Minor}), 132.8 (CH_{Ar Major}), 132.0 (C_{Ar Minor}), 131.9 (C_{Ar Major}), 130.85 (CH=CH_{2 Minor}), 130.80 (CH_{Ar Minor}), 130.6 (CH=CH_{2 Major}), 130.2 (CH_{Ar Tosyl Major} and CH_{Ar Tosyl Minor}), 128.5 (C_{Ar Minor}), 127.5 (CH_{Ar Tosyl Major}), 127.4 (CH_{Ar Tosyl Minor}), 124.8 (C_{Ar Major}), 122.8 (CH=CH_{2 Minor}), 122.48 (CH=CH_{2 Major}), 122.45 (q, $J = 275$ Hz, CF_{3 Major} and CF_{3 Minor}), 122.39 (q, $J = 276$ Hz, CF_{3 Major} and CF_{3 Minor}), 118.0 (CH_{Ar Major}), 117.72 (C_{Ar Major}), 117.69 (CH_{Ar Minor}), 109.6 (C \equiv N_{Minor}), 109.0 (C \equiv N_{Major}), 101.3 (C-NO_{2 Minor}), 99.9 (C-NO_{2 Major}), 74.1 (Ts-N-CH_{Minor}), 74.0 (Ts-N-CH_{Major}), 64.5 (C-(CO₂CH₂CF₃)_{2 Minor}), 63.7 (C-(CO₂CH₂CF₃)_{2 Major}), 62.8 – 61.6 (m, CH₂CF_{3 Major} and CH₂CF_{3 Minor}), 54.0 (CH-CH=CH_{2 Minor}), 50.0 (CH-CH=CH_{2 Major}), 40.0 (CH-CH_{2 Minor}), 37.5 (CH-CH_{2 Major}), 21.7 (CH_{3 Major} and CH_{3 Minor}) ppm. **¹⁹F NMR** (470 Hz, CDCl₃): δ –73.50 (t, $J = 8.5$ Hz, CF_{3 Minor}), –73.60 (t, $J = 8.0$ Hz, CF_{3 Major}), –73.69 (t, $J = 8.0$ Hz, CF_{3 Minor}), –73.72 (t, $J = 7.5$ Hz, CF_{3 Major}) ppm. **IR** (Neat): 2232, 1754, 1555, 1373, 1287,

1241, 1169, 1089, 1066 cm^{-1} . HRMS (ESI) m/z : $[\text{M} + \text{Na}]^+$ Calcd for $\text{C}_{27}\text{H}_{21}\text{F}_6\text{N}_3\text{O}_8\text{SNa}$ 684.0851; Found 684.0836.

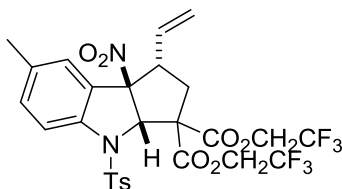
Bis(2,2,2-trifluoroethyl)(3aS,8bR)-7,8b-dinitro-4-tosyl-1-vinyl-1,3a,4,8b-tetrahydrocyclopenta[b]indole-3,3(2H)-dicarboxylate (108f/108f')



Based on the typical procedure, the title compound was obtained as a colourless oil film (29.6 mg, 0.0434 mmol) in 73% yield after column chromatography (20% ethyl acetate in hexane). $^1\text{H NMR}$ (400 MHz, CDCl_3): δ 8.38 (dd, $J = 9.0, 2.0$ Hz, 3H, 1 \times CH_{Ar} Major and 2 \times CH_{Ar} Minor), 8.24 (d, $J = 2.0$ Hz, 1H, CH_{Ar} Major), 7.88 – 7.84 (m, 2H, CH_{Ar} Major and CH_{Ar} Minor), 7.58 (d, $J = 4.2$ Hz, 2H, CH_{Ar} Minor), 7.51 (d, $J = 8.4$ Hz, 2H, CH_{Ar} Major), 7.21 (d, $J = 8.0$ Hz, 4H, 2 \times CH_{Ar} Major and 2 \times CH_{Ar} Minor), 6.37 (s, 1H, Ts-N-CH Minor), 6.35 (s, 1H, Ts-N-CH Major), 5.81 (ddd, $J = 17.3, 10.2, 7.2$ Hz, 1H, $\text{CH}=\text{CH}_2$ Major), 5.55 – 5.45 (m, 2H, $\text{CH}=\text{CH}_2$ Minor and $\text{CH}=\text{CH}_2$ Major), 5.38 – 5.33 (m, 2H, $\text{CH}=\text{CH}_2$ Minor), 5.24 (d, $J = 17.2$ Hz, 1H, $\text{CH}=\text{CH}_2$ Major), 4.99 – 4.90 (m, 1H, OCH_2CF_3 Major), 4.88 – 4.68 (m, 1H of OCH_2CF_3 Major and 2H of OCH_2CF_3 Minor), 4.62 – 4.51 (m, 2H, OCH_2CF_3 Major and OCH_2CF_3 Minor), 4.49 – 4.39 (m, 2H, OCH_2CF_3 Major and OCH_2CF_3 Minor), 3.49 (app q, $J = 6.8$ Hz, 1H, $\text{CH}-\text{CH}=\text{CH}_2$ Minor), 3.37 (dt, $J = 14.4, 6.4$ Hz, 1H, $\text{CH}-\text{CH}=\text{CH}_2$ Major), 2.71 (dd, $J = 14.0, 6.4$ Hz, 1H, $\text{CH}-\text{CH}_2$ Minor), 2.59 (dd, $J = 18.0, 4.8$ Hz, 1H, $\text{CH}-\text{CH}_2$ Major), 2.48 (dd, $J = 14.0, 8.8$ Hz, 1H, $\text{CH}-\text{CH}_2$ Minor), 2.37 (s, 6H, CH_3 Tosyl Major and CH_3 Tosyl Minor), 2.29 (app t, $J = 14.0$ Hz, 1H, $\text{CH}-\text{CH}_2$ Major) ppm. $^{13}\text{C NMR}$ (100MHz, CDCl_3): δ 167.3 (C=O Major), 167.2 (C=O Minor), 165.8 (C=O Minor), 164.3 (C=O Major), 149.0 (C_{Ar}

Major), 147.1 (C_{Ar} Minor), 146.4 (C_{Ar} Major), 146.3 (C_{Ar} Minor), 144.8 (C_{Ar} Major), 132.0 (C_{Ar} Minor), 131.9 (C_{Ar} Major), 130.7 (CH=CH₂ Minor), 130.4 (CH=CH₂ Major), 130.3 (CH_{Ar} Tosyl Major and CH_{Ar} Tosyl Minor), 128.4 (C_{Ar} Minor), 128.2 (CH_{Ar} Major), 128.0 (CH_{Ar} Minor), 127.5 (CH_{Ar} Tosyl Major), 127.4 (CH_{Ar} Tosyl Minor), 124.8 (C_{Ar} Major), 124.7 (CH_{Ar} Major), 122.9 (CH=CH₂ Minor), 122.8 (CH_{Ar} Minor), 122.6 (CH=CH₂ Major), 122.44 (q, *J* = 275 Hz, CF₃ Major and CF₃ Minor), 122.37 (q, *J* = 276 Hz, CF₃ Major and CF₃ Minor), 117.1 (CH_{Ar} Major), 116.9 (CH_{Ar} Minor), 101.1 (C-NO₂ Minor), 99.6 (C-NO₂ Major), 74.6 (Ts-N-CH Major and Ts-N-CH Minor), 64.5 (C-(CO₂CH₂CF₃)₂ Minor), 63.7 (C-(CO₂CH₂CF₃)₂ Major), 62.8 – 61.6 (m, CH₂CF₃ Major and CH₂CF₃ Minor), 53.7 (CH-CH=CH₂ Minor), 49.8 (CH-CH=CH₂ Major), 39.9 (CH-CH₂ Minor), 37.5 (CH-CH₂ Major), 21.7 (CH₃ Major and CH₃ Minor) ppm. ¹⁹F NMR (470 Hz, CDCl₃): δ -73.50 (t, *J* = 8.5 Hz, CF₃ Minor), -73.59 (t, *J* = 8.0 Hz, CF₃ Major), -73.67 (t, *J* = 8.5 Hz, CF₃ Minor), -73.71 (t, *J* = 8.9 Hz, CF₃ Major) ppm. IR (Neat): 1753, 1558, 1529, 1375, 1344, 1287, 1248, 1165, 1085 cm⁻¹. HRMS (ESI) *m/z*: [M + Na]⁺ Calcd for C₂₆H₂₁F₆N₃O₁₀SNa 704.0750; Found 704.0750.

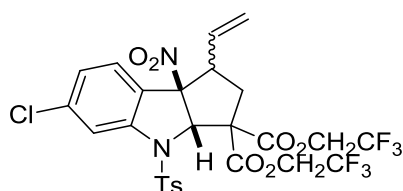
*Bis(2,2,2-trifluoroethyl)(3a*S*,8*b**R*)-7-methyl-8*b*-nitro-4-tosyl-1-vinyl-1,3*a*,4,8*b*-tetrahydrocyclopenta[*b*]indole-3,3(2*H*)-dicarboxylate (108*g*)*



Based on the typical procedure, the title compound was obtained as an off-white solid (30.3 mg, 0.0466 mmol) in 78% yield after column chromatography (20 – 30% ethyl acetate in hexane). The major isomer was isolated by recrystallization in methanol. ¹H NMR (400 MHz, CDCl₃): δ 7.62 (d, *J* = 8.0 Hz, 1H, CH_{Ar}), 7.43 (d, *J* = 8.0 Hz, 2H,

CH_{Ar}), 7.30 – 7.27 (m, 1H, CH_{Ar}), 7.13 (d, *J* = 8.0 Hz, 3H, CH_{Ar}), 6.21 (d, *J* = 1.2 Hz, 1H, Ts-N-CH), 5.76 (ddd, *J* = 17.4, 10.2, 7.6 Hz, 1H, CH=CH₂), 5.31 (d, *J* = 10.4 Hz, 1H, CH=CH₂), 5.17 (d, *J* = 17.2 Hz, 1H, CH=CH₂), 5.02 – 4.93 (m, 1H, OCH₂CF₃), 4.85 – 4.76 (m, 1H, OCH₂CF₃), 4.57 – 4.48 (m, 1H, OCH₂CF₃), 4.47 – 4.38 (m, 1H, OCH₂CF₃), 3.28 (dt, *J* = 16.0, 5.6 Hz, 1H, CH-CH=CH₂), 2.45 (ddd, *J* = 13.6, 5.6, 1.2 Hz, 1H, CH-CH₂), 2.34 (s, 6H, CH₃), 2.28 (app t, *J* = 14.0 Hz, 1H, CH-CH₂) ppm. ¹³C NMR (100 MHz, CDCl₃): δ 167.8 (C=O), 164.5 (C=O), 145.3 (C_{Ar}), 141.8 (C_{Ar}), 135.4 (C_{Ar}), 133.2 (CH_{Ar}), 132.2 (C_{Ar}), 131.7 (CH=CH₂), 129.8 (CH_{Ar}Tosyl), 128.7 (CH_{Ar}), 127.7 (CH_{Ar} Tosyl), 124.0 (C_{Ar}), 121.1 (CH=CH₂), 117.6 (CH_{Ar}), 100.9 (C-NO₂), 73.7 (Ts-N-CH), 63.7 (C-(CO₂CH₂CF₃)₂), 62.1 (q, *J* = 38.0 Hz, CH₂CF₃), 61.9 (q, *J* = 37.0 Hz, CH₂CF₃), 50.3 (CH-CH=CH₂), 37.4 (CH-CH₂), 21.6 (CH₃), 21.2 (CH₃) ppm. ¹⁹F NMR (470 Hz, CDCl₃): δ -73.62 (t, *J* = 8.0 Hz, CF₃), -73.75 (t, *J* = 8.5 Hz, CF₃) ppm. IR (Neat): 1751, 1550, 1486, 1419, 1370, 1285, 1244, 1158, 1092, 1071 cm⁻¹. HRMS (ESI) *m/z*: [M + Na]⁺ Calcd for C₂₇H₂₄F₆N₂O₈SNa 673.1055; Found 673.1056. **Melting point:** 199.5 – 202.6 °C.

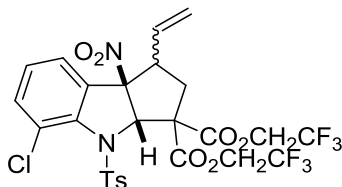
Bis(2,2,2-trifluoroethyl) (3aS,8bR)-6-chloro-8b-nitro-4-tosyl-1-vinyl-1,3a,4,8b-tetrahydrocyclopenta[b]indole-3,3(2H)-dicarboxylate (108i/108i')



Based on the typical procedure, the title compound was obtained as a colourless oil (34.1 mg, 0.0508 mmol) in 88% yield after column chromatography (30% diethyl ether in hexane). ¹H NMR (500 MHz, CDCl₃): δ 7.76 (d, *J* = 1.5 Hz, 1H, CH_{Ar} Major), 7.73 (s, 1H,

CH_{Ar} Minor), 7.55 (d, $J = 8.0$ Hz, 2H, CH_{Ar} Minor), 7.47 (d, $J = 8.0$ Hz, 2H, CH_{Ar} Major), 7.30 (d, $J = 8.0$ Hz, 2H, CH_{Ar} Major and CH_{Ar} Minor), 7.19 – 7.14 (m, 6H, 3 × CH_{Ar} Major and 3 × CH_{Ar} Minor), 6.29 (s, 1H, Ts-N-CH_{Minor}), 6.24 (s, 1H, Ts-N-CH_{Major}), 5.73 (ddd, $J = 17.3$, 10.3, 7.5 Hz, 1H, CH=CH₂ Major), 5.50 – 5.43 (m, 1H, CH=CH₂ Minor), 5.33 (d, $J = 10.5$ Hz, 1H, CH=CH₂ Major), 5.29 – 5.24 (m, 2H, CH=CH₂ Minor), 5.18 (d, $J = 17.0$ Hz, 1H, CH=CH₂ Major), 5.01 – 4.94 (m, 1H, OCH₂CF₃ Major), 4.88 – 4.74 (m, 1H of OCH₂CF₃ Major and 2H of OCH₂CF₃ Minor), 4.58 – 4.50 (m, 2H, OCH₂CF₃ Major and OCH₂CF₃ Minor), 4.46 – 4.39 (m, 2H, OCH₂CF₃ Major and OCH₂CF₃ Minor), 3.42 (app q, $J = 7.0$ Hz, 1H, CH-CH=CH₂ Minor), 3.29 (dt, $J = 14.0$, 6.5 Hz, 1H, CH-CH=CH₂ Major), 2.67 (dd, $J = 13.5$, 6.5 Hz, 1H, CH-CH₂ Minor), 2.50 (dd, $J = 13.8$, 5.0 Hz, 1H, CH-CH₂ Major), 2.43 – 2.40 (m, 1H, CH-CH₂ Minor), 2.36 (s, 6H, CH₃ Tosyl Major and CH₃ Tosyl Minor), 2.29 (app t, $J = 14.0$ Hz, 1H, CH-CH₂ Major) ppm. **¹³C NMR** (125 MHz, CDCl₃): δ 167.6 (C=O), 164.4 (C=O), 145.8 (C_{Ar}), 145.2 (C_{Ar}), 138.7 (C_{Ar}), 131.9 (C_{Ar}), 131.2 (CH=CH₂), 130.1 (CH_{Ar} Tosyl), 129.3 (CH_{Ar}), 127.7 (CH_{Ar} Tosyl), 125.7 (CH_{Ar}), 122.5 (q, $J = 276.3$ Hz, CF₃), 122.4 (q, $J = 276.3$ Hz, CF₃), 122.3 (C_{Ar}), 121.6 (CH=CH₂), 118.0 (CH_{Ar}), 100.3 (C-NO₂), 74.0 (Ts-N-CH), 63.7 (C-(CO₂CH₂CF₃)₂), 62.1 (q, $J = 36.3$ Hz, CH₂CF₃), 62.0 (q, $J = 36.3$ Hz, CH₂CF₃), 50.1 (CH-CH=CH₂), 37.4 (CH-CH₂), 21.7 (CH₃) ppm. **¹⁹F NMR** (470 Hz, CDCl₃): δ -73.54 (t, $J = 8.5$ Hz, CF₃ Minor), -73.62 (t, $J = 8.9$ Hz, CF₃ Major), -73.69 (t, $J = 8.5$ Hz, CF₃ Minor), -73.74 (t, $J = 7.5$ Hz, CF₃ Major) ppm. **IR** (Neat): 1757, 1751, 1551, 1417, 1373, 1288, 1238, 1173, 1153 cm⁻¹. **HRMS** (ESI) m/z : [M + Na]⁺ Calcd for C₂₆H₂₁ClF₆N₂O₈SNa 693.0509; Found 693.0501.

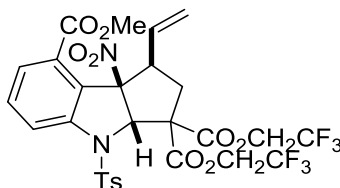
Bis(2,2,2-trifluoroethyl) (3*aS*,8*bR*)-5-chloro-8*b*-nitro-4-tosyl-1-vinyl-1,3*a*,4,8*b*-tetrahydrocyclopenta[*b*]indole-3,3(2*H*)-dicarboxylate (108*j*/108*j'*)



Based on the typical procedure, the title compound was obtained as beige solid (32.7 mg, 0.0487 mmol) in 88% yield after column chromatography (20 – 40% ethyl acetate in hexane). **¹H NMR** (500 MHz, CDCl₃): δ 7.56 – 7.17 (m, 14H, CH_{Ar} Major and CH_{Ar} Minor), 6.40 (s, 1H, Ts-N-CH_{Minor}), 6.38 (s, 1H, Ts-N-CH_{Major}), 5.62 (ddd, *J* = 17.4, 10.3, 7.5 Hz, 1H, CH=CH₂ Major), 5.50 – 5.42 (m, 1H, CH=CH₂ Minor), 5.30 (d, *J* = 10.0 Hz, 1H, CH=CH₂ Major), 5.24 – 5.21 (m, 2H, CH=CH₂ Minor), 5.10 (d, *J* = 15.0 Hz, 1H, CH=CH₂ Major), 5.01 – 4.94 (m, 1H, OCH₂CF₃ Major), 4.84 – 4.73 (m, 3H, OCH₂CF₃ Major and OCH₂CF₃ Minor), 4.57 – 4.42 (m, 2H, OCH₂CF₃ Major and OCH₂CF₃ Minor), 4.25 – 4.11 (m, 2H, OCH₂CF₃ Major and OCH₂CF₃ Minor), 3.36 – 3.24 (m, 2H, CH-CH=CH₂ Major and CH-CH=CH₂ Minor), 2.49 (dd, *J* = 13.8, 7.0 Hz, 1H, CH-CH₂ Minor), 2.40 (s, 6H, CH₃ Tosyl Major and CH₃ Tosyl Minor), 2.34 (dd, *J* = 14.0, 5.5 Hz, 1H, CH-CH₂ Major), 2.26 (dd, *J* = 14.0, 8.5 Hz, 1H, CH-CH₂ Minor), 2.06 (app t, *J* = 14.0 Hz, 1H, CH-CH₂ Major) ppm. **¹³C NMR** (100 MHz, CDCl₃): δ 167.6 (C=O Major), 167.4 (C=O Minor), 165.7 (C=O Minor), 164.3 (C=O Major), 146.0 (C_{Ar} Major), 145.7 (C_{Ar} Minor), 141.6 (C_{Ar} Major), 139.8 (C_{Ar} Minor), 134.1 (C_{Ar} Minor), 133.9 (CH_{Ar} Major), 133.5 (CH_{Ar} Minor), 132.3 (C_{Ar} Minor), 132.1 (C_{Ar} Major), 131.5 (CH=CH₂ Minor), 130.9 (CH=CH₂ Major), 130.0 (CH_{Ar} Tosyl Major), 129.8 (CH_{Ar} Tosyl Minor), 128.9 (CH_{Ar} Minor), 128.6 (C_{Ar} Major), 128.5 (CH_{Ar} Tosyl Minor), 128.4 (CH_{Ar} Tosyl Major), 127.64 (CH_{Ar} Major), 127.61 (CH_{Ar} Major), 127.1 (C_{Ar} Major), 126.9 (C_{Ar} Minor), 125.0 (CH_{Ar} Minor), 122.4 (q, *J* = 276 Hz, CF₃ Major and CF₃ Minor), 122.3 (q, *J* = 276 Hz, CF₃ Major and CF₃

Minor), 122.0 (CH=CH₂ Minor), 121.7 (CH=CH₂ Major), 101.2 (C-NO₂ Minor), 100.7 (C-NO₂ Major), 74.4 (Ts-N-CH Minor), 74.0 (Ts-N-CH Major), 64.3 (C-(CO₂CH₂CF₃)₂ Minor), 63.7 (C-(CO₂CH₂CF₃)₂ Major), 62.7 – 61.5 (m, CH₂CF₃ Major and CH₂CF₃ Minor), 54.7 (CH-CH=CH₂ Minor), 51.7 (CH-CH=CH₂ Major), 38.4 (CH-CH₂ Minor), 36.8 (CH-CH₂ Major), 21.7 (CH₃ Major and CH₃ Minor) ppm. **¹⁹F NMR** (470 Hz, CDCl₃): δ -73.63 - -73.78 (m, CF₃ Major and CF₃ Minor) ppm. **IR** (Neat): 1757, 1559, 1465, 1457, 1378, 1288, 1241, 1172 cm⁻¹. **HRMS** (ESI) m/z: [M + Na]⁺ Calcd for C₂₆H₂₁ClF₆N₂O₈SNa 693.0509; Found 693.0504.

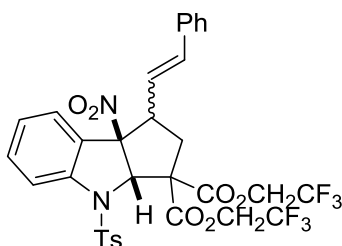
8-Methyl 3,3-bis(2,2,2-trifluoroethyl) (1S,3aS,8bR)-8b-nitro-4-tosyl-1-vinyl-1,3a,4,8b-tetrahydrocyclopenta[b]indole-3,3,8(2H)-tricarboxylate (108k')



Based on the typical procedure with the exclusion of tetrabutylammonium iodide, the title compound was obtained as a colourless oil (34.0 mg, 0.0490 mmol) in 88% yield after column chromatography (20 – 30% ethyl acetate in hexane). **¹H NMR** (400 MHz, CDCl₃): δ 7.96 (dd, *J* = 8.4, 0.8 Hz, 1H, CH_{Ar}), 7.73 (dd, *J* = 7.6, 0.8 Hz, 1H, CH_{Ar}), 7.55 (t, *J* = 8.0 Hz, 1H, CH_{Ar}), 7.49 (d, *J* = 8.4 Hz, 2H, CH_{Ar} Tosyl), 7.17 (d, *J* = 8.0 Hz, 2H, CH_{Ar} Tosyl), 6.03 (s, 1H, Ts-N-CH), 6.00 – 5.91 (m, 1H, CH=CH₂), 5.09 (d, *J* = 10.4 Hz, 1H, CH=CH₂), 5.08 (d, *J* = 16.8 Hz, 1H, CH=CH₂), 4.87 – 4.74 (m, 2H, OCH₂CF₃), 4.57 – 4.47 (m, 1H, OCH₂CF₃), 4.46 – 4.37 (m, 1H, OCH₂CF₃), 3.81 (app q, *J* = 7.2 Hz, 1H, CH-CH=CH₂), 3.75 (s, 3H, OCH₃), 2.65 (dd, *J* = 14.0, 8.0 Hz, 1H, CH-CH₂), 2.54 (dd, *J* = 16.0, 8.0 Hz, 1H, CH-CH₂), 2.35 (s, 3H, CH₃ Tosyl) ppm. **¹³C NMR** (100 MHz, CDCl₃): δ 167.7 (C=O), 165.9 (C=O), 165.7 (C=O), 145.7 (C_{Ar}), 143.9 (C_{Ar}), 133.9 (CH=CH₂),

132.1 (C_{Ar}), 132.0 (CH_{Ar}), 130.0 (CH_{Ar} Tosyl), 129.4 (C_{Ar}), 128.2 (CH_{Ar}), 127.71 (CH_{Ar} Tosyl), 127.66 (C_{Ar}), 122.5 (q, *J* = 280 Hz, CF₃), 122.4 (q, *J* = 280 Hz, CF₃), 121.4 (CH_{Ar}), 119.0 (CH=CH₂), 102.2 (C-NO₂), 76.7 (Ts-N-CH), 64.1 (C-(CO₂CH₂CF₃)₂), 62.6 – 61.1 (m, CH₂CF₃), 53.3 (CH-CH=CH₂), 52.5 (OCH₃), 40.7 (CH-CH₂), 21.6 (CH₃ Tosyl) ppm. **¹⁹F NMR** (470 Hz, CDCl₃): δ -73.79 - -73.84 (m, CF₃) ppm. **IR** (Neat): 1753, 1733, 1731, 1557, 1371, 1286, 1242, 1169, 1089 cm⁻¹. **HRMS** (ESI) *m/z*: [M + Na]⁺ Calcd for C₂₈H₂₄F₆N₂O₁₀SNa 717.0954; Found 717.0950.

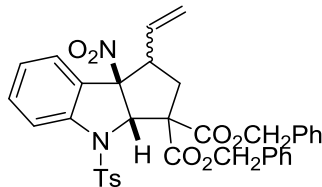
*Bis(2,2,2-trifluoroethyl)(3a*S*,8b*R*)-8b-nitro-1-styryl-4-tosyl-1,3a,4,8b-tetrahydrocyclopenta[*b*]indole-3,3(2*H*)-dicarboxylate (112/112')*



Based on the typical procedure, the title compound was obtained as a colourless film (29.2 mg, 0.0410 mmol) in 73% yield after column chromatography (20% ethyl acetate in hexane). **¹H NMR** (500 MHz, CDCl₃): δ 7.78 – 7.12 (m, 26H, CH_{Ar} Major and CH_{Ar} Minor), 6.57 (d, *J* = 15.0 Hz, 1H, CH=CH-Ph Minor), 6.46 (d, *J* = 15.0 Hz, 1H, CH=CH-Ph Major), 6.35 (s, 1H, Ts-N-CH Minor), 6.27 (s, 1H, Ts-N-CH Major), 6.01 (dd, *J* = 15.0, 10.0 Hz, 1H, CH=CH-Ph Major), 5.78 (dd, *J* = 15.0, 10.0 Hz, 1H, CH=CH-Ph Minor), 5.03 – 4.96 (m, 1H, OCH₂CF₃ Major), 4.86 – 4.73 (m, 1H of OCH₂CF₃ Major and 2H of OCH₂CF₃ Minor), 4.60 – 4.52 (m, 2H, OCH₂CF₃ Major and OCH₂CF₃ Minor), 4.50 – 4.42 (m, 2H, OCH₂CF₃ Major and OCH₂CF₃ Minor), 3.62 (app q, *J* = 10.0 Hz, 1H, CH-CH=CH₂ Minor), 3.48 (dt, *J* = 15.0, 10.0 Hz, 1H, CH-CH=CH₂ Major), 2.73 (dd, *J* = 12.5, 5.0 Hz, 1H, CH-CH₂ Minor), 2.56 (dd, *J* =

15.0, 5.0 Hz, 1H, CH-CH₂ Major), 2.48 (dd, *J* = 12.5, 5.0 Hz, 1H, CH-CH₂ Minor), 2.38 (app t, *J* = 15.0 Hz, 1H, CH-CH₂ Major), 2.33 (s, 3H, CH₃ Major), 2.32 (s, 3H, CH₃ Minor) ppm. **¹³C NMR** (125 MHz, CDCl₃): δ 167.74 (C=O Major), 167.66 (C=O Minor), 166.0 (C=O Minor), 164.5 (C=O Major), 145.5 (C_{Ar} Major), 145.4 (C_{Ar} Minor), 144.2 (C_{Ar} Major), 142.2 (C_{Ar} Minor), 136.6 (CH=CH-Ph Minor), 135.8 (C_{Ar} Major), 135.6 (C_{Ar} Minor), 135.5 (CH=CH-Ph Major), 132.3 (CH_{Ar} Major), 132.1 (C_{Ar} Major and CH_{Ar} Minor), 129.9 (CH_{Ar} Tosyl Major and CH_{Ar} Tosyl Minor), 128.8 (CH_{Ar} Major), 128.7 (CH_{Ar} Minor), 128.6 (CH_{Ar} Minor), 128.5 (2 × CH_{Ar} Major), 128.0 (C_{Ar} Minor), 127.7 (CH_{Ar} Tosyl Major), 127.6 (CH_{Ar} Tosyl Minor), 126.7 (CH_{Ar} Minor), 126.5 (CH_{Ar} Major), 126.4 (CH_{Ar} Minor), 126.2 (CH_{Ar} Minor), 125.4 (CH_{Ar} Major), 124.1 (C_{Ar} Major), 122.6 (q, *J* = 275 Hz, CF₃ Major and CF₃ Minor), 122.5 (q, *J* = 275 Hz, CF₃ Major and CF₃ Minor), 122.5 (CH=CH-Ph Major), 122.3 (CH=CH-Ph Minor), 118.0 (CH_{Ar} Major), 117.6 (CH_{Ar} Minor), 102.3 (C-NO₂ Minor), 101.3 (C-NO₂ Major), 73.6 (Ts-N-CH Major and Ts-N-CH Minor), 64.8 (C-(CO₂CH₂CF₃)₂ Minor), 63.9 (C-(CO₂CH₂CF₃)₂ Major), 62.6 – 61.5 (m, CH₂CF₃ Major and CH₂CF₃ Minor), 53.6 (CH-CH=Ph Minor), 49.9 (CH-CH=Ph Major), 40.3 (CH-CH₂ Minor), 38.0 (CH-CH₂ Major), 21.6 (CH₃ Major and CH₃ Minor) ppm. **¹⁹F NMR** (470 Hz, CDCl₃): δ -73.48 (t, *J* = 8.0 Hz, CF₃ Minor), -73.59 (t, *J* = 8.0 Hz, CF₃ Major), -73.67 - -73.73 (m, CF₃ Major and CF₃ Minor) ppm. **IR** (Neat): 1752, 1549, 1464, 1417, 1370, 1286, 1246, 1170, 1089, 1071 cm⁻¹. **HRMS** (ESI) *m/z*: [M + Na]⁺ Calcd for C₃₂H₂₆F₆N₂O₈SNa 735.1212; Found 735.1186.

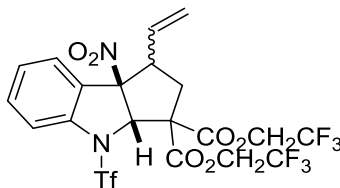
*Dibenzyl (3a*S*,8b*R*)-8b-nitro-4-tosyl-1-vinyl-1,3a,4,8b-tetrahydrocyclopenta[*b*]indole-3,3(2*H*)-dicarboxylate (113/113')*



Based on the typical procedure, the title compound was obtained as a colourless film (18.0 mg, 0.0276 mmol) in 48% yield after column chromatography (20 – 50% ethyl acetate in hexane). **¹H NMR** (400 MHz, CDCl₃): δ 7.75 (d, *J* = 8.4 Hz, 1H, CH_{Ar} Major), 7.64 (d, *J* = 8.0 Hz, 1H, CH_{Ar} Minor), 7.51 – 7.06 (m, 34H, CH_{Ar} Major and CH_{Ar} Minor), 6.40 (s, 1H, Ts-N-CH Minor), 6.33 (s, 1H, Ts-N-CH Major), 5.74 (ddd, *J* = 17.4, 10.2, 7.6 Hz, 1H, CH=CH₂ Major), 5.48 – 5.39 (m, 1H of CH=CH₂ Major and 1H of CH=CH₂ Minor), 5.30 – 5.06 (m, 11H, 1 × CH=CH₂ Major, 2 × OCH₂ Major, 1 × CH=CH₂ Minor and 2 × OCH₂ Minor), 3.40 (app q, *J* = 8.0 Hz, 1H, CH-CH=CH₂ Minor), 3.24 (dt, *J* = 14.4, 6.4 Hz, 1H, CH-CH=CH₂ Major), 2.59 (dd, *J* = 13.6, 6.8 Hz, 1H, CH-CH₂ Minor), 2.43 (dd, *J* = 13.6, 5.2 Hz, 1H, CH-CH₂ Major), 2.37 – 2.29 (m, 7H, CH₃ Major, CH₃ Minor and CH-CH₂ Minor), 2.22 (app t, *J* = 14.0 Hz, 1H, CH-CH₂ Major) ppm. **¹³C NMR** (100 MHz, CDCl₃): δ 169.40 (C=O Major), 169.37 (C=O Minor), 167.5 (C=O Minor), 166.3 (C=O Major), 145.0 (C_{Ar} Major), 144.9 (C_{Ar} Minor), 144.4 (C_{Ar} Major), 142.5 (C_{Ar} Minor), 135.2 (C_{Ar} Major), 135.0 (C_{Ar} Minor), 134.9 (C_{Ar} Minor), 134.7 (C_{Ar} Major), 132.8 (C_{Ar} Minor), 132.6 (C_{Ar} Major), 132.5 (CH=CH₂ Minor), 132.2 (CH=CH₂ Major), 132.0 (CH_{Ar} Major), 131.9 (CH_{Ar} Minor), 129.7 (CH_{Ar} Major and CH_{Ar} Minor), 128.58 (CH_{Ar} Major), 128.56 (CH_{Ar} Major), 128.55 (CH_{Ar} Major), 128.50 (CH_{Ar} Minor), 128.48 (CH_{Ar} Minor), 128.4 (CH_{Ar} Major), 128.3 (C_{Ar} Minor), 128.2 (CH_{Ar} Minor), 127.7 (CH_{Ar} Major), 127.6 (CH_{Ar} Minor), 126.3 (CH_{Ar} Minor), 125.9 (CH_{Ar} Minor), 125.1 (CH_{Ar} Major), 124.4 (C_{Ar} Major), 121.0 (CH=CH₂ Minor), 120.6 (CH=CH₂ Major), 118.1 (CH_{Ar} Major), 117.7 (CH_{Ar} Minor), 102.6 (C-

NO₂ Minor), 101.1 (C-NO₂ Major), 73.7 (Ts-N-CH Major), 73.3 (Ts-N-CH Minor), 68.6 (OCH₂ Major), 68.4 (OCH₂ Major), 68.3 (OCH₂ Minor), 68.2 (OCH₂ Minor), 65.0 (C-(CO₂Bn)₂ Minor), 64.2 (C-(CO₂Bn)₂ Major), 53.6 (CH-CH=CH₂ Minor), 50.4 (CH-CH=CH₂ Major), 39.6 (CH-CH₂ Minor), 37.6 (CH-CH₂ Major), 21.6 (CH₃ Major and CH₃ Minor) ppm. **IR** (Neat): 1730, 1550, 1456, 1368, 1269, 1241, 1170, 1089, 1068 cm⁻¹. **HRMS** (ESI) m/z: [M + Na]⁺ Calcd for C₃₆H₃₂N₂O₈SNa 675.1777; Found 675.1780.

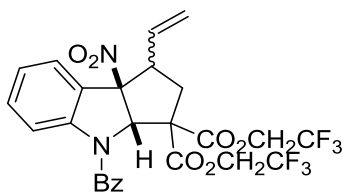
*Bis(2,2,2-trifluoroethyl) (3a*S*,8b*R*)-8b-nitro-4-((trifluoromethyl)sulfonyl)-1-vinyl-1,3a,4,8b-tetrahydrocyclopenta[*b*]indole-3,3(2*H*)-dicarboxylate (114a/114a')*



Based on the typical procedure, the title compound was obtained as a white solid (18.3 mg, 0.0298 mmol) in 61% yield after column chromatography (20% ethyl acetate in hexane). **¹H NMR** (400 MHz, CDCl₃): δ 7.73 (d, *J* = 8.0 Hz, 1H, CH_{Ar}), 7.64 (d, *J* = 8.0 Hz, 1H, CH_{Ar}), 7.58 – 7.49 (m, 4H, CH_{Ar}), 7.40 – 7.31 (m, 2H, CH_{Ar}), 6.56 (s, 1H, Tf-N-CH), 6.49 (s, 1H, Tf-N-CH), 5.90 (ddd, *J* = 17.3, 10.2, 7.2 Hz, 1H, CH=CH₂), 5.64 (ddd, *J* = 17.6, 9.2, 8.4 Hz, 1H, CH=CH₂), 5.43 – 5.36 (m, 3H, CH=CH₂), 5.30 (d, *J* = 20.0 Hz, 1H, CH=CH₂), 4.89 – 4.49 (m, 6H, OCH₂CF₃), 4.40 – 4.28 (m, 2H, OCH₂CF₃), 3.54 – 3.44 (m, 2H, CH-CH=CH₂), 2.75 (dd, *J* = 13.6, 6.4 Hz, 1H, CH-CH₂), 2.59 (ddd, *J* = 14.0, 5.6, 1.2 Hz, 1H, CH-CH₂), 2.53 (dd, *J* = 13.6, 9.2 Hz, 1H, CH-CH₂), 2.33 (app t, *J* = 14.0 Hz, 1H, CH-CH₂) ppm. **¹³C NMR** (125 MHz, CDCl₃): δ 167.0 (C=O), 166.8 (C=O), 165.3 (C=O), 164.5 (C=O), 141.4 (C_{Ar}), 139.6 (C_{Ar}), 133.0 (CH_{Ar}), 132.7 (CH_{Ar}), 131.3 (CH=CH₂), 131.0 (CH=CH₂), 129.1 (CH_{Ar}), 127.2 (CH_{Ar}), 127.1 (CH_{Ar}), 127.0 (C_{Ar}),

126.5 (CH_{Ar}), 123.1 (C_{Ar}), 122.5 (CH=CH₂), 122.33 (q, *J* = 275 Hz, CF₃), 122.31 (q, *J* = 275 Hz, CF₃), 122.2 (q, *J* = 275 Hz, CF₃), 122.1 (q, *J* = 275 Hz, CF₃), 121.9 (CH=CH₂), 115.9 (CH_{Ar}), 115.5 (CH_{Ar}), 101.6 (C-NO₂), 100.5 (C-NO₂), 74.7 (Tf-N-CH), 74.3 (Tf-N-CH), 64.0 (C-(CO₂CH₂CF₃)₂), 63.5 (C-(CO₂CH₂CF₃)₂), 62.7 – 61.3 (m, CH₂CF₃), 53.4 (CH-CH=CH₂), 50.0 (CH-CH=CH₂), 40.0 (CH-CH₂), 37.9 (CH-CH₂) ppm. **¹⁹F NMR** (470 Hz, CDCl₃): δ -71.39 (s, N-SO₂-CF₃ Major), -72.11 (s, N-SO₂-CF₃ Minor), -73.52 (t, *J* = 8.0 Hz, CH₂CF₃ Minor), -73.61 (t, *J* = 8.5 Hz, CH₂CF₃ Major), -73.74 - -73.80 (m, CH₂CF₃ Major and CH₂CF₃ Minor) ppm. **IR** (Neat): 1756, 1559, 1465, 1412, 1350, 1286, 1222, 1168, 1142, 1073 cm⁻¹. **HRMS** (ESI) *m/z*: [M + Na]⁺ Calcd for C₂₀H₁₅F₉N₂O₈SNa 637.0303; Found 637.0276.

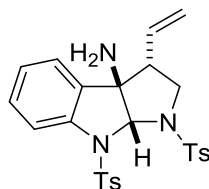
*Bis(2,2,2-trifluoroethyl)(3a*S*,8b*R*)-4-benzoyl-8b-nitro-1-vinyl-1,3a,4,8b tetrahydrocyclopenta[*b*]indole-3,3(2*H*)-dicarboxylate (114*b*/114*b*)*



Based on the typical procedure, the title compound was obtained as a colourless oil (7.00 mg, 0.0119 mmol) in 21% yield. NMR data consistent with literature.⁶² **IR** (Neat): 1751, 1749, 1658, 1550, 1480, 1379, 1349, 1281, 1158 cm⁻¹ (IR provided as not previously reported in the literature).

4.5.4 Chemical transformation of cyclopenta[*b*]indoline derivatives

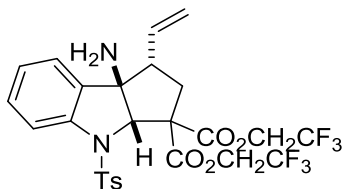
(3*S*,3*aS*,8*aS*)-1,8-Ditosyl-3-vinyl-2,3,8,8*a*-tetrahydropyrrolo[2,3-*b*]indol-3*a*(1*H*)-amine
(116)



Zinc powder (92.7 mg, 1.42 mmol, 21.5 equiv) was slowly added to a solution of **115**⁶¹ (35.6 mg, 0.0660 mmol, 1 equiv) and trimethylsilyl chloride (0.170 mL, 1.34 mmol, 20.3 equiv) in methanol at 0 °C. After stirring the reaction suspension at 0 °C for 1 h, the suspension was filtered and washed with methanol (2 × 2.5 mL) then dichloromethane (2 × 2.5 mL). After the filtrate was washed with saturated sodium bicarbonate solution (15 mL), organic fraction was isolated while aqueous fraction was extracted with dichloromethane (3 × 15 mL). The combined organic fractions were dried over sodium sulfate and concentrated under reduced pressure. Column chromatography was performed to yield the title compound as a white solid (24.6 mg, 0.0483 mmol, 73% yield). ¹H NMR (500 MHz, CDCl₃): δ 7.99 (d, *J* = 8.5 Hz, 2H, CH_{Ar} Tosyl), 7.69 (d, *J* = 8.5 Hz, 2H, CH_{Ar} Tosyl), 7.60 (d, *J* = 8.5 Hz, 1H, CH_{Ar}), 7.34 – 7.29 (m, 3H, CH_{Ar} Tosyl & CH_{Ar}), 7.18 (d, *J* = 8 Hz, 2H CH_{Ar} Tosyl), 7.08 (d, *J* = 7 Hz, 1H CH_{Ar}), 7.03 (t, *J* = 7 Hz, 1H CH_{Ar}), 6.46 (s, 1H, TsN-CH-NTs), 5.43 – 5.36 (m, 1H, CH=CH₂), 5.17 (d, *J* = 10 Hz, 1H, CH=CH₂), 5.11 (d, *J* = 17 Hz, 1H, CH=CH₂), 4.47 (d, *J* = 22 Hz, 2H, NH₂), 3.79 (dd, *J* = 11.8, 6.5 Hz, 1H, CH₂-NTs), 3.10 (m, 1H, CH-CH=CH₂), 2.77 (t, *J* = 12 Hz, 1H, CH₂-NTs), 2.43 (s, 3H, CH₃), 2.34 (s, 3H, CH₃) ppm. ¹³C NMR (125 MHz, CDCl₃): δ 144.4 (C_{Ar}), 143.7 (C_{Ar}), 143.3 (C_{Ar}), 137.2 (C_{Ar}), 134.4 (C_{Ar}), 132.8 (CH=CH₂), 130.3 (CH_{Ar}), 129.6 (CH_{Ar} Tosyl), 129.5 (CH_{Ar} Tosyl), 127.9 (CH_{Ar} Tosyl), 127.6 (CH_{Ar} Tosyl), 126.7 (CH_{Ar}), 126.6(C_{Ar}),

124.0(CH_{Ar}), 119.6 (CH=CH₂), 116.2 (CH_{Ar}), 82.0 (TsN-CH-NTs), 80.5 (C-NH₂), 50.6 (CH₂-NTs), 49.2 (CH-CH=CH₂), 21.61 (CH₃), 21.57 (CH₃) ppm. **IR** (Neat): 3510, 3504, 1363, 1340, 1172 cm⁻¹. **HRMS** (ESI) m/z: [M + Na]⁺ Calcd for C₂₆H₂₇N₃O₄S₂Na 532.1341; Found 532.1364. **Melting point**: 177.4 – 179.8 °C.

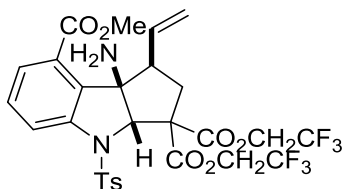
*Bis(2,2,2-trifluoroethyl)(3a*S*,8b*R*)-8b-amino-4-tosyl-1-vinyl-1,3a,4,8b-tetrahydrocyclopenta[*b*]indole-3,3(2*H*)-dicarboxylate (117a)*



A solution of **108a** (30.1 mg, 47.3 μmol, 1 equiv) and trimethylsilyl chloride (0.150 mL, 128 mg, 1.18 mmol, 25 equiv) in methanol was cooled to 0 °C prior to the slow addition of zinc powder (62.4 mg, 0.954 mmol, 20 equiv). After the reaction was stirred at 0 °C for 2 h 20 mins, another portion of trimethylsilyl chloride (0.0500 mL, 42.8 mg, 0.394 mmol, 8 equiv) was added and the reaction was stirred at room temperature for 2 h then 70 °C for 30 mins. The reaction was cooled to room temperature and filtered. The insoluble solid was washed with methanol (1 mL) and dichloromethane (3 × 1 mL). The filtrate and the combined washings were treated with saturated sodium bicarbonate solution (10 mL) and diluted with dichloromethane (10 mL). The organic fraction was isolated and the aqueous fraction was extracted with dichloromethane (2 × 10 mL). The combined organic fractions were dried over sodium sulfate then concentrated under reduced pressure. ¹H NMR analysis of the crude residue revealed that approximately 66% conversion was completed. In order to maximise the conversion, a solution of the crude residue and trimethylsilyl chloride (0.100 mL, 85.6 mg, 0.788 mmol, 17 equiv) in

methanol (1 mL) was cooled to 0 °C prior to the slow addition of zinc powder (33.5 mg, 0.512 mmol, 11 equiv). The reaction was stirred for 35 mins at 0 °C then filtered. Washing and extraction were carried out as previous. After column chromatography (40% ethyl acetate in hexane), the title compound was obtained as a colourless oil film (22.0 mg, 36.3 μ mol) in 77% yield. **¹H NMR** (400 MHz, CDCl₃): δ 7.71 (d, J = 8.0 Hz, 1H, CH_{Ar}), 7.55 (d, J = 8.0 Hz, 2H, CH_{Ar}), 7.38 – 7.34 (m, 1H, CH_{Ar}), 7.16 (d, J = 8.0 Hz, 2H, CH_{Ar}), 7.09 – 7.03 (m, 2H, CH_{Ar}), 5.72 (ddd, J = 17.4, 10.0, 7.2 Hz, 1H, CH=CH₂), 5.61 (s, 1H, Ts-N-CH), 5.19 (d, J = 8.0 Hz, 1H, CH=CH₂), 5.08 (d, J = 16.0 Hz, 1H, CH=CH₂), 5.01 – 4.91 (m, 1H, OCH₂CF₃), 4.81 – 4.72 (m, 1H, OCH₂CF₃), 4.53 – 4.37 (m, 2H, OCH₂CF₃), 4.08 (bs, 2H, NH₂), 2.85 (dt, J = 16.0, 4.0 Hz, 1H, CH-CH=CH₂), 2.35 – 2.30 (m, 4H, CH₃ and CH-CH₂), 2.19 (app t, J = 16.0 Hz, 1H, CH-CH₂) ppm. **¹³C NMR** (100 MHz, CDCl₃): δ 168.6 (C=O), 165.6 (C=O), 144.7 (C_{Ar}), 143.7 (C_{Ar}), 134.7 (CH=CH₂), 133.3 (C_{Ar}), 130.6 (CH_{Ar}), 129.5 (CH_{Ar} Tosyl), 128.7 (C_{Ar}), 127.7 (CH_{Ar} Tosyl), 126.7 (CH_{Ar}), 124.8 (CH_{Ar}), 122.7 (q, J = 280 Hz, CF₃), 122.6 (q, J = 280 Hz, CF₃), 118.5 (CH=CH₂), 117.6 (CH_{Ar}), 79.7 (C-NH₂), 70.5 (Ts-N-CH), 63.4 (C-(CO₂CH₂CF₃)₂), 61.7 (q, J = 40.0 Hz, CH₂CF₃), 61.6 (q, J = 40.0 Hz, CH₂CF₃), 45.1 (CH-CH=CH₂), 36.3 (CH-CH₂), 21.5 (CH₃) ppm. **¹⁹F NMR** (470 Hz, CDCl₃): δ -73.62 (t, J = 8.0 Hz, CF₃), -73.71 (t, J = 8.5 Hz, CF₃) ppm. **IR** (Neat): 3510, 3263, 1751, 1598, 1459, 1412, 1363, 1286, 1164, 1092, 1065 cm⁻¹. **HRMS** (ESI) m/z : [M + Na]⁺ Calcd for C₂₆H₂₄F₆N₂O₆SNa 629.1157; Found 629.1144.

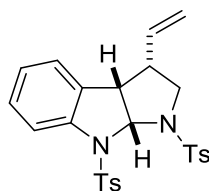
8-Methyl 3,3-bis(2,2,2-trifluoroethyl) (1S,3aS,8bR)-8b-amino-4-tosyl-1-vinyl-1,3a,4,8b-tetrahydrocyclopenta[b]indole-3,3,8(2H)-tricarboxylate (117k')



Zinc powder (76.7 mg, 1.17 mmol, 23 equiv) was slowly added to a solution of **108k'** (36.0 mg, 51.8 μmol , 1 equiv), trimethylsilyl chloride (0.140 mL, 0.120 g, 1.10 mmol, 21 equiv) in methanol (0.6 mL) at 0 °C. After stirring the reaction suspension at 0 °C for 30 mins, the suspension was filtered and the solids were washed with dichloromethane (3 \times 1 mL). The filtrate was diluted with dichloromethane (10 mL) and treated with saturated sodium bicarbonate solution (5 mL). Organic fraction was isolated and aqueous fraction was extracted with dichloromethane (2 \times 10 mL). The combined organic fractions were dried over magnesium sulfate and concentrated under reduced pressure. After column chromatography (40% ethyl acetate in hexane), the title compound was collected as a colourless oil (31.1 mg, 46.8 μmol) in 90% yield. $^1\text{H NMR}$ (400 MHz, CDCl_3): δ 7.98 (dd, $J = 8.2, 0.8$ Hz, 1H, CH_{Ar}), 7.70 – 7.66 (m, 3H, CH_{Ar}), 7.40 (t, $J = 8.0$ Hz, 1H, CH_{Ar}), 7.19 (d, $J = 8.0$ Hz, CH_{Ar}), 5.76 – 5.66 (m, 1H, $\text{CH}=\text{CH}_2$), 5.56 (s, 1H, Ts-N-CH), 5.09 – 5.05 (m, 2H, $\text{CH}=\text{CH}_2$), 4.92 – 4.75 (m, 2H, OCH_2CF_3), 4.49 – 4.34 (m, 2H, OCH_2CF_3), 3.83 (s, 3H, OCH_3), 3.20 – 3.14 (m, 1H, $\text{CH}-\text{CH}=\text{CH}_2$), 2.52 (dd, $J = 13.6, 7.2$ Hz, 1H, $\text{CH}-\text{CH}_2$), 2.36 – 2.32 (m, 4H, $\text{CH}-\text{CH}_2$ and CH_3 Tosyl) ppm. $^{13}\text{C NMR}$ (100 MHz, CDCl_3): δ 168.9 (C=O), 167.3 (C=O), 166.5 (C=O), 144.7 (C_{Ar}), 144.1 (C_{Ar}), 134.4 ($\text{CH}=\text{CH}_2$), 133.9 (C_{Ar}), 133.8 (C_{Ar}), 129.9 (CH_{Ar}), 129.6 (CH_{Ar} Tosyl), 128.1 (CH_{Ar} Tosyl), 127.62 (C_{Ar}), 127.59 (CH_{Ar}), 122.7 (q, $J = 275.0$ Hz, CF_3), 120.6 (CH_{Ar}), 118.1 ($\text{CH}=\text{CH}_2$), 80.2 (C-NH₂), 74.6 (Ts-N-CH), 64.8 (C-($\text{CO}_2\text{CH}_2\text{CF}_3$)₂), 61.7 (q, $J = 40.0$ Hz, OCH_2CF_3), 61.5 (q, $J = 40.0$ Hz, OCH_2CF_3), 52.9 ($\text{CH}-\text{CH}=\text{CH}_2$), 52.6 (OCH_3), 40.8 ($\text{CH}-\text{CH}_2$), 21.6 (CH_3

_{Tosyl}) ppm. ¹⁹F NMR (470 Hz, CDCl₃): δ -73.57 (t, *J* = 7.0 Hz, CF₃), -73.58 (t, *J* = 7.5 Hz, CF₃) ppm. IR (Neat): 1751, 1715, 1445, 1363, 1279, 1162, 1090 cm⁻¹. HRMS (ESI) *m/z*: [M + H]⁺ Calcd for C₂₈H₂₇F₆N₂O₈S 665.1392; Found 665.1415.

(3*R*,8*aS*)-1,8-Ditosyl-3-vinyl-1,2,3,3*a*,8,8*a*-hexahydropyrrolo[2,3-*b*]indole (**118**)

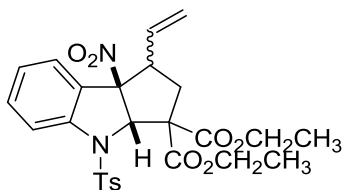


0.2 M AIBN (0.440 mL, 0.0880 mmol, 1.2 equiv) was added to a solution of **115**⁶¹ (40.9 mg, 75.8 μmol, 1 equiv) and tributyltin hydride (40.0 μL, 43.3 mg, 149 μmol, 2 equiv) in toluene (1 mL). After the reaction was heated at 80 °C for 48 h, the reaction was cooled to room temperature then CCl₄ (0.150 mL) was added and left stirring for 40 mins. The reaction was poured into saturated potassium fluoride solution (15 mL) and extracted with ethyl acetate. After drying the organic fraction with sodium sulfate, the solution was concentrated under reduced pressure. NMR analysis indicated that no conversion had occurred therefore the reaction crude was resubjected to the same reaction condition for a longer time of 96 h. Column chromatography (35% ethyl acetate in hexane) was performed to yield the title compound as a white solid (23.4 mg, 47.3 μmol) in 62% yield.

¹H NMR (500 MHz, CDCl₃): δ 7.96 (d, *J* = 8.0 Hz, 2H, CH_{Ar Tosyl}), 7.59 (d, *J* = 8.0 Hz, 2H, CH_{Ar Tosyl}), 7.52 (d, *J* = 8.5 Hz, 1H, CH_{Ar}), 7.32 (d, *J* = 8.0 Hz, 2H, CH_{Ar Tosyl}), 7.22 – 7.16 (m, 3H, CH_{Ar Tosyl} & CH_{Ar}), 7.03 (d, *J* = 7.5 Hz, 1H, CH_{Ar}), 6.98 (t, *J* = 7.5 Hz, 1H, CH_{Ar}), 6.44 (d, *J* = 7.0 Hz, 1H, N-CH-N), 5.50 (dt, *J* = 16.5, 9.5 Hz, 1H, CH=CH₂), 5.16 – 5.11 (m, 2H, CH=CH₂), 3.73 (dd, *J* = 11.3, 7.0 Hz, 1H, CH₂-NTs), 3.68 (t, *J* = 8.0 Hz,

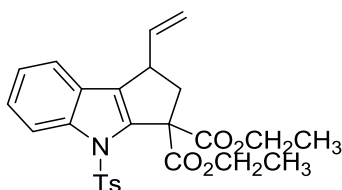
1H, CH-CH-CH=CH₂), 3.07 – 3.00 (m, 1H, CH-CH=CH₂), 2.69 (t, *J* = 11.5 Hz, 1H, CH₂-NTs), 2.44 (s, 3H, CH₃), 2.35 (s, 3H, CH₃) ppm. ¹³C NMR (125 MHz, CDCl₃): δ 144.2 (C_{Ar}), 143.5 (C_{Ar}), 142.2 (C_{Ar}), 137.4 (C_{Ar}), 134.5 (C_{Ar}), 133.7 (CH=CH₂), 129.6 (CH_{Ar}), 129.5 (CH_{Ar}), 128.6 (CH_{Ar}), 128.3 (C_{Ar}), 127.7 (CH_{Ar}), 127.4 (CH_{Ar}), 126.7 (CH_{Ar}), 124.1 (CH_{Ar}), 118.8 (CH=CH₂), 116.5 (CH_{Ar}), 81.1 (N-CH-N), 50.4 (N-CH₂), 49.7 (CH-CH-CH=CH₂), 47.6 (CH-CH=CH₂), 21.60 (CH₃), 21.56 (CH₃) ppm. IR (Neat): 1355, 1345, 1168, 1161, 1091, 1003 cm⁻¹. HRMS (ESI) *m/z*: [M + Na]⁺ Calcd for C₂₆H₂₆N₂O₄S₂Na 517.1232; Found 517.1221. **Melting point**: 171.1 – 175.3 °C.

*Diethyl (3a*S*,8b*R*)-8b-nitro-4-tosyl-1-vinyl-1,3a,4,8b-tetrahydrocyclopenta[*b*]indole-3,3(2*H*)-dicarboxylate (107a/107a')*



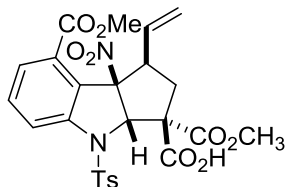
A suspension of **108a/108a'** (mixture of diastereomers, 28.3 mg, 44.5 μmol, 1 equiv) and potassium carbonate (14.1 mg, 102 μmol, 2.3 equiv) in ethanol (3 mL) was stirred overnight at room temperature. The reaction was diluted with water (5 mL). Organic fraction was isolated and aqueous fraction was extracted with diethyl ether (3 × 10 mL). Combined organic fractions were washed with brine (5 mL) and dried over sodium sulfate. After column chromatography (20% ethyl acetate in hexane), the title compound was collected as a white oil film (18.8 mg, 35.6 μmol) in 80% yield. The data collected for this compound matches that obtained for the direct cycloaddition.

Diethyl 4-tosyl-1-vinyl-1,4-dihydrocyclopenta[b]indole-3,3(2H)-dicarboxylate (119)



A suspension of **107a** (19.8 mg, 37.5 μmol , 1 equiv), sodium chloride (4.80 mg, 82.0 μmol , 2.2 equiv) and water (1 drop) in DMSO (0.500 mL) was heated in a microwave reactor at 170 $^{\circ}\text{C}$ for 5 mins. The reaction was diluted with water (4 mL) then extracted with ethyl acetate (3×10 mL). The combined organic extracts were dried over sodium sulfate and concentrated under reduced pressure. After column chromatography (20% ethyl acetate in hexane), the title compound was obtained as an off-white oil film (9.00 mg, 18.7 μmol) in 50% yield. **^1H NMR** (400 MHz, CDCl_3): δ 7.89 (d, $J = 8.4$ Hz, 2H, CH_{Ar}), 7.60 (dd, $J = 7.0, 1.6$ Hz, 1H, CH_{Ar}), 7.43 – 7.40 (m, 1H, CH_{Ar}), 7.23 (d, $J = 8.0$ Hz, 2H, CH_{Ar}), 7.20 – 7.13 (m, 2H, CH_{Ar}), 5.91 (ddd, $J = 17.3, 9.4, 8.0$ Hz, 1H, $\text{CH}=\text{CH}_2$), 5.22 (d, $J = 17.2$ Hz, 1H, $\text{CH}=\text{CH}_2$), 5.11 (d, $J = 10.0$ Hz, 1H, $\text{CH}=\text{CH}_2$), 4.31 – 4.17 (m, 4H, OCH_2CH_3), 3.88 (app q, $J = 6.0$ Hz, 1H, $\text{CH}-\text{CH}=\text{CH}_2$), 3.46 (dd, $J = 13.2, 7.6$ Hz, 1H, $\text{CH}-\text{CH}_2$), 2.93 (dd, $J = 12.8, 5.6$ Hz, 1H, $\text{CH}-\text{CH}_2$), 2.34 (s, 3H, CH_3 Tosyl), 1.29 (t, $J = 7.2$ Hz, 6H, OCH_2CH_3) ppm. **^{13}C NMR** (100 MHz, CDCl_3): δ 170.2 (C=O), 169.5 (C=O), 144.6 (C_{Ar}), 140.0 (C_{Ar}), 139.1 (C_{Ar}), 138.8 ($\text{CH}=\text{CH}_2$), 136.1 (C_{Ar}), 130.8 (C_{Ar}), 129.6 (CH_{Ar} Tosyl), 127.7 (CH_{Ar} Tosyl), 125.4 (C_{Ar}), 124.5 (CH_{Ar}), 123.0 (CH_{Ar}), 119.8 (CH_{Ar}), 116.0 ($\text{CH}=\text{CH}_2$), 114.3 (CH_{Ar}), 62.5 ($\text{C}-(\text{CO}_2\text{Et})_2$), 62.1 (OCH_2CH_3), 48.3 ($\text{CH}-\text{CH}_2$), 40.9 ($\text{CH}-\text{CH}=\text{CH}_2$), 21.6 (CH_3 Tosyl), 14.0 (OCH_2CH_3) ppm. **IR** (Neat): 1727, 1446, 1366, 1252, 1173 cm^{-1} . **HRMS** (ESI) m/z : $[\text{M} + \text{Na}]^+$ Calcd for $\text{C}_{26}\text{H}_{27}\text{NO}_6\text{SNa}$ 504.1457; Found 504.1475.

(1*R*,3*S*,3*aS*,8*bR*)-3,8-Bis(methoxycarbonyl)-8*b*-nitro-4-tosyl-1-vinyl-1,2,3,3*a*,4,8*b*-hexahydrocyclopenta[*b*]indole-3-carboxylic acid (**120**)



Ammonia solution (7 N in methanol, 2 mL) was added to **108k'** (33.5 mg, 48.2 mmol) at 5 °C. The reaction solution was stirred at 5 °C for 1 h then concentrated under reduced pressure. After column chromatography (5% methanol in dichloromethane), the title compound was obtained as a white solid (16.3 mg, 29.9 mmol) in 62% yield. **¹H NMR** (500 MHz, CDCl₃): δ 7.98 (d, *J* = 5.0 Hz, 1H, CH_{Ar}), 7.72 (d, *J* = 10.0 Hz, 1H, CH_{Ar}), 7.54 (t, *J* = 10.0 Hz, 1H, CH_{Ar}), 7.47 (d, *J* = 10.0 Hz, 2H, CH_{Ar Tosyl}), 7.17 (d, *J* = 5.0 Hz, 2H, CH_{Ar Tosyl}), 6.05 (ddd, *J* = 17.3, 9.8, 8.0 Hz, 1H, CH=CH₂), 5.90 (s, 1H, Ts-N-CH), 5.80 (bs, 1H, CO₂H), 5.08 (t, *J* = 15.0 Hz, 2H, CH=CH₂), 3.83 – 3.78 (m, 1H, CH-CH=CH₂), 3.74 (s, 3H, OCH₃), 3.57 (s, 3H, OCH₃), 2.78 (dd, *J* = 15.0, 10.0 Hz, 1H, CH-CH₂), 2.49 (dd, *J* = 15.0, 10.0 Hz, 1H, CH-CH₂), 2.35 (s, 3H, CH_{3 Tosyl}) ppm. **¹³C NMR** (100 MHz, CDCl₃): δ 171.4 (C=O), 170.2 (C=O), 165.8 (C=O), 145.7 (C_{Ar}), 143.9 (C_{Ar}), 135.2 (CH=CH₂), 132.3 (C_{Ar}), 131.6 (CH_{Ar}), 130.0 (CH_{Ar}), 129.7 (C_{Ar}), 128.7 (C_{Ar}), 128.0 (CH_{Ar}), 127.5 (CH_{Ar}), 120.7 (CH_{Ar}), 118.1 (CH=CH₂), 103.0 (C-NO₂), 78.2 (Ts-N-CH), 64.0 (C-CO₂H), 52.82 (CH-CH=CH₂ or OCH₃), 52.77 (CH-CH=CH₂ or OCH₃), 52.6 (OCH₃), 41.2 (CH-CH₂), 21.7 (CH_{3 Tosyl}) ppm. **IR** (Neat): 3438, 3196, 2954, 1730, 1688, 1685, 1553, 1436, 1374, 1294, 1238, 1173 cm⁻¹. **LRMS** (ESI) = 567, (M+Na)⁺. **Melting point**: 194.3 – 196.4 °C.

4.5.5 X-ray crystallographic information

Crystals of **108a** and **120** were recrystallised from dichloromethane/methanol and dichloromethane, respectively. Data for **108a** and **120** were collected at 100 K on crystals mounted on a Hampton Scientific cryoloop on Bruker QUEST. The structures were solved by intrinsic phasing methods with SHELXT, refined using full-matrix least-squares routines against F^2 with SHELXL-2014,⁹³ and visualised using OLEX2.⁹⁴ All non-hydrogen atoms were refined anisotropically. All hydrogen atoms were placed in calculated positions and refined using a riding model with fixed C–H distances of 0.95 Å (sp^2 CH), 1.00 Å (CH), 0.99 Å (CH₂), 0.98 Å (CH₃). The thermal parameters of all hydrogen atoms were estimated as $U_{iso}(H) = 1.2U_{eq}(C)$ except for CH₃ where $U_{iso}(H) = 1.5U_{eq}(C)$. A summary of crystallographic data given below.

Crystal data for **108a**: C₂₆H₂₂N₂O₈F₆S ($M = 636.53$ g/mol): monoclinic, space group $P2_1/n$ (no. 14), $a = 10.893(2)$ Å, $b = 19.835(4)$ Å, $c = 12.801(3)$ Å, $\beta = 96.80(3)^\circ$, $V = 2746.3(10)$ Å³, $Z = 4$, $T = 100$ K, $\mu(\text{Cu K}\alpha) = 1.907$ mm⁻¹, $D_{calc} = 1.5393$ g/cm³, 25858 reflections measured ($8.26^\circ \leq 2\theta \leq 132.76^\circ$), 4761 unique ($R_{int} = 0.0448$, $R_{sigma} = 0.0303$) which were used in all calculations. The final R_1 was 0.0351 ($I \geq 2\sigma(I)$) and wR_2 was 0.0870 (all data).

Crystal data for **120**: C₂₅H₂₄NO₁₁S ($M = 544.54$ g/mol): triclinic, space group $P-1$ (no. 2), $a = 8.5498(19)$ Å, $b = 9.5122(13)$ Å, $c = 16.619(2)$ Å, $\alpha = 95.944(10)^\circ$, $\beta = 100.270(12)^\circ$, $\gamma = 107.515(14)^\circ$, $V = 1250.3(4)$ Å³, $Z = 2$, $T = 100(2)$ K, $\mu(\text{Cu K}\alpha) = 1.699$ mm⁻¹, $D_{calc} = 1.4463$ g/cm³, 41132 reflections measured ($5.48^\circ \leq 2\theta \leq 145.62^\circ$), 4913 unique ($R_{int} = 0.0364$, $R_{sigma} = 0.0197$) which were used in all calculations. The final R_1 was 0.0571 ($I \geq 2\sigma(I)$) and wR_2 was 0.1637 (all data).

4.6 References

- (1) Budynina, E. M.; Ivanov, K. L.; Sorokin, I. D.; Melnikov, M. Y. *Synthesis* **2017**, *49*, 3035.
- (2) Ganesh, V.; Chandrasekaran, S. *Synthesis* **2016**, *48*, 4347.
- (3) Reissig, H.-U.; Zimmer, R. *Chem. Rev.* **2003**, *103*, 1151.
- (4) Schneider, T. F.; Kaschel, J.; Werz, D. B. *Angew. Chem. Int. Ed.* **2014**, *53*, 5504.
- (5) Takano, S.; Iwabuchi, Y.; Ogasawara, K. *J. Am. Chem. Soc.* **1987**, *109*, 5523.
- (6) Sato, M.; Uchimarui, F. *Chem. Pharm. Bull. (Tokyo)* **1981**, *29*, 3134.
- (7) Danishefsky, S.; Rovnyak, G. *J. Org. Chem.* **1975**, *40*, 114.
- (8) Grover, H. K.; Emmett, M. R.; Kerr, M. A. *Org. Biomol. Chem.* **2015**, *13*, 655.
- (9) Allen, B. D. W.; Lakeland, C. P.; Harrity, J. P. A. *Chem. - Eur. J.* **2017**, *23*, 13830.
- (10) Liu, L.; Montgomery, J. *J. Am. Chem. Soc.* **2006**, *128*, 5348.
- (11) Bowman, R. K.; Johnson, J. S. *Org. Lett.* **2006**, *8*, 573.
- (12) Dieskau, A. P.; Holzwarth, M. S.; Plietker, B. *J. Am. Chem. Soc.* **2012**, *134*, 5048.
- (13) Moran, J.; Smith, A. G.; Carris, R. M.; Johnson, J. S.; Krische, M. J. *J. Am. Chem. Soc.* **2011**, *133*, 18618.
- (14) Trost, B. M.; Chan, D. M. T. *J. Am. Chem. Soc.* **1983**, *105*, 2315.
- (15) Shimizu, I.; Ohashi, Y.; Tsuji, J. *Tetrahedron Lett.* **1985**, *26*, 3825.
- (16) Mei, L.-y.; Wei, Y.; Xu, Q.; Shi, M. *Organometallics* **2012**, *31*, 7591.
- (17) Goldberg, A. F. G.; Stoltz, B. M. *Org. Lett.* **2011**, *13*, 4474.
- (18) Li, W.-K.; Liu, Z.-S.; He, L.; Kang, T.-R.; Liu, Q.-Z. *Asian J. Org. Chem.* **2015**, *4*, 28.
- (19) Wendt, J. A.; Gauvreau, P. J.; Bach, R. D. *J. Am. Chem. Soc.* **1994**, *116*, 9921.
- (20) Brooks, B. A.; Blair, E. M.; Finch, R.; Lant, A. F. *Br. J. Clin. Pharmacol.* **1980**, *10*, 249.
- (21) Wei, F.; Ren, C.-L.; Wang, D.; Liu, L. *Chem. - Eur. J.* **2015**, *21*, 2335.
- (22) Zlotos, D. P.; Tränkle, C.; Holzgrabe, U.; Gündisch, D.; Jensen, A. A. *J. Nat. Prod.* **2014**, *77*, 2006.
- (23) Liu, Y.-P.; Zhao, Y.-L.; Feng, T.; Cheng, G.-G.; Zhang, B.-H.; Li, Y.; Cai, X.-H.; Luo, X.-D. *J. Nat. Prod.* **2013**, *76*, 2322.
- (24) Jadulco, R.; Edrada, R. A.; Ebel, R.; Berg, A.; Schaumann, K.; Wray, V.; Steube, K.; Proksch, P. *J. Nat. Prod.* **2004**, *67*, 78.
- (25) Liu, Z.-S.; Li, W.-K.; Kang, T.-R.; He, L.; Liu, Q.-Z. *Org. Lett.* **2015**, *17*, 150.
- (26) Halskov, K. S.; Næsberg, L.; Tur, F.; Jørgensen, K. A. *Org. Lett.* **2016**, *18*, 2220.
- (27) Trost, B. M.; Jiang, C. *Synthesis* **2006**, *2006*, 369.
- (28) Hong, A. Y.; Stoltz, B. M. *Eur. J. Org. Chem.* **2013**, *2013*, 2745.
- (29) Quasdorf, K. W.; Overman, L. E. *Nature* **2014**, *516*, 181.
- (30) Næsberg, L.; Tur, F.; Meazza, M.; Blom, J.; Halskov, K. S.; Jørgensen, K. A. *Chem. Eur. J.* **2017**, *23*, 268.
- (31) Yuan, Z.; Wei, W.; Lin, A.; Yao, H. *Org. Lett.* **2016**, *18*, 3370.
- (32) Trost, B. M.; Morris, P. J.; Sprague, S. J. *J. Am. Chem. Soc.* **2012**, *134*, 17823.
- (33) Seeman, J. I. *Chem. Rev.* **1983**, *83*, 83.
- (34) Yamamoto, K.; Ishida, T.; Tsuji, J. *Chem. Lett.* **1987**, *16*, 1157.
- (35) Parsons, A. T.; Campbell, M. J.; Johnson, J. S. *Org. Lett.* **2008**, *10*, 2541.
- (36) Cao, R.; Zhang, J.; Zhou, H.; Yang, H.; Jiang, G. *Org. Biomol. Chem.* **2016**, *14*, 2191.
- (37) Garve, L. K. B.; Werz, D. B. *Org. Lett.* **2015**, *17*, 596.
- (38) Yin, J.; Hyland, C. J. T. *J. Org. Chem.* **2015**, *80*, 6529.
- (39) Repka, L. M.; Reisman, S. E. *J. Org. Chem.* **2013**, *78*, 12314.

- (40) Schallenberger, M. A.; Newhouse, T.; Baran, P. S.; Romesberg, F. E. *J. Antibiot.* **2010**, *63*, 685.
- (41) Lathrop, S. P.; Movassaghi, M. *Chem. Sci.* **2014**, *5*, 333.
- (42) Welmaker, G. S.; Sabalski, J. E.; Smith, M. D. US20020058689A1, 2002.
- (43) Ngantchou, I.; Nyasse, B.; Denier, C.; Blonski, C.; Hannaert, V.; Schneider, B. *Bioorg. Med. Chem. Lett.* **2010**, *20*, 3495.
- (44) Chapman, O. L.; Eian, G. L. *J. Am. Chem. Soc.* **1968**, *90*, 5329.
- (45) Gataullin, R. R.; Ishberdina, R. R.; Shitikova, O. V.; Minnigulov, F. F.; Spirikhin, L. V.; Abdrakhmanov, I. B. *Chem. Heterocycl. Compd.* **2006**, *42*, 1025.
- (46) Murphy, J. A.; Scott, K. A.; Sinclair, R. S.; Lewis, N. *Tetrahedron Lett.* **1997**, *38*, 7295.
- (47) Welmaker, G. S.; Sabalski, J. E. *Tetrahedron Lett.* **2004**, *45*, 4851.
- (48) Prasad, B. A. B.; Buechele, A. E.; Gilbertson, S. R. *Org. Lett.* **2010**, *12*, 5422.
- (49) Roche, S. P.; Youte Tendoung, J.-J.; Treguier, B. *Tetrahedron* **2015**, *71*, 3549.
- (50) Barluenga, J.; Tudela, E.; Ballesteros, A.; Tomas, M. *J. Am. Chem. Soc.* **2009**, *131*, 2096.
- (51) Lian, Y.; Davies, H. M. L. *J. Am. Chem. Soc.* **2010**, *132*, 440.
- (52) Jing, C.; Cheng, Q.-Q.; Deng, Y.; Arman, H.; Doyle, M. P. *Org. Lett.* **2016**, *18*, 4550.
- (53) Kerr, M. A.; Keddy, R. G. *Tetrahedron Lett.* **1999**, *40*, 5671.
- (54) England, D. B.; Kuss, T. D. O.; Keddy, R. G.; Kerr, M. A. *J. Org. Chem.* **2001**, *66*, 4704.
- (55) Xiong, H.; Xu, H.; Liao, S.; Xie, Z.; Tang, Y. *J. Am. Chem. Soc.* **2013**, *135*, 7851.
- (56) Trost, B. M.; Ehmke, V.; O'Keefe, B. M.; Bringley, D. A. *J. Am. Chem. Soc.* **2014**, *136*, 8213.
- (57) Awata, A.; Arai, T. *Angew. Chem. Int. Ed.* **2014**, *53*, 10462.
- (58) Mc Cartney, D.; Guiry, P. J. *Chem. Soc. Rev.* **2011**, *40*, 5122.
- (59) Beletskaya, I. P.; Cheprakov, A. V. *Chem. Rev.* **2000**, *100*, 3009.
- (60) Montgomery, T. P.; Johns, A. M.; Grubbs, R. H. *Catalysts* **2017**, *7*, 87.
- (61) Rivinoja, D. J.; Gee, Y. S.; Gardiner, M. G.; Ryan, J. H.; Hyland, C. J. T. *ACS Catal.* **2017**, *7*, 1053.
- (62) Laugeois, M.; Ling, J.; Féraud, C.; Michelet, V.; Ratovelomanana-Vidal, V.; Vitale, M. R. *Org. Lett.* **2017**, *19*, 2266.
- (63) Sherry, B. D.; Furstner, A. *Chem. Commun.* **2009**, 7116.
- (64) Pelkey, E. T.; Gribble, G. W. *Synthesis* **1999**, 1999, 1117.
- (65) Lee, J. Y.; Ha, H.; Bae, S.; Han, I.; Joo, J. M. *Adv. Synth. Catal.* **2016**, *358*, 3458.
- (66) Trost, B. M.; Toste, F. D. *J. Am. Chem. Soc.* **1999**, *121*, 4545.
- (67) Campeau, L.-C.; Fagnou, K. *Chem. Commun.* **2006**, 1253.
- (68) Fairlamb, I. J. S.; Kapdi, A. R.; Lee, A. F. *Org. Lett.* **2004**, *6*, 4435.
- (69) Moumne, R.; Lavielle, S.; Karoyan, P. *J. Org. Chem.* **2006**, *71*, 3332.
- (70) Zard, S. Z. *Radical Reactions in Organic Synthesis*; Oxford University Press, 2003.
- (71) Sharpe, R. J.; Johnson, J. S. *J. Org. Chem.* **2015**, *80*, 9740.
- (72) Bergman, J.; Venemalm, L. *Tetrahedron* **1992**, *48*, 759.
- (73) Aoki, K.; Murayama, K.; Nishiyama, H. *J. Chem. Soc., Chem. Commun.* **1995**, 2221.
- (74) Holder, J. C.; Zou, L.; Marziale, A. N.; Liu, P.; Lan, Y.; Gatti, M.; Kikushima, K.; Houk, K. N.; Stoltz, B. M. *J. Am. Chem. Soc.* **2013**, *135*, 14996.
- (75) Bird, M. BScAdv (Hons) Thesis, University of Wollongong, 2017.

- (76) Seiser, T.; Saget, T.; Tran, D. N.; Cramer, N. *Angew. Chem. Int. Ed.* **2011**, *50*, 7740.
- (77) Perrotta, D.; Racine, S.; Vuilleumier, J.; de Nanteuil, F.; Waser, J. *Org. Lett.* **2015**, *17*, 1030.
- (78) Vemula, N.; Stevens, A. C.; Schon, T. B.; Pagenkopf, B. L. *Chem. Commun.* **2014**, *50*, 1668.
- (79) Vemula, N.; Pagenkopf, B. L. *Eur. J. Org. Chem.* **2015**, *2015*, 4900.
- (80) Moustafa, M. M. A. R.; Stevens, A. C.; Machin, B. P.; Pagenkopf, B. L. *Org. Lett.* **2010**, *12*, 4736.
- (81) Moustafa, M. M. A. R.; Pagenkopf, B. L. *Org. Lett.* **2010**, *12*, 4732.
- (82) Parsons, A. T.; Johnson, J. S. *J. Am. Chem. Soc.* **2009**, *131*, 14202.
- (83) Labadie, S. S.; Parmer, C. *Synth. Commun.* **2011**, *41*, 1752.
- (84) Swissman, N.; Jacoby, J. *Clin. Pharmacol. Ther.* **1964**, *5*, 136.
- (85) Ando, M.; Buechi, G.; Ohnuma, T. *J. Am. Chem. Soc.* **1975**, *97*, 6880.
- (86) Mei, L.-y.; Wei, Y.; Xu, Q.; Shi, M. *Organometallics* **2013**, *32*, 3544.
- (87) Takacs, J. M.; Xu, Z.; Jiang, X.-t.; Leonov, A. P.; Theriot, G. C. *Org. Lett.* **2002**, *4*, 3843.
- (88) Kurisaki, T.; Naniwa, T.; Yamamoto, H.; Imagawa, H.; Nishizawa, M. *Tetrahedron Lett.* **2007**, *48*, 1871.
- (89) Arisawa, M.; Terada, Y.; Takahashi, K.; Nakagawa, M.; Nishida, A. *J. Org. Chem.* **2006**, *71*, 4255.
- (90) Stokes, B. J.; Liu, S.; Driver, T. G. *J. Am. Chem. Soc.* **2011**, *133*, 4702.
- (91) Ren, W.; Yamane, M. *J. Org. Chem.* **2010**, *75*, 8410.
- (92) Raimer, B.; Wartmann, T.; Jones, P. G.; Lindel, T. *Eur. J. Org. Chem.* **2014**, *2014*, 5509.
- (93) Sheldrick, G. *Acta Crystallogr., Sect. A* **2015**, *71*, 3.
- (94) Dolomanov, O. V.; Bourhis, L. J.; Gildea, R. J.; Howard, J. A. K.; Puschmann, H. *J. Appl. Crystallogr.* **2009**, *42*, 339.

Appendix 1

Supporting figure for Chapter 2

Design and synthesis of a novel dual-action prodrug to target glioblastoma multiforme
via lysine-specific demethylase 1 (LSD1) inhibition and glutathione depletion

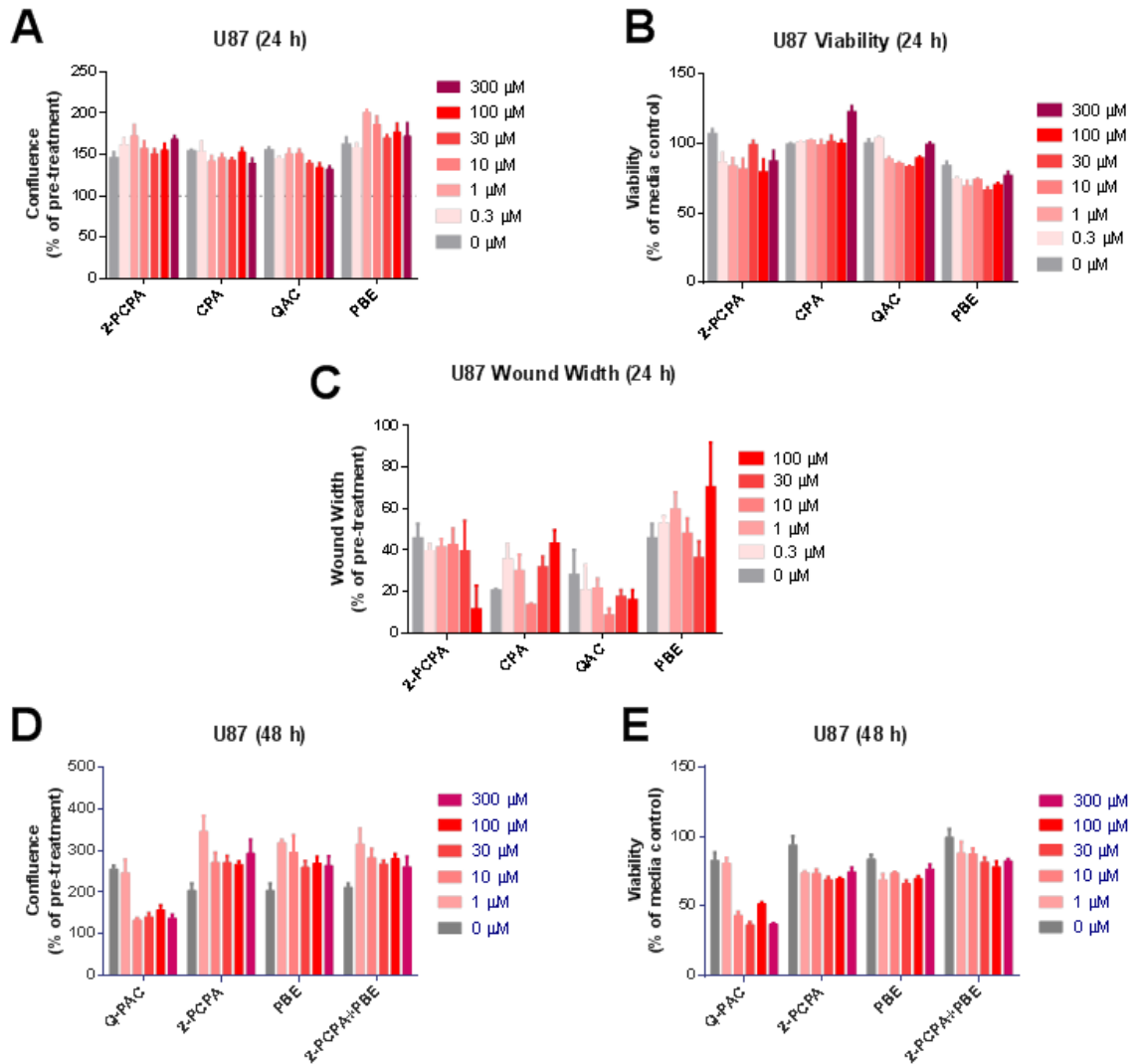


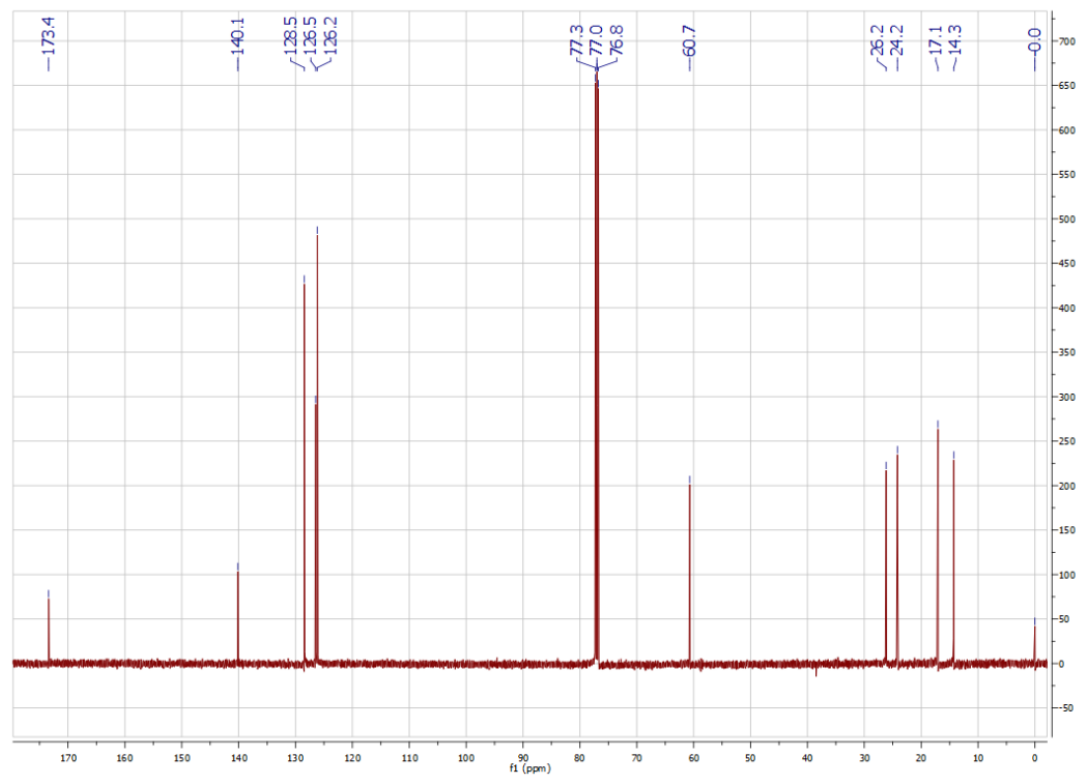
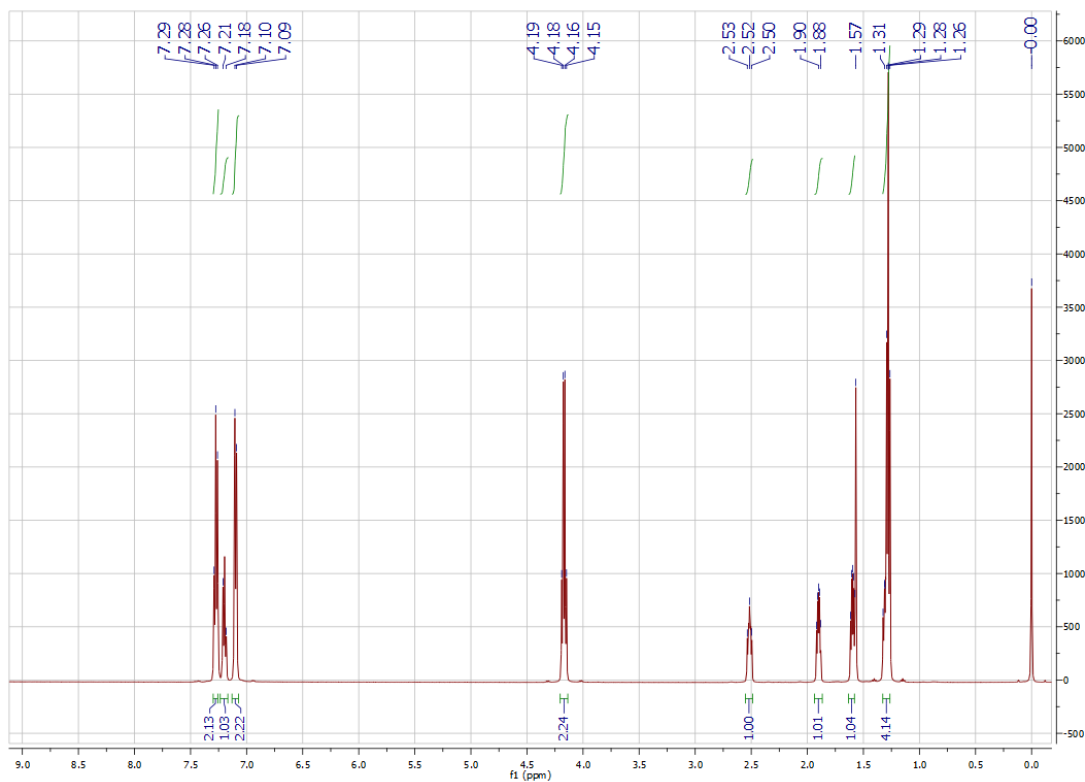
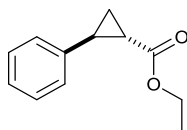
Figure A1: U87 cells show no response to Q-PAC constituent molecules. U87 cultures were treated with the components of Q-PAC (2-PCPA, CPA and PBE) and the phenyl-free control compound QAC, with their confluence (A), viability (B) and migration (C) assessed after 24 h ($n=4$ per concentration). (D-E) Co-treatment with 2-PCPA and PBE did not affect confluence (D) or viability (E) of U87 cultures over a 48 h period ($n=3$ per concentration). Data represent mean \pm SEM, * $P<0.05$, ** $P<0.01$, *** $P<0.001$, **** $P<0.0001$ compared to vehicle control.

Appendix 2

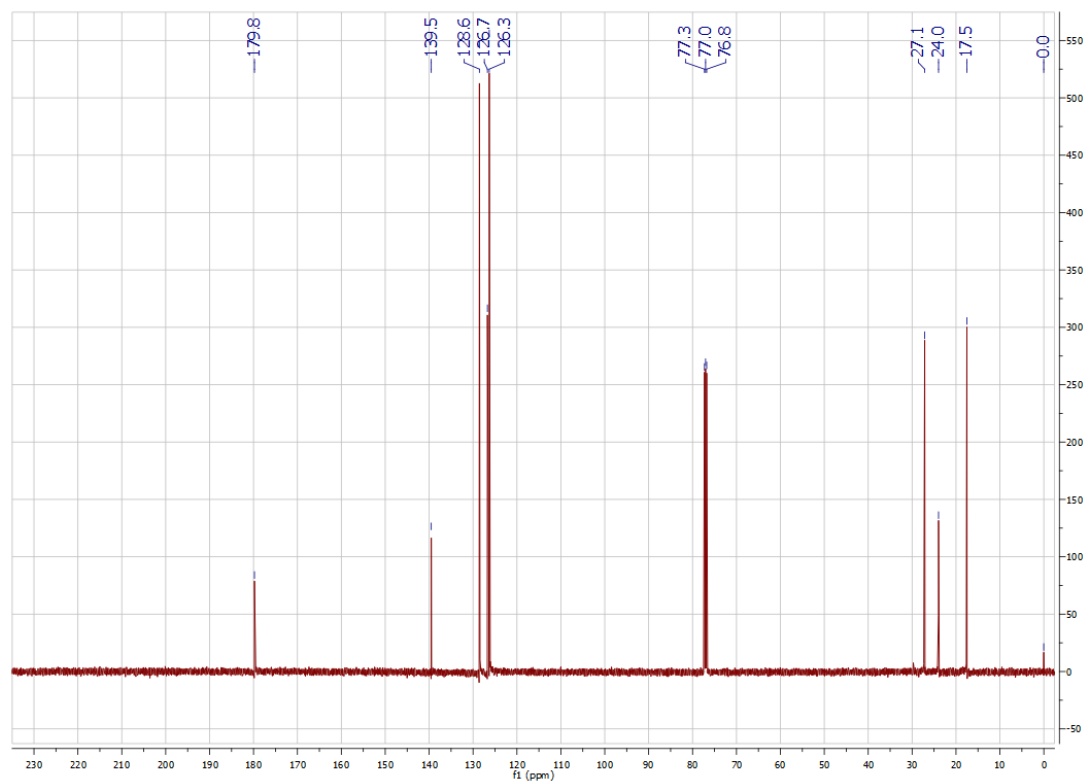
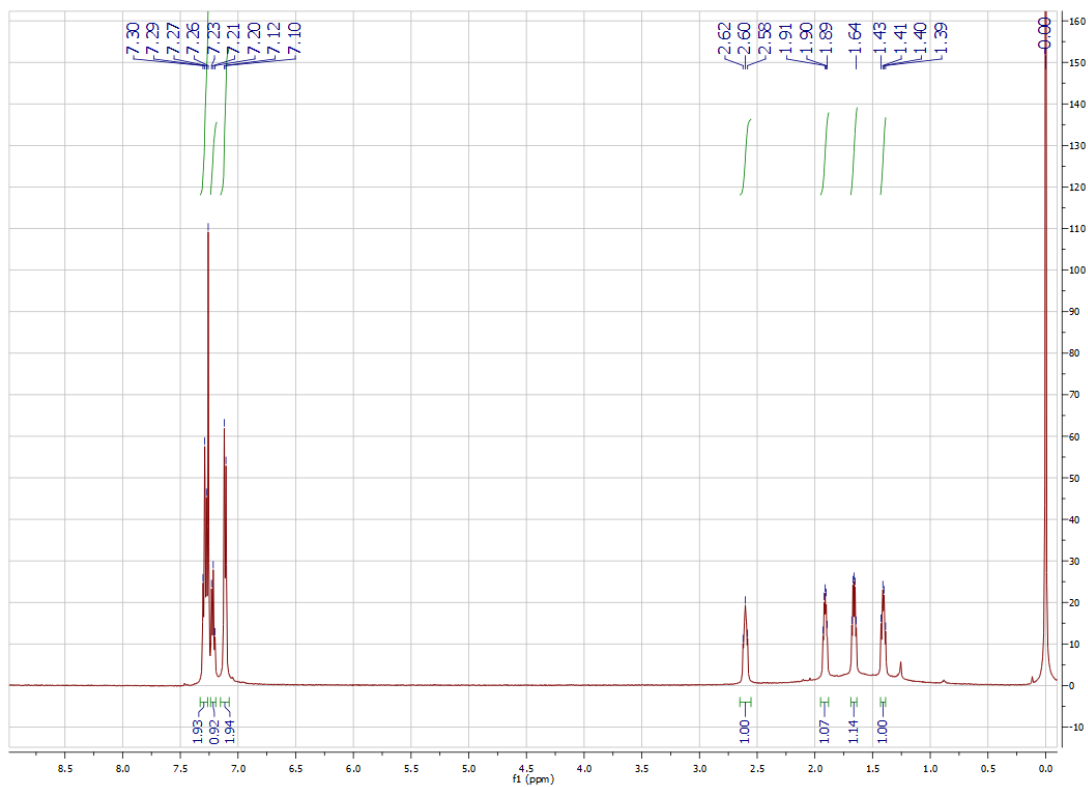
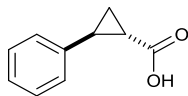
NMR spectra for Chapter 2

Design and synthesis of a novel dual-action prodrug to target glioblastoma multiforme
via lysine-specific demethylase 1 (LSD1) inhibition and glutathione depletion

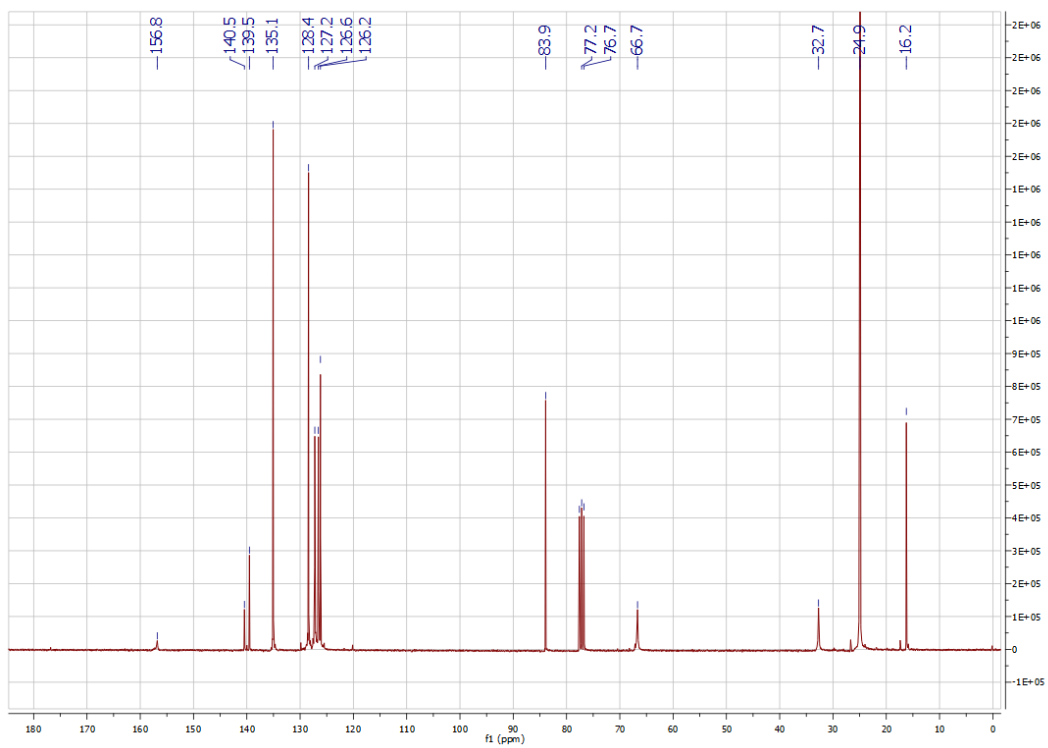
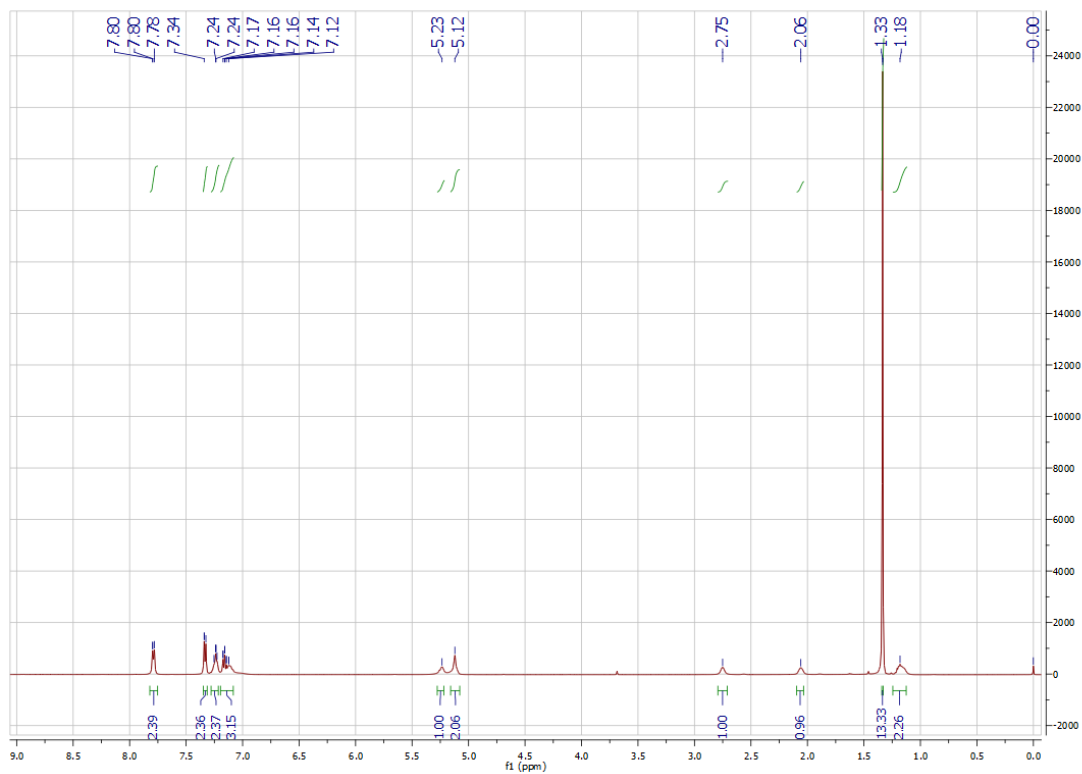
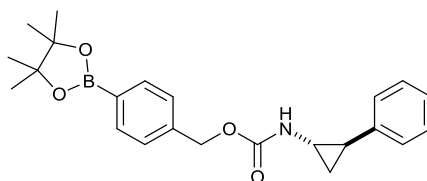
Ethyl 2-phenylcyclopropane-1-carboxylate (**16a**)



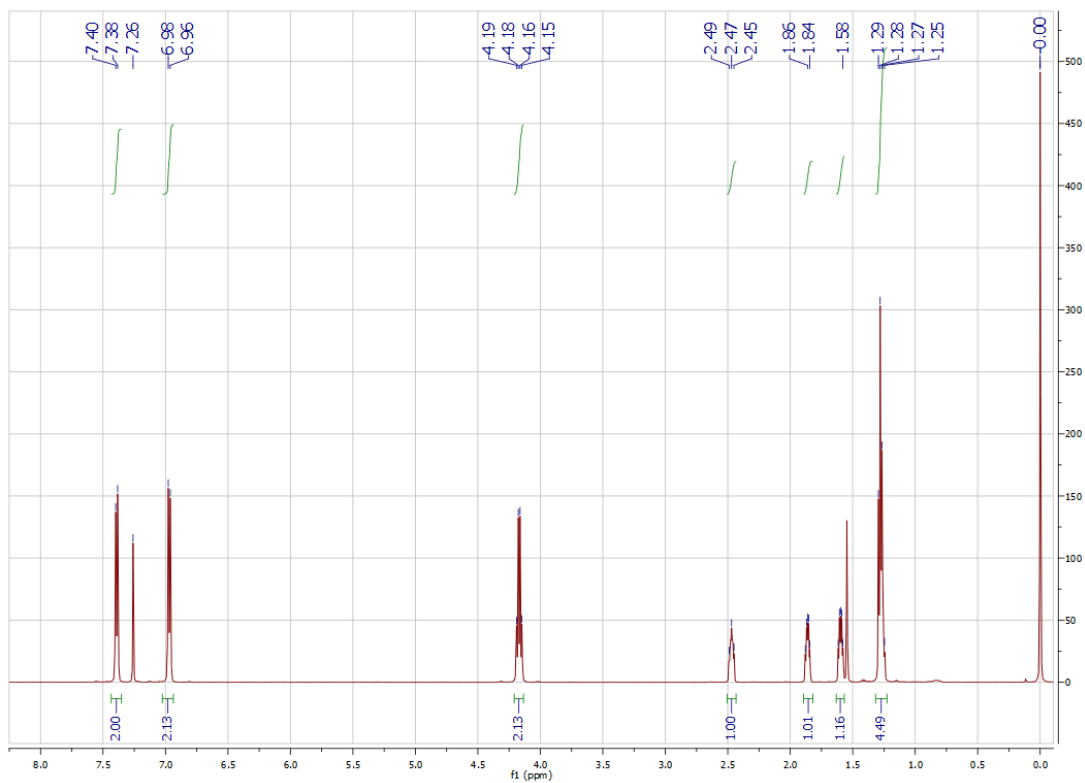
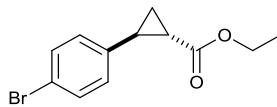
2-Phenylcyclopropane-1-carboxylic acid (**17a**)



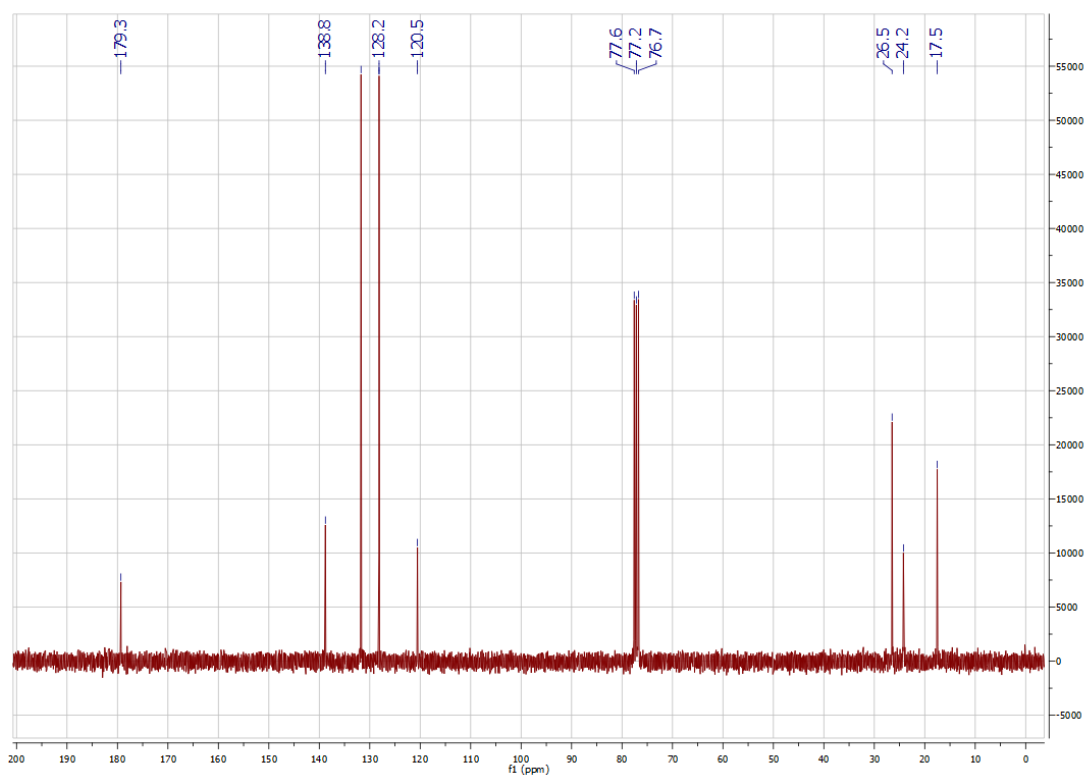
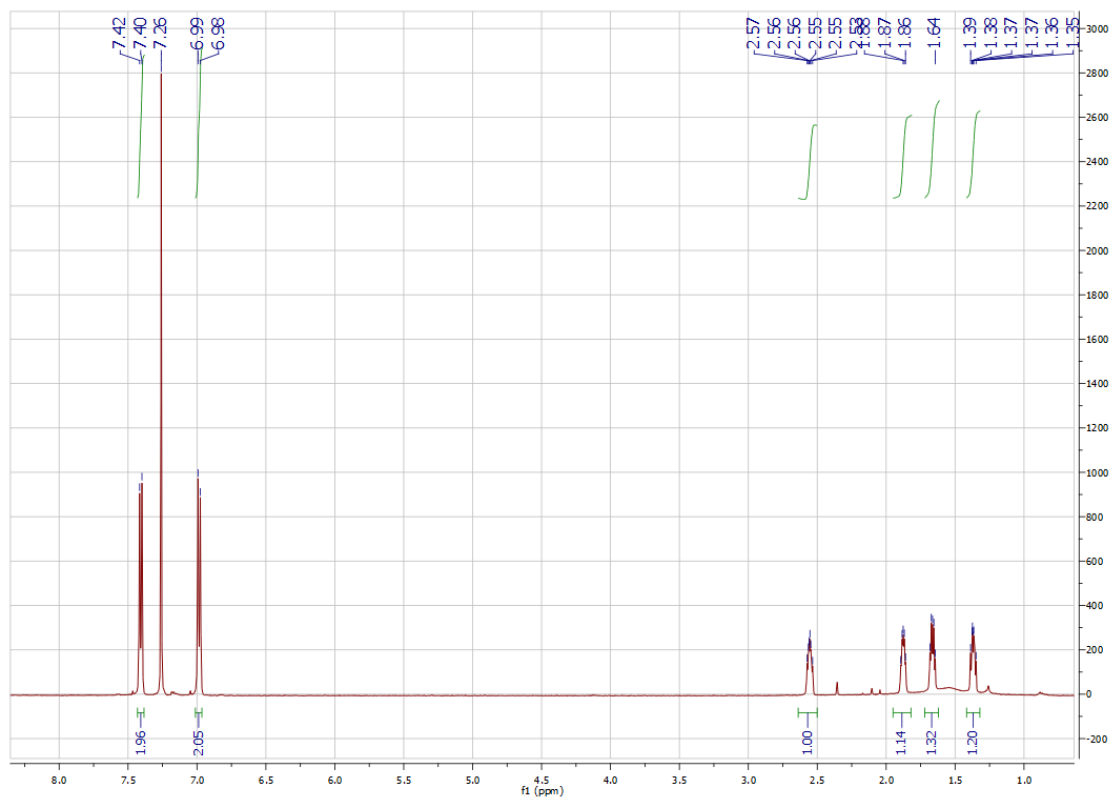
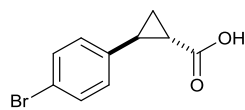
4-(4,4,5,5-Tetramethyl-1,3,2-dioxaborolan-2-yl)benzyl (2-phenylcyclopropyl)carbamate (Q-PAC)



Ethyl 2-(4-bromophenyl)cyclopropane-1-carboxylate (**16b**)

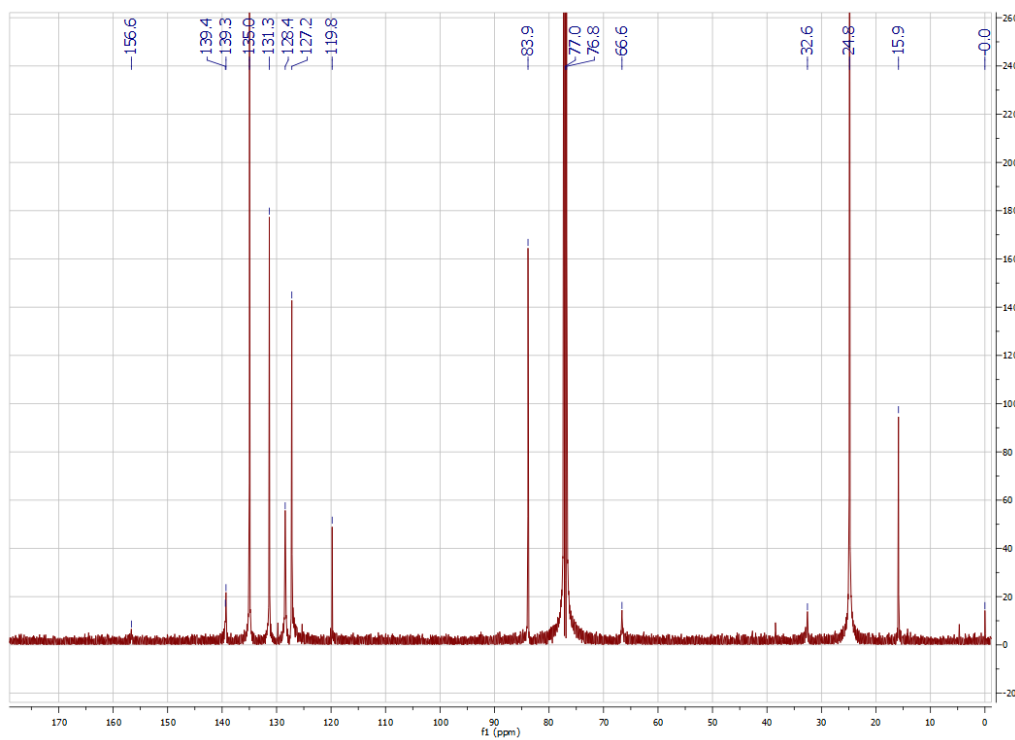
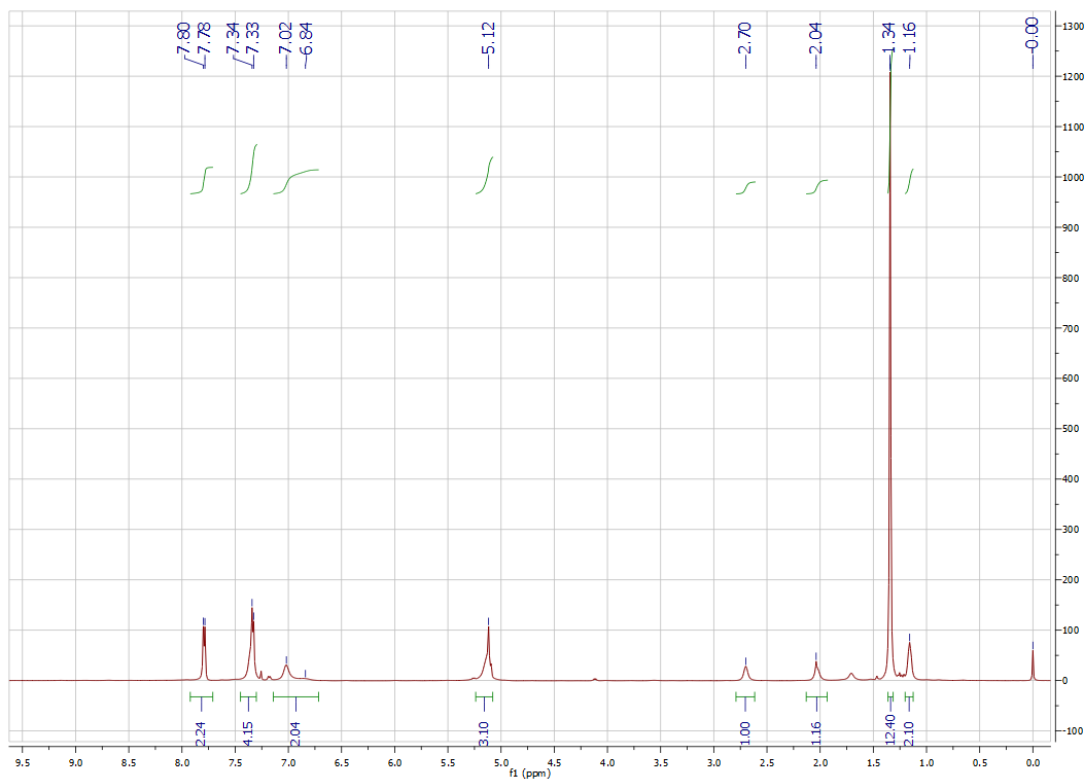
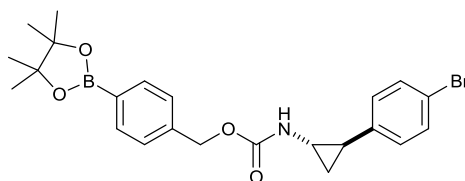


2-(4-Bromophenyl)cyclopropane-1-carboxylic acid (**17b**)

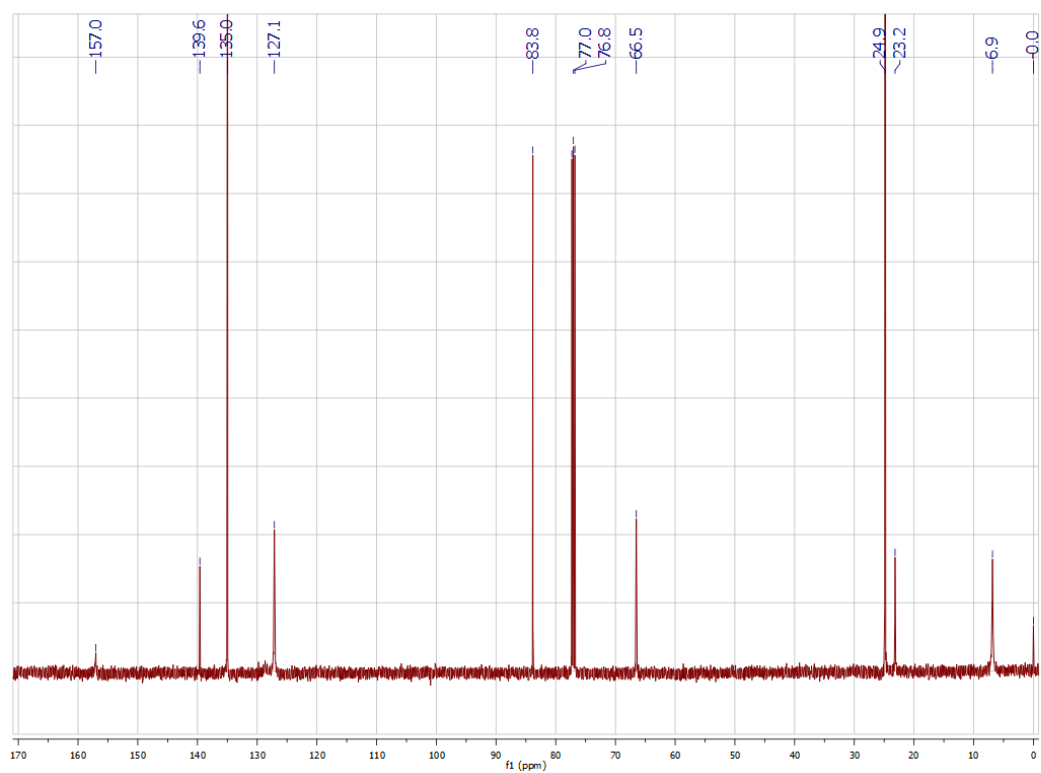
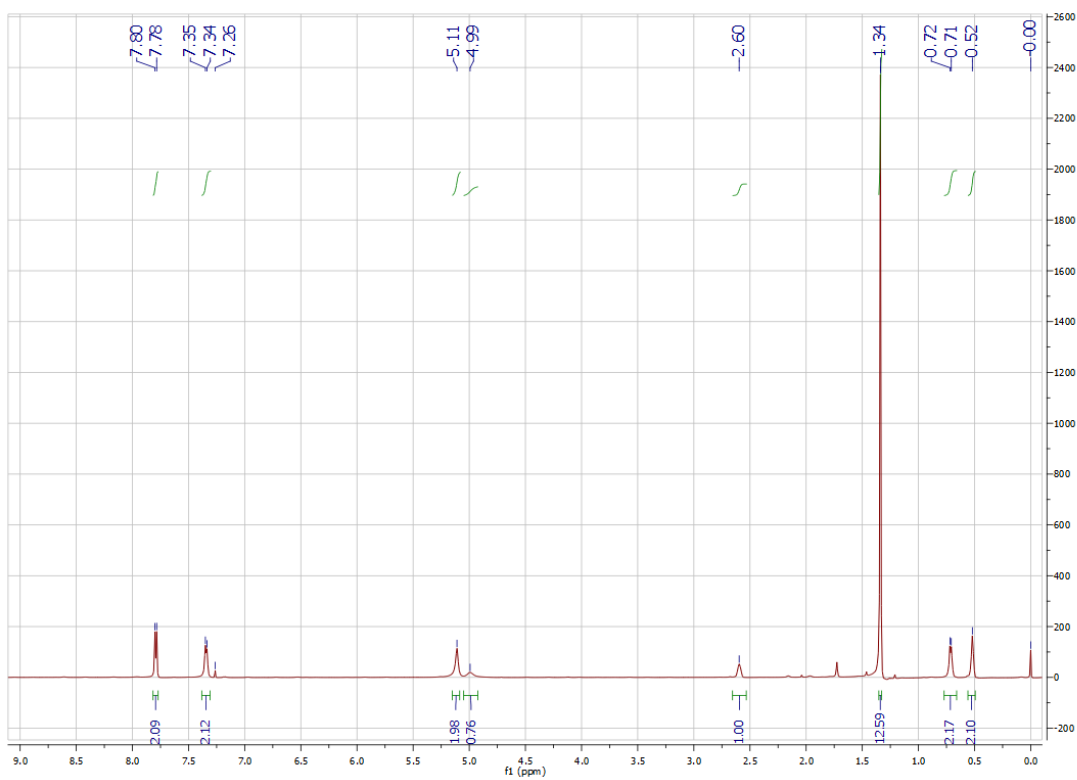
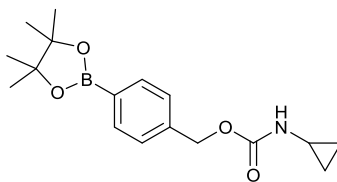


4-(4,4,5,5-Tetramethyl-1,3,2-dioxaborolan-2-yl)benzyl
bromophenyl)cyclopropyl)carbamate (Q-BrAC)

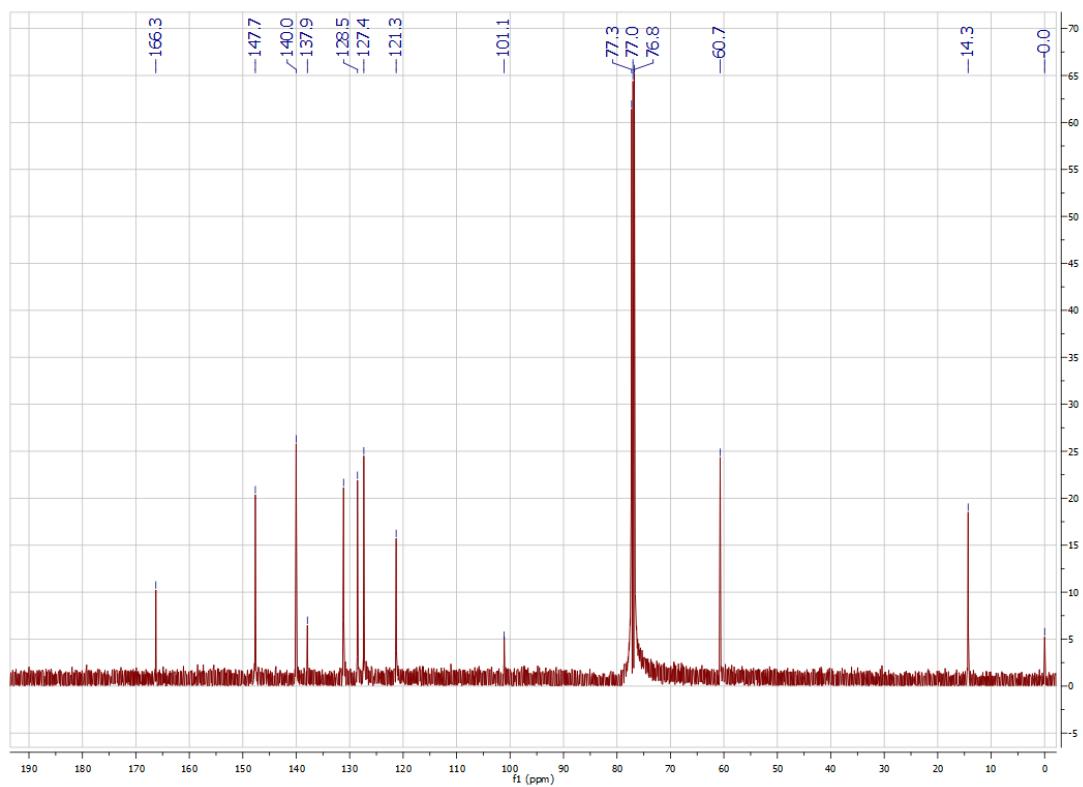
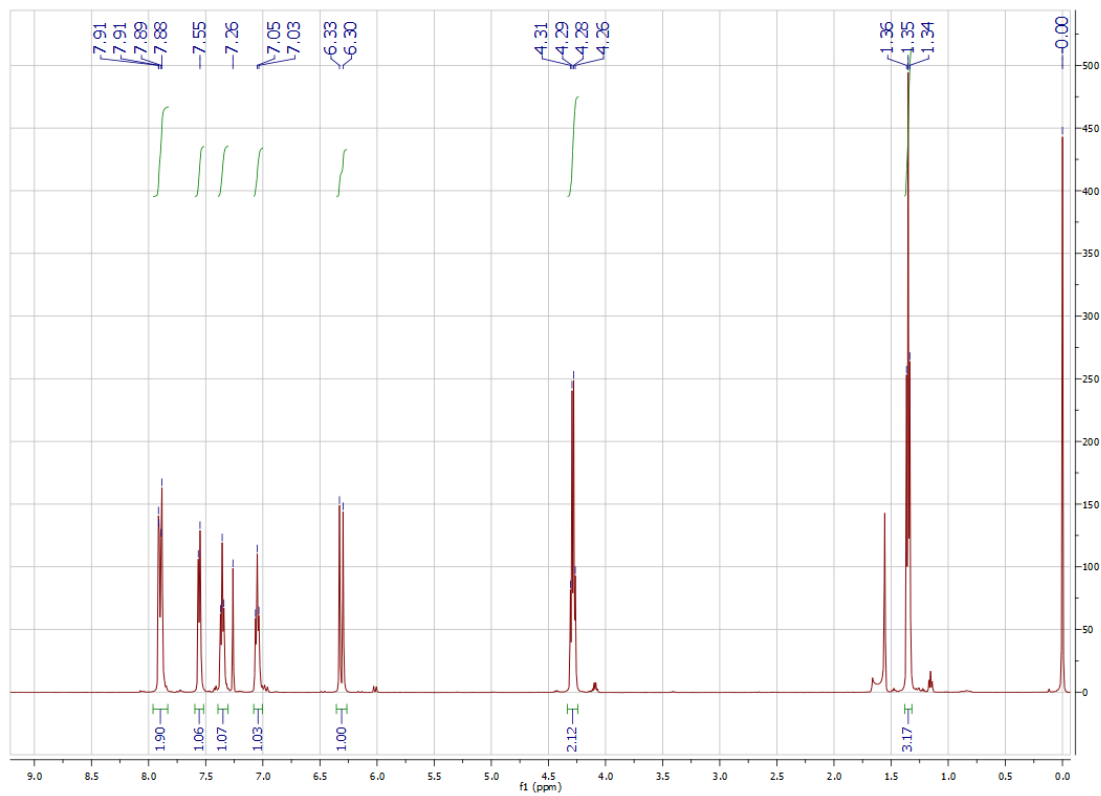
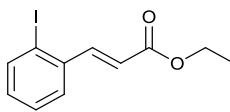
(2-(4-



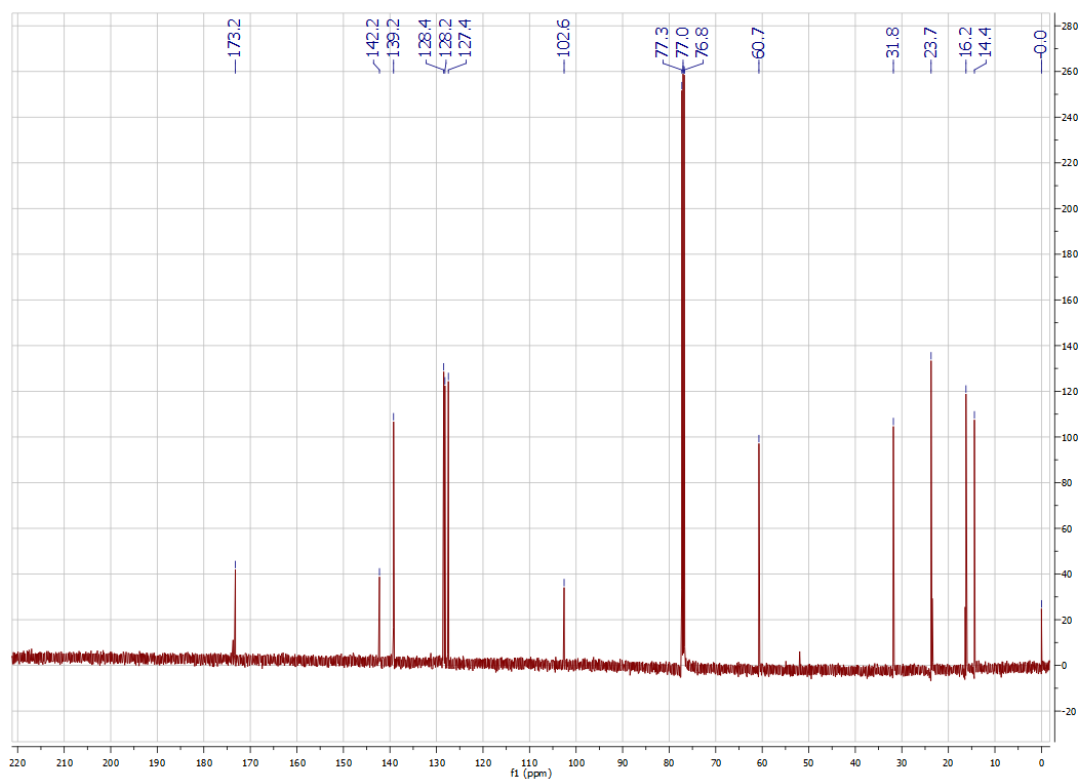
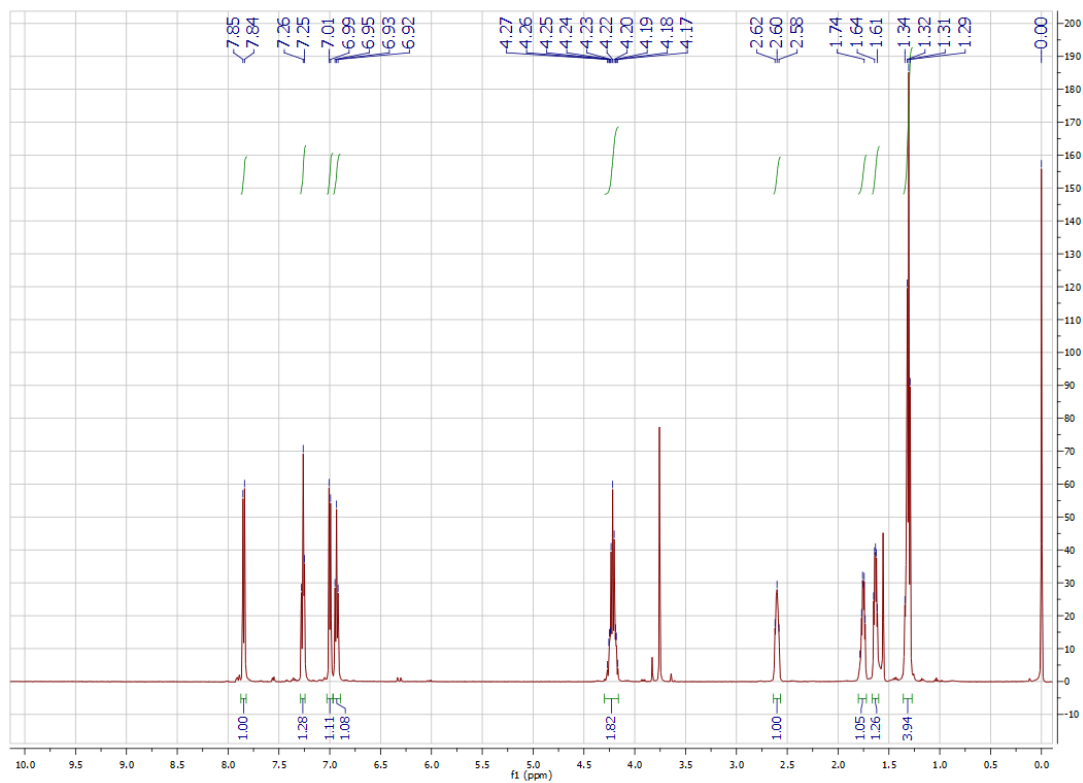
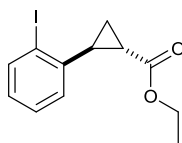
4-(4,4,5,5-tetramethyl-1,3,2-dioxaborolan-2-yl)benzyl cyclopropylcarbamate (QAC)



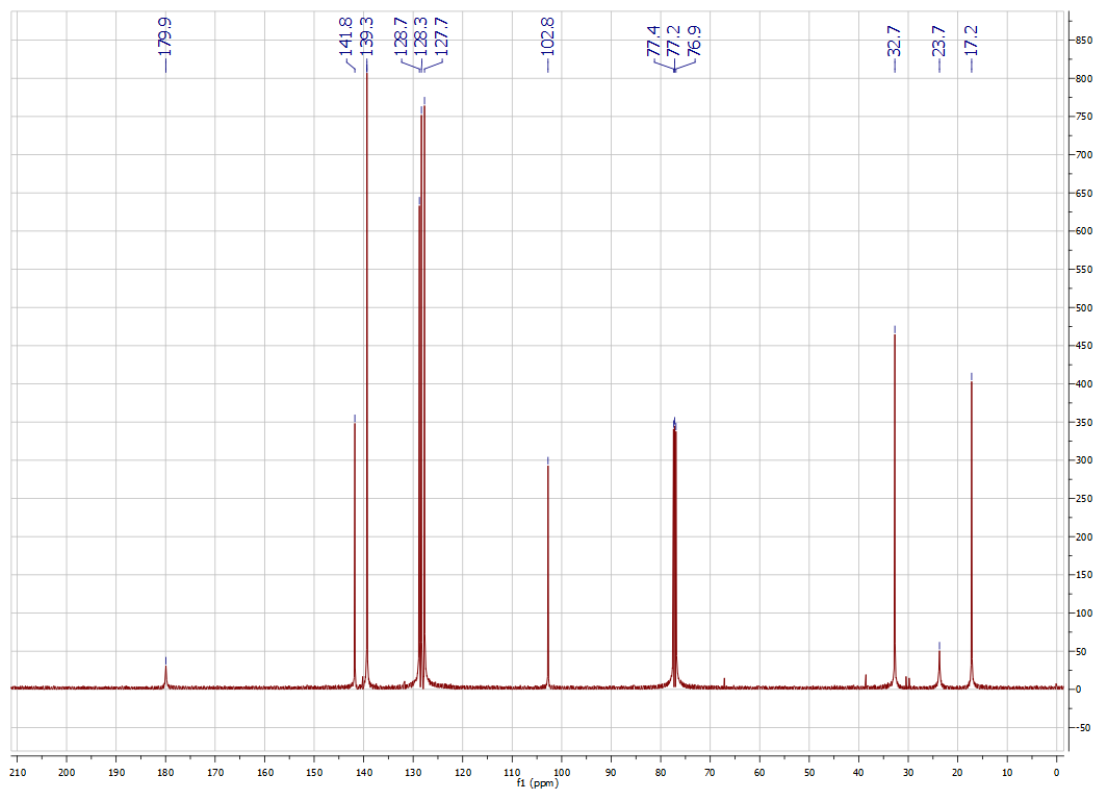
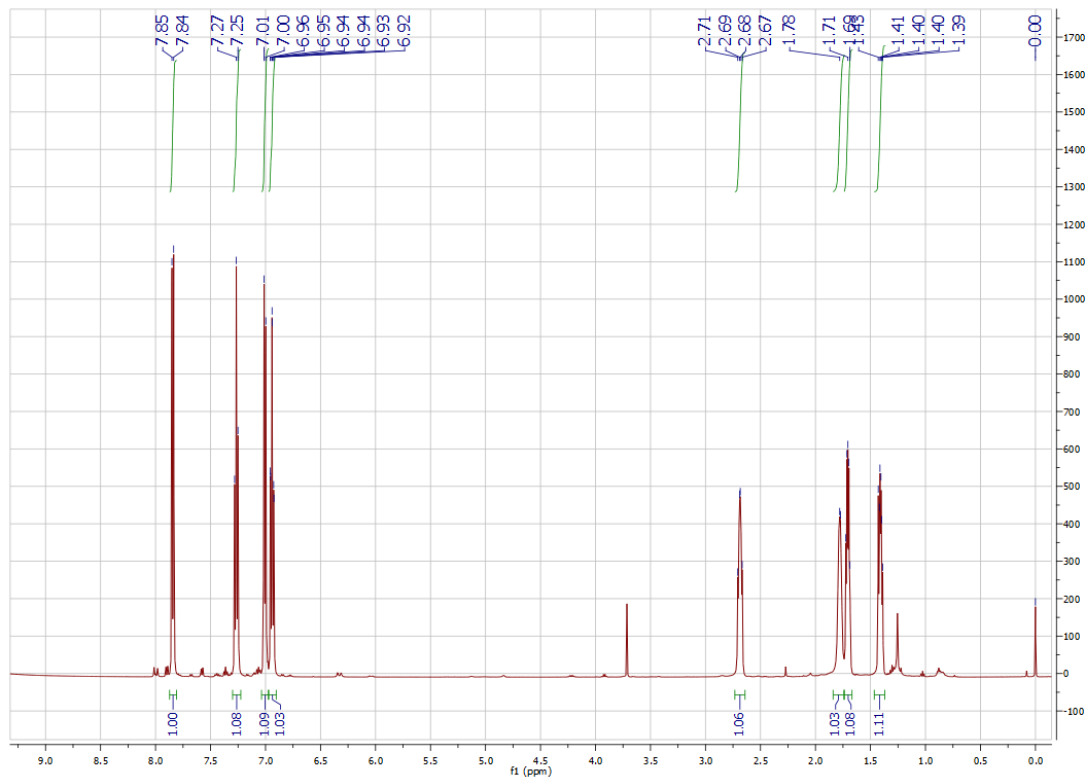
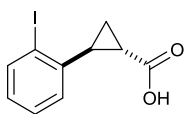
Ethyl (E)-3-(2-iodophenyl)acrylate



Ethyl 2-(2-iodophenyl)cyclopropane-1-carboxylate

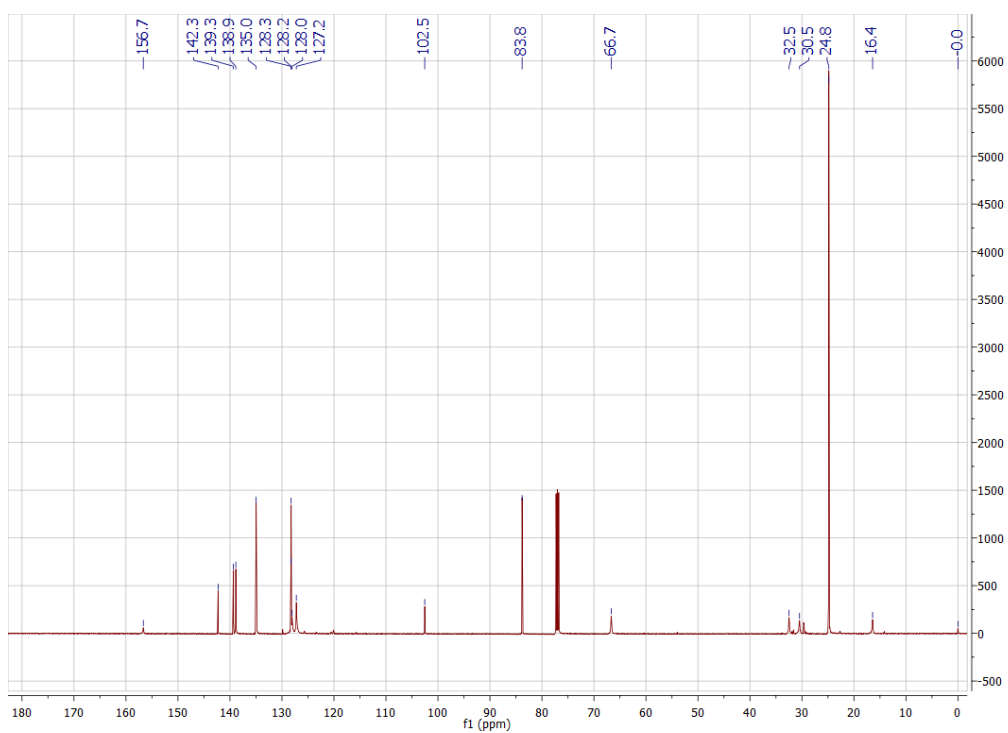
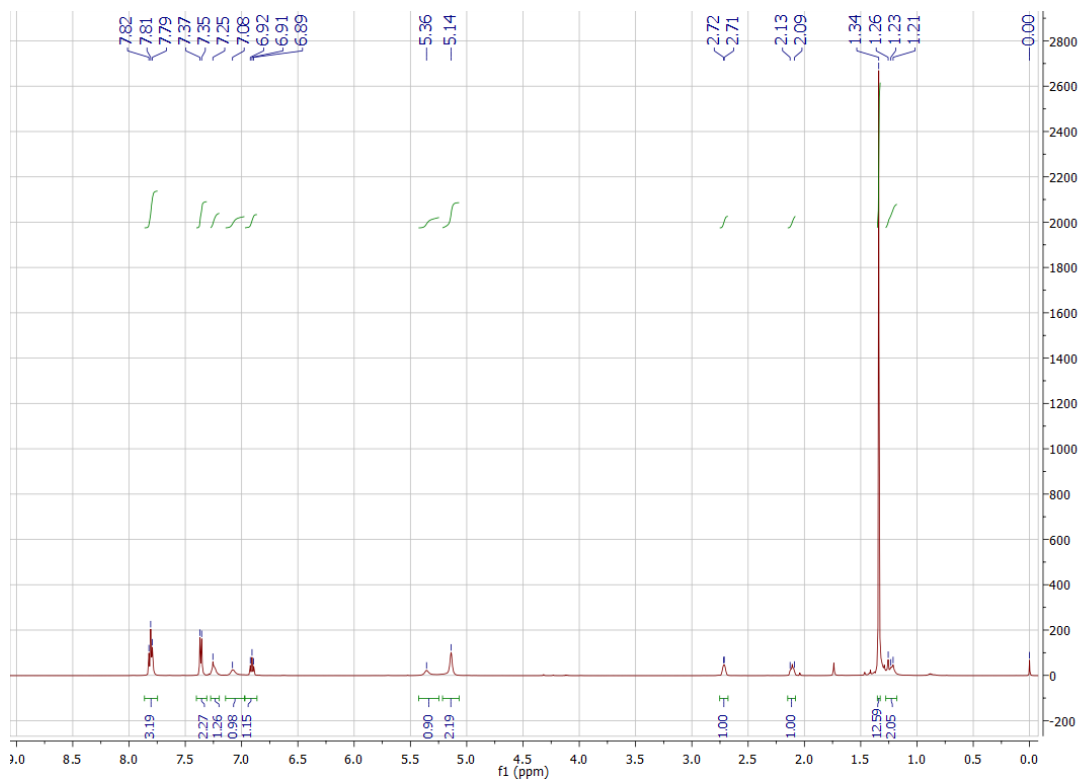
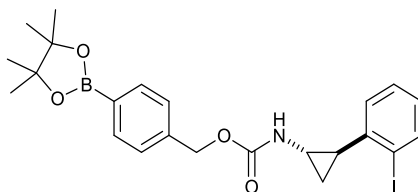


2-(2-Iodophenyl)cyclopropane-1-carboxylic acid

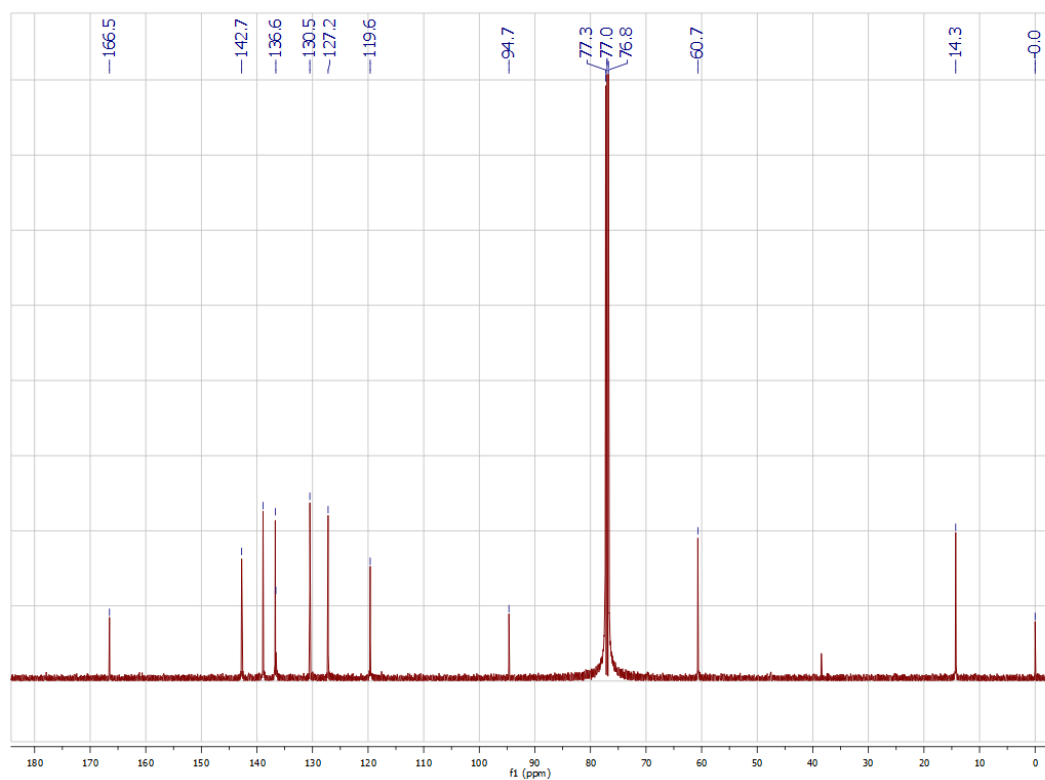
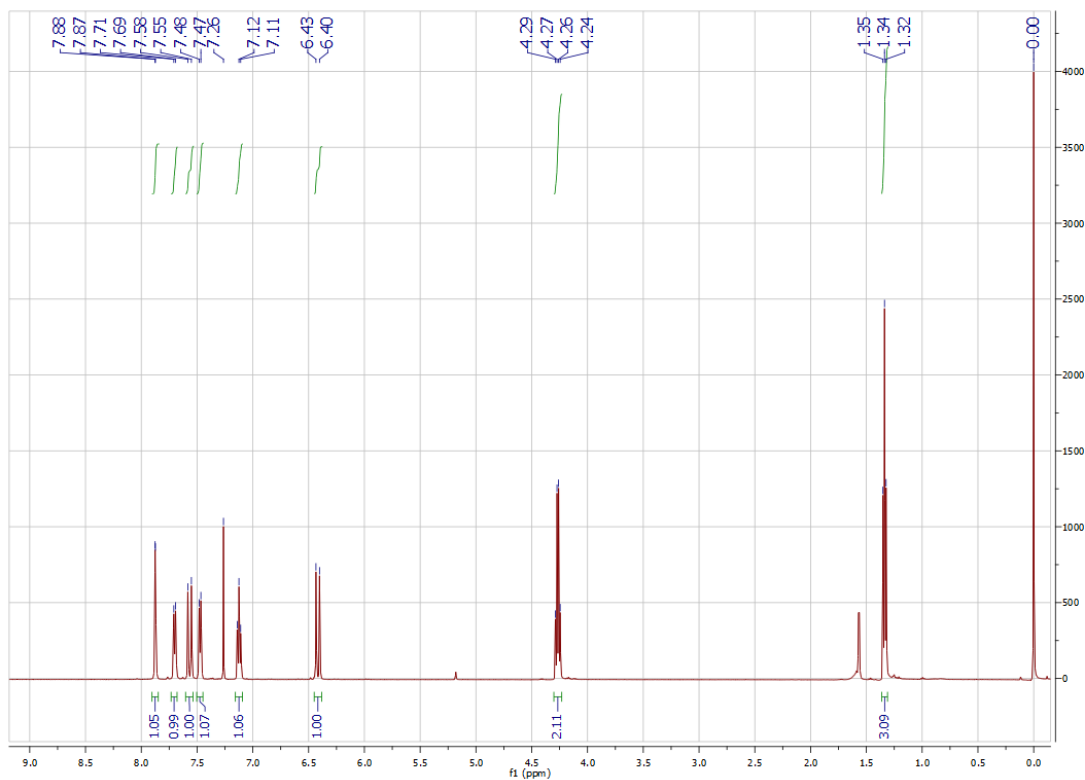
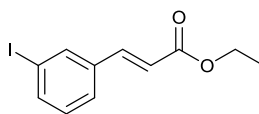


4-(4,4,5,5-Tetramethyl-1,3,2-dioxaborolan-2-yl)benzyl
(2-(2-iodophenyl)cyclopropyl)carbamate (Q-2IAC)

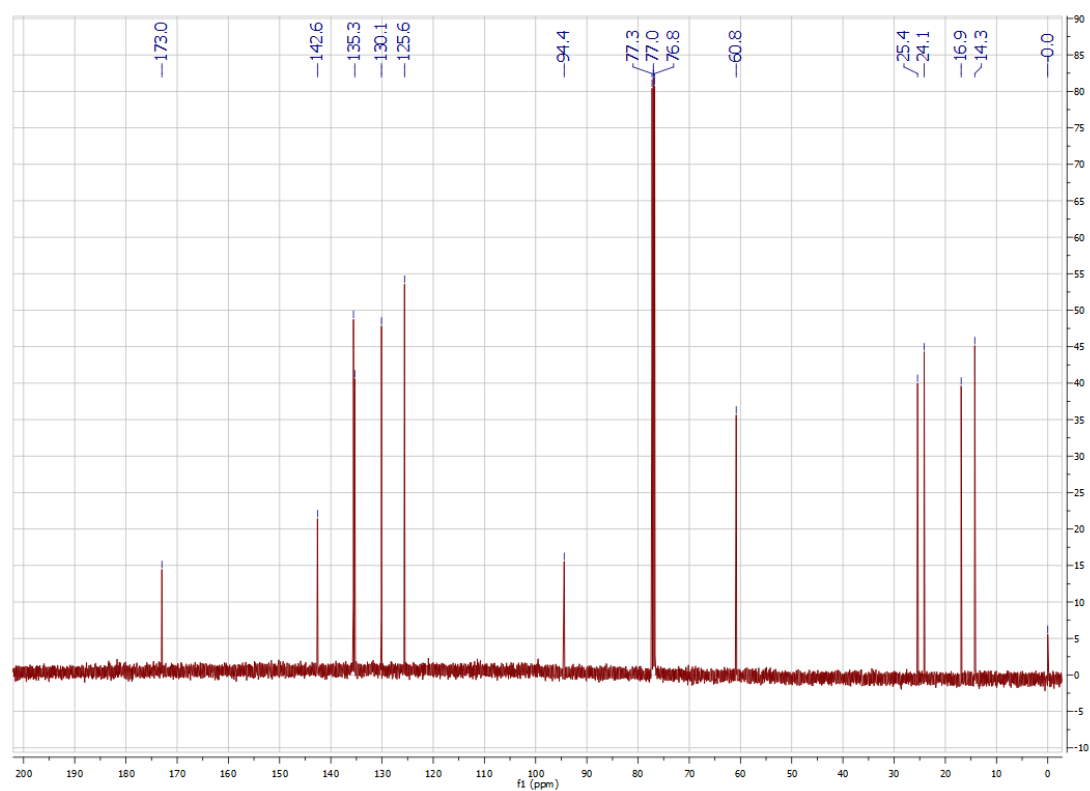
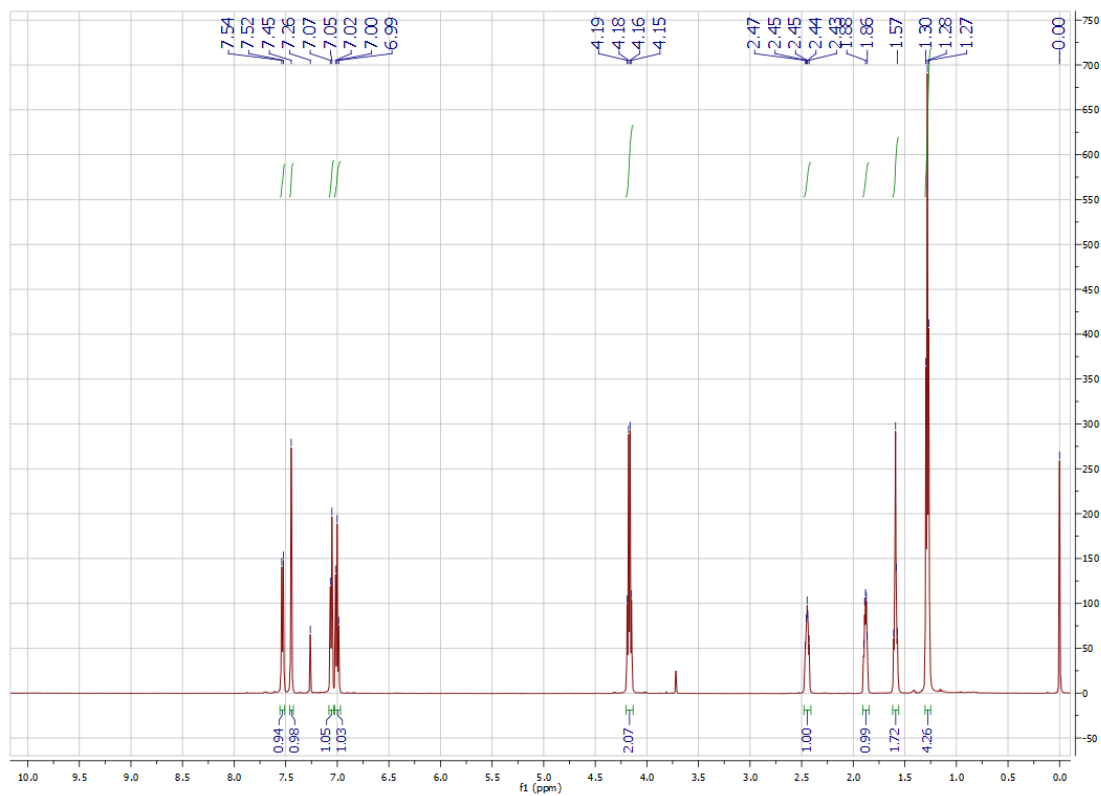
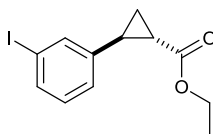
(2-(2-



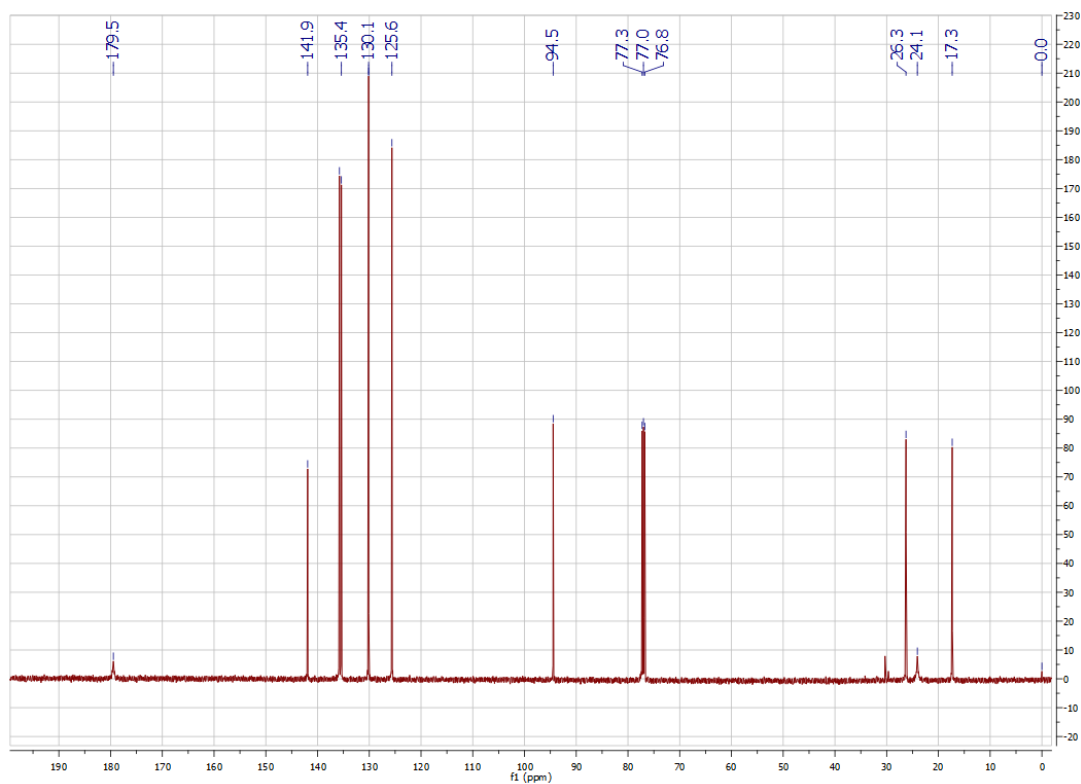
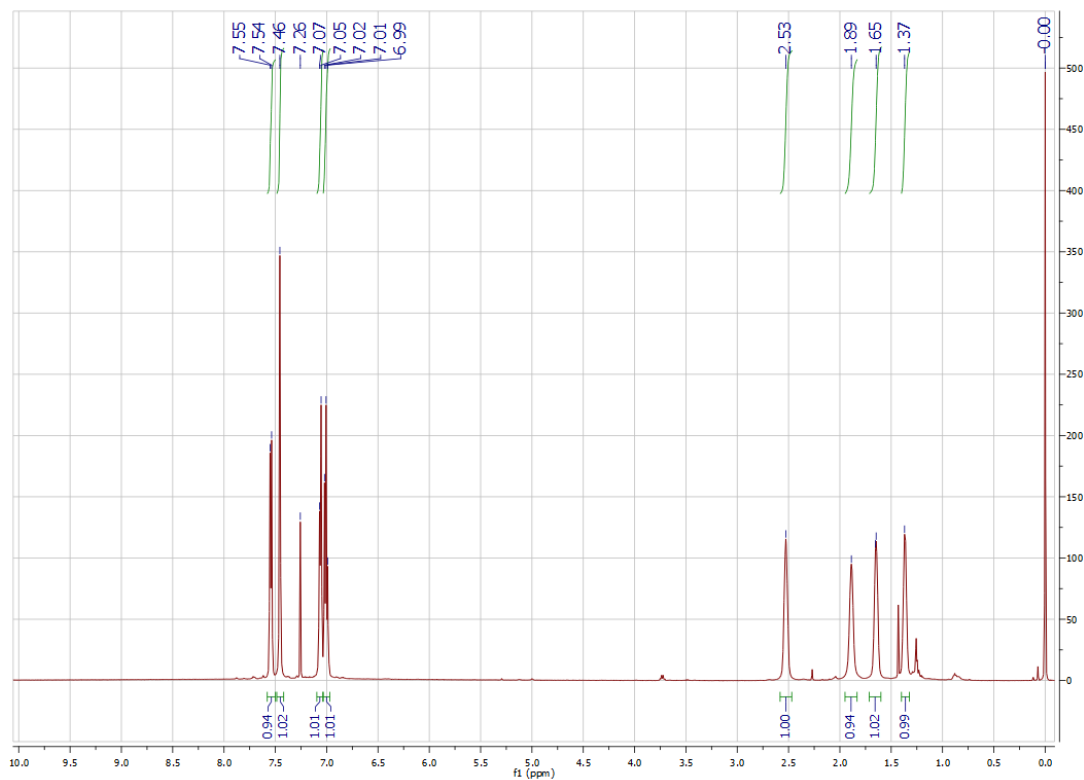
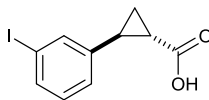
Ethyl (E)-3-(3-iodophenyl)acrylate



Ethyl 2-(3-iodophenyl)cyclopropane-1-carboxylate

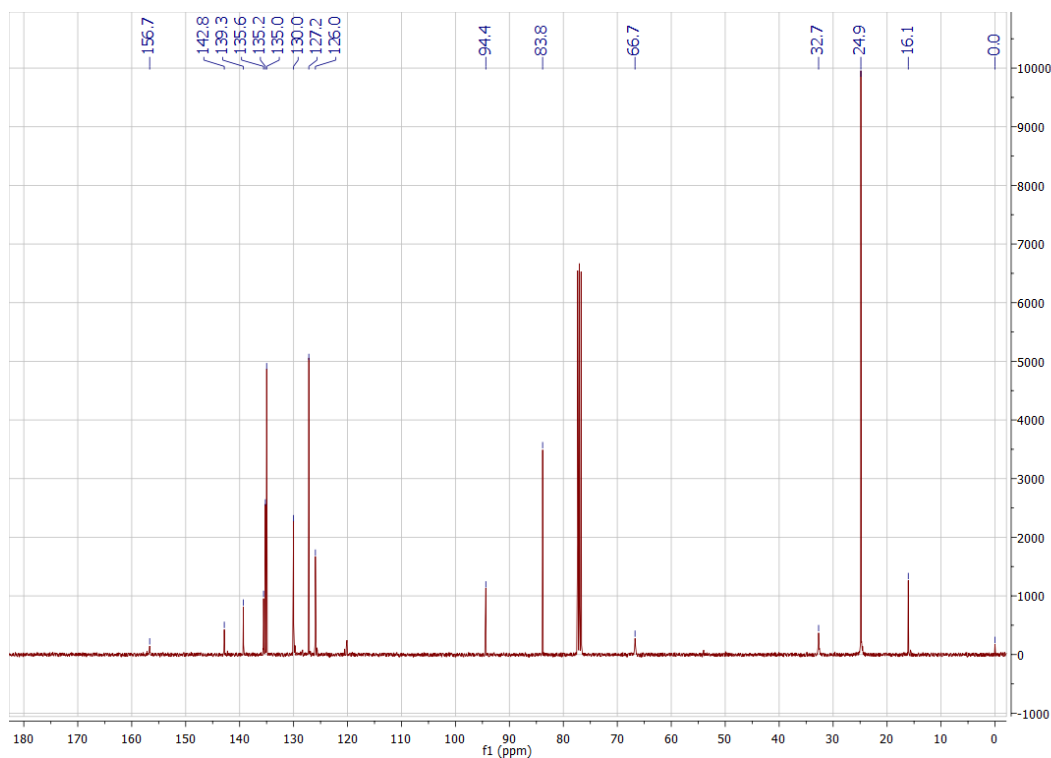
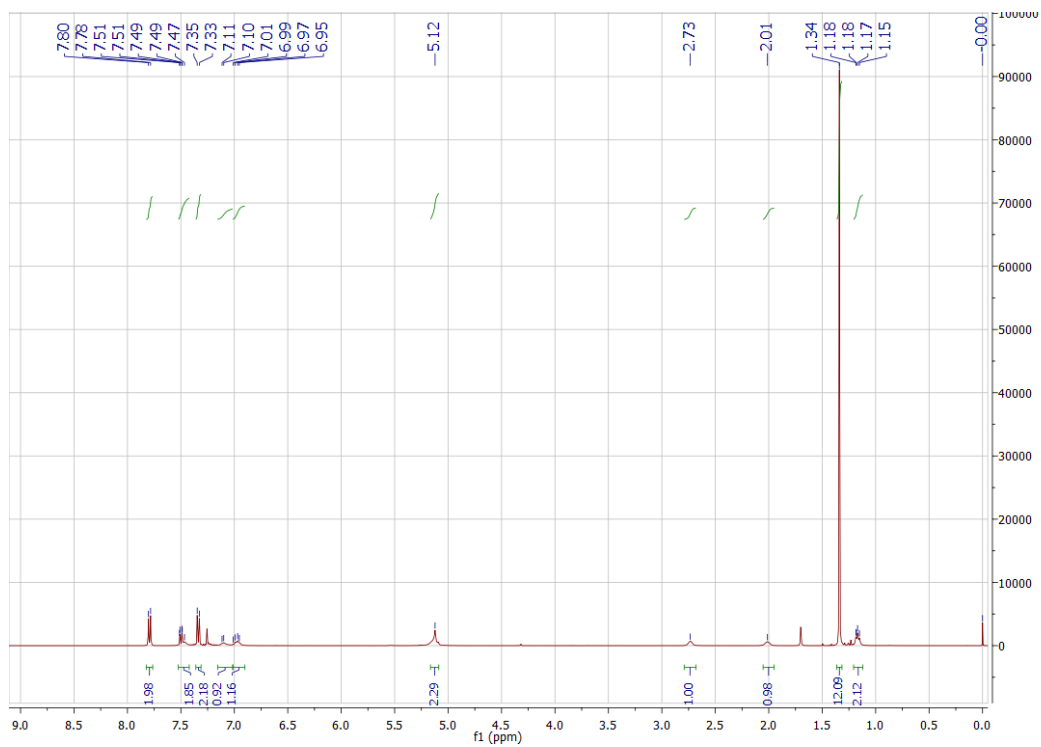
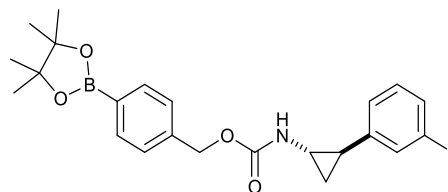


2-(3-Iodophenyl)cyclopropane-1-carboxylic acid

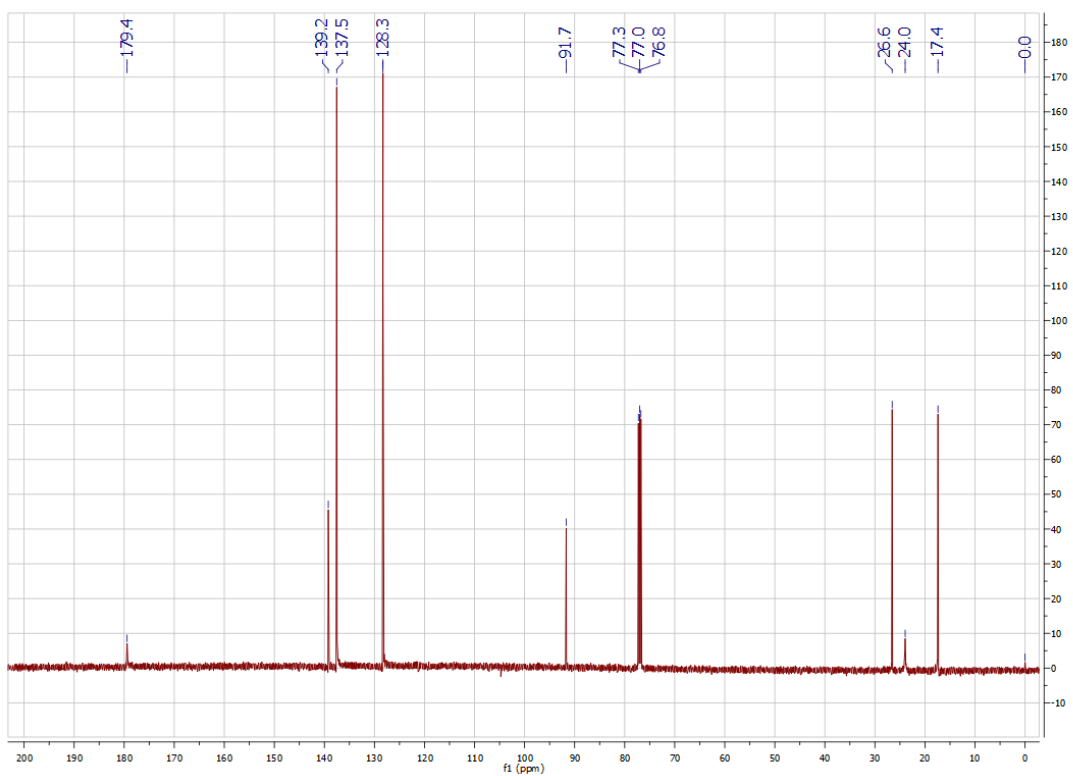
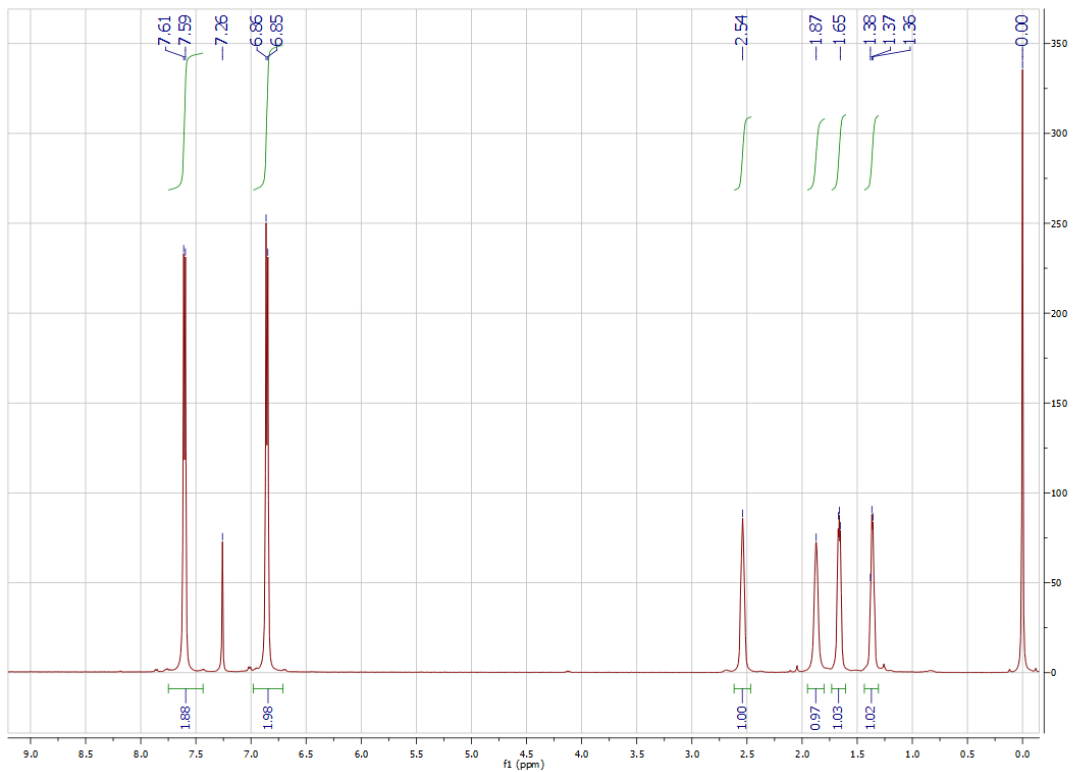
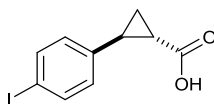


4-(4,4,5,5-Tetramethyl-1,3,2-dioxaborolan-2-yl)benzyl
iodophenyl)cyclopropyl)carbamate (Q-3IAC)

(2-(3-

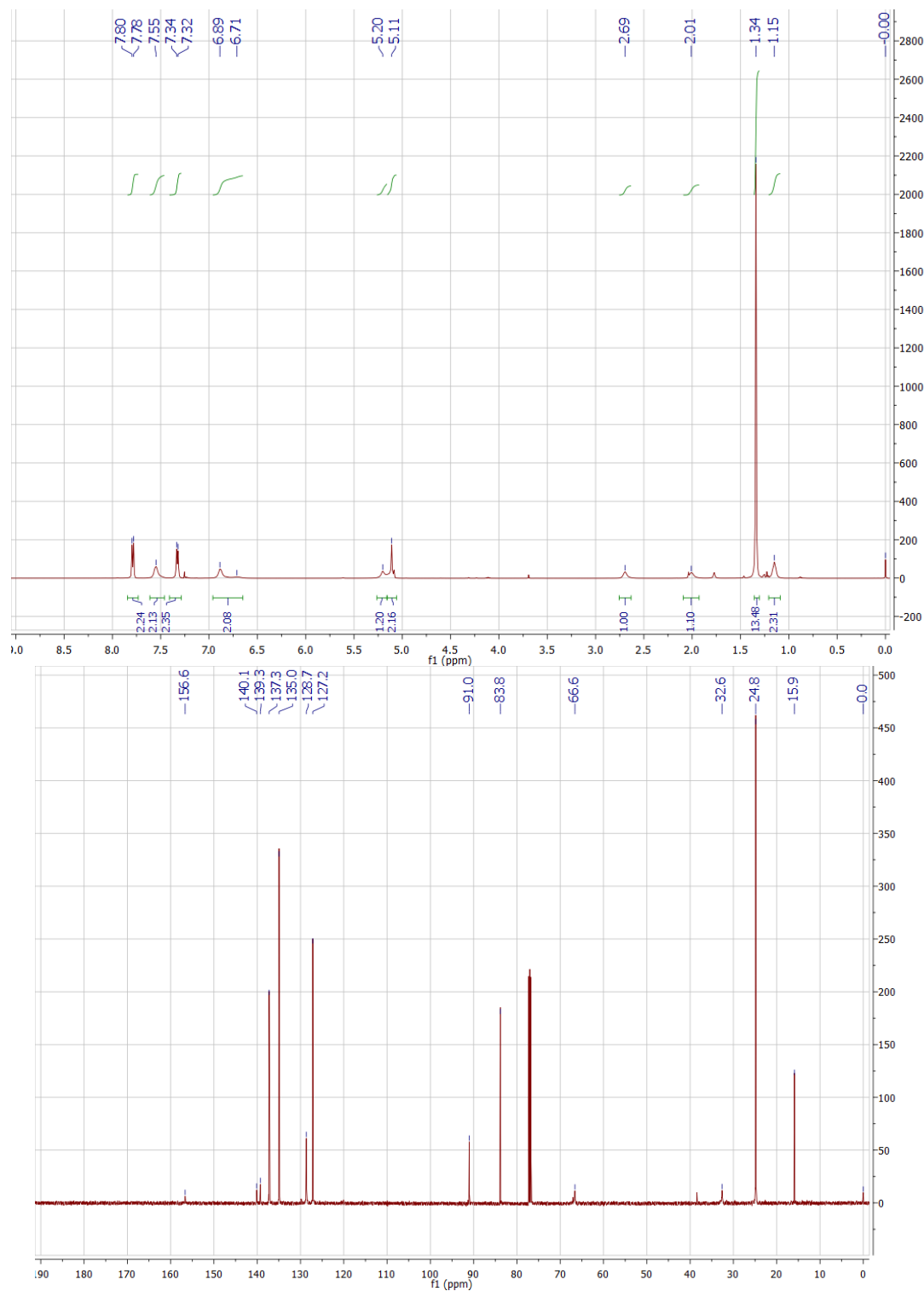
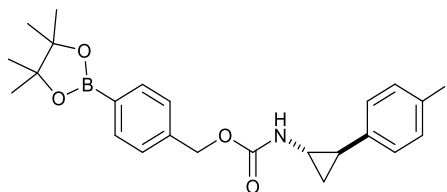


2-(4-Iodophenyl)cyclopropane-1-carboxylic acid (17c)

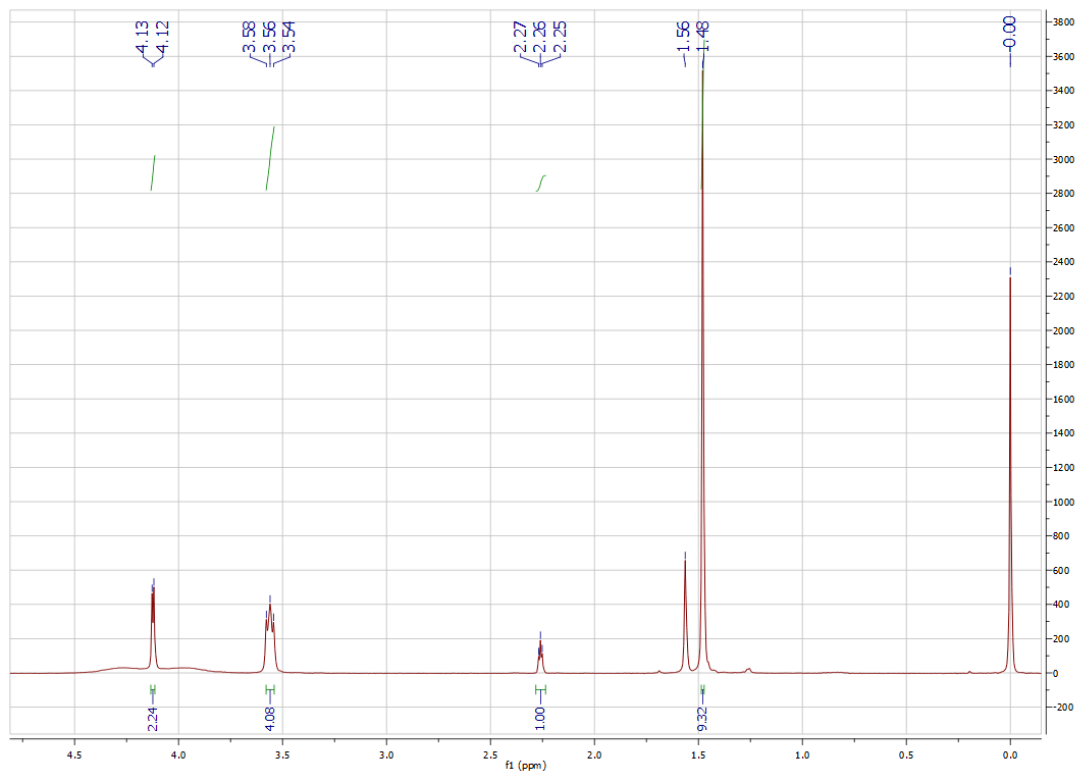
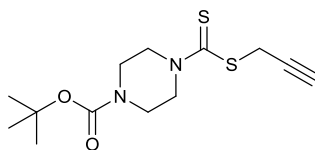


4-(4,4,5,5-Tetramethyl-1,3,2-dioxaborolan-2-yl)benzyl
(2-(4-iodophenyl)cyclopropyl)carbamate (Q-4IAC)

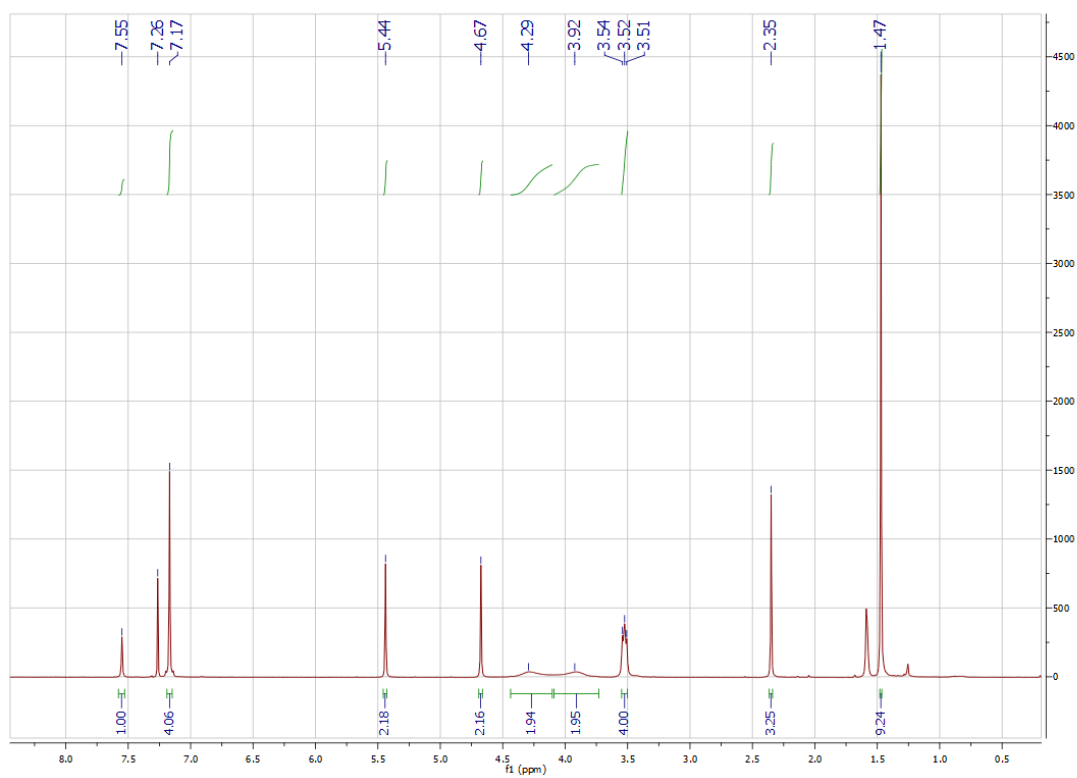
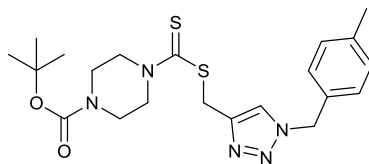
(2-(4-



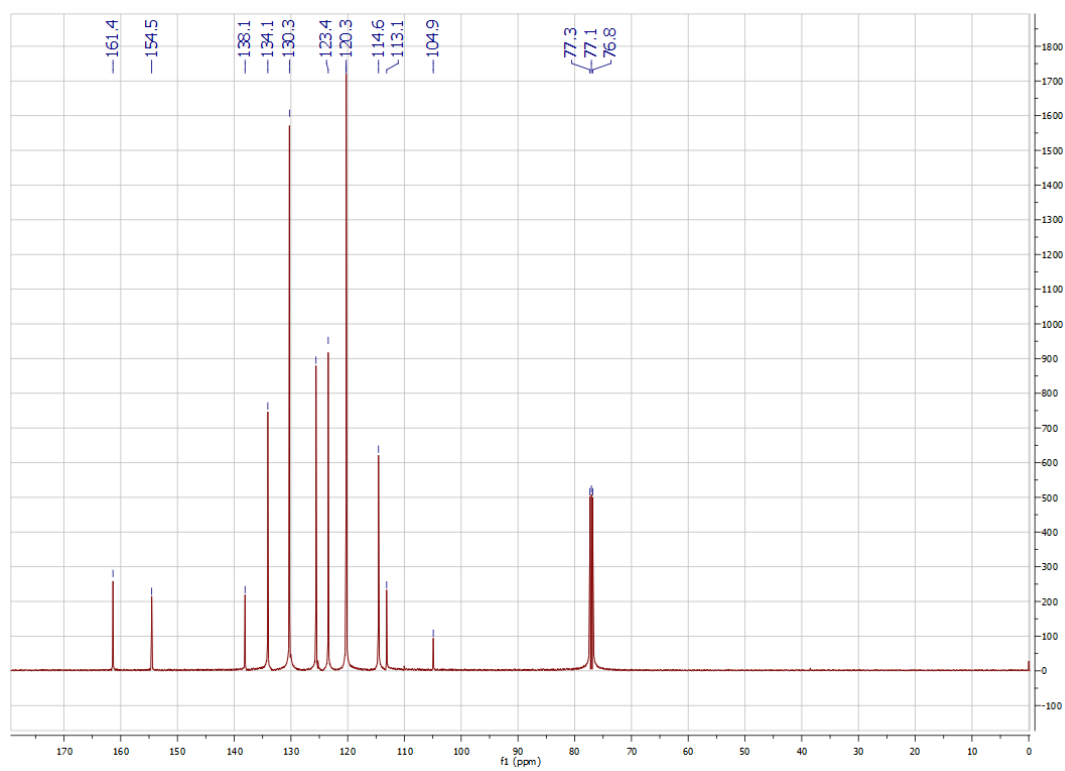
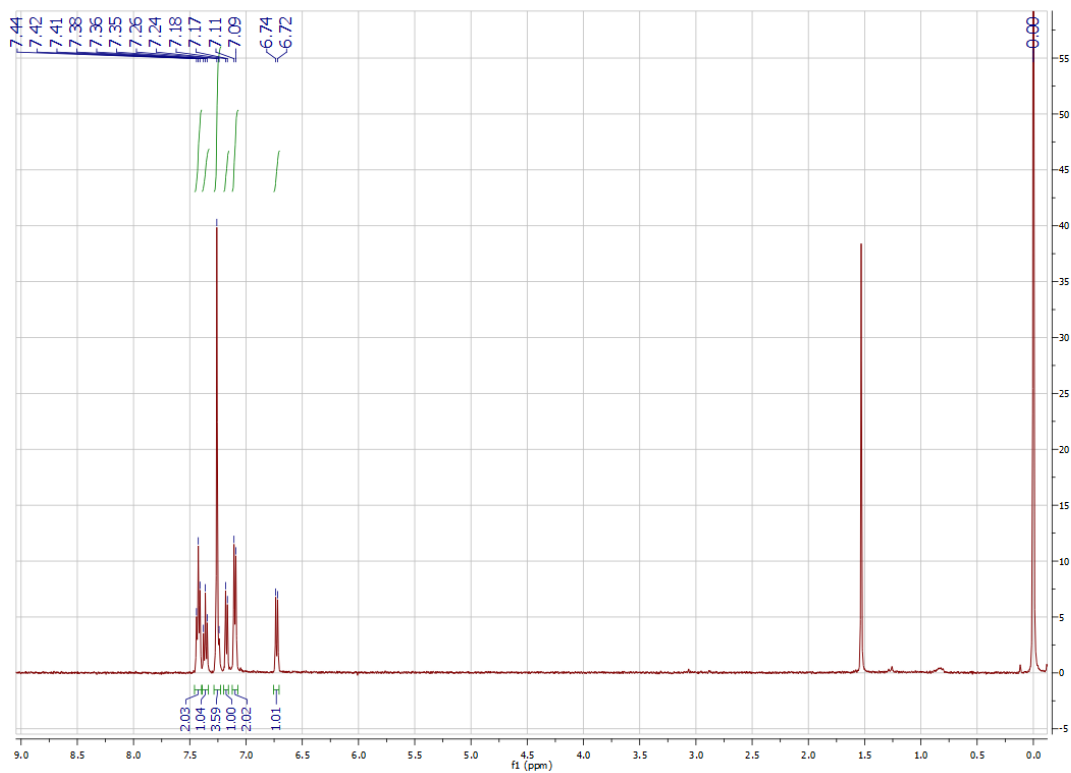
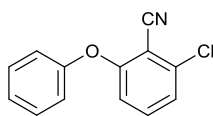
tert-Butyl 4-((prop-2-yn-1-ylthio)carbonothioyl)piperazine-1-carboxylate (**19**)



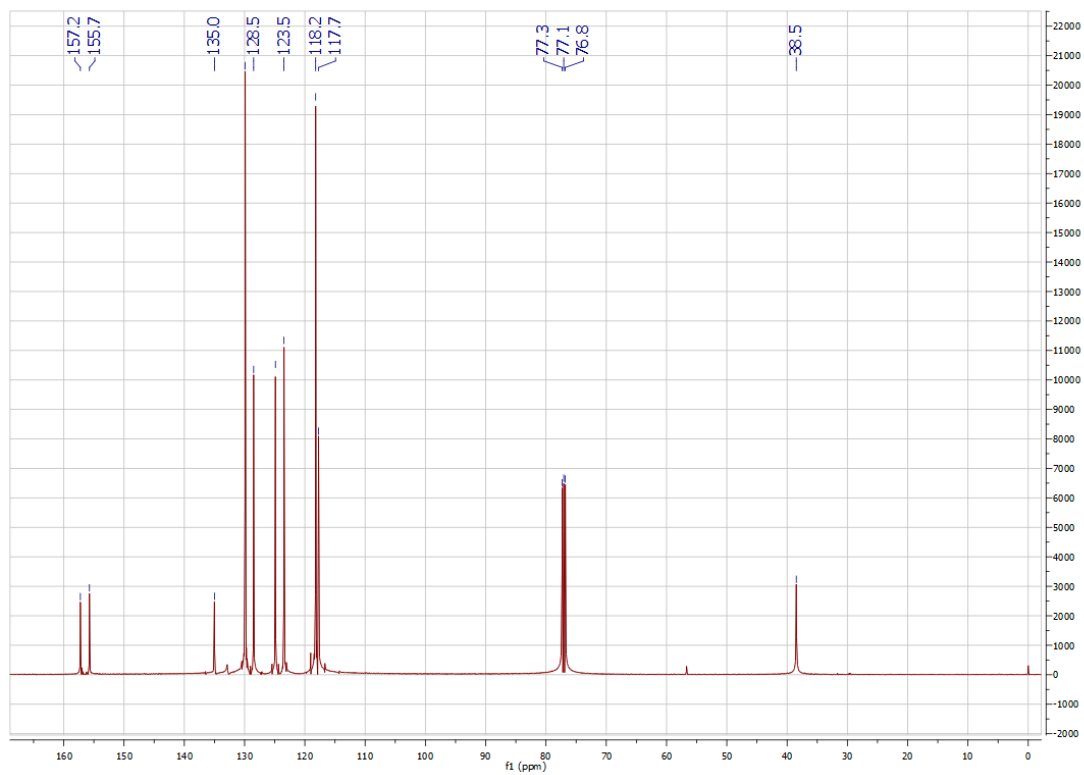
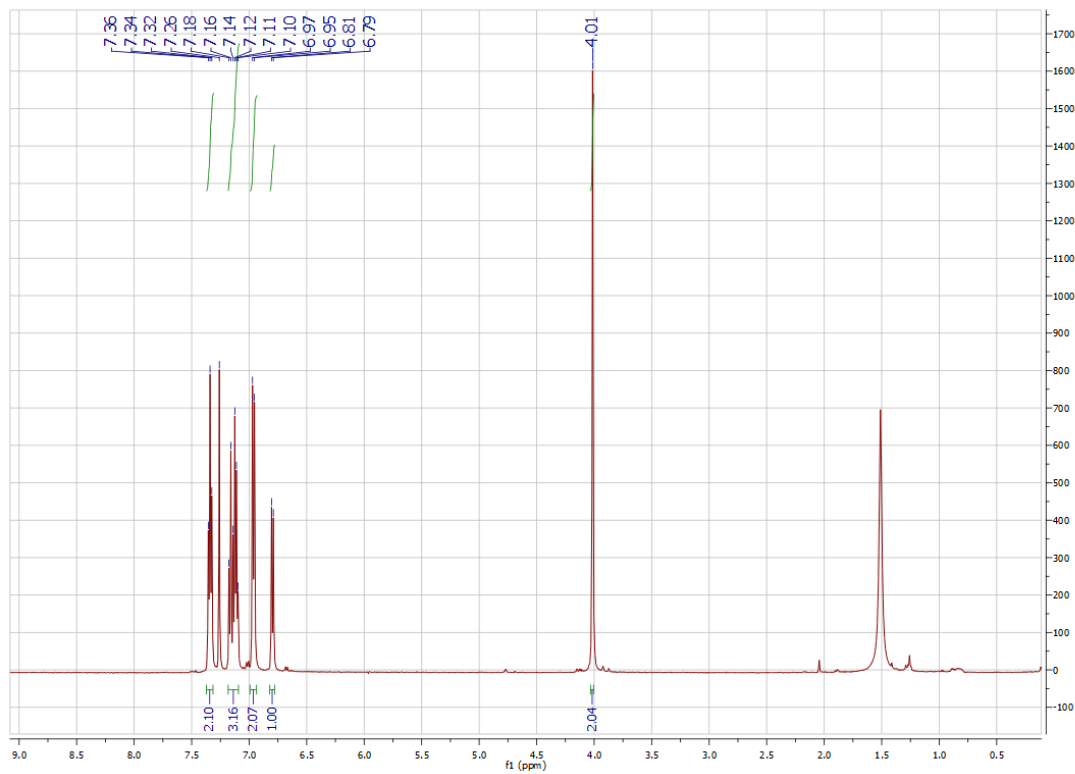
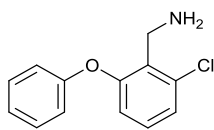
tert-Butyl 4-(((1-(4-methylbenzyl)-1H-1,2,3-triazol-4-yl)-methylthio)carbonothioyl)piperazine-1-carboxylate (**11**)



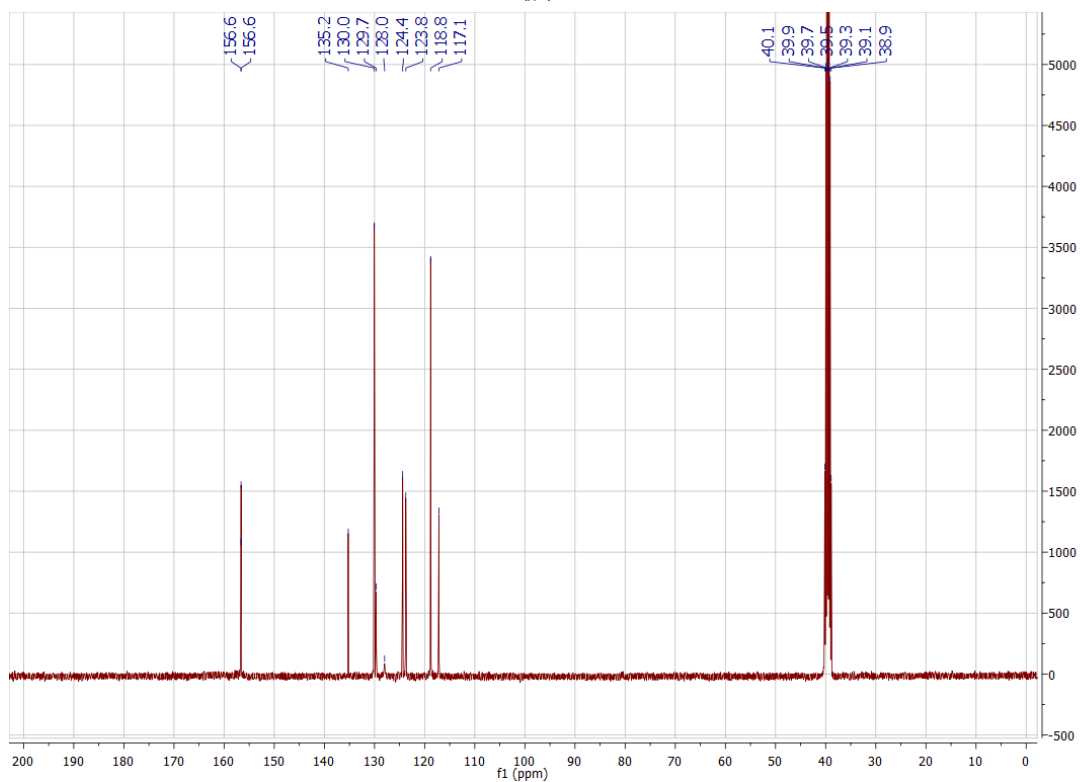
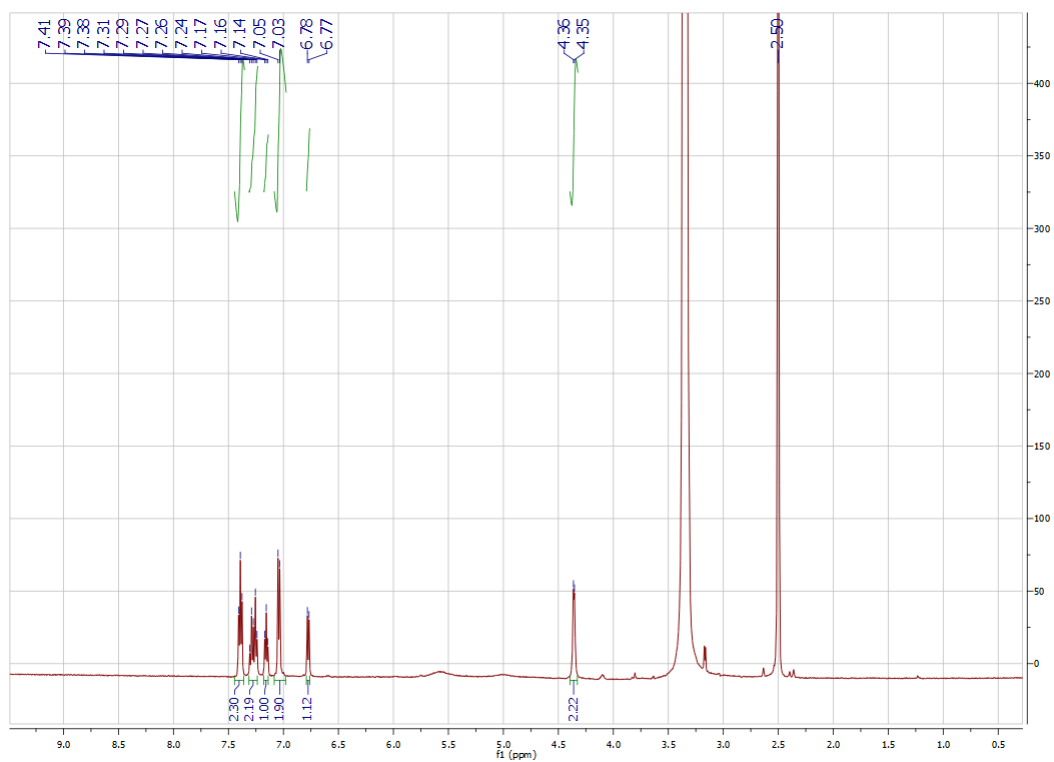
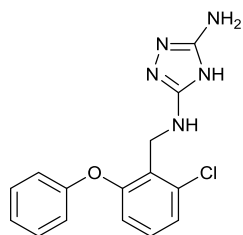
2-Chloro-6-phenoxybenzonitrile (21)



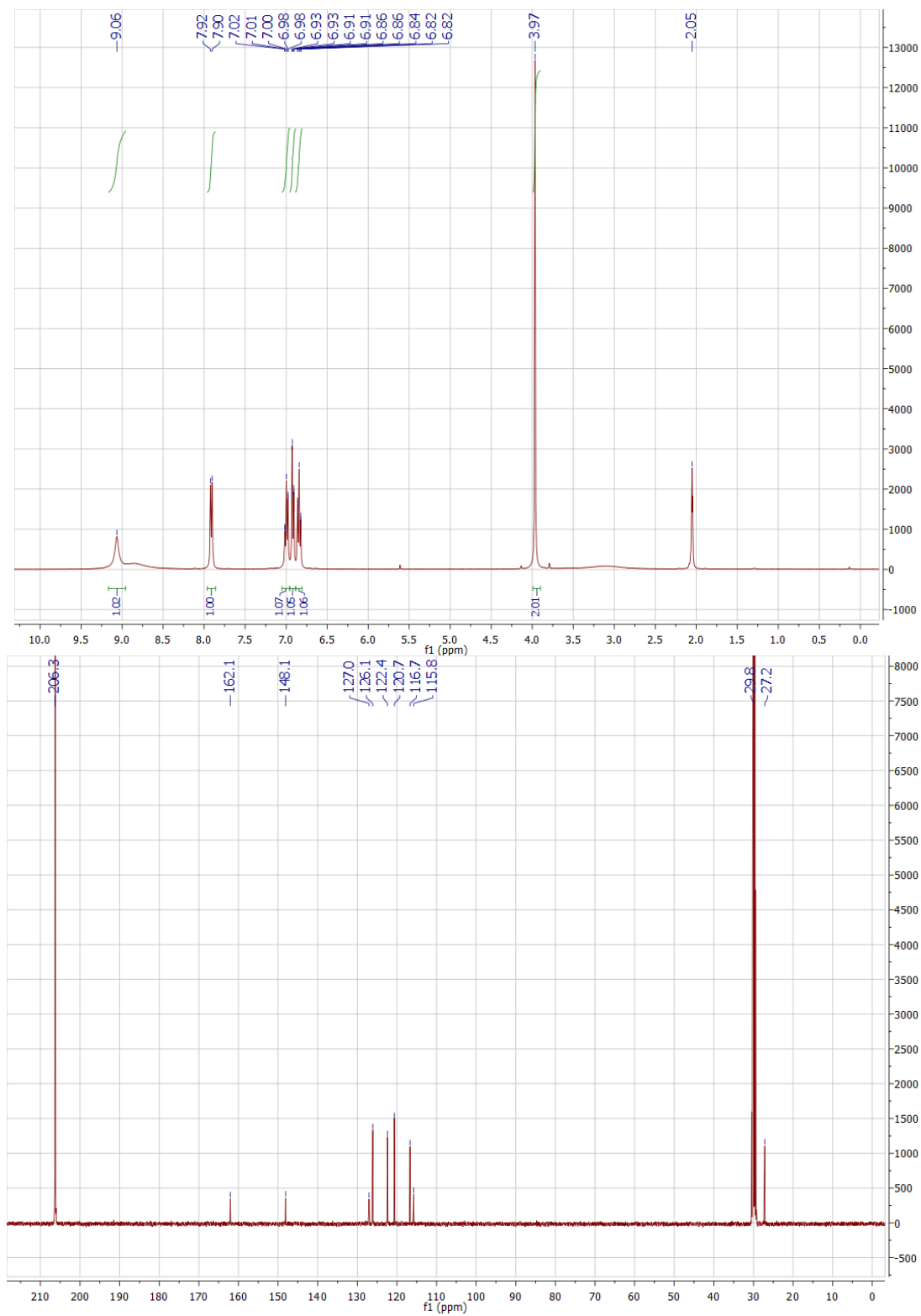
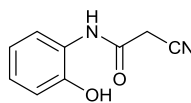
(2-Chloro-6-phenoxyphenyl)methanamine (22)



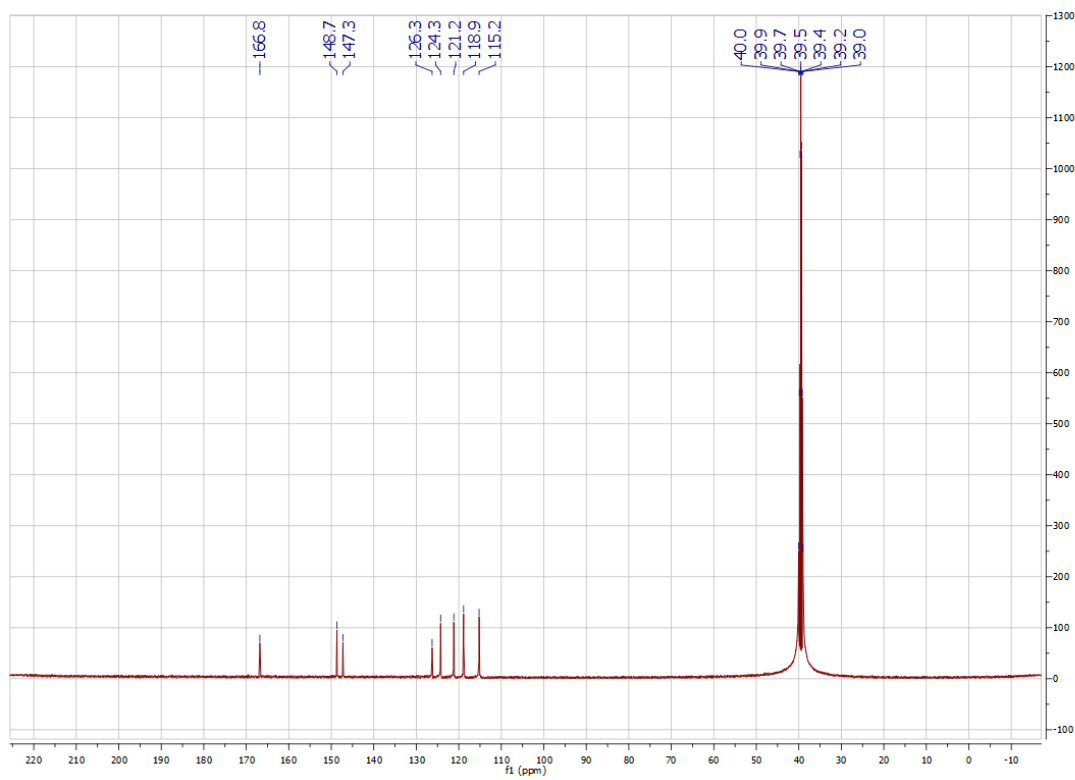
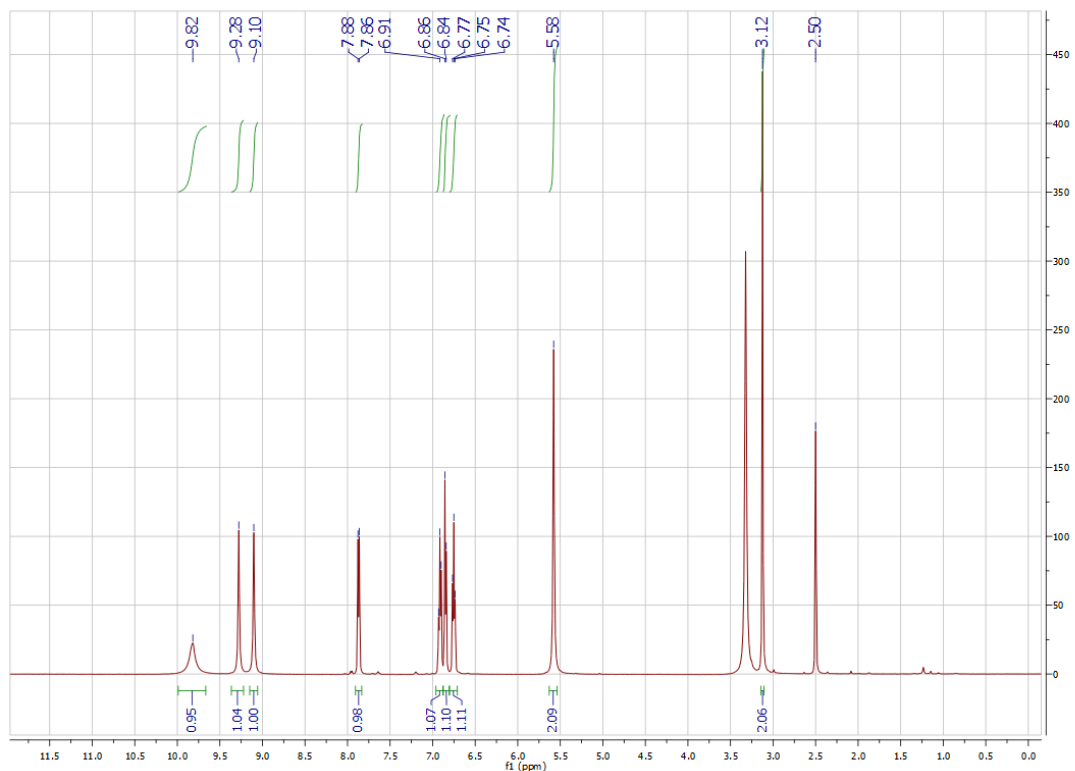
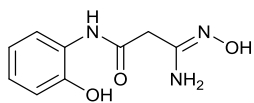
*N*³-(2-Chloro-6-phenoxybenzyl)-4*H*-1,2,4-triazole-3,5-diamine (**12**)



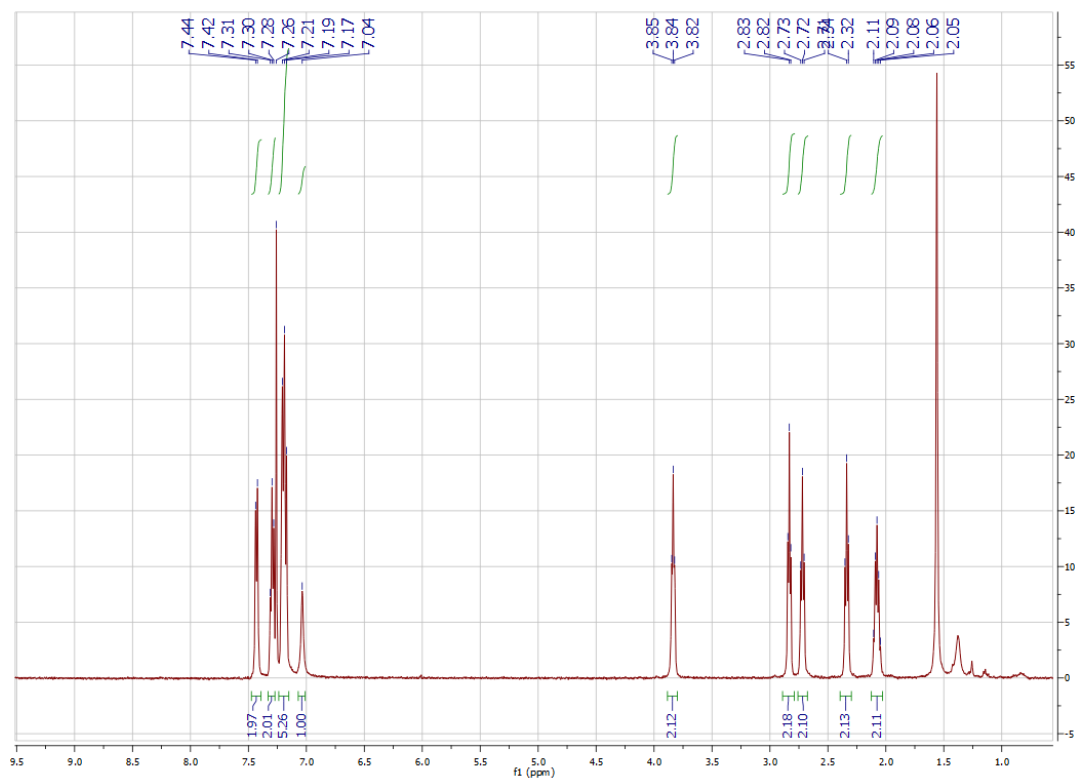
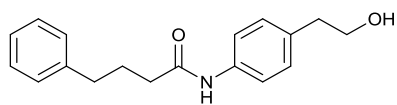
2-Cyano-N-(2-hydroxyphenyl)acetamide (23)



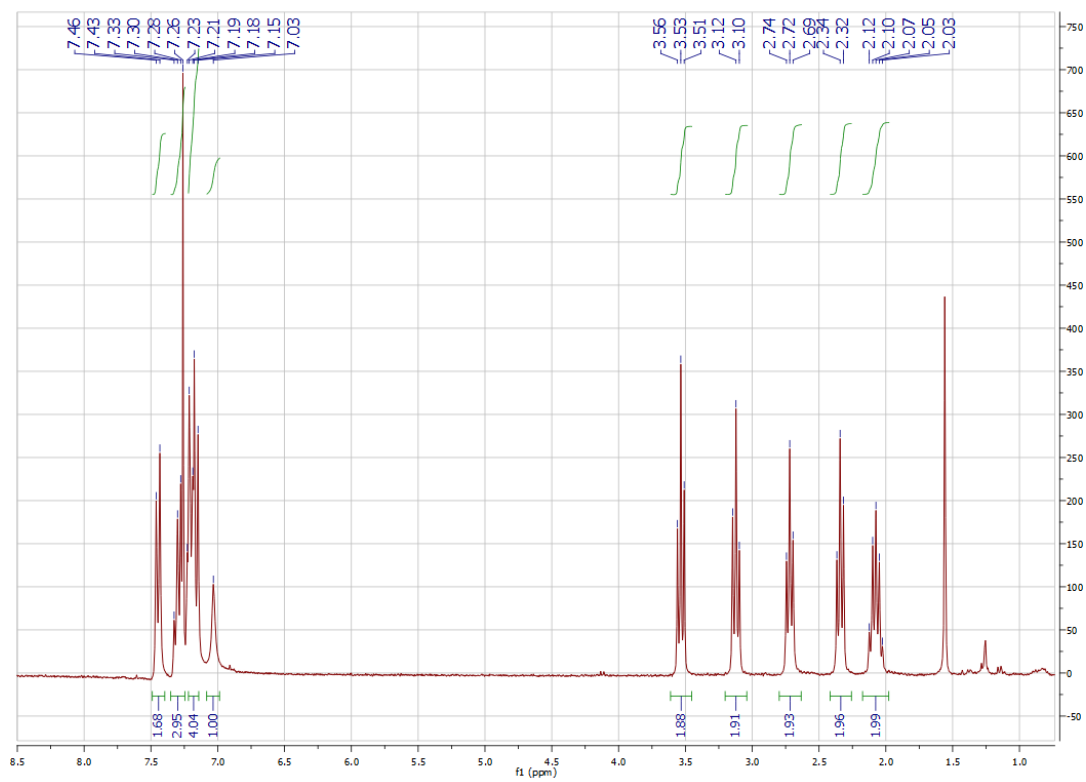
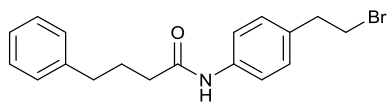
(3-Amino-3-(hydroxyimino)-N-[2-(hydroxyl)phenyl]propanamide) (13)



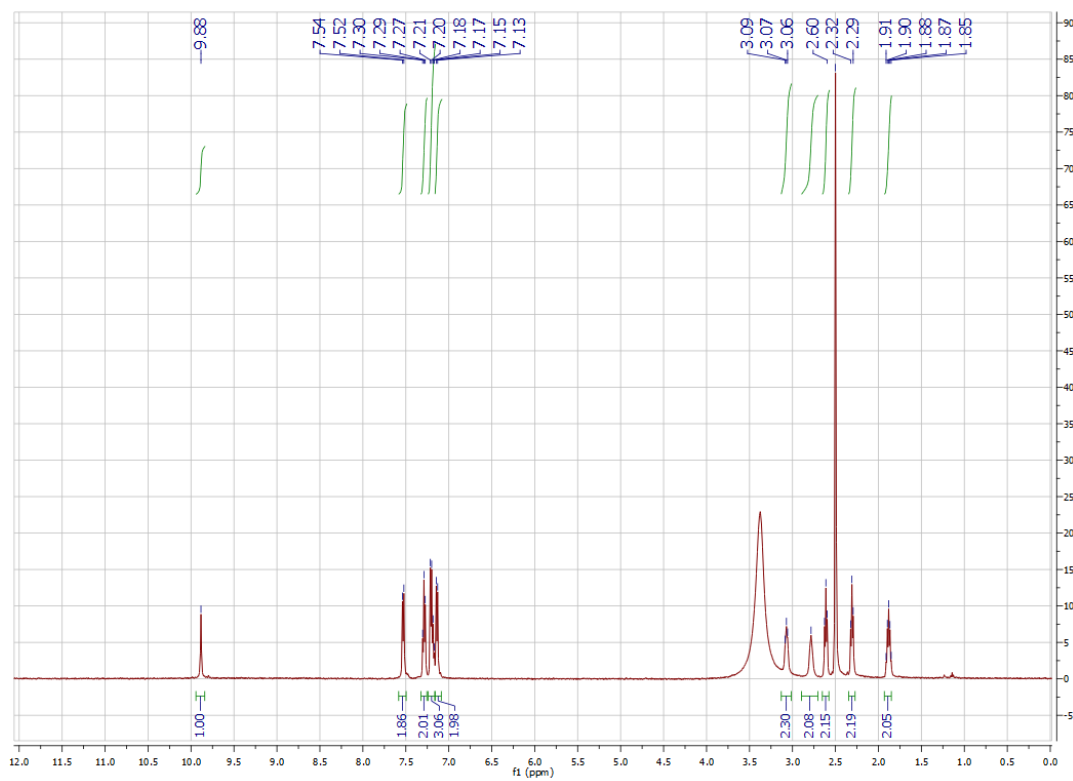
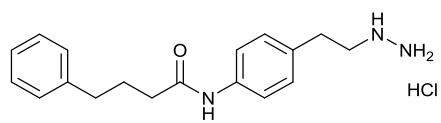
N-(4-(2-Hydroxyethyl)phenyl)-4-phenylbutanamide (**25**)



N-(4-(2-Bromoethyl)phenyl)-4-phenylbutanamide



Bizine

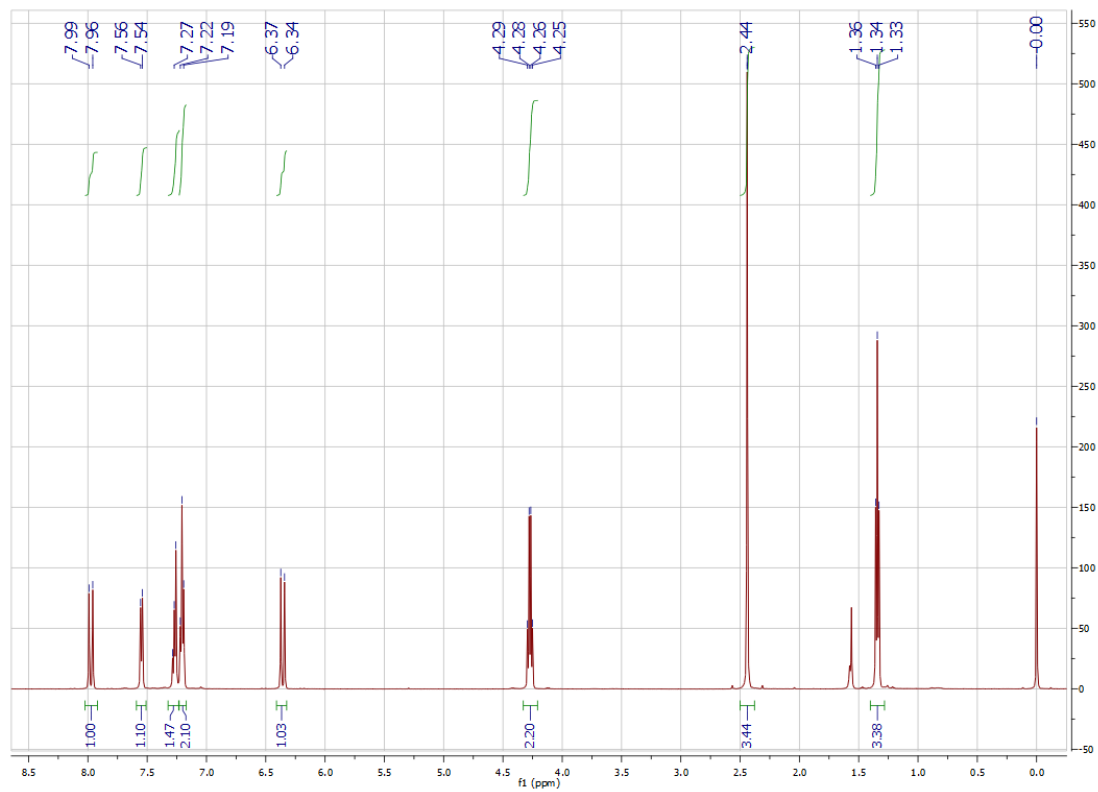
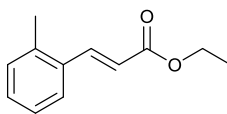


Appendix 3

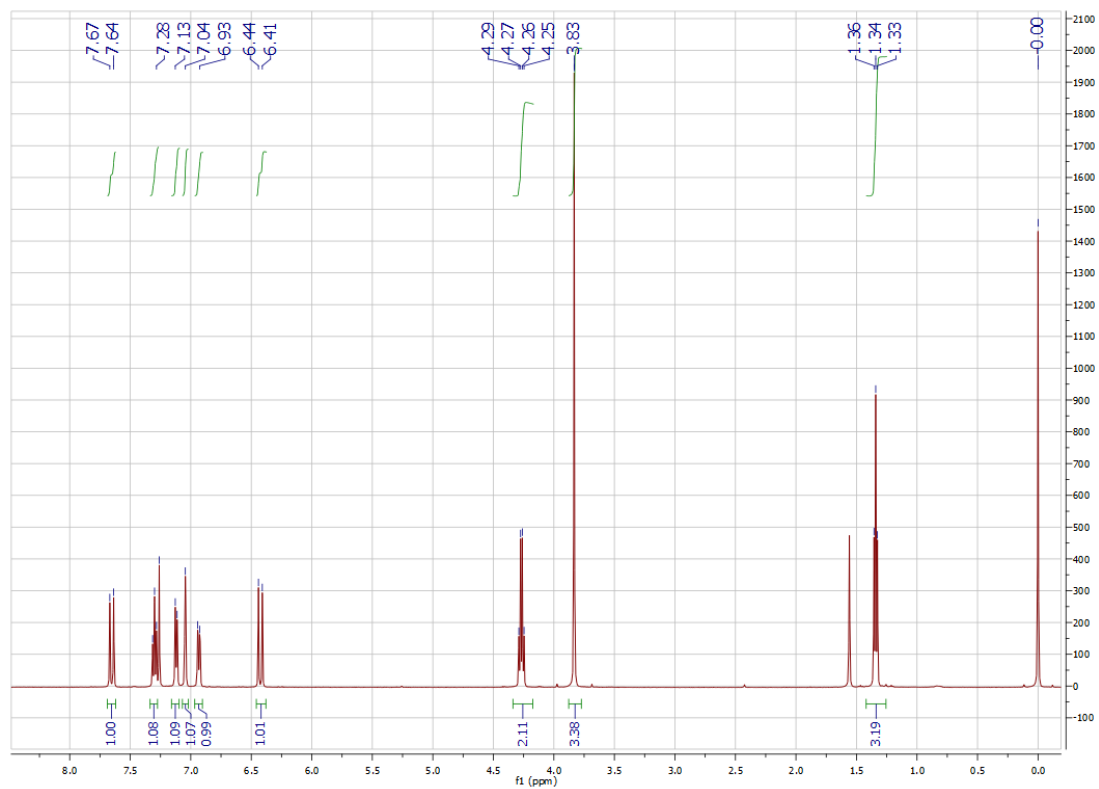
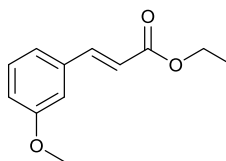
NMR spectra for Chapter 3

Synthesis and biological evaluation of metallocene derivatives of cyclopropylamines

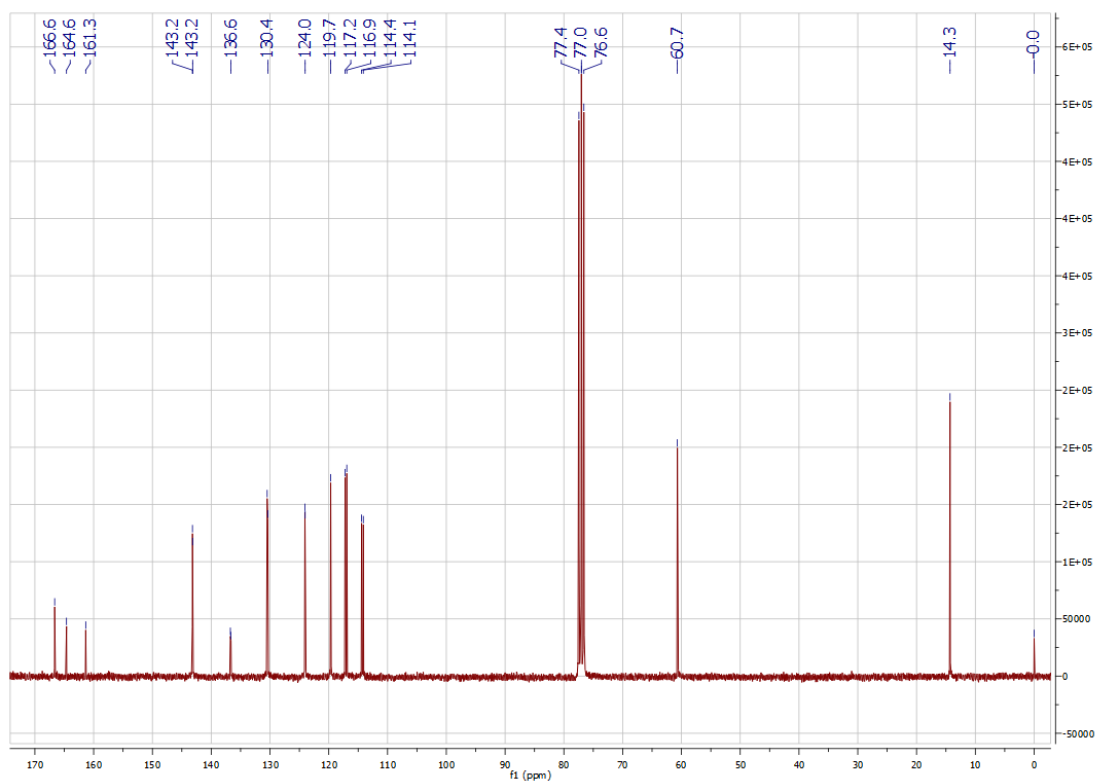
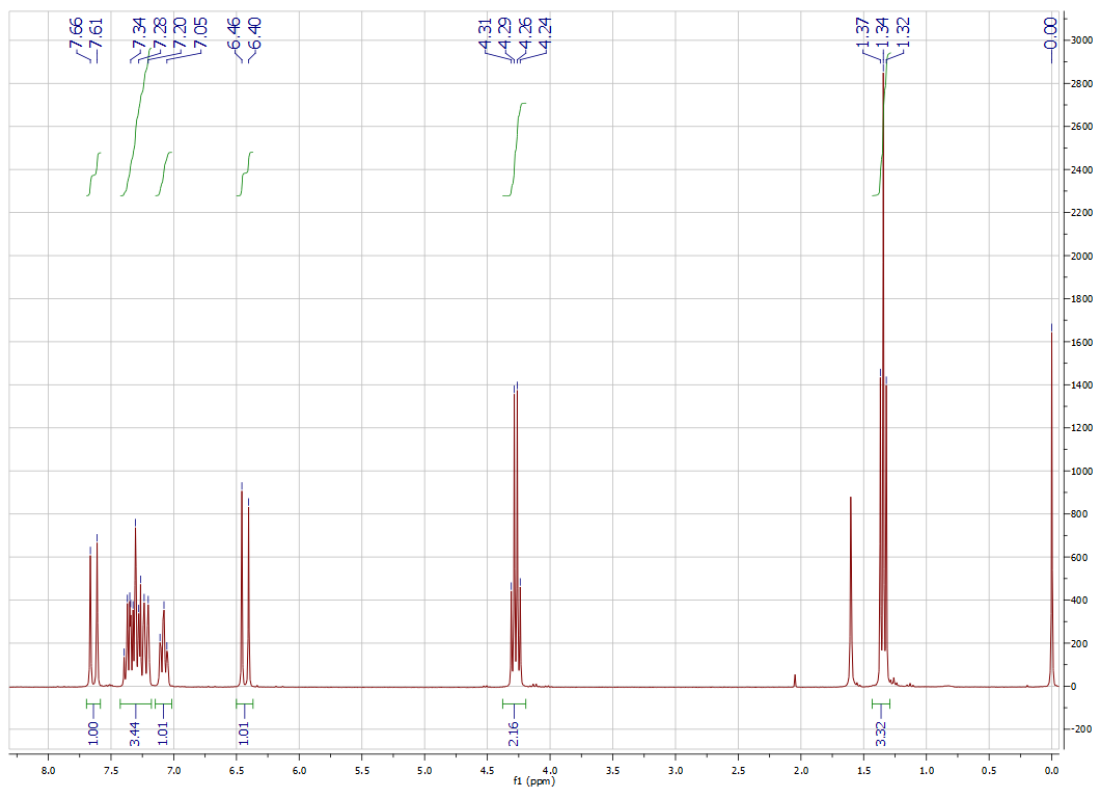
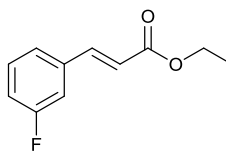
Ethyl (E)-3-(o-tolyl)-2-propenoate (59b)



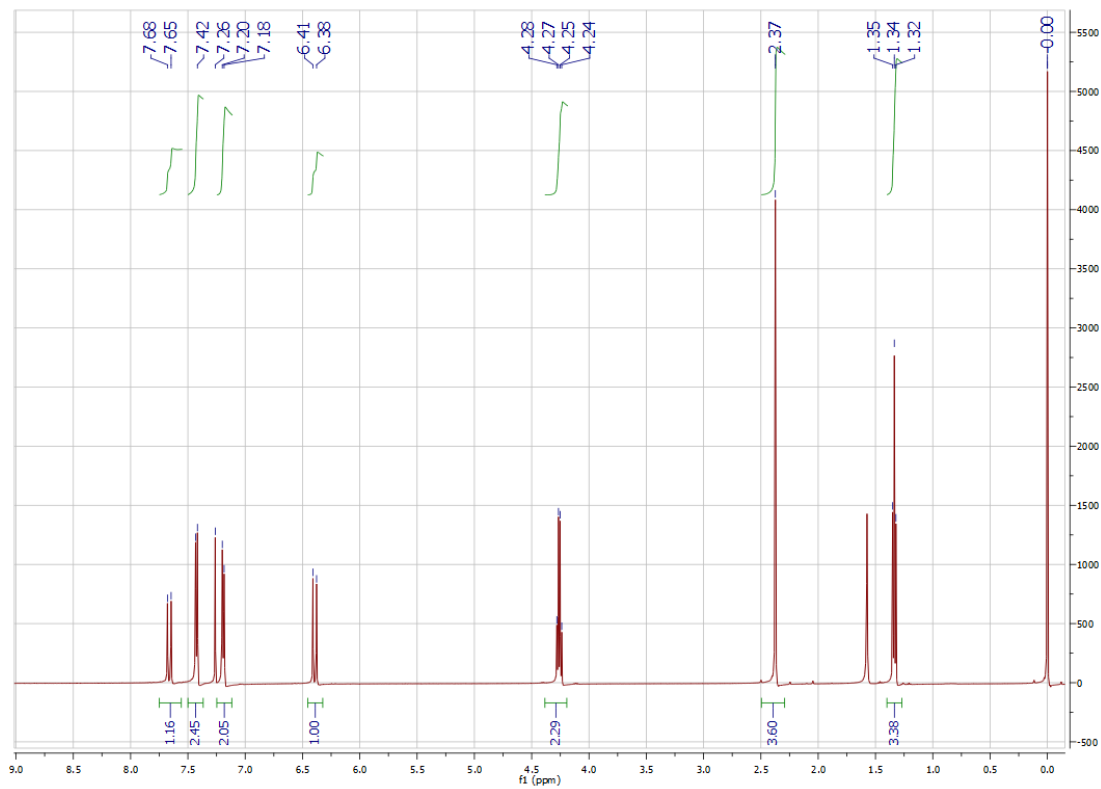
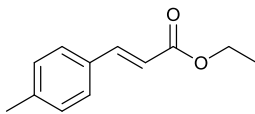
Ethyl (E)-3-(m-methoxyphenyl)-2-propenoate (59c)



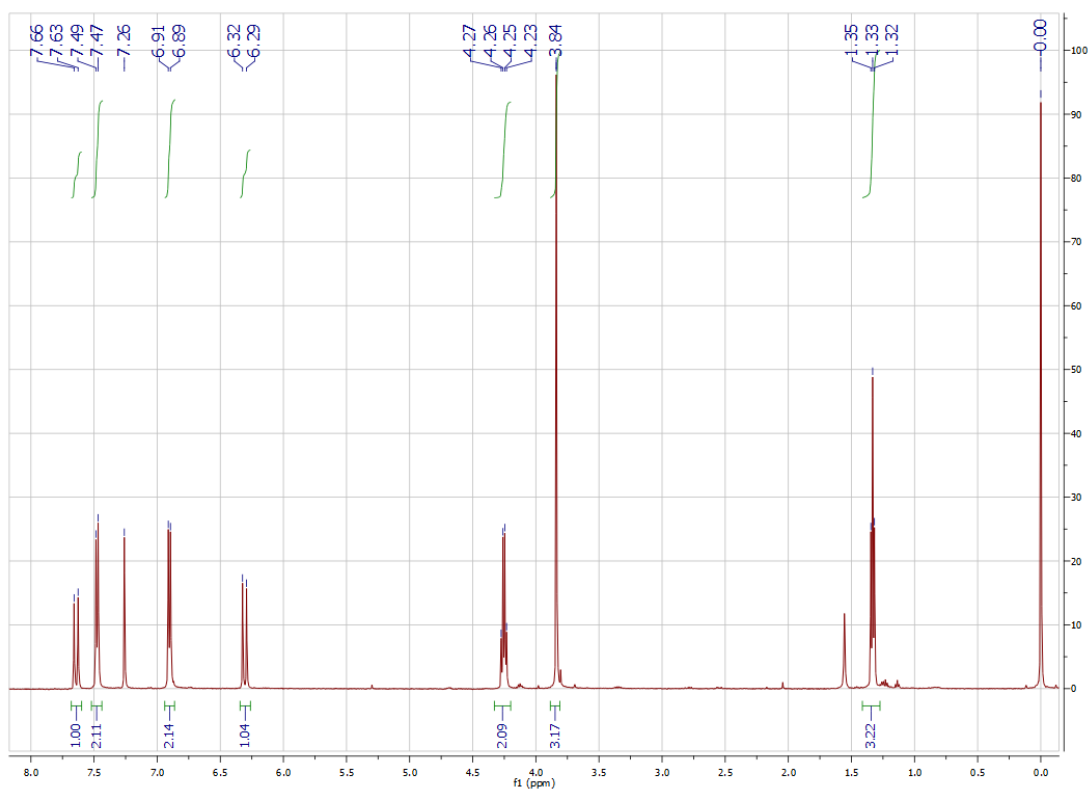
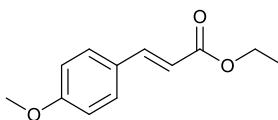
Ethyl (E)-3-(m-fluorophenyl)-2-propenoate (59d)



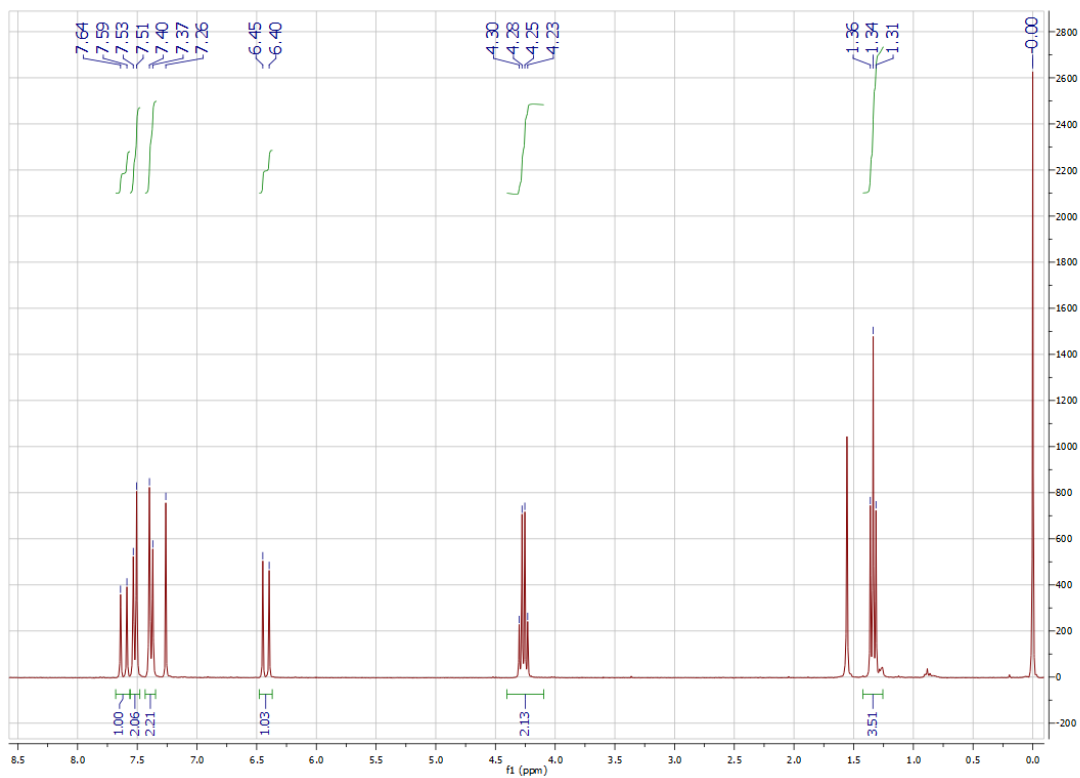
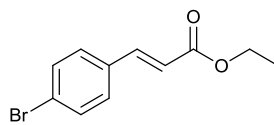
Ethyl (E)-3-(p-tolyl)-2-propenoate (59e)



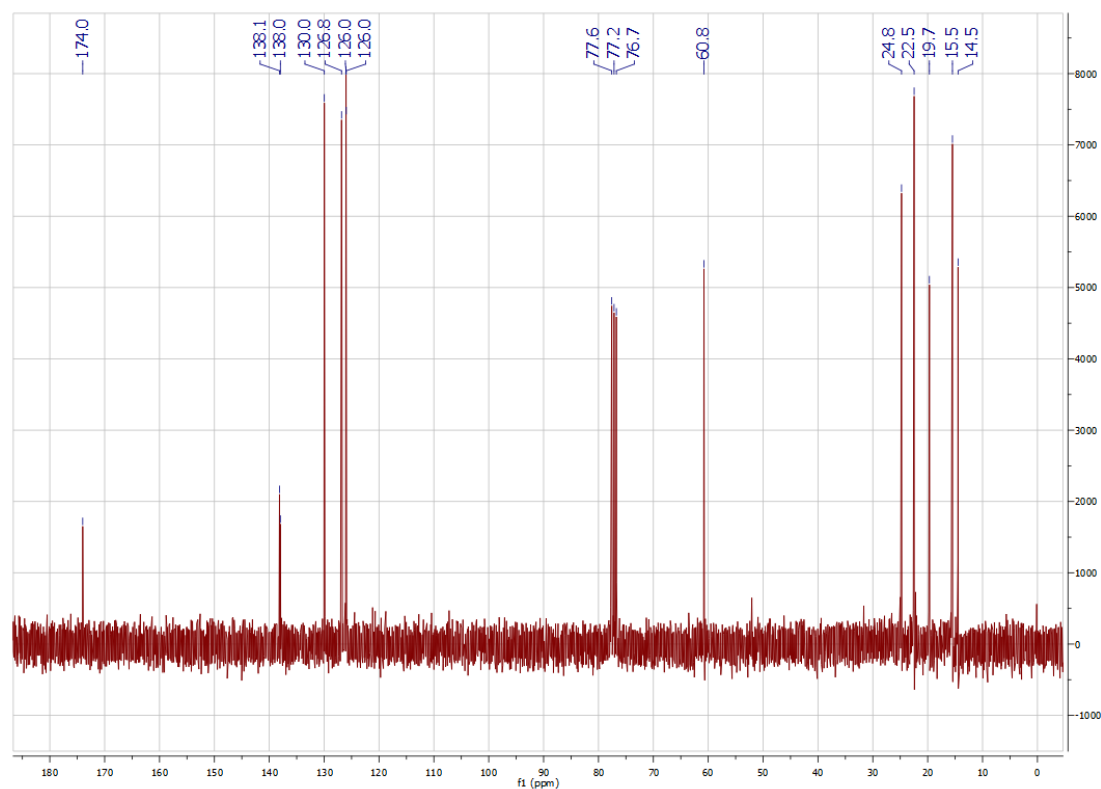
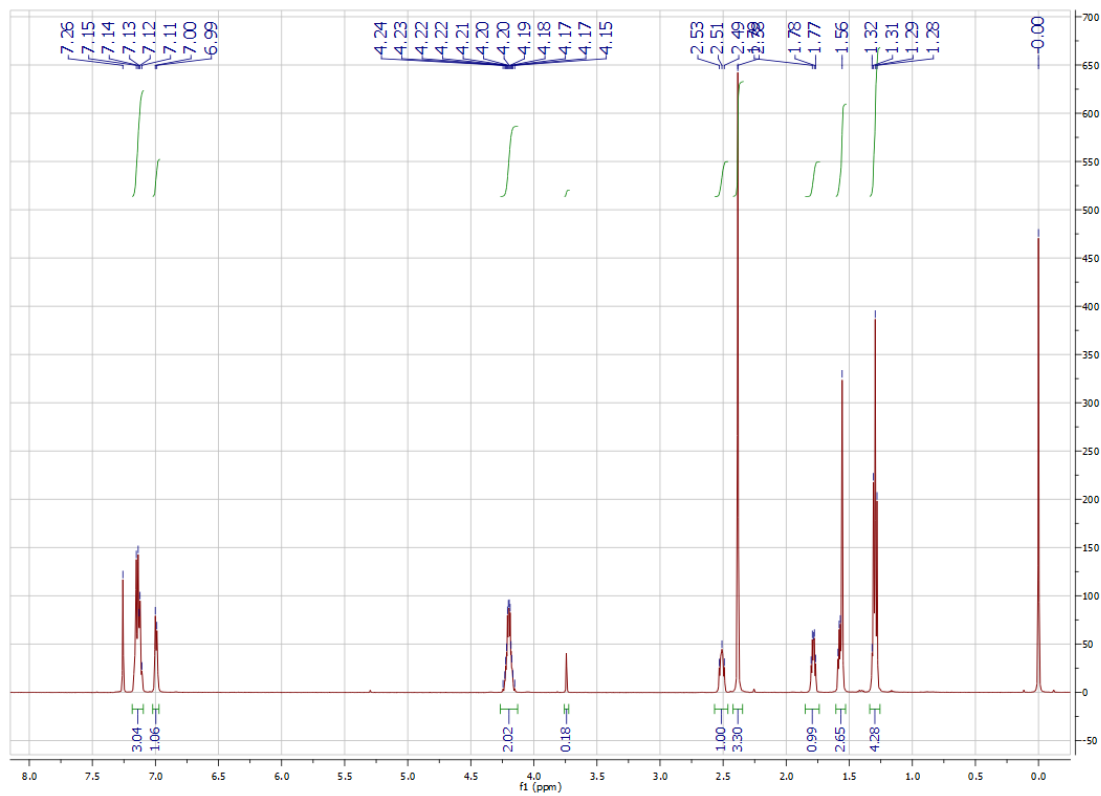
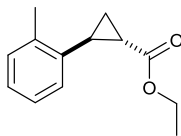
Ethyl (E)-3-(p-methoxyphenyl)-2-propenoate (59f)



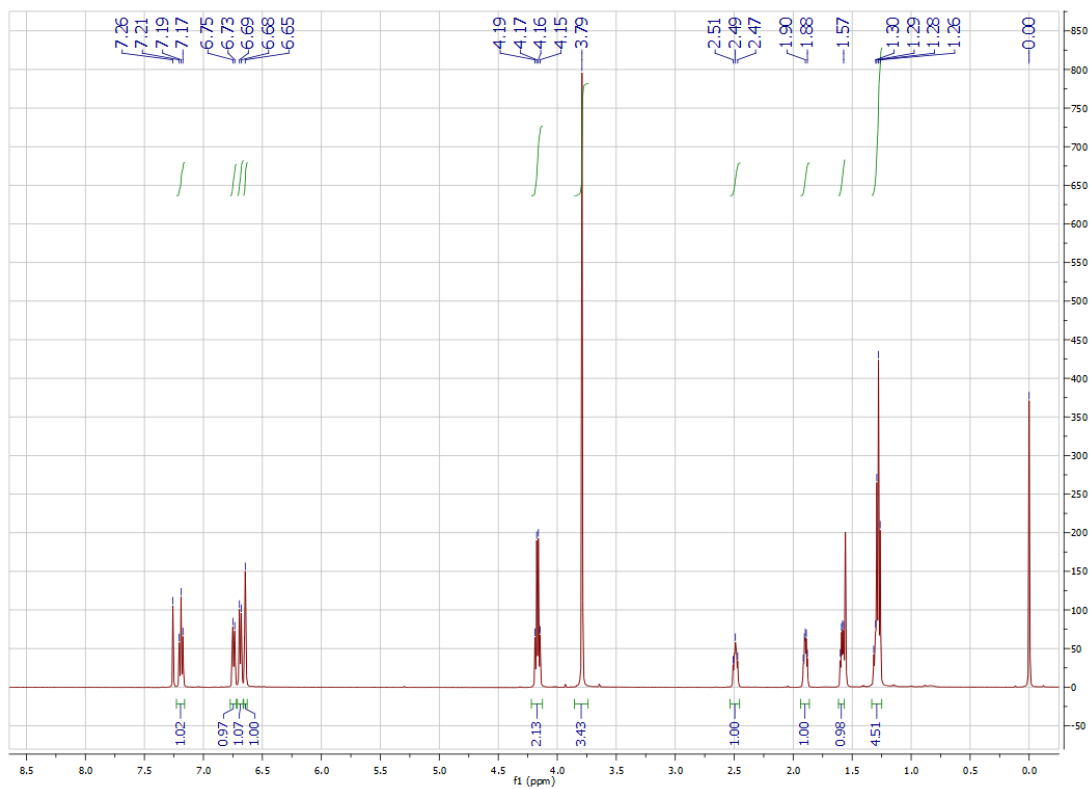
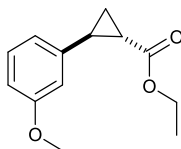
Ethyl (E)-3-(p-bromophenyl)-2-propenoate (59g)



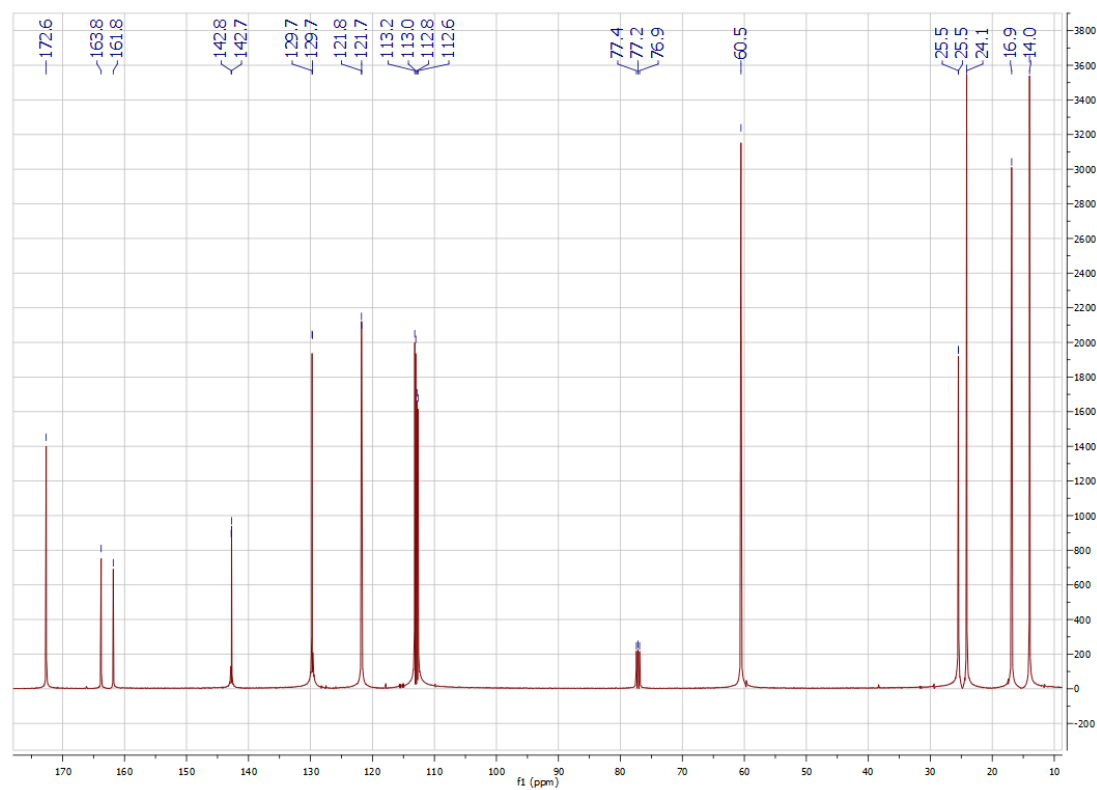
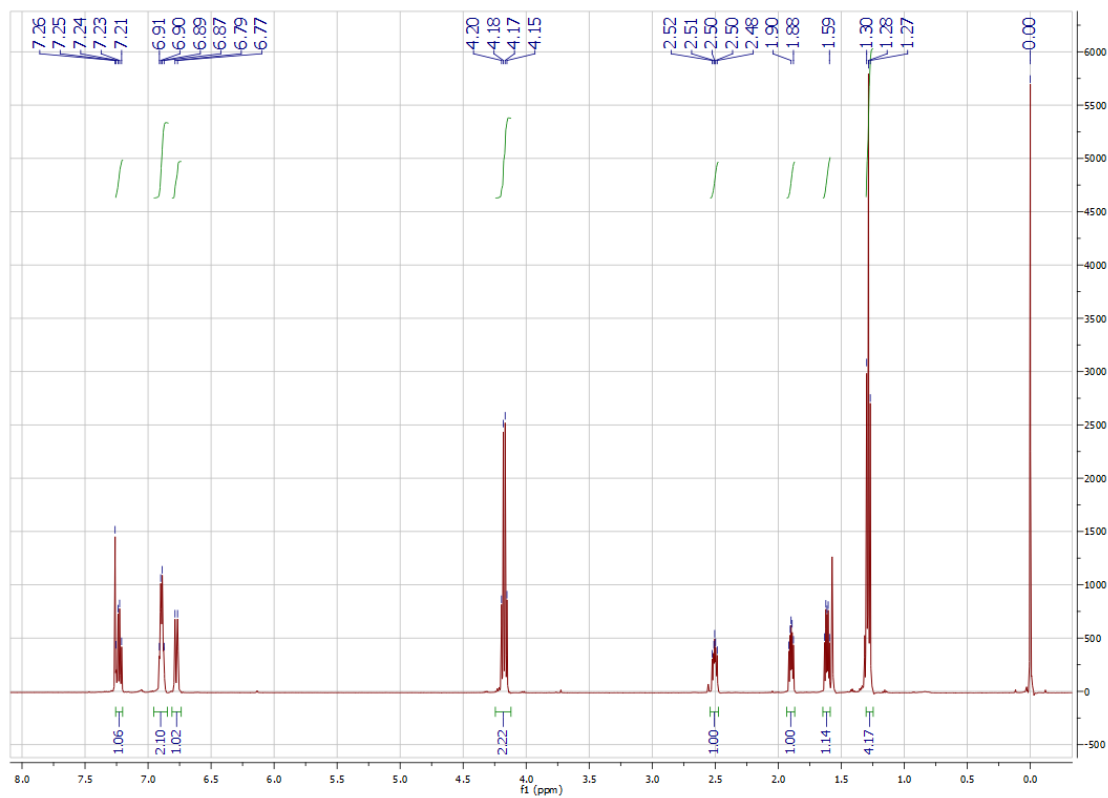
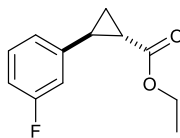
Ethyl 2-(*o*-tolyl)cyclopropane-1-carboxylate (**60b**)



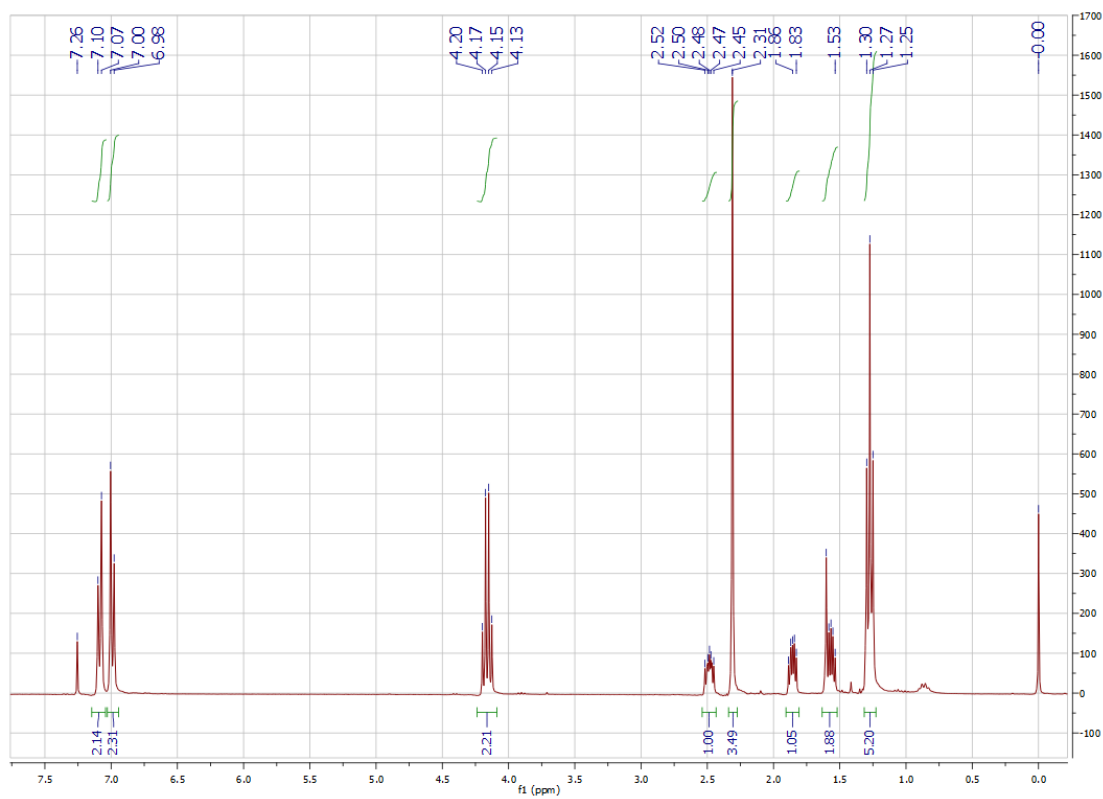
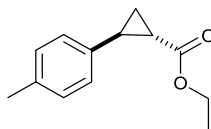
Ethyl 2-(*m*-methoxyphenyl)cyclopropane-1-carboxylate (**60c**)



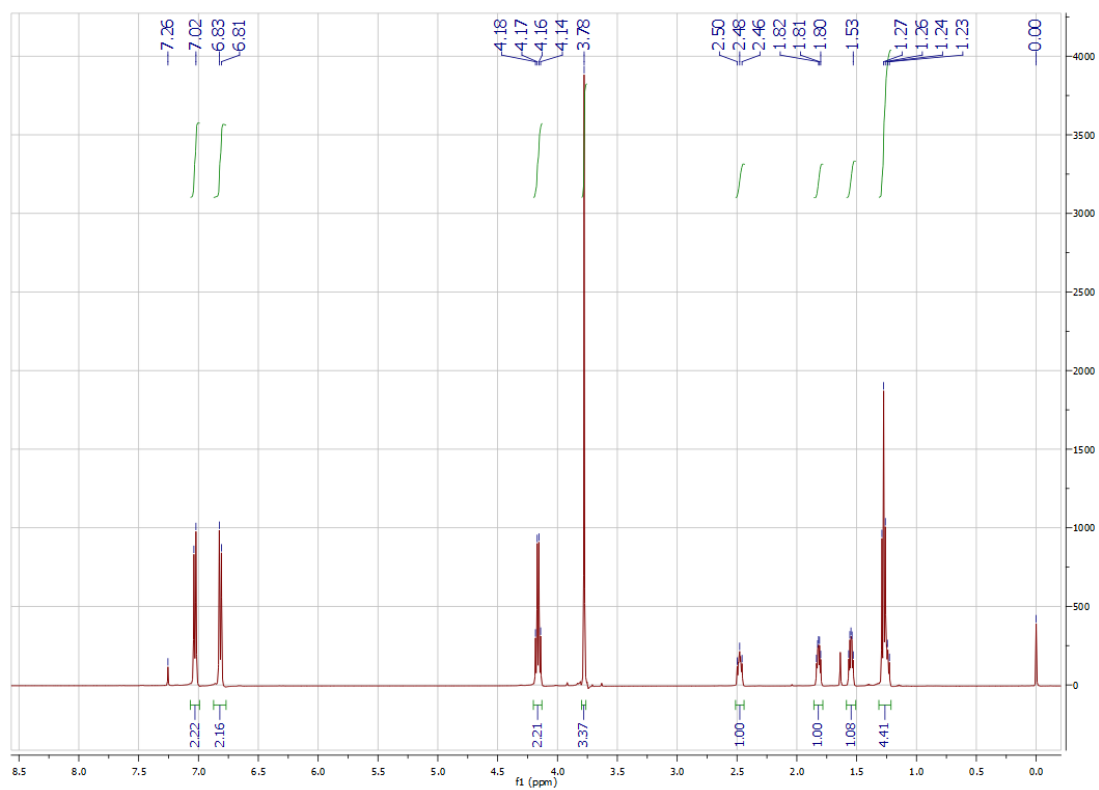
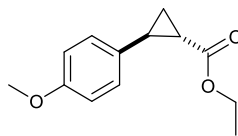
Ethyl 2-(*m*-fluorophenyl)cyclopropane-1-carboxylate (**60d**)



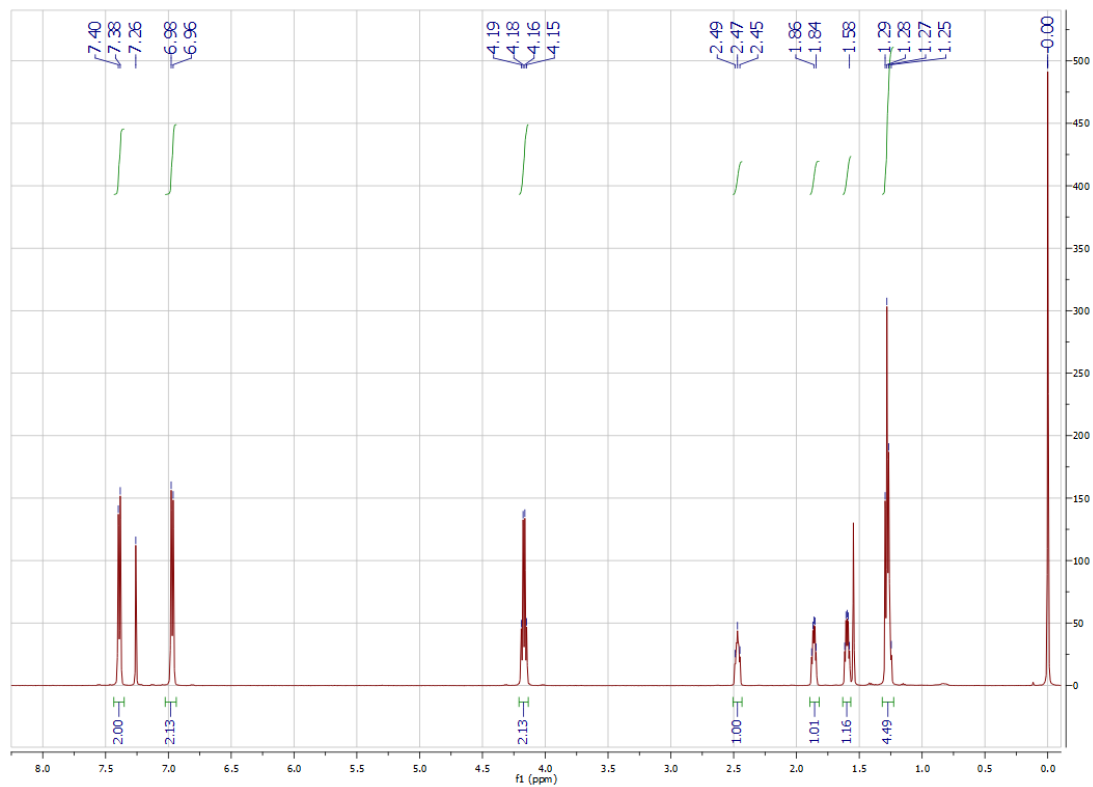
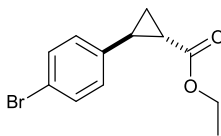
Ethyl 2-(p-tolyl)cyclopropane-1-carboxylate (60e)



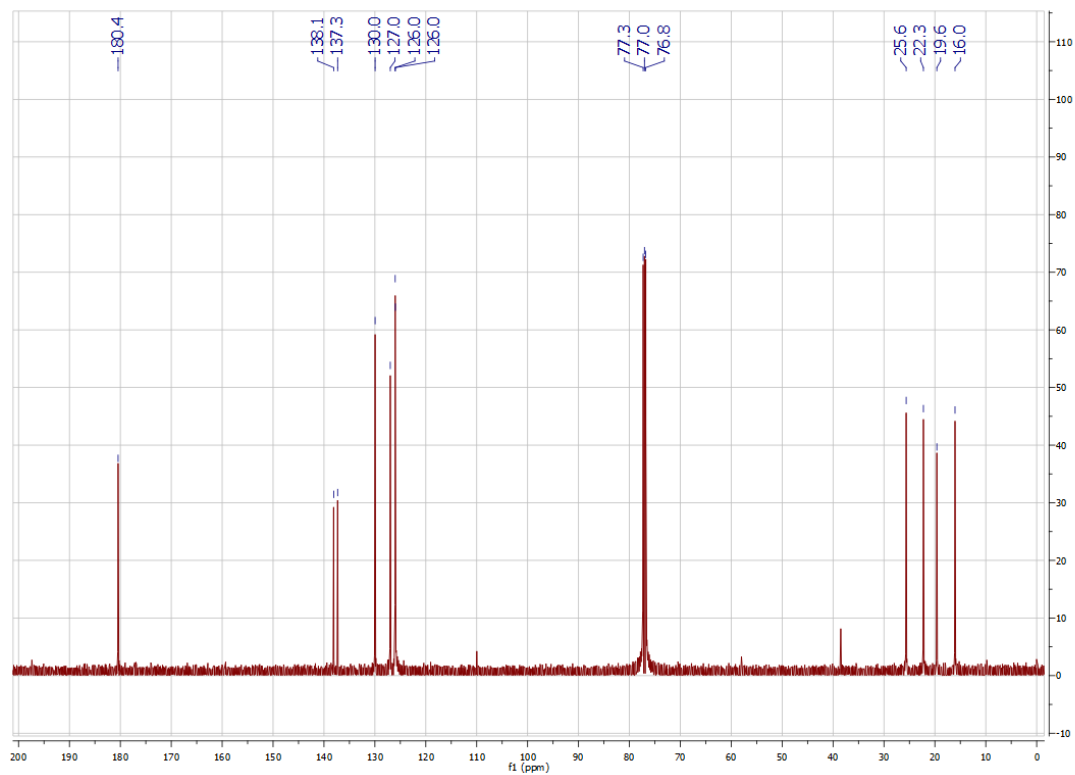
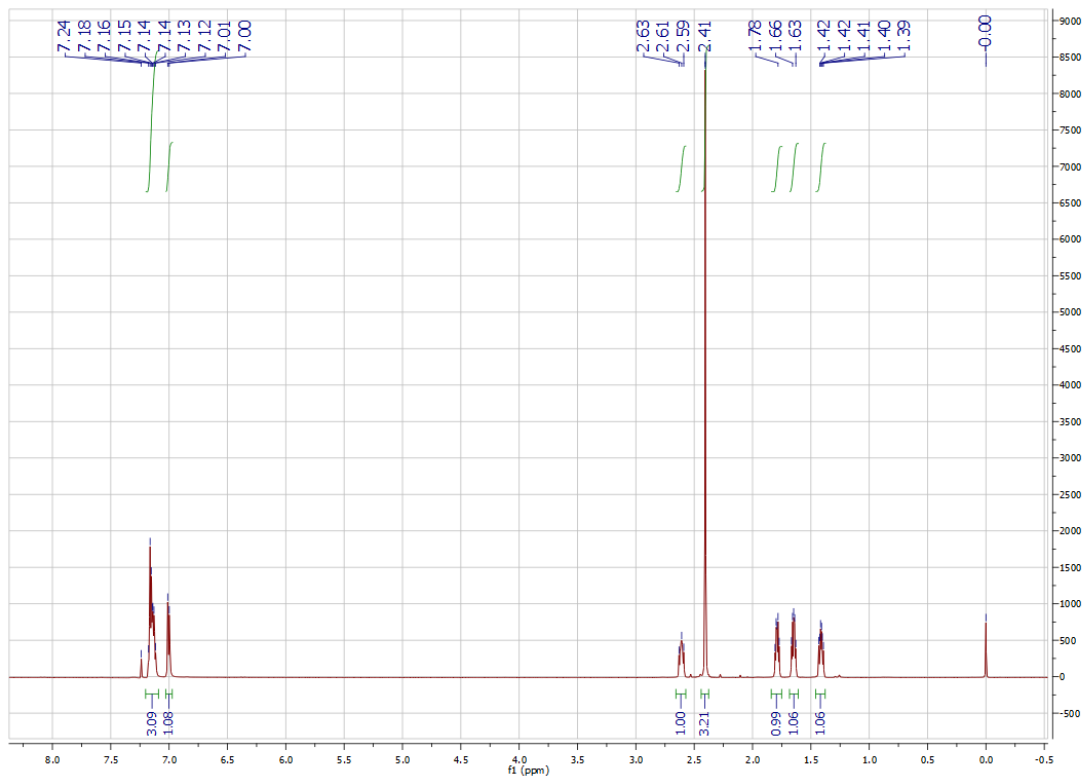
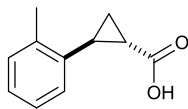
Ethyl 2-(p-methoxyphenyl)cyclopropane-1-carboxylate (60f)



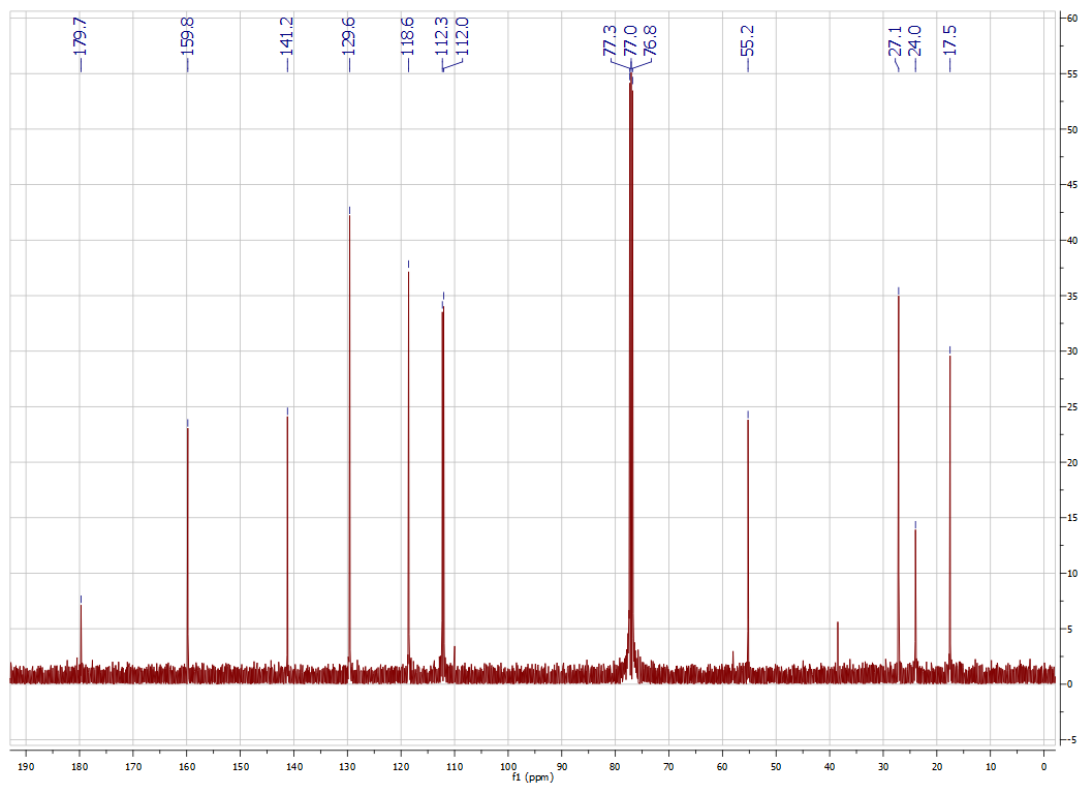
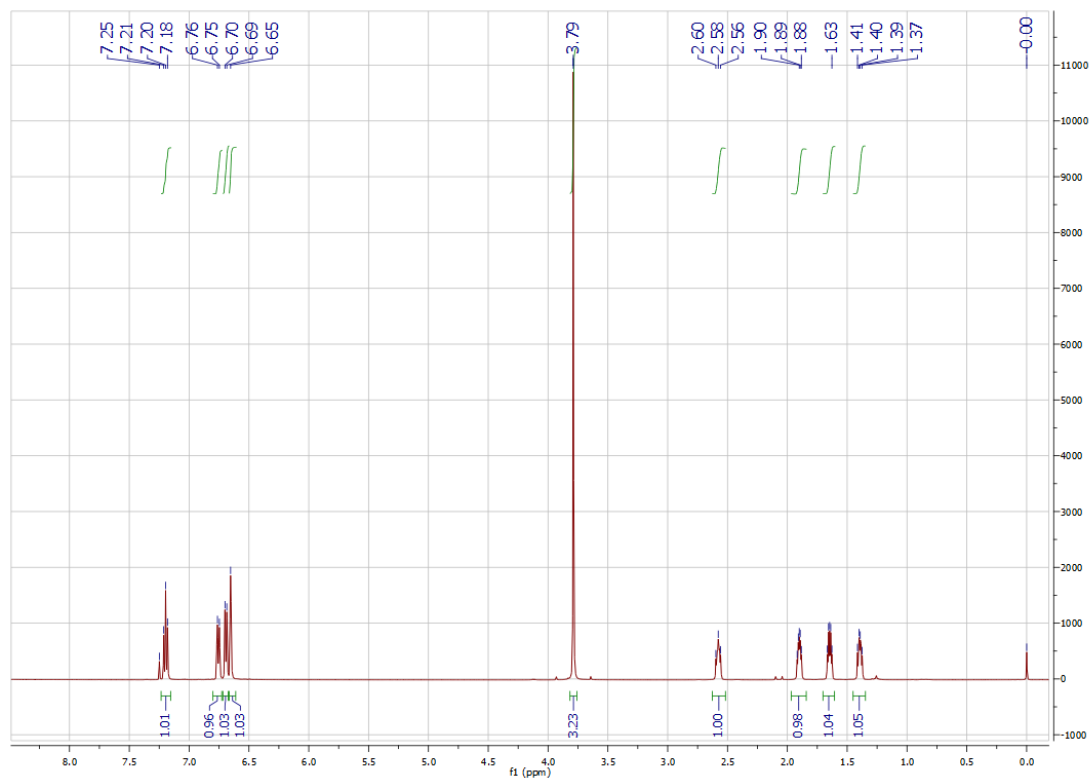
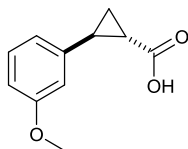
Ethyl 2-(p-bromophenyl)cyclopropane-1-carboxylate (60g)



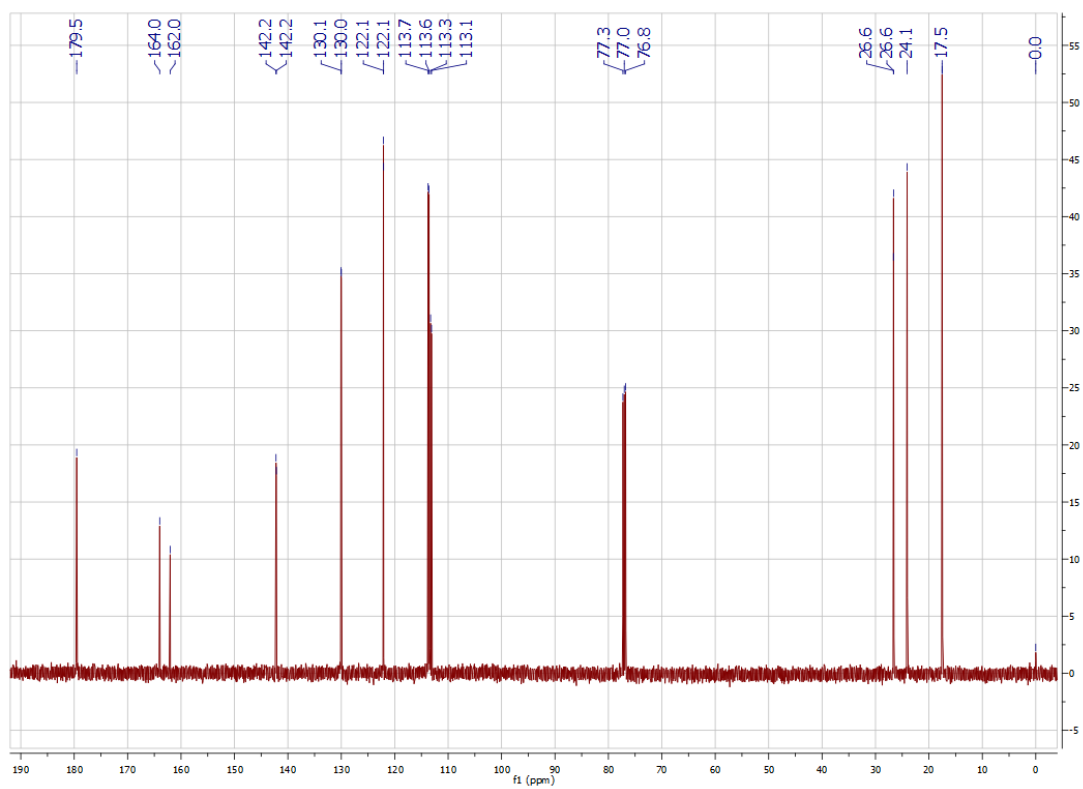
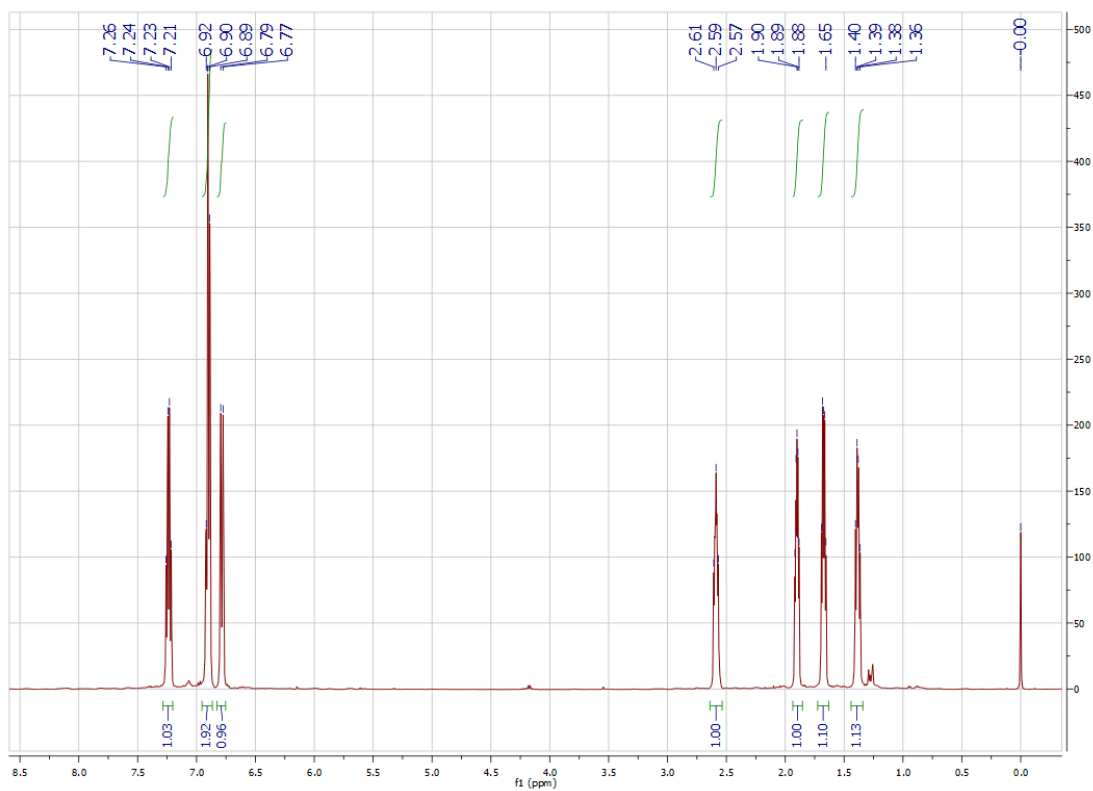
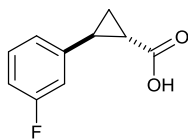
2-(*o*-Tolyl)cyclopropane-1-carboxylic acid (**61b**)



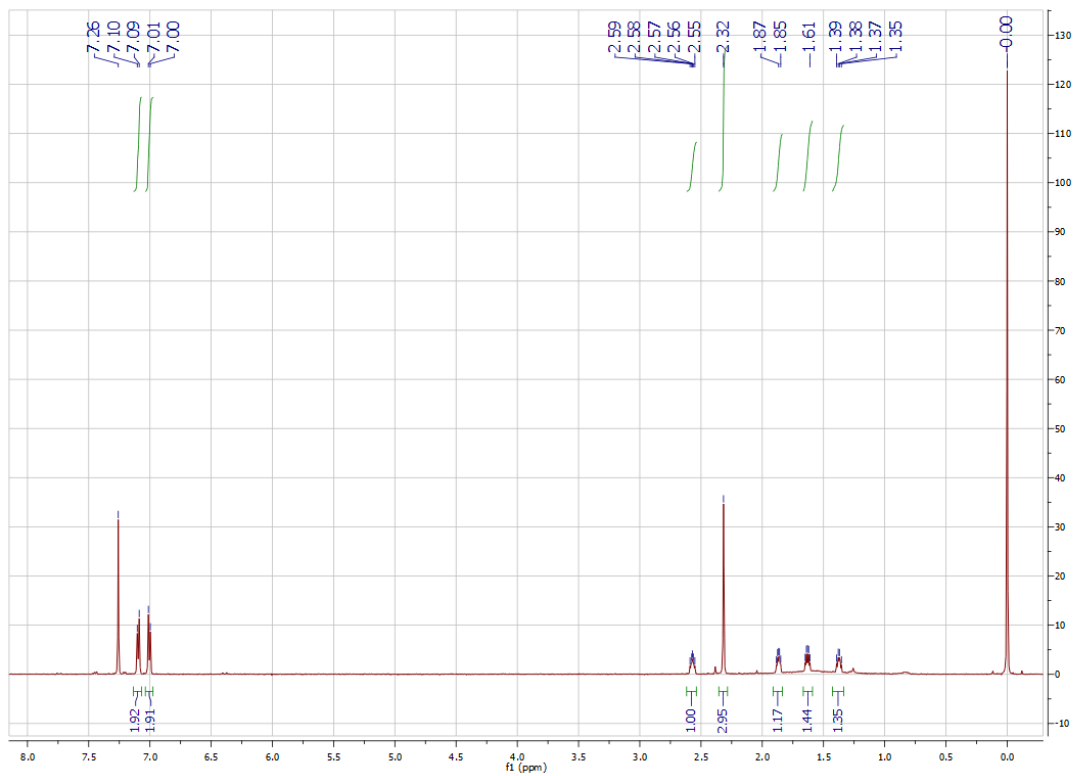
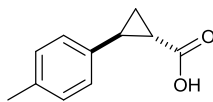
2-(*m*-Methoxyphenyl)cyclopropane-1-carboxylic acid (**61c**)



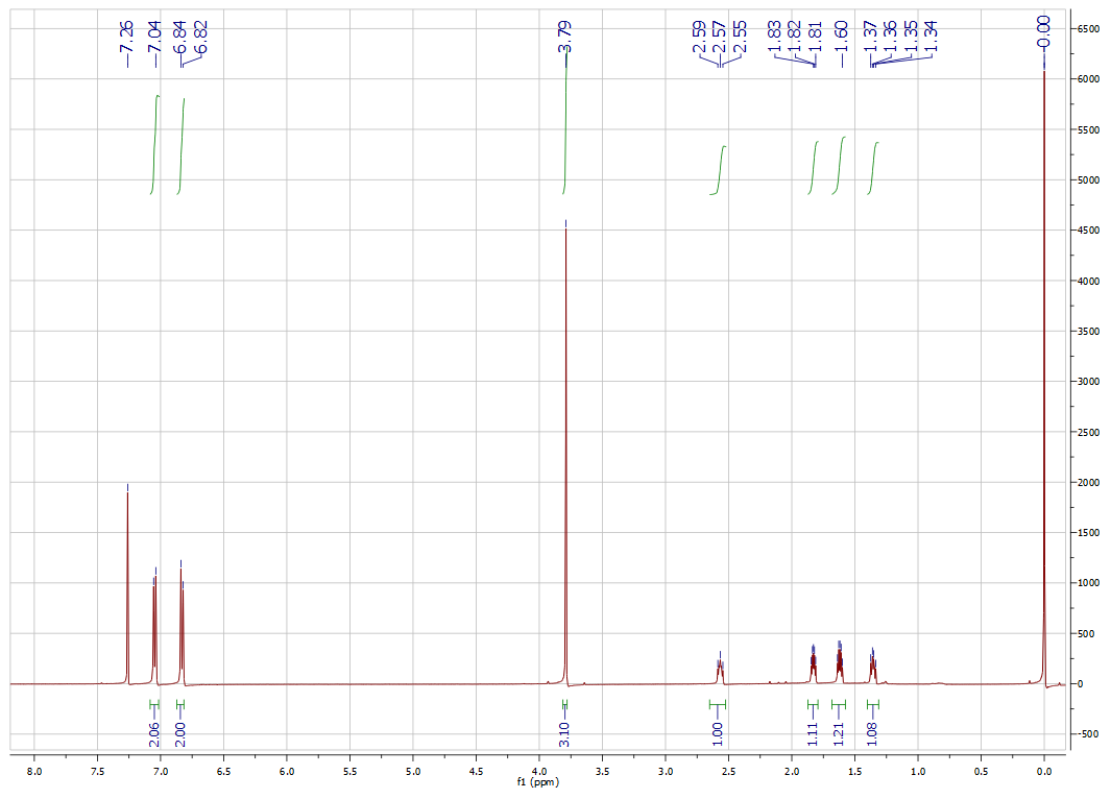
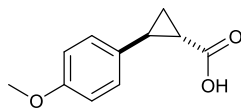
2-(*m*-Fluorophenyl)cyclopropane-1-carboxylic acid (**61d**)



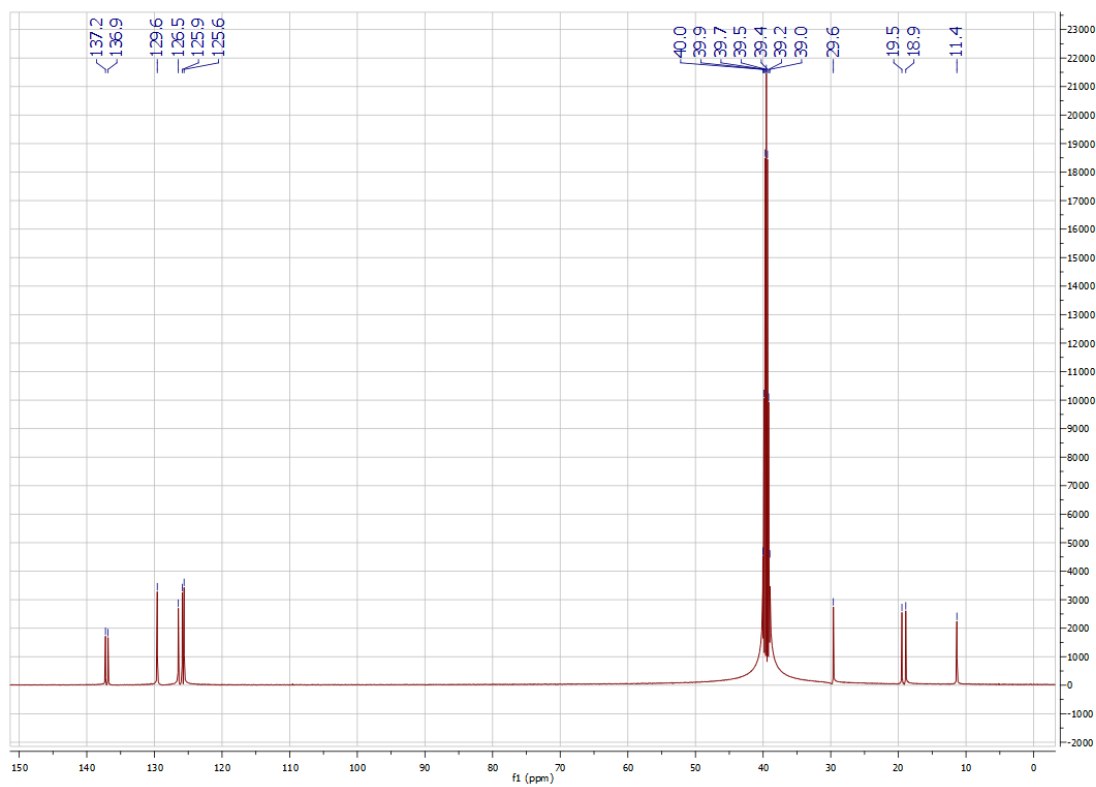
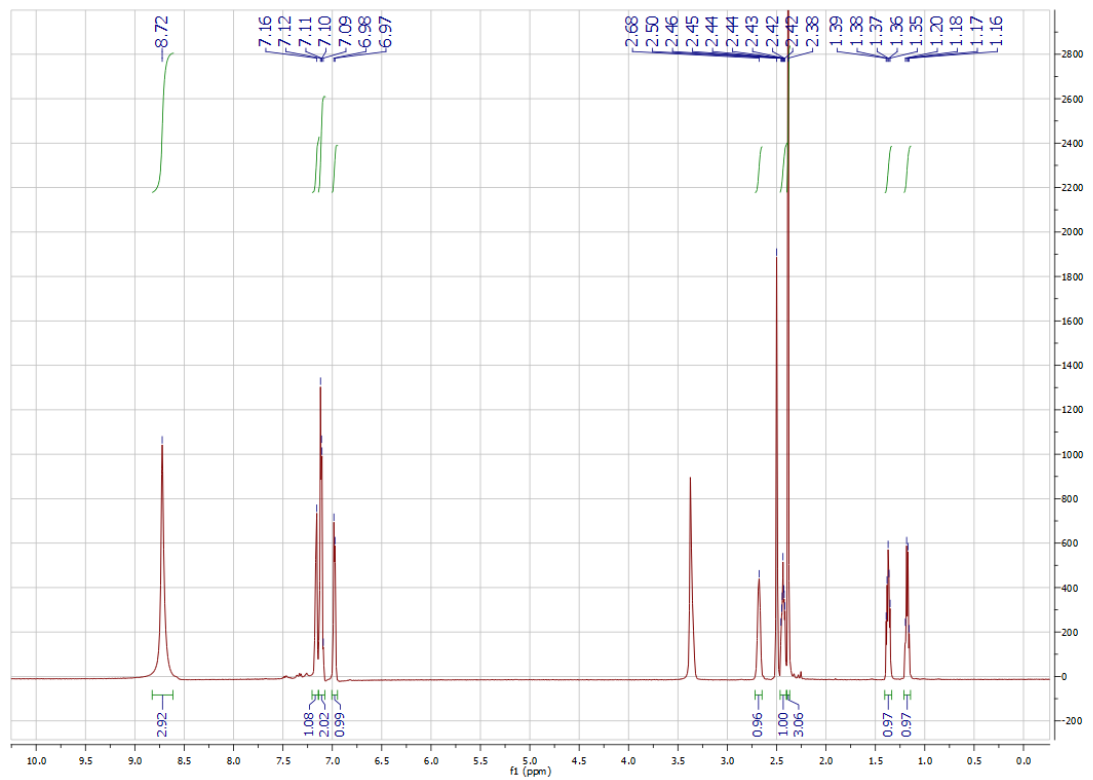
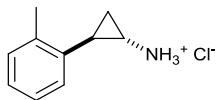
2-(*p*-Tolyl)cyclopropane-1-carboxylic acid (**61e**)



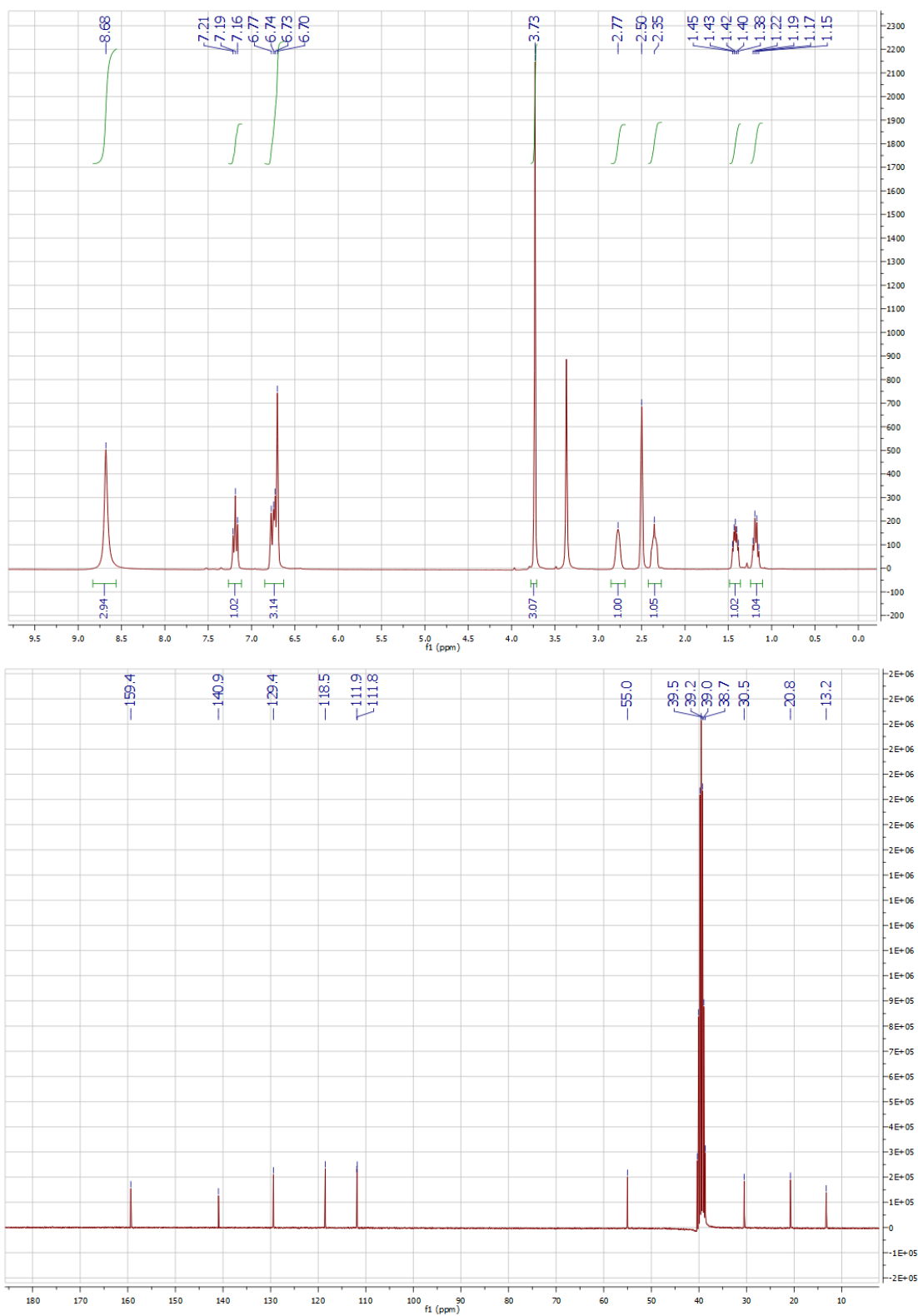
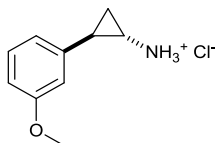
2-(*p*-Methoxyphenyl)cyclopropane-1-carboxylic acid (**61f**)



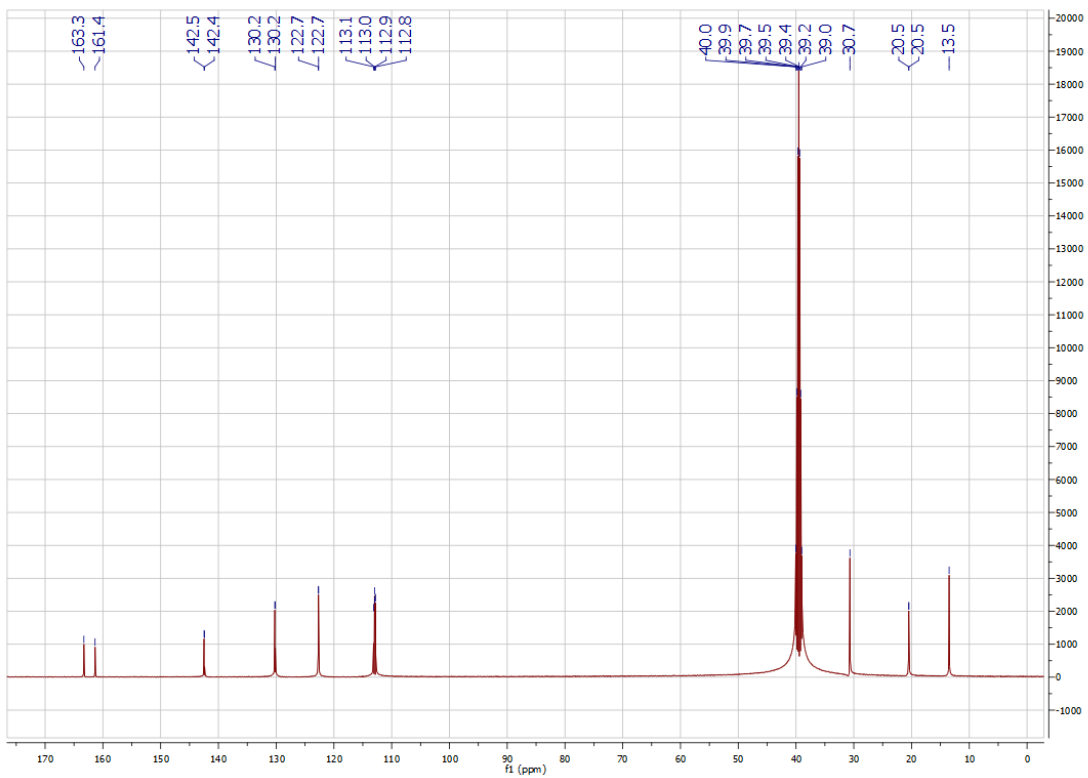
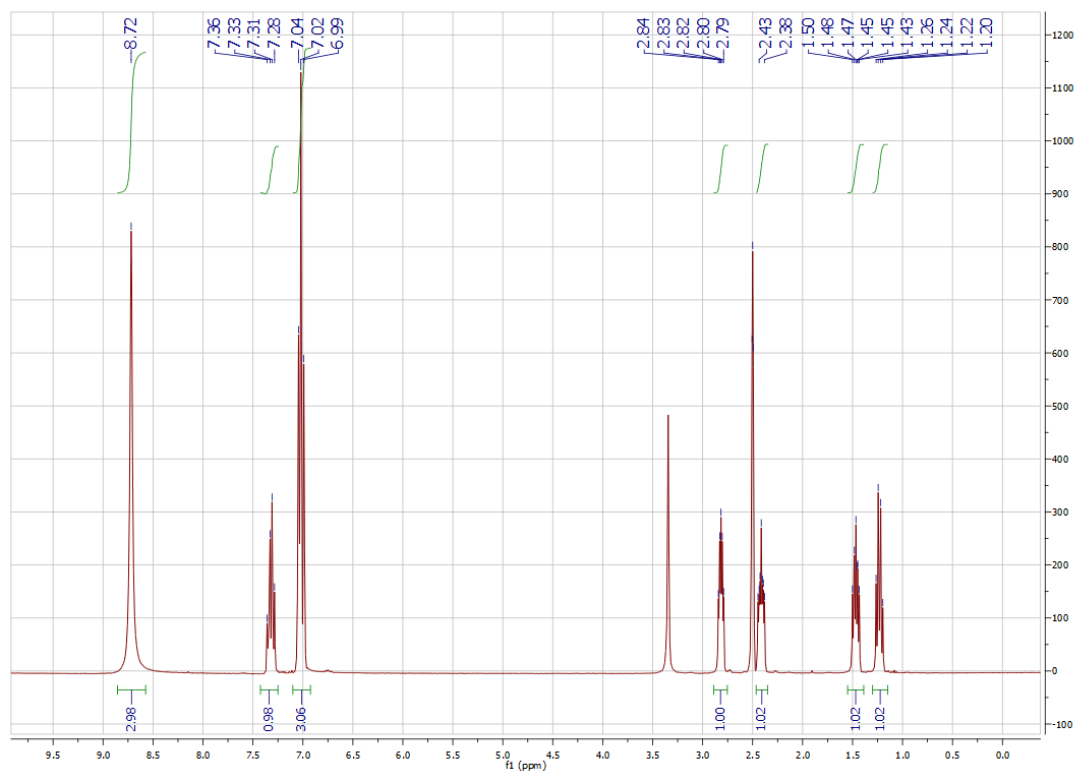
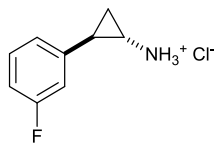
2-(*o*-Tolyl)cyclopropylamine hydrochloride (**62b**)



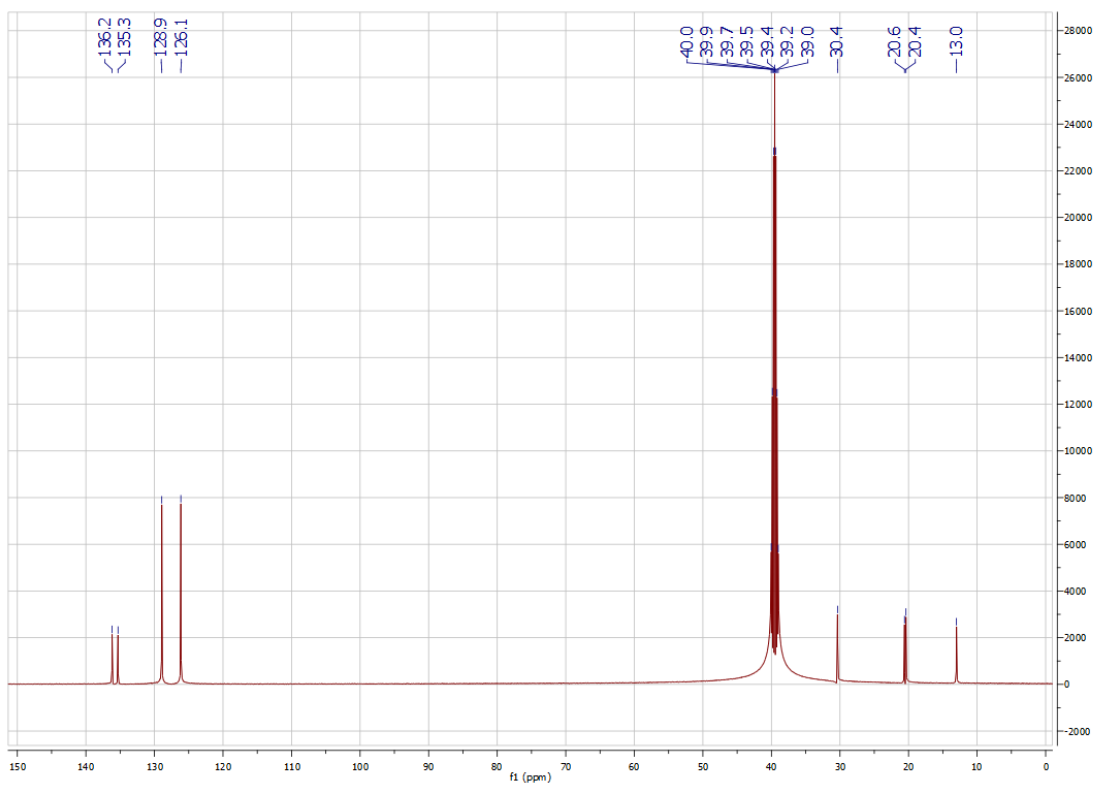
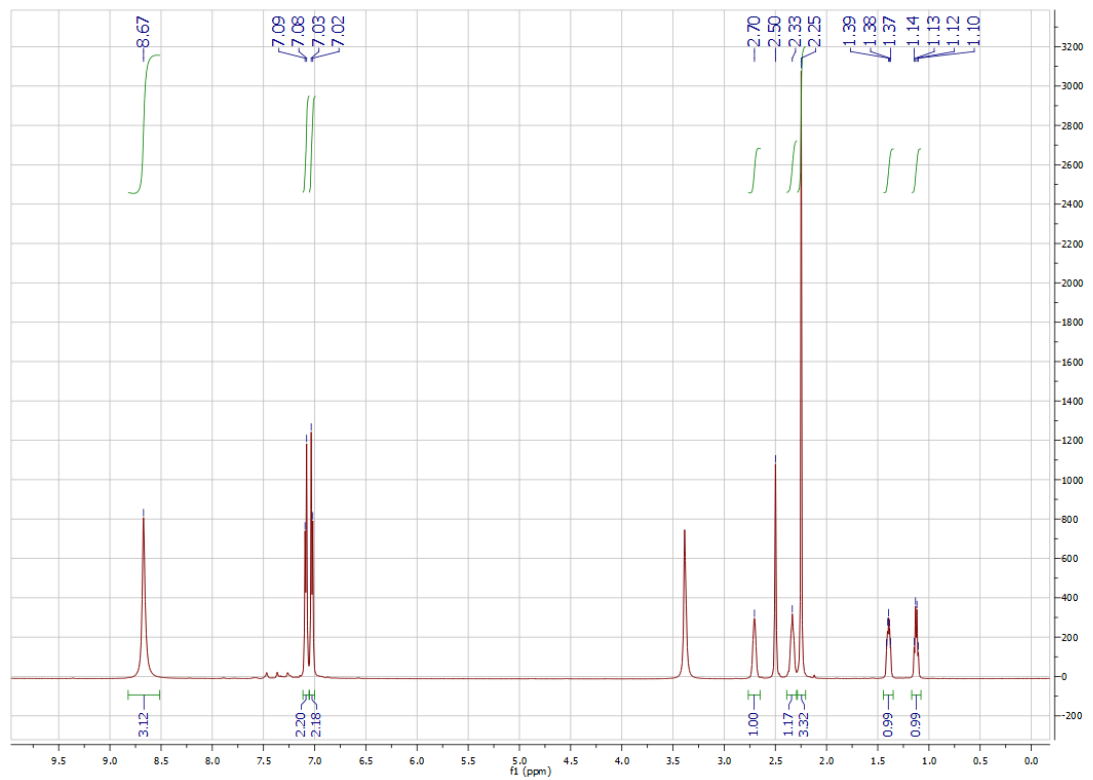
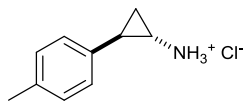
2-(*m*-Methoxyphenyl)cyclopropylamine hydrochloride (**62c**)



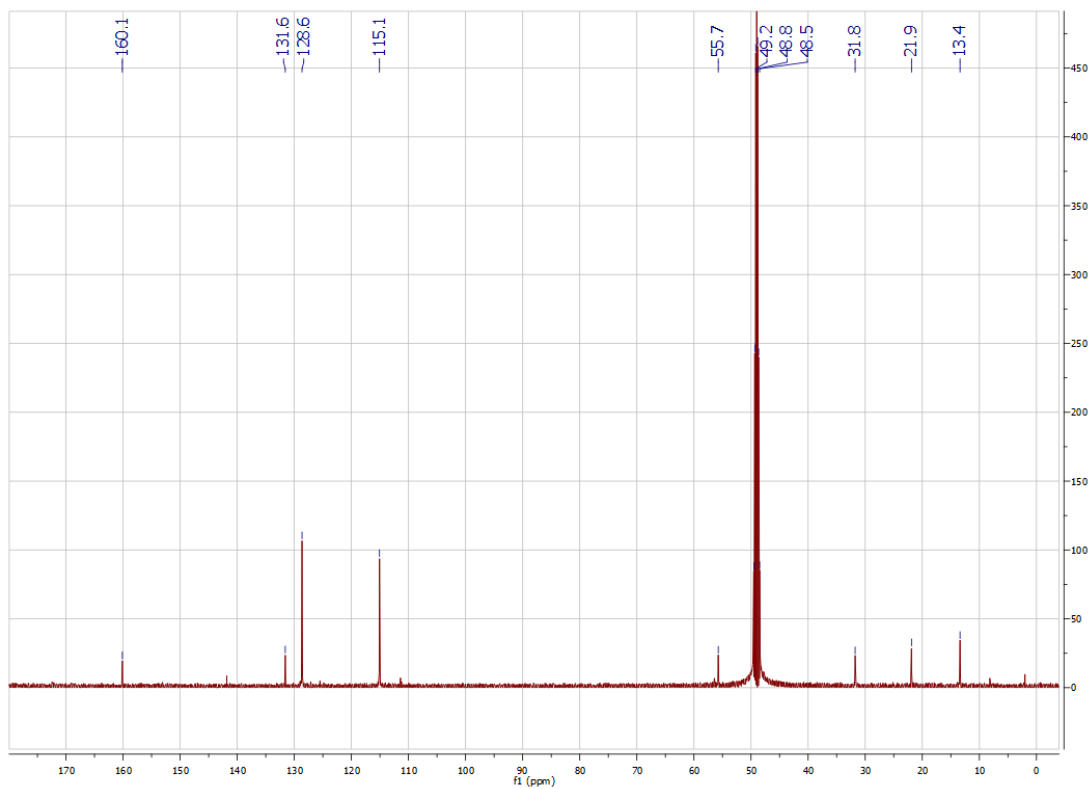
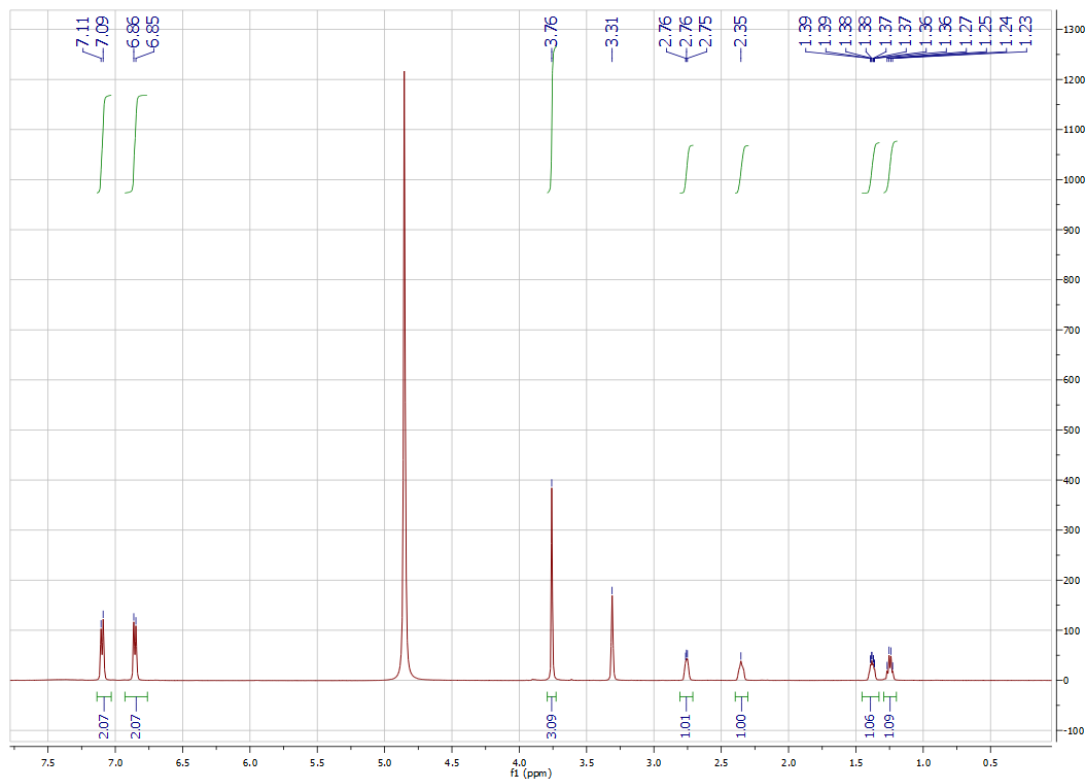
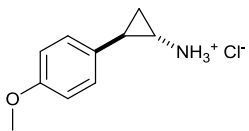
2-(*m*-Fluorophenyl)cyclopropylamine hydrochloride (**62d**)



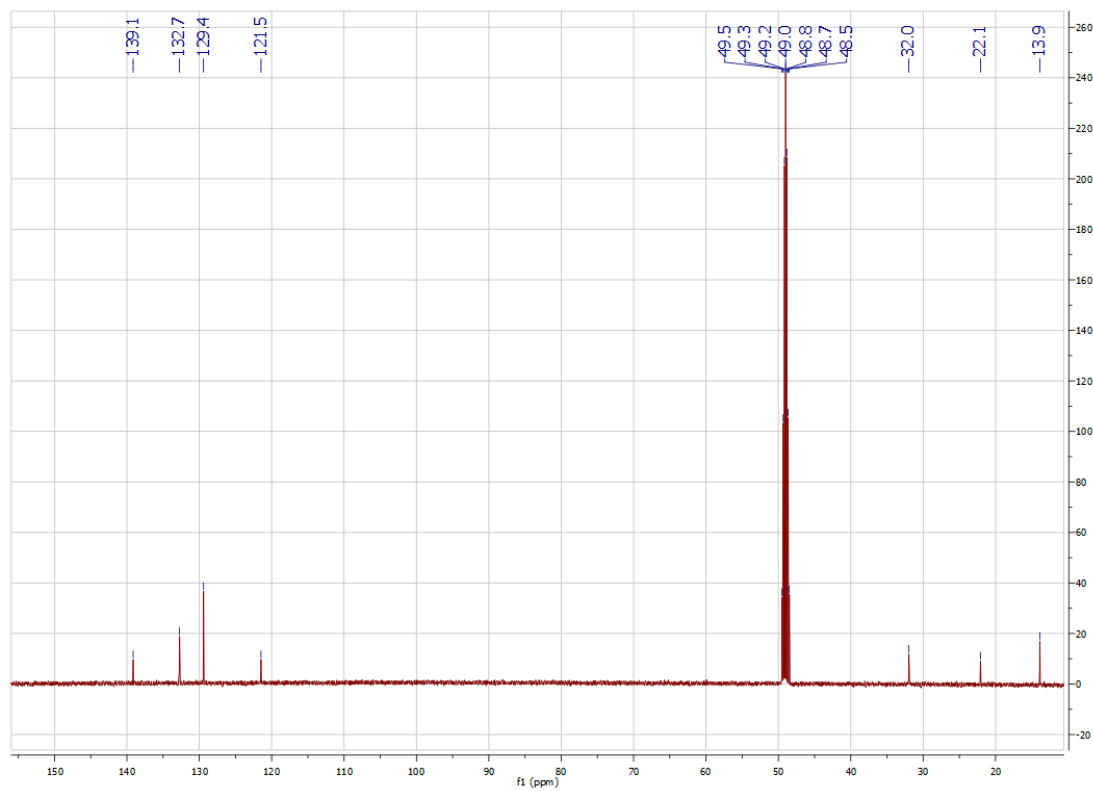
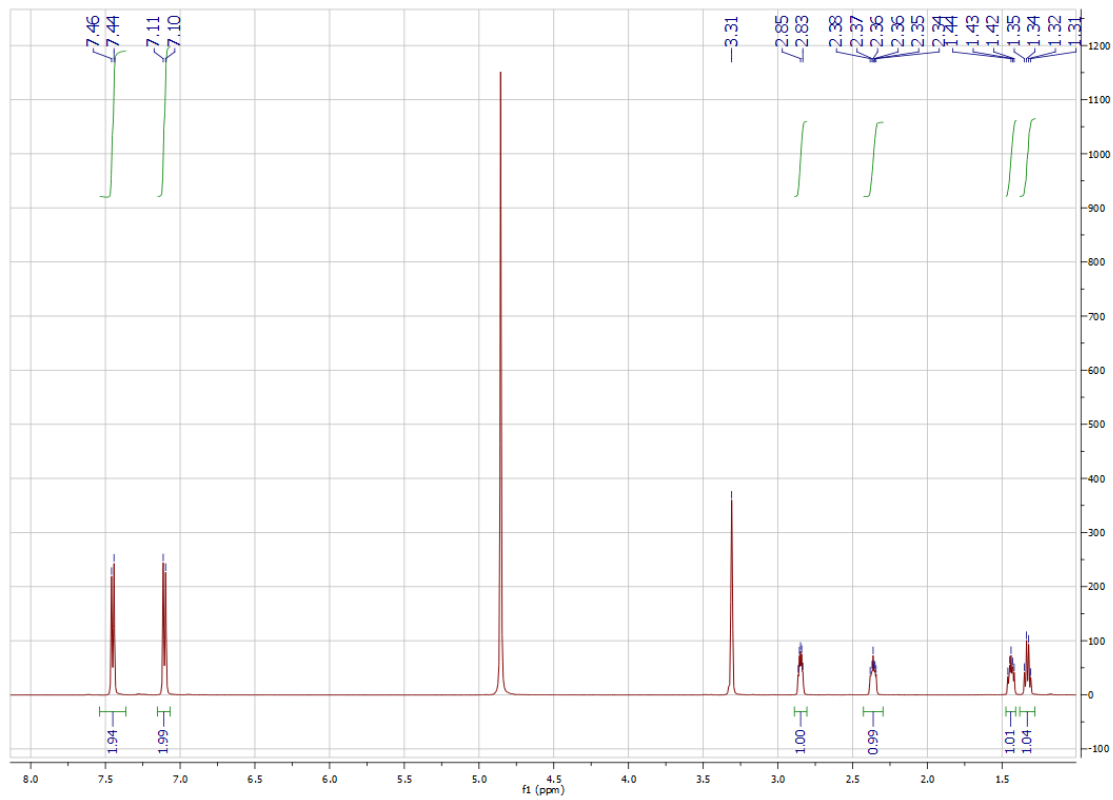
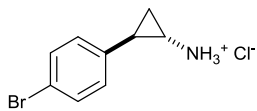
2-(*p*-Tolyl)cyclopropylamine hydrochloride (**62e**)



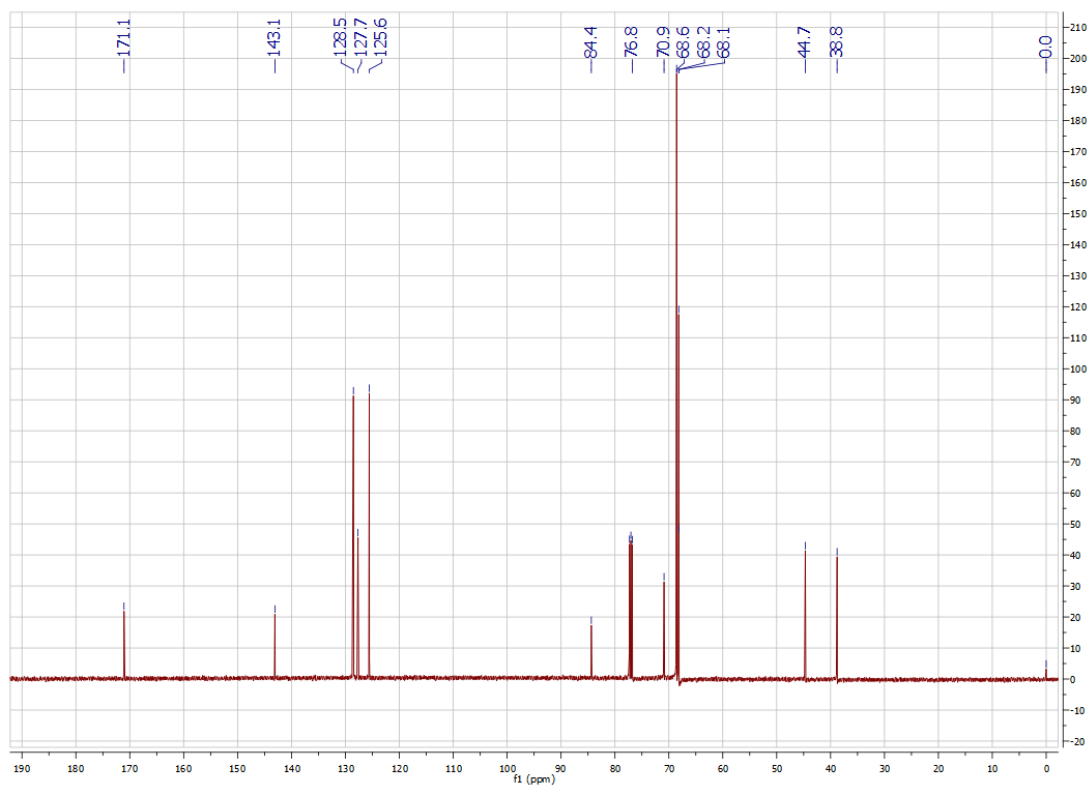
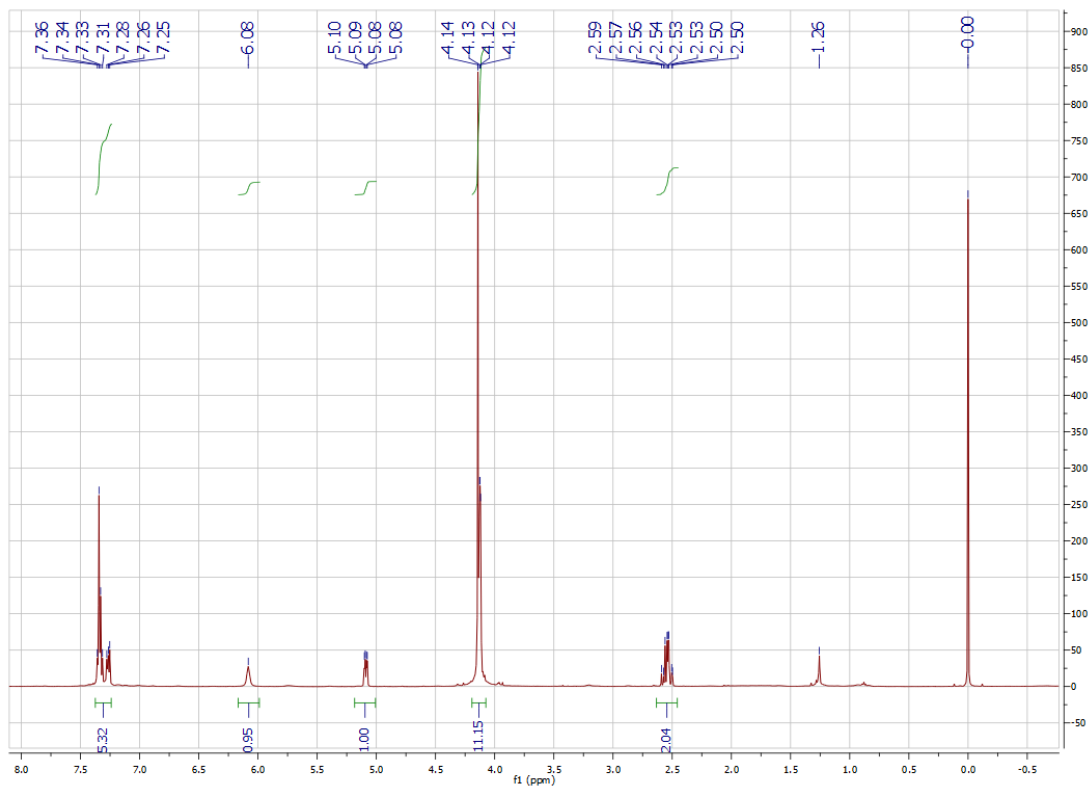
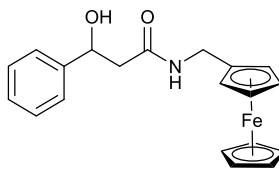
2-(p-Methoxyphenyl)cyclopropylamine hydrochloride (62f)



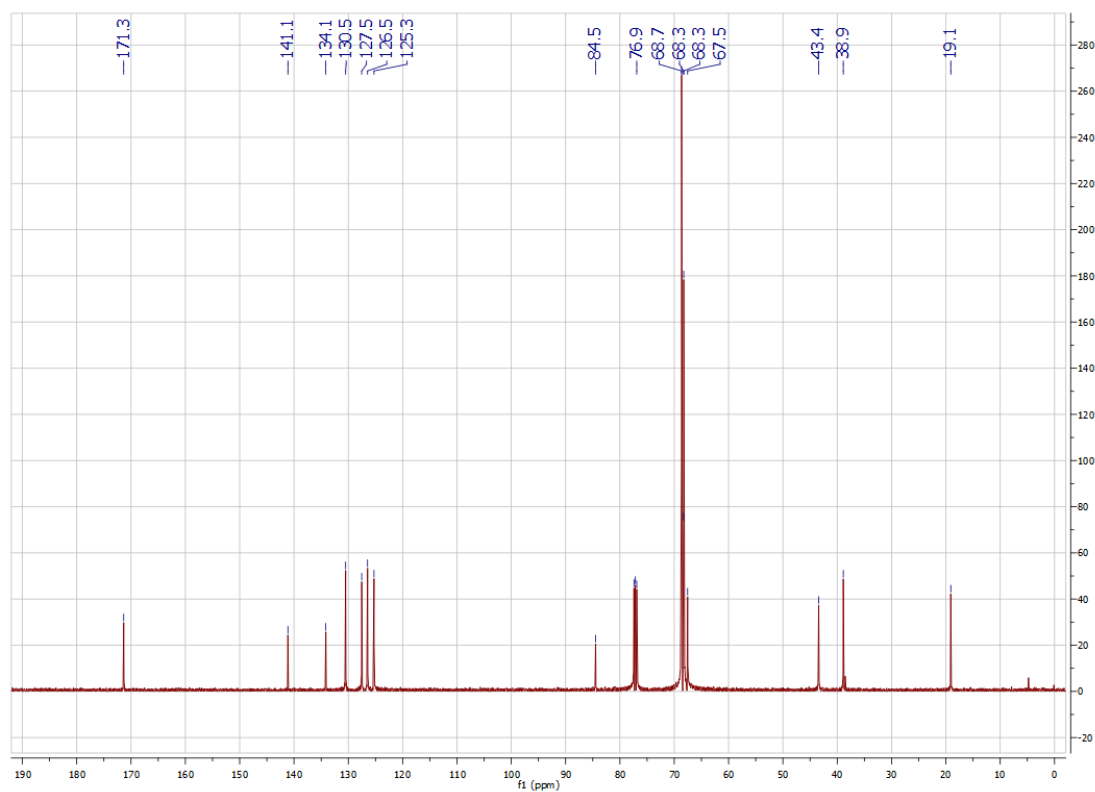
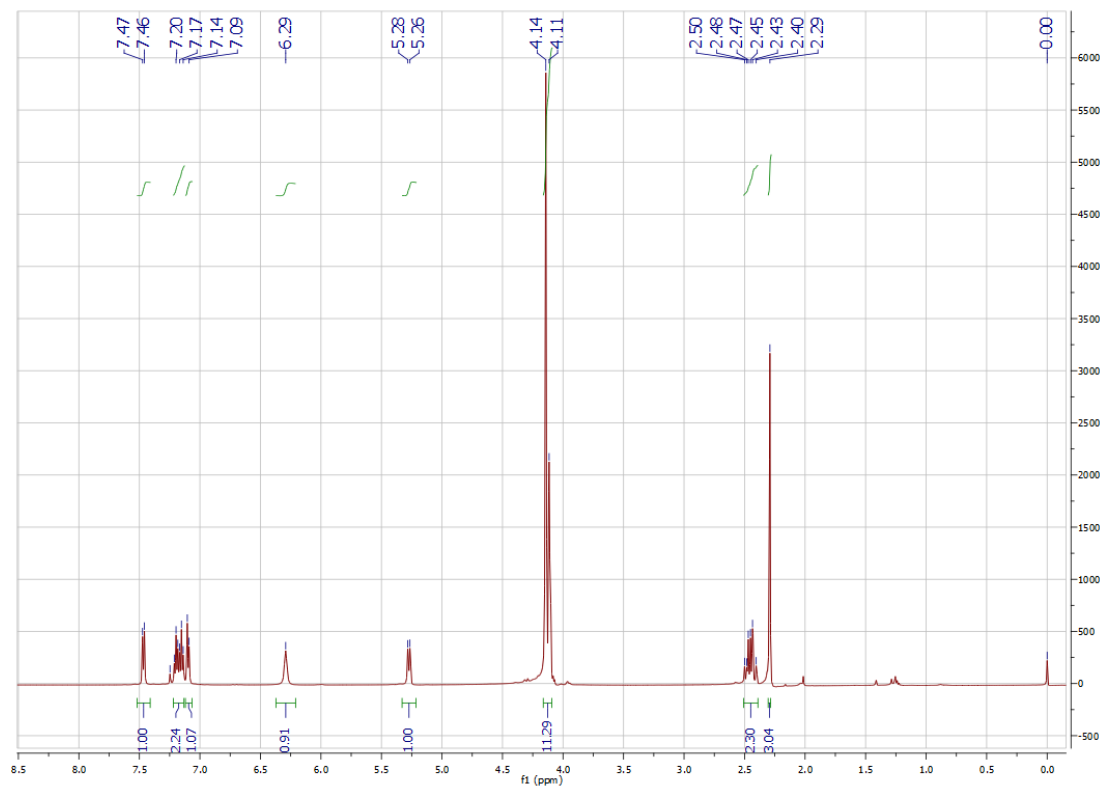
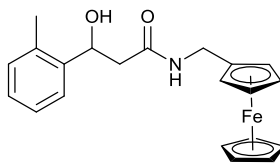
2-(p-Bromophenyl)cyclopropylamine hydrochloride (62g)



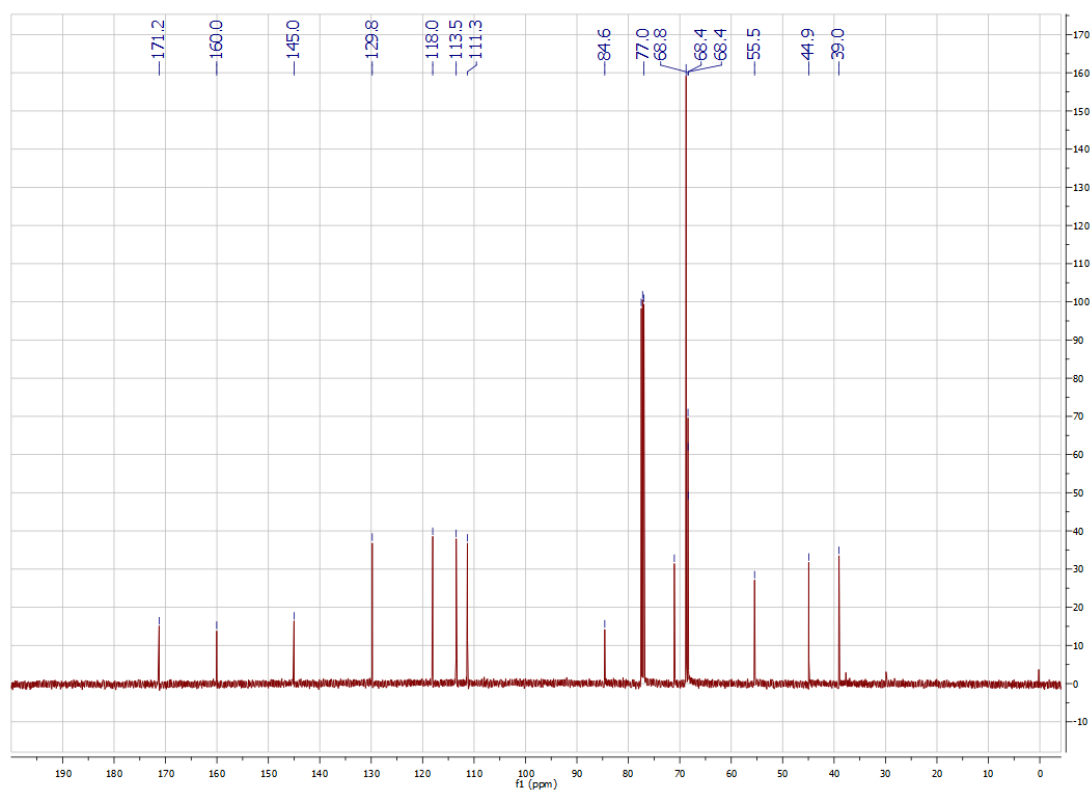
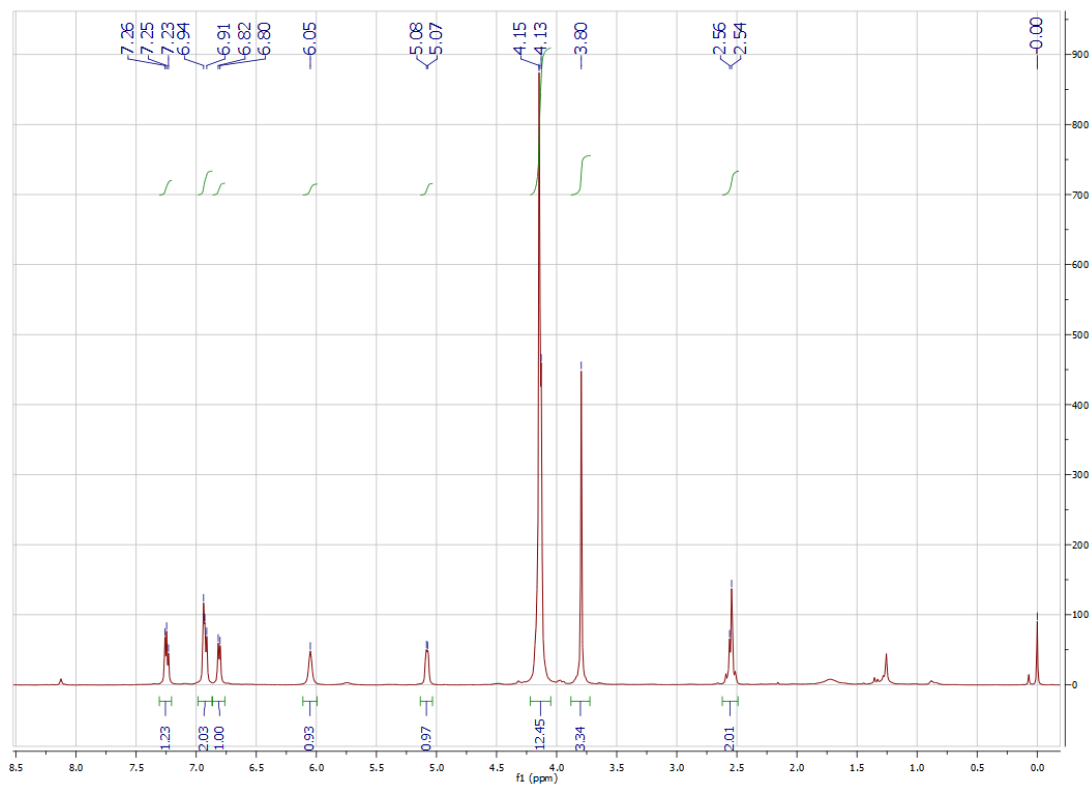
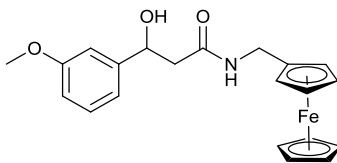
N-(Ferrocenylmethyl)-3-hydroxy-3-phenylpropanamide (**65a**)



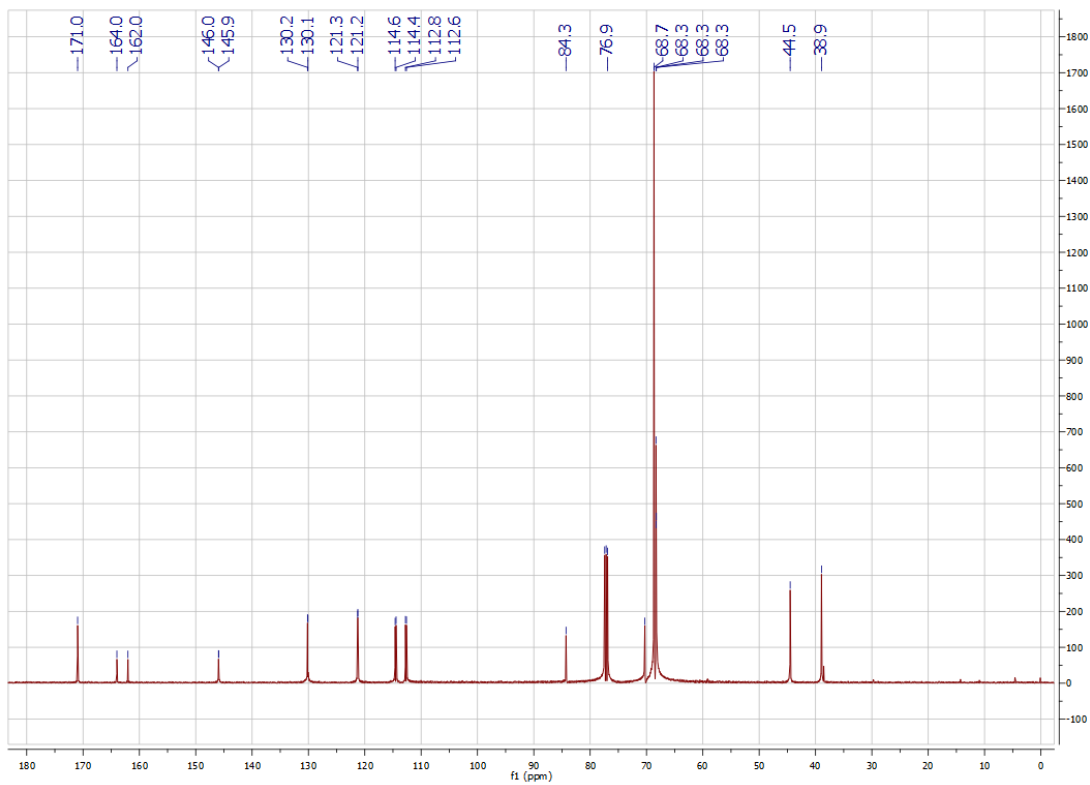
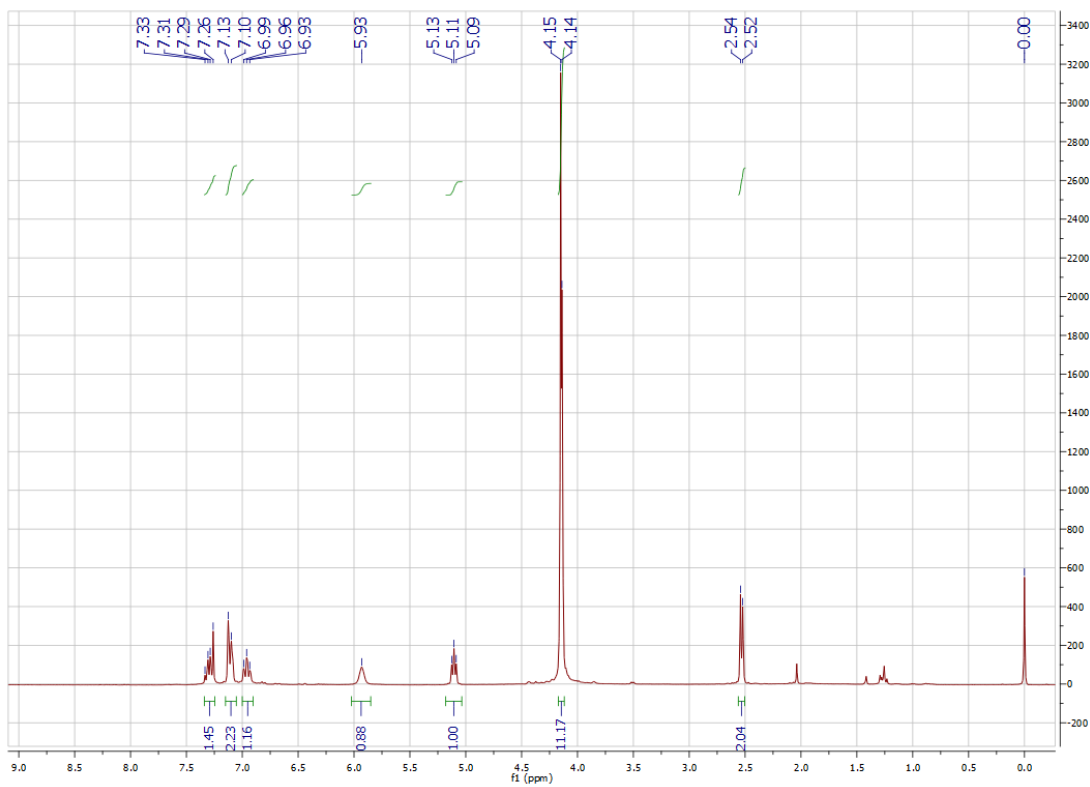
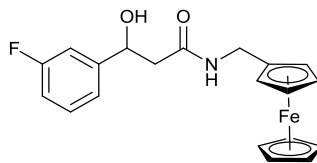
N-(Ferrocenylmethyl)-3-hydroxy-3-(*o*-methylphenyl)propanamide (**65b**)



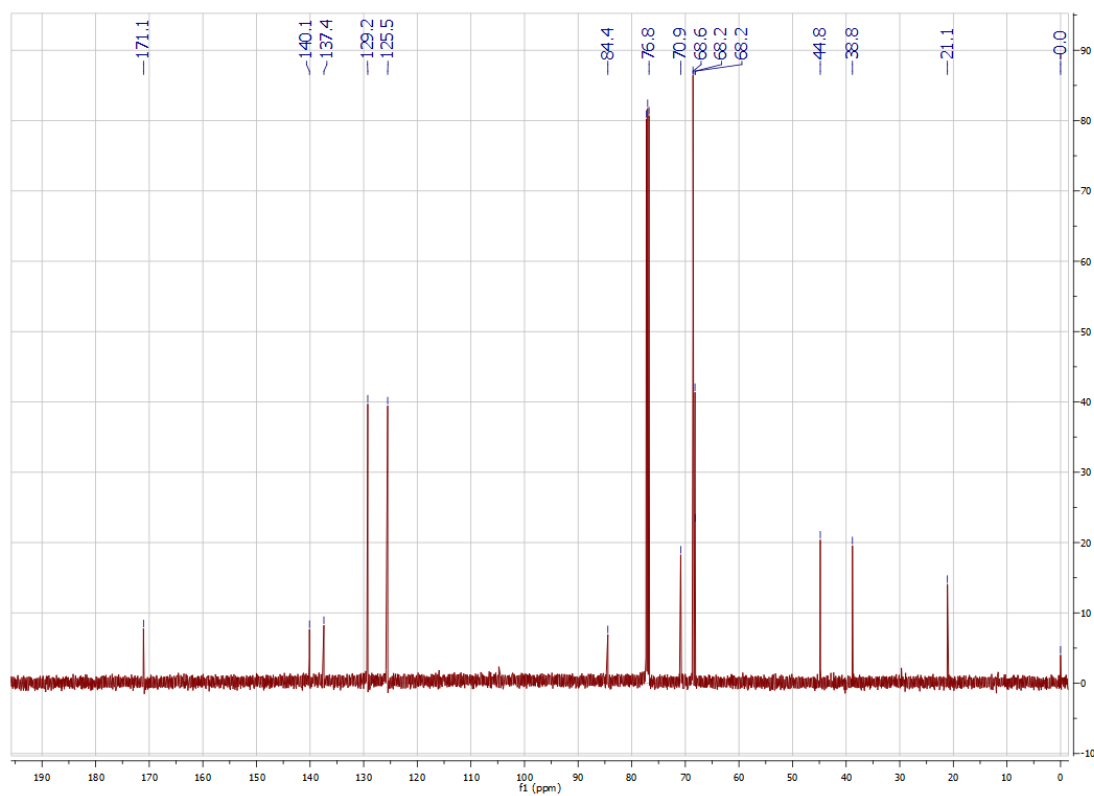
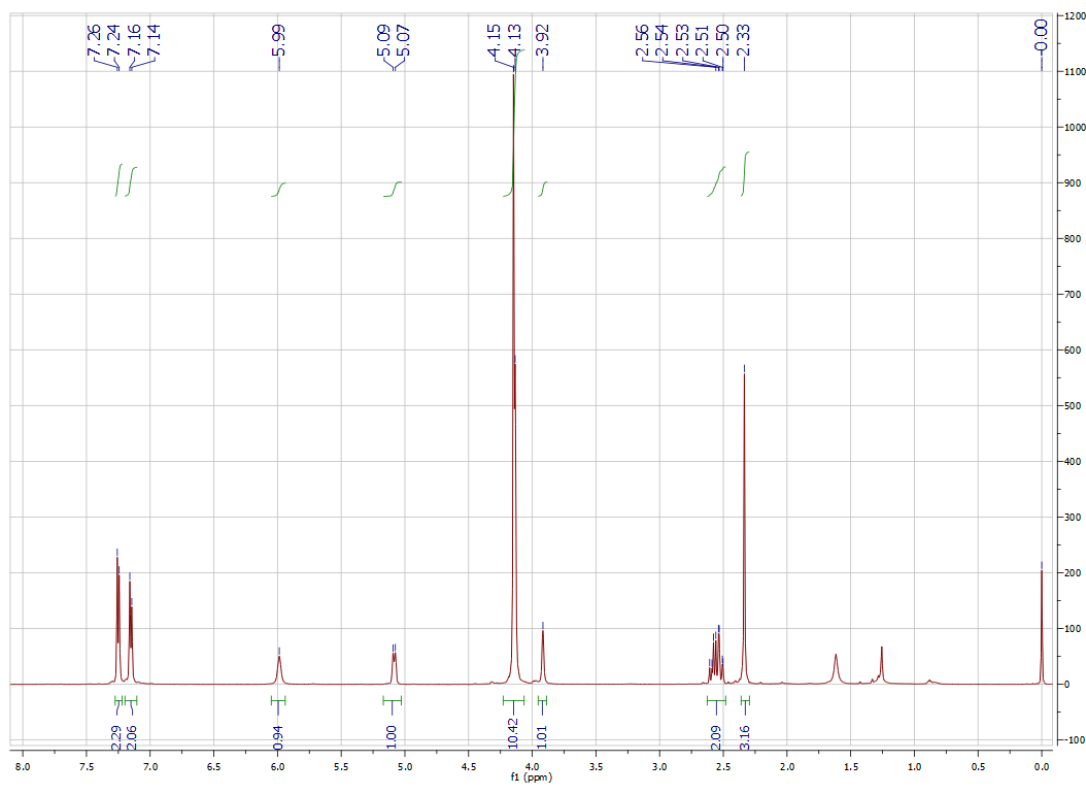
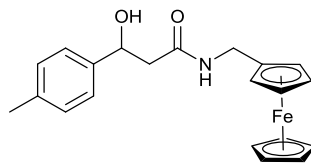
N-(Ferrocenylmethyl)-3-hydroxy-3-(*m*-methoxyphenyl)propanamide (**65c**)



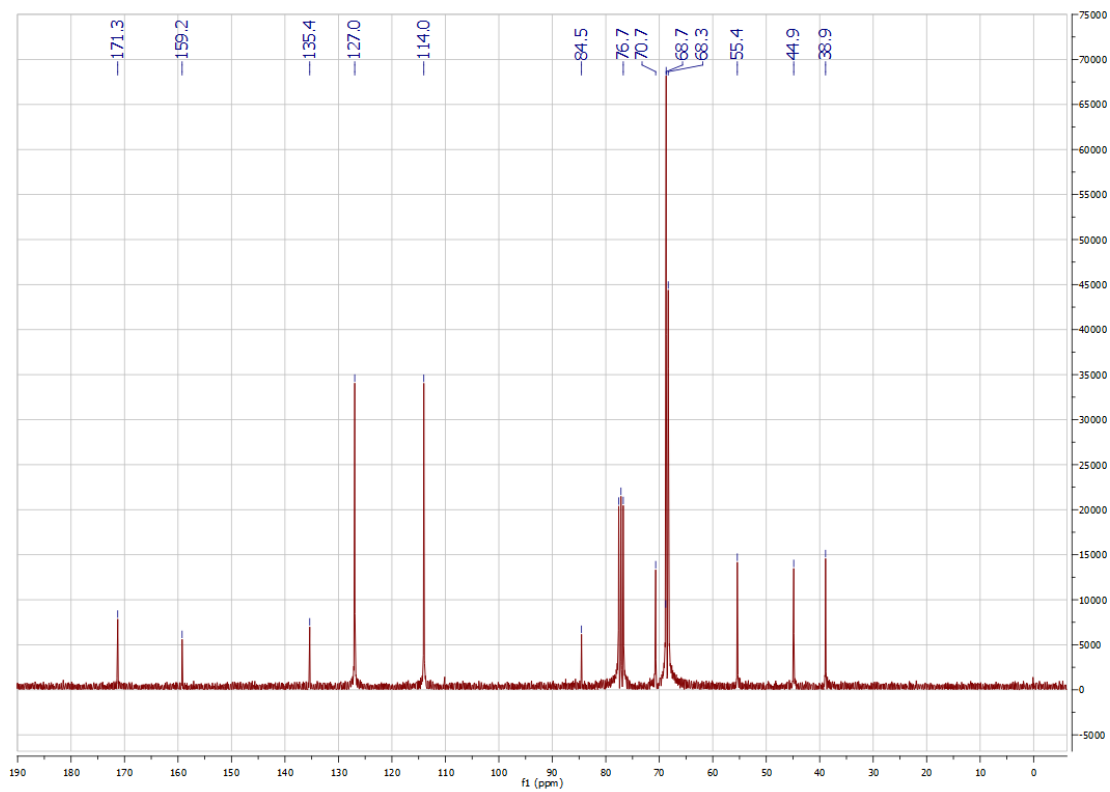
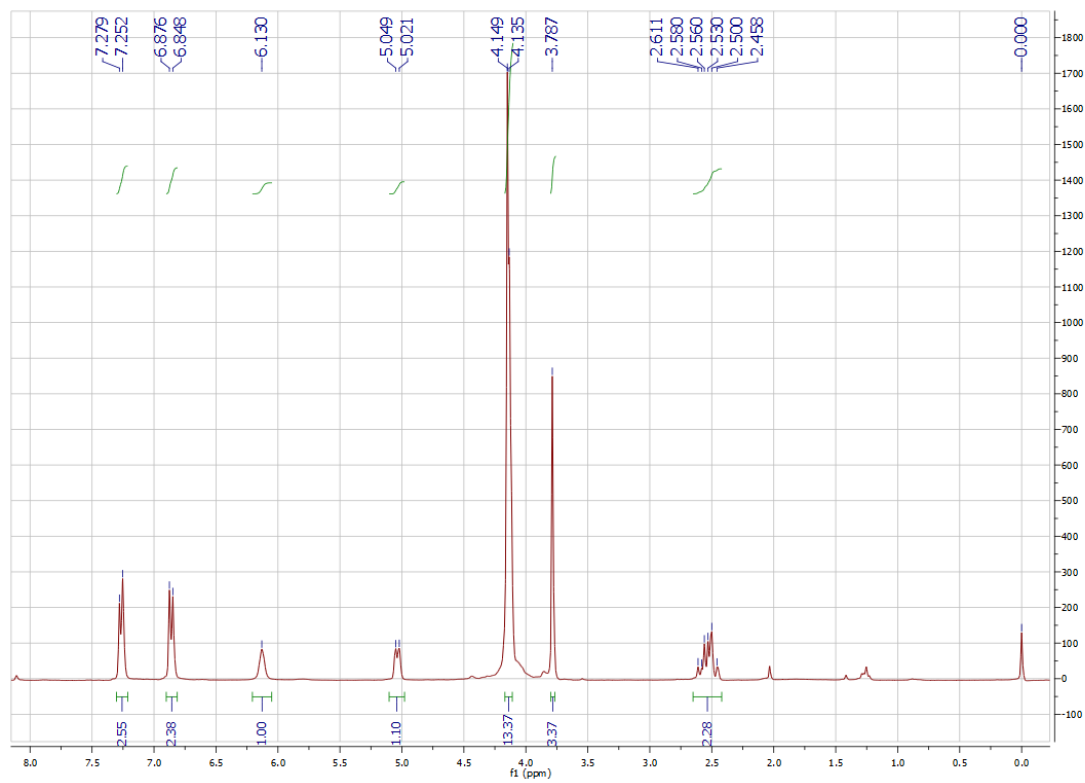
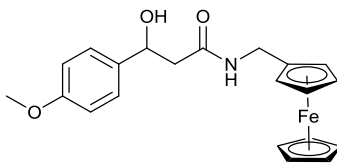
N-(Ferrocenylmethyl)-3-hydroxy-3-(*m*-fluorophenyl)propanamide (**65d**)



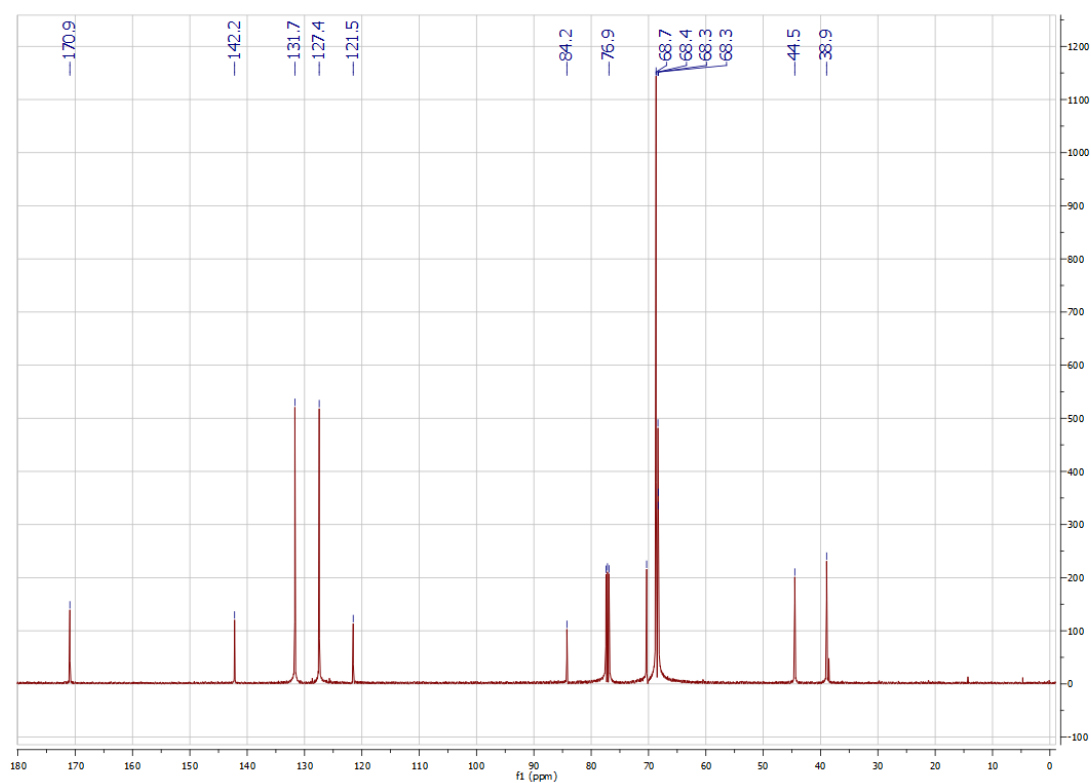
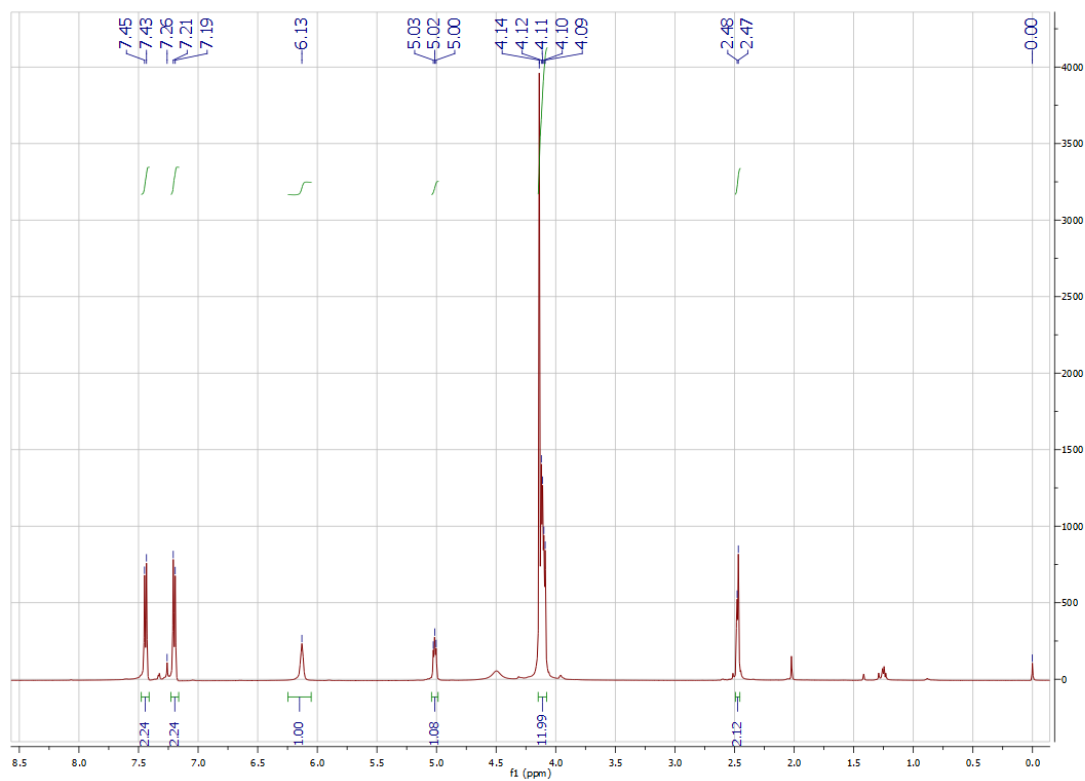
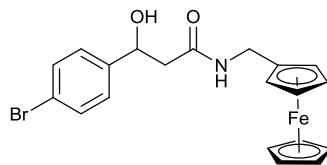
N-(Ferrocenylmethyl)-3-hydroxy-3-(*p*-methylphenyl)propanamide (**65e**)



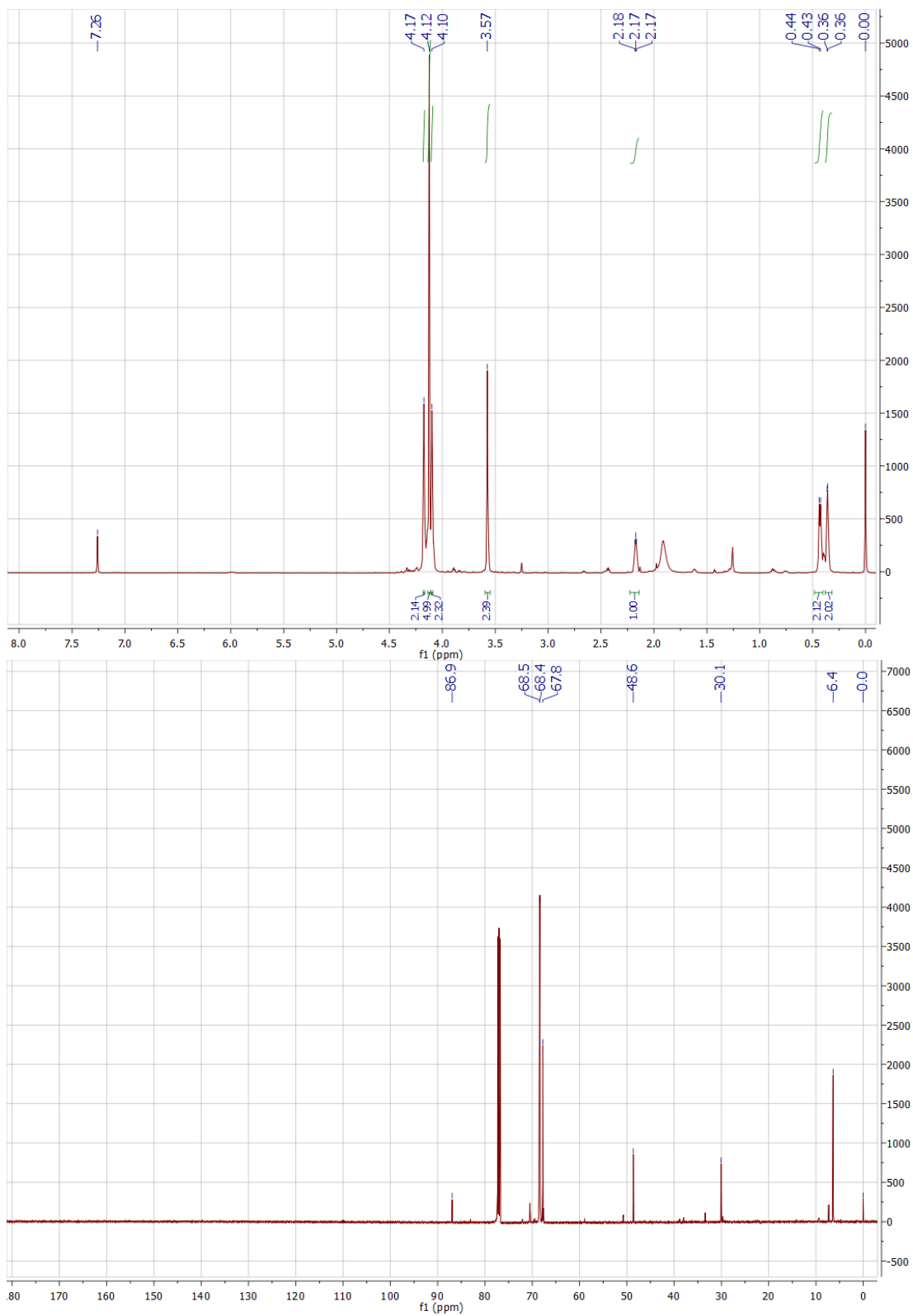
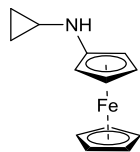
N-(Ferrocenylmethyl)-3-hydroxy-3-(*p*-methoxyphenyl)propanamide (65f)



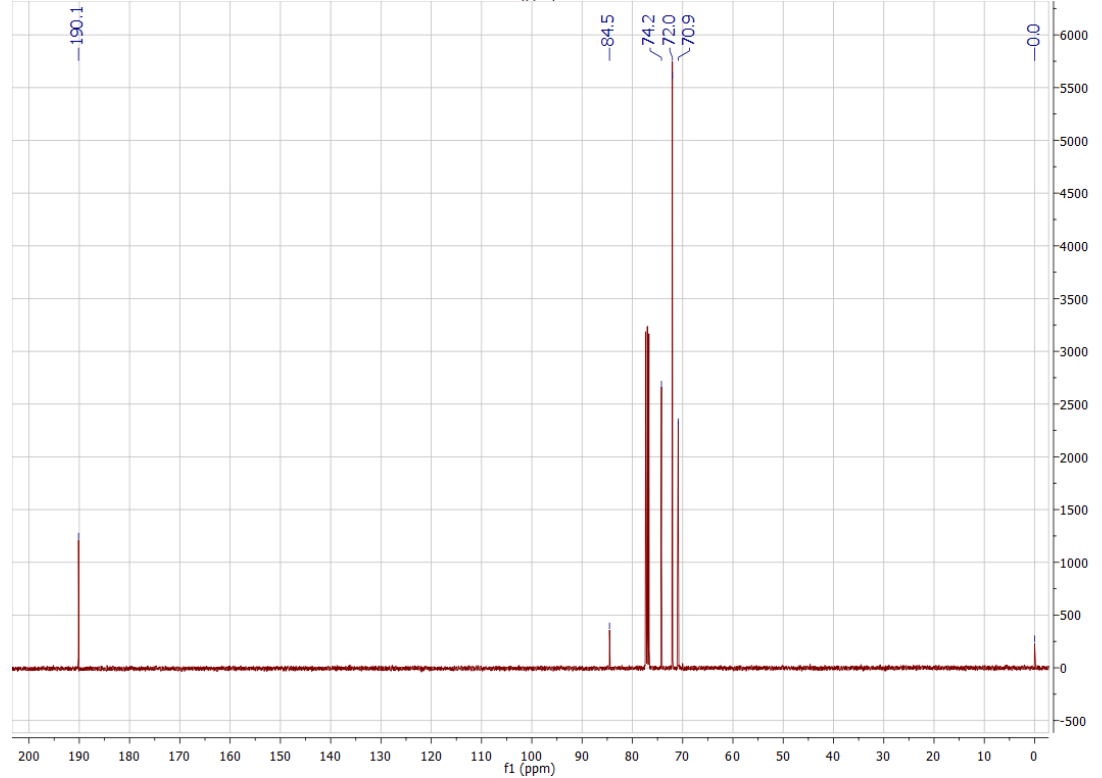
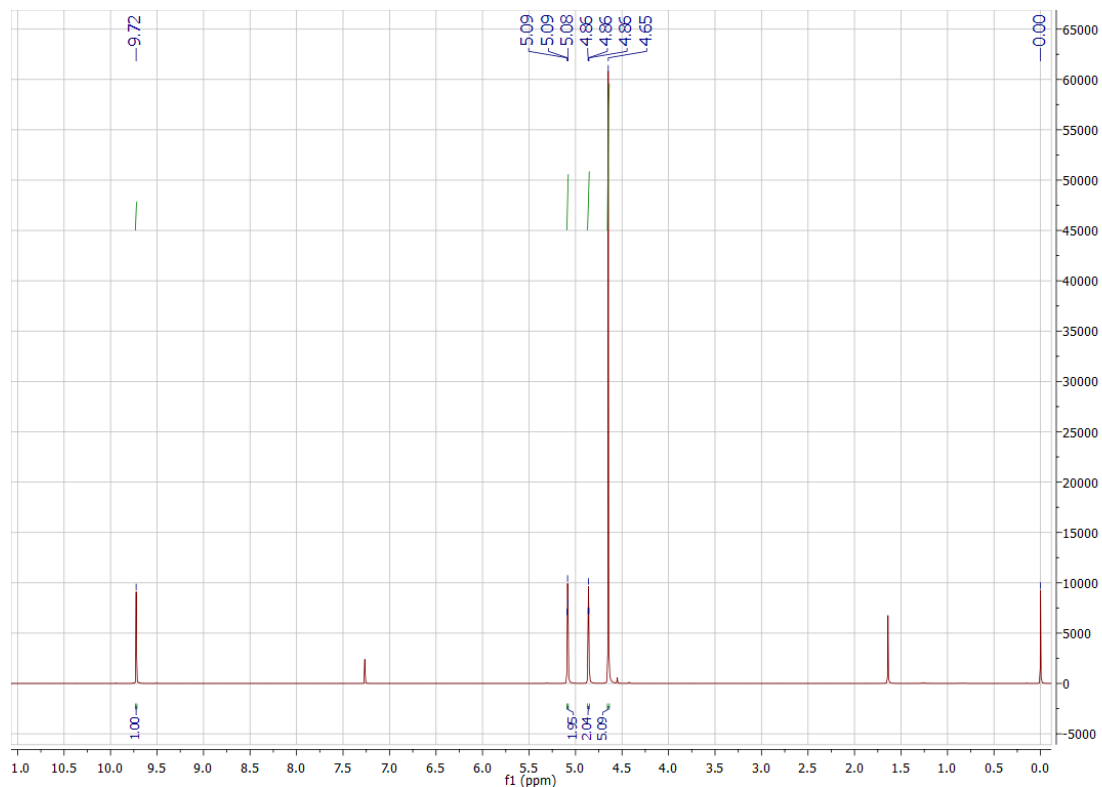
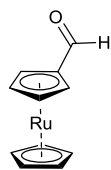
N-(Ferrocenylmethyl)-3-hydroxy-3-(*p*-bromophenyl)propanamide (65g)



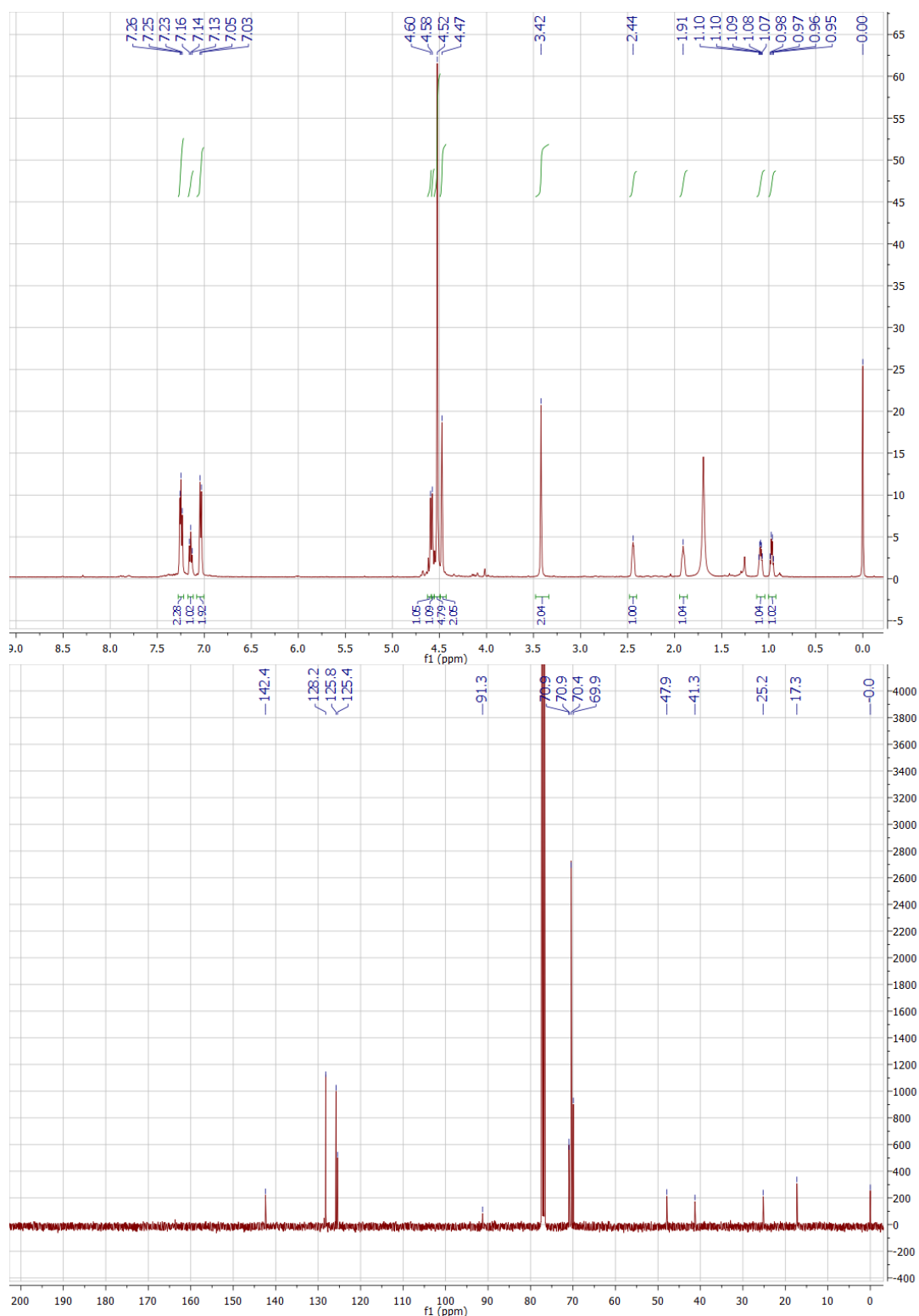
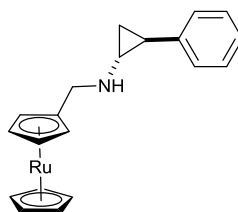
N-(Ferrocenylmethyl)-cyclopropylamine (73)



Ruthenocenecarboxaldehyde (75)



N-(Ruthenocenylmethyl)-2-phenylcyclopropan-1-amine (76)

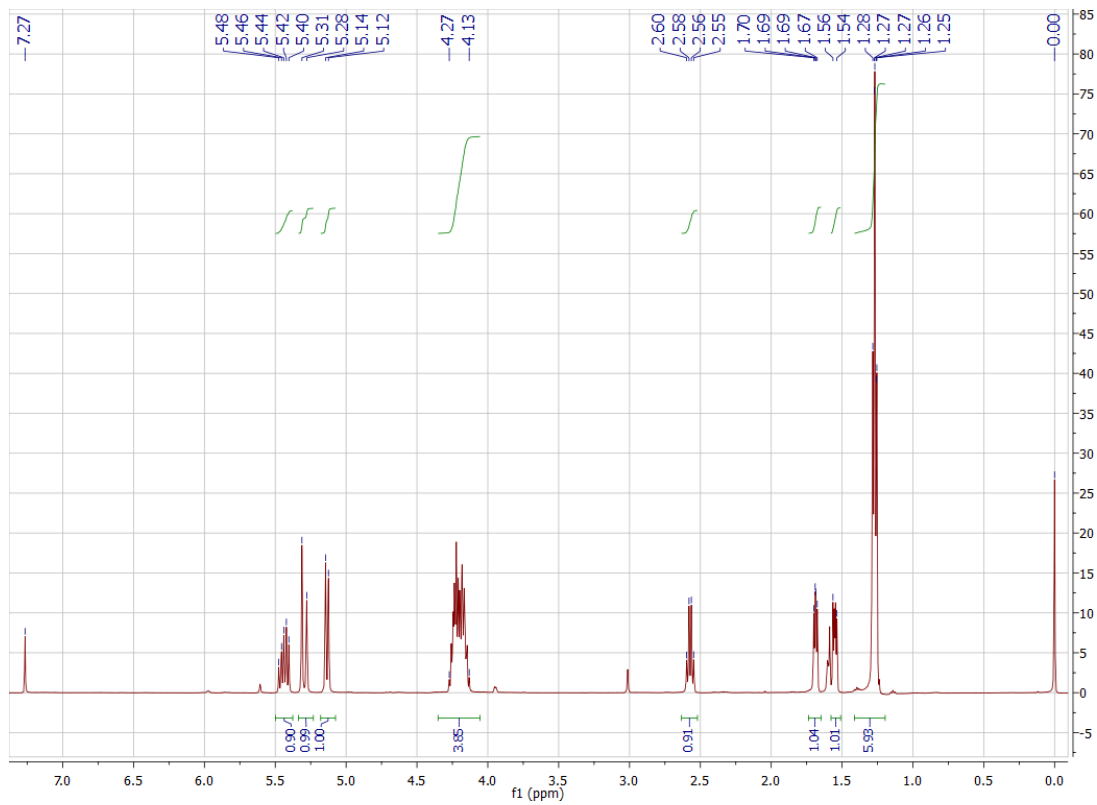
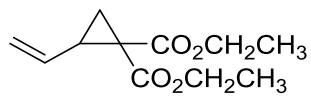


Appendix 4

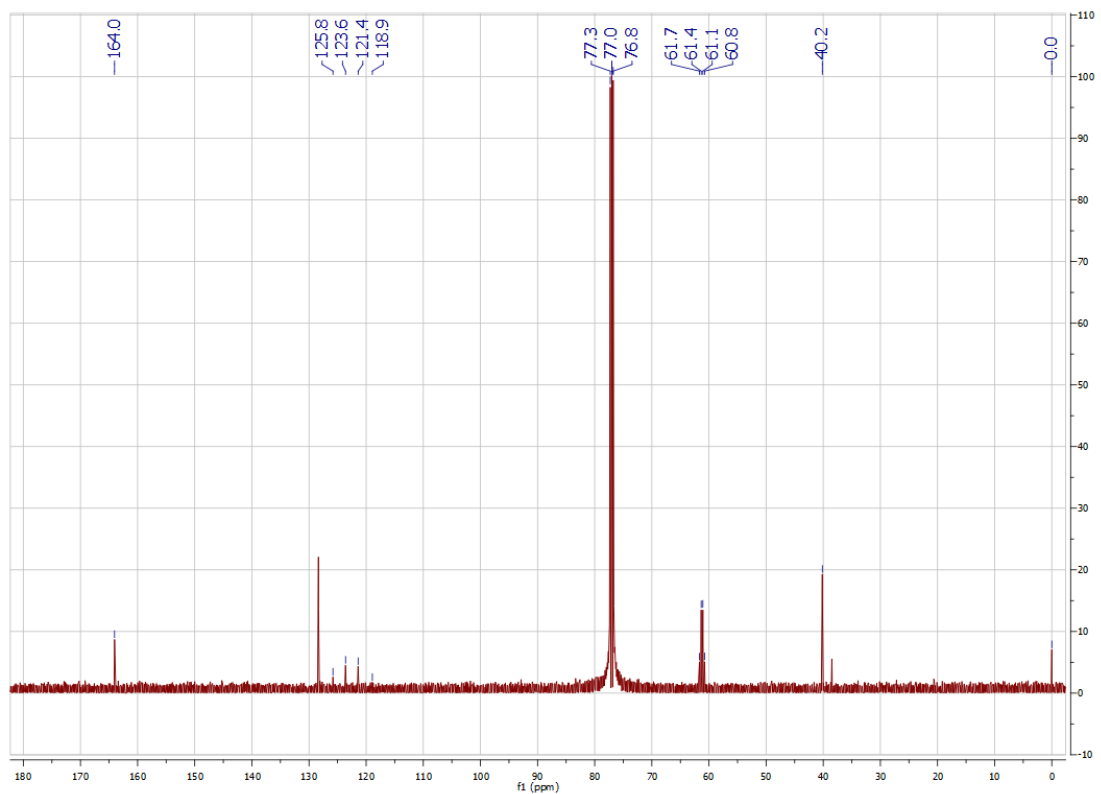
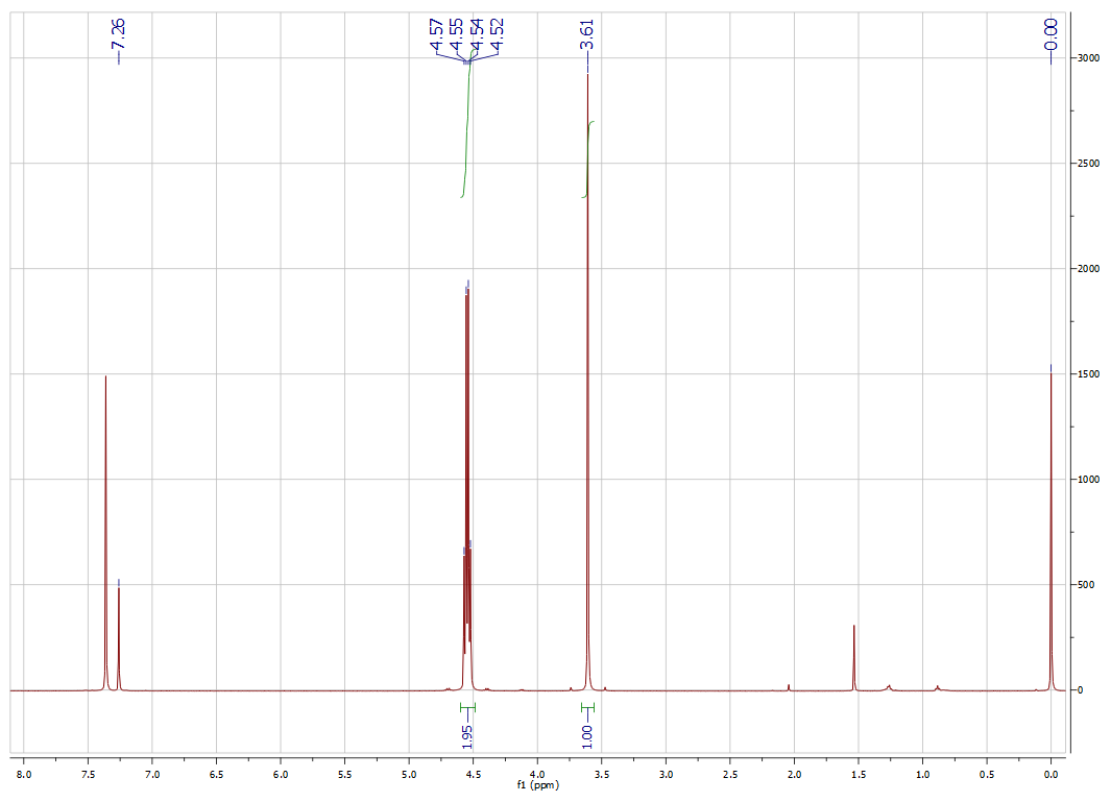
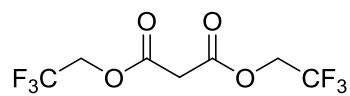
NMR spectra for Chapter 4

Palladium-catalysed dearomative [3 + 2] cycloaddition of 3-nitroindoles with
vinylcyclopropane dicarboxylates

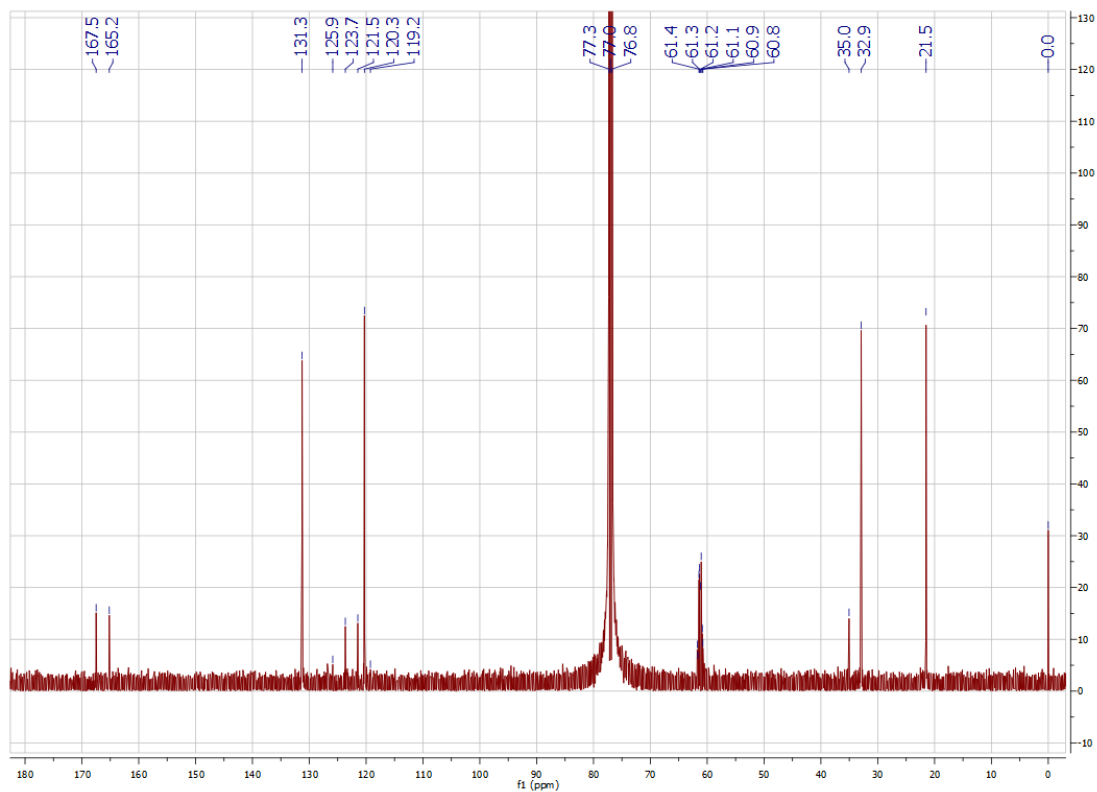
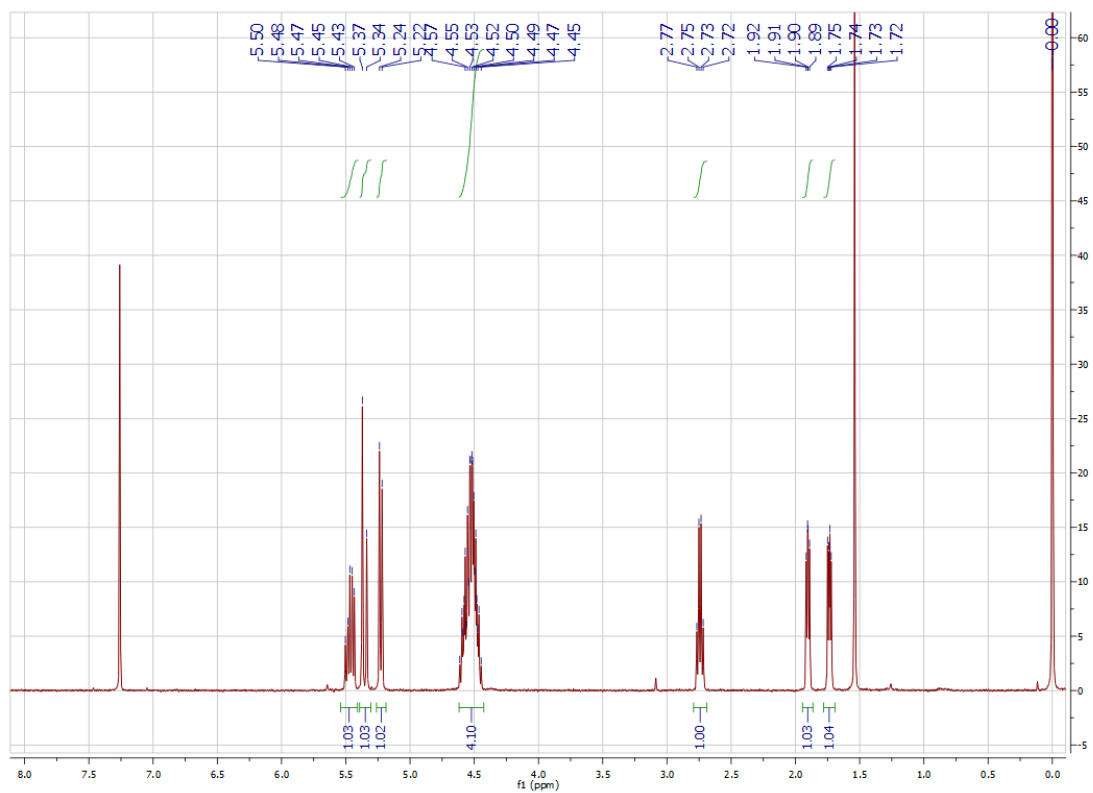
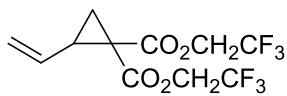
¹H NMR of Diethyl 2-vinylcyclopropane-1,1-dicarboxylate (**104**)



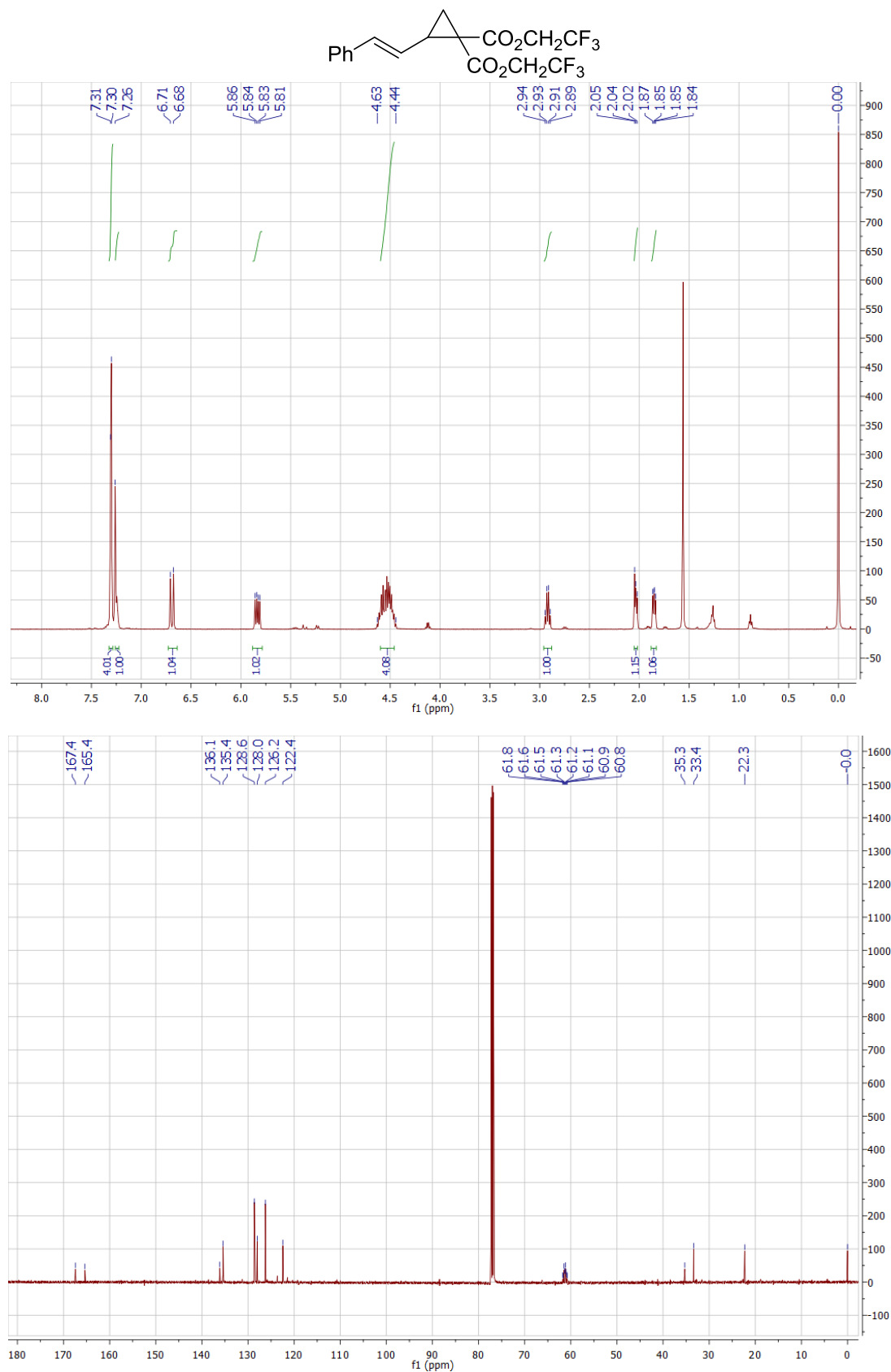
^1H & ^{13}C NMR of Bis(2,2,2-trifluoroethyl) malonate



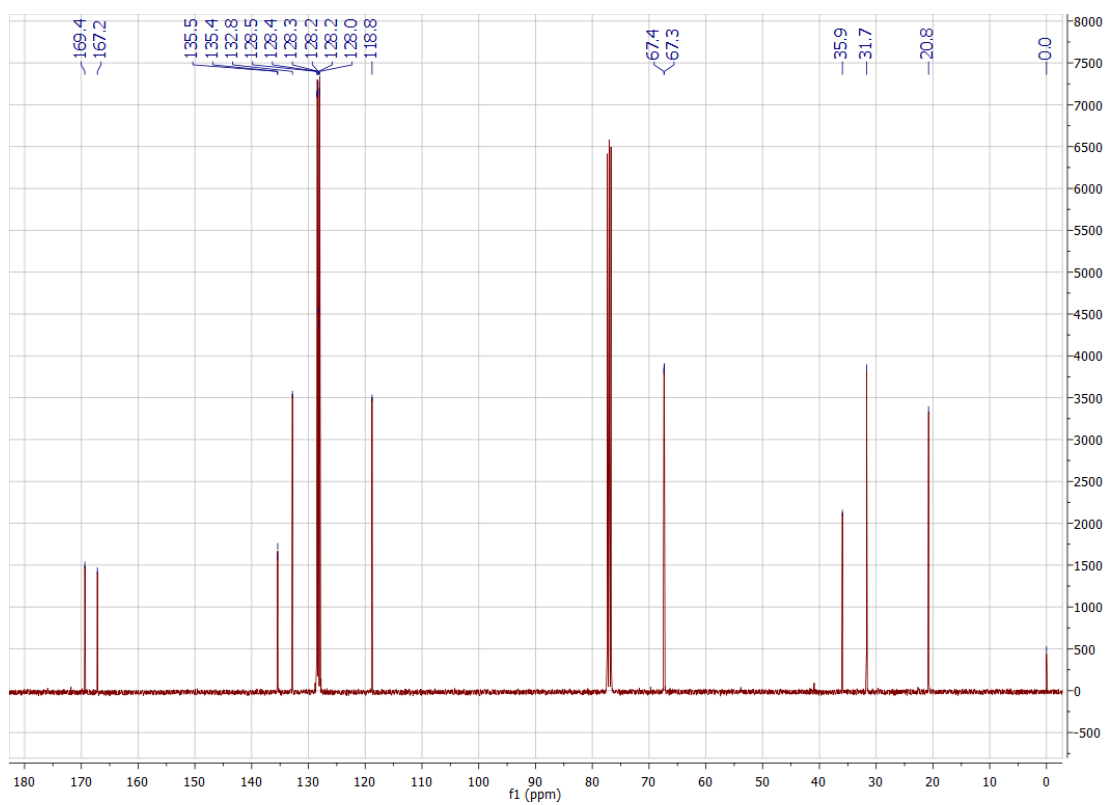
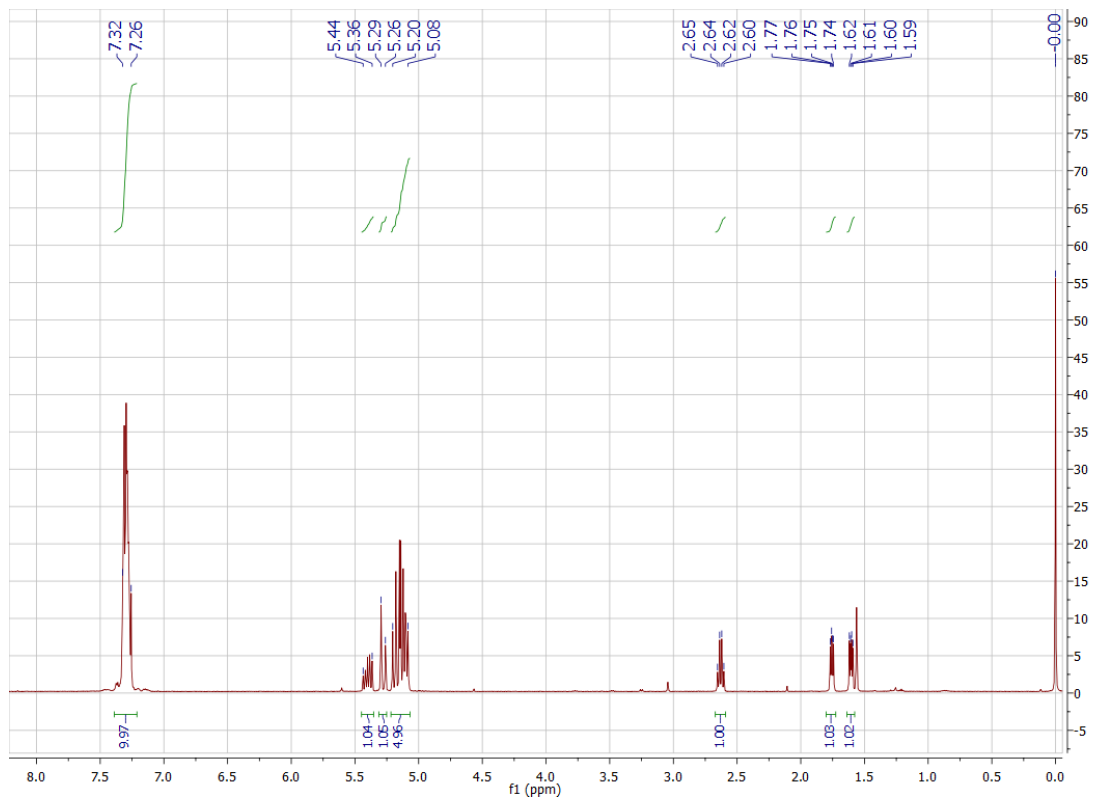
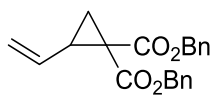
^1H & ^{13}C NMR of Bis(2,2,2-trifluoroethyl) 2-vinylcyclopropane-1,1-dicarboxylate (**105**)



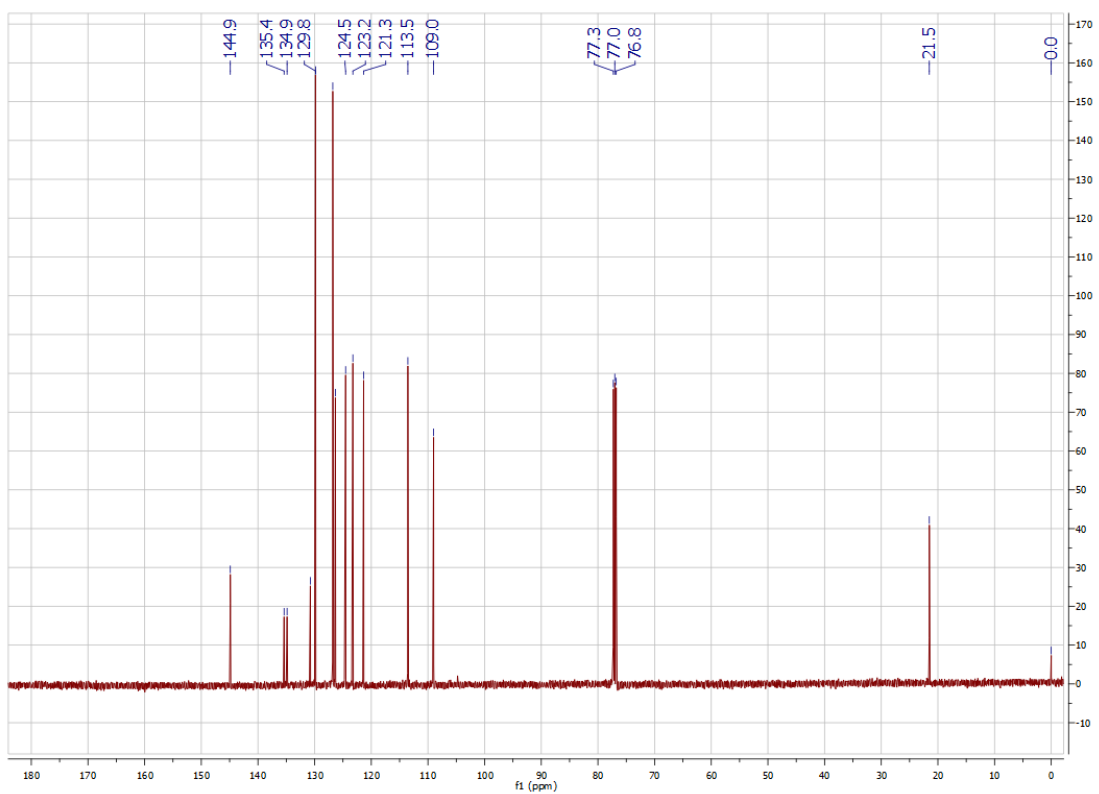
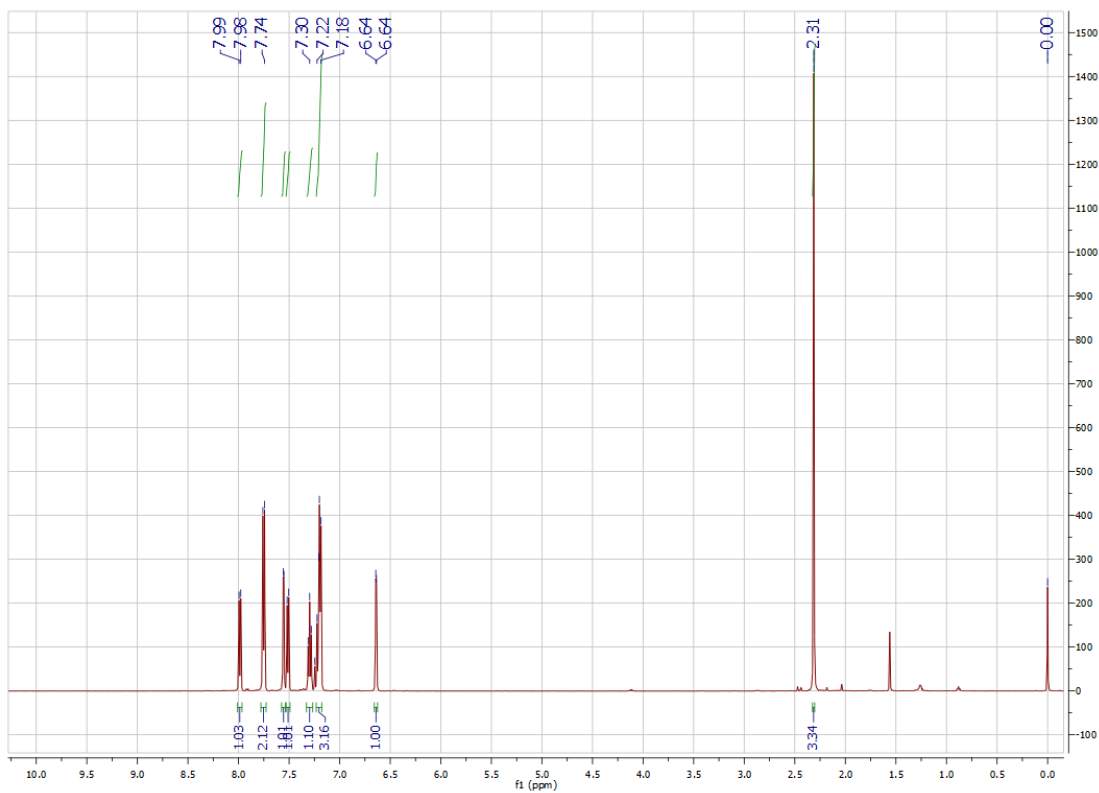
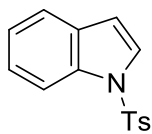
¹H & ¹³C NMR of Bis(2,2,2-trifluoroethyl) (E)-2-styrylcyclopropane-1,1-dicarboxylate (110)



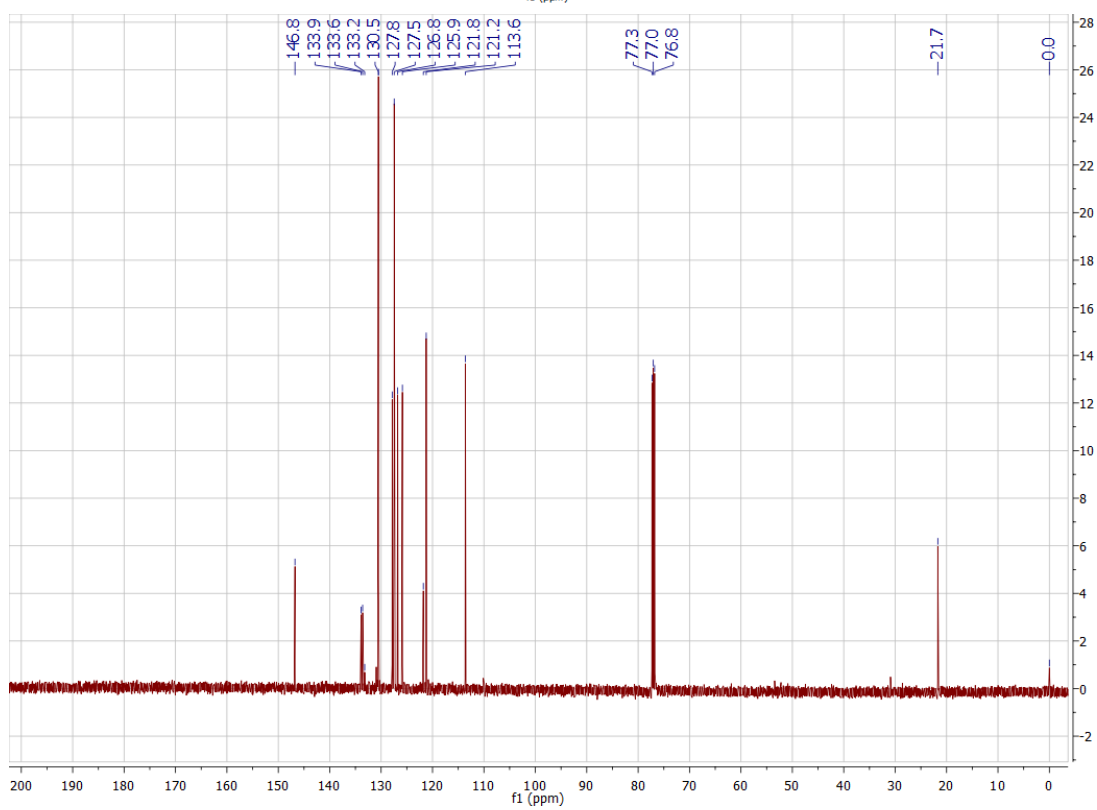
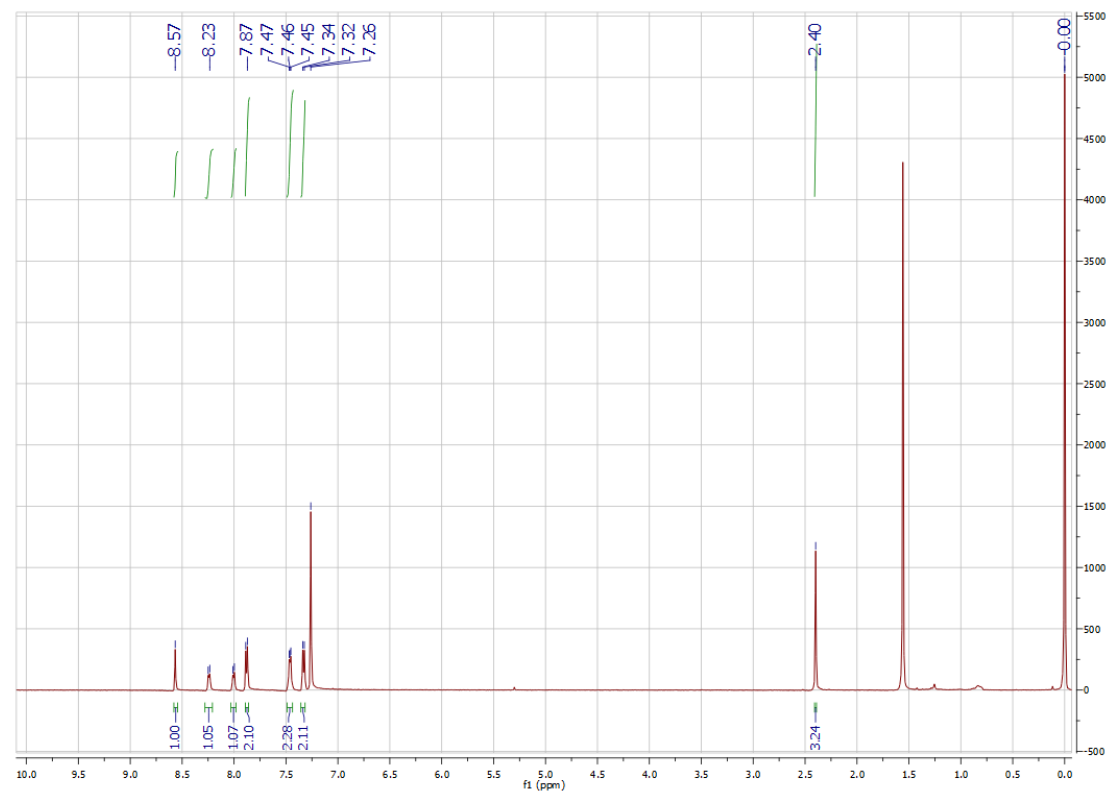
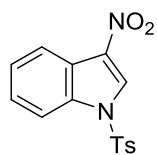
^1H & ^{13}C NMR of Dibenzyl 2-vinylcyclopropane-1,1-dicarboxylate (**111**)



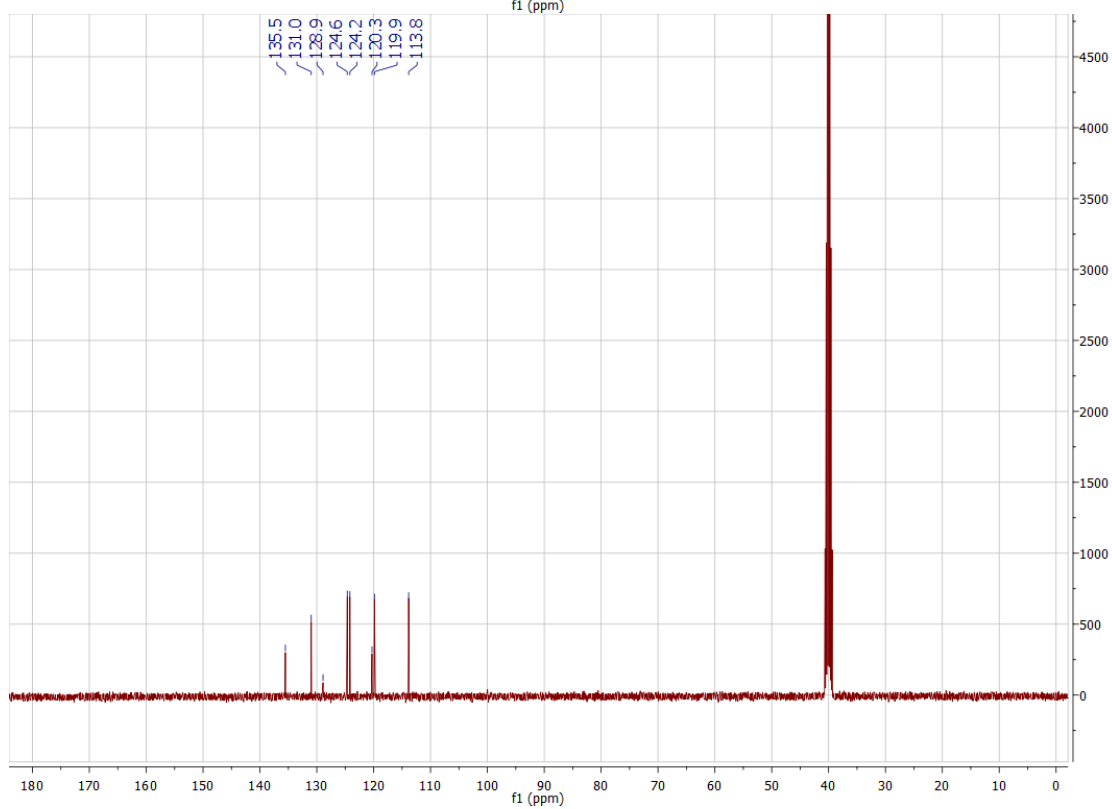
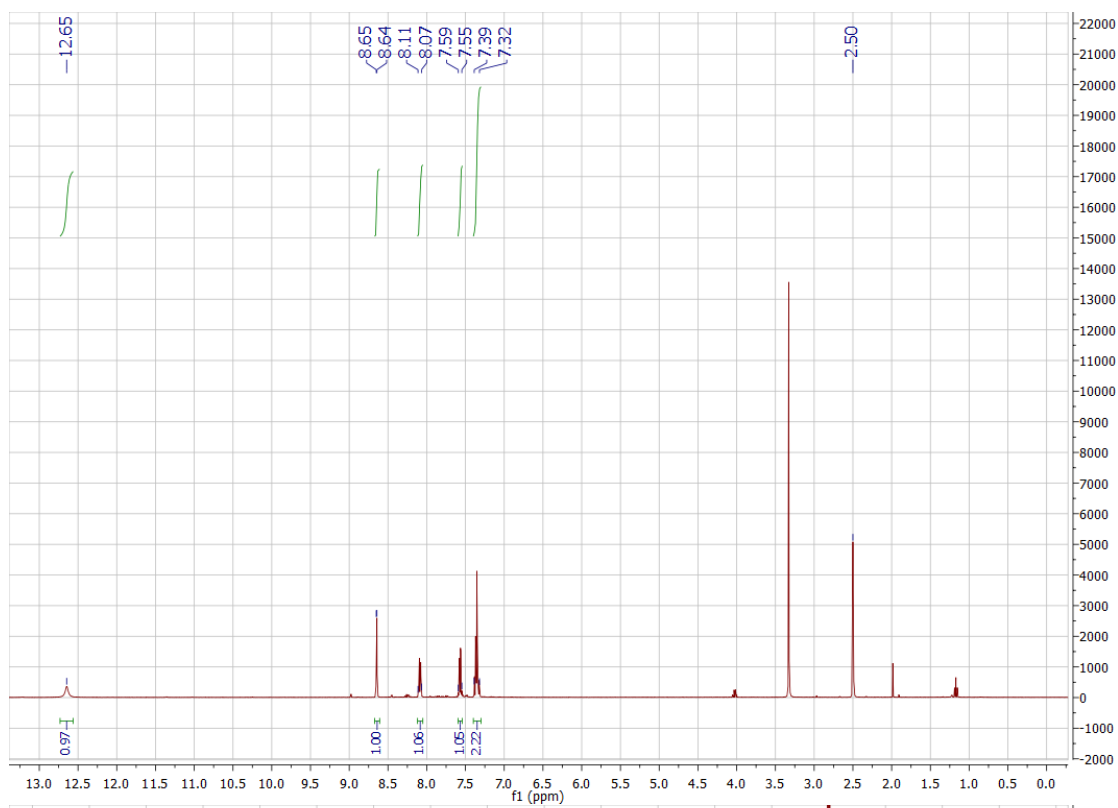
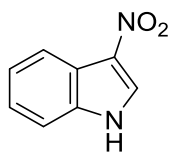
^1H & ^{13}C NMR of 1-Tosyl-1H-indole



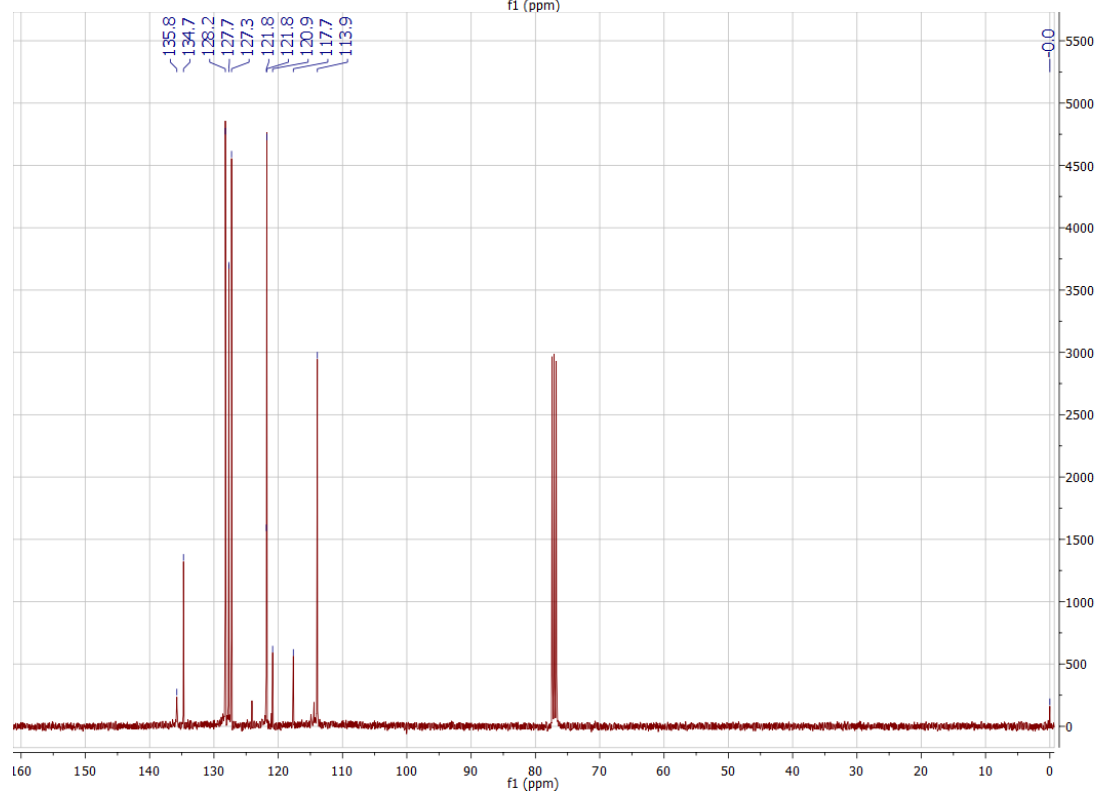
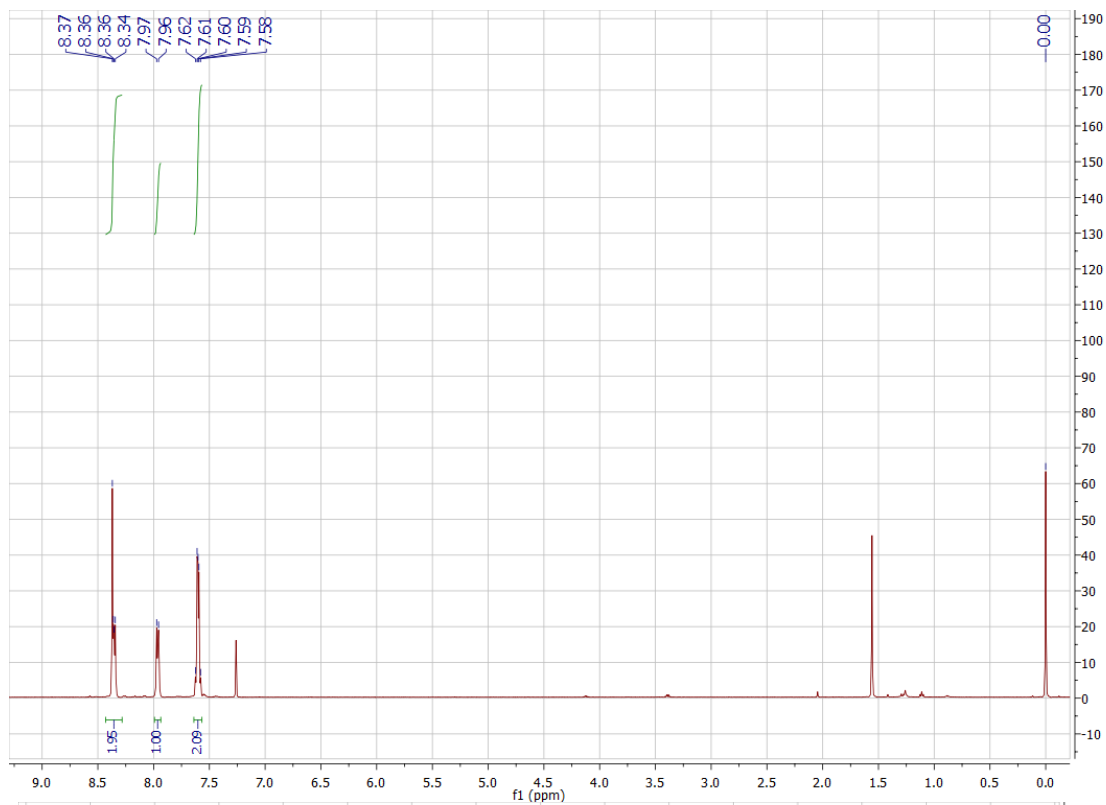
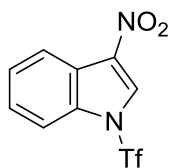
^1H & ^{13}C NMR of 3-Nitro-1-tosyl-1H-indole (106a)



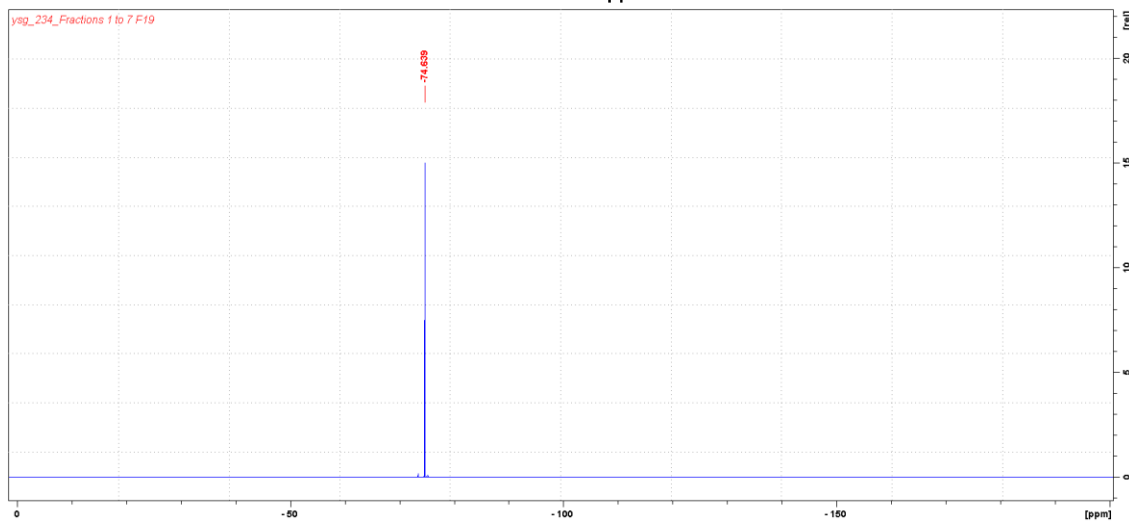
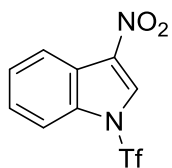
^1H & ^{13}C NMR of 3-Nitro-1H-indole



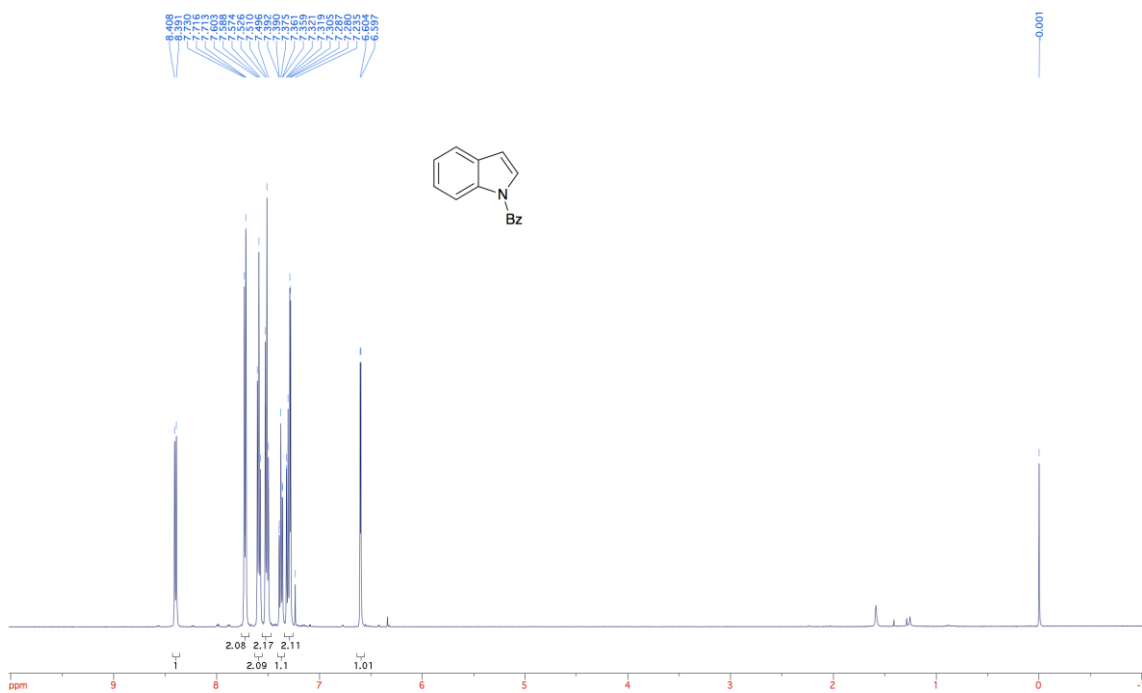
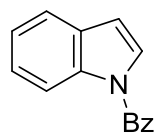
^1H & ^{13}C NMR of 3-Nitro-1-((trifluoromethyl)sulfonyl)-1H-indole (**109a**)



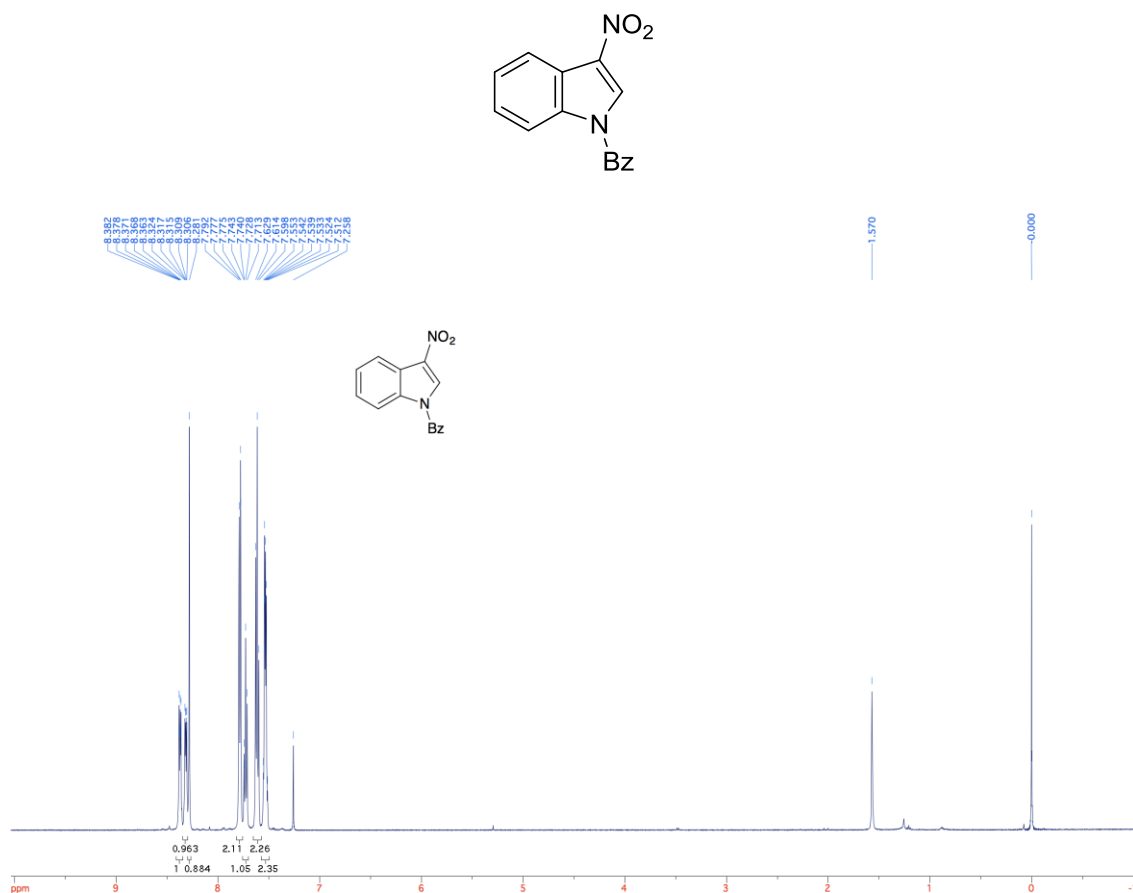
^{19}F NMR of 3-Nitro-1-((trifluoromethyl)sulfonyl)-1H-indole (**109a**)



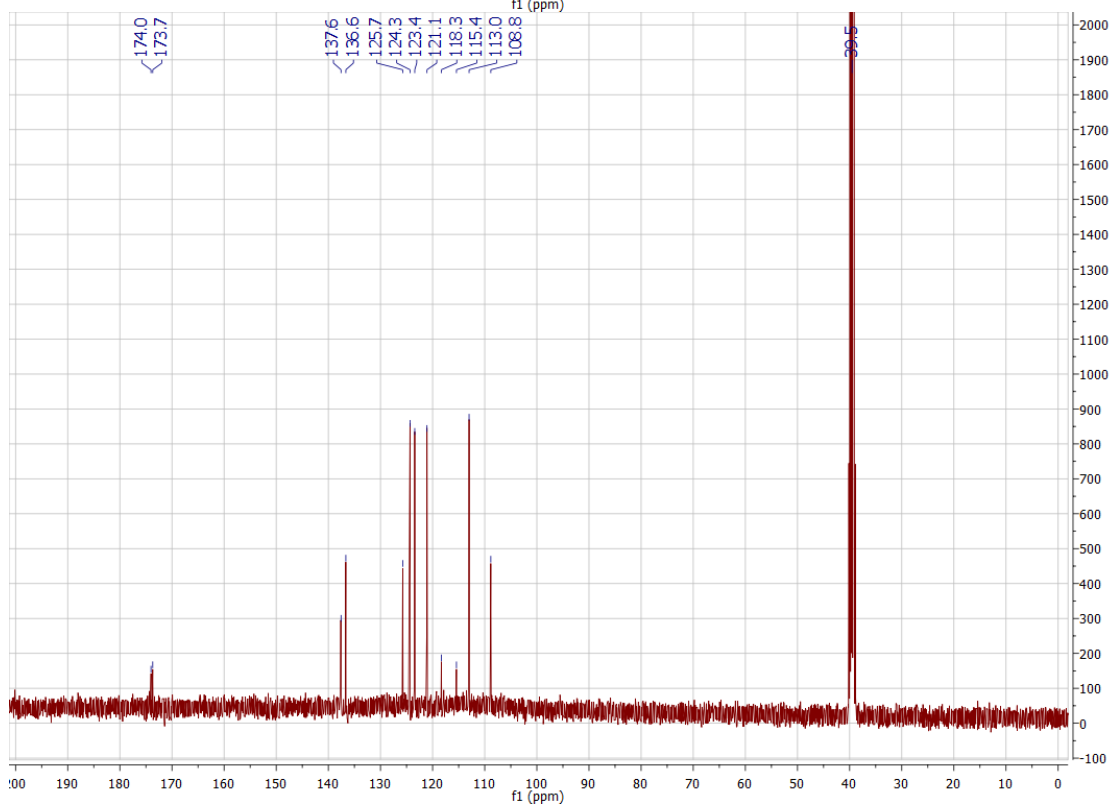
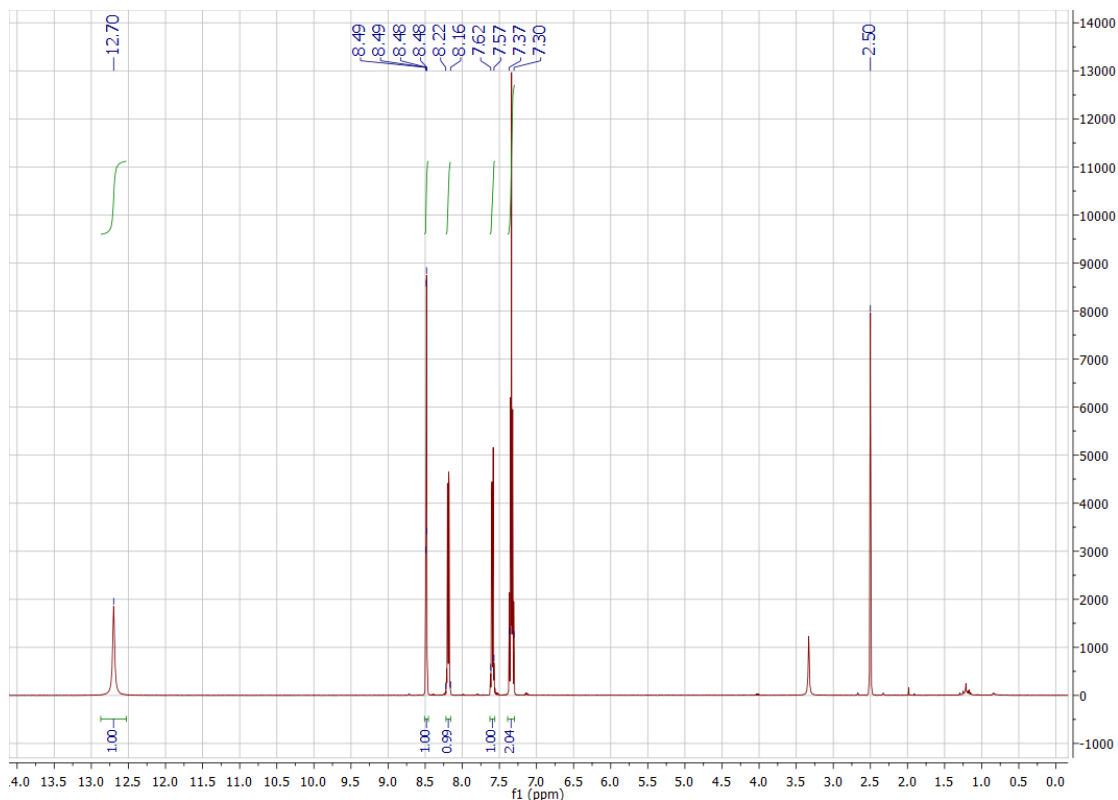
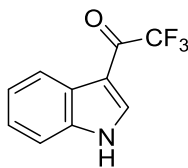
¹H NMR of (1H-Indol-1-yl)(phenyl)methanone



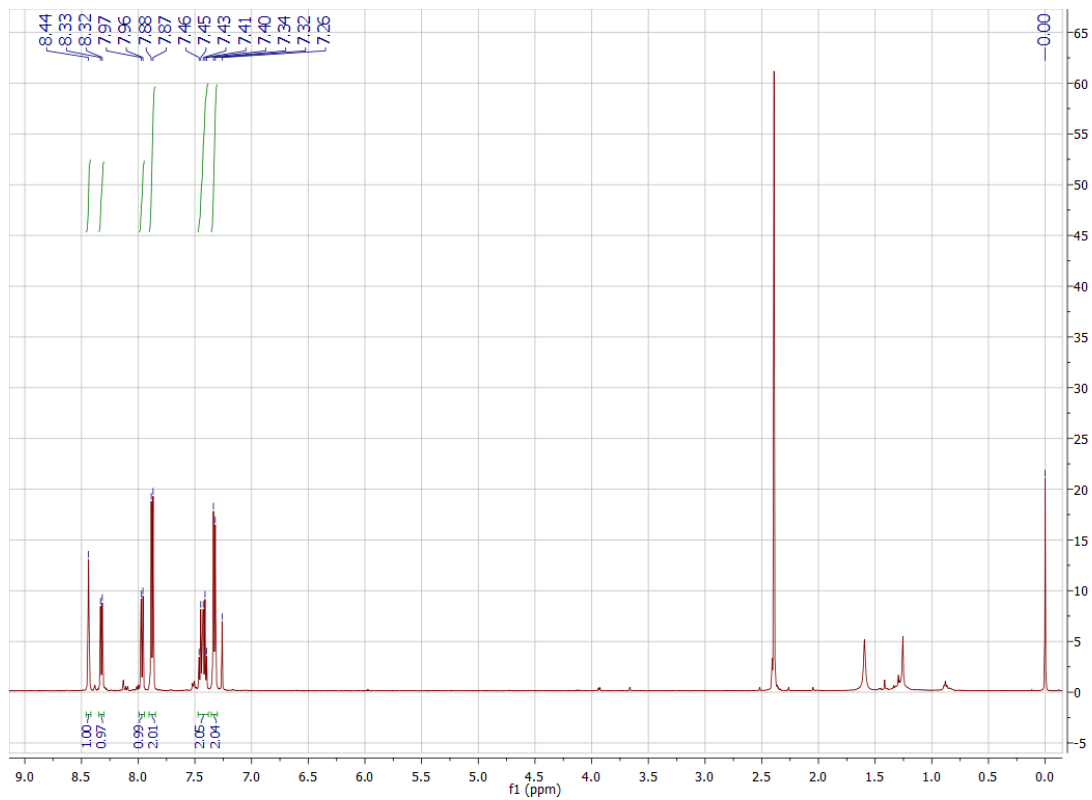
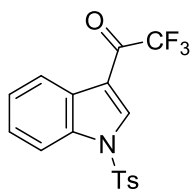
¹H NMR of (3-Nitro-1H-indol-1-yl)(phenyl)methanone (**109b**)



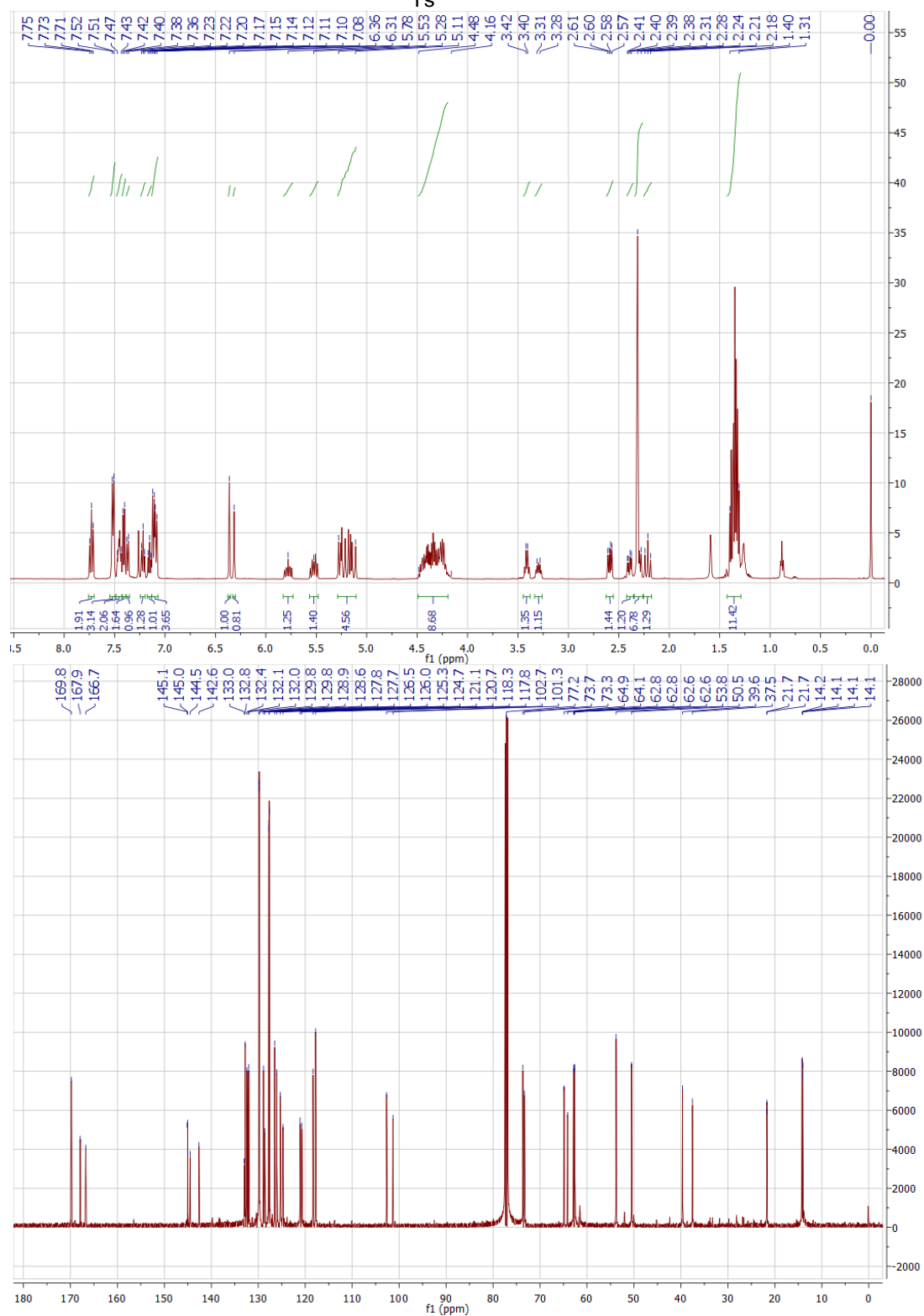
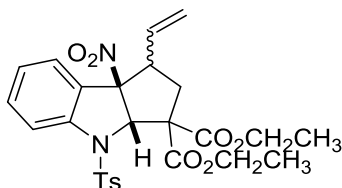
^1H & ^{13}C NMR of 2,2,2-Trifluoro-1-(1H-indol-3-yl)ethan-1-one



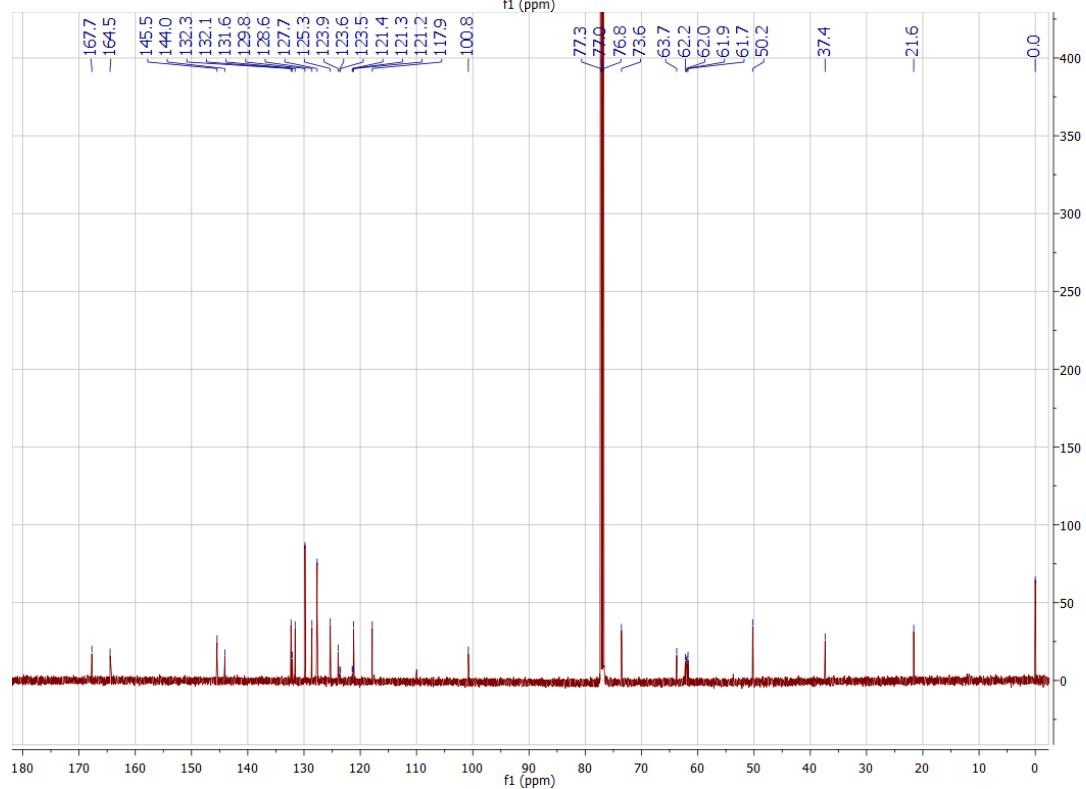
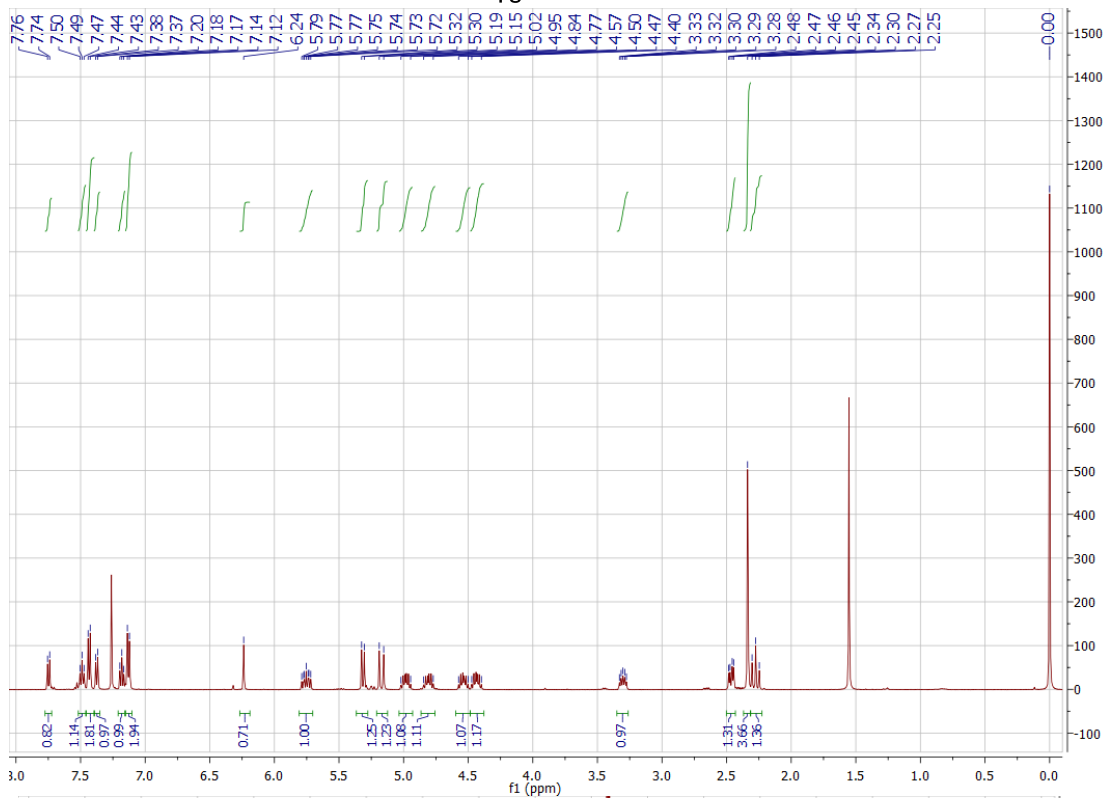
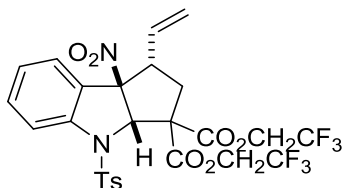
¹H NMR of 2,2,2-Trifluoro-1-(1-tosyl-1H-indol-3-yl)ethan-1-one (**109d**)



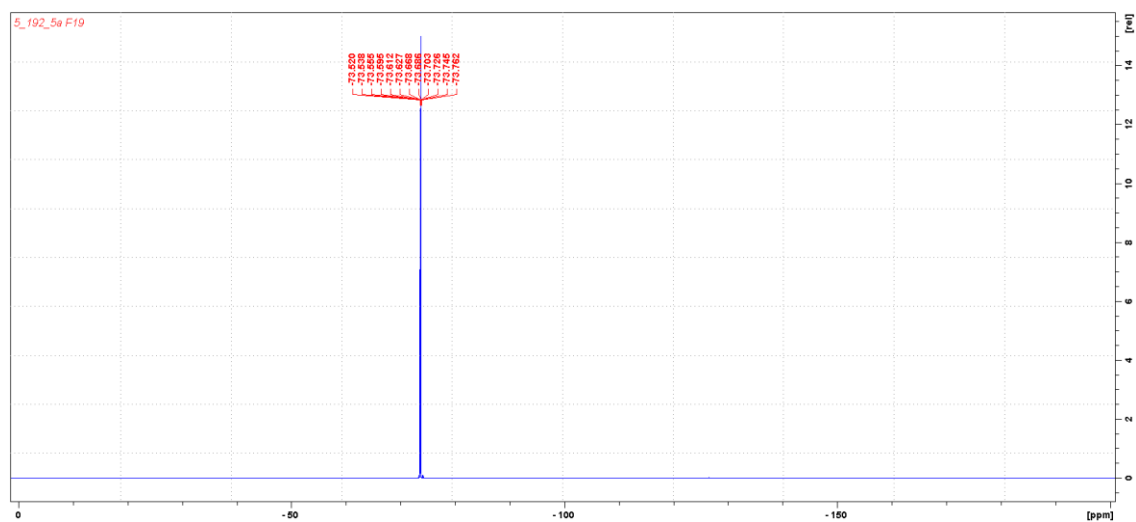
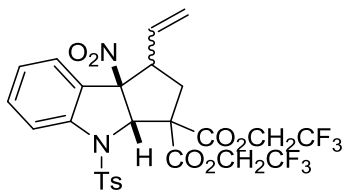
¹H & ¹³C NMR of Diethyl (1*S*,3*aS*,8*bR*)-8*b*-nitro-4-tosyl-1-vinyl-1,3*a*,4,8*b*-tetrahydrocyclopenta[*b*]indole-3,3(2*H*)-dicarboxylate (107*a*/107*a'*)



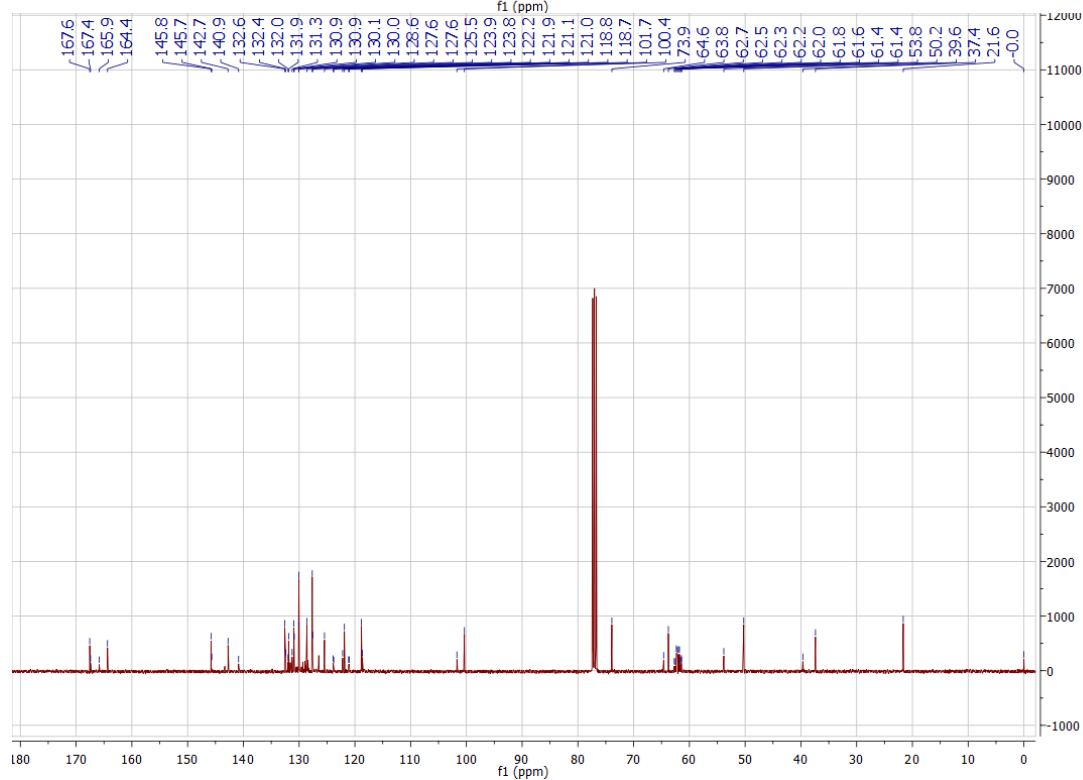
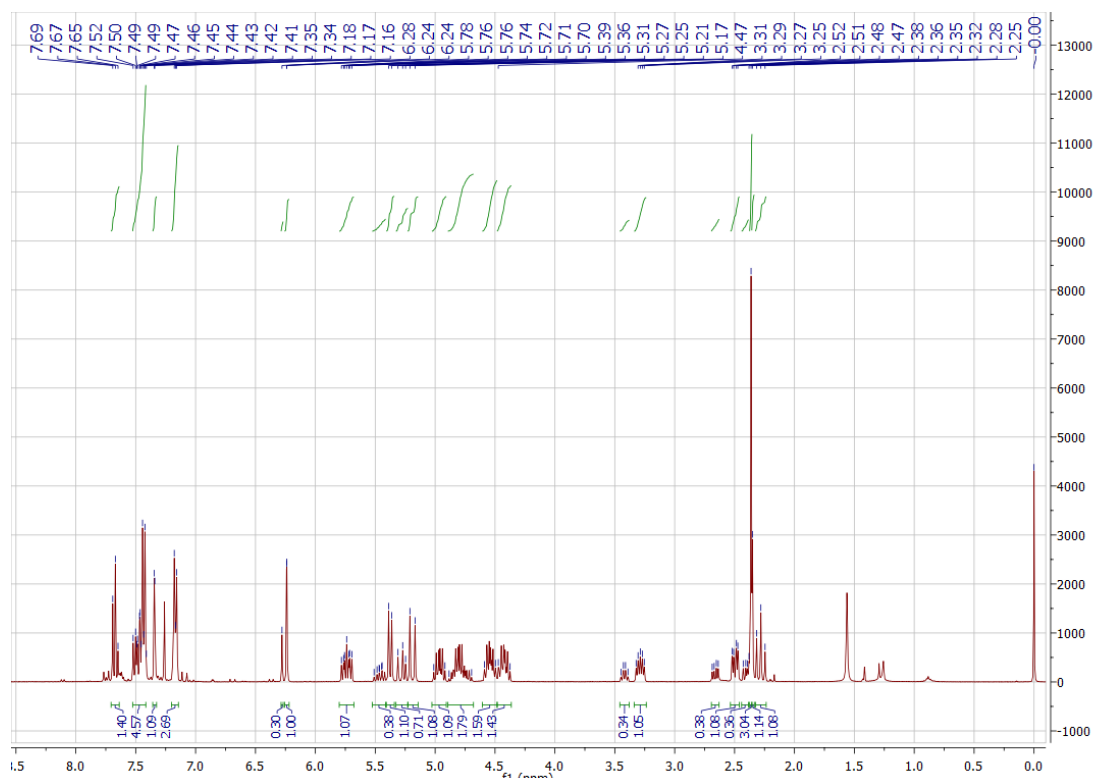
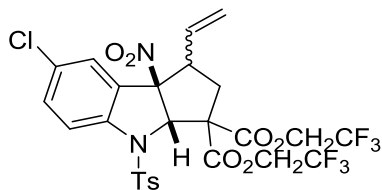
¹H & ¹³C NMR of Bis(2,2,2-trifluoroethyl) (3a*S*,8*bR*)-8*b*-nitro-4-tosyl-1-vinyl-1,3*a*,4,8*b*-tetrahydrocyclopenta[*b*]indole-3,3(2*H*)-dicarboxylate (**108a**)



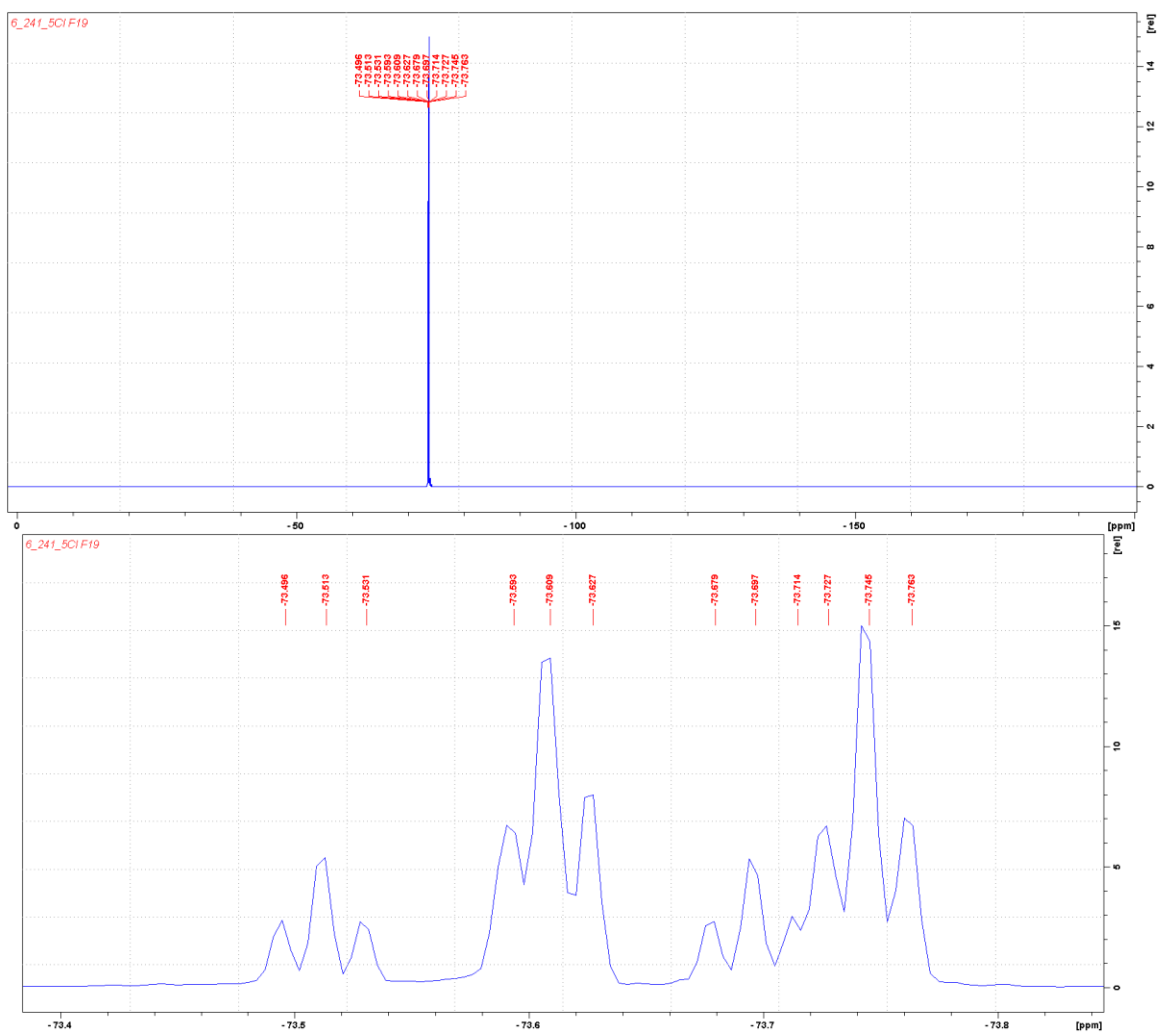
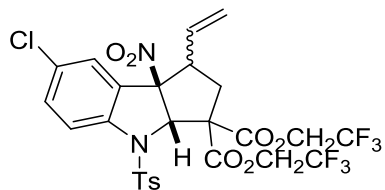
^{19}F NMR of Bis(2,2,2-trifluoroethyl) (3*a*S,8*b*R)-8*b*-nitro-4-tosyl-1-vinyl-1,3*a*,4,8*b*-tetrahydrocyclopenta[*b*]indole-3,3(2*H*)-dicarboxylate (108*a*/108*a'*)



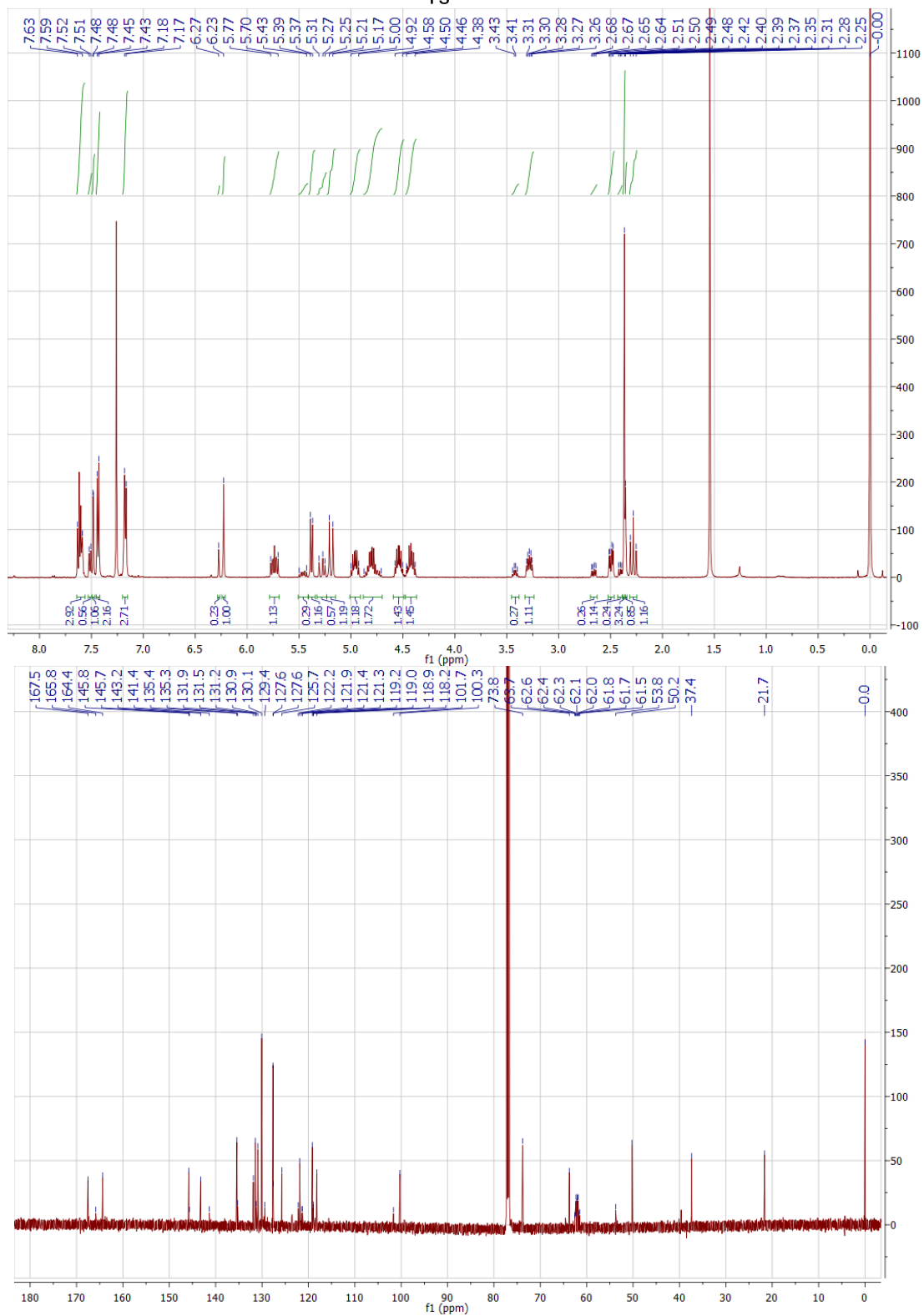
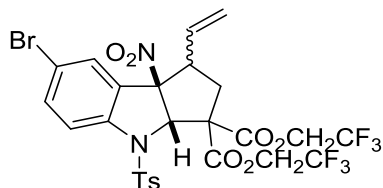
¹H & ¹³C NMR of Bis(2,2,2-trifluoroethyl) (3*a*S,8*b*R)-7-chloro-8*b*-nitro-4-tosyl-1-vinyl-1,3*a*,4,8*b*-tetrahydrocyclopenta[*b*]indole-3,3(2*H*)-dicarboxylate (108*b*/108*b'*)



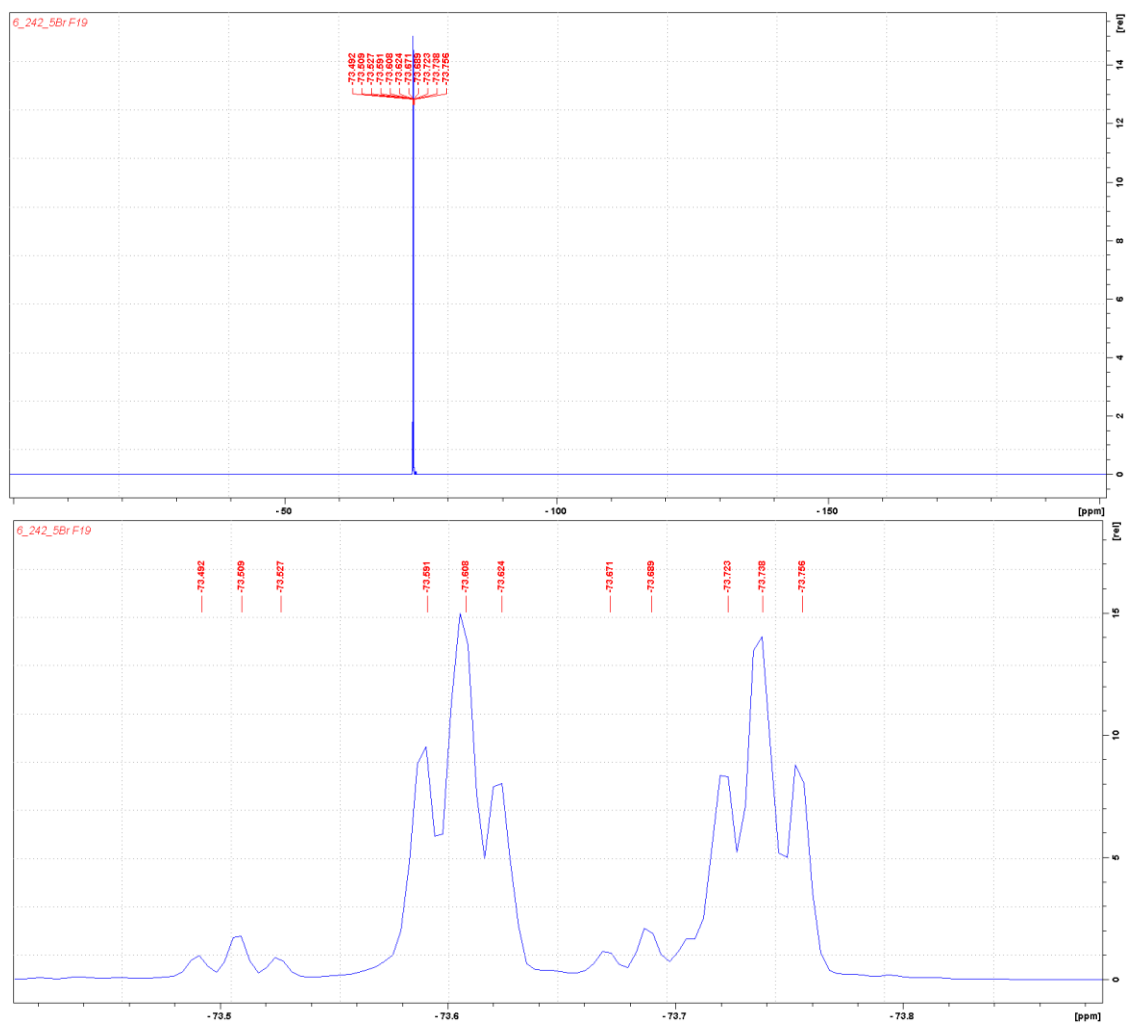
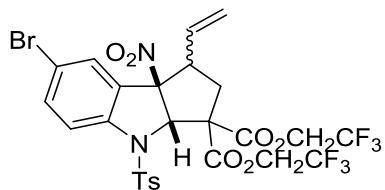
¹⁹F NMR of Bis(2,2,2-trifluoroethyl) (3*aS*,8*bR*)-7-chloro-8*b*-nitro-4-tosyl-1-vinyl-1,3*a*,4,8*b*-tetrahydrocyclopenta[*b*]indole-3,3(2*H*)-dicarboxylate (108*b*/108*b'*)



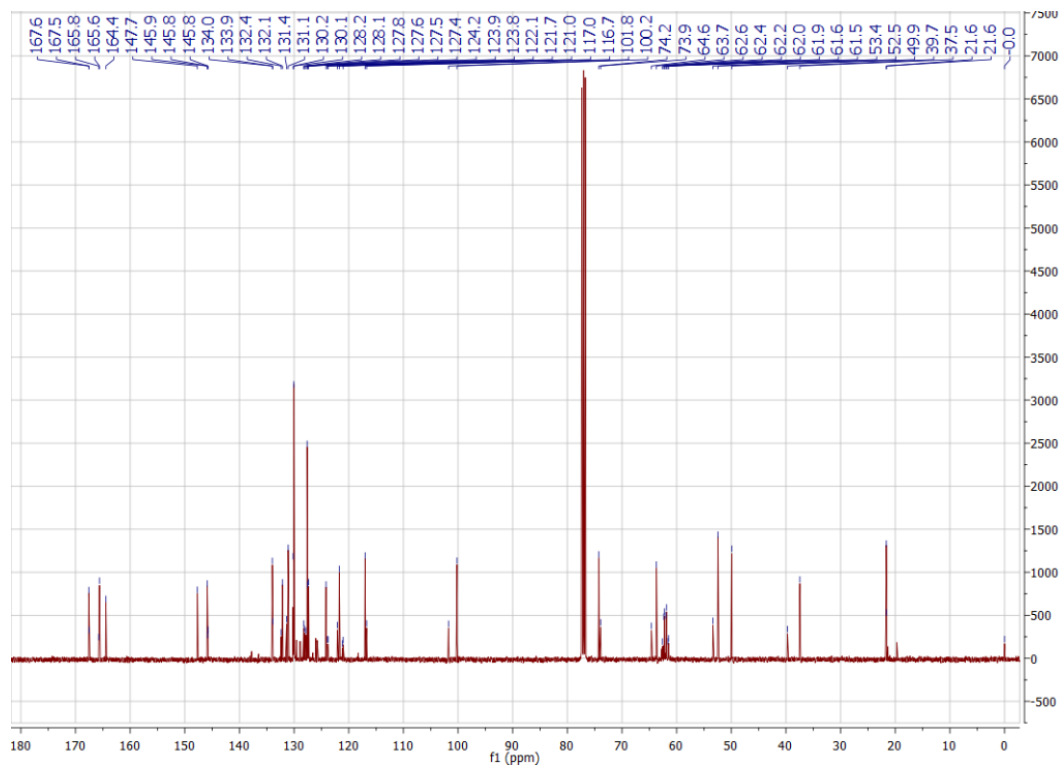
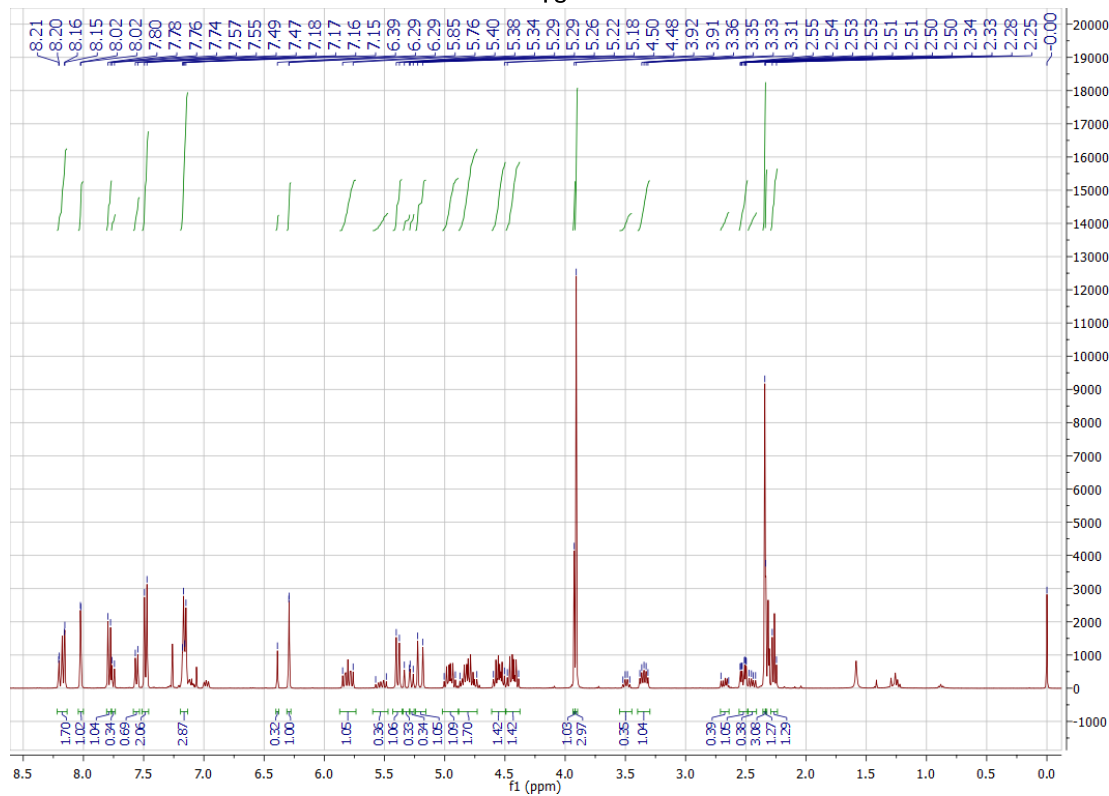
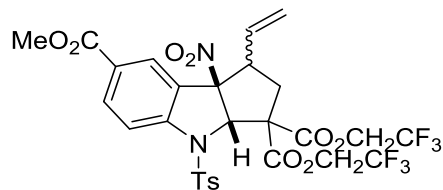
¹H & ¹³C NMR of Bis(2,2,2-trifluoroethyl) (3a*S*,8*b**R*)-7-bromo-8*b*-nitro-4-tosyl-1-vinyl-1,3*a*,4,8*b*-tetrahydrocyclopenta[*b*]indole-3,3(2*H*)-dicarboxylate (108*c*/108*c'*)



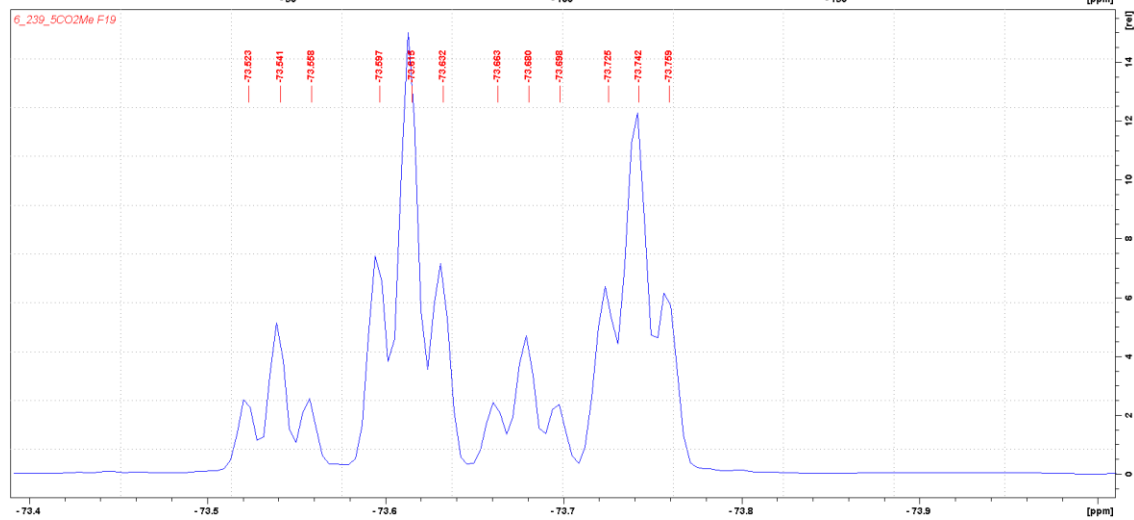
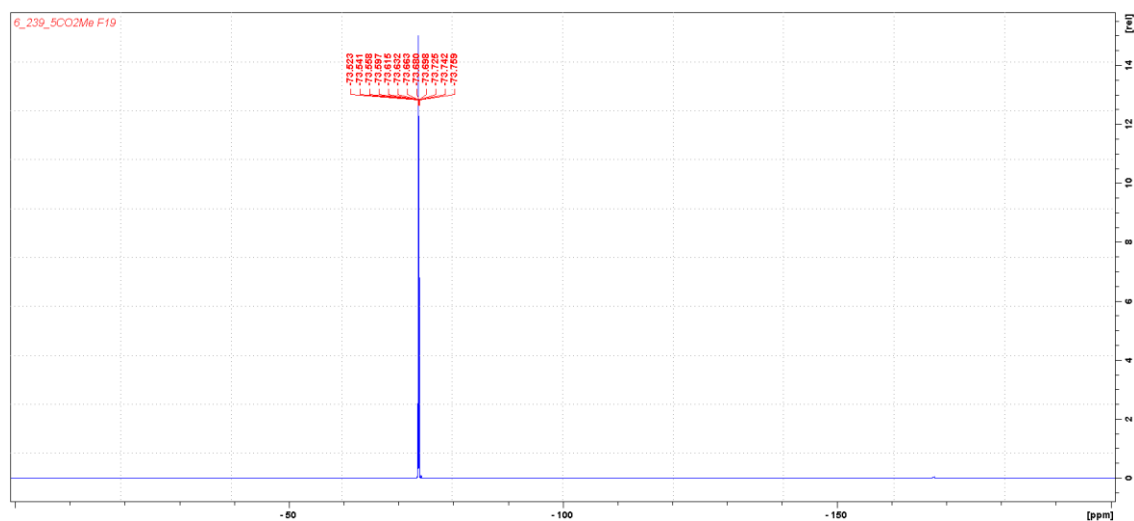
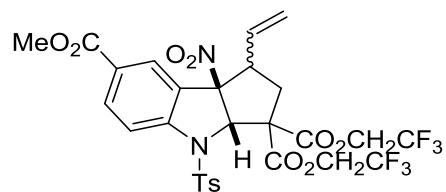
^{19}F NMR of Bis(2,2,2-trifluoroethyl) (3*aS*,8*bR*)-7-bromo-8*b*-nitro-4-tosyl-1-vinyl-1,3*a*,4,8*b*-tetrahydrocyclopenta[*b*]indole-3,3(2*H*)-dicarboxylate (108*c*/108*c'*)



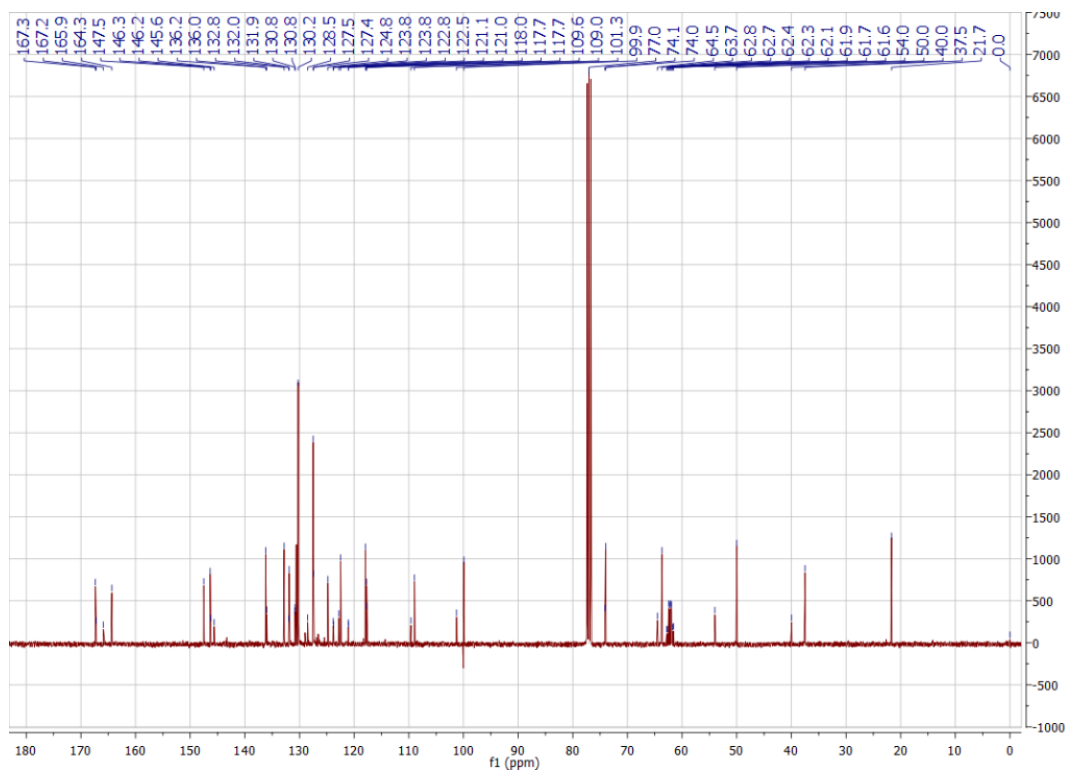
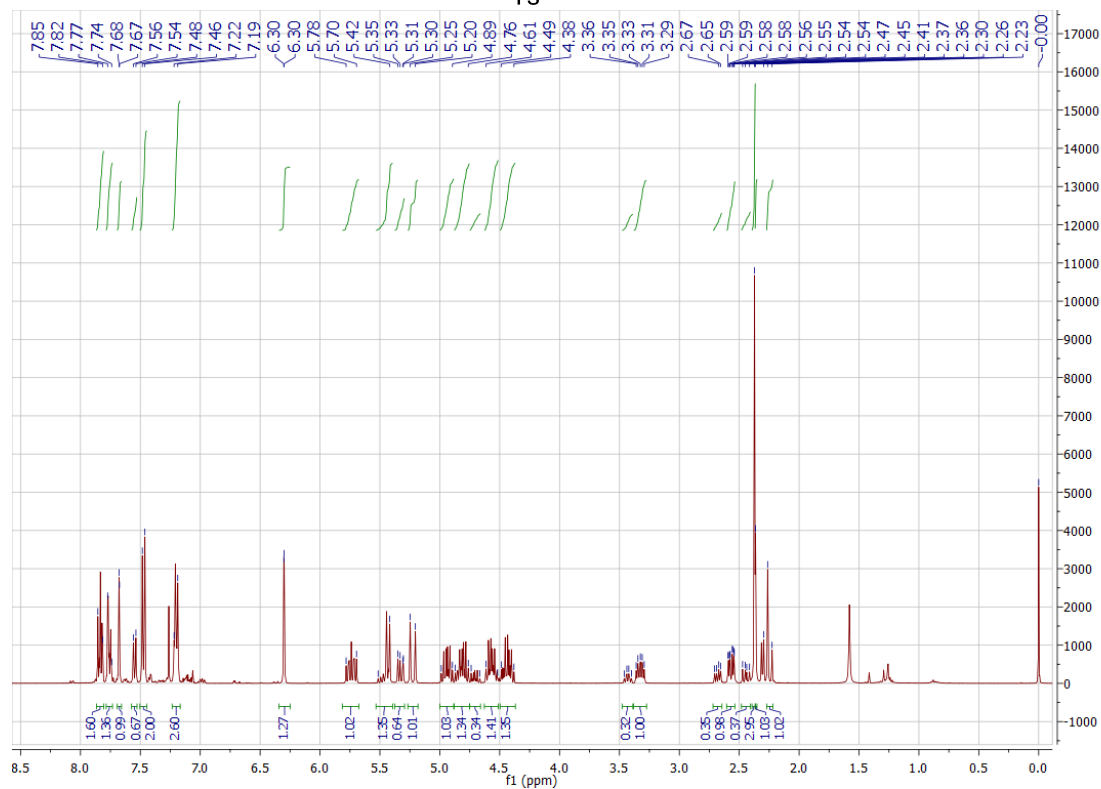
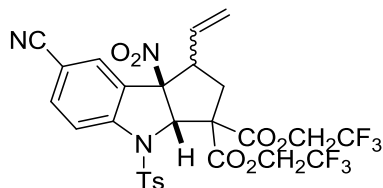
*¹H & ¹³C NMR of 7-Methyl 3,3-bis(2,2,2-trifluoroethyl) (3a*S*,8*bR*)-8*b*-nitro-4-tosyl-1-vinyl-1,3*a*,4,8*b*-tetrahydrocyclopenta[*b*]indole-3,3,7(2*H*)-tricarboxylate (108*d*/108*d'*)*



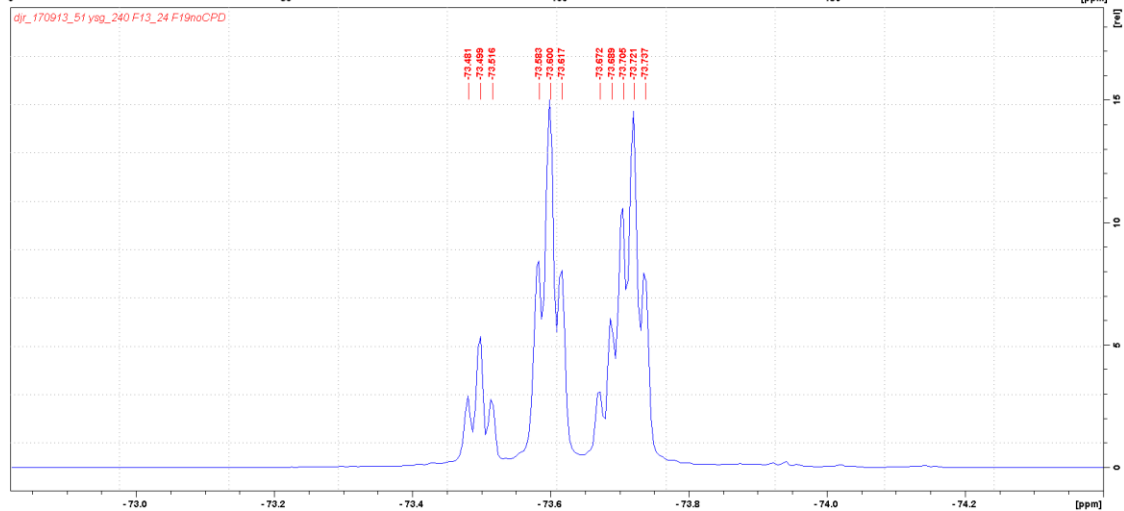
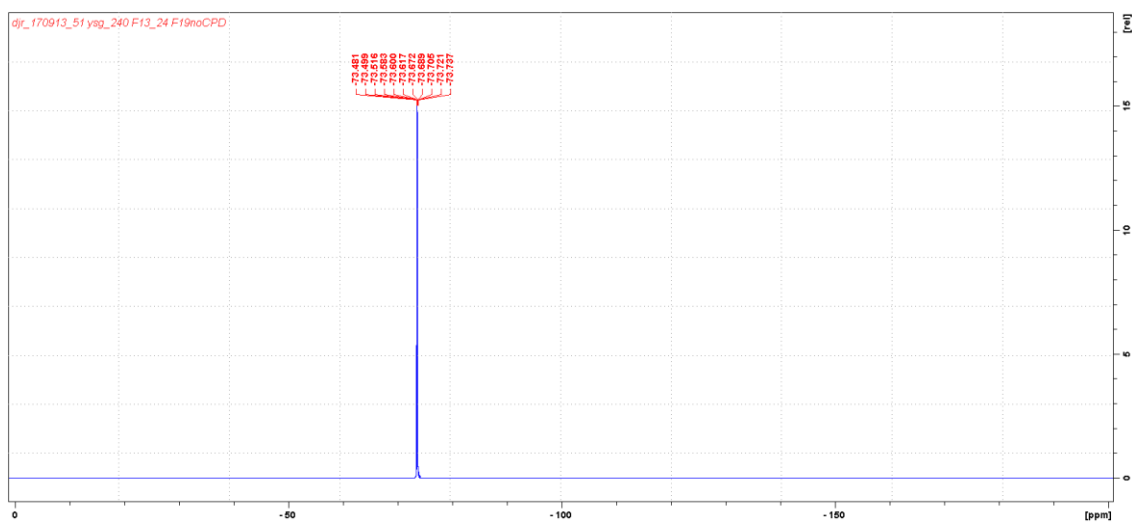
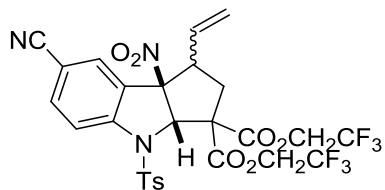
^{19}F NMR of 7-Methyl 3,3-bis(2,2,2-trifluoroethyl) (3*aS*,8*bR*)-8*b*-nitro-4-tosyl-1-vinyl-1,3*a*,4,8*b*-tetrahydrocyclopenta[*b*]indole-3,3,7(2*H*)-tricarboxylate (108*d*/108*d'*)



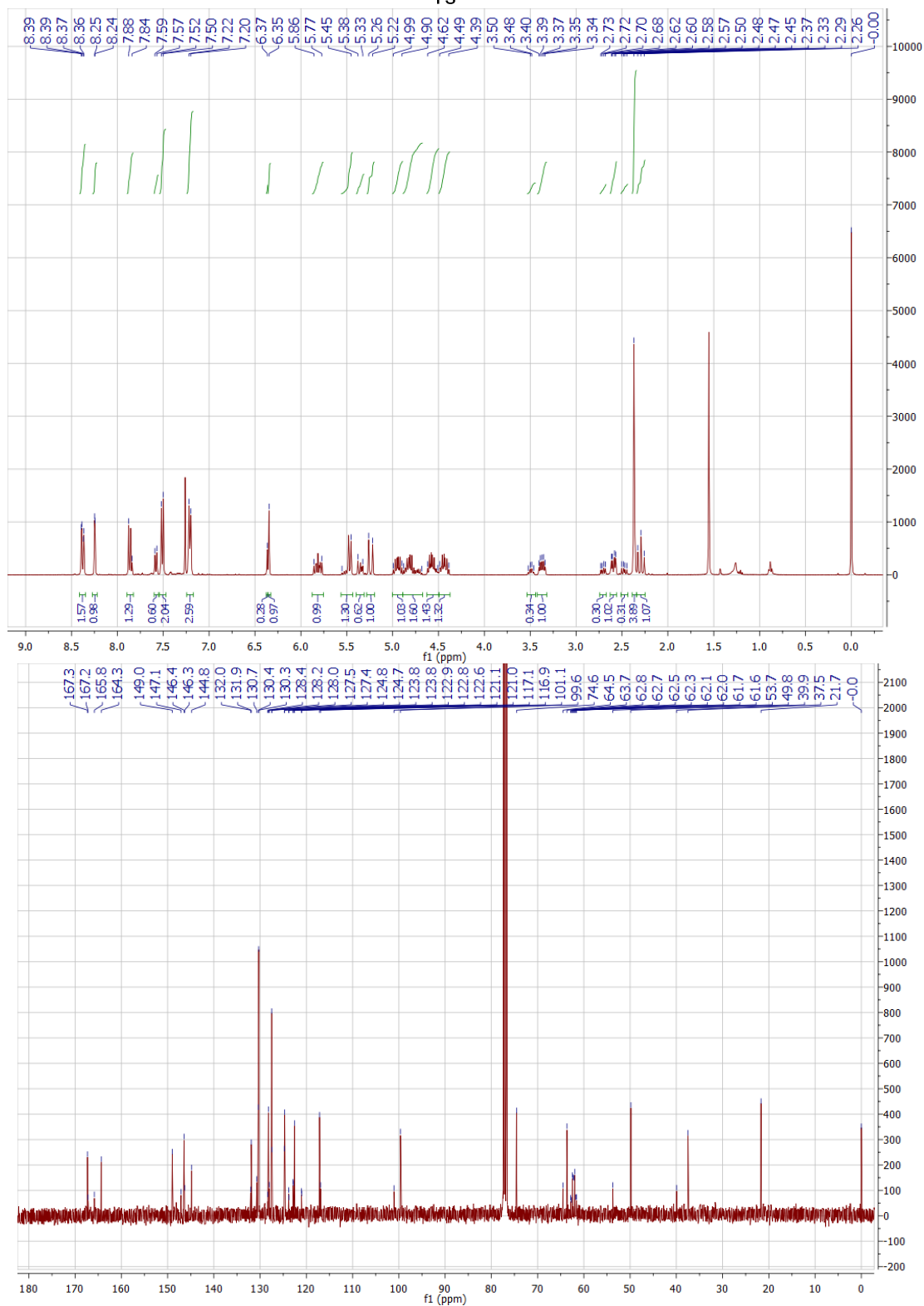
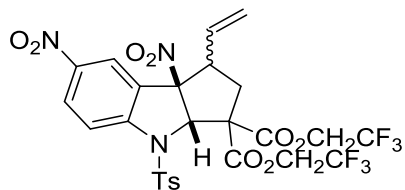
¹H & ¹³C NMR of Bis(2,2,2-trifluoroethyl) (3aS,8bR)-7-cyano-8b-nitro-4-tosyl-1-vinyl-1,3a,4,8b-tetrahydrocyclopenta[b]indole-3,3(2H)-dicarboxylate (108e/108e')



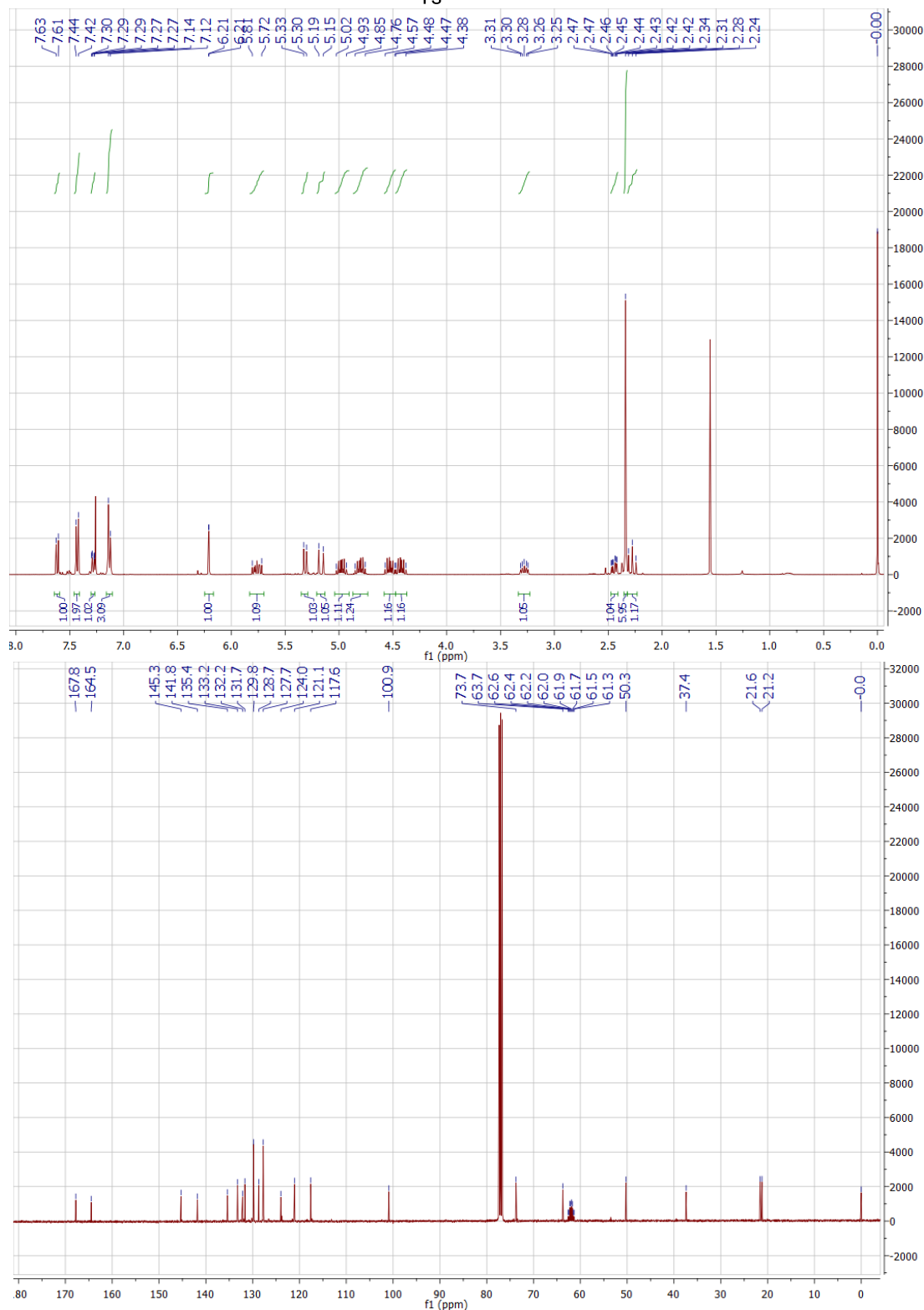
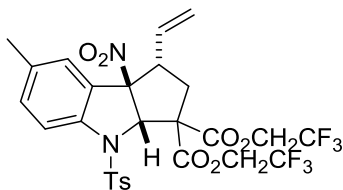
^{19}F NMR of Bis(2,2,2-trifluoroethyl) (3*a*S,8*b*R)-7-cyano-8*b*-nitro-4-tosyl-1-vinyl-1,3*a*,4,8*b*-tetrahydrocyclopenta[*b*]indole-3,3(2*H*)-dicarboxylate (108*e*/108*e'*)



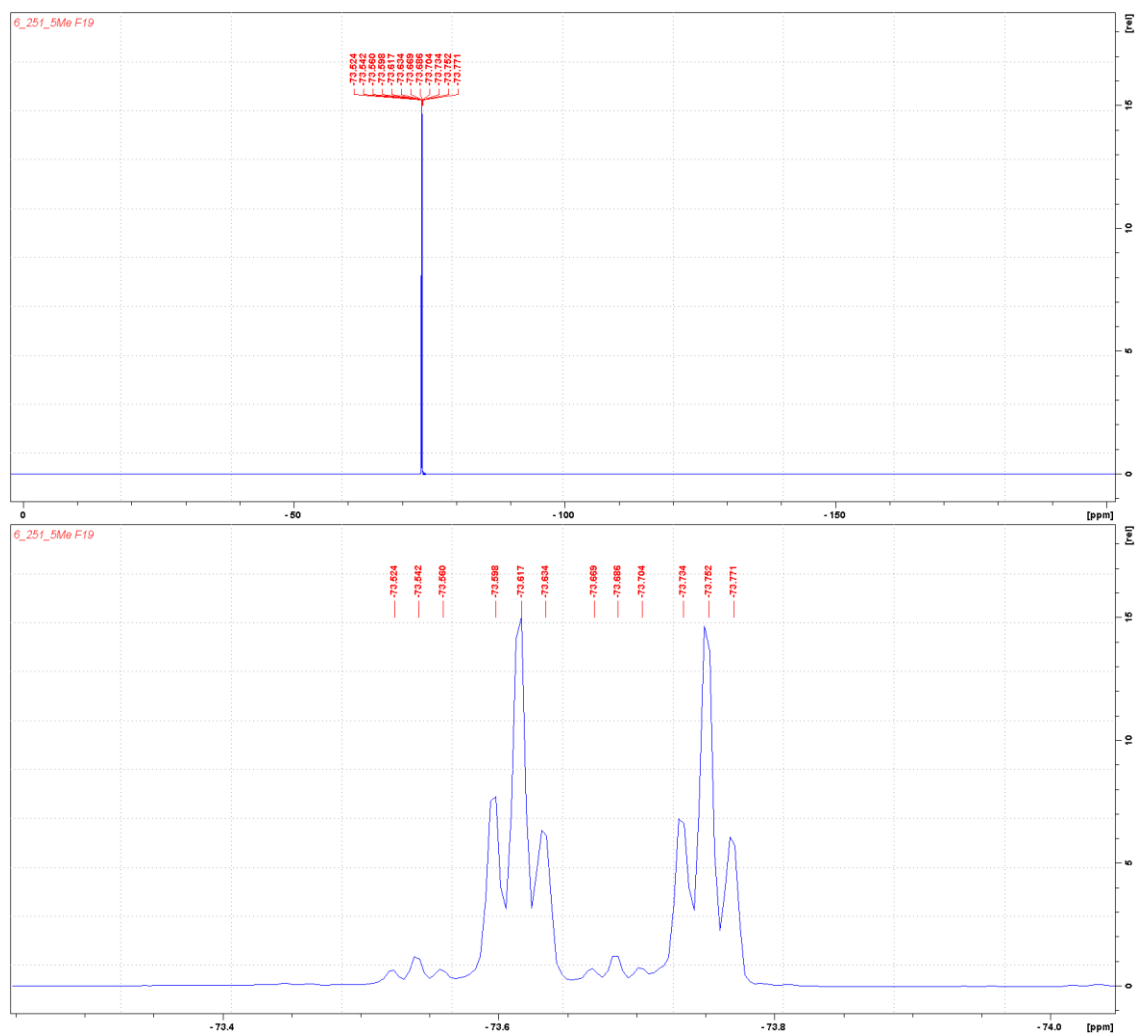
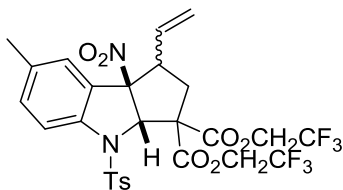
¹H & ¹³C NMR of Bis(2,2,2-trifluoroethyl) (3a*S*,8*bR*)-7,8*b*-dinitro-4-tosyl-1-vinyl-1,3*a*,4,8*b*-tetrahydrocyclopenta[*b*]indole-3,3(2*H*)-dicarboxylate (108*f*/108*f*)



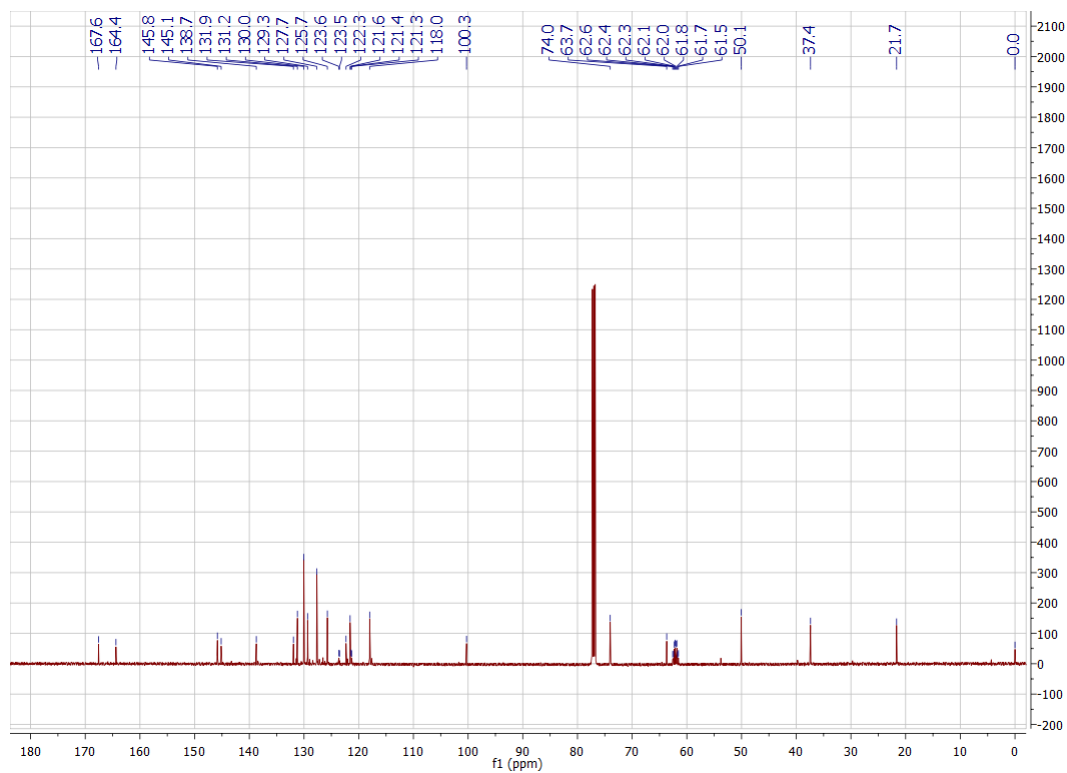
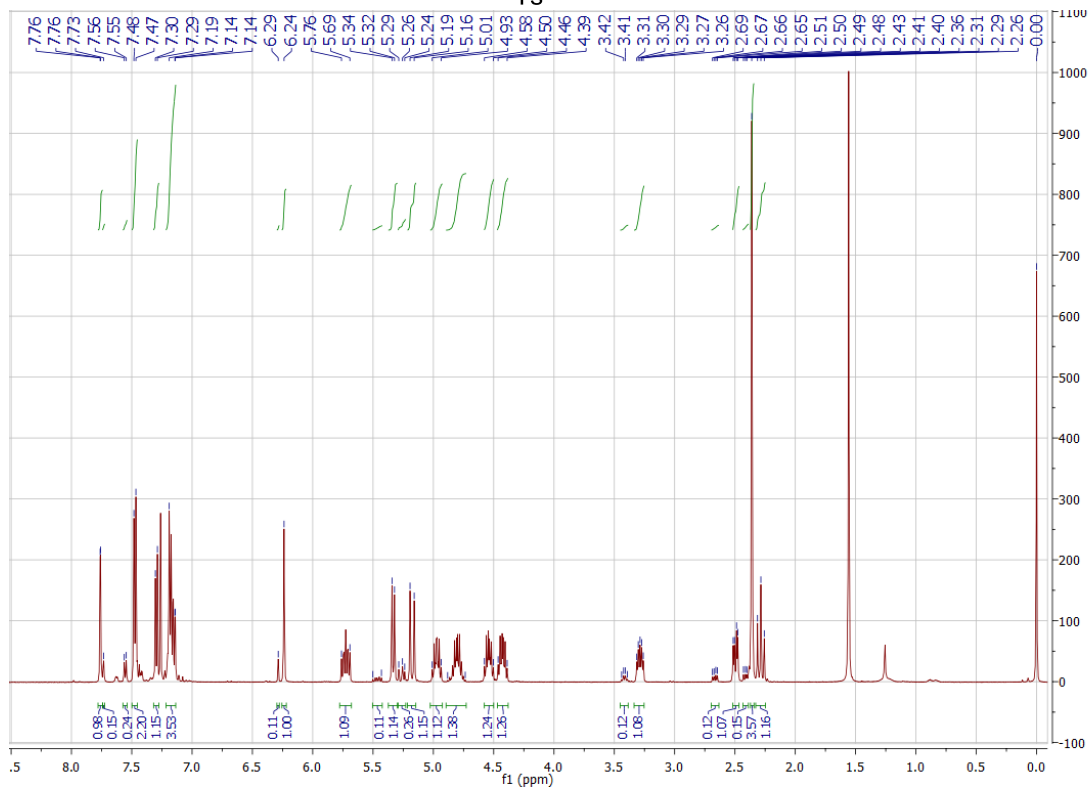
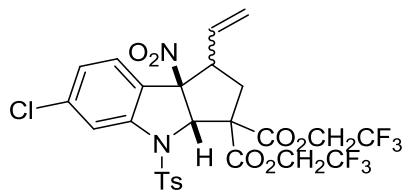
¹H & ¹³C NMR of Bis(2,2,2-trifluoroethyl) (3a*S*,8*bR*)-7-methyl-8*b*-nitro-4-tosyl-1-vinyl-1,3*a*,4,8*b*-tetrahydrocyclopenta[*b*]indole-3,3(2*H*)-dicarboxylate (**108g**)



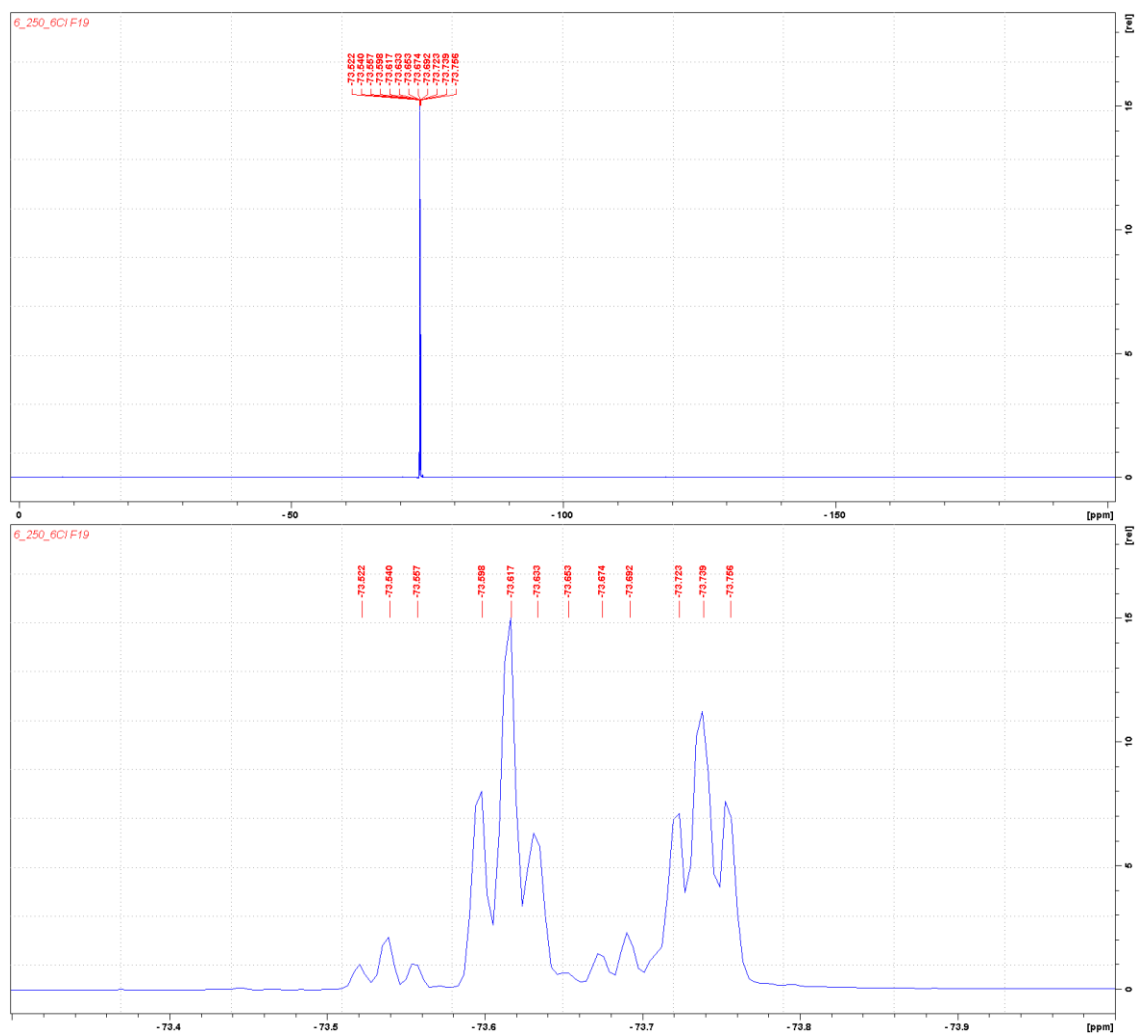
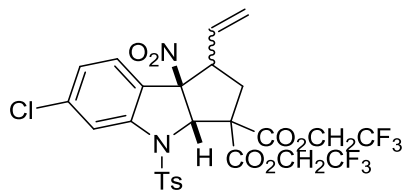
^{19}F NMR of Bis(2,2,2-trifluoroethyl) (3a*S*,8*bR*)-7-methyl-8*b*-nitro-4-tosyl-1-vinyl-1,3*a*,4,8*b*-tetrahydrocyclopenta[*b*]indole-3,3(2*H*)-dicarboxylate (108*g*/108*g*')



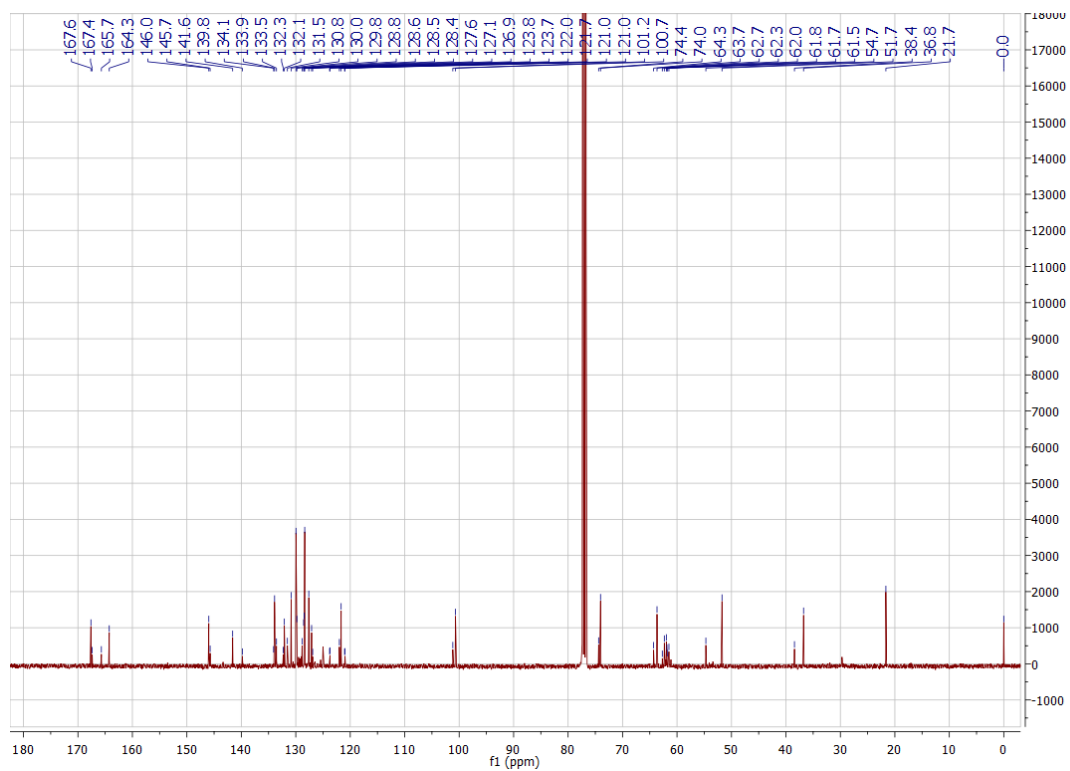
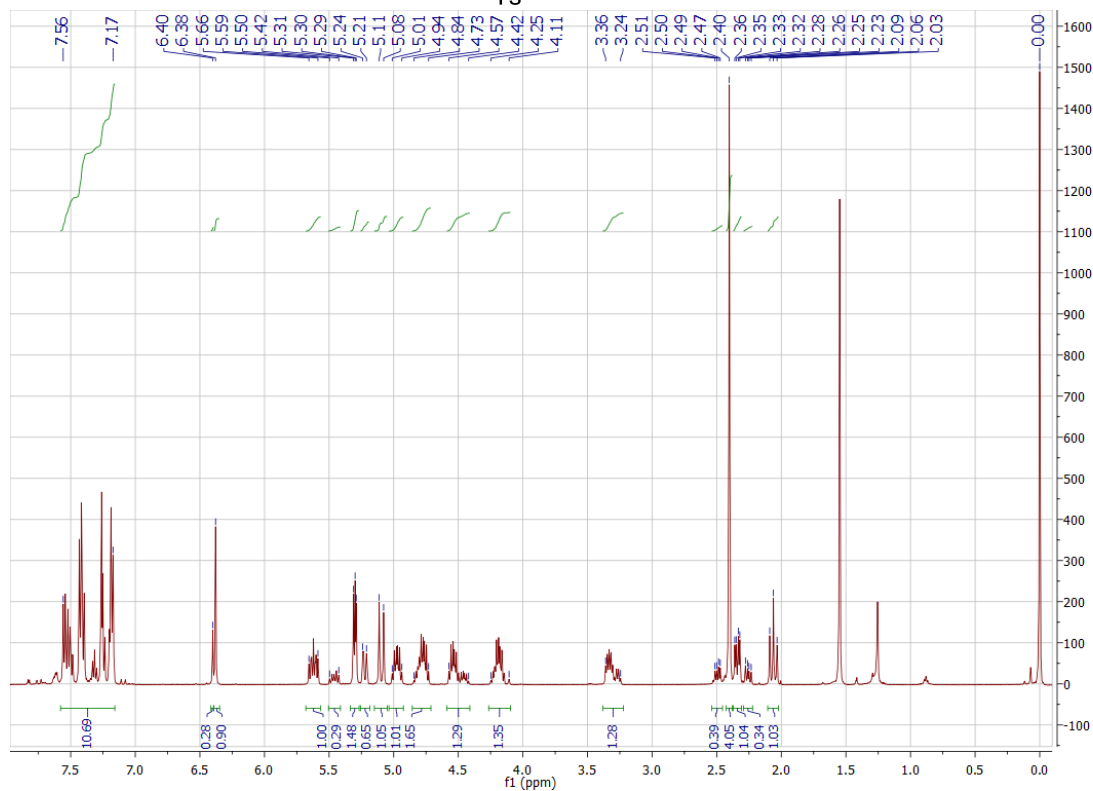
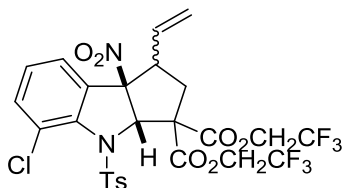
¹H & ¹³C NMR of Bis(2,2,2-trifluoroethyl) (3a*S*,8*bR*)-6-chloro-8*b*-nitro-4-tosyl-1-vinyl-1,3*a*,4,8*b*-tetrahydrocyclopenta[*b*]indole-3,3(2*H*)-dicarboxylate (108*i*/108*i'*)



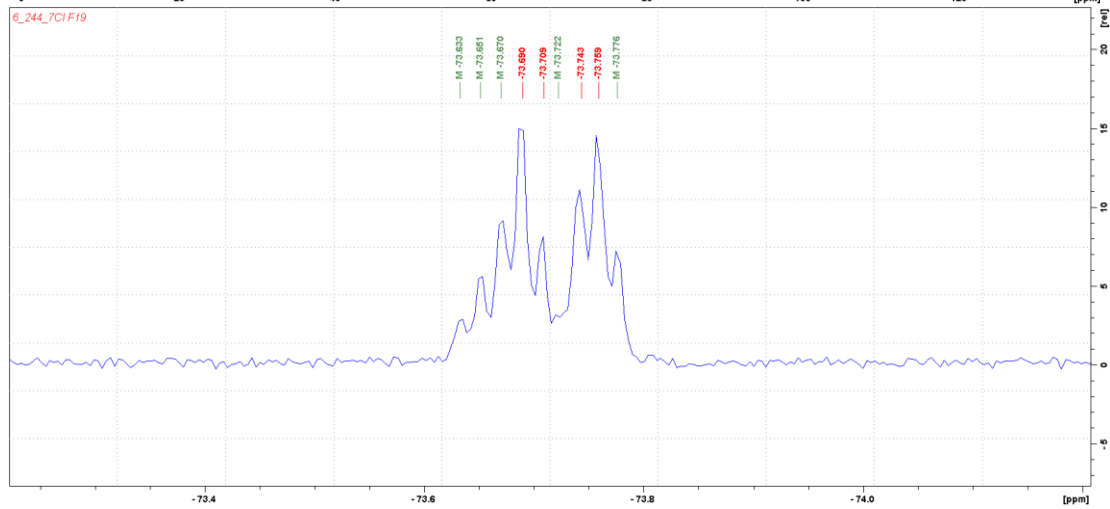
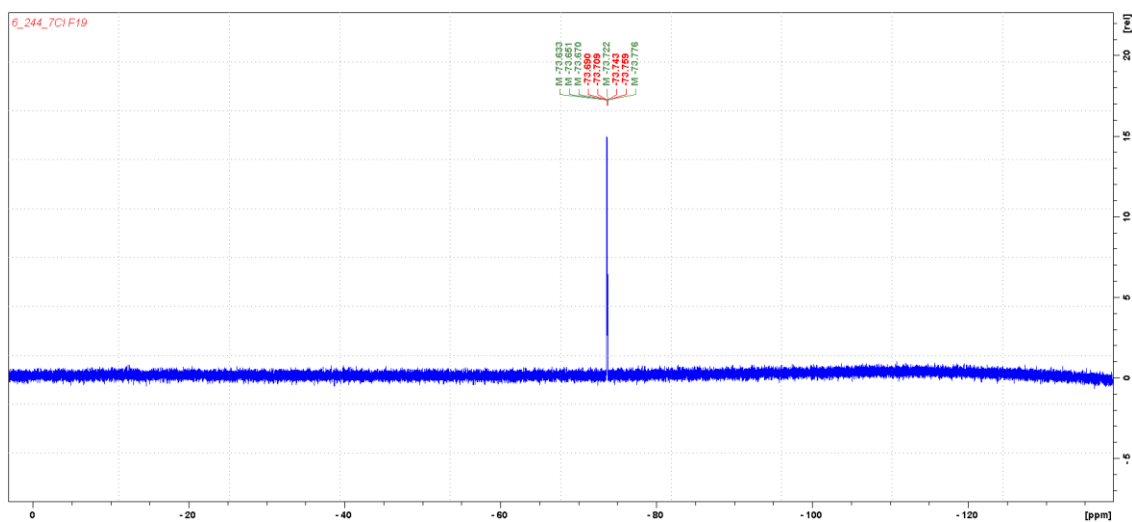
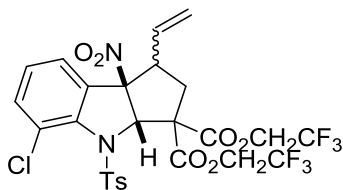
^{19}F NMR of Bis(2,2,2-trifluoroethyl) (3a*S*,8*b*R)-6-chloro-8*b*-nitro-4-tosyl-1-vinyl-1,3*a*,4,8*b*-tetrahydrocyclopenta[*b*]indole-3,3(2*H*)-dicarboxylate (108*i*/108*i'*)



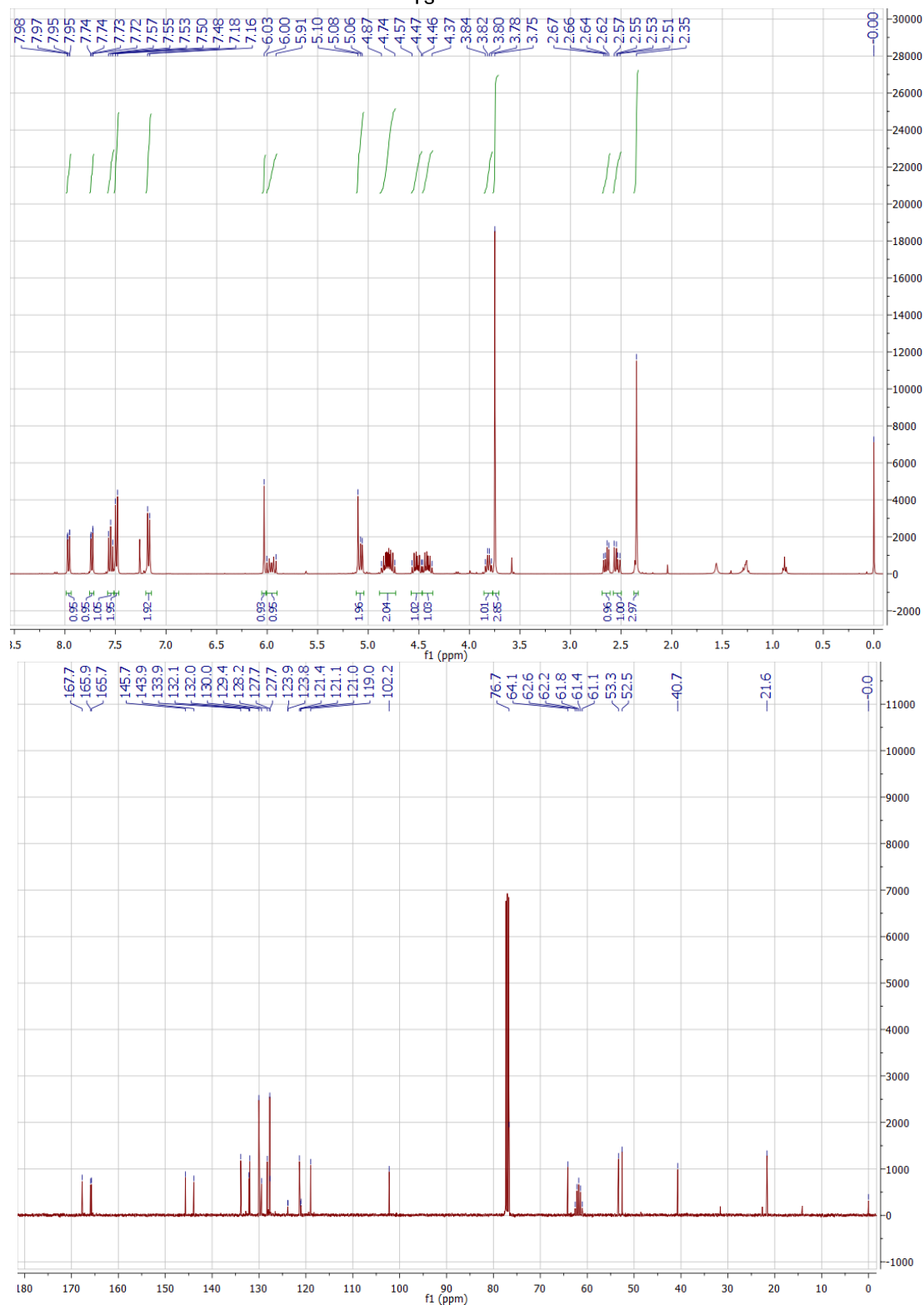
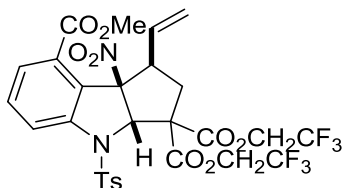
¹H & ¹³C NMR of Bis(2,2,2-trifluoroethyl) (3aS,8bR)-5-chloro-8b-nitro-4-tosyl-1-vinyl-1,3a,4,8b-tetrahydrocyclopenta[b]indole-3,3(2H)-dicarboxylate (108j/108j')



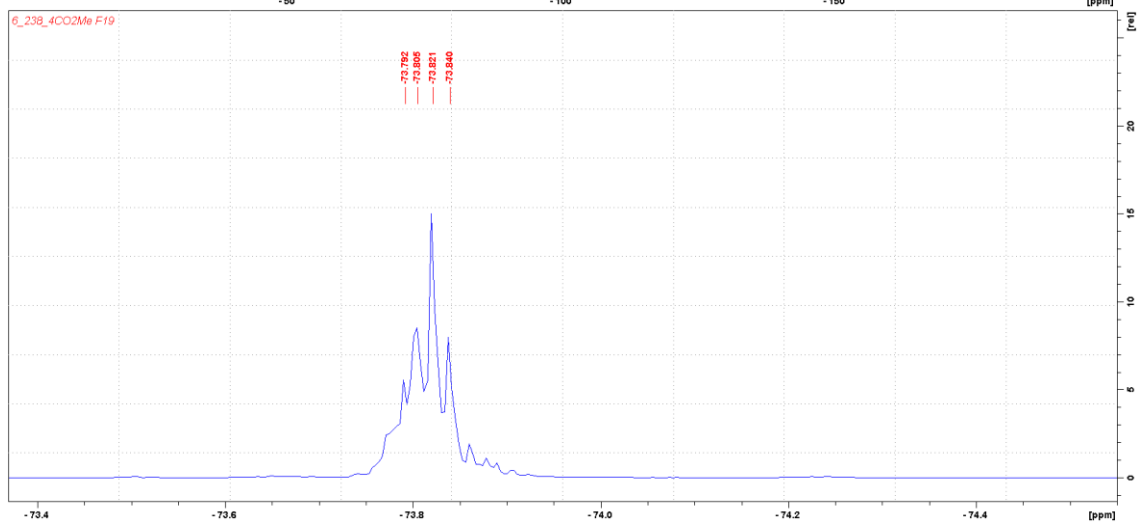
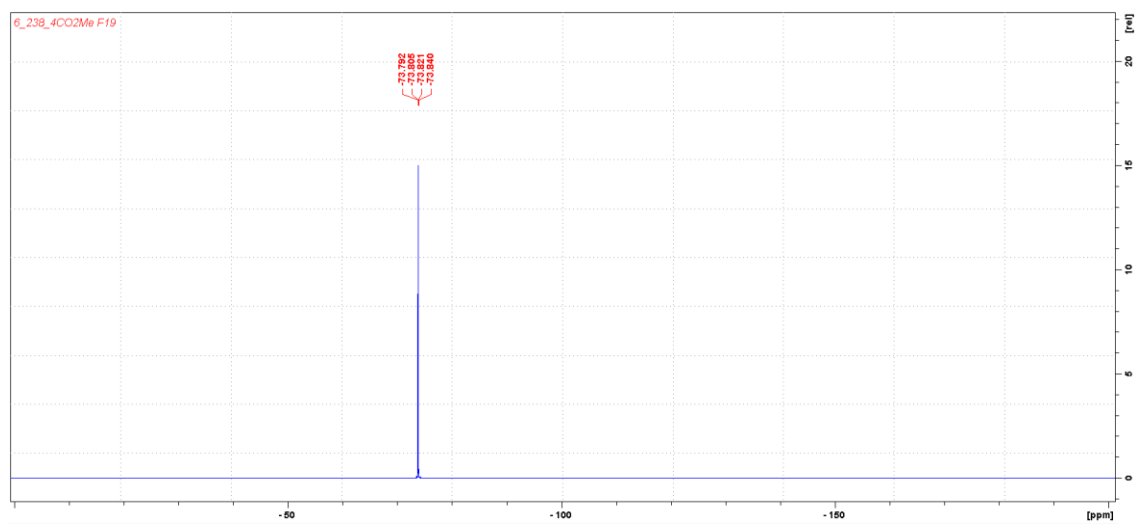
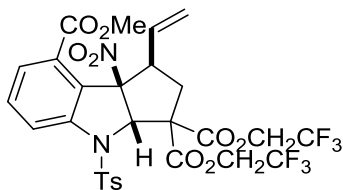
^{19}F NMR of Bis(2,2,2-trifluoroethyl) (3*a*S,8*b*R)-5-chloro-8*b*-nitro-4-tosyl-1-vinyl-1,3*a*,4,8*b*-tetrahydrocyclopenta[*b*]indole-3,3(2*H*)-dicarboxylate (108*j*/108*j'*)



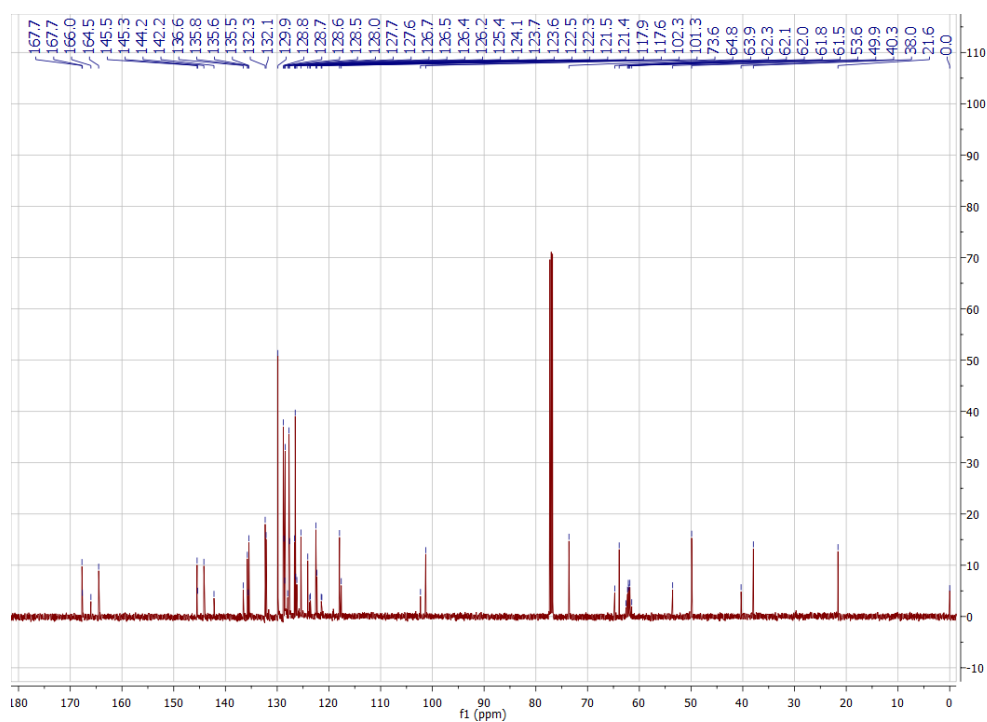
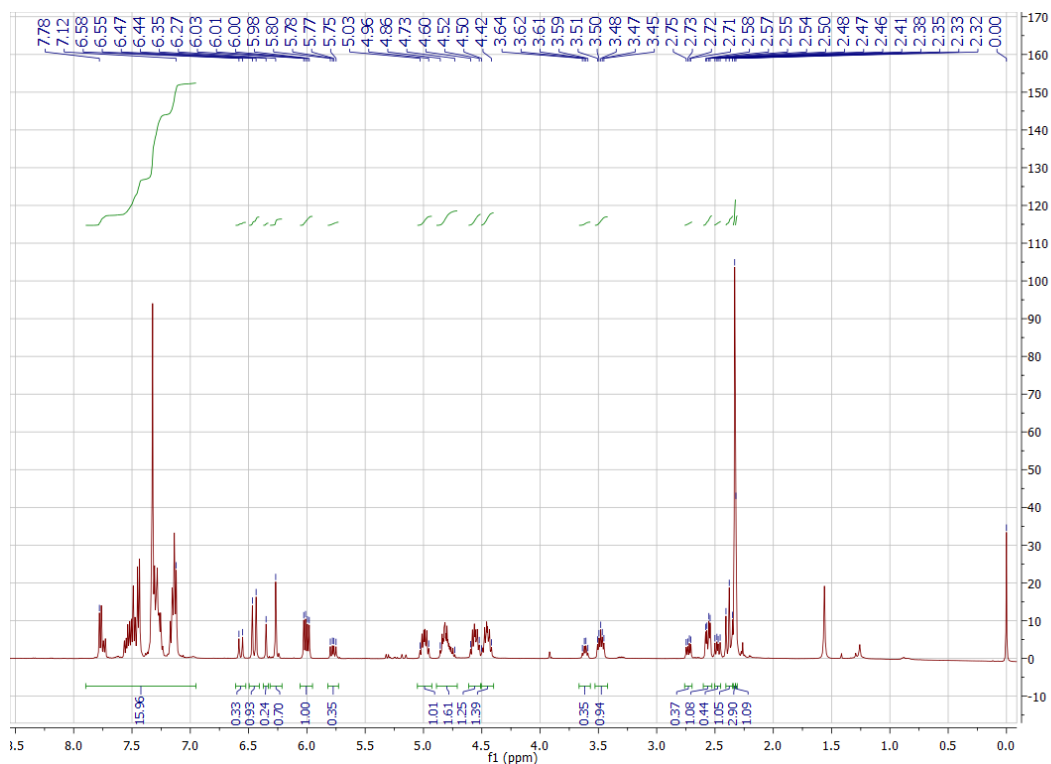
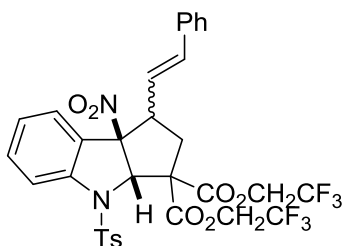
^1H & ^{13}C NMR of 8-Methyl 3,3-bis(2,2,2-trifluoroethyl) (3a*S*,8*bR*)-8*b*-nitro-4-tosyl-1-vinyl-1,3*a*,4,8*b*-tetrahydrocyclopenta[*b*]indole-3,3,8(2*H*)-tricarboxylate (**108k'**)



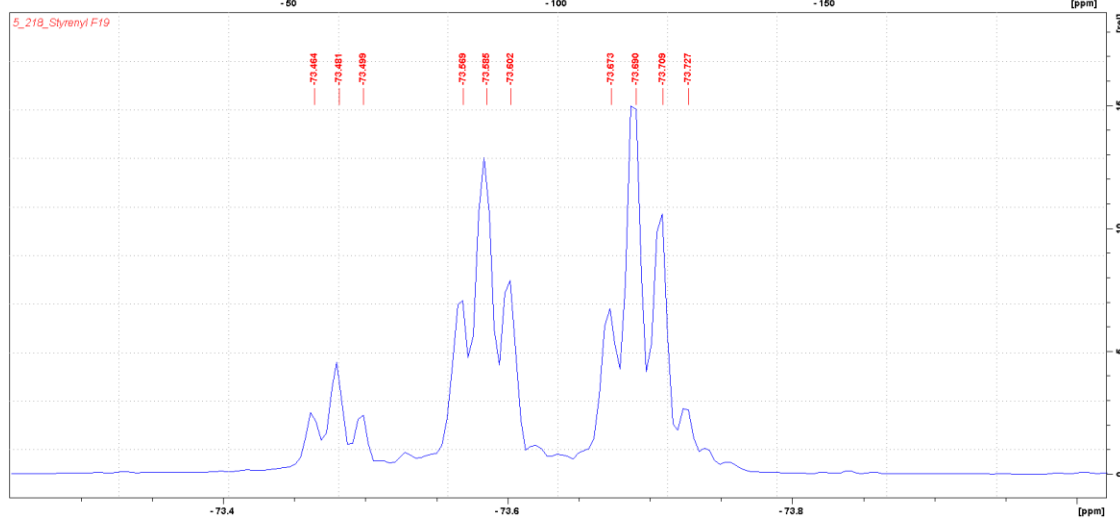
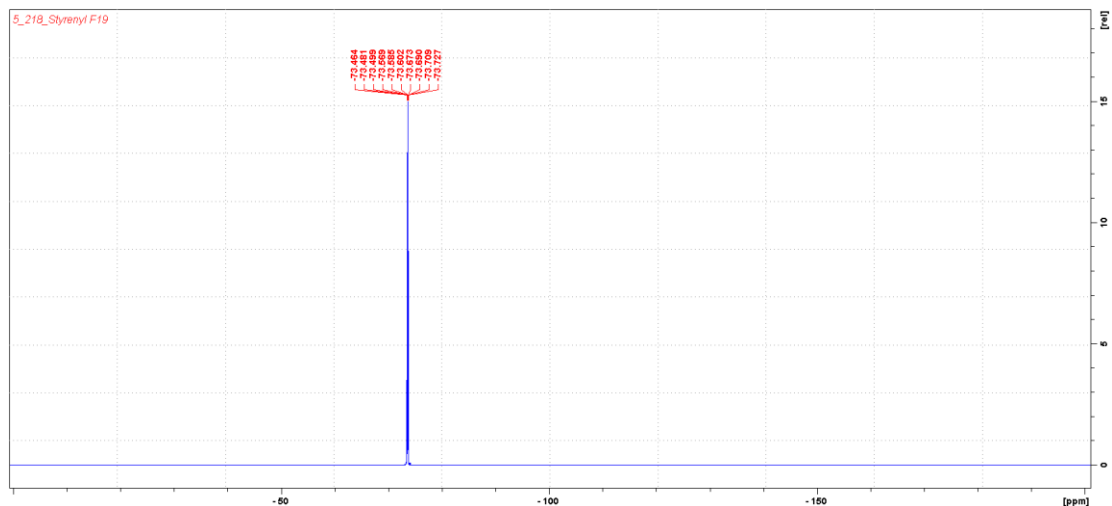
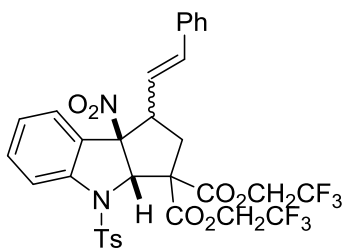
^{19}F NMR of 8-Methyl 3,3-bis(2,2,2-trifluoroethyl) (3*aS*,8*bR*)-8*b*-nitro-4-tosyl-1-vinyl-1,3*a*,4,8*b*-tetrahydrocyclopenta[*b*]indole-3,3,8(2*H*)-tricarboxylate(108*k'*)



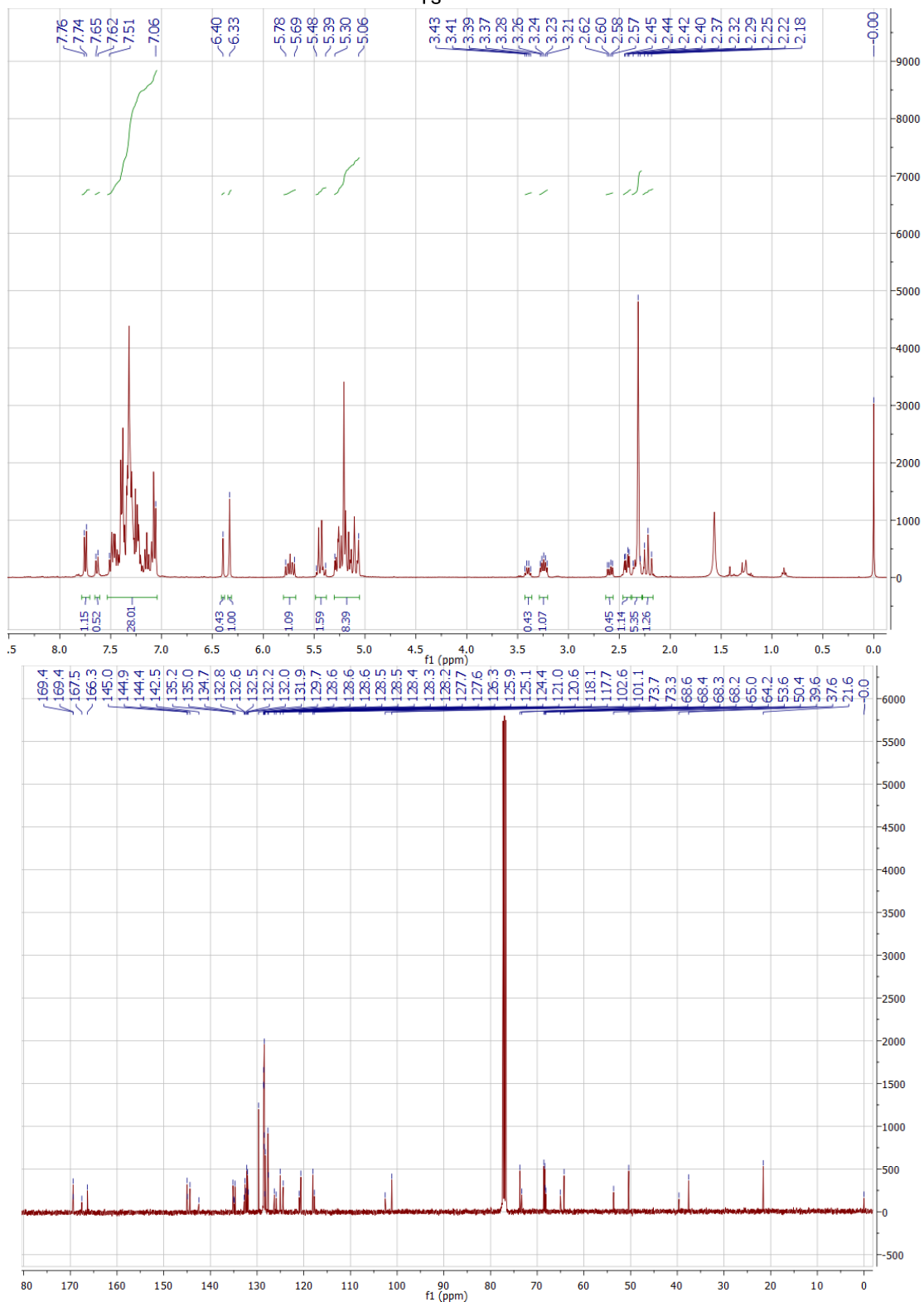
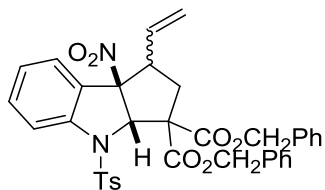
¹H & ¹³C NMR of Bis(2,2,2-trifluoroethyl) (3a*S*,8*bR*)-8*b*-nitro-1-styryl-4-tosyl-1,3*a*,4,8*b*-tetrahydrocyclopenta[*b*]indole-3,3(2*H*)-dicarboxylate (112/112')



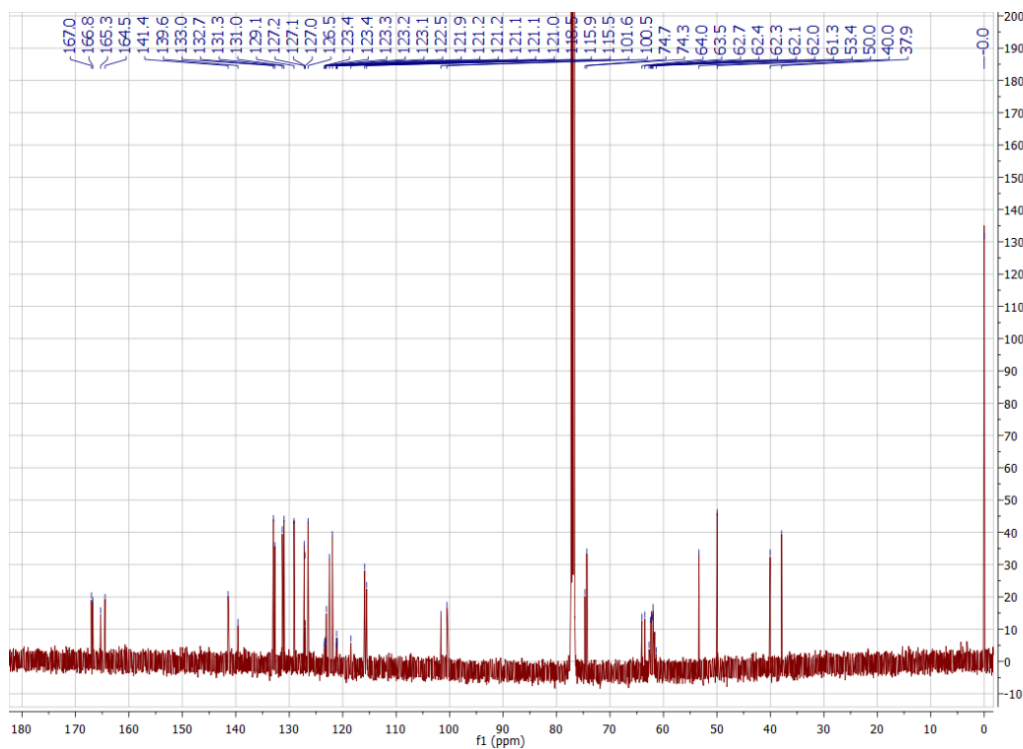
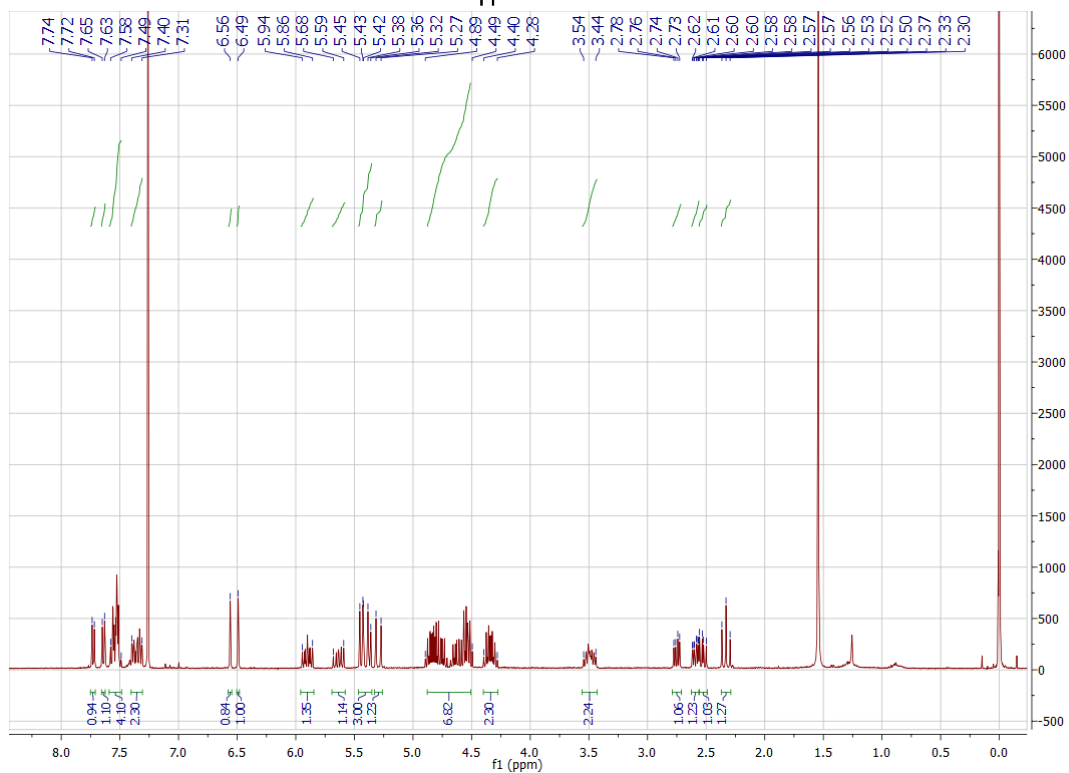
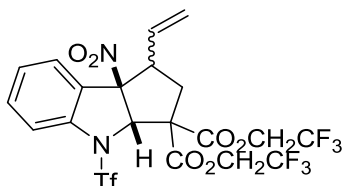
^{19}F NMR of Bis(2,2,2-trifluoroethyl) (3*a*S,8*b*R)-8*b*-nitro-1-styryl-4-tosyl-1,3*a*,4,8*b*-tetrahydrocyclopenta[*b*]indole-3,3(2*H*)-dicarboxylate (112/112')



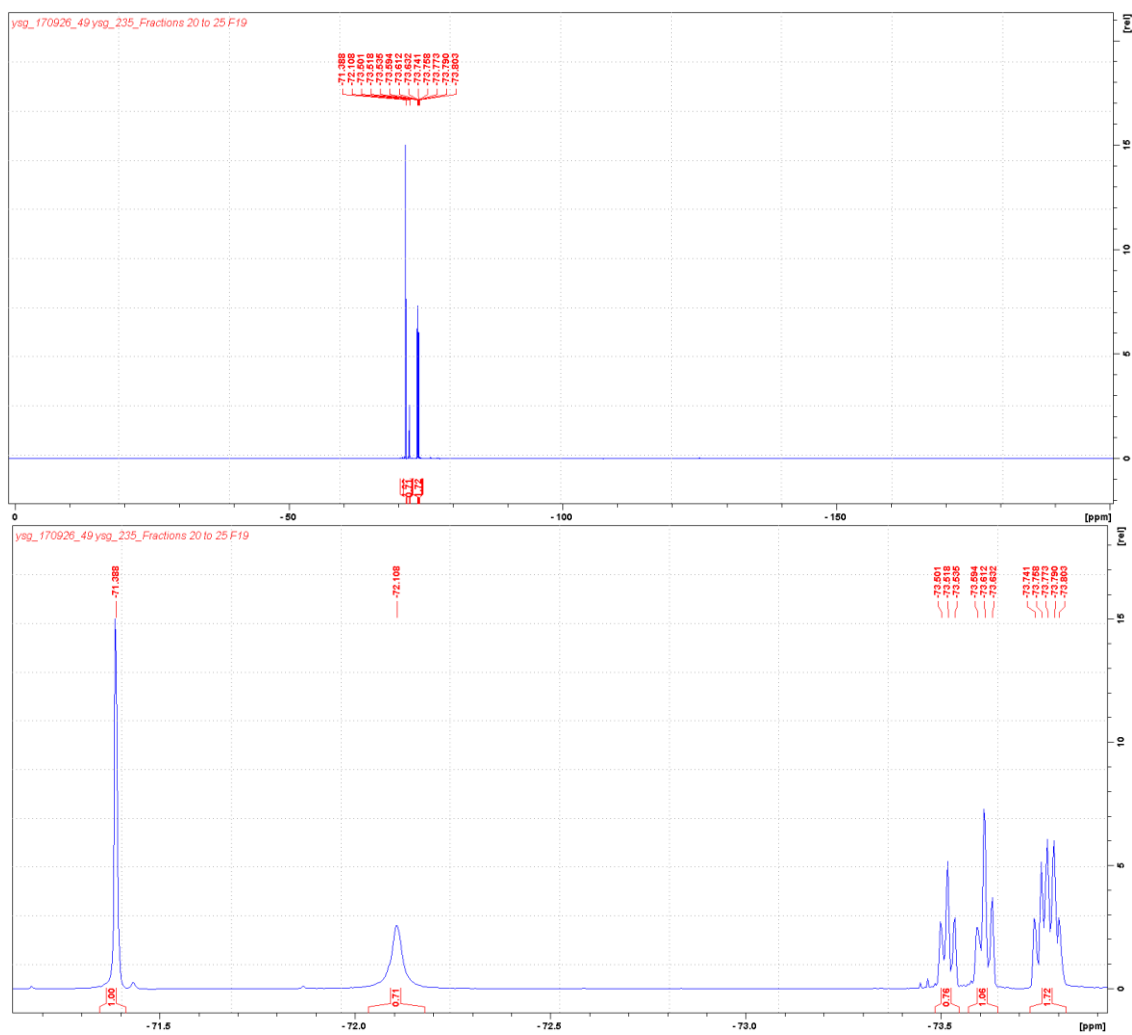
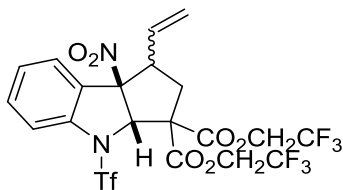
^1H & ^{13}C NMR of Dibenzyl (3a*S*,8*bR*)-8*b*-nitro-4-tosyl-1-vinyl-1,3*a*,4,8*b*-tetrahydrocyclopenta[*b*]indole-3,3(2*H*)-dicarboxylate (**113/113'**)



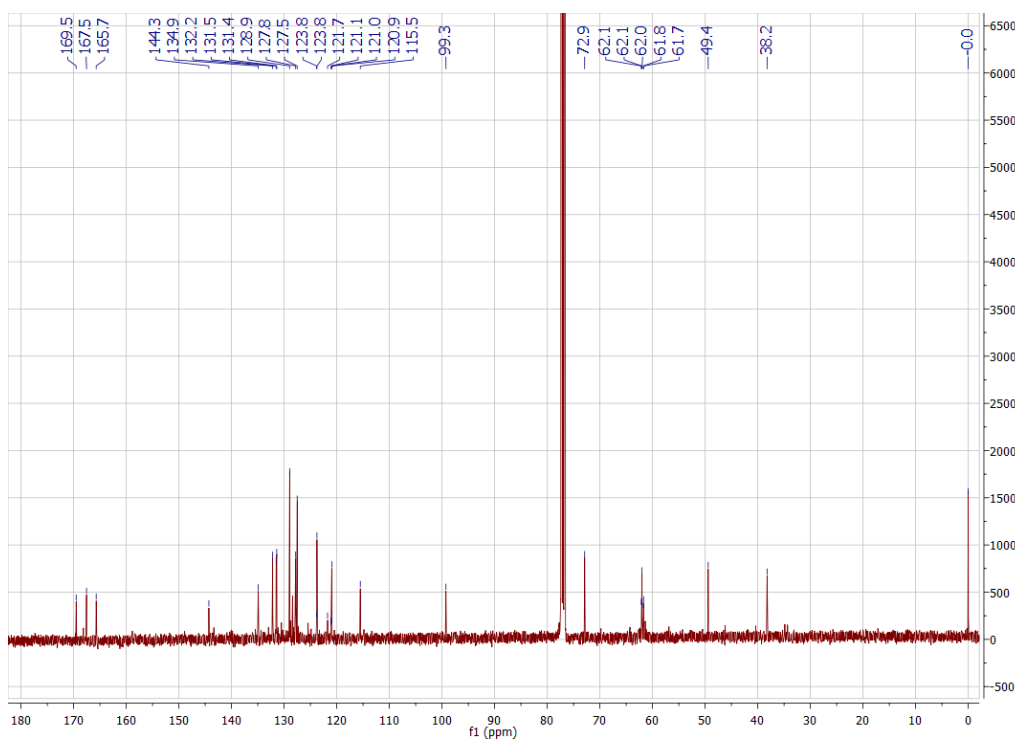
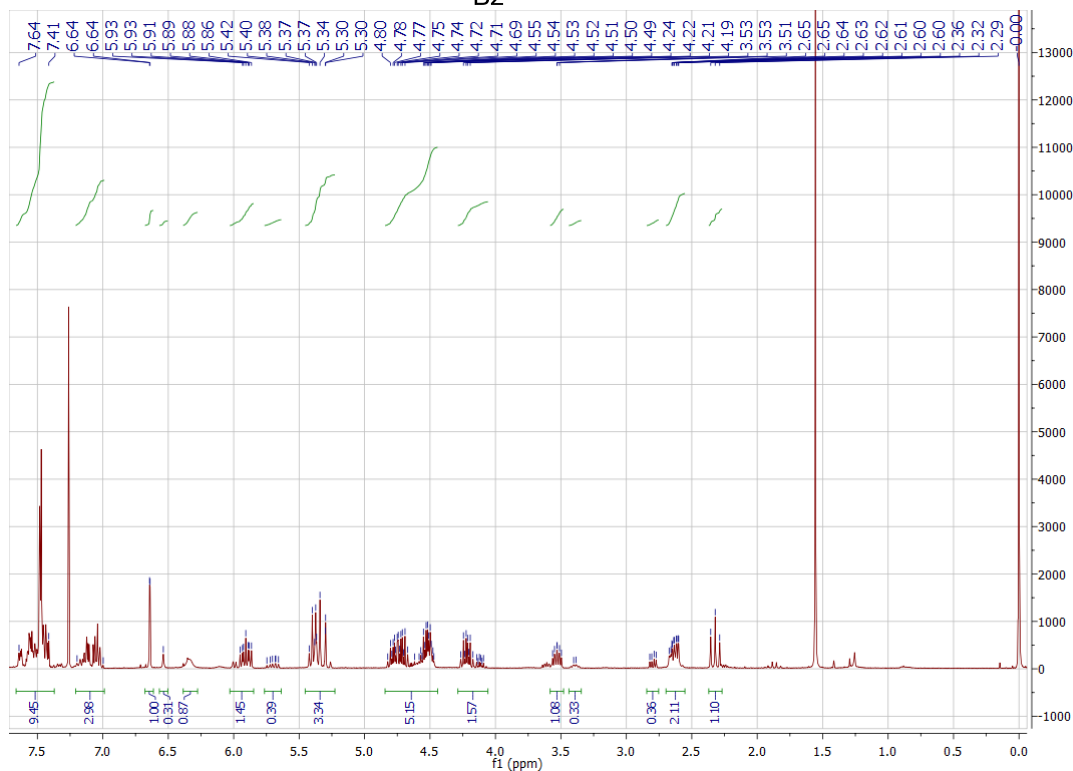
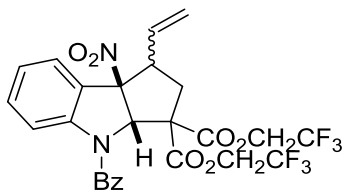
^1H & ^{13}C NMR of Bis(2,2,2-trifluoroethyl) (3a*S*,8b*R*)-8b-nitro-4-((trifluoromethyl)sulfonyl)-1-vinyl-1,3a,4,8b-tetrahydrocyclopenta[*b*]indole-3,3(2*H*)-dicarboxylate (114a/114a')



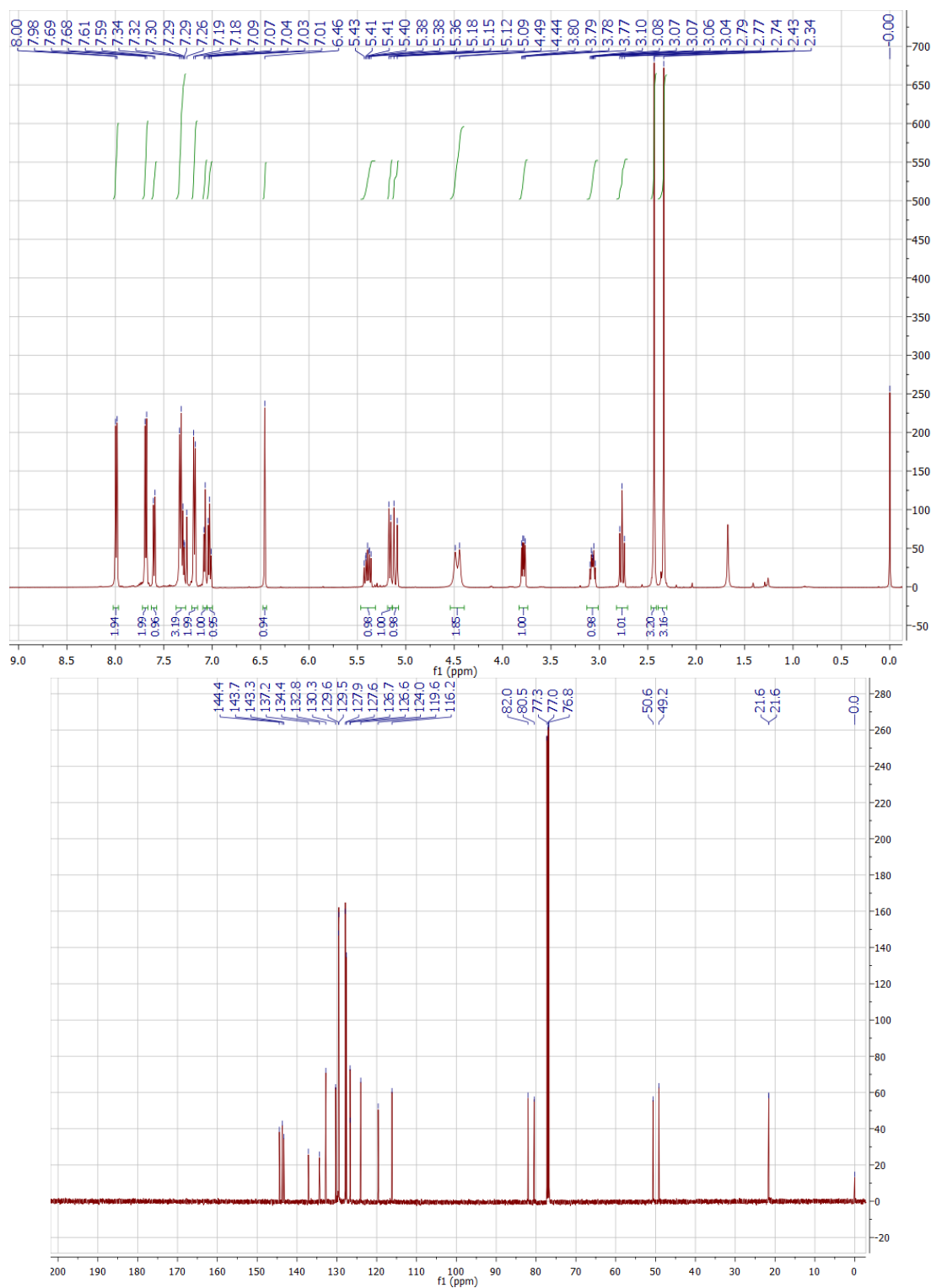
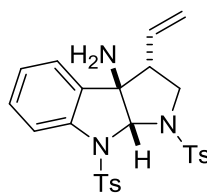
¹⁹F NMR of Bis(2,2,2-trifluoroethyl) (3a*S*,8b*R*)-8b-nitro-4-((trifluoromethyl)sulfonyl)-1-vinyl-1,3a,4,8b-tetrahydrocyclopenta[*b*]indole-3,3(2*H*)-dicarboxylate (114a/114a')



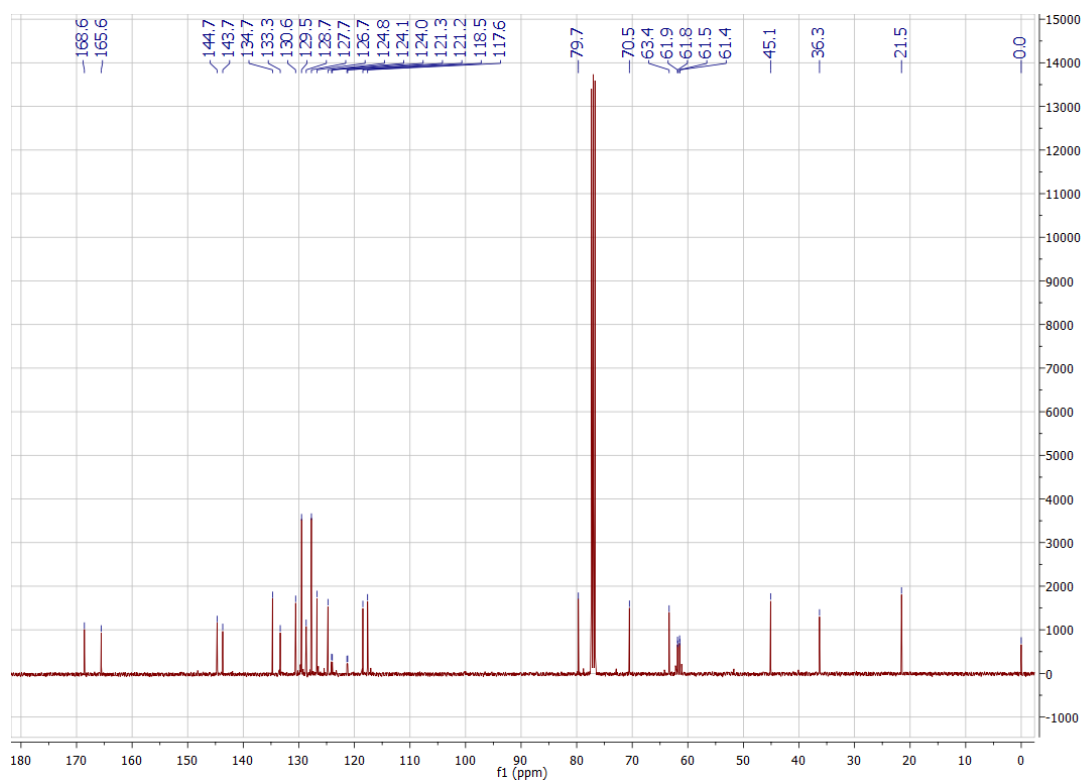
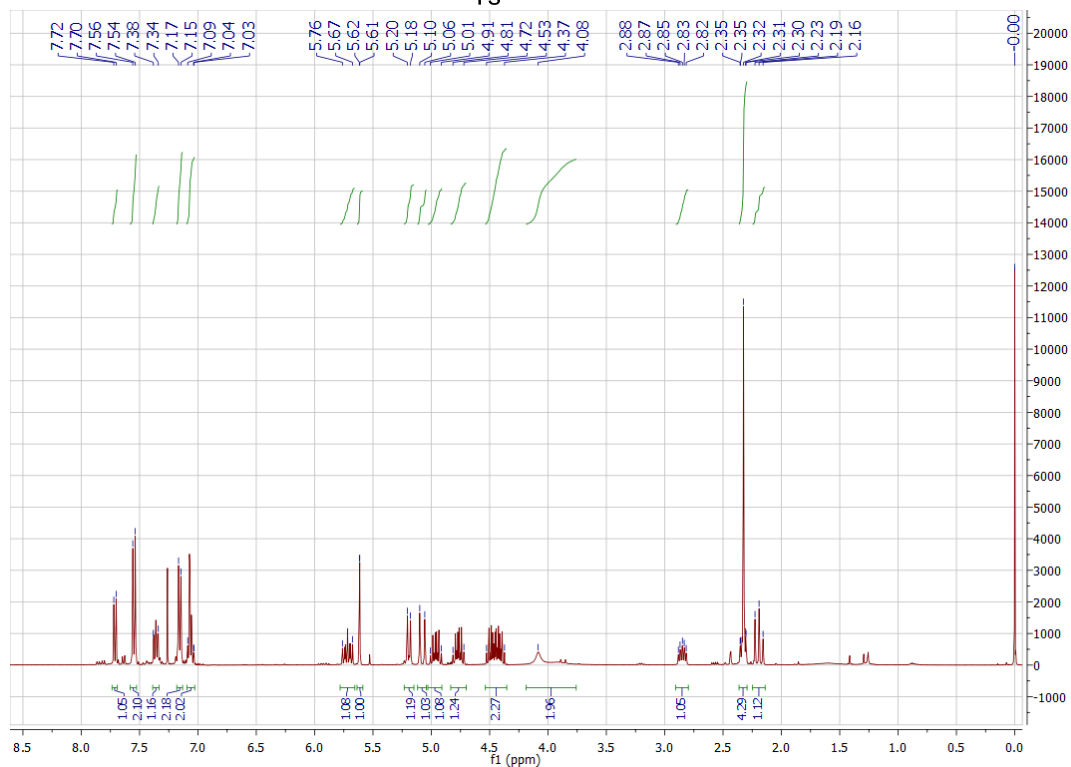
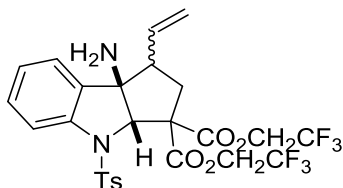
^1H & ^{13}C NMR of Bis(2,2,2-trifluoroethyl) (3*a*S,8*b*R)-4-benzoyl-8*b*-nitro-1-vinyl-1,3*a*,4,8*b*-tetrahydrocyclopenta[*b*]indole-3,3(2*H*)-dicarboxylate (114*b*/114*b'*)



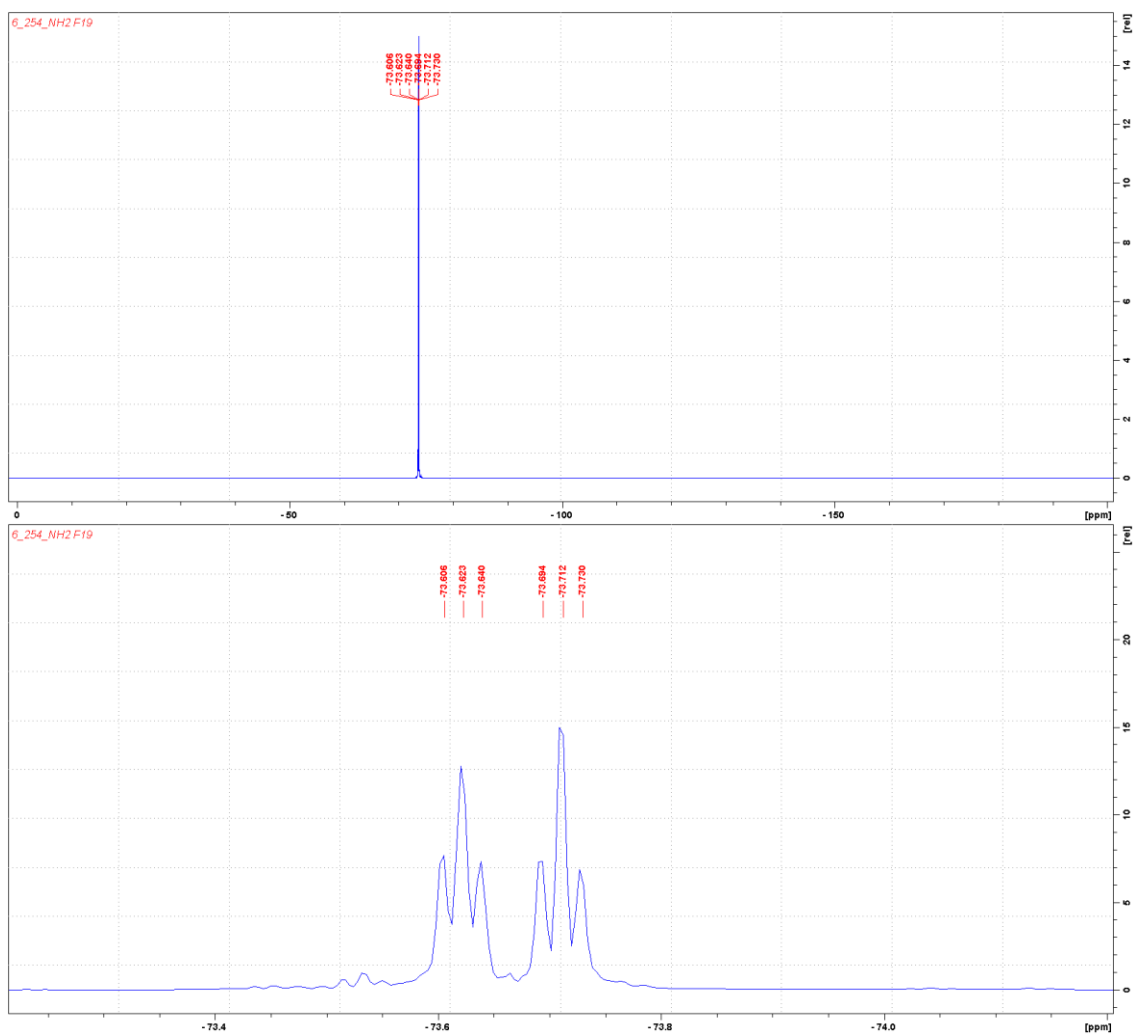
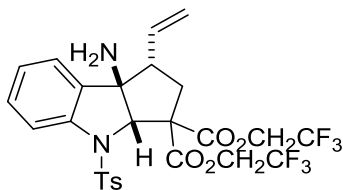
^1H & ^{13}C NMR of (3*S*,3*aS*,8*aS*)-1,8-Ditosyl-3-vinyl-2,3,8,8*a*-tetrahydropyrrolo[2,3-*b*]indol-3*a*(1*H*)-amine (**116**)



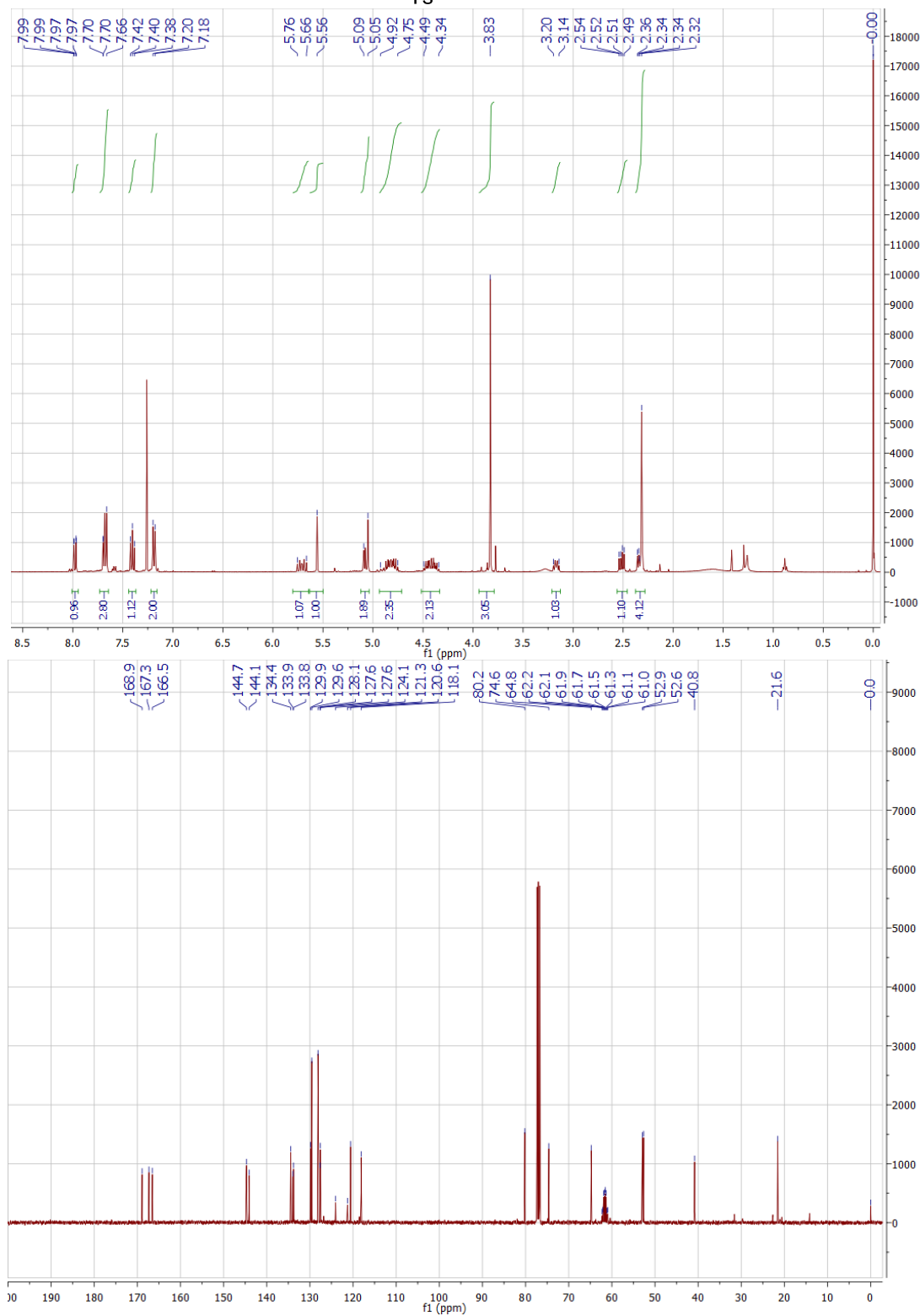
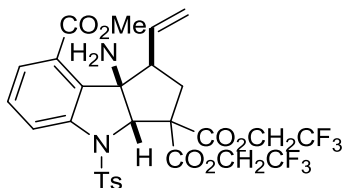
¹H & ¹³C NMR of Bis(2,2,2-trifluoroethyl) (3a*S*,8*bR*)-8*b*-amino-4-tosyl-1-vinyl-1,3*a*,4,8*b*-tetrahydrocyclopenta[*b*]indole-3,3(2*H*)-dicarboxylate (**117a**)



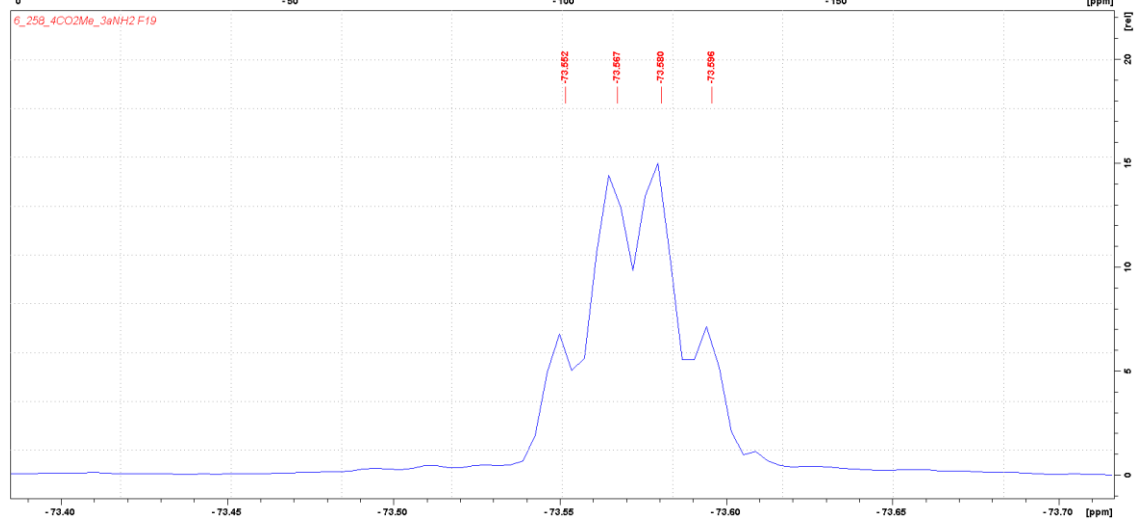
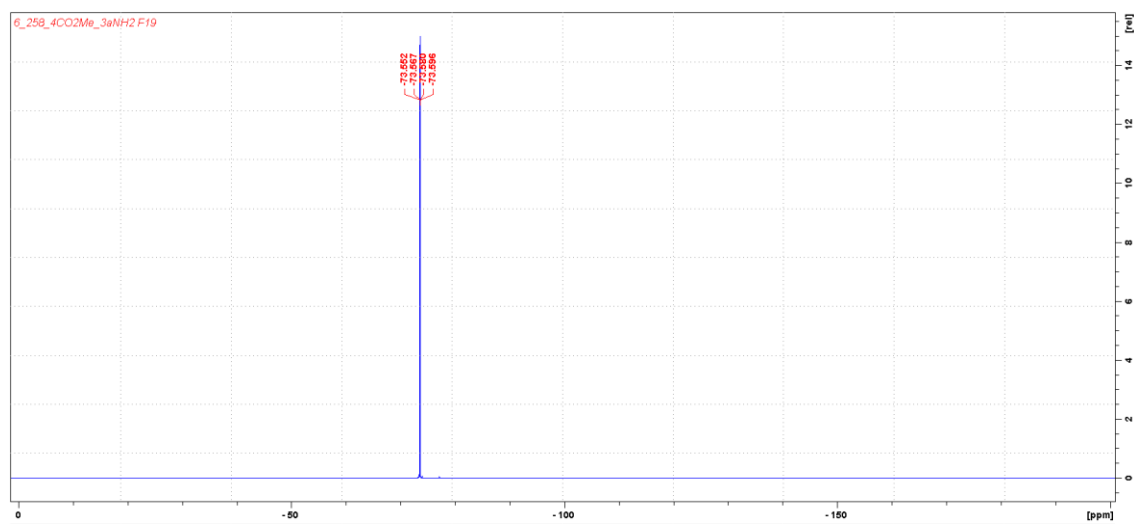
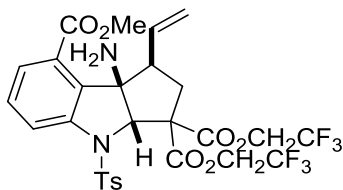
^{19}F NMR of Bis(2,2,2-trifluoroethyl) (3a*S*,8*bR*)-8*b*-amino-4-tosyl-1-vinyl-1,3*a*,4,8*b*-tetrahydrocyclopenta[*b*]indole-3,3(2*H*)-dicarboxylate (**117a**)



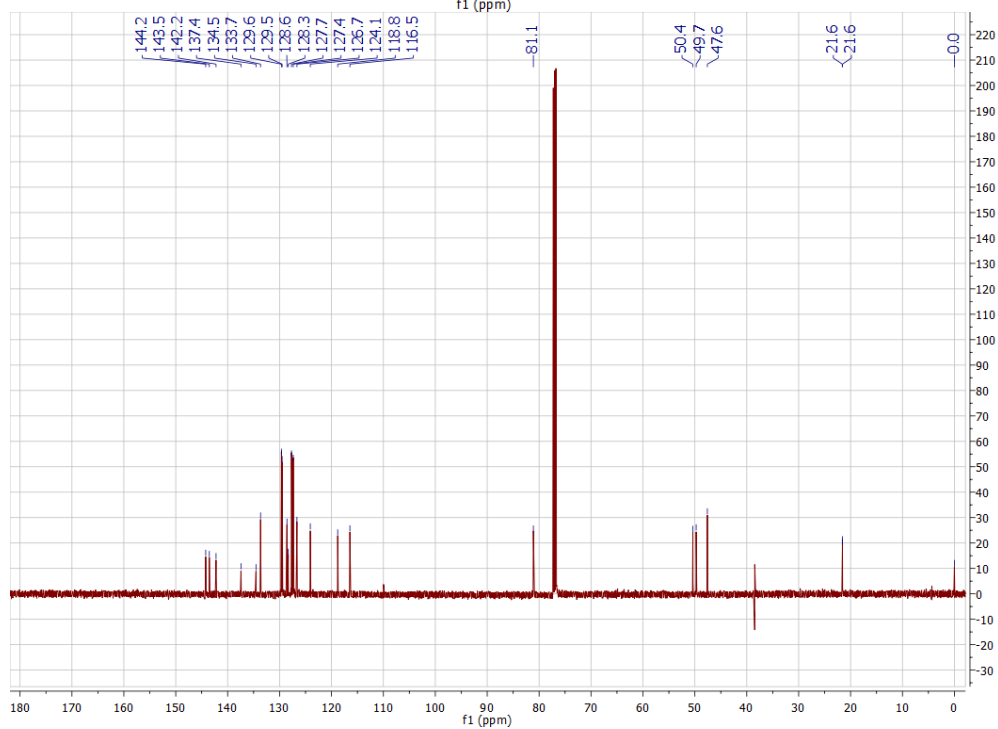
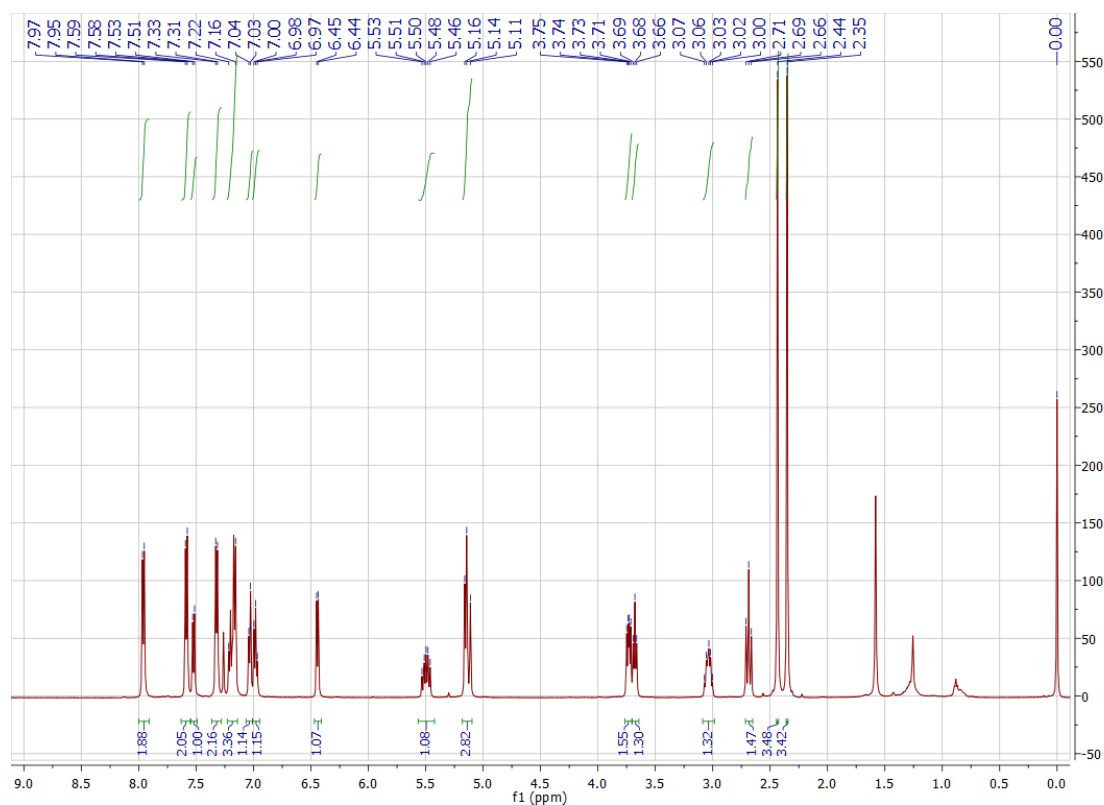
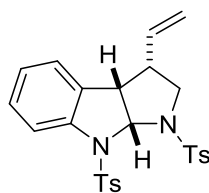
¹H & ¹³C NMR of 8-Methyl 3,3-bis(2,2,2-trifluoroethyl) (1*S*,3*aS*,8*bR*)-8*b*-amino-4-tosyl-1-vinyl-1,3*a*,4,8*b*-tetrahydrocyclopenta[*b*]indole-3,3,8(2*H*)-tricarboxylate (**117k'**)



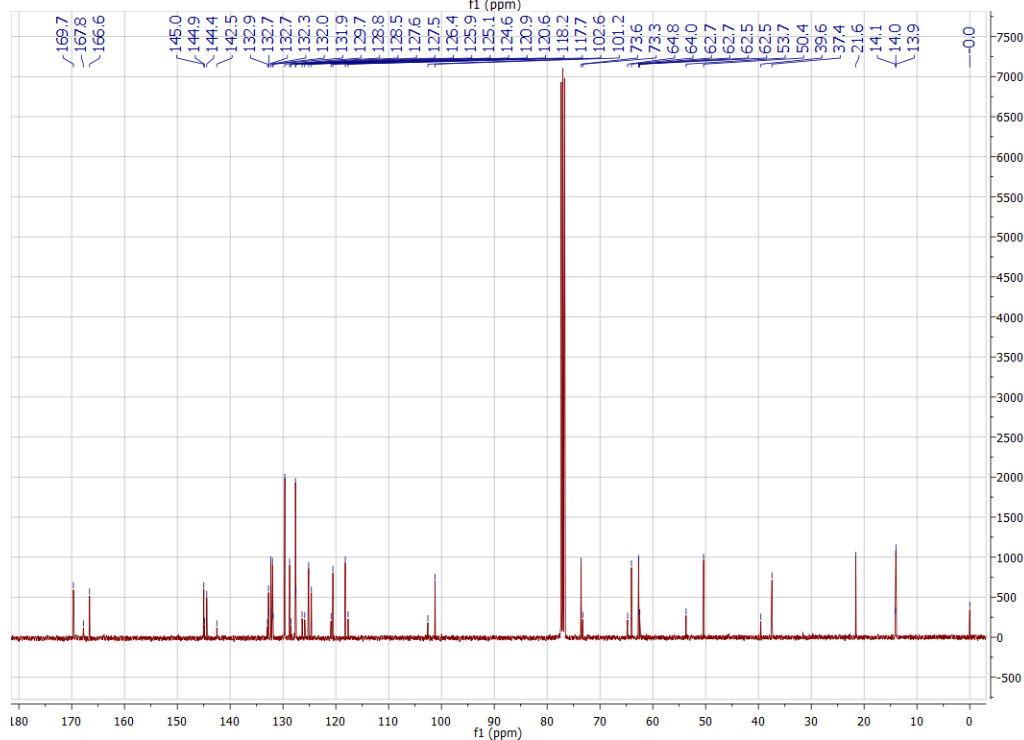
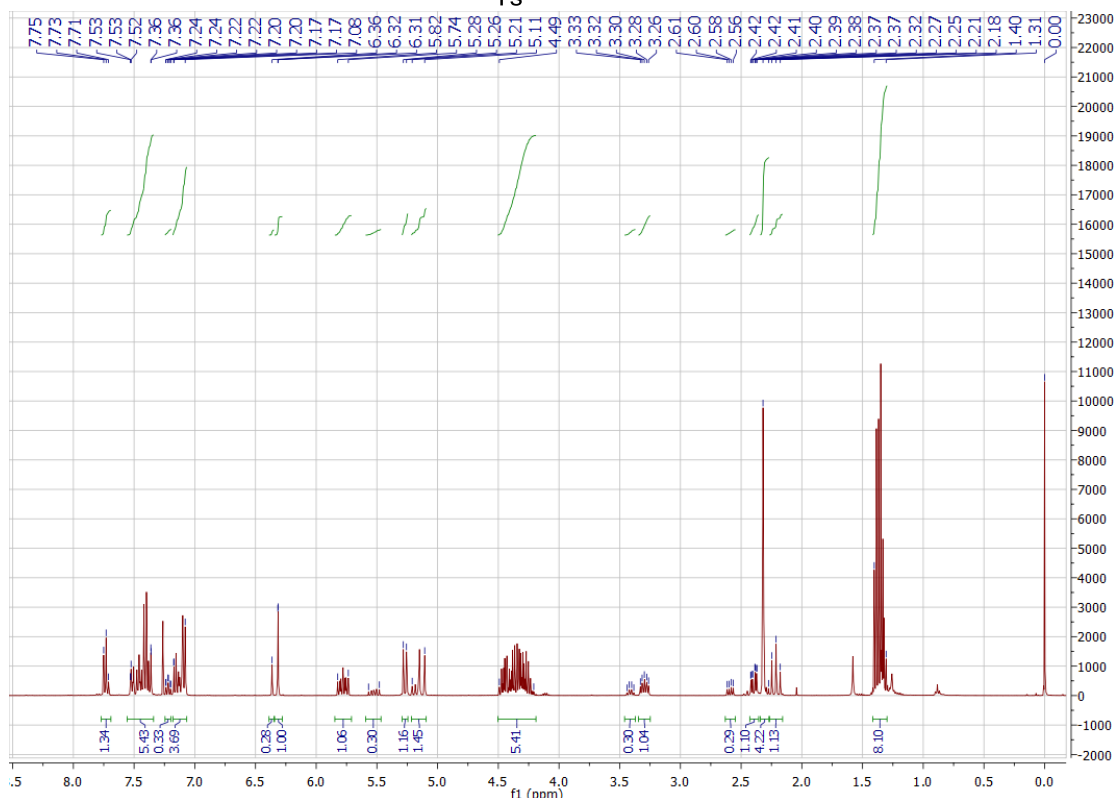
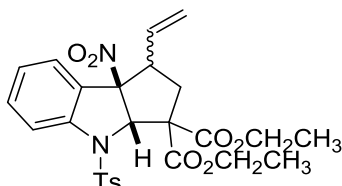
^{19}F NMR of 8-Methyl 3,3-bis(2,2,2-trifluoroethyl) (1*S*,3*aS*,8*bR*)-8*b*-amino-4-tosyl-1-vinyl-1,3*a*,4,8*b*-tetrahydrocyclopenta[*b*]indole-3,3,8(2*H*)-tricarboxylate (**117k'**)



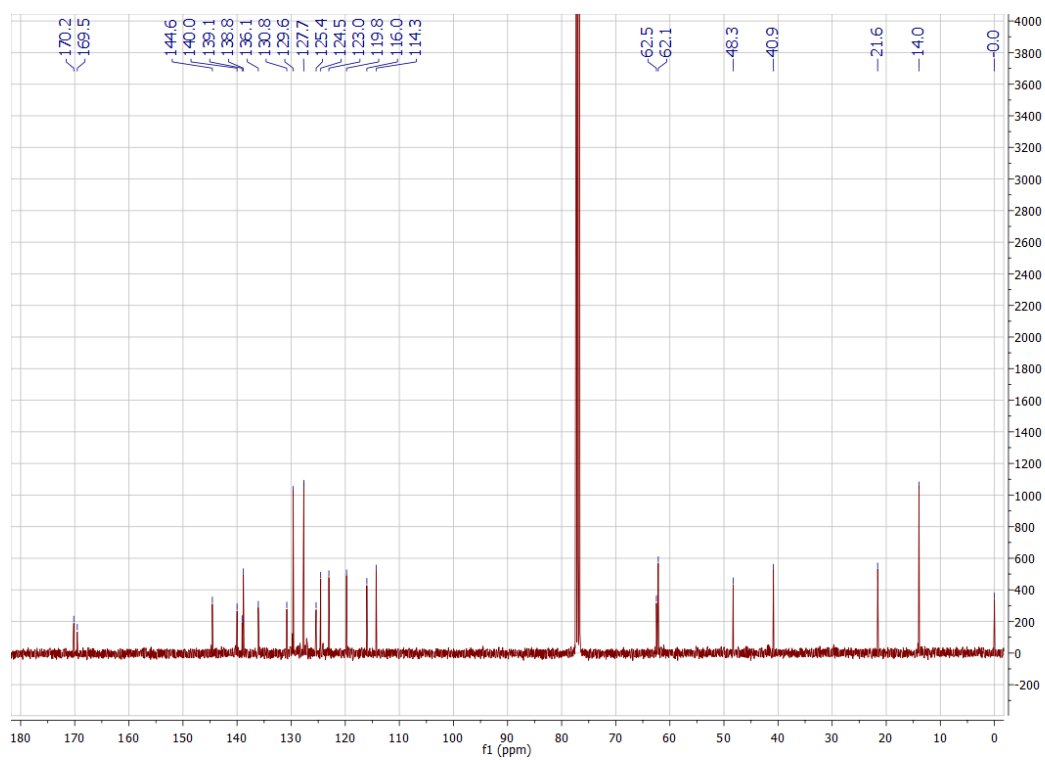
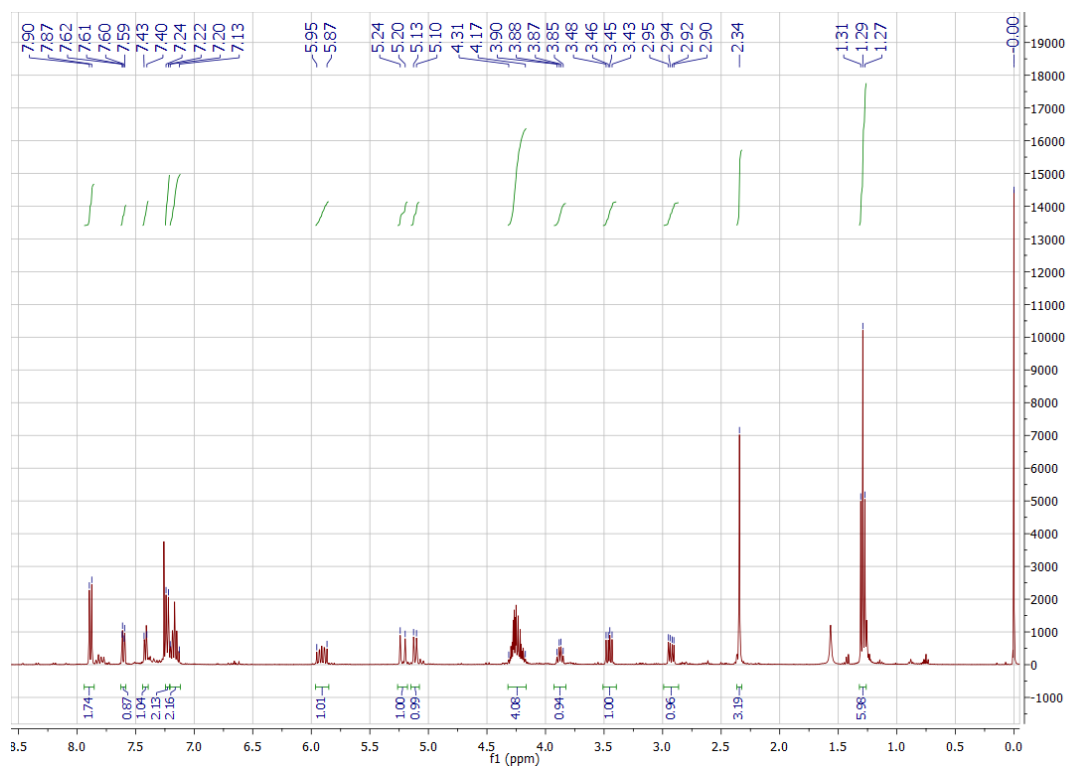
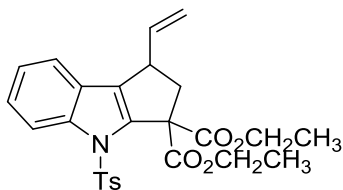
^1H & ^{13}C NMR of (3*R*,8*aS*)-1,8-Ditosyl-3-vinyl-1,2,3,3*a*,8,8*a*-hexahydropyrrolo[2,3-*b*]indole (**118**)



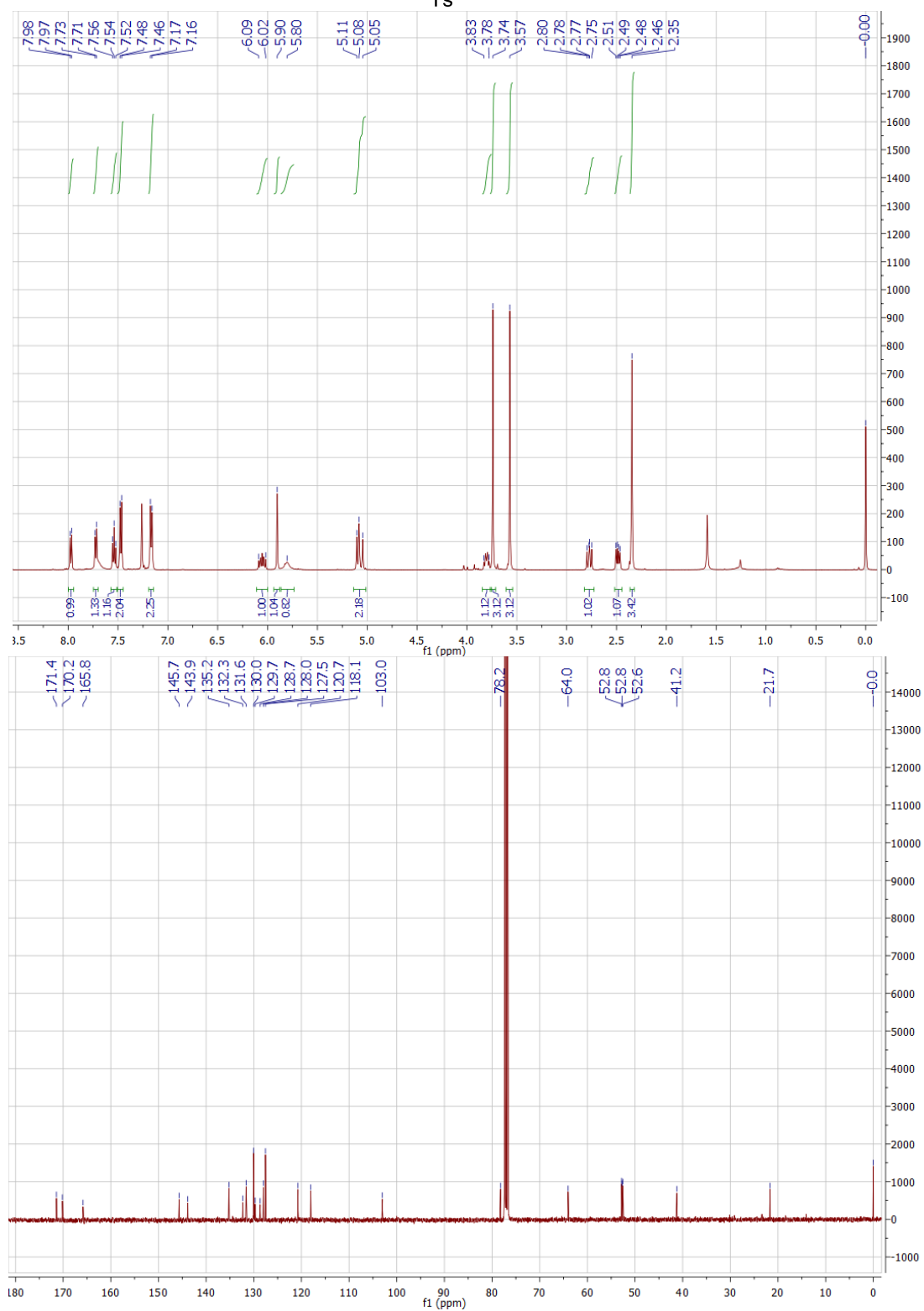
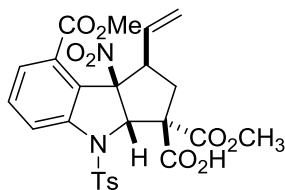
¹H & ¹³C NMR of Diethyl (3a*S*,8*bR*)-8*b*-nitro-4-tosyl-1-vinyl-1,3*a*,4,8*b*-tetrahydrocyclopenta[*b*]indole-3,3(2*H*)-dicarboxylate (107*a*/107*a'*) from transesterification



¹H & ¹³C NMR of Diethyl 4-tosyl-1-vinyl-1,4-dihydrocyclopenta[b]indole-3,3(2H)-dicarboxylate (119)



¹H & ¹³C NMR of (1R,3S,3aS,8bR)-3,8-Bis(methoxycarbonyl)-8b-nitro-4-tosyl-1-vinyl-1,2,3,3a,4,8b-hexahydrocyclopenta[b]indole-3-carboxylic acid (120)



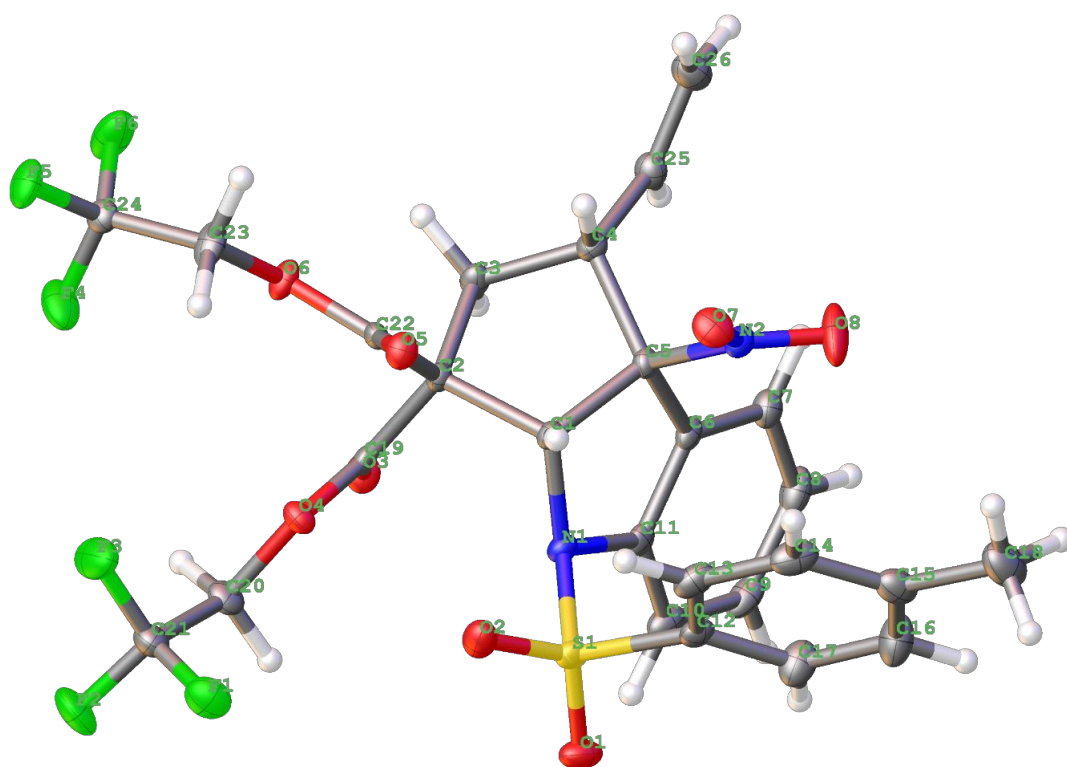


Figure A2: Thermal Ellipsoid Plot for the crystal structure of 108a. Thermal ellipsoids are shown at the 50% probability level. All methyl and aromatic-ring hydrogen atoms are omitted for clarity.

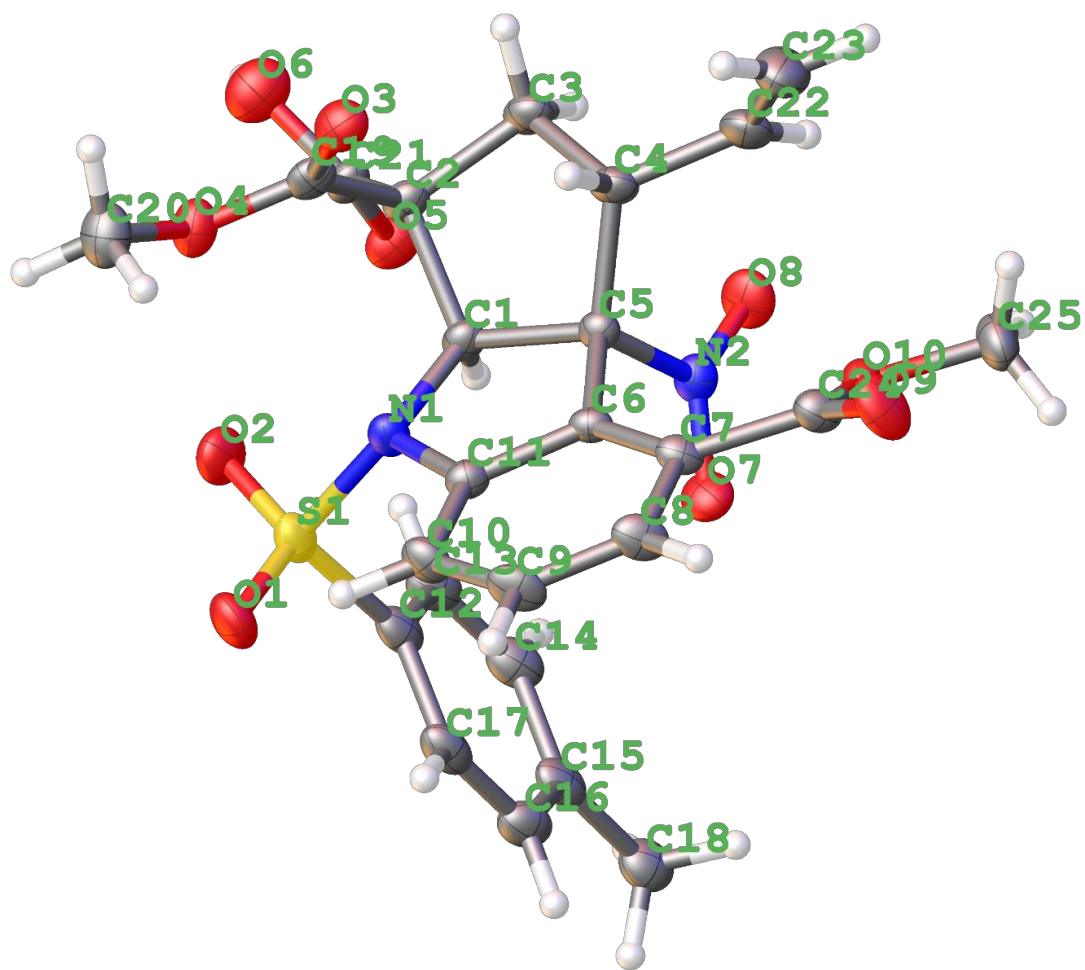


Figure A3: Thermal Ellipsoid Plot for the crystal structure of **120**. Thermal ellipsoids are shown at the 50% probability level. All methyl and aromatic-ring hydrogen atoms are omitted for clarity.

Appendix 5

Publications

- (1) Gee, Y. S.; Goertz, N. J. M.; Gardiner, M. G.; Hyland, C. J. T. *Org. Biomol. Chem.* **2016**, *14*, 2498.
- (2) Rivinoja, D. J.; Gee, Y. S.; Gardiner, M. G.; Ryan, J. H.; Hyland, C. J. T. *ACS Catal.* **2017**, *7*, 1053.
- (3) Gee, Y. S.; Rivinoja, D. J.; Wales, S. M.; Gardiner, M. G.; Ryan, J. H.; Hyland, C. J. T. *J. Org. Chem.* **2017**, *82*, 13517.

Articles 2 and 3 removed for copyright reasons. Please refer to the citation



Cite this: *Org. Biomol. Chem.*, 2016, **14**, 2498

Oxidative ring-opening of ferrocenylcyclopropylamines to *N*-ferrocenylmethyl β -hydroxyamides†

Yi Sing Gee,‡^a Neils J. M. Goertz,‡^a Michael G. Gardiner^b and Christopher J. T. Hyland*^a

Received 16th December 2015,

Accepted 20th January 2016

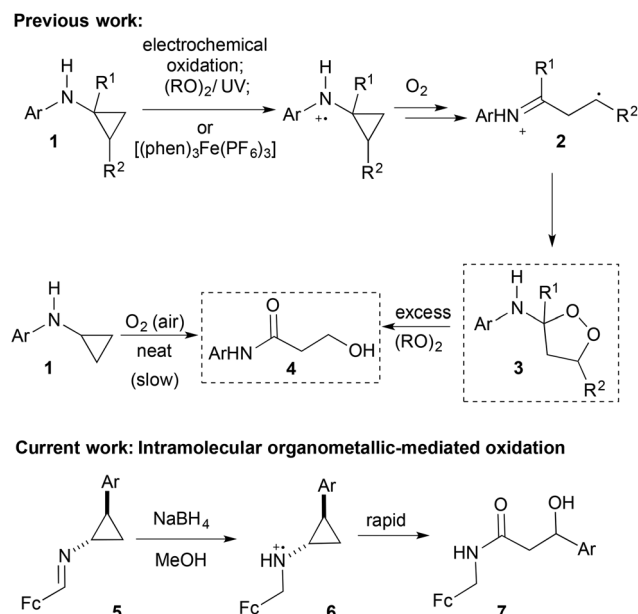
DOI: 10.1039/c5ob02577j

www.rsc.org/obc

The *in situ* reduction of ferrocenyl cyclopropylamines to the corresponding amines triggers a facile oxidative ring-opening to yield the formal four-electron oxidation products: *N*-ferrocenylmethyl β -hydroxyamides. This process is believed to proceed *via* generation of a ferrocenium ion in the presence of air, leading to facile formation of a distonic radical cation that is ultimately trapped by oxygen.

Introduction

Cyclopropylamines **1** are found in a broad variety of biologically active compounds, such as the antibiotics Ciprofloxacin, Moxifloxacin, Trovafloxacin and the antidepressant 2-phenylcyclopropylamine (2-PCPA).^{1,2} Therefore, much attention has been paid to understanding the reactivity of these important structures.^{3,4} Cyclopropylamines **1** can undergo characteristic, irreversible ring-opening reactions *via* a single-electron transfer mechanism to yield a distonic radical cation **2** (Scheme 1). This process is particularly important in biological systems; for example, 2-PCPA inhibits monoamine oxidase by flavin adenine dinucleotide (FAD) oxidation of the cyclopropylamine nitrogen and subsequent ring-opening to a distonic radical cation similar to **2**.⁵ The ability of cyclopropylamines to undergo this ring-opening process has also been seen when used as tools for studying biological amine-oxidation.^{6,7} Given this widespread importance, several groups have studied the ring-opening of cyclopropylamines initiated by single electron oxidation and subsequent reaction with oxygen (Scheme 1). Endoperoxides **3** derived from aminocyclopropanes **1** have been prepared by aerobic electrochemical oxidation⁸ as well as autocatalytic radical ring-opening under aerobic conditions using an oxidising agent $[(\text{phen})_3\text{Fe}(\text{PF}_6)_3]$ or hydrogen-abstracting agents $((\text{RO})_2/\text{UV})$ (Scheme 1).⁹ In the latter case, excess peroxide can convert the endoperoxide into



Scheme 1 Previous work on ring-opening of cyclopropylamines **1** initiated by oxidation of amine nitrogen and subsequent reaction with oxygen. Current study on the internal oxidation of ferrocenyl-aminocyclopropanes. Fc = ferrocene.

a simple β -hydroxyamide **4**. Epoxy-ketones can also be formed by CuCl_2 -catalysed oxygenation of 1-pyrrolidino[*n*,1,0]-bicycloalkanes.¹⁰ It has also been shown that *N*-cyclopropylanilines can undergo slow air oxidation under ambient conditions to yield simple β -hydroxyamides **4**.¹¹ However, to date we are unaware of any studies into the reactivity of organometallic derivatives of cyclopropylamines.

Ferrocene (Fc) can undergo reversible oxidation and this has rendered it important in bioorganometallic drugs, such as

^aSchool of Chemistry, University of Wollongong, Wollongong, NSW 2522, Australia.
E-mail: chris_hyland@uow.edu.au

^bSchool of Physical Sciences - Chemistry, University of Tasmania, Hobart, TAS 7001, Australia

† Electronic supplementary information (ESI) available. CCDC 1434659. For ESI and crystallographic data in CIF or other electronic format see DOI: 10.1039/c5ob02577j

‡ These authors contributed equally to this paper.

ferroquine¹² and ferrocifens.¹³ In ferrocifens it is likely that the active quinone methide form of the drug is only formed following oxidation of the ferrocene to the ferrocinium ion. As such, we postulated that cyclopropylamine-ferrocene conjugates could harness the redox ability of ferrocene to initiate oxidative ring-opening processes in the presence of air.

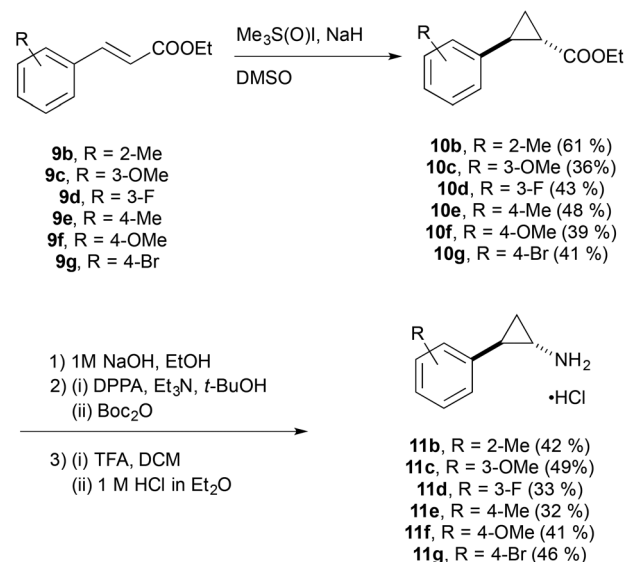
Given the importance of both the ferrocene moiety and cyclopropylamines in biological systems, understanding of these ring-opening processes could provide important information for the utilisation of organometallic derivatives of cyclopropylamines in biological applications. Herein, we describe the NaBH₄ initiated oxidative ring-opening of ferrocenyl cyclopropylimines **5** to *N*-ferrocenylmethyl β-hydroxyamides **7** (Scheme 1). This is the first process where ferrocene initiates an oxidative cyclopropane ring-opening, allowing synthesis of a series of novel organometallic β-hydroxyamides.

Results and discussion

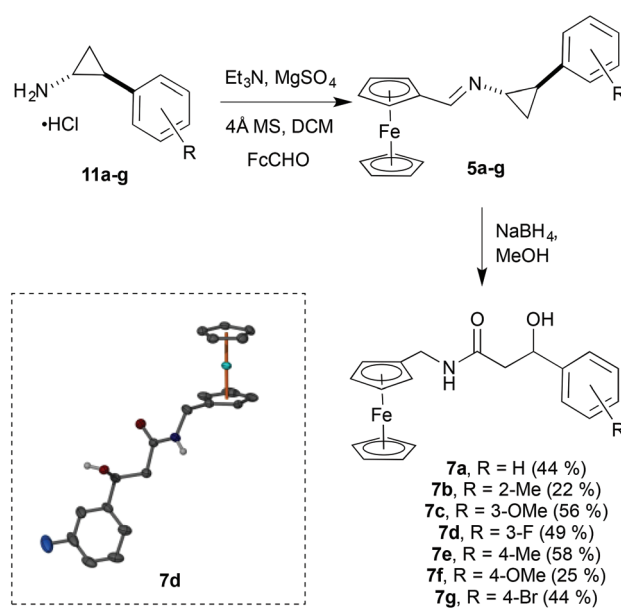
Work commenced with commercially available 2-PCPA, which was transformed to imine **5a** by condensation with ferrocene-carboxyaldehyde. Upon reduction of this imine with stoichiometric sodium borohydride none of the amine **8a** was observed – instead the ring-opened and oxidised *N*-ferrocenylmethyl β-hydroxyamide product **7a** was observed to form rapidly (Scheme 2). The same product was formed when Bu₃SnH on silica gel was used as the reducing agent.

It is of note that unlike the previously reported electrochemical and autocatalytic ring-opening reactions no dioxolane products were observed under these present conditions.

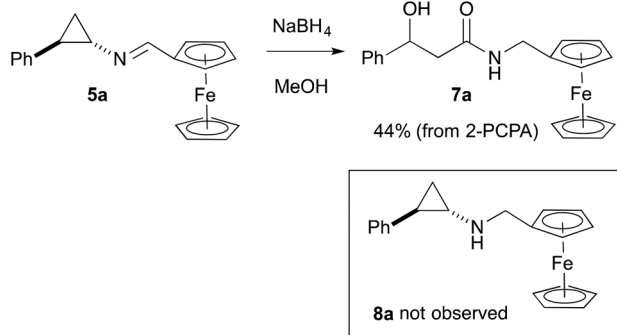
Following this intriguing result, a series of 2-PCPA analogues were prepared (Scheme 3). The procedure originated with cinnamic esters **9b–g**, which were subjected to Corey–Chaykovsky cyclopropanation to yield cyclopropanes **10b–g**. After basic hydrolysis, the carboxylic acids were converted to 2-PCPA analogues **11b–g** by a Curtius rearrangement and deprotection. These 2-PCPA analogues **11b–g** were then subjected to condensation with ferrocenecarboxyaldehyde to yield imines **5b–g** (Scheme 4). In all cases, treatment of these cyclopropylamines with sodium borohydride, gave the ring-opened *N*-fer-



Scheme 3 Syntheses of 2-PCPA derivatives.



Scheme 4 Reductive amination of ferrocenecarboxyaldehyde and 2-PCPA analogues **11a–g** to yield *N*-ferrocenylmethyl β-hydroxyamides **7a–g**. Molecular structure of **7d**. Thermal ellipsoids are shown at the 50% probability level. All methine, methylene and aromatic-ring hydrogen atoms are omitted for clarity. Intra-/intermolecular H-bonding is also not shown for clarity. The asymmetric unit contains another similar molecule of **7d**, featuring a 120° rotation of the C(methylene)–C(methine) bond to allow intramolecular H-bonding to the carbonyl carbon (C=O...H–O).



Scheme 2 Oxidative ring-opening of **5a** initiated by treatment with NaBH₄.

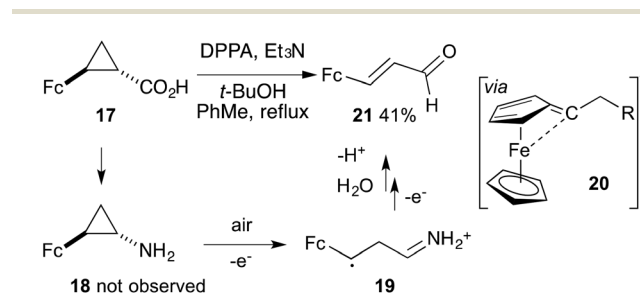
rocenylmethyl β-hydroxyamides **7b–g** (22–58% yield over two steps from the amine salt). A range of differently substituted aromatic groups, including *ortho*, *meta* and *para* substituents could be tolerated. The structure of **7d** was confirmed unambiguously by X-ray crystallography (Scheme 4).

Mechanistically, it is proposed that the ferrocene moiety plays a key role in the reaction, especially as the corresponding benzyl-derivatives have been reported to be air stable.¹⁴ Air-generated ferrocenium ions have been recently utilised as the terminal oxidant in asymmetric dehydrogenative Heck reactions.¹⁵ Therefore, it is proposed the ferrocenium ion **12**, generated *in situ* by air that acts as an internal oxidant to generate aminium radical **6** from cyclopropylamines **8**, which are the initial NaBH₄ reduction products (Fig. 1). Cyclopropane ring-opening of **6** then occurs exclusively by cleavage of the C1–C2 bond as this pathway gives the more stable benzylic carbon-centred radical. This is consistent with Wimalasena *et al.* who suggest the carbon-centered radical is a discrete intermediate in radical ring-opening of cyclopropylamines and therefore, ring-opening and molecular oxygen insertion are not concerted.⁹ The resulting distonic radical cation **13** is able to be trapped with dioxygen to give adduct **14** which can undergo 5-*exo-trig* cyclisation to radical cation **15**. The catalytic cycle is propagated by abstraction of an electron from **8** by radical cation **15**, which yields dioxolane **16** as an intermediate.

Dioxolane **16** is not observed for the current reaction, as it is likely isomerisation with concomitant O–O bond cleavage to yield *N*-ferrocenylmethyl β-hydroxyamides **7** is a facile process under basic conditions. This isomerisation step to the hydroxyamide could occur *via* several pathways. While it has been reported that 1,2-dioxolanes can undergo conversion to β-ketoalcohols in the presence of silica gel,¹⁶ in our case this is unlikely as signals corresponding to the hydroxyamide were observed in the ¹H NMR of the crude reaction material prior to contact with silica gel. Therefore, it is more likely that the isomerisation occurs *via* base-mediated¹⁷ or radical abstraction⁹ of H. Of these two possibilities the base-mediated mechanism

would appear more likely as no clear mechanism for generation of RO[•] is apparent and our conditions are intrinsically basic due to the presence of NaBH₄.

The analogue **18** of 2-PCPA, where the phenyl ring is replaced with ferrocene, also displays a strong propensity to undergo these ferrocene-mediated ring-opening processes (Scheme 5). When carboxylic acid **17** was subjected to a Curtius rearrangement, enal **21** was observed instead of cyclopropylamine **18**. The analogous cinnamaldehyde product has been reported to be obtained from the oxidation of 2-PCPA by horseradish peroxidase.¹⁸ Similarly to the 2-PCPA analogues **8**, it is thought that amine **18** is intrinsically unstable in the presence of air and likely undergoes a similar oxidation/ring-opening sequence. Interestingly, the distonic radical cation **19** does not appear to be trapped by molecular oxygen, preferring to undergo a second oxidation, then elimination and hydrolysis to the enal. The preference for oxidation to an α-ferrocenylcarbenium ion **20**, rather than trapping with molecular oxygen, may be related to the well-established stabilisation of



Scheme 5 Attempted Curtius rearrangement of **17** to yield enal **21**.

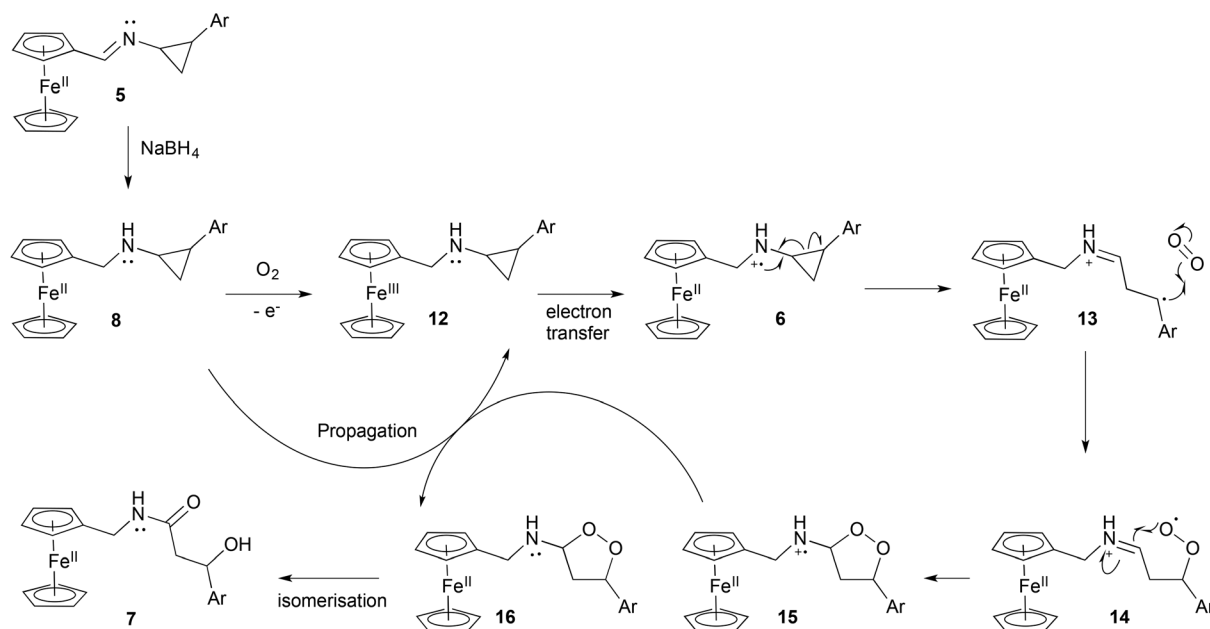


Fig. 1 Proposed mechanism of NaBH₄-initiated ring-opening-oxidation of cyclopropylamines **5**.

α -carbocations by ferrocene. Such systems show fulvene character and direct iron- α -carbon bonding.¹⁹

Conclusion

In conclusion, we have unveiled a novel ring-opening process of cyclopropylamine facilitated by the redox ability of ferrocene in air. This process yields novel *N*-ferrocenylmethyl β -hydroxyamides and provides information about the reactivity of organometallic cyclopropylamine derivatives. The increased reactivity of the ferrocenyl derivatives of 2-PCPA towards oxidation with molecular oxygen and ring-opening suggests the possibility of modulating aminocyclopropane reactivity with less-readily oxidised metallocene fragments. It may also be possible to employ ferrocene as a catalytic additive to enhance the oxidative ring-opening of aminocyclopropanes. It is worth noting that distonic radical cations can participate in useful reactions like [3 + 2] cycloadditions with olefins.²⁰ As such, the current method of generating such species under environmentally friendly conditions could lead to reaction with species other than molecular oxygen to obtain more complex organometallic compounds.

It is also the first report of a very facile conversion to the hydroxyamide skeleton by internal redox. As β -hydroxyamide products feature in bioactive compounds, such as Cruentaren A (antifungal)²¹ and Octreotide (growth hormone inhibitor),²² organometallic derivatives of this moiety are of potential interest to medicinal chemists.²³

Experimental

General information

Unless stated specifically, all chemicals were purchased from commercial suppliers and used without purification. All reactions were conducted in oven-dried glassware under nitrogen atmosphere. Reaction solvents were dried by passing through a column of activated alumina and then stored over 4 Å molecular sieves. Progress of reactions was tracked by TLC and was performed on aluminium backed silica gel sheets (Grace Davison, UV254). TLC plates were visualised under UV lamp at 254 nm and/or by treatment with one of the following TLC stains: Phosphomolybdic acid (PMA) stain: PMA (10 g), absolute EtOH (100 mL); Potassium permanganate stain: KMnO₄ (1.5 g), 10% NaOH (1.25 mL), water (200 mL); Vanillin stain: Vanillin (15 g), concentrated H₂SO₄ (2.5 mL), EtOH (250 mL). Preparative TLC was carried out on glass backed TLC plates with silica matrix. Column chromatography was performed using silica gel (40–75 μ m) as the solid phase. For NMR spectroscopy analytes were dissolved in deuterated chloroform or stated otherwise. NMR spectra for each compound were collected from one of the following instrument: Mercury 2000 spectrometer operates at 500 and 125 MHz for ¹H and ¹³C NMR respectively, or Varian spectrometer operates at 300 and 75 MHz for ¹H and ¹³C NMR respectively. NMR data are expressed in parts per million (ppm) and referenced to the

solvent (7.26 ppm for ¹H NMR and 77.16 ppm for ¹³C NMR). The following abbreviations are used to assign the multiplicity of the ¹H NMR signal: s = singlet; bs = broad singlet; d = doublet; t = triplet; q = quartet; quin = quintet; dd = doublet of doublets; m = multiplet. For mass spectroscopy analytes were dissolved in HPLC grade methanol. Spectra of low-resolution mass spectrometry were obtained from a Shimadzu LC-2010 mass spectrometer (ESI) or a Shimadzu QP5050 mass spectrometer (EI). High-resolution mass spectra were collected from a Waters Xevo G1 QTOF mass spectrophotometer (ESI or ASAP) or Thermo Scientific LTQ Orbitrap XL (ESI). Infrared spectra were obtained from a Shimadzu IRAffinity-1 Fourier transform infrared spectrophotometer with ATR attachment. Melting point measurements were taken on a Buchi M-560. The 2-PCPA derivatives (**11a–g**) were prepared according to literature procedures; their syntheses and characterisation are provided in the ESI.†

Typical procedure for the synthesis of *N*-ferrocenylmethyl β -hydroxyamides

Triethylamine (0.93 mmol, 1.9 equiv.) was added to a suspension of 2-PCPA derivative hydrochloride salt (0.48 mmol, 1 equiv.) and magnesium sulphate (1.82 mmol, 3.8 equiv.) in dry dichloromethane (4 mL). This mixture was stirred for 10 minutes before ferrocenecarboxaldehyde (0.58 mmol, 1.2 equiv.) was added. After 3 hours of stirring, another portion of ferrocenecarboxaldehyde (93.4 μ mol, 0.2 equiv.) and one spatula of magnesium sulphate were added. The mixture was allowed to stir overnight, after which another portion of ferrocenecarboxaldehyde (67.3 μ mol, 0.1 equiv.) and a spatula of magnesium sulphate were added. After 2 hours of stirring, dry toluene (8 mL) was added to precipitate triethylamine hydrochloride and the mixture was filtered. After removal of solvents under reduced pressure, more triethylamine hydrochloride precipitated out, therefore dry toluene (10 mL) was added and the mixture was filtered again. After removal of solvents, sodium borohydride (2.07 mmol, 4.3 equiv.) was added to the solution of crude imine mixture in dry methanol (5 mL) at –10 °C. After stirring for 15 minutes at –10 °C, the reaction was left stirring at room temperature. Another portion of sodium borohydride (0.78 mmol, 1.6 equiv.) was added after 45 min at –10 °C. After stirring for 15 minutes at –10 °C, the reaction solution was left stirring overnight at room temperature. The reaction was quenched with water (5 mL) and methanol was evaporated under reduced pressure. After the aqueous layer was extracted with ethyl acetate (3 \times 10 mL), the combined organic extracts were washed with brine (10 mL) and dried over magnesium sulphate. This crude mixture was subjected to column chromatography (typically 40–80% ethyl acetate in hexane), which yielded the *N*-ferrocenylmethyl β -hydroxyamides.

***N*-(Ferrocenylmethyl)-3-hydroxy-3-phenylpropanamide (7a)**. Obtained as a yellowish orange solid (77.8 mg, 0.21 mmol) in a 44% overall yield. ¹H NMR (500 MHz, CDCl₃): δ 7.36–7.25 (m, 5H), 6.08 (s, 1H), 5.09 (dd, *J* = 8.75, 3.5 Hz, 1H), 4.14–4.12 (m, 11H), 2.59–2.50 (m, 2H) ppm. ¹³C NMR (125 MHz, CDCl₃):

δ 171.1, 143.1, 128.5, 127.7, 125.6, 84.4, 70.9, 68.6, 68.2, 68.1, 44.7, 38.8 ppm. IR (Neat): 3300, 1646 cm^{-1} . HRMS (ASAP) Found: M, 363.0914. $\text{C}_{20}\text{H}_{21}\text{FeNO}_2$ requires M, 363.0922. Melting point: 114.7–116.9 °C.

N-(Ferrocenylmethyl)-3-hydroxy-3-(*o*-methylphenyl) propanamide (7b). Obtained as brownish orange solid (46.1 mg, 0.12 mmol) in a 22% overall yield. ^1H NMR (500 MHz, CDCl_3): δ 7.47 (d, $J = 7.5$ Hz, 1H), 7.21–7.14 (m, 2H), 7.10–7.09 (m, 1H), 6.29 (bs, 1H), 5.27 (d, $J = 9$ Hz, 1H), 4.14–4.12 (m, 11H), 2.50–2.40 (m, 2H), 2.29 (s, 3H) ppm. ^{13}C NMR (125 MHz, CDCl_3): δ 171.3, 141.1, 134.1, 130.5, 127.5, 126.5, 125.3, 84.5, 68.7, 68.3, 68.3, 67.5, 43.4, 38.9, 19.1 ppm. IR (Neat): 3305, 1636 cm^{-1} . HRMS (ESI) Found: M+, 377.10726. $\text{C}_{21}\text{H}_{23}\text{FeNO}_2$ requires M+, 377.10726. Melting point: 103.2–107.3 °C.

N-(Ferrocenylmethyl)-3-hydroxy-3-(*m*-methoxyphenyl) propanamide (7c). Obtained as a brownish orange solid (111.5 mg, 0.28 mmol) in a 56% overall yield. ^1H NMR (500 MHz, CDCl_3): δ 7.26–7.23 (m, 1H), 6.94–6.91 (m, 2H), 6.81 (d, $J = 8$ Hz, 1H), 6.05 (bs, 1H), 5.08–5.07 (m, 1H), 4.15–4.13 (m, 11H), 3.80 (s, 3H), 2.56–2.54 (m, 2H) ppm. ^{13}C NMR (125 MHz, CDCl_3): δ 171.2, 160.0, 145.0, 129.8, 118.0, 113.5, 111.3, 84.6, 71.1, 68.8, 68.4, 68.4, 68.4, 55.5, 44.9, 39.0 ppm. IR (Neat): 3310, 1647 cm^{-1} . HRMS (ESI) Found: (M + Na)+, 416.0918. $\text{C}_{21}\text{H}_{23}\text{NO}_3\text{Fe}$ requires (M + Na)+, 416.0925. Melting point: 83.2–86.8 °C.

N-(Ferrocenylmethyl)-3-hydroxy-3-(*m*-fluorophenyl) propanamide (7d). Obtained as a brown solid (35.2 mg, 0.09 mmol) in a 49% overall yield. ^1H NMR (300 MHz, CDCl_3): δ 7.33–7.26 (m, 1H), 7.13–7.10 (m, 2H), 6.99–6.93 (m, 1H), 5.93 (bs, 1H), 5.11 (t, $J = 6.3$ Hz, 1H), 4.15–4.14 (m, 11H), 2.53 (d, $J = 6$ Hz, 2H) ppm. ^{13}C NMR (125 MHz, CDCl_3): δ 171.0, 163.0 (d, $J = 245$ Hz), 145.9 (d, $J = 7.5$ Hz), 130.1 (d, $J = 8.75$ Hz), 121.2 (d, $J = 3.75$ Hz), 114.5 (d, $J = 21.25$ Hz), 112.7 (d, $J = 22.5$ Hz), 84.3, 70.3, 68.7, 68.3, 68.3, 68.3, 44.5, 38.9 ppm. IR (Neat): 3238, 1650 cm^{-1} . HRMS (ESI) Found: (M + Na)+, 404.0710. $\text{C}_{20}\text{H}_{20}\text{NO}_2\text{FFe}$ requires (M + Na)+, 404.0725. Melting point: 112.3–116.3 °C.

N-(Ferrocenylmethyl)-3-hydroxy-3-(*p*-methylphenyl) propanamide (7e). Obtained as a yellow oil (118.8 mg, 0.32 mmol) in 58% overall yield. ^1H NMR (500 MHz, CDCl_3): δ 7.25 (d, $J = 7.5$ Hz, 2H), 7.15 (d, $J = 8$ Hz, 2H), 5.99 (bs, 1H), 5.08 (d, $J = 8.5$ Hz, 1H), 4.15–4.13 (m, 11H), 3.92 (bs, 1H), 2.61–2.50 (m, 2H), 2.34 (s, 3H) ppm. ^{13}C NMR (125 MHz, CDCl_3): δ 171.1, 140.1, 137.4, 129.2, 125.5, 84.4, 70.9, 68.6, 68.2, 68.2, 44.8, 38.8, 21.1 ppm. IR (Neat): 3299, 1636 cm^{-1} . HRMS (ESI) Found: (M + Na)+, 400.0979. $\text{C}_{21}\text{H}_{23}\text{NO}_2\text{Fe}$ requires (M + Na)+, 400.0976.

N-(Ferrocenylmethyl)-3-hydroxy-3-(*p*-methoxyphenyl) propanamide (7f). Obtained as a yellowish orange solid in 25% yield. ^1H NMR (300 MHz, CDCl_3): δ 7.27 (d, $J = 8.1$ Hz, 2H), 6.86 (d, $J = 8.4$ Hz, 2H), 6.13 (bs, 1H), 5.04 (d, $J = 8.4$ Hz, 1H), 4.15–4.14 (m, 11H), 3.79 (s, 3H), 2.61–2.46 (m, 2H) ppm. ^{13}C NMR (75 MHz, CDCl_3): δ 171.3, 159.2, 135.4, 127.0, 114.0, 84.5, 70.7, 68.8, 68.7, 68.3, 55.4, 44.9, 38.9 ppm. IR (Neat): 3301, 1636 cm^{-1} . HRMS (ESI) Found: (M + Na)+, 416.0937. $\text{C}_{21}\text{H}_{23}\text{FeNO}_3$ requires (M + Na)+, 416.0925. Melting point: 80.5–83.8 °C.

N-(Ferrocenylmethyl)-3-hydroxy-3-(*p*-bromophenyl) propanamide (7g). Obtained as a yellowish orange solid (82.5 mg, 0.19 mmol) in a 44% overall yield. ^1H NMR (500 MHz, CDCl_3): δ 7.44 (d, $J = 8$ Hz, 2H), 7.20 (d, $J = 8.5$ Hz, 2H), 6.13 (bs, 1H), 5.03–5.00 (m, 1H), 4.14–4.09 (m, 11H), 2.48–2.47 (m, 2H) ppm. ^{13}C NMR (125 MHz, CDCl_3): δ 170.9, 142.2, 131.7, 127.4, 121.5, 84.2, 70.3, 68.7, 68.4, 68.3, 68.3, 44.5, 38.9 ppm. IR (Neat): 3302, 1636 cm^{-1} . HRMS (ESI) Found: (M + Na)+, 463.9934. $\text{C}_{20}\text{H}_{20}\text{BrFeNO}_2$ requires (M + Na)+, 463.9925. Melting point: 113.6–115.1 °C.

Acknowledgements

The University of Wollongong is gratefully acknowledged for the financial support of this research.

Notes and references

- 1 A. de Meijere, *Chem. Rev.*, 2003, **103**, 931.
- 2 C. Binda, M. Li, F. Hubálek, N. Restelli, D. E. Edmondson and A. Mattevi, *Proc. Natl. Acad. Sci. U. S. A.*, 2003, **100**, 9750.
- 3 B. Cao, D. Xiao and M. M. Joullié, *Org. Lett.*, 1999, **1**, 1799.
- 4 B. Denolf, S. Mangelinckx, K. W. Törnroos and N. De Kimpe, *Org. Lett.*, 2007, **9**, 187.
- 5 R. B. Silverman, *J. Biol. Chem.*, 1983, **258**, 14766.
- 6 M. A. Cerny and R. P. Hanzlik, *J. Am. Chem. Soc.*, 2006, **128**, 3346.
- 7 Q. Sun, R. Zhu, F. W. Foss and T. L. Macdonald, *Chem. Res. Toxicol.*, 2008, **21**, 711.
- 8 C. Madelaine, Y. Six and O. Buriez, *Angew. Chem., Int. Ed.*, 2007, **46**, 8046.
- 9 K. Wimalasena, H. B. Wickman and M. P. D. Mahindaratne, *Eur. J. Org. Chem.*, 2001, 3811.
- 10 T. Itoh, K. Kaneda and S. Teranishi, *Tetrahedron Lett.*, 1975, **16**, 2801.
- 11 A. Blackburn, D. M. Bowles, T. T. Curran and H. Kim, *Synth. Commun.*, 2012, **42**, 1855.
- 12 C. Biot, G. Glorian, L. A. Maciejewski, J. S. Brocard, O. Domarle, G. Blampain, P. Millet, A. J. Georges, H. Abessolo, D. Dive and J. Lebib, *J. Med. Chem.*, 1997, **40**, 3715.
- 13 M. Görmen, P. Pigeon, S. Top, E. A. Hillard, M. Huché, C. G. Hartinger, F. de Montigny, M.-A. Plamont, A. Vessières and G. Jaouen, *ChemMedChem*, 2010, **5**, 2039.
- 14 S. J. Cho, N. H. Jensen, T. Kurome, S. Kadari, M. L. Manzano, J. E. Malberg, B. Caldarone, B. L. Roth and A. P. Kozikowski, *J. Med. Chem.*, 2009, **52**, 1885.
- 15 C. Pi, Y. Li, X. Cui, H. Zhang, Y. Han and Y. Wu, *Chem. Sci.*, 2013, **4**, 2675.
- 16 (a) K. S. Feldman and R. E. Simpson, *Tetrahedron Lett.*, 1989, **30**, 6985–6988; (b) T. Iwama, H. Matsumoto, T. Ito, H. Shimizu and T. Kataoka, *Chem. Pharm. Bull.*, 1998, **46**, 913.
- 17 M. G. Zagorski and R. G. Salomon, *J. Am. Chem. Soc.*, 1980, **102**, 2501.

- 18 L. M. Sayre, R. T. Naismith, M. A. Bada, W. S. Li, M. E. Klein and M. D. Tennant, *Biochim. Biophys. Acta*, 1996, **1296**, 250.
- 19 K. Mütter, R. Fröhlich, C. Mück-Lichtenfeld, S. Grimme and M. Oestreich, *J. Am. Chem. Soc.*, 2011, **133**, 12442.
- 20 S. Maity, M. Zhu, R. S. Shinabery and N. Zheng, *Angew. Chem., Int. Ed.*, 2011, **51**, 222.
- 21 B. Kunze, H. Steinmetz, G. Höfle, M. Huss, H. Wiczorek and H. Reichenbach, *J. Antibiot.*, 2006, **59**, 664.
- 22 R. Cozzi and R. Attanasio, *Expert Rev. Clin. Pharmacol.*, 2012, **5**, 125.
- 23 H. Kakei, T. Nemoto, T. Ohshima and M. Shibasaki, *Angew. Chem., Int. Ed.*, 2004, **43**, 317.